ISSN 1948-5204 (online)

World Journal of *Gastrointestinal Oncology*

World J Gastrointest Oncol 2023 July 15; 15(7): 1105-1316

Published by Baishideng Publishing Group Inc

World Journal of Gastrointestinal Oncology

Contents

Monthly Volume 15 Number 7 July 15, 2023

REVIEW

MINIREVIEWS

ORIGINAL ARTICLE

Basic Study

Clinical and Translational Research

Case Control Study

Retrospective Cohort Study

World Journal of Gastrointestinal Oncology

Monthly Volume 15 Number 7 July 15, 2023

Contents

World Journal of Gastrointestinal Oncology

Monthly Volume 15 Number 7 July 15, 2023

Contents

ABOUT COVER

Editorial Board Member of *World Journal of Gastrointestinal Oncology*, Zhi-Fei Cao, MD, PhD, Assistant Professor, Research Assistant Professor, Department of Pathology, The Second Affiliated Hospital of Soochow University, Suzhou 215004, Jiangsu Province, China. hunancao@163.com

AIMS AND SCOPE

The primary aim of *World Journal of Gastrointestinal Oncology* (*WJGO*, *World J Gastrointest Oncol*) is to provide scholars and readers from various fields of gastrointestinal oncology with a platform to publish high-quality basic and clinical research articles and communicate their research findings online.

WJGO mainly publishes articles reporting research results and findings obtained in the field of gastrointestinal oncology and covering a wide range of topics including liver cell adenoma, gastric neoplasms, appendiceal neoplasms, biliary tract neoplasms, hepatocellular carcinoma, pancreatic carcinoma, cecal neoplasms, colonic neoplasms, colorectal neoplasms, duodenal neoplasms, esophageal neoplasms, gallbladder neoplasms, *etc*.

INDEXING/ABSTRACTING

The *WJGO* is now abstracted and indexed in PubMed, PubMed Central, Science Citation Index Expanded (SCIE, also known as SciSearch®), Journal Citation Reports/Science Edition, Scopus, Reference Citation Analysis, China National Knowledge Infrastructure, China Science and Technology Journal Database, and Superstar Journals Database. The 2023 edition of Journal Citation Reports® cites the 2022 impact factor (IF) for *WJGO* as 3.0; IF without journal self cites: 2.9; 5-year IF: 3.0; Journal Citation Indicator: 0.49; Ranking: 157 among 241 journals in oncology; Quartile category: Q3; Ranking: 58 among 93 journals in gastroenterology and hepatology; and Quartile category: Q3. The *WJGO*'s CiteScore for 2022 is 4.1 and Scopus CiteScore rank 2022: Gastroenterology is 71/149; Oncology is 197/366.

RESPONSIBLE EDITORS FOR THIS ISSUE

Production Editor: *Xiang-Di Zhang*; **Production Department Director:** *Xiang Li*; **Editorial Office Director:** *Jia-Ru Fan*.

NAME OF JOURNAL
World Journal of Gastrointestinal Oncology

ISSN
ISSN 1948-5204 (online)

LAUNCH DATE
February 15, 2009

FREQUENCY
Monthly

EDITORS-IN-CHIEF
Monjur Ahmed, Florin Burada

EDITORIAL BOARD MEMBERS
https://www.wjgnet.com/1948-5204/editorialboard.htm

PUBLICATION DATE
July 15, 2023

INSTRUCTIONS TO AUTHORS
https://www.wjgnet.com/bpg/gerinfo/204

GUIDELINES FOR ETHICS DOCUMENTS
https://www.wjgnet.com/bpg/GerInfo/287

GUIDELINES FOR NON-NATIVE SPEAKERS OF ENGLISH
https://www.wjgnet.com/bpg/gerinfo/240

PUBLICATION ETHICS
https://www.wjgnet.com/bpg/GerInfo/288

PUBLICATION MISCONDUCT
https://www.wjgnet.com/bpg/gerinfo/208

ARTICLE PROCESSING CHARGE
https://www.wjgnet.com/bpg/gerinfo/242

STEPS FOR SUBMITTING MANUSCRIPTS
https://www.wjgnet.com/bpg/GerInfo/239

ONLINE SUBMISSION
https://www.f6publishing.com

World Journal of Gastrointestinal Oncology

Submit a Manuscript: https://www.f6publishing.com

World J Gastrointest Oncol 2023 July 15; 15(7): 1105-1118

DOI: 10.4251/wjgo.v15.i7.1105

ISSN 1948-5204 (online)

REVIEW

Role of ferroptosis in esophageal cancer and corresponding immunotherapy

Xin Fan, Yan-Ting Fan, Hui Zeng, Xi-Qi Dong, Min Lu, Zhi-Yuan Zhang

Specialty type: Oncology

Provenance and peer review: Invited article; Externally peer reviewed.

Peer-review model: Single blind

Peer-review report's scientific quality classification

Grade A (Excellent): 0
Grade B (Very good): B, B
Grade C (Good): 0
Grade D (Fair): 0
Grade E (Poor): 0

P-Reviewer: Fu ZC, China; Hsu C, Taiwan

Received: December 28, 2022
Peer-review started: December 28, 2022
First decision: January 12, 2023
Revised: February 28, 2023
Accepted: April 24, 2023
Article in press: April 24, 2023
Published online: July 15, 2023

Xin Fan, Zhi-Yuan Zhang, Department of Otolaryngology-Head and Neck Surgery, The First Affiliated Hospital of Nanchang University, Nanchang 330000, Jiangxi Province, China

Yan-Ting Fan, Xi-Qi Dong, The First Clinical Medical College, Nanchang University, Nanchang 330000, Jiangxi Province, China

Hui Zeng, Department of Stomatology, The Second Affiliated Hospital of Nanchang University, Nanchang 330000, Jiangxi Province, China

Min Lu, Department of Emergency Medicine, Shangrao Hospital Affiliated to Nanchang University, Shangrao 334000, Jiangxi Province, China

Corresponding author: Zhi-Yuan Zhang, PhD, Doctor, Department of Otolaryngology-Head and Neck Surgery, The First Affiliated Hospital of Nanchang University, No. 17 Yongwaizheng Street, Donghu District, Nanchang 330000, Jiangxi Province, China. zzyent@126.com

Abstract

Esophageal cancer (EC) is one of the most common digestive system malignancies in the world. The combined modality treatment of EC is usually surgery and radiation therapy, however, its clinical efficacy for advanced patients is relatively limited. Ferroptosis, a new type of iron-dependent programmed cell death, is different from apoptosis, necrosis and autophagy. In recent years, many studies have further enlightened that ferroptosis plays an essential role in the occurrence, development and metastasis of tumors. Targeting ferroptosis stimulates a new direction for further exploration of oncologic treatment regimens. Furthermore, ferroptosis has a critical role in the immune microenvironment of tumors. This paper reviews the mechanism of ferroptosis and the ferroptosis research progress in the treatment of EC. We further elaborate the interaction between ferroptosis and immunotherapy, and the related mechanisms of ferroptosis participation in the immunotherapy of EC, so as to provide new directions and ideas for the treatment of EC.

Key Words: Esophageal cancer; Ferroptosis; Immunotherapy; Metastasis

Core Tip: Recent studies suggested that ferroptosis plays an important role in the development, progression and metastasis of esophageal cancer (EC). Meanwhile, ferroptosis influences the outcome of immunotherapy to some extent. This review aims to elucidate the mechanism of ferroptosis and the ferroptosis research progress in the treatment of EC. We further elaborate the interaction between ferroptosis and immunotherapy, and the related mechanisms of ferroptosis participation in the immunotherapy of EC, so as to provide new directions and ideas for the treatment of EC.

Citation: Fan X, Fan YT, Zeng H, Dong XQ, Lu M, Zhang ZY. Role of ferroptosis in esophageal cancer and corresponding immunotherapy. *World J Gastrointest Oncol* 2023; 15(7): 1105-1118
URL: https://www.wjgnet.com/1948-5204/full/v15/i7/1105.htm
DOI: https://dx.doi.org/10.4251/wjgo.v15.i7.1105

INTRODUCTION

Esophageal cancer (EC) is a common malignancy of the digestive system with 604000 new cases and 544000 new deaths per year[1]. EC can be classified into two major subtypes: Esophageal adenocarcinoma (EAC) and esophageal squamous cell carcinoma (ESCC). ESCC is the major subgroup, making up almost 90 percent of total cases, and common in East to Central Asia[2]. Under multi-modality management, esophagectomy, endoscopic treatment, radiotherapy, and chemotherapy are the main theraputic strategies for patients with EC. The standard treatment for locally advanced EC uses neoadjuvant radiotherapy followed by esophagectomy; however, the 5-year overall survival rate for EC is less than 20%[3,4].

Iron-dependent form of regulated cell death, known as ferroptosis, was first proposed by Dixon *et al*[5] in 2012. Ferroptosis results in smaller intracellular mitochondria, increased membrane density, and reduced cristae, accompanied by the accumulation of lipid peroxides combined with the production of reactive oxygen species (ROS). Initially, it was considered that inhibition of cystine uptake abnormalized the antioxidant system of cells, leading to iron-dependent oxidative death[5]. Later studies have confirmed that ferroptosis can be induced through various pathways such as glutathione peroxidase 4 (GPX4) inhibition, intracellular iron accumulation, oxidative attack by lipoxygenase (LOX), and targeting of NRF2[6-9] (Figure 1). A study in 2021 showed that 5-aminolevulinic acid (5-ALA) treatment inhibited GPX4 and HMOX1 overexpression, promoting ferroptosis in ESCC[10]. In the same year, Zhang *et al*[11] demonstrated that oridonin (Ori) inhibited glutathione synthesis in EC cells, thereby inducing ferroptosis to exert anticancer activity. Thus, targeting ferroptosis genes and related pathways may promote further research progress to control tumor growth.

More recently, immunotherapy in EC has become a hot topic. Immunotherapy complements the conventional treatment options, which shows great promise in unresectable or metastatic EC[12]. Immune checkpoint blockade (ICB) is increasingly at the front line of cancer treatment, often as monotherapy or in combination with radiotherapy. Immune checkpoints, such as programmed cell death 1 ligand 1 (PD-L1) and cytotoxic T lymphocyte-associated antigen-4 (CTLA-4), can be expressed on the surface of cancer cells and act tumor immune escape by binding to receptors on the surface of immune cells[13]. Based on this principle, commercially available immune checkpoint blockers (ICIs) include anti-CTLA-4 and anti-programmed cell death 1 (PD-1)/PD-L1[13]. Currently, PD-1 inhibitors have been utilized as first-line immunotherapy for advanced metastatic EC[14,15]. However, there are still limits to identify patients who would be most likely to benefit from ICB therapy.

The tumor immune microenvironment (TIME) can promote tumor progression as well as resist the immune response. Tumor immunosuppressive cells, regulatory T (Treg) cells, M2 macrophages, and migratory dendritic cells (DCs), play an important role in the immune escape of tumors[16]. Therefore, targeting these cells may enhance the antitumor immune effect. For example, Xu *et al*[17] found that Treg-specific ablation of GPX4 inhibited tumor growth and simultaneously enhanced antitumor immunity. One study reported that CD8+ T cells release Interferon-gamma (IFNγ), which promotes lipid peroxidation and ferroptosis in tumor cells[18]. This study, the first to connect immunity and ferroptosis at once, is a breakthrough discovery. In 2022, Luo *et al*[19] improved the effectiveness of radiotherapy in ESCC patients by targeting SCD1 to induce ferroptosis in ESCC cells and confer immunogenicity. It appears that the application of ferroptosis in immunotherapy for EC patients deserves further exploration.

In this review, we illustrate the research progress of ferroptosis in EC and try to explore the key role of ferroptosis in EC immunotherapy to provide novel directions and ideas for the treatment of EC.

THE MECHANISM OF FERROPTOSIS

Glutathione metabolism

Glutathione, a tripeptide containing γ-amide bond and sulfhydryl group, consists of glutamic acid, cysteine and glycine. Glutathione exists in both reduced (GSH) and oxidized (GSSG) forms, whereas GSH predominating in the physiological state. As an important member of the intracellular antioxidant system, GSH can directly quench oxidized substances while being oxidized itself to GSSG[20]. GPX4 as the fourth member of the selenium-containing GPX family, converts hydrogen peroxide (H_2O_2) and lipid hydroperoxide (Lipid-OOH), important drivers of ferroptosis, into water (H_2O) and

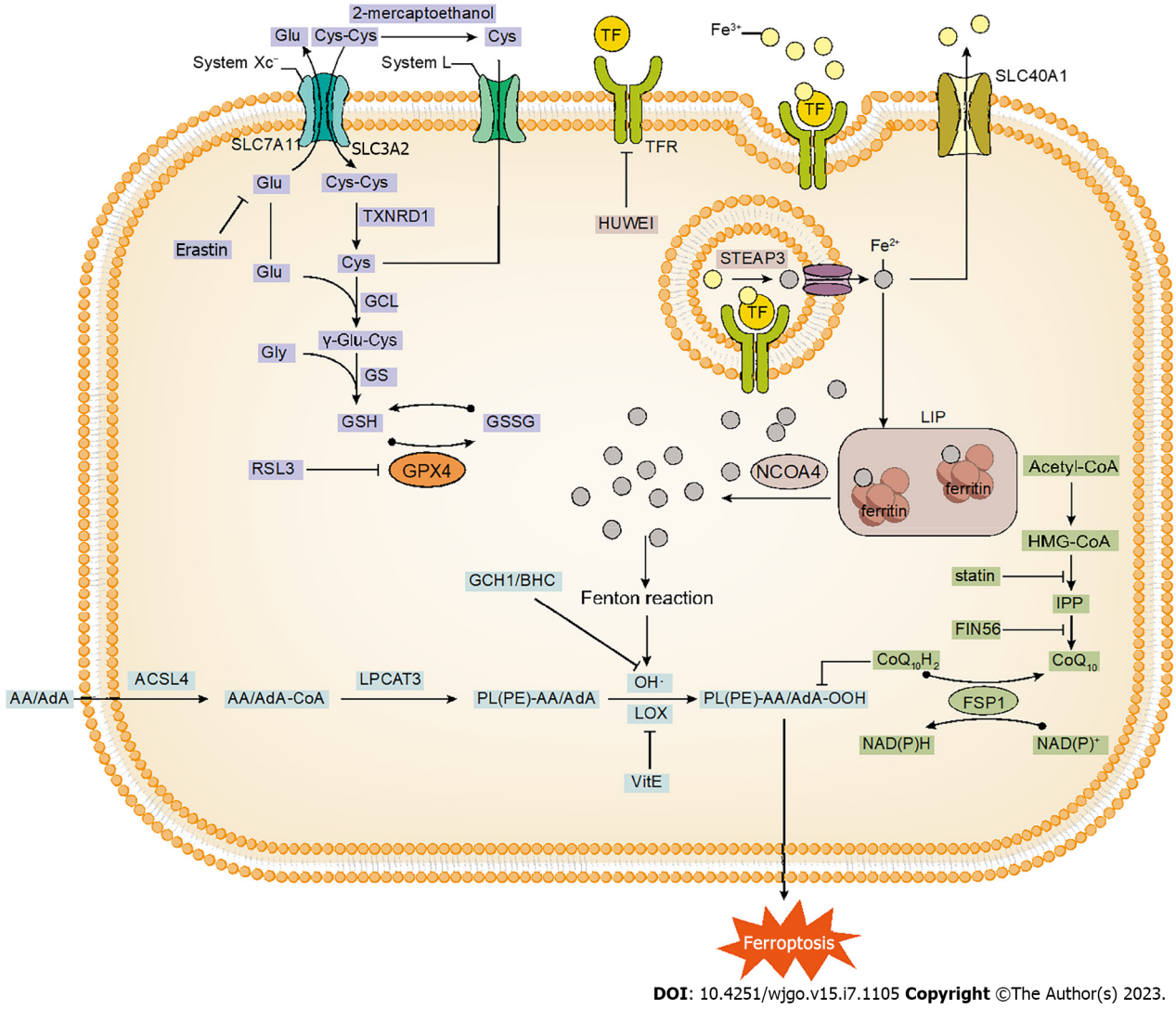

DOI: 10.4251/wjgo.v15.i7.1105

Figure 1 The process of ferroptosis, mainly including glutathione metabolism, iron metabolism and lipid peroxidation reaction.

lipid alcohol (Lipid-OH)[20]. This process effectively prevents the generation of toxic ROS and attenuates the occurrence of ferroptosis. Therefore, the reduction of GPX4 Levels in intracellular due to depletion of GSH can effectively induce the intracellular ferroptosis response. A 2014 study demonstrated that the lethality of all 12 ferroptosis inducers was affected by GPX4 expression and knockdown[6]. Affinity-based chemoproteomics displayed that RSL3 [(1S,3R)-RSL3] can bind specifically to GPX4, inhibit GPX4 enzyme activity, and lead to the accumulation of intracellular peroxides, thus triggering ferroptosis[6].

System Xc^- is a glutamate/cystine antiporter on cell surface, composed of SLC7A11 and SLC3A2. Cystine and glutamate are exchanged in and out of the cell in an equal proportion *via* System Xc^-, and then intracellular cystine is rapidly reduced to cysteine by thioredoxin reductase 1 (TXNRD1). Cysteine is the rate-limiting substrate for the synthesis of GSH. The GSH biosynthesis consists of two main steps: (1) Glutamate and cysteine synthesize dipeptide (γ-glutamyl-cysteine) catalyzed by glutamate-cysteine ligase (GCL); and (2) glutathione synthetase (GS) catalyzes the synthesis of GSH from dipeptide and glycine[21]. Consequently, it follows that acting on System Xc^- on the cell membrane becomes the primary mechanism for inducing ferroptosis. Erastin[5], sorafenib[22] can interfere with cystine uptake through targeted inhibition of the SLC7A11 subunit of System Xc^-, thus affecting GSH synthesis. High concentrations of extracellular glutamate also affect System Xc^-, preventing cystine input and leading to GSH depletion[23].

In addition, 2-mercaptoethanol converts extracellular cystine to cysteine and cysteine transfers into the cell *via* the L system, bypassing System Xc^- to participate in the synthesis of GSH[24]. In this way, certain cells can resist erastin-induced ferroptosis. In the study of Hayano *et al*[25], the loss of cysteinyl-tRNA synthetase induced the transsulfuration pathway and suppressed the ferroptosis induced by erastin.

The potential role of iron

Iron is an essential element for various organisms, and the deficiency or excess of iron can facilitate the development of various diseases. Accumulation of Fe^{2+} causes peroxidation of cells, further leading to cell death. Fe^{2+} generates ROS driving the production of lipid peroxides (LPO), which induces ferroptosis, mainly through Fenton reaction with H_2O_2: $Fe^{2+} + H_2O_2 \rightarrow Fe^{3+} + (OH)^- + OH\cdot$[26,27]. In addition to the production of LPO by the Fenton reaction, excess iron also

triggers the LPO generator through the GSH and iron redox coupling sequence to induce LPO independent with the Fenton reaction, triggering ferroptosis[28].

The balance of iron metabolism is maintained through four major processes: uptake, storage, utilization, and export. An imbalance in any of these processes can lead to a disruption of iron metabolism. Plasma Fe^{3+} binds to transferrin (TF) on the cell membrane, and TF carries Fe^{3+} further to the transferrin receptor (TFR)[29]. Subsequent endocytosis of vesicles formed by the plasma membrane transports the TF-Fe^{3+} complex into the cell. Fe^{3+} can be reduced intracellularly to Fe^{2+} by the iron reductase STEAP3[29]. The study showed that knockdown of TF led to reduced cell death and ROS after treatment and inhibited the induction of ferroptosis following siramesine and lapatinib treatment of breast cancer cells [7]. Targeted inhibition of TFR1 by HUWE1 significantly reduces ferroptosis in acute liver injury[30]. On the contrary, aberrant TF and ferritin upregulation triggers iron accumulation *via* IRP2-induced upregulation of TFR1[31]. Therefore, TF and TFR contribute to iron uptake and regulation of ferroptosis occurrence.

Fe^{2+} in the cytoplasm enters the labile iron pool (LIP) and the excess iron stably binds to ferritin in the form of Fe^{3+}. Whereas, nuclear receptor coactivator 4 (NCOA4) mediates ferritin phagocytosis and delivers ferritin to autolysosome, thereby allowing lysosomes to degrade ferritin and release iron transport proteins[32], suggesting the vital role of ferritin in ferroptosis. Hypoxia reduces intracellular free iron and increases mitochondrial ferritin expression, which can effectively protect from ferroptosis[33]. SLC40A1 mainly mediates iron export[29].

Lipid peroxidation reaction

Lipid peroxidation is a class of oxidative degradation of lipid reaction in which ROS reacts with the carbon-carbon double bonds of unsaturated lipids in biological membranes, leading to cellular damage. The final products of lipid peroxidation include malondialdehyde (MDA), and 4-hydroxynonenal (4-HNE). It most often affects polyunsaturated fatty acids (PUFAs), because they contain multiple double bonds. Exogenous monounsaturated fatty acids (MUFAs), on the other hand, inhibit the occurrence of lipid peroxidation reactions by a specific mechanism, whereby MUFAs promote the replacement of PUFAs from plasma membrane phospholipids in an ACSL3-dependent manner[34]. Arachidonic acid (AA) and adrenic acid (AdA) are the major PUFAs during ferroptosis. At present, lipid peroxidation mainly acts on esterified PUFAs rather than free PUFAs. Acyl-CoA synthetase long-chain family member 4 (ACSL4) and lysophosphatidylcholine acyltransferase 3 (LPCAT3) have been confirmed to be the key determinants of ferroptosis susceptibility [35,36]. ACSL4 transfers CoA to AA/AdA to form AA/AdA-CoA, while AA/AdA-CoA is esterified to PL(PE)-AA/AdA catalyzed by LPCAT3[37].

Phospholipids containing polyunsaturated fatty acyl groups (PL-PUFAs) can be oxidized by both enzymatic and non-enzymatic pathways. The non-enzymatic reaction occurs mainly through autoxidation of the Fenton reaction, which consists of three steps: (1) The free radicals (such as OH·) attack the hydrogen atom from the methylene carbon of PL-PUFA, which subtracts hydrogen from PL-PUFA, forming phospholipid free radicals (PL·); (2) PL· then reacts with oxygen to form phospholipid peroxide radical (PLOO·); and (3) PLOO· extracts the hydrogen atom from another PUFA to form phospholipid hydroperoxide (PLOOH). Unfortunately, the mechanism of the enzymatic reaction is not clear. One study has shown that the enzymatic reaction emphasizes the role of the LOX family[9]. LOX is a family of non-heme, iron-containing enzymes, and most LOXs consume free fatty acids as substrates. In contrast, 15-LOX directly oxygenates PL(PE)-AA/AdA to produce hydroperoxides, which functions in LPO and ferroptosis[37]. Tocopherols and tocotrienols strongly inhibit LOX and prevent ferroptosis, suggesting a role of the vitamin E family in the regulation of ferroptosis [37]. In addition, the knockdown of 15-LOX mediated by specific inhibitors and siRNA significantly suppressed cell death induced by erastin and RSL3[38]. Further, there could be alternative studies explaning the mechanism that cytochrome P450 oxidoreductase (POR) may promote lipid peroxidation by accelerating the cycling between Fe^{2+} and Fe^{3+} in the heme component of cytochrome P450 (CYP)[39].

Other metabolic pathways

Originally named apoptosis-inducing factor mitochondrial 2 (AIFM2), ferroptosis inhibitory protein 1 (FSP1) acts as the NAD(P)H-dependent oxidoreductase mediating the reduction of extra-mitochondrial coenzyme Q (CoQ), thus inhibiting lipid peroxidation reactions[40]. Acted as the lipophilic radical-trapping antioxidant (RTA), reduced CoQ captures lipid radicals as well as elevates the endogenous amounts of α-tocopherol[40,41]. CoQ, an effector molecule of FSP1, is a class of lipid-soluble quinones with side chains composed of different numbers of isoprene units. Normally found in the human body, CoQ10 containing 10 isoprene units is an important fat-soluble antioxidant *in vivo* and plays an important role in the anti-lipid peroxidation of ferroptosis. The synthesis of CoQ10 results in following steps: synthesis of the benzoquinone ring and isoprene side chains, assembly of CoQ, and modification of the benzoquinone ring[42]. Isoprene side chains are synthesized *via* the mevalonate (MVA) pathway. 3-hydroxy-3-methylglutaryl coenzyme A (HMG-CoA) is the key intermediate in the MVA pathway, and HMG-CoA undergoes a series of enzymatic reactions to form isopentenyl diphosphate (IPP), which in turn synthesizes isoprene side chains[42,43]. The target site of action of statins is HMG-CoA reductase, which can secondarily inhibit the synthesis of CoQ10 and also prevent the maturation of selenocysteine tRNA and the synthesis of GPX4[44]. As a consequence, besides their cholesterol-lowering activity, statins exert the induction of ferroptosis in tumors. In addition to degrading GPX4, FIN56 binds and activates squalene synthase, and farnesyl pyrophosphate (FPP) (an intermediate in CoQ10 synthesis by IPP) is correspondingly reduced, thereby inhibiting the CoQ10 synthesis process and enhancing susceptibility to ferroptosis[45].

Tetrahydrobiopterin (BH4), acted as RTA, protects cells from oxidation, regulates their redox status, and plays a synergistic role together with vitamin E[46]. Guanosine triphosphate cyclic hydrolase (GCH1), the rate-limiting enzyme for BH4 synthesis, was identified by the genome-wide CRISPR screen as a GPX4-independent ferroptosis suppressor gene [47]. Dihydrofolate reductase (DHFR) catalyzes the reduction of BH2 to BH4. The methotrexate (MTX) blocking DHFR acts in concert with GPX4 to induce ferroptosis[46].

Nuclear factor red lineage 2-related factor (NRF2) is a redox-sensitive transcription factor that may facilitate antioxidation and exert resistance to ferroptosis. NRF2 targets several antioxidant genes: NAD(P)H, glutathione S-transferase (GST), γ-glutamylcysteine synthase, heme oxygenase-1 (HO-1), *etc*.[48]. Keap1 can bind to NRF2 and plays a central role in ferroptosis by participating in iron and ROS metabolism through the p62-Keap1-NRF2 pathway[8].

THE FERROPTOSIS RESEARCH PROGRESS IN THE TREATMENT OF EC

The prognosis of EC predicted by ferroptosis-related genes

A systematic analysis by Zhu *et al*[49] determined that four ferroptosis-related genes (FRGs) (CARS1, GCLM, GLS2, and EMC2) held prognostic value for overall survival (OS) in EAC patients. GLS2, CARS1, and EMC2 all induced ferroptosis and were positively correlated with the prognosis of patients, whereas GCLM as the EAC oncogene exerted a suppressive effect on ferroptosis[49]. Lu *et al*[50] identified 45 FRGs in ESCC patients, among which SCP2, mitogen-activated protein kinase (MAPK), and PRKAA1 possessed strong prognostic value for ferroptosis. Seven FRGs (ALOX12, ALOX12B, ANGPTL7, DRD4, MAPK9, SLC38A1 and ZNF419) were selected as biomarkers in the study of Song *et al*[51], where ANGPTL7, MAPK9 and ZNF419 were risk genes, while ALOX12, ALOX12B, DRD4 and SLC38A1 were protective genes. Zhao *et al*[52] identified six signature genes from 117 genes for iron metabolism and ferroptosis associated with prognosis, CNV, TMB and immune cell infiltration in ESCC (PRNP, SLC3A2, SLC39A8 and SLC39A14 had a poor prognosis in ESCC patients, in contrast to ATP6V0A1 and LCN2). Lu *et al*[53] used TCGA and GEO databases to screen out three prognostically related differentially expressed immune-related ferroptosis genes (DDIT3, SLC2A3 and GCH1), all of which were risk factors for EC patients. Recently, centrosomal and spindle pole-associated protein (CSPP1) has been identified as a novel cancer biomarker. Several studies observed increased expression of CSPP1 in EC, whereas overexpression of CSPP1 inhibited ferroptosis while promoting tumor growth[54].

The FRGs screened in these studies possess an independent prognostic value and can predict the prognosis of EC patients. By targeting these genes, the treatment plan for EC patients can be continuously updated and improved. These findings also provide new ideas and perspectives for the clinical treatment of EC.

Therapeutic value of inhibition of the System Xc⁻ on the cell membrane for EC

System Xc $^-$ on the cell membrane mainly transfers extracellular cystine into the cell and participates in the subsequent GSH synthesis. Targeting SLC7A11 and SLC3A2 in System Xc$^-$ thus offers an effective way to induce ferroptosis and inhibit tumor proliferation and metastasis. The common chemotherapeutic drugs erastin, sulfasalazine, sorafenib, imidazole ketone erastin are based on this mechanism[5,22,55,56]. High levels of SLC7A11 expression are associated with resistance to radiotherapy, and cancer cells survive under the condition of oxidative stress by upregulating SLC7A11 expression, which mediates cystine uptake[57]. SLC7A11 is highly expressed in TE13 and KYSE170 cells, and knockdown of SLC7A11 using siRNA inhibits the G1-S phase, suggesting that SLC7A11 could be an independent prognostic factor for ESCC[58]. Furthermore, knockdown of SLC7A11 makes p53 knockout (p53-KO) cells susceptible to oxidative stress and restores the radiosensitivity of EAC to cancer therapeutic agents[59]. Inhibition of the SLC7A11-glutathione axis reduces cancer growth and overcomes tumor drug resistance. The mechanism of radioresistance mediated by NRF2, a transcription factor that regulates cellular antioxidation, is unknown. A study in 2021 revealed that activated NRF2 may directly bind to the promoter region of SLC7A11, regulate its transcription, and mediate the radioresistance of ESCC through SLC7A11-mediated ferroptosis inhibition[60]. Consequently, targeting the NRF2/SLC7A11/ferroptosis axis makes it possible to combat the drug resistance of EC and even other tumors in the future.

Most studies have focused on SLC7A11, with little research on SLC3A2. Ma *et al*[61] found that YTHDC2 could act as an endogenous ferroptosis inducer in lung adenocarcinoma (LUAD) and inhibited SLC3A2 *via* inhibiting HOXA13 in an indirect m6A manner. SLC3A2 facilitates osteosarcoma growth through the regulation of the PI3K/Akt signaling pathway[62]. A study by Li *et al*[63] similarly elaborated that overexpressed SNHG1 activated the Akt pathway by regulation of SLC3A2, thereby promoting sorafenib resistance. In summary, SLC3A2 may be a promising anticancer target in the future.

Therapeutic role of GPX4 inhibitors in EC

The expression level of GPX4 is significantly elevated in most tumors. The scavenging of cell membrane Lipid-OOH by GPX4 is the main mechanism of resistance to the occurrence of ferroptosis. Current GPX4 inhibitors in use contain (1S,3R)-RSL3, FIN56, and ML210 which inhibit GPX4 activity by binding to the active site of GPX4 or by degrading GPX4 [6,45,64]. A study showed that Hsp27 rescued EC stem cells from ferroptosis-induced cell death by upregulating GPX4, which was associated with poor prognosis in EC patients[65]. Western blot results suggested that DNAJB6a overexpression downregulated GPX4 and promoted ferroptosis in ESCC, thus playing an important anticancer role[66]. In the current study, the neuropeptide LGI1 receptor ADAM23 may lead to ferroptosis in ESCC cells due to the depletion of GPX4, SLC3A2 and SLC7A11[67]. Shishido *et al*[10] verified in RT-PCR and western blot experiments that 5-ALA restrained GPX4 and overexpressed HO-1 in ESCC tissues. 5-ALA induced ferroptosis in ESCC, suggesting a strong antitumor effect. In the RNA immunoprecipitation assay, OIP5-AS1 bound to GPX4, while OIP5-AS1 knockdown inhibited EC cell proliferation by downregulating GPX4[68].

Cancer cells in the high mesenchymal state are dependent on GPX4 for survival and are more sensitive to GPX4 inhibitors[69]. Therefore, the ability of GPX4 inhibitors to eliminate drug resistance in cancer cells is often combined with targeted therapy for tumors and radiotherapy as a way to prevent tumor recurrence. However, the combination of multiple drugs often generates greater side effects for patients. Hangauer *et al*[69] proposed that targeted therapy or

chemotherapy before or after treatment with GPX4 inhibitors, an alternating therapy that improves efficacy as well as reduces toxic side effects. Targeting GPX4 provides a new strategy for treating tumors.

Therapeutic role of competing endogenous RNAs associated with EC ferroptosis

Competing endogenous RNAs (ceRNA) is a hot research topic in recent years, which emphasizes a mutual regulatory mechanism between RNAs. CeRNA regulatory network links microRNA (miRNA), mRNA, long non-coding RNA (lncRNA), circular RNA (circRNA), *etc.* MiRNA silences mRNA by binding to miRNA response elements (MREs) located on mRNA[70]. CeRNAs (mainly lncRNA and circRNA) containing MREs regulate gene expression by competitively binding to miRNAs[70]. As biological markers, ceRNAs perform an active role in targeted cancer therapy[71,72]. It has been reported that miR-27a inhibited the occurrence of ESCC by targeting KRAS[73]. The expression level of miR-27a-3p increases following p53-KO, whereas TP53 is associated with sensitivity to ferroptosis[59,74]. The downregulation of miR-27a reversed multidrug resistance in ESCC[75]. CircBCAR3 (has_circ_0007624) is highly expressed in EC and upregulates transporter protein-1 (TNPO1) through the action of sponging miR-27a-3p, thus promoting EC cell proliferation, migration, invasion and ferroptosis in vitro[76]. Lu *et al*[53] found that TMEM161B-AS1 also sponged miR-27a-3p and upregulated the expression of GCH1, promoting EC development. This suggested that miR-27a-3p and TMEM161B-AS1 may affect the ferroptosis process in EC by regulating the GCH1/BH4/DHFR axis.

As previously described, ADAM23 induces ferroptosis in ESCC cells. Chen *et al*[67] investigated the ceRNA regulatory mechanism of ADAM23: ARHGEF26-AS1 increased ADAM23 expression by regulating the miR-372-3p/ADAM23 axis, thus upregulating the ferroptosis pathway. Yao *et al*[77] demonstrated that circPVT1 accelerated the cancer progression in ESCC by targeting the miR-30a-5p/FZD3 axis. In the experiment, circPVT1 was significantly upregulated in ESCC cells resistant to 5-fluorouracil, and the knockdown of circPVT1 increased ferroptosis by downregulating p-β-linked protein, GPX4 and SLC7A11. A recent study showed that SLC7A11 was regulated by miR-513a-3p, which is mediated by lncRNA BBOX1-AS1 in ESCC cells[78]. Silencing BBOX1-AS1 through miR-513a-3p/SLC7A11 axis could provide new insights into EC therapy. Circ0120816 acts as a sponge for miR-1305 to promote ESCC development, while miR-1305 exerts tumor suppressive effects in ESCC by directly targeting and inhibiting TXNRD1, a key enzyme in GSH synthesis[79]. Targeting circ0120816 may affect the initiation of ferroptosis by inhibiting the synthesis of GSH.

The study of ceRNAs is a hot topic today, which can explain the regulation of genes on a macroscopic level. Targeting any link of the ceRNA axis can interfere with the initiation of ferroptosis in EC. Studying the regulatory network of ceRNAs associated with ferroptosis develops a variety of new pathways for targeted therapy of esophageal tumors.

The role of chemoradiotherapy in ferroptosis on EC

In the case of patients with advanced EC who cannot undergo surgery, radiotherapy along with concurrent chemotherapy is often recommended[80]. However, resistance to radiotherapy often limits the prognosis of EC patients. Radiotherapy or chemotherapy has recently been discovered to induce ferroptosis in cancer patients, while increased ferroptosis enhances patients' sensitivity to radiotherapy. Lei *et al*[81] found that ionizing radiation (IR) induced expression of the ferroptosis marker gene PTGS2 in EC cells and that 4-HNE levels were elevated in EC cell line FLO-1 cells after IR treatment. Thus, IR induces lipid peroxidation, which makes EC cell lines attenuate the resistance to ferroptosis. Luo *et al*[19] revealed that MF-438 significantly improved the effectiveness of radiotherapy in ESCC by targeting stearoyl coenzyme desaturase (SCD1) to improve radiosensitivity. The team analyzed that SCD1 was responsible for the production of MUFAs (oleic and palmitoleic acids) which tended to reduce ferroptosis in tumor cells, suggesting a role for SCD1 resistance to ferroptosis. Oleic acid protects melanoma cells derived from lymph nodes from ferroptosis in an ACSL3-dependent manner. Ori, a diterpenoid extracted from rabdosia rubescens, has been demonstrated to possess anticancer activity and is curative in the treatment of EC. As is shown in the study by Fan *et al*[82], rabdosia rubescens significantly improved the survival rate of patients with early EC, while rabdosia rubescens also enhanced the effect of chemotherapy treatment in patients with advanced EC. It was shown that Ori could block the γ-glutamyl cycle in EC cells TE1 by inhibiting γ-glutamyl transpeptidase 1 (GGT1) activity and also covalently bound to cysteine to form conjugated Ori-cysteine[11]. As a result, Ori inhibits the cystine/GSH/GPX4 axis, thereby inducing ferroptosis and exerting antitumor activity. Brusatol, also a diterpenoid, inhibits the growth of EAC cells by targeting NRF2. And Brusatol alone or in combination with cisplatin (CDDP) induced significant lipid peroxidation and ferroptosis[83]. It is obvious that Brusatol alone or in conjunction with chemotherapy works primarily through ferroptosis. Eprenetapopt, the first TP53 inhibitor, has a better therapeutic effect in combination with the conventional anticancer drug (azacitidine)[84,85]. Fujihara *et al*[86] observed reduced levels of GSH in EC cells OACM5.1 following non-targeted metabolomic and label-free quantitative proteomic analyses of EC cells OACM5.1 treated with eprenetapopt. Eprenetapopt induces ferroptosis by triggering GSH depletion, thereby limiting tumor proliferation. In addition, the combination of glycine restriction and eprenetapopt significantly suppressed esophageal tumor growth and delayed the onset of disease, thus prolonging overall survival[86].

Some classical anticancer drugs can promote ferroptosis in various processes, such as blocking System Xc^-, depleting GSH, affecting GPX4 enzyme activity, *etc.* Currently, the induction of ferroptosis can inhibit tumor proliferation and effectively improve the prognosis of cancer patients. Chemoradiotherapy combined with ferroptosis treatment could be a novel approach to improve the sensitivity of tumors to chemoradiotherapy.

THE CROSSTALK BETWEEN FERROPTOSIS AND IMMUNOTHERAPY

Immunotherapy has been recognized as a promising modality in cancer treatment, including four major categories:

Adoptive cell therapy, ICIs, non-specific immune activators, and cancer vaccines. The mainstream application of ICIs in immunotherapy holds promise. ICIs block CTLA-4 and PD-1/PD-L1 immune checkpoints that limit immune escape of tumors[13]. However, only a minority of patients receive durable and stable therapeutic effects with ICIs, while limited clinical efficacy is the normality for most tumor patients. Recent findings indicate that CD8+ T cells could promote ferroptosis in tumor cells during cancer immunotherapy[18]. The crosstalk between ferroptosis and anti-tumor immunity may lead to new directions in cancer therapy.

TIME includes tumor cells, immune cells, and cytokines, *etc.* Immune cells such as T cells, B cells, macrophages, and neutrophils have a broad effect on human diseases. Ferroptosis, however, is a double-edged sword for immunotherapy, affecting immune cells in two different ways: promoting immune function on the one hand, weakening it on the other hand[87]. Consequently, the roles of ferroptosis-related pathways on different aspects of immune cell subsets have different effects on prognosis. Ferroptosis can affect the number of immune cells to suppress the immune function of immune cells. It has been found that T cell-specific GPX4-deficient mice, despite normal thymic T cell development, accumulated lipid peroxides and ferroptosis in peripheral T cells due to the lack of GPX4[88]. In contrast, selenium supplementation enhances GPX4 expression in T cells, protects follicular helper T (T_{FH}) cells from ferroptosis, thereby increasing T_{FH} cell numbers and promoting antibody response[89]. Ferroptosis also activates the immune function of immune cells. Cinnamaldehyde dimer (CDC), a GSH-depleting dimer, causes intracellular GSH depletion after the rupture in the cytoplasm. Zhou *et al*[90] reported that the combination of CDC and sorafenib resulted in a significant enhancement of ferroptosis in "cold" tumors, as well as triggering a strong immune response *in vivo* by stimulating the maturation of dendritic cells and the initiation of CD8+ T cells.

T cells consist of distinct subpopulations such as T helper (Th) cells, cytotoxic CD8+ T lymphocytes (CTLs), Treg cells, *etc.* CTLs are often considered to release perforin and granzyme and induced FasL-mediated apoptosis so as to kill tumor cells[91]. However, CD8+ T cells have been confirmed to downregulate the expression of two subunits of System Xc^-, SLC3A2 and SLC7A11, thus inhibiting cystine uptake of tumor cells and facilitating ferroptosis in tumors. The specific mechanism is that IFNγ released by CD8+ T cells activates the janus kinase (JAK) and signal transducer and activator of transcription (STAT) 1-mediated signaling pathway, whereas STAT1 can bind to the transcriptional start site of SLC7A11 [18] (Figure 2). The Ataxia- Telangiectasia mutated gene (ATM) activated after radiotherapy can synergistically suppress SLC7A11 with activated CD8+ T cells[92]. The same team also demonstrated that naive human and mouse CD4 and CD8 T cells were relatively insensitive to cell death induced by erastin or RSL3, whereas tumor cells were susceptible to ferroptosis[18]. IFNγ produced by CD8+ T cells also stimulates ACSL4 and alters lipid patterns of tumor cells, thereby increasing AA incorporation into phospholipids containing C16 and C18 acyl chains. Low doses of AA enhance the antitumor immune effect of ICIs by enhancing tumor ferroptosis[93]. On the other hand, CD36 mediates the uptake of fatty acids on tumor-infiltrating CD8+ T cells, inducing lipid peroxidation and ferroptosis, leading to reduced cytotoxic cytokine production and impaired antitumor capacity. Blocking CD36 restores the antitumor activity of CD8+ T cells and exerts a greater antitumor effect in combination with PD-1 antibodies[94]. Treg cells, known as suppressor T cells at the early stage, exhibit immunosuppressive effects. A recent study showed that deletion of GPX4 mediated ferroptosis of Treg cells in response to T cell receptor (TCR)/CD28 co-stimulation, which inhibited tumor growth and simultaneously enhanced antitumor immunity. Likewise, GPX4-deficient Treg cells mediated the output of mitochondrial superoxide and interleukin-1β (IL-1β) that facilitated Th17 cell responses[17]. Therefore, inducing Treg cells to undergo ferroptosis may become a novel avenue for immunotherapy.

Tumor-associated macrophages (TAMs) play a key role in cancer progression, divided into two subtypes: Classically activated M1 macrophages and alternatively activated M2 macrophages. M1 macrophages play an antitumor role; M2 macrophages promote tumor proliferation, invasion, metastasis, and angiogenesis[95]. Hence, the primary object of immunotherapy is to convert M2 macrophages in an immunosuppressed state to M1 macrophages with tumor-killing activity. The ability of macrophages to engulf and remove dead cells contributes to the efficiency of immunotherapy. 1-steaoryl-2-15-HpETE-sn-glycero-3-phosphatidylethanolamine (SAPE-OOH), acted as an "eat me" signal on the surface of ferroptotic cells, targets the TLR2 receptor on macrophages that improves the phagocytosis and clearance ability of macrophages to ferroptotic cells[96]. M1 macrophages produce high NO• production due to a higher content of inducible NO synthase (iNOS) than M2 macrophages. iNOS/NO• can substitute the role of GPX4 to inhibit RSL3-induced ferroptosis. Thus, M1 polarized macrophages are highly resistant to ferroptosis, while M2 macrophages lacking iNOS show high sensitivity to ferroptosis[97]. The application of ferroptosis in M1 macrophages is often used for anticancer therapy. A biomimetic magnetosome composed of Fe_3O_4 magnetic nanocluster (NC) as the core and TGF-β inhibitor (Ti) and PD-1 antibody (Pa) as the coat enters the tumor and increases H_2O_2 in polarized M1 macrophages, thus promoting the Fenton reaction with Fe ions released from the magnetosome. The application of this magnetosome promotes ferroptosis in the tumor, and the exposed tumor antigen in turn promotes an immune response[98]. Currently, nanoparticle (NP) is frequently used for ferroptosis and to enhance immune efficacy. Hsieh *et al*[99] reported that zero-valent-iron nanoparticle (ZVI-NP) enhanced the degradation of NRF2 and triggered ferroptosis in lung cancer cells through oxidative stress and lipid peroxidation. ZVI-NP induced the polarization of TAM towards the M1 phenotype that increased the cytotoxic function of CD8+ T cells and decreased the Treg cell ratio, thereby enhancing antitumor immunity. The biomimetic magnetic nanoparticles Fe_3O_4-SAS@PLT, triggering ferroptosis pathway by inhibiting System Xc^-, that mediated ferroptosis not only induced tumor-specific immune response but also repolarized M2 macrophages to M1 phenotype[100].

DC, a powerful antigen-presenting cell that activates CTL, contributes importantly to the maintenance of the immune environment. As a nuclear receptor involved in the regulation of lipid metabolism, PPARG/PPARγ is responsible for RSL3-induced ferroptosis in DC. Ferroptotic DCs fail to secrete pro-inflammatory cytokines (TNF and IL6) and lose the ability to express MHC class I in response to maturation signals of lipopolysaccharide, and even fail to induce IFNG/IFNγ production by CD8+ T cells[101]. Taken together, ferroptosis occurring in DCs limits antitumor immunity.

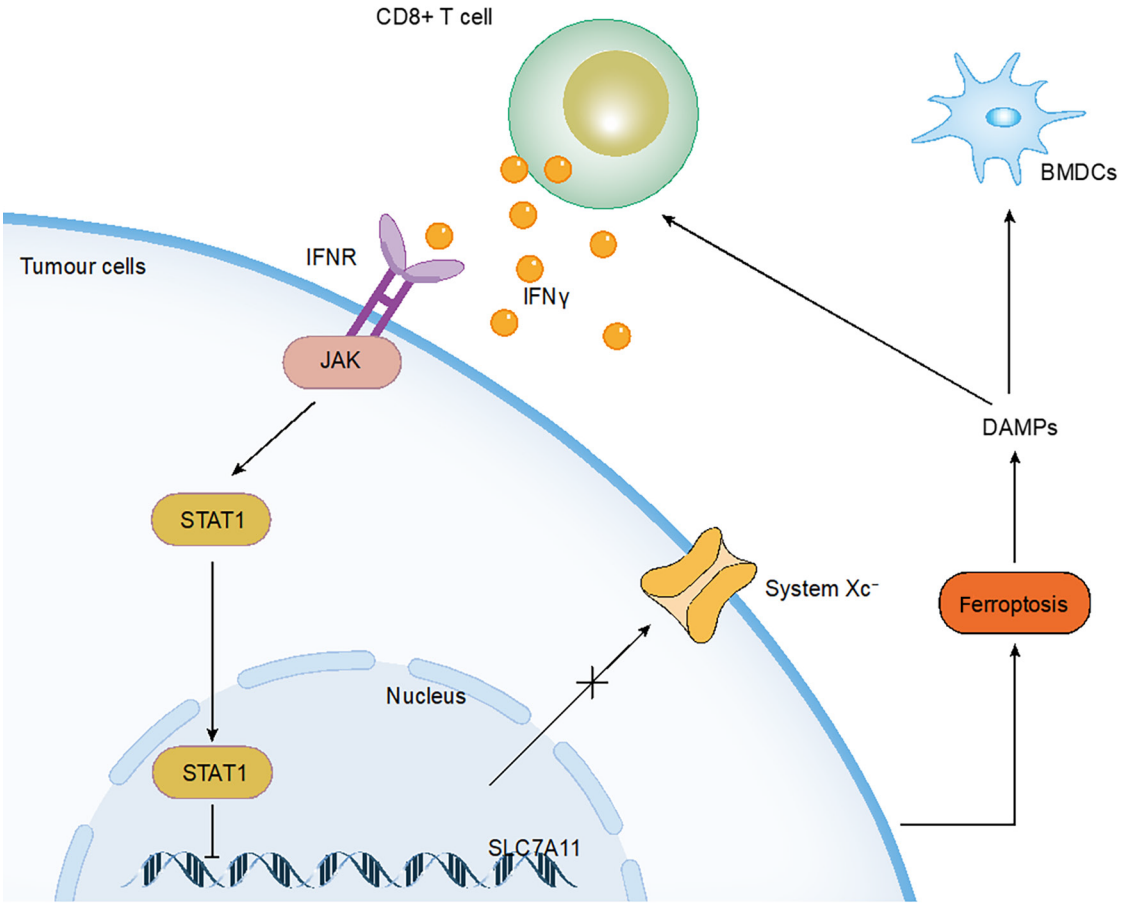

DOI: 10.4251/wjgo.v15.i7.1105

Figure 2 The crosstalk between ferroptosis and immunotherapy. The IFNγ released by CD8+ T cells activates ferroptosis in tumor cells through the JAK/STAT1 pathway. Ferroptotic tumor cells then release DAMPs which contributes to immune activation. IFN: Interferon; DAMPs: Damage-associated molecular patterns.

Immunogenic cell death (ICD) is the anti-tumor immune response of the organism caused by the conversion of non-immunogenicity to immunogenicity[102]. Cancer cells generate a series of endogenous danger signals during this process, which are called damage-associated molecular patterns (DAMPs). DAMPs mainly include calreticulin (CRT), high mobility group protein 1 (HMGB1), ATP, and so on[103,104]. Lately, HMGB1 is shown to be a DAMP released by ferroptotic cells in an autophagy-dependent manner. Ferroptosis activators, including erastin, sorafenib, RSL3, and FIN56, induce HMGB1 release in both cancer and non-cancer cells[103]. Therefore, probing the immunogenicity of ferroptotic cancer cells broadens the scope of immunogenicity that offers new possibilities for cancer therapy. Efimova *et al*[105] were the first to demonstrate that ferroptosis-induced ICD in both *vivo* and *vitro*. Ferroptotic cells promote phenotypic maturation of bone marrow-derived dendritic cells (BMDCs) and induce vaccination-like effects in immuno-competent mice (Figure 2). Meanwhile, ATP and HMGB1 were shown to be immunogenic signals for early ferroptotic cancer cells[105]. Acidity-activatable dynamic nanoparticles significantly recruited tumor-infiltrating T lymphocytes for IFN γ secretion, sensitizing tumor cells to RSL-3-induced ferroptosis and thus triggering the immunogenicity in ferroptotic tumor cells[106]. Unfortunately, no advanced ferroptotic cancer cells have been observed to be immunogenic. Therefore, the study of the immunogenicity of ferroptotic cancer cells remains a difficult problem today.

THE MECHANISM OF FERROPTOSIS IN THE IMMUNOTHERAPY OF EC

In recent years, breakthroughs have been made in the application of immunotherapy of EC patients. Pembrolizumab (the PD-1 inhibitor) plus chemotherapy (cisplatin and 5-fluorouracil) was approved for the first-line treatment of advanced EC [14]. However, more sufficient evidence-based medical evidence is still needed for immunotherapy in the first-line treatment. In the field of basic cancer research, there have been many studies exploring the role of ferroptosis in cancer immunotherapy. Therefore, the utilization of ferroptosis in immunotherapy provides a new option for the personalized treatment of EC patients. A number of studies exhibited that FRG signature was observed to be closely associated with immunity in EC. Lu *et al*[50] investigated immune cell infiltration in the tumor microenvironment using the CIBERSORT and ESTIMATE algorithms and found that CD8 T cells, CD4 memory-activated T cells, and M0, M1, and M2 in ESCC patients macrophages were significantly correlated with the screened ferroptosis gene signature[50]. Zhu *et al*'s analysis results showed differences in immune status between high and low risk groups of EAC patients, with higher levels of DC

and CD8 + T cells in the low risk group. In addition, the FRGs (GCLM, GLS2) were significantly associated with CD8+ T cells[49]. This suggests to us that ferroptosis may interact with CD8+ T cells to regulate the immune response in EAC patients. In the study by Song *et al*[51], the ferroptosis signature consisting of seven FRGs was found to be associated with most immune checkpoints, such as MAPK9 interacting with CTLA-4 and SLC38A1 blocking the effectiveness of PD-L1 antibodies. Niu *et al*[107] evaluated the level of immune cell infiltration for ferroptosis and iron metabolism-associated lncRNAs in TCGA and GEO cohorts, respectively, demonstrating the role of ferroptosis-associated lncRNAs in the regulation of immune infiltration in ESCC[107]. Meanwhile, by studying ten ferroptosis-associated lncRNAs, Zhu *et al*[108] also revealed significant differences in the TIME of ESCC patients between high- and low-risk groups, as well as the differences in the clinical benefits reaped. Hence, ferroptosis-associated lncRNAs may become immunotherapeutic targets for EC patients. While Lu *et al*[50] innovatively constructed a prognostic model of EC patients consisting of immune-related FRGs, which closely linked immunity and ferroptosis. The team detected that EC patients in the high-risk group benefited more from ICIs, which provided a personalized immunotherapy regimen for EC patients.

Key genes in the ferroptosis process play an important role in cancer progression, such as GPX4, SLC7A11, and FSP1. Recently, the expression levels of these genes were found to correlate with immune infiltration in pan-cancer. Shi *et al*[109] found that in EC, GPX4 expression was significantly associated with macrophage and DC infiltration, and AIFM2 expression was significantly associated with CD4 T cell infiltration. Simultaneously, GPX4 expression was positively correlated with the expression levels of monocyte markers (including CD14 and CD115) and M2 macrophage markers (including VSIG4 and MS4A4A) in EC. To summary, there may be a close interaction between GPX4 and macrophages in EC patients.

It seems that the ICD induces antitumor efficacy in EC patients. Zhang *et al*[110] integrated different cell death signals in ESCC and classified patients into different ICD subtypes. Transcriptomic and proteomic characterization of patients showed that cell death signals, such as ferroptosis, were positively correlated with immune activation in ESCC. A recent study explored the immunogenicity of targeting SCD1-induced ferroptotic ESCC cells. Ferroptotic ESCC cells contribute to DC activation; inhibition of SCD1, a novel ICD inducer, effectively improves the prognosis of ESCC patients[19]. Triggering the immunogenicity of ferroptotic cancer cells could lead to the discovery of new therapeutic targets, a promising therapeutic strategy in patients with EC. However, there are few reports on the immunogenicity of ferroptotic cancer cells in EC. Thus, more experimental studies and clinical validation are required to stimulate the immunogenicity of ferroptotic cancer cells in EC.

CONCLUSION

Patients with advanced EC are often treated with concurrent chemoradiotherapy, plus surgery. However, EC has a poor prognosis due to the development of resistance to chemoradiotherapy. The role of ferroptosis in a variety of cancers has been revealed. Based on the keywords "esophageal cancer" and "ferroptosis", we searched the PubMed database. Most of the studies on ferroptosis in EC are based on FRGs screened by the database, which may have independent prognostic value as protective and risk factors for EC patients, respectively. Some chemotherapeutic agents, such as erastin, sulfasalazine, sorafenib, as well as IR can induce ferroptosis. In turn, targeting essential points in the ferroptosis pathway also induces EC sensitivity to radiotherapy, such as inhibition of SLC7A11 to overcome radioresistance. Ferroptosis combined with radiotherapy could be a viable option for EC therapeutics. Currently, anticancer therapy for EC can promote ferroptosis in cancer cells and inhibit the proliferation of esophageal tumors by targeting System Xc-, GPX4, NRF2, *etc*. Moreover, the study of the ceRNA regulatory network of ferroptosis in EC may explain the gene regulation process from a macroscopic perspective, thus providing more possibilities for the treatment of EC patients.

Immunotherapy has been reported more frequently in EC. Meanwhile, studies have been conducted to elaborate on the complex mechanisms between ferroptosis and immunotherapy. During our search for articles related to the role of ferroptosis in EC, we identified that there was a close correlation between FRGs and immune infiltration. In addition, key genes in the process of ferroptosis were also associated with immunity. However, little has been reported about the mechanisms of ferroptosis in EC immunotherapy. Only a few reports were revealed to elaborate on the immunogenicity of ferroptotic EC cells. Induction of ferroptosis in cancer cells may promote the expression of their immunogenicity and in turn the anticancer activity of immune cells. Ferroptosis-related immunogenicity seems to broaden the scope of EC immunotherapy, which provides personalized treatment options for EC patients.

Since ferroptosis in EC has been studied mainly by some screening FRGs, future research should focus on the study of ferroptosis regulatory mechanisms. We can focus on one or two genes and explore their mechanisms of action in EC from different histologies (genomics, transcriptomics, proteomics, methylomics, lipidomics and metabolomics), followed by experimental validation. The research on ferroptosis in tumor immunotherapy is still in its infancy. Taken together, it is needed for us to further explore the mechanisms of ferroptosis-related immunogenicity in EC in the future to find more evidence of ferroptosis in the immunotherapy of EC patients.

FOOTNOTES

Author contributions: Fan X and Fan YT drafted the manuscript; Zeng H, Dong XQ, Lu M and Zhang ZY contributed to the editing of the manuscript; all authors contributed to the article and approved the submitted version.

Supported by the Central Funds Guiding the Local Science and Technology Development of China, No. 20221ZDG020066.

Conflict-of-interest statement: The authors have no conflicts of interest to declare.

Country/Territory of origin: China

ORCID number: Min Lu 0000-0003-0636-2240; Zhi-Yuan Zhang 0000-0001-6422-4431.

S-Editor: Yan JP
L-Editor: A
P-Editor: Yu HG

REFERENCES

1 **Sung H**, Ferlay J, Siegel RL, Laversanne M, Soerjomataram I, Jemal A, Bray F. Global Cancer Statistics 2020: GLOBOCAN Estimates of Incidence and Mortality Worldwide for 36 Cancers in 185 Countries. *CA Cancer J Clin* 2021; **71**: 209-249 [PMID: 33538338 DOI: 10.3322/caac.21660]
2 **Abnet CC**, Arnold M, Wei WQ. Epidemiology of Esophageal Squamous Cell Carcinoma. *Gastroenterology* 2018; **154**: 360-373 [PMID: 28823862 DOI: 10.1053/j.gastro.2017.08.023]
3 **Pennathur A**, Luketich JD, Landreneau RJ, Ward J, Christie NA, Gibson MK, Schuchert M, Cooper K, Land SR, Belani CP. Long-term results of a phase II trial of neoadjuvant chemotherapy followed by esophagectomy for locally advanced esophageal neoplasm. *Ann Thorac Surg* 2008; **85**: 1930-6; discussion 1936 [PMID: 18498797 DOI: 10.1016/j.athoracsur.2008.01.097]
4 **Pennathur A**, Gibson MK, Jobe BA, Luketich JD. Oesophageal carcinoma. *Lancet* 2013; **381**: 400-412 [PMID: 23374478 DOI: 10.1016/S0140-6736(12)60643-6]
5 **Dixon SJ**, Lemberg KM, Lamprecht MR, Skouta R, Zaitsev EM, Gleason CE, Patel DN, Bauer AJ, Cantley AM, Yang WS, Morrison B 3rd, Stockwell BR. Ferroptosis: an iron-dependent form of nonapoptotic cell death. *Cell* 2012; **149**: 1060-1072 [PMID: 22632970 DOI: 10.1016/j.cell.2012.03.042]
6 **Yang WS**, SriRamaratnam R, Welsch ME, Shimada K, Skouta R, Viswanathan VS, Cheah JH, Clemons PA, Shamji AF, Clish CB, Brown LM, Girotti AW, Cornish VW, Schreiber SL, Stockwell BR. Regulation of ferroptotic cancer cell death by GPX4. *Cell* 2014; **156**: 317-331 [PMID: 24439385 DOI: 10.1016/j.cell.2013.12.010]
7 **Ma S**, Henson ES, Chen Y, Gibson SB. Ferroptosis is induced following siramesine and lapatinib treatment of breast cancer cells. *Cell Death Dis* 2016; **7**: e2307 [PMID: 27441659 DOI: 10.1038/cddis.2016.208]
8 **Sun X**, Ou Z, Chen R, Niu X, Chen D, Kang R, Tang D. Activation of the p62-Keap1-NRF2 pathway protects against ferroptosis in hepatocellular carcinoma cells. *Hepatology* 2016; **63**: 173-184 [PMID: 26403645 DOI: 10.1002/hep.28251]
9 **Yang WS**, Kim KJ, Gaschler MM, Patel M, Shchepinov MS, Stockwell BR. Peroxidation of polyunsaturated fatty acids by lipoxygenases drives ferroptosis. *Proc Natl Acad Sci U S A* 2016; **113**: E4966-E4975 [PMID: 27506793 DOI: 10.1073/pnas.1603244113]
10 **Shishido Y**, Amisaki M, Matsumi Y, Yakura H, Nakayama Y, Miyauchi W, Miyatani K, Matsunaga T, Hanaki T, Kihara K, Yamamoto M, Tokuyasu N, Takano S, Sakamoto T, Honjo S, Hasegawa T, Fujiwara Y. Antitumor Effect of 5-Aminolevulinic Acid Through Ferroptosis in Esophageal Squamous Cell Carcinoma. *Ann Surg Oncol* 2021; **28**: 3996-4006 [PMID: 33210267 DOI: 10.1245/s10434-020-09334-4]
11 **Zhang J**, Wang N, Zhou Y, Wang K, Sun Y, Yan H, Han W, Wang X, Wei B, Ke Y, Xu X. Oridonin induces ferroptosis by inhibiting gamma-glutamyl cycle in TE1 cells. *Phytother Res* 2021; **35**: 494-503 [PMID: 32869425 DOI: 10.1002/ptr.6829]
12 **van Rossum PSN**, Mohammad NH, Vleggaar FP, van Hillegersberg R. Treatment for unresectable or metastatic oesophageal cancer: current evidence and trends. *Nat Rev Gastroenterol Hepatol* 2018; **15**: 235-249 [PMID: 29235549 DOI: 10.1038/nrgastro.2017.162]
13 **Topalian SL**, Drake CG, Pardoll DM. Immune checkpoint blockade: a common denominator approach to cancer therapy. *Cancer Cell* 2015; **27**: 450-461 [PMID: 25858804 DOI: 10.1016/j.ccell.2015.03.001]
14 **Sun JM**, Shen L, Shah MA, Enzinger P, Adenis A, Doi T, Kojima T, Metges JP, Li Z, Kim SB, Cho BC, Mansoor W, Li SH, Sunpaweravong P, Maqueda MA, Goekkurt E, Hara H, Antunes L, Fountzilas C, Tsuji A, Oliden VC, Liu Q, Shah S, Bhagia P, Kato K; KEYNOTE-590 Investigators. Pembrolizumab plus chemotherapy versus chemotherapy alone for first-line treatment of advanced oesophageal cancer (KEYNOTE-590): a randomised, placebo-controlled, phase 3 study. *Lancet* 2021; **398**: 759-771 [PMID: 34454674 DOI: 10.1016/S0140-6736(21)01234-4]
15 **Li ZC**, Sun YT, Lai MY, Zhou YX, Qiu MZ. Efficacy and safety of PD-1 inhibitors combined with chemotherapy as first-line therapy for advanced esophageal cancer: A systematic review and network meta-analysis. *Int Immunopharmacol* 2022; **109**: 108790 [PMID: 35504202 DOI: 10.1016/j.intimp.2022.108790]
16 **Binnewies M**, Roberts EW, Kersten K, Chan V, Fearon DF, Merad M, Coussens LM, Gabrilovich DI, Ostrand-Rosenberg S, Hedrick CC, Vonderheide RH, Pittet MJ, Jain RK, Zou W, Howcroft TK, Woodhouse EC, Weinberg RA, Krummel MF. Understanding the tumor immune microenvironment (TIME) for effective therapy. *Nat Med* 2018; **24**: 541-550 [PMID: 29686425 DOI: 10.1038/s41591-018-0014-x]
17 **Xu C**, Sun S, Johnson T, Qi R, Zhang S, Zhang J, Yang K. The glutathione peroxidase Gpx4 prevents lipid peroxidation and ferroptosis to sustain Treg cell activation and suppression of antitumor immunity. *Cell Rep* 2021; **35**: 109235 [PMID: 34133924 DOI: 10.1016/j.celrep.2021.109235]
18 **Wang W**, Green M, Choi JE, Gijón M, Kennedy PD, Johnson JK, Liao P, Lang X, Kryczek I, Sell A, Xia H, Zhou J, Li G, Li J, Li W, Wei S, Vatan L, Zhang H, Szeliga W, Gu W, Liu R, Lawrence TS, Lamb C, Tanno Y, Cieslik M, Stone E, Georgiou G, Chan TA, Chinnaiyan A, Zou W. CD8(+) T cells regulate tumour ferroptosis during cancer immunotherapy. *Nature* 2019; **569**: 270-274 [PMID: 31043744 DOI: 10.1038/s41586-019-1170-y]

19 **Luo H**, Wang X, Song S, Wang Y, Dan Q, Ge H. Targeting stearoyl-coa desaturase enhances radiation induced ferroptosis and immunogenic cell death in esophageal squamous cell carcinoma. *Oncoimmunology* 2022; **11**: 2101769 [PMID: 35859734 DOI: 10.1080/2162402X.2022.2101769]

20 **Lushchak VI**. Glutathione homeostasis and functions: potential targets for medical interventions. *J Amino Acids* 2012; **2012**: 736837 [PMID: 22500213 DOI: 10.1155/2012/736837]

21 **Lu SC**. Glutathione synthesis. *Biochim Biophys Acta* 2013; **1830**: 3143-3153 [PMID: 22995213 DOI: 10.1016/j.bbagen.2012.09.008]

22 **Yuan S**, Wei C, Liu G, Zhang L, Li J, Li L, Cai S, Fang L. Sorafenib attenuates liver fibrosis by triggering hepatic stellate cell ferroptosis *via* HIF-1α/SLC7A11 pathway. *Cell Prolif* 2022; **55**: e13158 [PMID: 34811833 DOI: 10.1111/cpr.13158]

23 **Dixon SJ**, Patel DN, Welsch M, Skouta R, Lee ED, Hayano M, Thomas AG, Gleason CE, Tatonetti NP, Slusher BS, Stockwell BR. Pharmacological inhibition of cystine-glutamate exchange induces endoplasmic reticulum stress and ferroptosis. *Elife* 2014; **3**: e02523 [PMID: 24844246 DOI: 10.7554/eLife.02523]

24 **Ishii T**, Bannai S, Sugita Y. Mechanism of growth stimulation of L1210 cells by 2-mercaptoethanol in vitro. Role of the mixed disulfide of 2-mercaptoethanol and cysteine. *J Biol Chem* 1981; **256**: 12387-12392 [PMID: 7298664]

25 **Hayano M**, Yang WS, Corn CK, Pagano NC, Stockwell BR. Loss of cysteinyl-tRNA synthetase (CARS) induces the transsulfuration pathway and inhibits ferroptosis induced by cystine deprivation. *Cell Death Differ* 2016; **23**: 270-278 [PMID: 26184909 DOI: 10.1038/cdd.2015.93]

26 **Toyokuni S**. Iron and carcinogenesis: from Fenton reaction to target genes. *Redox Rep* 2002; **7**: 189-197 [PMID: 12396663 DOI: 10.1179/135100002125000596]

27 **Shen Z**, Liu T, Li Y, Lau J, Yang Z, Fan W, Zhou Z, Shi C, Ke C, Bregadze VI, Mandal SK, Liu Y, Li Z, Xue T, Zhu G, Munasinghe J, Niu G, Wu A, Chen X. Fenton-Reaction-Acceleratable Magnetic Nanoparticles for Ferroptosis Therapy of Orthotopic Brain Tumors. *ACS Nano* 2018; **12**: 11355-11365 [PMID: 30375848 DOI: 10.1021/acsnano.8b06201]

28 **He YJ**, Liu XY, Xing L, Wan X, Chang X, Jiang HL. Fenton reaction-independent ferroptosis therapy *via* glutathione and iron redox couple sequentially triggered lipid peroxide generator. *Biomaterials* 2020; **241**: 119911 [PMID: 32143060 DOI: 10.1016/j.biomaterials.2020.119911]

29 **Chen X**, Li J, Kang R, Klionsky DJ, Tang D. Ferroptosis: machinery and regulation. *Autophagy* 2021; **17**: 2054-2081 [PMID: 32804006 DOI: 10.1080/15548627.2020.1810918]

30 **Wu Y**, Jiao H, Yue Y, He K, Jin Y, Zhang J, Wei Y, Luo H, Hao Z, Zhao X, Xia Q, Zhong Q. Ubiquitin ligase E3 HUWE1/MULE targets transferrin receptor for degradation and suppresses ferroptosis in acute liver injury. *Cell Death Differ* 2022; **29**: 1705-1718 [PMID: 35260822 DOI: 10.1038/s41418-022-00957-6]

31 **Sze SCW**, Zhang L, Zhang S, Lin K, Ng TB, Ng ML, Lee KF, Lam JKW, Zhang Z, Yung KKL. Aberrant Transferrin and Ferritin Upregulation Elicits Iron Accumulation and Oxidative Inflammaging Causing Ferroptosis and Undermines Estradiol Biosynthesis in Aging Rat Ovaries by Upregulating NF-Kb-Activated Inducible Nitric Oxide Synthase: First Demonstration of an Intricate Mechanism. *Int J Mol Sci* 2022; **23** [PMID: 36293552 DOI: 10.3390/ijms232012689]

32 **Mancias JD**, Wang X, Gygi SP, Harper JW, Kimmelman AC. Quantitative proteomics identifies NCOA4 as the cargo receptor mediating ferritinophagy. *Nature* 2014; **509**: 105-109 [PMID: 24695223 DOI: 10.1038/nature13148]

33 **Fuhrmann DC**, Mondorf A, Beifuß J, Jung M, Brüne B. Hypoxia inhibits ferritinophagy, increases mitochondrial ferritin, and protects from ferroptosis. *Redox Biol* 2020; **36**: 101670 [PMID: 32810738 DOI: 10.1016/j.redox.2020.101670]

34 **Magtanong L**, Ko PJ, To M, Cao JY, Forcina GC, Tarangelo A, Ward CC, Cho K, Patti GJ, Nomura DK, Olzmann JA, Dixon SJ. Exogenous Monounsaturated Fatty Acids Promote a Ferroptosis-Resistant Cell State. *Cell Chem Biol* 2019; **26**: 420-432.e9 [PMID: 30686757 DOI: 10.1016/j.chembiol.2018.11.016]

35 **Dixon SJ**, Winter GE, Musavi LS, Lee ED, Snijder B, Rebsamen M, Superti-Furga G, Stockwell BR. Human Haploid Cell Genetics Reveals Roles for Lipid Metabolism Genes in Nonapoptotic Cell Death. *ACS Chem Biol* 2015; **10**: 1604-1609 [PMID: 25965523 DOI: 10.1021/acschembio.5b00245]

36 **Doll S**, Proneth B, Tyurina YY, Panzilius E, Kobayashi S, Ingold I, Irmler M, Beckers J, Aichler M, Walch A, Prokisch H, Trümbach D, Mao G, Qu F, Bayir H, Füllekrug J, Scheel CH, Wurst W, Schick JA, Kagan VE, Angeli JP, Conrad M. ACSL4 dictates ferroptosis sensitivity by shaping cellular lipid composition. *Nat Chem Biol* 2017; **13**: 91-98 [PMID: 27842070 DOI: 10.1038/nchembio.2239]

37 **Kagan VE**, Mao G, Qu F, Angeli JP, Doll S, Croix CS, Dar HH, Liu B, Tyurin VA, Ritov VB, Kapralov AA, Amoscato AA, Jiang J, Anthonymuthu T, Mohammadyani D, Yang Q, Proneth B, Klein-Seetharaman J, Watkins S, Bahar I, Greenberger J, Mallampalli RK, Stockwell BR, Tyurina YY, Conrad M, Bayır H. Oxidized arachidonic and adrenic PEs navigate cells to ferroptosis. *Nat Chem Biol* 2017; **13**: 81-90 [PMID: 27842066 DOI: 10.1038/nchembio.2238]

38 **Shintoku R**, Takigawa Y, Yamada K, Kubota C, Yoshimoto Y, Takeuchi T, Koshiishi I, Torii S. Lipoxygenase-mediated generation of lipid peroxides enhances ferroptosis induced by erastin and RSL3. *Cancer Sci* 2017; **108**: 2187-2194 [PMID: 28837253 DOI: 10.1111/cas.13380]

39 **Zou Y**, Li H, Graham ET, Deik AA, Eaton JK, Wang W, Sandoval-Gomez G, Clish CB, Doench JG, Schreiber SL. Cytochrome P450 oxidoreductase contributes to phospholipid peroxidation in ferroptosis. *Nat Chem Biol* 2020; **16**: 302-309 [PMID: 32080622 DOI: 10.1038/s41589-020-0472-6]

40 **Bersuker K**, Hendricks JM, Li Z, Magtanong L, Ford B, Tang PH, Roberts MA, Tong B, Maimone TJ, Zoncu R, Bassik MC, Nomura DK, Dixon SJ, Olzmann JA. The CoQ oxidoreductase FSP1 acts parallel to GPX4 to inhibit ferroptosis. *Nature* 2019; **575**: 688-692 [PMID: 31634900 DOI: 10.1038/s41586-019-1705-2]

41 **Kamzalov S**, Sumien N, Forster MJ, Sohal RS. Coenzyme Q intake elevates the mitochondrial and tissue levels of Coenzyme Q and alpha-tocopherol in young mice. *J Nutr* 2003; **133**: 3175-3180 [PMID: 14519806 DOI: 10.1093/jn/133.10.3175]

42 **Pallotti F**, Bergamini C, Lamperti C, Fato R. The Roles of Coenzyme Q in Disease: Direct and Indirect Involvement in Cellular Functions. *Int J Mol Sci* 2021; **23** [PMID: 35008564 DOI: 10.3390/ijms23010128]

43 **Miziorko HM**. Enzymes of the mevalonate pathway of isoprenoid biosynthesis. *Arch Biochem Biophys* 2011; **505**: 131-143 [PMID: 20932952 DOI: 10.1016/j.abb.2010.09.028]

44 **Zhu PF**, Wang MX, Chen ZL, Yang L. Targeting the Tumor Microenvironment: A Literature Review of the Novel Anti-Tumor Mechanism of Statins. *Front Oncol* 2021; **11**: 761107 [PMID: 34858839 DOI: 10.3389/fonc.2021.761107]

45 **Shimada K**, Skouta R, Kaplan A, Yang WS, Hayano M, Dixon SJ, Brown LM, Valenzuela CA, Wolpaw AJ, Stockwell BR. Global survey of cell death mechanisms reveals metabolic regulation of ferroptosis. *Nat Chem Biol* 2016; **12**: 497-503 [PMID: 27159577 DOI: 10.1038/nchembio.2079]

46 **Soula M**, Weber RA, Zilka O, Alwaseem H, La K, Yen F, Molina H, Garcia-Bermudez J, Pratt DA, Birsoy K. Metabolic determinants of cancer cell sensitivity to canonical ferroptosis inducers. *Nat Chem Biol* 2020; **16**: 1351-1360 [PMID: 32778843 DOI:

10.1038/s41589-020-0613-y]
47 **Kraft VAN**, Bezjian CT, Pfeiffer S, Ringelstetter L, Müller C, Zandkarimi F, Merl-Pham J, Bao X, Anastasov N, Kössl J, Brandner S, Daniels JD, Schmitt-Kopplin P, Hauck SM, Stockwell BR, Hadian K, Schick JA. GTP Cyclohydrolase 1/Tetrahydrobiopterin Counteract Ferroptosis through Lipid Remodeling. *ACS Cent Sci* 2020; **6**: 41-53 [PMID: 31989025 DOI: 10.1021/acscentsci.9b01063]
48 **Gao B**, Doan A, Hybertson BM. The clinical potential of influencing Nrf2 signaling in degenerative and immunological disorders. *Clin Pharmacol* 2014; **6**: 19-34 [PMID: 24520207 DOI: 10.2147/CPAA.S35078]
49 **Zhu L**, Yang F, Wang L, Dong L, Huang Z, Wang G, Chen G, Li Q. Identification the ferroptosis-related gene signature in patients with esophageal adenocarcinoma. *Cancer Cell Int* 2021; **21**: 124 [PMID: 33602233 DOI: 10.1186/s12935-021-01821-2]
50 **Lu T**, Xu R, Li Q, Zhao JY, Peng B, Zhang H, Guo JD, Zhang SQ, Li HW, Wang J, Zhang LY. Systematic profiling of ferroptosis gene signatures predicts prognostic factors in esophageal squamous cell carcinoma. *Mol Ther Oncolytics* 2021; **21**: 134-143 [PMID: 33981829 DOI: 10.1016/j.omto.2021.02.011]
51 **Song J**, Liu Y, Guan X, Zhang X, Yu W, Li Q. A Novel Ferroptosis-Related Biomarker Signature to Predict Overall Survival of Esophageal Squamous Cell Carcinoma. *Front Mol Biosci* 2021; **8**: 675193 [PMID: 34291083 DOI: 10.3389/fmolb.2021.675193]
52 **Zhao M**, Li M, Zheng Y, Hu Z, Liang J, Bi G, Bian Y, Sui Q, Zhan C, Lin M, Wang Q. Identification and analysis of a prognostic ferroptosis and iron-metabolism signature for esophageal squamous cell carcinoma. *J Cancer* 2022; **13**: 1611-1622 [PMID: 35371305 DOI: 10.7150/jca.68568]
53 **Lu M**, Li J, Fan X, Xie F, Fan J, Xiong Y. Novel Immune-Related Ferroptosis Signature in Esophageal Cancer: An Informatics Exploration of Biological Processes Related to the TMEM161B-AS1/hsa-miR-27a-3p/GCH1 Regulatory Network. *Front Genet* 2022; **13**: 829384 [PMID: 35281840 DOI: 10.3389/fgene.2022.829384]
54 **Wang W**, Zhang J, Wang Y, Xu Y, Zhang S. Identifies microtubule-binding protein CSPP1 as a novel cancer biomarker associated with ferroptosis and tumor microenvironment. *Comput Struct Biotechnol J* 2022; **20**: 3322-3335 [PMID: 35832625 DOI: 10.1016/j.csbj.2022.06.046]
55 **Gout PW**, Buckley AR, Simms CR, Bruchovsky N. Sulfasalazine, a potent suppressor of lymphoma growth by inhibition of the x(c)- cystine transporter: a new action for an old drug. *Leukemia* 2001; **15**: 1633-1640 [PMID: 11587223 DOI: 10.1038/sj.leu.2402238]
56 **Zhang Y**, Tan H, Daniels JD, Zandkarimi F, Liu H, Brown LM, Uchida K, O'Connor OA, Stockwell BR. Imidazole Ketone Erastin Induces Ferroptosis and Slows Tumor Growth in a Mouse Lymphoma Model. *Cell Chem Biol* 2019; **26**: 623-633.e9 [PMID: 30799221 DOI: 10.1016/j.chembiol.2019.01.008]
57 **Koppula P**, Zhang Y, Zhuang L, Gan B. Amino acid transporter SLC7A11/xCT at the crossroads of regulating redox homeostasis and nutrient dependency of cancer. *Cancer Commun (Lond)* 2018; **38**: 12 [PMID: 29764521 DOI: 10.1186/s40880-018-0288-x]
58 **Shiozaki A**, Iitaka D, Ichikawa D, Nakashima S, Fujiwara H, Okamoto K, Kubota T, Komatsu S, Kosuga T, Takeshita H, Shimizu H, Nako Y, Sasagawa H, Kishimoto M, Otsuji E. xCT, component of cysteine/glutamate transporter, as an independent prognostic factor in human esophageal squamous cell carcinoma. *J Gastroenterol* 2014; **49**: 853-863 [PMID: 23771433 DOI: 10.1007/s00535-013-0847-5]
59 **Eichelmann AK**, Mayne GC, Chiam K, Due SL, Bastian I, Butz F, Wang T, Sykes PJ, Clemons NJ, Liu DS, Michael MZ, Karapetis CS, Hummel R, Watson DI, Hussey DJ. Mutant p53 Mediates Sensitivity to Cancer Treatment Agents in Oesophageal Adenocarcinoma Associated with MicroRNA and SLC7A11 Expression. *Int J Mol Sci* 2021; **22** [PMID: 34074015 DOI: 10.3390/ijms22115547]
60 **Feng L**, Zhao K, Sun L, Yin X, Zhang J, Liu C, Li B. SLC7A11 regulated by NRF2 modulates esophageal squamous cell carcinoma radiosensitivity by inhibiting ferroptosis. *J Transl Med* 2021; **19**: 367 [PMID: 34446045 DOI: 10.1186/s12967-021-03042-7]
61 **Ma L**, Zhang X, Yu K, Xu X, Chen T, Shi Y, Wang Y, Qiu S, Guo S, Cui J, Miao Y, Tian X, Du L, Yu Y, Xia J, Wang J. Targeting SLC3A2 subunit of system X(C)(-) is essential for m(6)A reader YTHDC2 to be an endogenous ferroptosis inducer in lung adenocarcinoma. *Free Radic Biol Med* 2021; **168**: 25-43 [PMID: 33785413 DOI: 10.1016/j.freeradbiomed.2021.03.023]
62 **Zhu B**, Cheng D, Hou L, Zhou S, Ying T, Yang Q. SLC3A2 is upregulated in human osteosarcoma and promotes tumor growth through the PI3K/Akt signaling pathway. *Oncol Rep* 2017; **37**: 2575-2582 [PMID: 28350098 DOI: 10.3892/or.2017.5530]
63 **Li W**, Dong X, He C, Tan G, Li Z, Zhai B, Feng J, Jiang X, Liu C, Jiang H, Sun X. LncRNA SNHG1 contributes to sorafenib resistance by activating the Akt pathway and is positively regulated by miR-21 in hepatocellular carcinoma cells. *J Exp Clin Cancer Res* 2019; **38**: 183 [PMID: 31053148 DOI: 10.1186/s13046-019-1177-0]
64 **Eaton JK**, Furst L, Ruberto RA, Moosmayer D, Hilpmann A, Ryan MJ, Zimmermann K, Cai LL, Niehues M, Badock V, Kramm A, Chen S, Hillig RC, Clemons PA, Gradl S, Montagnon C, Lazarski KE, Christian S, Bajrami B, Neuhaus R, Eheim AL, Viswanathan VS, Schreiber SL. Selective covalent targeting of GPX4 using masked nitrile-oxide electrophiles. *Nat Chem Biol* 2020; **16**: 497-506 [PMID: 32231343 DOI: 10.1038/s41589-020-0501-5]
65 **Liu CC**, Li HH, Lin JH, Chiang MC, Hsu TW, Li AF, Yen DH, Hsu HS, Hung SC. Esophageal Cancer Stem-like Cells Resist Ferroptosis-Induced Cell Death by Active Hsp27-GPX4 Pathway. *Biomolecules* 2021; **12** [PMID: 35053196 DOI: 10.3390/biom12010048]
66 **Jiang B**, Zhao Y, Shi M, Song L, Wang Q, Qin Q, Song X, Wu S, Fang Z, Liu X. DNAJB6 Promotes Ferroptosis in Esophageal Squamous Cell Carcinoma. *Dig Dis Sci* 2020; **65**: 1999-2008 [PMID: 31701262 DOI: 10.1007/s10620-019-05929-4]
67 **Chen C**, Zhao J, Liu JN, Sun C. Mechanism and Role of the Neuropeptide LGI1 Receptor ADAM23 in Regulating Biomarkers of Ferroptosis and Progression of Esophageal Cancer. *Dis Markers* 2021; **2021**: 9227897 [PMID: 35003396 DOI: 10.1155/2021/9227897]
68 **Hou J**, Huang Q, Fan Z, Sang H, Wu S, Cheng S, Li Q. LncRNA OIP5-AS1 Knockdown Facilitated the Ferroptosis and Immune Evasion by Modulating the GPX4 in Oesophageal Carcinoma. *Comput Math Methods Med* 2022; **2022**: 8103198 [PMID: 35872956 DOI: 10.1155/2022/8103198]
69 **Hangauer MJ**, Viswanathan VS, Ryan MJ, Bole D, Eaton JK, Matov A, Galeas J, Dhruv HD, Berens ME, Schreiber SL, McCormick F, McManus MT. Drug-tolerant persister cancer cells are vulnerable to GPX4 inhibition. *Nature* 2017; **551**: 247-250 [PMID: 29088702 DOI: 10.1038/nature24297]
70 **Tay Y**, Rinn J, Pandolfi PP. The multilayered complexity of ceRNA crosstalk and competition. *Nature* 2014; **505**: 344-352 [PMID: 24429633 DOI: 10.1038/nature12986]
71 **Cheng DL**, Xiang YY, Ji LJ, Lu XJ. Competing endogenous RNA interplay in cancer: mechanism, methodology, and perspectives. *Tumour Biol* 2015; **36**: 479-488 [PMID: 25604144 DOI: 10.1007/s13277-015-3093-z]
72 **Qi X**, Zhang DH, Wu N, Xiao JH, Wang X, Ma W. ceRNA in cancer: possible functions and clinical implications. *J Med Genet* 2015; **52**: 710-718 [PMID: 26358722 DOI: 10.1136/jmedgenet-2015-103334]
73 **Zhu L**, Wang Z, Fan Q, Wang R, Sun Y. microRNA-27a functions as a tumor suppressor in esophageal squamous cell carcinoma by targeting KRAS. *Oncol Rep* 2014; **31**: 280-286 [PMID: 24154848 DOI: 10.3892/or.2013.2807]

74 **Thompson LR**, Oliveira TG, Hermann ER, Chowanadisai W, Clarke SL, Montgomery MR. Distinct TP53 Mutation Types Exhibit Increased Sensitivity to Ferroptosis Independently of Changes in Iron Regulatory Protein Activity. *Int J Mol Sci* 2020; **21** [PMID: 32942535 DOI: 10.3390/ijms21186751]

75 **Zhang H**, Li M, Han Y, Hong L, Gong T, Sun L, Zheng X. Down-regulation of miR-27a might reverse multidrug resistance of esophageal squamous cell carcinoma. *Dig Dis Sci* 2010; **55**: 2545-2551 [PMID: 19960259 DOI: 10.1007/s10620-009-1051-6]

76 **Xi Y**, Shen Y, Wu D, Zhang J, Lin C, Wang L, Yu C, Yu B, Shen W. CircBCAR3 accelerates esophageal cancer tumorigenesis and metastasis *via* sponging miR-27a-3p. *Mol Cancer* 2022; **21**: 145 [PMID: 35840974 DOI: 10.1186/s12943-022-01615-8]

77 **Yao W**, Wang J, Meng F, Zhu Z, Jia X, Xu L, Zhang Q, Wei L. Circular RNA CircPVT1 Inhibits 5-Fluorouracil Chemosensitivity by Regulating Ferroptosis Through MiR-30a-5p/FZD3 Axis in Esophageal Cancer Cells. *Front Oncol* 2021; **11**: 780938 [PMID: 34966683 DOI: 10.3389/fonc.2021.780938]

78 **Pan C**, Chen G, Zhao X, Xu X, Liu J. lncRNA BBOX1-AS1 silencing inhibits esophageal squamous cell cancer progression by promoting ferroptosis *via* miR-513a-3p/SLC7A11 axis. *Eur J Pharmacol* 2022; **934**: 175317 [PMID: 36216119 DOI: 10.1016/j.ejphar.2022.175317]

79 **Li X**, Song L, Wang B, Tao C, Shi L, Xu M. Circ0120816 acts as an oncogene of esophageal squamous cell carcinoma by inhibiting miR-1305 and releasing TXNRD1. *Cancer Cell Int* 2020; **20**: 526 [PMID: 33292234 DOI: 10.1186/s12935-020-01617-w]

80 **Kelsen DP**, Ilson DH. Chemotherapy and combined-modality therapy for esophageal cancer. *Chest* 1995; **107**: 224S-232S [PMID: 7781398 DOI: 10.1378/chest.107.6_supplement.224s]

81 **Lei G**, Zhang Y, Koppula P, Liu X, Zhang J, Lin SH, Ajani JA, Xiao Q, Liao Z, Wang H, Gan B. The role of ferroptosis in ionizing radiation-induced cell death and tumor suppression. *Cell Res* 2020; **30**: 146-162 [PMID: 31949285 DOI: 10.1038/s41422-019-0263-3]

82 **Fan QX**, Wang R, Wang RL. Clinical efficacy of treatment by Rabdosia rubescens alone or in combination chemotherapy for esophageal cancer. *Shijie Huaren Xiaohua Zazhi* 2007; **15**: 2534-2537

83 **Ballout F**, Lu H, Chen Z, Hu T, Chen L, Washington MK, El-Rifai W, Peng D. Targeting NRF2 Sensitizes Esophageal Adenocarcinoma Cells to Cisplatin through Induction of Ferroptosis and Apoptosis. *Antioxidants (Basel)* 2022; **11** [PMID: 36290582 DOI: 10.3390/antiox11101859]

84 **Sallman DA**, DeZern AE, Garcia-Manero G, Steensma DP, Roboz GJ, Sekeres MA, Cluzeau T, Sweet KL, McLemore A, McGraw KL, Puskas J, Zhang L, Yao J, Mo Q, Nardelli L, Al Ali NH, Padron E, Korbel G, Attar EC, Kantarjian HM, Lancet JE, Fenaux P, List AF, Komrokji RS. Eprenetapopt (APR-246) and Azacitidine in TP53-Mutant Myelodysplastic Syndromes. *J Clin Oncol* 2021; **39**: 1584-1594 [PMID: 33449813 DOI: 10.1200/JCO.20.02341]

85 **Cluzeau T**, Sebert M, Rahmé R, Cuzzubbo S, Lehmann-Che J, Madelaine I, Peterlin P, Bève B, Attalah H, Chermat F, Miekoutima E, Rauzy OB, Recher C, Stamatoullas A, Willems L, Raffoux E, Berthon C, Quesnel B, Loschi M, Carpentier AF, Sallman DA, Komrokji R, Walter-Petrich A, Chevret S, Ades L, Fenaux P. Eprenetapopt Plus Azacitidine in TP53-Mutated Myelodysplastic Syndromes and Acute Myeloid Leukemia: A Phase II Study by the Groupe Francophone des Myélodysplasies (GFM). *J Clin Oncol* 2021; **39**: 1575-1583 [PMID: 33600210 DOI: 10.1200/JCO.20.02342]

86 **Fujihara KM**, Zhang BZ, Jackson TD, Ogunkola MO, Nijagal B, Milne JV, Sallman DA, Ang CS, Nikolic I, Kearney CJ, Hogg SJ, Cabalag CS, Sutton VR, Watt S, Fujihara AT, Trapani JA, Simpson KJ, Stojanovski D, Leimkühler S, Haupt S, Phillips WA, Clemons NJ. Eprenetapopt triggers ferroptosis, inhibits NFS1 cysteine desulfurase, and synergizes with serine and glycine dietary restriction. *Sci Adv* 2022; **8**: eabm9427 [PMID: 36103522 DOI: 10.1126/sciadv.abm9427]

87 **Chen X**, Kang R, Kroemer G, Tang D. Ferroptosis in infection, inflammation, and immunity. *J Exp Med* 2021; **218** [PMID: 33978684 DOI: 10.1084/jem.20210518]

88 **Matsushita M**, Freigang S, Schneider C, Conrad M, Bornkamm GW, Kopf M. T cell lipid peroxidation induces ferroptosis and prevents immunity to infection. *J Exp Med* 2015; **212**: 555-568 [PMID: 25824823 DOI: 10.1084/jem.20140857]

89 **Yao Y**, Chen Z, Zhang H, Chen C, Zeng M, Yunis J, Wei Y, Wan Y, Wang N, Zhou M, Qiu C, Zeng Q, Ong HS, Wang H, Makota FV, Yang Y, Yang Z, Deng J, Shen C, Xia Y, Yuan L, Lian Z, Deng Y, Guo C, Huang A, Zhou P, Shi H, Zhang W, Yi H, Li D, Xia M, Fu J, Wu N, de Haan JB, Shen N, Liu Z, Yu D. Selenium-GPX4 axis protects follicular helper T cells from ferroptosis. *Nat Immunol* 2021; **22**: 1127-1139 [PMID: 34413521 DOI: 10.1038/s41590-021-00996-0]

90 **Zhou Z**, Liang H, Yang R, Yang Y, Dong J, Di Y, Sun M. Glutathione Depletion-Induced Activation of Dimersomes for Potentiating the Ferroptosis and Immunotherapy of "Cold" Tumor. *Angew Chem Int Ed Engl* 2022; **61**: e202202843 [PMID: 35238124 DOI: 10.1002/anie.202202843]

91 **Bossi G**, Griffiths GM. Degranulation plays an essential part in regulating cell surface expression of Fas ligand in T cells and natural killer cells. *Nat Med* 1999; **5**: 90-96 [PMID: 9883845 DOI: 10.1038/4779]

92 **Lang X**, Green MD, Wang W, Yu J, Choi JE, Jiang L, Liao P, Zhou J, Zhang Q, Dow A, Saripalli AL, Kryczek I, Wei S, Szeliga W, Vatan L, Stone EM, Georgiou G, Cieslik M, Wahl DR, Morgan MA, Chinnaiyan AM, Lawrence TS, Zou W. Radiotherapy and Immunotherapy Promote Tumoral Lipid Oxidation and Ferroptosis *via* Synergistic Repression of SLC7A11. *Cancer Discov* 2019; **9**: 1673-1685 [PMID: 31554642 DOI: 10.1158/2159-8290.CD-19-0338]

93 **Liao P**, Wang W, Kryczek I, Li X, Bian Y, Sell A, Wei S, Grove S, Johnson JK, Kennedy PD, Gijón M, Shah YM, Zou W. CD8(+) T cells and fatty acids orchestrate tumor ferroptosis and immunity *via* ACSL4. *Cancer Cell* 2022; **40**: 365-378.e6 [PMID: 35216678 DOI: 10.1016/j.ccell.2022.02.003]

94 **Ma X**, Xiao L, Liu L, Ye L, Su P, Bi E, Wang Q, Yang M, Qian J, Yi Q. CD36-mediated ferroptosis dampens intratumoral CD8(+) T cell effector function and impairs their antitumor ability. *Cell Metab* 2021; **33**: 1001-1012.e5 [PMID: 33691090 DOI: 10.1016/j.cmet.2021.02.015]

95 **Pan Y**, Yu Y, Wang X, Zhang T. Tumor-Associated Macrophages in Tumor Immunity. *Front Immunol* 2020; **11**: 583084 [PMID: 33365025 DOI: 10.3389/fimmu.2020.583084]

96 **Luo X**, Gong HB, Gao HY, Wu YP, Sun WY, Li ZQ, Wang G, Liu B, Liang L, Kurihara H, Duan WJ, Li YF, He RR. Oxygenated phosphatidylethanolamine navigates phagocytosis of ferroptotic cells by interacting with TLR2. *Cell Death Differ* 2021; **28**: 1971-1989 [PMID: 33432112 DOI: 10.1038/s41418-020-00719-2]

97 **Kapralov AA**, Yang Q, Dar HH, Tyurina YY, Anthonymuthu TS, Kim R, St Croix CM, Mikulska-Ruminska K, Liu B, Shrivastava IH, Tyurin VA, Ting HC, Wu YL, Gao Y, Shurin GV, Artyukhova MA, Ponomareva LA, Timashev PS, Domingues RM, Stoyanovsky DA, Greenberger JS, Mallampalli RK, Bahar I, Gabrilovich DI, Bayır H, Kagan VE. Redox lipid reprogramming commands susceptibility of macrophages and microglia to ferroptotic death. *Nat Chem Biol* 2020; **16**: 278-290 [PMID: 32080625 DOI: 10.1038/s41589-019-0462-8]

98 **Zhang F**, Li F, Lu GH, Nie W, Zhang L, Lv Y, Bao W, Gao X, Wei W, Pu K, Xie HY. Engineering Magnetosomes for Ferroptosis/Immunomodulation Synergism in Cancer. *ACS Nano* 2019; **13**: 5662-5673 [PMID: 31046234 DOI: 10.1021/acsnano.9b00892]

99 **Hsieh CH**, Hsieh HC, Shih FS, Wang PW, Yang LX, Shieh DB, Wang YC. An innovative NRF2 nano-modulator induces lung cancer

ferroptosis and elicits an immunostimulatory tumor microenvironment. *Theranostics* 2021; **11**: 7072-7091 [PMID: 34093872 DOI: 10.7150/thno.57803]

100 **Jiang Q**, Wang K, Zhang X, Ouyang B, Liu H, Pang Z, Yang W. Platelet Membrane-Camouflaged Magnetic Nanoparticles for Ferroptosis-Enhanced Cancer Immunotherapy. *Small* 2020; **16**: e2001704 [PMID: 32338436 DOI: 10.1002/smll.202001704]

101 **Han L**, Bai L, Qu C, Dai E, Liu J, Kang R, Zhou D, Tang D, Zhao Y. PPARG-mediated ferroptosis in dendritic cells limits antitumor immunity. *Biochem Biophys Res Commun* 2021; **576**: 33-39 [PMID: 34478917 DOI: 10.1016/j.bbrc.2021.08.082]

102 **Kroemer G**, Galluzzi L, Kepp O, Zitvogel L. Immunogenic cell death in cancer therapy. *Annu Rev Immunol* 2013; **31**: 51-72 [PMID: 23157435 DOI: 10.1146/annurev-immunol-032712-100008]

103 **Wen Q**, Liu J, Kang R, Zhou B, Tang D. The release and activity of HMGB1 in ferroptosis. *Biochem Biophys Res Commun* 2019; **510**: 278-283 [PMID: 30686534 DOI: 10.1016/j.bbrc.2019.01.090]

104 **Krysko DV**, Garg AD, Kaczmarek A, Krysko O, Agostinis P, Vandenabeele P. Immunogenic cell death and DAMPs in cancer therapy. *Nat Rev Cancer* 2012; **12**: 860-875 [PMID: 23151605 DOI: 10.1038/nrc3380]

105 **Efimova I**, Catanzaro E, Van der Meeren L, Turubanova VD, Hammad H, Mishchenko TA, Vedunova MV, Fimognari C, Bachert C, Coppieters F, Lefever S, Skirtach AG, Krysko O, Krysko DV. Vaccination with early ferroptotic cancer cells induces efficient antitumor immunity. *J Immunother Cancer* 2020; **8** [PMID: 33188036 DOI: 10.1136/jitc-2020-001369]

106 **Song R**, Li T, Ye J, Sun F, Hou B, Saeed M, Gao J, Wang Y, Zhu Q, Xu Z, Yu H. Acidity-Activatable Dynamic Nanoparticles Boosting Ferroptotic Cell Death for Immunotherapy of Cancer. *Adv Mater* 2021; **33**: e2101155 [PMID: 34170581 DOI: 10.1002/adma.202101155]

107 **Niu R**, Zhao F, Dong Z, Li Z, Li S. A stratification system of ferroptosis and iron-metabolism related LncRNAs guides the prediction of the survival of patients with esophageal squamous cell carcinoma. *Front Oncol* 2022; **12**: 1010074 [PMID: 36185246 DOI: 10.3389/fonc.2022.1010074]

108 **Zhu J**, Zhao Y, Wu G, Zhang X, Chen Q, Yang B, Guo X, Ji S, Gu K. Ferroptosis-Related lncRNA Signature Correlates with the Prognosis, Tumor Microenvironment, and Therapeutic Sensitivity of Esophageal Squamous Cell Carcinoma. *Oxid Med Cell Longev* 2022; **2022**: 7465880 [PMID: 35903713 DOI: 10.1155/2022/7465880]

109 **Shi ZZ**, Tao H, Fan ZW, Song SJ, Bai J. Prognostic and Immunological Role of Key Genes of Ferroptosis in Pan-Cancer. *Front Cell Dev Biol* 2021; **9**: 748925 [PMID: 34722530 DOI: 10.3389/fcell.2021.748925]

110 **Zhang Y**, Chen Y. Stratification From Heterogeneity of the Cell-Death Signal Enables Prognosis Prediction and Immune Microenvironment Characterization in Esophageal Squamous Cell Carcinoma. *Front Cell Dev Biol* 2022; **10**: 855404 [PMID: 35493093 DOI: 10.3389/fcell.2022.855404]

World Journal of Gastrointestinal Oncology

Submit a Manuscript: https://www.f6publishing.com

World J Gastrointest Oncol 2023 July 15; 15(7): 1119-1134

DOI: 10.4251/wjgo.v15.i7.1119

ISSN 1948-5204 (online)

REVIEW

Core fucosylation and its roles in gastrointestinal glycoimmunology

Nian-Zhu Zhang, Li-Fen Zhao, Qian Zhang, Hui Fang, Wan-Li Song, Wen-Zhe Li, Yu-Song Ge, Peng Gao

Specialty type: Immunology

Provenance and peer review: Invited article; Externally peer reviewed.

Peer-review model: Single blind

Peer-review report's scientific quality classification

Grade A (Excellent): A
Grade B (Very good): 0
Grade C (Good): C
Grade D (Fair): 0
Grade E (Poor): 0

P-Reviewer: Miyoshi E, Japan; Wang Q, China

Received: January 18, 2023
Peer-review started: January 18, 2023
First decision: February 24, 2023
Revised: February 28, 2023
Accepted: May 8, 2023
Article in press: May 8, 2023
Published online: July 15, 2023

Nian-Zhu Zhang, Li-Fen Zhao, Peng Gao, Clinical Laboratory, The Second Hospital of Dalian Medical University, Dalian 116023, Liaoning Province, China

Qian Zhang, Department of Cell Therapy, Shanghai Tianze Yuntai Biomedical Co., Ltd., Shanghai 200100, China

Hui Fang, Graduate School of Comprehensive Human Sciences, University of Tsukuba, Tsukuba 305-0005, Ibaraki, Japan

Wan-Li Song, Wen-Zhe Li, Guangdong Provincial Key Laboratory of Infectious Diseases and Molecular Immunopathology, Shantou University Medical College, Shantou 515041, Guangdong Province, China

Yu-Song Ge, Department of Neurology, The Second Hospital of Dalian Medical University, Dalian 116023, Liaoning Province, China

Corresponding author: Peng Gao, MD, PhD, Director, Professor, Clinical Laboratory, The Second Hospital of Dalian Medical University, No. 467 Zhongshan Road, Shahekou District, Dalian 116023, Liaoning Province, China. gaop@dicp.ac.cn

Abstract

Glycosylation is a common post-translational modification in eukaryotic cells. It is involved in the production of many biologically active glycoproteins and the regulation of protein structure and function. Core fucosylation plays a vital role in the immune response. Most immune system molecules are core fucosylated glycoproteins such as complements, cluster differentiation antigens, immunoglobulins, cytokines, major histocompatibility complex molecules, adhesion molecules, and immune molecule synthesis-related transcription factors. These core fucosylated glycoproteins play important roles in antigen recognition and clearance, cell adhesion, lymphocyte activation, apoptosis, signal transduction, and endocytosis. Core fucosylation is dominated by fucosyltransferase 8 (Fut8), which catalyzes the addition of α-1,6-fucose to the innermost GlcNAc residue of N-glycans. Fut8 is involved in humoral, cellular, and mucosal immunity. Tumor immunology is associated with aberrant core fucosylation. Here, we summarize the roles and potential modulatory mechanisms of Fut8 in various immune processes of the gastrointestinal system.

Key Words: Fucosyltransferase 8; Core fucosylation; Glycoimmunology; Gastrointestinal tumor immunology; T cell signal pathway

Core Tip: Core fucosylation is driven by fucosyltransferase 8 (Fut8), which catalyzes the addition of α-1,6-fucose to the innermost GlcNAc residue of N-glycans. Core fucosylation plays a vital role in immune responses. Most immune system molecules are core fucosylated glycoproteins that play important roles in antigen recognition and clearance, cell adhesion, lymphocyte activation, apoptosis, signal transduction, and endocytosis. Fut8 is involved in humoral immune responses, cellular immunity, mucosal immunity, and tumor immunology. Here, we summarize the roles and potential modulatory mechanisms of Fut8 in various immune responses of the gastrointestinal system.

Citation: Zhang NZ, Zhao LF, Zhang Q, Fang H, Song WL, Li WZ, Ge YS, Gao P. Core fucosylation and its roles in gastrointestinal glycoimmunology. *World J Gastrointest Oncol* 2023; 15(7): 1119-1134
URL: https://www.wjgnet.com/1948-5204/full/v15/i7/1119.htm
DOI: https://dx.doi.org/10.4251/wjgo.v15.i7.1119

INTRODUCTION

Glycosylation is a vital post-transcriptional modification involving the addition of glycans to proteins *via* chemical bonds [1]. This process occurs in the secretory pathway and affects most intracellular protein folding and trafficking[2]. N-glycosylation and O-glycosylation are the two main types of glycosylation[3]. N-linked glycosylation, also called N-glycosylation, refers to the attachment of an oligosaccharide sugar molecule to a nitrogen atom in the asparagine residue of a protein molecule[4]. In contrast, O-glycosylation refers to the attachment of a sugar molecule to the oxygen atom of a serine or threonine residue[5]. Both N-glycosylation- and O-glycosylation commonly occur during post-translational modifications[6]. Diverse proteins participate in immunological processes, most of which are glycosylated. Glycoimmunology refers to the research on the interactions between glycans and glycan-binding proteins involved in various immune responses and biological/pathological effects[7]. Glycoproteins are also effectors of the immune system, because protein glycosylation promotes immune cell migration throughout the body. Glycosylation is closely associated with pathogen recognition, immune cell homeostasis, and inflammation[8]. In addition, glycosylation is involved in the folding, quality control, maturity, packaging, antigen presentation, assembly of the T cell receptor (TCR) complex and peptide-loaded major histocompatibility complex (p-MHC) antigens, and stability of immune molecules[9]. Previous studies reported that glycans on T cells, immune molecules, and pathogens can influence cellular signal transduction[10-12]. Glycoproteins are key components of the innate and adaptive immune responses[9].

Abnormal glycosylation has been observed in many immune system diseases[1]. O-glycosylation plays a vital role in T cell immunity[13]. Moreover, abnormal O-glycan expression levels in leukomonocytes and cancer cells have been reported in acquired immunodeficiency syndrome, Wiskott–Aldrich syndrome, and T lymphocytic leukemia[3,12,14-17]. Excess core 2 O-glycosylation in T cells reduces primary T cell responses and impairs the interaction between antigen-presenting cells (APC) and T cells, which reduces the production of cytokines, resulting in reduced T cell activation. Core 2 O-glycans serve as a critical backbone for selectin ligand carbohydrate structures[18] and are involved in the adhesion and development of white blood cells[19]. N-Glycosylation mediates innate immune system recognition, inflammation, and autoimmune diseases[20]. Branching and number of N-glycans influence cell proliferation and differentiation[21]. Patients with rheumatoid arthritis (RA) exhibit altered N-glycosylation of immunoglobulin G (IgG). Low N-glycosylation of CD55 (DAF) and CD59 has been observed in RA and inflammation. Furthermore, patients with systemic lupus erythematosus (SLE) display altered N-glycosylation levels in T cells. Decreased synthesis of mannosyl (alpha-1,6-)-glycoproteinbeta-1,6-N-acetyl-glucosaminyltransferase (MGAT5) is observed in autoimmune diseases, whereas it is increased in malignancies[22].

Fucosylation is widely involved in oligosaccharide modifications, which play an essential role in immune-related diseases and cancer, and is often accompanied by the disordered expression of fucosyltransferases (FUTs)[9,23-24,27]. As the sole glycosyltransferase, Fut8 catalyzes the fucose residue transfer *via* the α1,6-linkage from GDP-fucose (GDP-Fuc) to the innermost N-acetylglucosamine (GlcNAc) residue of N-glycans in the Golgi apparatus of mammalian cells[28] (Figure 1). The core fucose levels of proteins depend on the substrate GDP-Fuc and its transportation to the Golgi apparatus[29]. After core fucosylation, proteins exhibit different spatial structures and biological activities. Core-fucosylated glycoproteins are widely expressed in mammalian tissues, and their aberrant expression is observed under pathological conditions[30]. Fut8 is involved in many types of immune-related diseases and immune responses, such as the humoral immune response, T cell signal transduction, $CD4^+$ T cell activation, $CD8^+$ cytotoxic T cell (CTL) activation, and benign and malignant biological regulation of the gastrointestinal system. Almost all innate and adaptive immune molecules are glycoproteins[31]. Aberrant core fucosylation is one of the most important glycosylation events and has been observed in many immune-related diseases. Most immunoglobulins, clusters of differentiation (CDs), adhesive molecules, soluble and membrane-type lectin receptors, cytokines and their receptors, complement T and B cell receptors (BCRs), and MHCs are core fucosylated proteins. Programmed cell death protein-1 (PD-1, CD279) (NM-005018) is one of the most important immune inhibitory receptors expressed on tumor-infiltrating T cells (TILs). Mass spectrometry has shown that PD-1 is a typical core-fucosylated protein containing four core-fucosylated N-glycans: N^{49}, N^{58}, N^{74}, and N^{116}

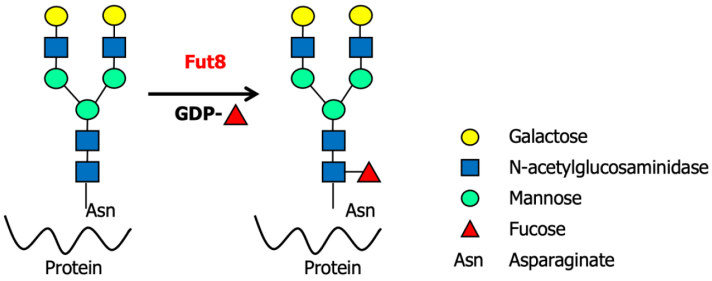

DOI: 10.4251/wjgo.v15.i7.1119 **Copyright** ©The Author(s) 2023.

Figure 1 The reaction was catalyzed by fucosyltransferase 8. Fucosyltransferase 8 transfers an L-fucose reside from GDP-β-L-fucose onto the innermost GDP-fucose to the innermost N-acetylglucosamine of an N-glycan to form an α-1,6 linkage. Fut8: Fucosyltransferase 8.

[32]. Loss of core fucosylation in PD-1 decreases its expression in CTL, leading to more efficient activation, cytotoxicity, and tumor eradication[33].

Gastrointestinal cancers, mostly colorectal cancer, esophageal cancer (OC), gastric cancer (GC), pancreatic cancer (PC), hepatocellular cancer (HCC), and biliary tract cancers, are the most common causes of cancer mortality worldwide, with significant associated morbidity[34]. Core fucosylation is widely involved in the development of neoplasms of the digestive system. Oral squamous cell carcinoma[35], esophageal squamous cell carcinoma (ESCC)[36], hepatocellular carcinoma[37], and PC[38] were all accompanied with high levels of core fucosylation. A high level of core fucosylation is also observed in colon (also known as bowel) cancer, which is the 3rd most common cancer worldwide (2022)[39,40]. Unlike other tumors, the level of core fucosylation is decreased in GC, and upregulation of core fucosylation can inhibit the proliferation of human GC cells[41]. High levels of Fut8 expression have also been observed in other tumors, such as non-small cell lung cancer, ovarian cancer, prostate cancer, melanoma, and breast cancer, and are associated with unfavorable prognosis[42-46].

Multiple complex mechanisms are involved in Fut8 immunoregulation of gastrointestinal diseases. This review provides an overview of the effect of core fucosylation on glycoimmunology in gastrointestinal diseases.

CORE FUCOSYLATION ON GASTROINTESTINAL CELLULAR IMMUNE MODULATION

T cells can be adoptively transferred from an immunized organism to a native organism to modulate cell-mediated immunity, which involves cell-mediated clearance mechanisms. The cell-mediated immune response is required in the process of elimination during intracellular infectious agents, such as viruses and certain bacteria (*e.g.*, Mycobacterium tuberculosis or Listeria monocytogenes)-induced infection. APC and T helper (Th) cells participate in this response to recognize infected cells. T-cell antigen recognition plays an essential role in both cellular and humoral immunity. After antigen recognition, Th cells release cytokines and chemokines and orchestrate subsequent reactions involving other immune cells, such as natural killer (NK) cells, macrophages, and CTL, to trigger T cell activation.

During T cell recognition and activation, molecules on the surface of CD4$^+$ and CD8$^+$ T cells bind to their respective class II and class I MHC ligands on APC[47]. Moreover, TCR and its co-receptors, CD4 and CD8, participate in the T cell recognition of pMHC ligands. Previous studies have reported that core fucosylation modulates the activation of CD4, CD8, and T-cell receptors.

Core fucosylation on T cell activation via TCR

Proper T cell activation promotes T cell migration to the periphery, where CTLs are found to infect cells and release toxic substances, and Th cells undergo further differentiation into subtypes. However, excessive T cell activation leads to a series of immune system disorders[48]. This abnormal activation was accompanied by changes in core fucosylation levels. SLE is a severe autoimmune disease characterized by the production of autoantibodies and subsequent inflammatory disorders[49]. Gastrointestinal symptoms, including acute abdominal pain (owing to pleurisy and peritonitis), diffuse abdominal pain, epigastric pain, epigastric pain with vomiting and chronic constipation, and diffuse abdominal pain with bleeding from the rectum, probably occur during SLE[50]. The onset and development of SLE pathogenesis are accompanied by excessive activation of CD4$^+$ T cells[51]. Higher core fucosylation levels and IgG antinuclear antibody expression have been observed in the sera of patients with SLE and are related to the severity of SLE[56]. Hyperactivity of B cells in SLE is also T cell-dependent[52]. Increased core fucosylation in patients with SLE has also been correlated with CD4$^+$ T-cell activation[53]. However, the correlation between core fucosylation and SLE-related gastrointestinal symptoms requires further investigation.

Experimental autoimmune encephalomyelitis (EAE), an activated CD4$^+$ T cell-mediated autoimmune disease model [54], shows slower and mild EAE symptoms and recovers body weight reduction after losing core fucosylation in mice [56]. Loss of core fucosylation markedly reduced the proliferation of CD4$^+$ T cells. Viral or bacterial infections and adverse reactions to medications leading to gastrointestinal symptoms are common among patients with SLE. SLE-related gastrointestinal symptoms cannot be ignored since their severity could cause the death of patients if not treated properly. Among all SLE-related gastrointestinal symptoms, lupus mesenteric vasculitis occurs most commonly, accompanied by

intestinal pseudo-obstruction, acute pancreatitis protein-losing enteropathy, and other rare complications such as inflammatory bowel diseases and celiac disease[55]. Both SLE and EAE models indicate that the lack of core fucosylation reduces $CD4^+$ T cell activation and consequently ameliorates symptoms[56].

$CD4^+$ T cell activation and differentiation are involved in the establishment and control of protective adaptive immune responses establishing and controlling[57]. Core fucosylation participates in all three stages of $CD4^+$ T-cell activation. First, core fucosylation is essential for structural formation of TCRs. Second, core fucosylation of TCR increases the recognition of pMHC and further promotes the $CD4^+$ T cell activation threshold and efficient TCR-pMHC-II contact[56]. De-core fucosylation suppresses IgG class switching by impairing $CD4^+$ T cell activation and signal transduction *via* TCR [56]. Fucose-specific lectins[58] might participate in T-B cell interactions[56]. Determining the mechanism by which core fucosylation influences $CD4^+$ T cell activation is vital for the treatment of SLE-related gastrointestinal symptoms. De-core fucosylated $CD4^+$ T cell infusion may be a useful intervention for the treatment of SLE-related gastrointestinal symptoms. Future studies should attempt to verify the effects of core fucosylation on SLE using mouse models.

Core fucosylation on T-B cell interaction

Glycosylation of membrane proteins participates in multiple cellular processes, such as immunological recognition, intercellular interactions, and cell signal transduction[59]. The interaction between $CD4^+$ T and B cells is important for optimal responses in adaptive immunity[60]. Fucose-specific lectins may be involved in the T-B cell interactions[56]. Genes related to TCR complex formation (CD3e, CD4, CD8, and CD40L), T cell activation (CD3e, CD4, CD8, and CD40L), and B cell activation (CD79a and CD81) exhibited reduced expression after the loss of core fucosylation in mouse models. A series of cell signaling molecules, such as MAPKKK, Vav1, PIK3, PKC, and Cyclin D3, also show decreased expression after the inhibition of core fucosylation[56]. Inhibition of core fucosylation attenuates T-B cell interactions *via* TCR-pMHC and consequently reduces $CD4^+$ T cell activation. Core fucosylation is necessary for efficient coalescence of lipid rafts during T-B cell contact. The main characteristics of the lipid raft included high concentrations of cholesterol, glycosphingolipid, GPI-anchored proteins, and parts of signal transduction-related molecules[25,26]. Efficient $CD4^+$ T cell activation requires the membrane compartmentalization of lipid rafts. Lipid raft coalescence and Ag-BCR endocytosis were substantially reduced following inhibition of core fucosylation[61].

Core fucosylation on Toll-like receptors recognition and signaling in macrophages

Receptor fucosylation is critical for BCR antigen recognition and antibody production[61] as well as Toll-like receptor (TLR) recognition and signaling through the scavenger receptor dendritic cell-specific ICAM-grabbing non-integrin[62, 63]. CD14 and TLRs are important pattern recognition molecules involved in innate immunity. TLRs serve as bridges between non-specific and specific immunity. CD14, a GPI anchored protein, was involved in governing lipopolysaccharide-induced dimerization of TLR4/myeloid differentiation factor 2 (MD2) complex, subsequent internalization of TLR4 and the activation of the Toll/IL-1R domain-containing adaptor-inducing IFN-β (TRIF)-dependent pathway[64]. CD14 and TLR4 receptor complexes are heavily glycosylated proteins with nine and two potential N-glycosylation sites, respectively[65,66]. Core fucose was essential for CD14-dependent TLR4 internalization and IFN-β production but not TLR4/MD2 activation and dimerization in mouse macrophage activity[64,67].

TLR2, another important component of the TLRs family, mediates the recognition of various G^+ bacterial cell wall components. In innate immunity, CD14 cooperates with TLR2/TLR4 to mediate the body's response to various pathogenic components[68]. The immune response of TLR2 and TLR4 is impaired after the loss of core fucosylation in macrophages. Compared to wild-type bone marrow cells, Fut8 knockout exhibited much higher resistance to inflammation in dextran sodium sulfate (DSS)-induced experimental colitis. Core fucose is essential for CD14- dependent TLR4 and TLR2 signaling in murine macrophages, leading to DSS-induced experimental colitis[67]. Screening compounds or small-molecule inhibitors that can inhibit core fucosylation of the CD14/TLR2/TLR4 signaling pathway could be a new strategy for the treatment of colitis. The modes of administration and dosage should first be tested in mouse models.

CORE FUCOSYLATION ON GASTROINTESTINAL MUCOSAL IMMUNE MODULATION

The mucosal immune system is the largest component of the immune system, and protects the main sites of infectious threats[69]. Core fucosylation is involved in the mucosal immune response, which is required for antiserum production during *Salmonella enterica subspp. enterica serovar Typhi* (*S. Typhi*) infection[70]. Secretory immunoglobulin A (sIgA) is the first line of defense against bacterial penetration and immunoprotecting against Salmonella infection[71]. The loss of core fucosylation results in suppressed sIgA production, which leads to increased susceptibility to pathogens. During *S. Typhi* infection, decreased T and B cell activation-related gene expression was observed after the inhibition of core fucosylation. Loss of core fucosylation suppresses the humoral immune response in *S. Typhi* infection[70].

sIgA is the main antibody of local mucosal anti-infection immunity and is frequently found in body fluids, such as saliva, tears, colostrum, nasal and bronchial secretions, gastric and intestinal fluids, urine, and sweat. In addition to the intestinal mucosal immunity, the influence of core fucosylation on other types of mucosal immunity remains largely unknown. Mucosal immunity differs from systemic immunity at structural, cellular, molecular, and functional levels. The mucosa-associated lymphoid tissues represented a highly compartmentalized immunological system and functioned essentially from the systemic immune apparatus independently[72]. Developing compounds that protect core fucosylation in specific mucosal systems against a variety of microbial pathogens is discussed in the table.

Fucosylated carbohydrate moieties in intestinal epithelial cells (IECs) are involved in creating an environmental niche for commensal and pathogenic bacteria. Core fucosylation is ubiquitously expressed in the intestinal mucosa and has strong effects on gut microbiota. After infection with *S. Typhi*, the levels of core fucosylation in IECs were upregulated, accompanied by an increased abundance of beneficial microorganisms such as *Akkermansia spp*. and *Lactobacillus*. Loss of core fucosylation increases the susceptibility of IECs to *S. Typhi*. During the infection of *S. Typhi*, the elevated core fucosylation level of IECs was mediated by the Wnt/β-catenin signaling pathway. Core fucosylation of IECs upregulates the biological antagonism of the intestinal microbiota to protect against *S. Typhi* infection[73].

CORE FUCOSYLATION ON GASTROINTESTINAL TUMOR IMMUNE MODULATION

Glycoproteomic and microarray analyses have revealed that Fut8 globally modifies surface antigens, receptors, and adhesion molecules and is involved in the regulation of dozens of genes associated with malignancy[74], suggesting that Fut8 contributes to gastrointestinal tumor progression through multiple mechanisms.

Core fucosylation on antibody-dependent cellular cytotoxicity

The antibody-dependent cellular cytotoxicity (ADCC) effector function of antibodies has been applied in oncotherapy and used to increase the clinical efficacy *in vivo*[75,76]. Therapeutic antibodies may modulate effector functions through the Fc receptor, and ADCC was affected by the Fc oligosaccharide structure[77,78]. *In vitro* and *in vivo* experiments have indicated that antibodies lacking core fucosylated Fc receptors exhibit stronger efficacy than core fucosylated antibodies [79-81]. Therapeutic antibodies that lack core fucosylation can evade inhibitory effects to achieve optimal ADCC[78,82-85]. The lack of core fucosylation of Fc oligosaccharides markedly enhances ADCC and is related to advanced antitumor efficacy *in vivo*[86]. Core fucose-deleted IgGs and N-glycan-reconstructed antibodies can be used in advanced antibody-based cancer immunotherapies. Defucosylated antibodies such as rituximab and trastuzumab, *etc.*, were considered promising next-generation therapeutics that can enhance ADCC activity (https://www.sciencedirect.com/topics/biochemistry-genetics-and-molecular-biology/fut8). Okazaki *et al*[87] reported that the loss of core fucosylation in the N-glycans of IgG1 molecules enhanced ADCC activity by 50-100 folds. Core fucosylation can modify physicochemical functions to regulate immunoglobulin function of immunoglobulins[87].

Core fucosylation on the expression of inhibitory receptors

During tumorigenic progression, CTLs experience dysfunction and exhaustion owing to immune-related tolerance and immunosuppression within the tumor microenvironment, favoring adaptive immune resistance. CTLs are key factors in eliminating tumorigenic cells during immune responses[33]. PD-1 was a receptor in the CD28 family of co-stimulatory molecules[88]. Upon interaction with its two ligands, programmed cell death 1 ligand 1 (PD-L1) or PD-L2 to T cells, PD-1 produces inhibitory signals[89]. PD-1 is a core fucosylated glycoprotein with four N-linked glycosylation sites[32], whereas the four N-linked glycosylation sites in PD-L1 (NM-001267706) are N^{35}, N^{192}, N^{200}, and N^{219}[90]. Blocking the core fucosylation of PD-1 inhibits its expression on CTL, which enhances the activation and anti-tumor activity of CTL[33]. Furthermore, the E3 ubiquitin ligase FBXO38 mainly mediates PD-1 polyubiquitination at Lys233[91]. Loss of core fucosylation increases the binding of FBXO38 to PD-1 and subsequent PD-1 degradation through the 26S proteasome to promote PD-1 ubiquitination (Figure 2)[33]. In conclusion, ubiquitination is regulated by core fucosylation, which is involved in tumor immunology[92].

PD-1/PD-L1 blockade immunotherapy has been utilized for gastrointestinal malignancies, including biliary tract, esophageal, colorectal, stomach, liver, pancreatic, and anal cancers[93]. The regulation of inhibitory receptor-mediated T cell dysfunction is vital in immunotherapy for gastrointestinal malignancies. The role of the core fucosylation of PD-1 and PD-L1 in the modulation of gastrointestinal cancer remains largely unknown. The effect of core fucosylation on other inhibitory receptors requires further investigation. In addition to PD-1, de-core fucosylation of other receptors, such as antigen 4 (CTLA-4), T-cell immunoglobulin, mucin-domain containing-3 (TIM-3), lymphocyte activation gene-3 (LAG-3), and T-cell immunoglobulin, and ITIM domain (TIGIT), has been investigated. To compare the effects of de-core fucosylation and PD-1/PD-L1 blockade, immunotherapy in a gastrointestinal cancer mouse model is essential.

Core fucosylation on the modulation of the epithelial to mesenchymal transition process

Fut8 inhibition suppresses highly metastatic breast cancer cell invasion and the ability to metastasize to the lung[46]. Epithelial to mesenchymal transition (EMT) is involved in cancer cell metastasis, wherein epithelial cells are transformed into mesenchymal cells to enhance cell dynamics, migration, and invasion[46]. E-cadherin/β-catenin signaling pathway could be activated by transforming growth factor β1 (TGF-β1) to regulate the EMT process. The TGF-β1 signaling pathway led to a deficiency in E-cadherin expression, allowing β-catenin translocation from the plasma membrane into the nucleus, and complexes with lymphoid enhancer-binding factor 1 (LEF-1)/T cell factor (TCF) to promote EMT[94,95]. Fut8 is a direct target of the transcription factor LEF-1, which regulates Fut8 levels. The promoter 1 region of Fut8 5′-UTR included multiple LEF-1/TCF binding sites which participated in the E-cadherin/β-catenin/LEF-1 signaling axis to regulate Fut8 expression during EMT[74,96] (Figure 3). Core fucosylation triggered TGF-β signaling and EMT, which subsequently stimulated the invasion and metastasis of cancer cells[46]. Caveolin-1 (Cav-1), a critical structural protein, could activate Wnt/β-catenin signaling to promote Fut8 expression which led to the proliferation and invasion of HCC [97]. Fut8 was also a driver for the progression of hepatocyte growth factor (HGF)-induced EMT, which was partially blocked by silencing of Fut8 in HCC cells. HGF or TGF-β1 treatment of HCC cells can increase the expression of glycosyltransferase Fut8 to up-regulate the core fucosylation of N-glycans, especially at the glycosylation site Asn-201 on

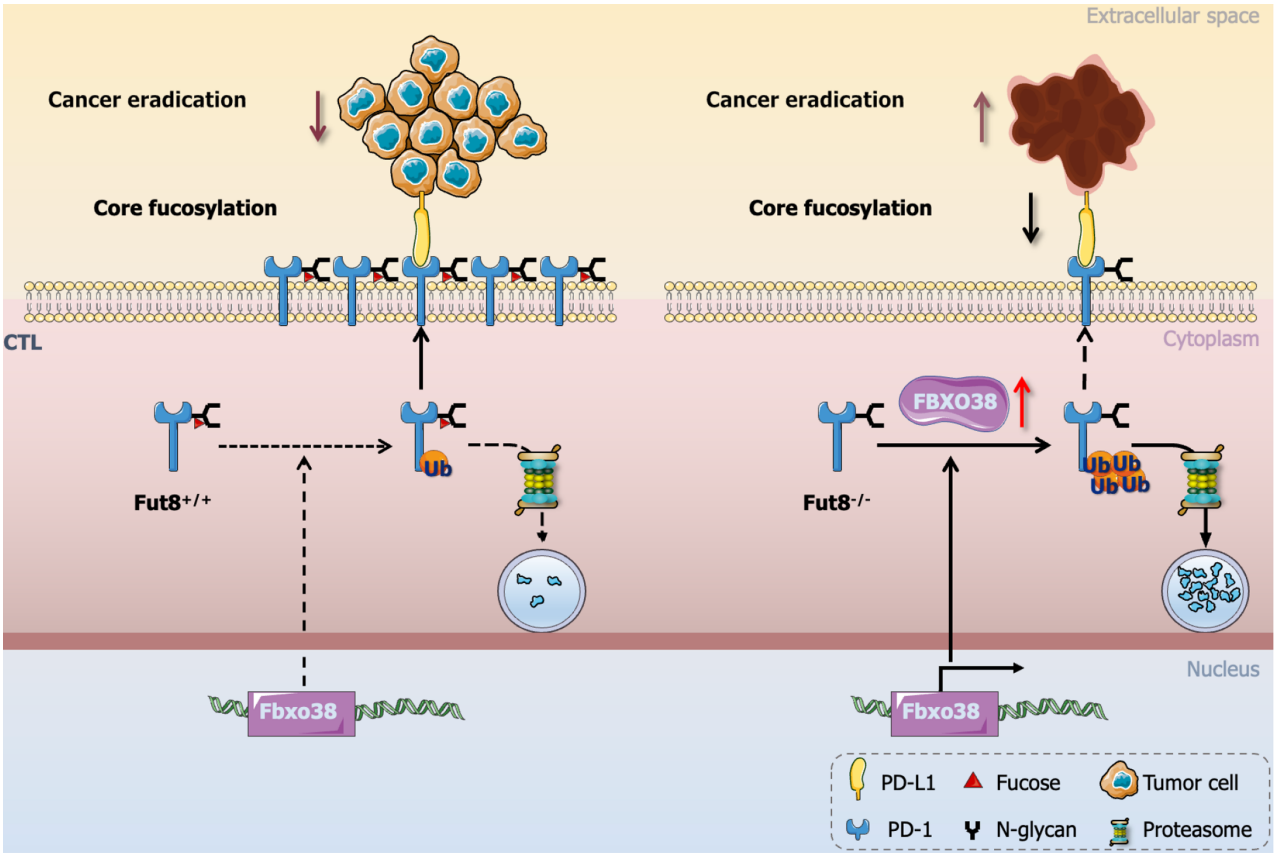

DOI: 10.4251/wjgo.v15.i7.1119

Figure 2 Programmed cell death 1 core fucosylation in tumorigenesis. Loss of core fucosylation catalyzed by fucosyltransferase 8 significantly enhanced CD8$^+$ cytotoxic T cell activation and cytotoxicity by increasing programmed cell death 1 (PD-1) ubiquitination which in turn led to the degradation of PD-1 in the proteasome and more efficient. PD-1: Programmed cell death 1; PD-L1: Programmed cell death 1 ligand 1; Fut8: Fucosyltransferase 8; CTL: Cytotoxic T cell. This figure was summarized and modified from Zhang *et al*[33].

glycoproteins including the folate receptor α (FOLR1)[98]. Core fucosylation of FOLR1 can enhance folate uptake capacity to promote EMT progression in HCC cells[98].

In colorectal cancer, there also existed high levels of Fut8 and E-cadherin protein expression. The enzymatic activity of Fut8 is involved in the appearance of a low-molecular-weight population of E-cadherin and regulates the total amount of E-cadherin[99]. The low-molecular-weight population of E-cadherin significantly increased after the overexpression of Fut8[99]. Core fucosylation participates in changes in N-glycosylation patterns in E-cadherin, stabilization of cell-cell contacts, and regulation of metastatic potential in colorectal cancer[99]. In colorectal cancer, liver metastasis is the most common incident, with a probability of at least 25%, which leads to colorectal liver metastases[100]. Decreased core fucosylation in colorectal cancer may positively influence tumor growth and metastasis. Exploring small molecules, miRNAs, and medicines that could target and downregulate the expression of Fut8 will make sense of the hepatic metastasis of colonic carcinoma.

TGF-β receptors I (TβRI) and II (TβRII) were highly glycosylated proteins. The TGF-β receptor was also modulated by core fucosylation modification[101]. Core fucosylation markedly facilitated functions of the heteromeric complexes of Tβ RII and TβRI to promote ligand binding and downstream signaling[46]. Loss of core fucosylation impaired the binding of TGF-β to its receptor[46] and inhibited the phosphorylation of regulatory Smad2 and Smad3 (R-Smads) to restrain TGF-β signal transduction(Figure 2). In conclusion, core fucosylation of TGF-β receptors modulated the receptor functions and a series of biological functions[102].

Core fucosylation on the modulation of epidermal growth factor receptor and hepatocyte growth factor receptor and biological functions

Functional growth factor receptors, such as hepatocyte growth factor receptor (HGFR) and epidermal growth factor receptor (EGFR) are regulated by core fucosylation[103,104]. EGFR, a type I transmembrane protein belonging to the ErbB family of receptor tyrosine kinases (RTKs) was activated following binding with peptide growth factors of the EGF family of proteins. Evidence suggests that the high expression of EGFR and EGF-like peptides is associated with the pathogenesis and progression of human carcinomas[37]. De-core fucosylation attenuates responses to EGF and HGF, and blocks EGF-induced phosphorylation of EGFR in hepatocellular carcinoma[37].

Ligand-receptor binding is also essential for core fucosylation between EGF and EGFR, whereas the expression levels of EGFR are not influenced by core fucosylation on the cell surface. Core fucosylation of EGFR is closely related to cancer immunotherapy, which could modulate cellular sensitivity to immunotherapeutic agents. Cells with high Fut8 expression

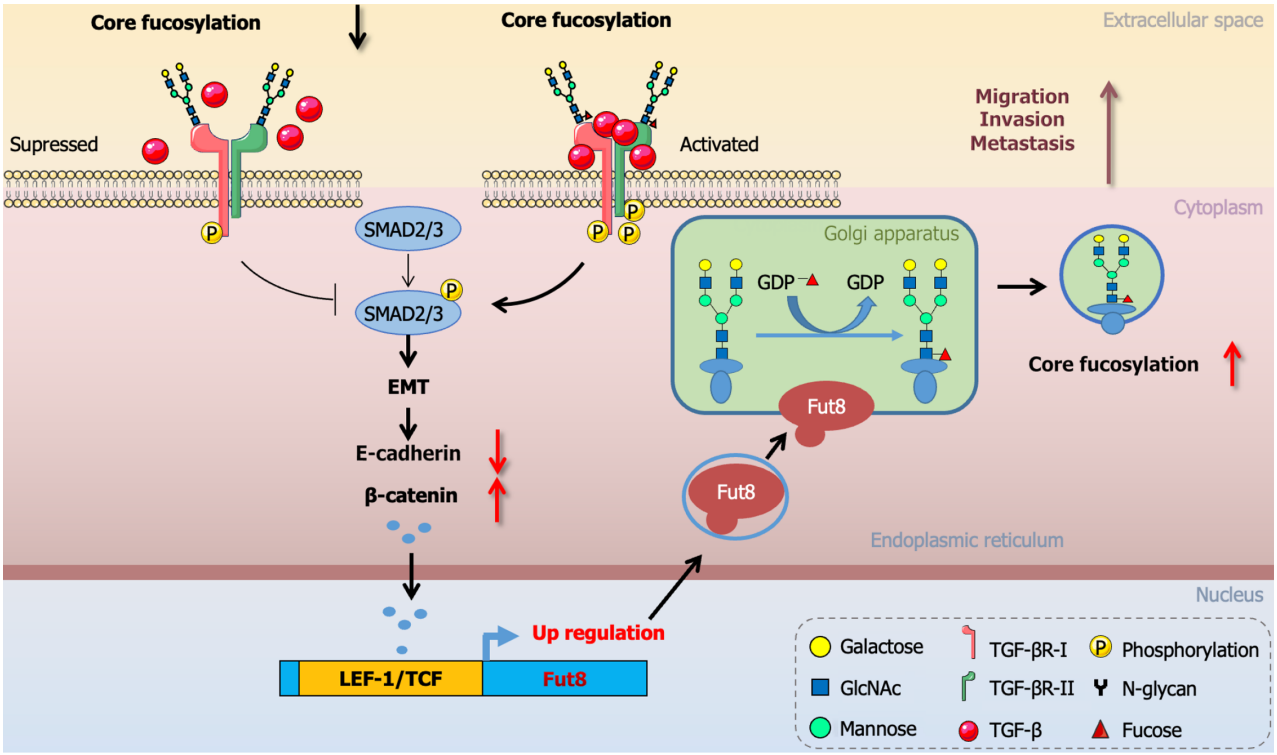

DOI: 10.4251/wjgo.v15.i7.1119

Figure 3 Core fucosylation modulated epithelial to mesenchymal transition during cancer progression. Loss of core fucosylation impaired the binding of transforming growth factor β to its receptor and inhibited the phosphorylation of regulatory Smad2 and Smad3. During epithelial to mesenchymal transition, the expression of E-cadherin was suppressed, resulting in the accumulation of β-catenin in the nucleus, where it complexed with lymphoid enhancer-binding factor 1 to transactivate fucosyltransferase 8 expression. The core fucosylation level on surface molecules of cancer cells was increased which promoted cancer cell malignant biological properties involving migration, invasion, and metastasis. EMT: Epithelial to mesenchymal transition; TCF: T cell factor; LEF: Lymphoid enhancer-binding factor 1; TGF: Transforming growth factor. This figure was summarized and modified from Tu *et al*[46], Chen *et al*[74], and Lin *et al*[101].

were more sensitive to gefitinib, an EGFR-specific tyrosine kinase inhibitor (EGFR-TKI)[106]. Collectively, core fucosylation plays a vital role in EGFR-mediated biological functions[103].

Fucosylation on the modulation of mitogen-activated protein kinase signal pathway

The mitogen-activated protein kinase (MAPK) pathway participates in the regulation of gene expression, cellular growth, and survival[107]. Abnormal MAPK signaling may induce increased or uncontrolled cell proliferation and apoptosis resistance, leading to oncogenesis[105]. The activation of phosphorylated ERK1/2 and p38 MAPK is involved in tumor cell proliferation and migration[108,109]. Loss of fucosylation suppresses the activation of the ERK1/2 and p38 MAPK signaling pathways, which inhibits carcinoma invasion. Therefore, fucosylation participates in the MAPK signaling pathway activation to modulate biological processes[110].

O-fucosylation is another type of fucosylation modification that is involved in embryonic development. Protein O-fucosyltransferase 1 (poFUT1) is an essential enzyme that catalyzes the synthesis of protein O-fucosylation. poFUT1 promotes trophoblast proliferation by increasing cell cycle progression and promoting cells in the S-phase *via* activating the MAPK and PI3K/Akt signaling pathways. Activated MAPK and PI3K/Akt signaling pathways are accompanied by increased expression of cyclin D1, cyclin E, CDK 2, CDK 4, and pRb, and decreased levels of the cyclin-dependent kinase inhibitors p21 and p27[111]. However, the influence of core fucosylated N-glycoproteins on the MAPK signaling pathway during tumorigenesis remains largely unknown.

Core fucosylation on the modulation of PI3K-AKT-NF-κB signal pathway

The hepatitis C virus (HCV) is a major cause of chronic liver disease and hepatocellular carcinoma[112]. HCV infection could induce Fut8 expression to promote hepatocellular carcinoma proliferation by activating PI3K-AKT-NF-κB signaling [113]. HCV also stimulates the expression of multidrug resistance-related protein 1 (MRP1) and drug-resistant protein P-glycoprotein (P-GP) and enhances the chemoresistance of HCC to 5-fluorouracil (5-FU)[113]. Inhibition of the PI3K/AKT pathway by its specific inhibitor wortmannin or by small interfering RNA (siRNA) of AKT resulted in decreased MDR of 5-FU chemoresistance in HCC cells, partly through the downregulation of MRP1[114]. In cancer treatment, Fut8 may play a role in reversing chemotherapy resistance and may serve as a therapeutic target.

Core fucosylation on the modulation of cancer cell stemness

Cancer stem cells (CSC) were responsible for cancer reconstitution and propagation. CSCs possess self-renewal, differentiation, and proliferative abilities similar to those of normal stem cells. Cancer stemness, the stem cell-like phenotype of

cancer cells, plays an important role in various aspects of carcinogenesis. During anticancer therapies, CSCs exhibited resistant effects, leading to subsequent relapse[115]. Fut8 is required for stemness maintenance in tumorigenic cells[116]. Fut8 deficiency downregulates the stemness of cancer cells, which decreases the expression of CSC-related biomarkers, such as EpCAM, CD133, c-Met, and CXCR4[117]. Fut8-catalyzed α-1,6-fucosylation also promoted stemness induced by fentanyl, an opioid analgesic widely used in cancer patients[118].

Core fucosylation on cancerous radio-resistance

Radioresistance is a major factor affecting the success of radiation therapy for ESCC[119]. There was a high level of core fucosylation in patients with radioresistant ESCC, which led to a poor prognosis. Fut8 inhibition increases the radiosensitivity of radioresistant ESCC cells and suppresses tumor growth and formation[119]. As a key regulatory tumor-associated antigen, native CD147 from human cancer tissue contains a high percentage of core fucosylated structures (28.8%) analyzed *via* N-linked glycan profiling[120]. In ESCC cells, the inhibition of CD147 partly reversed Fut8-induced radioresistance[119]. Collectively, core fucosylation plays a vital role in the radiosensitivity of ESCC.

Modulation of core fucosylation via microRNA, long non-coding RNA, and circular RNAs on gastrointestinal Tumor

MicroRNAs (miRNAs) and long non-coding RNA (lncRNAs) play vital roles in the post-transcriptional regulation of genes *via* gene imprinting, chromosome remodeling, and cell cycle regulation. The antisense RNA 1 of LEF1, LEF1-AS1, is a newly identified highly conserved lncRNA encoded on the plus strand of LEF1 on chromosome 4q25, which can modulate LEF1 expression[121]. LEF1-AS1 mediated Fut8 Level through activation of Wnt/β-catenin/LEF1 pathway, thereby resulting in β-catenin nuclear translocation. LEF1-AS1 silencing hinders tumorigenesis and lung and liver metastases of colon cancer cells in vivo, while overexpressed of Fut8 abolished the suppressive effect of LEF1-AS1 repression on the biological behavior of colon cancer cells[121]. Furthermore, miR-198 was shown to target the 3'UTR of Fut8 directly to downregulate Fut8 expression at both mRNA and protein levels and suppressed the proliferation and invasion of colorectal carcinoma[122]. In hepatocarcinoma cells, miR-122 and miR-34a were downregulated in spontaneous human hepatocarcinoma which could specifically interact with and regulate the 3'UTR of Fut8[123]. MiR-122-5p, as a post-transcriptional regulator of Fut8, inhibits the expression of Fut8 and suppresses the proliferation and migration of intrahepatic cholangiocarcinoma cells *via* the PI3K/AKT signaling pathway[124].

Circular RNAs (circRNAs) regulate cancer development *via* multiple mechanisms, including miRNA sponges, modulation of the Wnt signaling pathway, and EMT[125]. CircRNA cFUT8 promotes HCC development by binding free miR-548c and inhibiting the miR-548c/FUT8 regulatory axis[126].

MiRNAs are promising therapeutic targets for cancer treatment[127]. CircRNAs, such as miRNA sponges, protein scaffolding, or autophagy regulators, interact with RNA-binding proteins (RBP) to act as potential biomarkers for cancer prevention, diagnosis, and therapeutic targets[128]. Screening out more miRNAs and circRNAs targeting Fut8 both in scientific research and in the clinical treatment of gastrointestinal diseases, could be a directional research area.

MODULATION OF CORE FUCOSYLATION ON T CELL IMMUNOREGULATION

The results of the current study showed that Fut8 played a pivotal role in T and B cell activation. $CD4^+$ T cells represent a unique branch of the adaptive immune system that is crucial for achieving a regulated and effective immune response against pathogens and their proper functioning is vital for survival[129]. $CD4^+$ T cells perform multiple functions, including activation of cells of the innate immune system, B-lymphocytes, CTLs, and non-immune cells, and play a critical role in the suppression of immune reactions[129]. However, several uncertainties remain. Fut8 participates in the contact between TCR and pMHC and subsequent $CD4^+$ T cell activation. Owing to the complexity of the *in vivo* environment, we cannot simply assume that malfunction of the TCR signaling pathway is the only reason for T cell activation. Functions of Fut8 on the interaction of $CD4^+$ T cells with other APCs (such as dendritic cells and macrophages) are also important issues to be explored. SLE is characterized by the overproduction of autoantibodies, mainly IgG[130]. The pathogenesis of SLE is accompanied by hyper $CD4^+$ T cell metabolism[49,131,132]. Core fucosylation is associated with SLE severity and is significantly increased in the $CD4^+$ T cells of patients with SLE. Hyper core fucosylation-induced $CD4^+$ T cell activation could be involved in the development of SLE[56]. To further explore how core fucosylation modulates other cell types in the adaptive immune system, the entire function of SLE therapy may be an urgent project.

Core fucosylation is essential for $CD4^+$ T cell activation *via* TCR and affects the geometry and conformation of TCR-pMHC clusters in T-B cell interactions. The loss of core fucosylation enhances the anticancer activity of $CD8^+$ CTLs in lung adenocarcinoma. The IL-2 pathway is involved in immune cell activation and downstream effects[133], which may pave the way for further therapeutic developments. In the IL-2/ IL-2 receptor (IL-2R) pathway, the low-affinity IL-2 receptor, IL-2Rβγ, tended to be expressed on $CD8^+$ T cells and NK cells, while the high-affinity heterotrimeric IL-2-receptor alpha beta gamma subunits (IL-2Rαβγ) were constitutively expressed by Tregs[134]. Researchers have determined that IL-2 has pleiotropic effects; at high concentrations, IL-2 causes the expansion and activation of cytotoxic $CD8^+$ effector T cells, whereas at low concentrations, IL-2 expands and activates Tregs[135] which is the dual and seemingly opposing activity during tumor eradication. NKTR-214 is a CD122-biased IL-2R agonist that stimulates the proliferation of anticancer immune cells *in vivo* by targeting CD122-specific receptors on the surfaces of NK, $CD4^+$ T, and $CD8^+$ T cells. CD122, also known as the IL-2Rβ subunit, was an important signaling receptor known to increase the proliferation of these effector T cells. In preclinical and clinical studies, NKTR-214 treatment led to rapid expansion and mobilization of these cells into the microenvironment. Given that the mRNA expression of IL-2 was upregulated in $Fut8^{-/-}$OT-I CTLs, IL-2-induced FBXO38 expression resulted in enhanced PD-1 ubiquitination, which was correlated with lower PD-1 protein abundance

on the surface of activated CTLs. We hypothesize Fut8 may also participate in IL-2R subunit regulation and function, which subsequently influences CTL activation.

Physiologically, there may be an equilibrium of core fucosylation on the TCR and the inhibitory receptor PD-1 to regulate T cell activation. Our study is the first revealed that Fut8 inhibition promoted $CD8^+$ T cell activation while inhibiting TCR-pMHC contact and subsequent $CD4^+$ T cell activation. The complexity of *in vivo* conditions makes it impossible to determine the final influence of Fut8 on tumor immunology. $CD8^+$ T cells mainly participate in tumor eradication, whereas $CD4^+$ T cells are involved in immunoregulation. Although the study identified the role of Fut8 in $CD4^+$ T-cell activation during SLE and the anticancer activity of CTL in lung adenocarcinoma, the influence of Fut8 on $CD4^+$ T-cells during cancer progression remains largely unknown. The balance between specific and degenerate T cell recognition by pMHC-II has important implications for protective immunity *vs* autoimmunity.

FUT8 INHIBITOR AND GASTROINTESTINAL ONCOTHERAPY

Fucosylation, which regulates the biological functions of adhesion molecules and growth factor receptors[136,137]. Many types of fucosyltransferases (FucTs), the GDP-Fuc synthesis pathway, and GDP-Fuc transporters participate in the regulation of fucosylation. The inhibition of FucT activity by FucT inhibitors represents a potential strategy for cancer immunotherapy. The metabolic fucosylation inhibitor 2-fluoro-L-fucose (2F-Fuc) inhibits natural GDP-Fuc production by blocking fucosylation *via* endogenous salvage pathways[138]. 2F-Fuc affects the functions of both immune and tumor cells. Blocking core fucosylation of $CD8^+$ CTL *via* 2F-Fuc downregulates PD-1 expression and enhances CTL activation and tumor eradication[32]. Beyond this mechanism, 2F-Fuc inhibited the binding affinity of galectin-3 to glycoproteins, which could promote TCR signaling pathways and dendritic cell maturation by reducing the threshold for lattice disruption by peptide-MHC with easier TCR engagement (Abstract 4005: Understanding the mechanism of 2FF-induced immune modulation). 2F-Fuc enhances the immune-dependent protective effects of lymphoma vaccines[139].

2F-Fuc can also inhibit fucosylation and modulate tumor cell function. Core fucosylation of a series of membrane glycoproteins, integrin β1, and EGFR could be inhibited by 2F-Fuc treatment, which suppressed the phosphorylation of downstream signal molecules like EGFR, AKT, ERK, and FAK. Proliferation, migration, and tumor formation in human cancer cells are consequently suppressed by 2F-Fuc treatment[140].

Core fucosylated proteins are crucial components of the gastrointestinal immune system that modulate the immunoregulation of various immune processes and immune-related gastrointestinal diseases. Abnormal core fucosylation has been observed in several immune processes. Thus, given the unfavorable regulation of immune-related diseases by core fucosylation, Fut8 inhibitors should be developed. 2F-Fuc inhibits fucosylation of proteins. In total, 13 FUT genes have been identified in the human genome. Different genes encode different fucosyltransferases with various functions. Core fucosylation is an important modification of the N-glycan core structure, forming the α-1,6 fucosylation of the GlcNAc residue linked to asparagine, which is catalyzed by Fut8. The inhibition of core fucosylation has shown great therapeutic potential in a series of diseases, and is an important first step towards the development of future inhibitors. Compared to 2F-Fuc, the specific Fut8 inhibitor had a more precise function towards immunoregulation, with minor side effects on the entire gastrointestinal immune system.

Chimeric antigen receptor (CAR) T-cell therapy is an innovative form of cancer immunotherapy in which autologous T cells are genetically modified to express chimeric receptors encoding antigen-specific single-chain variable fragments and co-stimulatory molecules[141]. Although numerous advances have been made in CAR-T cell therapy for hematological tumors, this technology remains ineffective for treating solid cancers, especially gastrointestinal tumors. These shortcomings include on-target, off-tumor toxicity, a paucity of tumor-specific antigen targets, T cell exhaustion in the gastrointestinal tumor microenvironment, and low infiltration of immune cells into gastrointestinal solid tumor niches [142]. Thus, progress in gastrointestinal tumor immunology and improvements in the manufacturing of cell products have promoted the development of cellular immunotherapies. High expression of inhibitory receptors, such as PD-1, on the surface of T cells is modulated by core fucosylation. Inhibitors with smaller molecules can penetrate to the inner tumor tissue more easily. In comparison to monotherapy, CAR-T cell therapy combined with a Fut8 inhibitor may improve the therapeutic effect, especially in solid tumors such as gastrointestinal tumors.

CONCLUSION

Core fucosylation plays a major role in gastrointestinal glycoimmunology (Table 1). Owing to the complicated regulation of core fucosylation in a variety of immune-related gastrointestinal diseases and cancers, other regulatory mechanisms involved in core fucosylation modifications also need to be explored. Future studies should aim to identify the detailed and complex regulatory mechanisms and therapeutic effects of Fut8 on more kinds of gastrointestinal system-related immune cells and immune diseases.

Table 1 Abnormal core fucosylation in gastrointestinal diseases

Types of immune modulation	Mechanism	Patterns of modulation	Disease	Ref.
Core fucosylation on gastrointestinal cellular immune modulation	Core fucosylation modulated T cell activation *via* TCR	Higher core fucosylation level existed in the sera of SLE patients and related to the severity of SLE. Increased core fucosylation in SLE patients was also correlated with $CD4^+$ T cell activation	SLE	[51,53]
	Core fucosylation modulated TLRs recognition and signaling in macrophages	Core fucose was essential for CD14- dependent TLR4 and TLR2 signaling in murine macrophage activity, leading to DSS-induced experimental colitis	DSS-induced experimental colitis	[67]
Core fucosylation on gastrointestinal humoral immune modulation	Core fucosylation modulated humoral immune response	Loss of core fucosylation suppressed the humoral immune response in *S. Typhi* infection and resulted in suppressed sIgA production, which led to increased susceptibility to pathogens	*S. Typhi* infection	[70]
Core fucosylation on gastrointestinal tumor immune modulation	Core fucosylation modulated EMT	Caveolin-1 (Cav-1) could activate Wnt/β-catenin signaling to promote Fut8 expression which led to the proliferation and invasion of HCC	HCC	[97]
		Fut8 was a driver for the progress of hepatocyte growth factor (HGF)-induced EMT which was partially blocked by the silencing of Fut8 in HCC cells	HCC	[98]
		Core fucosylation on FOLR1 could enhance the folate uptake capacity to finally promote the EMT progress of HCC cells	HCC	[98]
		The low molecular weight population of E-cadherin was significantly increased after overexpression of Fut8, which resulted in an enhancement in cell–cell adhesion	Colorectal cancer	[99]
	Core fucosylation modulated EGFR and HGFR and biological functions	De-core fucosylation attenuated responses to EGF and HGF and blocked the EGF-induced phosphorylation of the EGFR in hepatocellular carcinoma	HCC	[37]
	Core fucosylation modulated PI3K-AKT-NF-κB signal pathway	HCV infection induced Fut8 expression to promote hepatocellular carcinoma proliferation by activating PI3K-AKT-NF-κB signaling	HCC	[113]
	Core fucosylation modulated cancerous radioresistance	Fut8 inhibition increased the radiosensitivity of radioresistant ESCC cells and suppressed the growth and formation of tumors	ESCC	[119]
	Modulation of core fucosylation *via* microRNA, long non-coding RNA, and circular RNAs	LEF1-AS1 (lncRNA) silence hindered the tumorigenesis, and lung and liver metastasis of colon cancer cells *in vivo*, while overexpressed Fut8 abolished the suppressive impact of LEF1-AS1 repression on the biological behavior of colorectal cancer cells	Colorectal cancer	[121]
		MiR-198 targeted the 3'UTR of Fut8 directly to downregulate Fut8 expression at both mRNA and protein levels and suppressed the proliferation and invasion of colorectal carcinoma	Colorectal cancer	[122]
		MiR-122 and miR-34a were downregulated in spontaneous human hepatocarcinoma which could specifically interact with and regulate the 3'UTR of Fut8	HCC	[123]
		MiR-122-5p inhibited the expression of Fut8 and suppressed the proliferation and migration ability of the intrahepatic cholangiocarcinoma cell line *via* PI3K/AKT signaling pathway	Intrahepatic cholangiocarcinoma	[124]
		CircRNA cFUT8 promoted HCC development by binding free miR-548c and inhibiting the miR-548c/FUT8 regulatory axis	HCC	[126]

Mechanisms and patterns of different types of gastrointestinal immune modulation included cellular, humoral, and tumor immune modulation after modification with core fucosylation. The related diseases were also listed with the references. HCC: Hepatocellular cancer; EMT: Epithelial to mesenchymal transition; Fut8: Fucosyltransferase 8; CTL: Cytotoxic T cell; HCV: Hepatitis C virus; EGFR: Epidermal growth factor receptor; HGFR: Hepatocyte growth factor receptor; SLE: Systemic lupus erythematosus; ESCC: Esophageal squamous cell carcinoma. TLRs: Toll-like receptors; *S. typhimurium: Salmonella typhimurium.*

FOOTNOTES

Author contributions: Zhang NZ and Zhao LF contributed equally to this work and wrote the manuscript; Gao P revised the review; Li WZ and Ge YS designed the structure of review; Zhang Q, Fang H, and Song WL prepared the figures and table; all authors have read and approve the final manuscript.

Supported by the National Natural Science Foundation of China, No. 32171279; Natural Science Foundation of Liaoning Province, No. 2022-BS-254, and No. 2022-MS-317; and the Project of Dalian Medical Science Research, No. 2012026.

Conflict-of-interest statement: The authors declare no commercial or financial conflict of interest.

Country/Territory of origin: China

ORCID number: Nian-Zhu Zhang 0000-0001-7140-2419; Peng Gao 0000-0001-6932-5370.

S-Editor: Yan JP
L-Editor: A
P-Editor: Zhang XD

REFERENCES

1 **Zhu Y**, Hart GW. Nutrient regulation of the flow of genetic information by O-GlcNAcylation. *Biochem Soc Trans* 2021; **49**: 867-880 [PMID: 33769449 DOI: 10.1042/BST20200769]
2 **Hülsmeier AJ**, Welti M, Hennet T. Glycoprotein maturation and the UPR. *Methods Enzymol* 2011; **491**: 163-182 [PMID: 21329800 DOI: 10.1016/B978-0-12-385928-0.00010-9]
3 **Essentials of Glycobiology**. Varki A, Cummings RD, Esko JD, Freeze HH, Stanley P, Bertozzi CR, Hart GW, Etzler ME, Editors. Cold Spring Harbor (NY): Cold Spring Harbor Laboratory Press, 2009
4 **Jefferis R**. Recombinant Proteins and Monoclonal Antibodies. *Adv Biochem Eng Biotechnol* 2021; **175**: 281-318 [PMID: 29071407 DOI: 10.1007/10_2017_32]
5 **Khairnar A**, Sunsunwal S, Babu P, Ramya TNC. Novel serine/threonine-O-glycosylation with N-acetylneuraminic acid and 3-deoxy-D-manno-octulosonic acid by bacterial flagellin glycosyltransferases. *Glycobiology* 2021; **31**: 288-306 [PMID: 32886756 DOI: 10.1093/glycob/cwaa084]
6 **Abu-Qarn M**, Eichler J, Sharon N. Not just for Eukarya anymore: protein glycosylation in Bacteria and Archaea. *Curr Opin Struct Biol* 2008; **18**: 544-550 [PMID: 18694827 DOI: 10.1016/j.sbi.2008.06.010]
7 **Colomb F**, Giron LB, Trbojevic-Akmacic I, Lauc G, Abdel-Mohsen M. Breaking the Glyco-Code of HIV Persistence and Immunopathogenesis. *Curr HIV/AIDS Rep* 2019; **16**: 151-168 [PMID: 30707400 DOI: 10.1007/s11904-019-00433-w]
8 **van Kooyk Y**, Rabinovich GA. Protein-glycan interactions in the control of innate and adaptive immune responses. *Nat Immunol* 2008; **9**: 593-601 [PMID: 18490910 DOI: 10.1038/ni.f.203]
9 **Rudd PM**, Wormald MR, Dwek RA. Glycosylation and the immune system. *J Protein Chem* 1998; **17**: 519 [PMID: 9723723]
10 **Garg A**, Barnes PF, Roy S, Quiroga MF, Wu S, García VE, Krutzik SR, Weis SE, Vankayalapati R. Mannose-capped lipoarabinomannan- and prostaglandin E2-dependent expansion of regulatory T cells in human Mycobacterium tuberculosis infection. *Eur J Immunol* 2008; **38**: 459-469 [PMID: 18203140 DOI: 10.1002/eji.200737268]
11 **Ma Y**, Chen H, Wang Q, Luo F, Yan J, Zhang XL. IL-24 protects against Salmonella typhimurium infection by stimulating early neutrophil Th1 cytokine production, which in turn activates CD8+ T cells. *Eur J Immunol* 2009; **39**: 3357-3368 [PMID: 19830736 DOI: 10.1002/eji.200939678]
12 **Zhang XL**. Roles of glycans and glycopeptides in immune system and immune-related diseases. *Curr Med Chem* 2006; **13**: 1141-1147 [PMID: 16719775 DOI: 10.2174/092986706776360897]
13 **Chang YH**, Weng CL, Lin KI. O-GlcNAcylation and its role in the immune system. *J Biomed Sci* 2020; **27**: 57 [PMID: 32349769 DOI: 10.1186/s12929-020-00648-9]
14 **Lefebvre JC**, Giordanengo V, Limouse M, Doglio A, Cucchiarini M, Monpoux F, Mariani R, Peyron JF. Altered glycosylation of leukosialin, CD43, in HIV-1-infected cells of the CEM line. *J Exp Med* 1994; **180**: 1609-1617 [PMID: 7964449 DOI: 10.1084/jem.180.5.1609]
15 **Brockhausen I**, Kuhns W, Schachter H, Matta KL, Sutherland DR, Baker MA. Biosynthesis of O-glycans in leukocytes from normal donors and from patients with leukemia: increase in O-glycan core 2 UDP-GlcNAc:Gal beta 3 GalNAc alpha-R (GlcNAc to GalNAc) beta(1-6)-N-acetylglucosaminyltransferase in leukemic cells. *Cancer Res* 1991; **51**: 1257-1263 [PMID: 1997166]
16 **Huang MM**, Tsuboi S, Wong A, Yu XJ, Oh-Eda M, Derry JM, Francke U, Fukuda M, Weinberg KI, Kohn DB. Expression of human Wiskott-Aldrich syndrome protein in patients' cells leads to partial correction of a phenotypic abnormality of cell surface glycoproteins. *Gene Ther* 2000; **7**: 314-320 [PMID: 10694812 DOI: 10.1038/sj.gt.3301085]
17 **Essentials of Glycobiology**. Varki A, Cummings RD, Esko JD, Stanley P, Hart GW, Aebi M, Darvill AG, Kinoshita T, Packer NH, Prestegard JH, Schnaar RL, Seeberger PH, Editors. Cold Spring Harbor (NY): Cold Spring Harbor Laboratory Press, 2015
18 **Ellies LG**, Tsuboi S, Petryniak B, Lowe JB, Fukuda M, Marth JD. Core 2 oligosaccharide biosynthesis distinguishes between selectin ligands essential for leukocyte homing and inflammation. *Immunity* 1998; **9**: 881-890 [PMID: 9881978 DOI: 10.1016/s1074-7613(00)80653-6]
19 **Tsuboi S**, Fukuda M. Roles of O-linked oligosaccharides in immune responses. *Bioessays* 2001; **23**: 46-53 [PMID: 11135308 DOI:

10.1002/1521-1878(200101)23:1<46::Aid-bies1006>3.0.Co;2-3]
20 **Green RS**, Stone EL, Tenno M, Lehtonen E, Farquhar MG, Marth JD. Mammalian N-glycan branching protects against innate immune self-recognition and inflammation in autoimmune disease pathogenesis. *Immunity* 2007; **27**: 308-320 [PMID: 17681821 DOI: 10.1016/j.immuni.2007.06.008]
21 **Lau KS**, Partridge EA, Grigorian A, Silvescu CI, Reinhold VN, Demetriou M, Dennis JW. Complex N-glycan number and degree of branching cooperate to regulate cell proliferation and differentiation. *Cell* 2007; **129**: 123-134 [PMID: 17418791 DOI: 10.1016/j.cell.2007.01.049]
22 **Li D**, Li Y, Wu X, Li Q, Yu J, Gen J, Zhang XL. Knockdown of Mgat5 inhibits breast cancer cell growth with activation of CD4+ T cells and macrophages. *J Immunol* 2008; **180**: 3158-3165 [PMID: 18292539 DOI: 10.4049/jimmunol.180.5.3158]
23 **Li J**, Hsu HC, Mountz JD, Allen JG. Unmasking Fucosylation: from Cell Adhesion to Immune System Regulation and Diseases. *Cell Chem Biol* 2018; **25**: 499-512 [PMID: 29526711 DOI: 10.1016/j.chembiol.2018.02.005]
24 **Miyoshi E**, Noda K, Yamaguchi Y, Inoue S, Ikeda Y, Wang W, Ko JH, Uozumi N, Li W, Taniguchi N. The alpha1-6-fucosyltransferase gene and its biological significance. *Biochim Biophys Acta* 1999; **1473**: 9-20 [PMID: 10580126 DOI: 10.1016/s0304-4165(99)00166-x]
25 **Dykstra M**, Cherukuri A, Sohn HW, Tzeng SJ, Pierce SK. Location is everything: lipid rafts and immune cell signaling. *Annu Rev Immunol* 2003; **21**: 457-481 [PMID: 12615889 DOI: 10.1146/annurev.immunol.21.120601.141021]
26 **Cheng PC**, Brown BK, Song W, Pierce SK. Translocation of the B cell antigen receptor into lipid rafts reveals a novel step in signaling. *J Immunol* 2001; **166**: 3693-3701 [PMID: 11238609 DOI: 10.4049/jimmunol.166.6.3693]
27 **Zhang K**, Wang H. [Role of Fucosylation in Cancer]. *Zhongguo Fei Ai Za Zhi* 2016; **19**: 760-765 [PMID: 27866519 DOI: 10.3779/j.issn.1009-3419.2016.11.07]
28 **Wilson JR**, Williams D, Schachter H. The control of glycoprotein synthesis: N-acetylglucosamine linkage to a mannose residue as a signal for the attachment of L-fucose to the asparagine-linked N-acetylglucosamine residue of glycopeptide from alpha1-acid glycoprotein. *Biochem Biophys Res Commun* 1976; **72**: 909-916 [PMID: 985526 DOI: 10.1016/s0006-291x(76)80218-5]
29 **Norton PA**, Mehta AS. Expression of genes that control core fucosylation in hepatocellular carcinoma: Systematic review. *World J Gastroenterol* 2019; **25**: 2947-2960 [PMID: 31249452 DOI: 10.3748/wjg.v25.i23.2947]
30 **Wang X**, Inoue S, Gu J, Miyoshi E, Noda K, Li W, Mizuno-Horikawa Y, Nakano M, Asahi M, Takahashi M, Uozumi N, Ihara S, Lee SH, Ikeda Y, Yamaguchi Y, Aze Y, Tomiyama Y, Fujii J, Suzuki K, Kondo A, Shapiro SD, Lopez-Otin C, Kuwaki T, Okabe M, Honke K, Taniguchi N. Dysregulation of TGF-beta1 receptor activation leads to abnormal lung development and emphysema-like phenotype in core fucose-deficient mice. *Proc Natl Acad Sci U S A* 2005; **102**: 15791-15796 [PMID: 16236725 DOI: 10.1073/pnas.0507375102]
31 **Rudd PM**, Elliott T, Cresswell P, Wilson IA, Dwek RA. Glycosylation and the immune system. *Science* 2001; **291**: 2370-2376 [PMID: 11269318 DOI: 10.1126/science.291.5512.2370]
32 **Okada M**, Chikuma S, Kondo T, Hibino S, Machiyama H, Yokosuka T, Nakano M, Yoshimura A. Blockage of Core Fucosylation Reduces Cell-Surface Expression of PD-1 and Promotes Anti-tumor Immune Responses of T Cells. *Cell Rep* 2017; **20**: 1017-1028 [PMID: 28768188 DOI: 10.1016/j.celrep.2017.07.027]
33 **Zhang N**, Li M, Xu X, Zhang Y, Liu Y, Zhao M, Li P, Chen J, Fukuda T, Gu J, Jin X, Li W. Loss of core fucosylation enhances the anticancer activity of cytotoxic T lymphocytes by increasing PD-1 degradation. *Eur J Immunol* 2020; **50**: 1820-1833 [PMID: 32460355 DOI: 10.1002/eji.202048543]
34 **Abdul-Latif M**, Townsend K, Dearman C, Shiu KK, Khan K. Immunotherapy in gastrointestinal cancer: The current scenario and future perspectives. *Cancer Treat Rev* 2020; **88**: 102030 [PMID: 32505807 DOI: 10.1016/j.ctrv.2020.102030]
35 **Chang SC**, Lin WL, Chang YF, Lee CT, Wu JS, Hsu PH, Chang CF. Glycoproteomic identification of novel plasma biomarkers for oral cancer. *J Food Drug Anal* 2019; **27**: 483-493 [PMID: 30987719 DOI: 10.1016/j.jfda.2018.12.008]
36 **Sadeghzadeh Z**, Khosravi A, Jazi MS, Asadi J. Upregulation of Fucosyltransferase 3, 8 and protein O-Fucosyltransferase 1, 2 genes in esophageal cancer stem-like cells (CSLCs). *Glycoconj J* 2020; **37**: 319-327 [PMID: 32157457 DOI: 10.1007/s10719-020-09917-z]
37 **Wang Y**, Fukuda T, Isaji T, Lu J, Im S, Hang Q, Gu W, Hou S, Ohtsubo K, Gu J. Loss of α1,6-fucosyltransferase inhibits chemical-induced hepatocellular carcinoma and tumorigenesis by down-regulating several cell signaling pathways. *FASEB J* 2015; **29**: 3217-3227 [PMID: 25873065 DOI: 10.1096/fj.15-270710]
38 **Watanabe K**, Ohta M, Yada K, Komori Y, Iwashita Y, Kashima K, Inomata M. Fucosylation is associated with the malignant transformation of intraductal papillary mucinous neoplasms: a lectin microarray-based study. *Surg Today* 2016; **46**: 1217-1223 [PMID: 26754572 DOI: 10.1007/s00595-015-1299-8]
39 **Muinelo-Romay L**, Villar-Portela S, Cuevas Alvarez E, Gil-Martín E, Fernández-Briera A. α(1,6)Fucosyltransferase expression is an independent prognostic factor for disease-free survival in colorectal carcinoma. *Hum Pathol* 2011; **42**: 1740-1750 [PMID: 21652057 DOI: 10.1016/j.humpath.2011.01.021]
40 **Siegel RL**, Miller KD, Fuchs HE, Jemal A. Cancer statistics, 2022. *CA Cancer J Clin* 2022; **72**: 7-33 [PMID: 35020204 DOI: 10.3322/caac.21708]
41 **Zhao YP**, Xu XY, Fang M, Wang H, You Q, Yi CH, Ji J, Gu X, Zhou PT, Cheng C, Gao CF. Decreased core-fucosylation contributes to malignancy in gastric cancer. *PLoS One* 2014; **9**: e94536 [PMID: 24732908 DOI: 10.1371/journal.pone.0094536]
42 **Lv X**, Song J, Xue K, Li Z, Li M, Zahid D, Cao H, Wang L, Song W, Ma T, Gu J, Li W. Core fucosylation of copper transporter 1 plays a crucial role in cisplatin-resistance of epithelial ovarian cancer by regulating drug uptake. *Mol Carcinog* 2019; **58**: 794-807 [PMID: 30614075 DOI: 10.1002/mc.22971]
43 **Wang X**, Chen J, Li QK, Peskoe SB, Zhang B, Choi C, Platz EA, Zhang H. Overexpression of α (1,6) fucosyltransferase associated with aggressive prostate cancer. *Glycobiology* 2014; **24**: 935-944 [PMID: 24906821 DOI: 10.1093/glycob/cwu051]
44 **Agrawal P**, Fontanals-Cirera B, Sokolova E, Jacob S, Vaiana CA, Argibay D, Davalos V, McDermott M, Nayak S, Darvishian F, Castillo M, Ueberheide B, Osman I, Fenyö D, Mahal LK, Hernando E. A Systems Biology Approach Identifies FUT8 as a Driver of Melanoma Metastasis. *Cancer Cell* 2017; **31**: 804-819.e7 [PMID: 28609658 DOI: 10.1016/j.ccell.2017.05.007]
45 **Honma R**, Kinoshita I, Miyoshi E, Tomaru U, Matsuno Y, Shimizu Y, Takeuchi S, Kobayashi Y, Kaga K, Taniguchi N, Dosaka-Akita H. Expression of fucosyltransferase 8 is associated with an unfavorable clinical outcome in non-small cell lung cancers. *Oncology* 2015; **88**: 298-308 [PMID: 25572677 DOI: 10.1159/000369495]
46 **Tu CF**, Wu MY, Lin YC, Kannagi R, Yang RB. FUT8 promotes breast cancer cell invasiveness by remodeling TGF-β receptor core fucosylation. *Breast Cancer Res* 2017; **19**: 111 [PMID: 28982386 DOI: 10.1186/s13058-017-0904-8]
47 **Miceli MC**, Parnes JR. The roles of CD4 and CD8 in T cell activation. *Semin Immunol* 1991; **3**: 133-141 [PMID: 1909592]
48 **Dimeloe S**, Burgener AV, Grählert J, Hess C. T-cell metabolism governing activation, proliferation and differentiation; a modular view.

Immunology 2017; **150**: 35-44 [PMID: 27479920 DOI: 10.1111/imm.12655]
49 **Yin Y**, Choi SC, Xu Z, Perry DJ, Seay H, Croker BP, Sobel ES, Brusko TM, Morel L. Normalization of CD4+ T cell metabolism reverses lupus. *Sci Transl Med* 2015; **7**: 274ra18 [PMID: 25673763 DOI: 10.1126/scitranslmed.aaa0835]
50 **Fawzy M**, Edrees A, Okasha H, El Ashmaui A, Ragab G. Gastrointestinal manifestations in systemic lupus erythematosus. *Lupus* 2016; **25**: 1456-1462 [PMID: 27055518 DOI: 10.1177/0961203316642308]
51 **Ohmes J**, Comdühr S, Akbarzadeh R, Riemekasten G, Humrich JY. Dysregulation and chronicity of pathogenic T cell responses in the pre-diseased stage of lupus. *Front Immunol* 2022; **13**: 1007078 [PMID: 36389689 DOI: 10.3389/fimmu.2022.1007078]
52 **Mao L**, Hou H, Wu S, Zhou Y, Wang J, Yu J, Wu X, Lu Y, Mao L, Bosco MJ, Wang F, Sun Z. TIGIT signalling pathway negatively regulates CD4(+) T-cell responses in systemic lupus erythematosus. *Immunology* 2017; **151**: 280-290 [PMID: 28108989 DOI: 10.1111/imm.12715]
53 **Sun Y**, Li Z, Liang W, Zhang Y, Song W, Song J, Xue K, Wang M, Sun W, Gu J, Li M, Li W. A novel immunochromatographic strips assay for rapid and simple detection of systemic lupus erythematosus. *Sci Rep* 2020; **10**: 14178 [PMID: 32843681 DOI: 10.1038/s41598-020-71137-0]
54 **McCarthy DP**, Richards MH, Miller SD. Mouse models of multiple sclerosis: experimental autoimmune encephalomyelitis and Theiler's virus-induced demyelinating disease. *Methods Mol Biol* 2012; **900**: 381-401 [PMID: 22933080 DOI: 10.1007/978-1-60761-720-4_19]
55 **Tian XP**, Zhang X. Gastrointestinal involvement in systemic lupus erythematosus: insight into pathogenesis, diagnosis and treatment. *World J Gastroenterol* 2010; **16**: 2971-2977 [PMID: 20572299 DOI: 10.3748/wjg.v16.i24.2971]
56 **Liang W**, Mao S, Sun S, Li M, Li Z, Yu R, Ma T, Gu J, Zhang J, Taniguchi N, Li W. Core Fucosylation of the T Cell Receptor Is Required for T Cell Activation. *Front Immunol* 2018; **9**: 78 [PMID: 29434598 DOI: 10.3389/fimmu.2018.00078]
57 **Reed J**, Wetzel SA. CD4(+) T Cell Differentiation and Activation. *Methods Mol Biol* 2018; **1803**: 335-351 [PMID: 29882148 DOI: 10.1007/978-1-4939-8549-4_20]
58 **Lehrman MA**, Hill RL. The binding of fucose-containing glycoproteins by hepatic lectins. Purification of a fucose-binding lectin from rat liver. *J Biol Chem* 1986; **261**: 7419-7425 [PMID: 3711093]
59 **Chen R**, Seebun D, Ye M, Zou H, Figeys D. Site-specific characterization of cell membrane N-glycosylation with integrated hydrophilic interaction chromatography solid phase extraction and LC-MS/MS. *J Proteomics* 2014; **103**: 194-203 [PMID: 24721674 DOI: 10.1016/j.jprot.2014.03.040]
60 **Tay C**, Kanellakis P, Hosseini H, Cao A, Toh BH, Bobik A, Kyaw T. B Cell and CD4 T Cell Interactions Promote Development of Atherosclerosis. *Front Immunol* 2019; **10**: 3046 [PMID: 31998318 DOI: 10.3389/fimmu.2019.03046]
61 **Li W**, Yu R, Ma B, Yang Y, Jiao X, Liu Y, Cao H, Dong W, Liu L, Ma K, Fukuda T, Liu Q, Ma T, Wang Z, Gu J, Zhang J, Taniguchi N. Core fucosylation of IgG B cell receptor is required for antigen recognition and antibody production. *J Immunol* 2015; **194**: 2596-2606 [PMID: 25694612 DOI: 10.4049/jimmunol.1402678]
62 **Gringhuis SI**, Kaptein TM, Wevers BA, van der Vlist M, Klaver EJ, van Die I, Vriend LE, de Jong MA, Geijtenbeek TB. Fucose-based PAMPs prime dendritic cells for follicular T helper cell polarization *via* DC-SIGN-dependent IL-27 production. *Nat Commun* 2014; **5**: 5074 [PMID: 25278262 DOI: 10.1038/ncomms6074]
63 **Gringhuis SI**, Kaptein TM, Wevers BA, Mesman AW, Geijtenbeek TB. Fucose-specific DC-SIGN signalling directs T helper cell type-2 responses *via* IKKε- and CYLD-dependent Bcl3 activation. *Nat Commun* 2014; **5**: 3898 [PMID: 24867235 DOI: 10.1038/ncomms4898]
64 **Iijima J**, Kobayashi S, Kitazume S, Kizuka Y, Fujinawa R, Korekane H, Shibata T, Saitoh SI, Akashi-Takamura S, Miyake K, Miyoshi E, Taniguchi N. Core fucose is critical for CD14-dependent Toll-like receptor 4 signaling. *Glycobiology* 2017; **27**: 1006-1015 [PMID: 28973141 DOI: 10.1093/glycob/cwx075]
65 **da Silva Correia J**, Ulevitch RJ. MD-2 and TLR4 N-linked glycosylations are important for a functional lipopolysaccharide receptor. *J Biol Chem* 2002; **277**: 1845-1854 [PMID: 11706042 DOI: 10.1074/jbc.M109910200]
66 **Meng J**, Parroche P, Golenbock DT, McKnight CJ. The differential impact of disulfide bonds and N-linked glycosylation on the stability and function of CD14. *J Biol Chem* 2008; **283**: 3376-3384 [PMID: 18057002 DOI: 10.1074/jbc.M707640200]
67 **Nakayama K**, Wakamatsu K, Fujii H, Shinzaki S, Takamatsu S, Kitazume S, Kamada Y, Takehara T, Taniguchi N, Miyoshi E. Core fucose is essential glycosylation for CD14-dependent Toll-like receptor 4 and Toll-like receptor 2 signalling in macrophages. *J Biochem* 2019; **165**: 227-237 [PMID: 30445455 DOI: 10.1093/jb/mvy098]
68 **Takeuchi O**, Hoshino K, Kawai T, Sanjo H, Takada H, Ogawa T, Takeda K, Akira S. Differential roles of TLR2 and TLR4 in recognition of gram-negative and gram-positive bacterial cell wall components. *Immunity* 1999; **11**: 443-451 [PMID: 10549626 DOI: 10.1016/s1074-7613(00)80119-3]
69 **Russell MW**, Moldoveanu Z, Ogra PL, Mestecky J. Mucosal Immunity in COVID-19: A Neglected but Critical Aspect of SARS-CoV-2 Infection. *Front Immunol* 2020; **11**: 611337 [PMID: 33329607 DOI: 10.3389/fimmu.2020.611337]
70 **Zahid D**, Zhang N, Fang H, Gu J, Li M, Li W. Loss of core fucosylation suppressed the humoral immune response in Salmonella typhimurium infected mice. *J Microbiol Immunol Infect* 2021; **54**: 606-615 [PMID: 32146162 DOI: 10.1016/j.jmii.2020.02.006]
71 **Jia S**, Zhang W, Tan X, He W, Wang W. The distribution of SIgA and IgG antibody-secreting cells in the palatine tonsils of Bactrian camels (Camelus bactrianus) of different ages. *Histol Histopathol* 2017; **32**: 511-521 [PMID: 27605252 DOI: 10.14670/HH-11-808]
72 **Holmgren J**, Czerkinsky C. Mucosal immunity and vaccines. *Nat Med* 2005; **11**: S45-S53 [PMID: 15812489 DOI: 10.1038/nm1213]
73 **Hao S**, Fan Q, Bai Y, Fang H, Zhou J, Fukuda T, Gu J, Li M, Li W. Core Fucosylation of Intestinal Epithelial Cells Protects Against Salmonella Typhi Infection *via* Up-Regulating the Biological Antagonism of Intestinal Microbiota. *Front Microbiol* 2020; **11**: 1097 [PMID: 32528455 DOI: 10.3389/fmicb.2020.01097]
74 **Chen CY**, Jan YH, Juan YH, Yang CJ, Huang MS, Yu CJ, Yang PC, Hsiao M, Hsu TL, Wong CH. Fucosyltransferase 8 as a functional regulator of nonsmall cell lung cancer. *Proc Natl Acad Sci U S A* 2013; **110**: 630-635 [PMID: 23267084 DOI: 10.1073/pnas.1220425110]
75 **Clynes RA**, Towers TL, Presta LG, Ravetch JV. Inhibitory Fc receptors modulate in vivo cytotoxicity against tumor targets. *Nat Med* 2000; **6**: 443-446 [PMID: 10742152 DOI: 10.1038/74704]
76 **Cartron G**, Dacheux L, Salles G, Solal-Celigny P, Bardos P, Colombat P, Watier H. Therapeutic activity of humanized anti-CD20 monoclonal antibody and polymorphism in IgG Fc receptor FcgammaRIIIa gene. *Blood* 2002; **99**: 754-758 [PMID: 11806974 DOI: 10.1182/blood.v99.3.754]
77 **Carter P**. Improving the efficacy of antibody-based cancer therapies. *Nat Rev Cancer* 2001; **1**: 118-129 [PMID: 11905803 DOI: 10.1038/35101072]
78 **Kanda Y**, Yamada T, Mori K, Okazaki A, Inoue M, Kitajima-Miyama K, Kuni-Kamochi R, Nakano R, Yano K, Kakita S, Shitara K, Satoh M.

Comparison of biological activity among nonfucosylated therapeutic IgG1 antibodies with three different N-linked Fc oligosaccharides: the high-mannose, hybrid, and complex types. *Glycobiology* 2007; **17**: 104-118 [PMID: 17012310 DOI: 10.1093/glycob/cwl057]

79 **Niwa R**, Sakurada M, Kobayashi Y, Uehara A, Matsushima K, Ueda R, Nakamura K, Shitara K. Enhanced natural killer cell binding and activation by low-fucose IgG1 antibody results in potent antibody-dependent cellular cytotoxicity induction at lower antigen density. *Clin Cancer Res* 2005; **11**: 2327-2336 [PMID: 15788684 DOI: 10.1158/1078-0432.Ccr-04-2263]

80 **Niwa R**, Natsume A, Uehara A, Wakitani M, Iida S, Uchida K, Satoh M, Shitara K. IgG subclass-independent improvement of antibody-dependent cellular cytotoxicity by fucose removal from Asn297-linked oligosaccharides. *J Immunol Methods* 2005; **306**: 151-160 [PMID: 16219319 DOI: 10.1016/j.jim.2005.08.009]

81 **Suzuki E**, Niwa R, Saji S, Muta M, Hirose M, Iida S, Shiotsu Y, Satoh M, Shitara K, Kondo M, Toi M. A nonfucosylated anti-HER2 antibody augments antibody-dependent cellular cytotoxicity in breast cancer patients. *Clin Cancer Res* 2007; **13**: 1875-1882 [PMID: 17363544 DOI: 10.1158/1078-0432.Ccr-06-1335]

82 **Iida S**, Misaka H, Inoue M, Shibata M, Nakano R, Yamane-Ohnuki N, Wakitani M, Yano K, Shitara K, Satoh M. Nonfucosylated therapeutic IgG1 antibody can evade the inhibitory effect of serum immunoglobulin G on antibody-dependent cellular cytotoxicity through its high binding to FcgammaRIIIa. *Clin Cancer Res* 2006; **12**: 2879-2887 [PMID: 16675584 DOI: 10.1158/1078-0432.Ccr-05-2619]

83 **Mori K**, Iida S, Yamane-Ohnuki N, Kanda Y, Kuni-Kamochi R, Nakano R, Imai-Nishiya H, Okazaki A, Shinkawa T, Natsume A, Niwa R, Shitara K, Satoh M. Non-fucosylated therapeutic antibodies: the next generation of therapeutic antibodies. *Cytotechnology* 2007; **55**: 109-114 [PMID: 19003000 DOI: 10.1007/s10616-007-9103-2]

84 **Preithner S**, Elm S, Lippold S, Locher M, Wolf A, da Silva AJ, Baeuerle PA, Prang NS. High concentrations of therapeutic IgG1 antibodies are needed to compensate for inhibition of antibody-dependent cellular cytotoxicity by excess endogenous immunoglobulin G. *Mol Immunol* 2006; **43**: 1183-1193 [PMID: 16102830 DOI: 10.1016/j.molimm.2005.07.010]

85 **Nechansky A**, Schuster M, Jost W, Siegl P, Wiederkum S, Gorr G, Kircheis R. Compensation of endogenous IgG mediated inhibition of antibody-dependent cellular cytotoxicity by glyco-engineering of therapeutic antibodies. *Mol Immunol* 2007; **44**: 1815-1817 [PMID: 17011625 DOI: 10.1016/j.molimm.2006.08.013]

86 **Imai-Nishiya H**, Mori K, Inoue M, Wakitani M, Iida S, Shitara K, Satoh M. Double knockdown of alpha1,6-fucosyltransferase (FUT8) and GDP-mannose 4,6-dehydratase (GMD) in antibody-producing cells: a new strategy for generating fully non-fucosylated therapeutic antibodies with enhanced ADCC. *BMC Biotechnol* 2007; **7**: 84 [PMID: 18047682 DOI: 10.1186/1472-6750-7-84]

87 **Okazaki A**, Shoji-Hosaka E, Nakamura K, Wakitani M, Uchida K, Kakita S, Tsumoto K, Kumagai I, Shitara K. Fucose depletion from human IgG1 oligosaccharide enhances binding enthalpy and association rate between IgG1 and FcgammaRIIIa. *J Mol Biol* 2004; **336**: 1239-1249 [PMID: 15037082 DOI: 10.1016/j.jmb.2004.01.007]

88 **Dai S**, Jia R, Zhang X, Fang Q, Huang L. The PD-1/PD-Ls pathway and autoimmune diseases. *Cell Immunol* 2014; **290**: 72-79 [PMID: 24908630 DOI: 10.1016/j.cellimm.2014.05.006]

89 **Cho H**, Kang H, Lee HH, Kim CW. Programmed Cell Death 1 (PD-1) and Cytotoxic T Lymphocyte-Associated Antigen 4 (CTLA-4) in Viral Hepatitis. *Int J Mol Sci* 2017; **18** [PMID: 28703774 DOI: 10.3390/ijms18071517]

90 **Li CW**, Lim SO, Xia W, Lee HH, Chan LC, Kuo CW, Khoo KH, Chang SS, Cha JH, Kim T, Hsu JL, Wu Y, Hsu JM, Yamaguchi H, Ding Q, Wang Y, Yao J, Lee CC, Wu HJ, Sahin AA, Allison JP, Yu D, Hortobagyi GN, Hung MC. Glycosylation and stabilization of programmed death ligand-1 suppresses T-cell activity. *Nat Commun* 2016; **7**: 12632 [PMID: 27572267 DOI: 10.1038/ncomms12632]

91 **Meng X**, Liu X, Guo X, Jiang S, Chen T, Hu Z, Liu H, Bai Y, Xue M, Hu R, Sun SC, Zhou P, Huang X, Wei L, Yang W, Xu C. FBXO38 mediates PD-1 ubiquitination and regulates anti-tumour immunity of T cells. *Nature* 2018; **564**: 130-135 [PMID: 30487606 DOI: 10.1038/s41586-018-0756-0]

92 **Chamoto K**, Yaguchi T, Tajima M, Honjo T. Insights from a 30-year journey: function, regulation and therapeutic modulation of PD1. *Nat Rev Immunol* 2023 [DOI: 10.1038/s41577-023-00867-9]

93 **Long J**, Lin J, Wang A, Wu L, Zheng Y, Yang X, Wan X, Xu H, Chen S, Zhao H. PD-1/PD-L blockade in gastrointestinal cancers: lessons learned and the road toward precision immunotherapy. *J Hematol Oncol* 2017; **10**: 146 [PMID: 28774337 DOI: 10.1186/s13045-017-0511-2]

94 **Medici D**, Hay ED, Goodenough DA. Cooperation between snail and LEF-1 transcription factors is essential for TGF-beta1-induced epithelial-mesenchymal transition. *Mol Biol Cell* 2006; **17**: 1871-1879 [PMID: 16467384 DOI: 10.1091/mbc.e05-08-0767]

95 **Kim K**, Lu Z, Hay ED. Direct evidence for a role of beta-catenin/LEF-1 signaling pathway in induction of EMT. *Cell Biol Int* 2002; **26**: 463-476 [PMID: 12095232 DOI: 10.1006/cbir.2002.0901]

96 **Lee HS**, Park MH, Yang SJ, Park KC, Kim NS, Kim YS, Kim DI, Yoo HS, Choi EJ, Yeom YI. Novel candidate targets of Wnt/beta-catenin signaling in hepatoma cells. *Life Sci* 2007; **80**: 690-698 [PMID: 17157329 DOI: 10.1016/j.lfs.2006.10.024]

97 **Zhang C**, Wu Q, Huang H, Chen X, Huang T, Li W, Zhang J, Liu Y. Caveolin-1 upregulates Fut8 expression by activating the Wnt/β-catenin pathway to enhance HCC cell proliferative and invasive ability. *Cell Biol Int* 2020; **44**: 2202-2212 [PMID: 32710651 DOI: 10.1002/cbin.11426]

98 **Jia L**, Li J, Li P, Liu D, Shen J, Zhu B, Ma C, Zhao T, Lan R, Dang L, Li W, Sun S. Site-specific glycoproteomic analysis revealing increased core-fucosylation on FOLR1 enhances folate uptake capacity of HCC cells to promote EMT. *Theranostics* 2021; **11**: 6905-6921 [PMID: 34093861 DOI: 10.7150/thno.56882]

99 **Osumi D**, Takahashi M, Miyoshi E, Yokoe S, Lee SH, Noda K, Nakamori S, Gu J, Ikeda Y, Kuroki Y, Sengoku K, Ishikawa M, Taniguchi N. Core fucosylation of E-cadherin enhances cell-cell adhesion in human colon carcinoma WiDr cells. *Cancer Sci* 2009; **100**: 888-895 [PMID: 19302290 DOI: 10.1111/j.1349-7006.2009.01125.x]

100 **Martin J**, Petrillo A, Smyth EC, Shaida N, Khwaja S, Cheow HK, Duckworth A, Heister P, Praseedom R, Jah A, Balakrishnan A, Harper S, Liau S, Kosmoliaptsis V, Huguet E. Colorectal liver metastases: Current management and future perspectives. *World J Clin Oncol* 2020; **11**: 761-808 [PMID: 33200074 DOI: 10.5306/wjco.v11.i10.761]

101 **Lin H**, Wang D, Wu T, Dong C, Shen N, Sun Y, Xie H, Wang N, Shan L. Blocking core fucosylation of TGF-β1 receptors downregulates their functions and attenuates the epithelial-mesenchymal transition of renal tubular cells. *Am J Physiol Renal Physiol* 2011; **300**: F1017-F1025 [PMID: 21228108 DOI: 10.1152/ajprenal.00426.2010]

102 **Venkatachalam MA**, Weinberg JM. New wrinkles in old receptors: core fucosylation is yet another target to inhibit TGF-β signaling. *Kidney Int* 2013; **84**: 11-14 [PMID: 23812359 DOI: 10.1038/ki.2013.95]

103 **Wang X**, Gu J, Ihara H, Miyoshi E, Honke K, Taniguchi N. Core fucosylation regulates epidermal growth factor receptor-mediated intracellular signaling. *J Biol Chem* 2006; **281**: 2572-2577 [PMID: 16316986 DOI: 10.1074/jbc.M510893200]

104 **Wang Y**, Fukuda T, Isaji T, Lu J, Gu W, Lee HH, Ohkubo Y, Kamada Y, Taniguchi N, Miyoshi E, Gu J. Loss of α1,6-fucosyltransferase suppressed liver regeneration: implication of core fucose in the regulation of growth factor receptor-mediated cellular signaling. *Sci Rep* 2015; **5**: 8264 [PMID: 25652335 DOI: 10.1038/srep08264]

105 **Anjum J**, Mitra S, Das R, Alam R, Mojumder A, Emran TB, Islam F, Rauf A, Hossain MJ, Aljohani ASM, Abdulmonem WA, Alsharif KF, Alzahrani KJ, Khan H. A renewed concept on the MAPK signaling pathway in cancers: Polyphenols as a choice of therapeutics. *Pharmacol Res* 2022; **184**: 106398 [PMID: 35988867 DOI: 10.1016/j.phrs.2022.106398]

106 **Matsumoto K**, Yokote H, Arao T, Maegawa M, Tanaka K, Fujita Y, Shimizu C, Hanafusa T, Fujiwara Y, Nishio K. N-Glycan fucosylation of epidermal growth factor receptor modulates receptor activity and sensitivity to epidermal growth factor receptor tyrosine kinase inhibitor. *Cancer Sci* 2008; **99**: 1611-1617 [PMID: 18754874 DOI: 10.1111/j.1349-7006.2008.00847.x]

107 **Knight T**, Irving JA. Ras/Raf/MEK/ERK Pathway Activation in Childhood Acute Lymphoblastic Leukemia and Its Therapeutic Targeting. *Front Oncol* 2014; **4**: 160 [PMID: 25009801 DOI: 10.3389/fonc.2014.00160]

108 **Chen L**, Mayer JA, Krisko TI, Speers CW, Wang T, Hilsenbeck SG, Brown PH. Inhibition of the p38 kinase suppresses the proliferation of human ER-negative breast cancer cells. *Cancer Res* 2009; **69**: 8853-8861 [PMID: 19920204 DOI: 10.1158/0008-5472.CAN-09-1636]

109 **Zhou X**, Liu Y, You J, Zhang H, Zhang X, Ye L. Myosin light-chain kinase contributes to the proliferation and migration of breast cancer cells through cross-talk with activated ERK1/2. *Cancer Lett* 2008; **270**: 312-327 [PMID: 18710790 DOI: 10.1016/j.canlet.2008.05.028]

110 **Carrascal MA**, Silva M, Ramalho JS, Pen C, Martins M, Pascoal C, Amaral C, Serrano I, Oliveira MJ, Sackstein R, Videira PA. Inhibition of fucosylation in human invasive ductal carcinoma reduces E-selectin ligand expression, cell proliferation, and ERK1/2 and p38 MAPK activation. *Mol Oncol* 2018; **12**: 579-593 [PMID: 29215790 DOI: 10.1002/1878-0261.12163]

111 **Liu C**, Liang X, Wang J, Zheng Q, Zhao Y, Khan MN, Liu S, Yan Q. Protein O-fucosyltransferase 1 promotes trophoblast cell proliferation through activation of MAPK and PI3K/Akt signaling pathways. *Biomed Pharmacother* 2017; **88**: 95-101 [PMID: 28103512 DOI: 10.1016/j.biopha.2017.01.026]

112 **Yeung CY**, Lee HC, Chan WT, Jiang CB, Chang SW, Chuang CK. Vertical transmission of hepatitis C virus: Current knowledge and perspectives. *World J Hepatol* 2014; **6**: 643-651 [PMID: 25276280 DOI: 10.4254/wjh.v6.i9.643]

113 **Li S**, Liu XY, Pan Q, Wu J, Liu ZH, Wang Y, Liu M, Zhang XL. Hepatitis C Virus-Induced FUT8 Causes 5-FU Drug Resistance in Human Hepatoma Huh7.5.1 Cells. *Viruses* 2019; **11** [PMID: 31022917 DOI: 10.3390/v11040378]

114 **Cheng L**, Luo S, Jin C, Ma H, Zhou H, Jia L. FUT family mediates the multidrug resistance of human hepatocellular carcinoma *via* the PI3K/Akt signaling pathway. *Cell Death Dis* 2013; **4**: e923 [PMID: 24232099 DOI: 10.1038/cddis.2013.450]

115 **Najafi M**, Farhood B, Mortezaee K. Cancer stem cells (CSCs) in cancer progression and therapy. *J Cell Physiol* 2019; **234**: 8381-8395 [PMID: 30417375 DOI: 10.1002/jcp.27740]

116 **Ma M**, Guo D, Tan Z, Du J, Guan F, Li X. Fucosyltransferase 8 regulation and breast cancer suppression by transcription factor activator protein 2γ. *Cancer Sci* 2021; **112**: 3190-3204 [PMID: 34036684 DOI: 10.1111/cas.14987]

117 **Liang C**, Fukuda T, Isaji T, Duan C, Song W, Wang Y, Gu J. α1,6-Fucosyltransferase contributes to cell migration and proliferation as well as to cancer stemness features in pancreatic carcinoma. *Biochim Biophys Acta Gen Subj* 2021; **1865**: 129870 [PMID: 33571582 DOI: 10.1016/j.bbagen.2021.129870]

118 **Yang HF**, Yu M, Jin HD, Yao JQ, Lu ZL, Yabasin IB, Yan Q, Wen QP. Fentanyl Promotes Breast Cancer Cell Stemness and Epithelial-Mesenchymal Transition by Upregulating α1, 6-Fucosylation *via* Wnt/β-Catenin Signaling Pathway. *Front Physiol* 2017; **8**: 510 [PMID: 28798691 DOI: 10.3389/fphys.2017.00510]

119 **Shen L**, Xia M, Deng X, Ke Q, Zhang C, Peng F, Dong X, Luo Z. A lectin-based glycomic approach identifies FUT8 as a driver of radioresistance in oesophageal squamous cell carcinoma. *Cell Oncol (Dordr)* 2020; **43**: 695-707 [PMID: 32474852 DOI: 10.1007/s13402-020-00517-5]

120 **Huang W**, Luo WJ, Zhu P, Tang J, Yu XL, Cui HY, Wang B, Zhang Y, Jiang JL, Chen ZN. Modulation of CD147-induced matrix metalloproteinase activity: role of CD147 N-glycosylation. *Biochem J* 2013; **449**: 437-448 [PMID: 23005037 DOI: 10.1042/BJ20120343]

121 **Qi Y**, Shan Y, Li S, Huang Y, Guo Y, Huang T, Zhao X, Jia L. LncRNA LEF1-AS1/LEF1/FUT8 Axis Mediates Colorectal Cancer Progression by Regulating α1, 6-Fucosylationvia Wnt/β-Catenin Pathway. *Dig Dis Sci* 2022; **67**: 2182-2194 [PMID: 34021424 DOI: 10.1007/s10620-021-07051-w]

122 **Wang M**, Wang J, Kong X, Chen H, Wang Y, Qin M, Lin Y, Xu J, Hong J, Chen YX, Zou W, Fang JY. MiR-198 represses tumor growth and metastasis in colorectal cancer by targeting fucosyl transferase 8. *Sci Rep* 2014; **4**: 6145 [PMID: 25174450 DOI: 10.1038/srep06145]

123 **Bernardi C**, Soffientini U, Piacente F, Tonetti MG. Effects of microRNAs on fucosyltransferase 8 (FUT8) expression in hepatocarcinoma cells. *PLoS One* 2013; **8**: e76540 [PMID: 24130780 DOI: 10.1371/journal.pone.0076540]

124 **Chen F**, Li Y, Aye L, Wu Y, Dong L, Yang Z, Gao Q, Zhang S. FUT8 is regulated by miR-122-5p and promotes malignancies in intrahepatic cholangiocarcinoma *via* PI3K/AKT signaling. *Cell Oncol (Dordr)* 2023; **46**: 79-91 [PMID: 36348252 DOI: 10.1007/s13402-022-00736-y]

125 **He J**, Xie Q, Xu H, Li J, Li Y. Circular RNAs and cancer. *Cancer Lett* 2017; **396**: 138-144 [PMID: 28342987 DOI: 10.1016/j.canlet.2017.03.027]

126 **Li C**, Xin Z, He L, Ning J, Lin K, Pan J, Rao J, Wang G, Zhu H. cFUT8 promotes liver cancer progression by miR-548c/FUT8 axis. *Signal Transduct Target Ther* 2021; **6**: 30 [PMID: 33500381 DOI: 10.1038/s41392-020-00393-3]

127 **Mollaei H**, Safaralizadeh R, Rostami Z. MicroRNA replacement therapy in cancer. *J Cell Physiol* 2019; **234**: 12369-12384 [PMID: 30605237 DOI: 10.1002/jcp.28058]

128 **Tang Q**, Hann SS. Biological Roles and Mechanisms of Circular RNA in Human Cancers. *Onco Targets Ther* 2020; **13**: 2067-2092 [PMID: 32210574 DOI: 10.2147/OTT.S233672]

129 **Luckheeram RV**, Zhou R, Verma AD, Xia B. CD4$^+$T cells: differentiation and functions. *Clin Dev Immunol* 2012; **2012**: 925135 [PMID: 22474485 DOI: 10.1155/2012/925135]

130 **Jost SA**, Tseng LC, Matthews LA, Vasquez R, Zhang S, Yancey KB, Chong BF. IgG, IgM, and IgA antinuclear antibodies in discoid and systemic lupus erythematosus patients. *ScientificWorldJournal* 2014; **2014**: 171028 [PMID: 24741342 DOI: 10.1155/2014/171028]

131 **Perl A**. Oxidative stress in the pathology and treatment of systemic lupus erythematosus. *Nat Rev Rheumatol* 2013; **9**: 674-686 [PMID: 24100461 DOI: 10.1038/nrrheum.2013.147]

132 **Morel L**. Immunometabolism in systemic lupus erythematosus. *Nat Rev Rheumatol* 2017; **13**: 280-290 [PMID: 28360423 DOI: 10.1038/nrrheum.2017.43]

133 **Osinalde N**, Moss H, Arrizabalaga O, Omaetxebarria MJ, Blagoev B, Zubiaga AM, Fullaondo A, Arizmendi JM, Kratchmarova I. Interleukin-2 signaling pathway analysis by quantitative phosphoproteomics. *J Proteomics* 2011; **75**: 177-191 [PMID: 21722762 DOI:

10.1016/j.jprot.2011.06.007]

134 **Doberstein SK**. Bempegaldesleukin (NKTR-214): a CD-122-biased IL-2 receptor agonist for cancer immunotherapy. *Expert Opin Biol Ther* 2019; **19**: 1223-1228 [PMID: 31652082 DOI: 10.1080/14712598.2019.1685489]

135 **Boyman O**, Kovar M, Rubinstein MP, Surh CD, Sprent J. Selective stimulation of T cell subsets with antibody-cytokine immune complexes. *Science* 2006; **311**: 1924-1927 [PMID: 16484453 DOI: 10.1126/science.1122927]

136 **Miyoshi E**, Moriwaki K, Nakagawa T. Biological function of fucosylation in cancer biology. *J Biochem* 2008; **143**: 725-729 [PMID: 18218651 DOI: 10.1093/jb/mvn011]

137 **Kondo J**, Sakata N, Morishita K, Hayashibara A, Sakon D, Takamatsu S, Asakura N, Suzuki T, Miyoshi E. Transcription factor SP1 regulates haptoglobin fucosylation *via* induction of GDP-fucose transporter 1 in the hepatoma cell line HepG2. *Biochem Biophys Rep* 2022; **32**: 101372 [PMID: 36313594 DOI: 10.1016/j.bbrep.2022.101372]

138 **Rillahan CD**, Antonopoulos A, Lefort CT, Sonon R, Azadi P, Ley K, Dell A, Haslam SM, Paulson JC. Global metabolic inhibitors of sialyl- and fucosyltransferases remodel the glycome. *Nat Chem Biol* 2012; **8**: 661-668 [PMID: 22683610 DOI: 10.1038/nchembio.999]

139 **Okeley NM**, Alley SC, Anderson ME, Boursalian TE, Burke PJ, Emmerton KM, Jeffrey SC, Klussman K, Law CL, Sussman D, Toki BE, Westendorf L, Zeng W, Zhang X, Benjamin DR, Senter PD. Development of orally active inhibitors of protein and cellular fucosylation. *Proc Natl Acad Sci U S A* 2013; **110**: 5404-5409 [PMID: 23493549 DOI: 10.1073/pnas.1222263110]

140 **Zhou Y**, Fukuda T, Hang Q, Hou S, Isaji T, Kameyama A, Gu J. Inhibition of fucosylation by 2-fluorofucose suppresses human liver cancer HepG2 cell proliferation and migration as well as tumor formation. *Sci Rep* 2017; **7**: 11563 [PMID: 28912543 DOI: 10.1038/s41598-017-11911-9]

141 **Toulouie S**, Johanning G, Shi Y. Chimeric antigen receptor T-cell immunotherapy in breast cancer: development and challenges. *J Cancer* 2021; **12**: 1212-1219 [PMID: 33442419 DOI: 10.7150/jca.54095]

142 **Xiao BF**, Zhang JT, Zhu YG, Cui XR, Lu ZM, Yu BT, Wu N. Chimeric Antigen Receptor T-Cell Therapy in Lung Cancer: Potential and Challenges. *Front Immunol* 2021; **12**: 782775 [PMID: 34790207 DOI: 10.3389/fimmu.2021.782775]

World Journal of Gastrointestinal Oncology

Submit a Manuscript: https://www.f6publishing.com

World J Gastrointest Oncol 2023 July 15; 15(7): 1135-1148

DOI: 10.4251/wjgo.v15.i7.1135

ISSN 1948-5204 (online)

REVIEW

Interaction mechanisms between autophagy and ferroptosis: Potential role in colorectal cancer

Xin-Ya Zeng, Xin-Ze Qiu, Jiang-Ni Wu, Sheng-Mei Liang, Jie-An Huang, Shi-Quan Liu

Specialty type: Biochemistry and molecular biology

Provenance and peer review: Unsolicited article; Externally peer reviewed.

Peer-review model: Single blind

Peer-review report's scientific quality classification

Grade A (Excellent): 0
Grade B (Very good): B, B
Grade C (Good): C, C, C
Grade D (Fair): 0
Grade E (Poor): 0

P-Reviewer: Bordonaro M, United States; Chen X, China; Sipos F, Hungary; Tzeng IS, Taiwan

Received: February 3, 2023
Peer-review started: February 3, 2023
First decision: March 14, 2023
Revised: March 28, 2023
Accepted: April 23, 2023
Article in press: April 23, 2023
Published online: July 15, 2023

Xin-Ya Zeng, Xin-Ze Qiu, Sheng-Mei Liang, Jie-An Huang, Shi-Quan Liu, Department of Gastroenterology, The Second Affiliated Hospital of Guangxi Medical University, Nanning 530000, Guangxi Zhuang Autonomous Region, China

Jiang-Ni Wu, Department of Pathology, The Second Affiliated Hospital of Guangxi Medical University, Nanning 530000, Guangxi Zhuang Autonomous Region, China

Corresponding author: Shi-Quan Liu, MD, PhD, Chief Doctor, Professor, Department of Gastroenterology, The Second Affiliated Hospital of Guangxi Medical University, No. 166 Daxuedong Road, Nanning 530000, Guangxi Zhuang Autonomous Region, China.
poempower@163.com

Abstract

Colorectal cancer (CRC) is a common malignancy that has the second highest incidence and mortality rate. Although there are many personalized treatment options for CRC, the therapeutic effects are ultimately limited by drug resistance. Studies have aimed to block the initiation and progression of CRC by inducing cell death to overcome this obstacle. Substantial evidence has indicated that both autophagy and ferroptosis play important regulatory roles in CRC. Autophagy, a lysosome-dependent process by which cellular proteins and organelles are degraded, is the basic mechanism for maintaining cell homeostasis. The duality and complexity of autophagy in cancer therapy is a hot topic of discussion. Ferroptosis, a regulated cell death pathway, is associated with iron accumulation-induced lipid peroxidation. The activation of ferroptosis can suppress CRC proliferation, invasion and drug resistance. Furthermore, recent studies have suggested an interaction between autophagy and ferroptosis. Autophagy can selectively degrade certain cellular contents to provide raw materials for ferroptosis, ultimately achieving antitumor and anti-drug resistance. Therefore, exploring the interaction between autophagy and ferroptosis could reveal novel ideas for the treatment of CRC. In this review, we describe the mechanisms of autophagy and ferroptosis, focusing on their roles in CRC and the crosstalk between them.

Key Words: Ferroptosis; Autophagy; Cell death; Colorectal cancer; Iron; Lipid peroxidation

Core Tip: Ferroptosis is a mode of cell death centered on iron accumulation and lipid peroxidation that plays a crucial role in colorectal cancer (CRC). Recently, an increasing number of studies have found that autophagy and ferroptosis have a cross-talk relationship in CRC. Enhancing the antitumor effect through autophagy-dependent ferroptosis will become a hot topic in medical biology. This review describes the mechanisms of autophagy and ferroptosis and their interactions in CRC with a goal of providing new strategies for the treatment of CRC.

Citation: Zeng XY, Qiu XZ, Wu JN, Liang SM, Huang JA, Liu SQ. Interaction mechanisms between autophagy and ferroptosis: Potential role in colorectal cancer. *World J Gastrointest Oncol* 2023; 15(7): 1135-1148
URL: https://www.wjgnet.com/1948-5204/full/v15/i7/1135.htm
DOI: https://dx.doi.org/10.4251/wjgo.v15.i7.1135

INTRODUCTION

Colorectal cancer (CRC) is the second most common cause of cancer-related death in both men and women. According to global cancer statistics, 52580 people in the United States will die from CRC in 2022[1]. At present, surgery is still the basis of CRC radical therapy. For unresectable metastatic CRC, systemic therapy, including cytotoxic chemotherapy, biologic therapy, immunotherapy, and their combinations, is the mainstay[2]. However, drug resistance in CRC significantly reduces the effectiveness of systemic treatment. Recently, an increasing number of studies have investigated methods to hinder the occurrence and development of CRC by targeted induction of different modes of cell death, such as apoptosis, necroptosis, pyroptosis, and ferroptosis[3].

Autophagy is a lysosome-dependent process for the degradation of proteins and organelles that involves the interaction of multiple protein complexes encoded by highly conserved autophagy-related (ATG) genes. Autophagy plays a central role in the maintenance of cellular homeostasis and is closely associated with human health and various diseases[4]. Current studies have shown that autophagy has a dual role in cancer, promotion or inhibition depending on the type of tumor cells, genetic background, stage of tumor progression and tumor microenvironment[5]. Nevertheless, the complex regulatory mechanisms still need further exploration. Thus, targeted autophagy has great potential in cancer therapy.

Ferroptosis is a mode of regulated cell death (RCD) centered on iron accumulation and lipid peroxidation. Originally in 2012, Dixon *et al*[6] discovered that erastin-induced death in RAS-mutant cancer cells could be prevented by iron chelators and antioxidants, and this iron-dependent mode of cell death was named ferroptosis. Unlike autophagy and other RCDs, such as necroptosis, the process of ferroptosis is lipid peroxidation-mediated plasma membrane damage catalyzed by iron accumulation. Morphologically, it is represented by obvious shrinkage of the mitochondria with increased membrane density, fewer or no mitochondrial cristae, and outer mitochondrial membrane rupture[7]. Because of its unique pathophysiological features, ferroptosis plays an important regulatory role in many diseases[8]. With the in-depth exploration of ferroptosis, relevant studies have indicated significant crosstalk between autophagy and ferroptosis [9-11]. The discovery of autophagy-dependent ferroptosis opens up new insights into cell death and holds great promise in the treatment of disease.

In this review, we summarized the mechanisms of autophagy and ferroptosis, as well as their roles in CRC. Next, we focused on the interaction between autophagy and ferroptosis in the context of CRC, aiming to provide new targets for clinical treatment.

AUTOPHAGY AND CRC

Mechanisms of autophagy

Depending on how cargo is delivered to lysosomes, autophagy can be classified as the following three types: Macroautophagy, microautophagy, and chaperone-mediated autophagy (CMA). Macroautophagy transports a bulk of cytoplasm or specific cargoes to lysosomes for degradation by forming autophagosomes with a double-membrane structure[12]. Microautophagy sequesters cell cytosolic components for lysosomal degradation through lysosomal membrane invagination[13,14]. CMA occurs only in mammalian cells and involves the crucial steps of chaperone-mediated identification and targeting of specific proteins to lysosomes[15]. Among the three different forms of autophagy, macroautophagy is the major regulatory mechanism that responds to environmental and physiological cues, so it is commonly referred to as 'autophagy'[16].

Autophagy is a dynamic process regulated by ATG proteins and can be divided into the following five distinct stages: Initiation, nucleation, elongation of the autophagosome membrane and autophagosome maturation, fusion of autophagosomes with lysosomes, and degradation of the vesicular contents[17]. The Unc-51-like kinase-1 (ULK1) complex, which includes the ULK1/FAK family–interacting protein of 200 kD (FIP200)/ATG13, is responsible for integrating nutrient and energy signals and controls the autophagy switch[18,19]. Upon receiving a starvation signal, the ULK1 complex becomes activated and phosphorylates beclin1 (BECN1) at Ser 14, progressing to the second stage of autophagy[20]. The class III phosphatidylinositol 3-kinase (PtdIns3K) complex is composed of VPS34 (phosphatidylinositol 3-kinase), VPS15 (the

adaptor of VPS34), BECN1 and ATG14 to generate phosphatidylinositol 3-phosphate (PI3P), which facilitates the nucleation of autophagosomal membranes[20,21]. Following nucleation, elongation of the autophagosomal membrane involves two ubiquitin-like (Ubl) conjugation systems: ATG12-ATG5-ATG16L and LC3-phosphatidylethanolamine (PE) [22]. The C-terminus of microtubule-associated protein one light chain 3 (LC3), a mammalian ortholog of yeast Atg8, is cleaved by ATG4 to form LC3-I[23,24]. LC3-I is conjugated to PE to generate LC3-II in the presence of ATG3, ATG7, and the ATG12-ATG5-ATG16L complex[24-26]. The autophagosomal membrane is continuously elongated, eventually forming an autophagosome with closed bilayer membrane structures. Subsequently, mature autophagosomes fuse with lysosomes to form autolysosomes, which decompose the contents of vesicles.

The role of autophagy in CRC

Whether autophagy is enhanced or inhibited is a topic of discussion in cancer treatment. The mechanisms of autophagy in cancer are complex and diverse, involving numerous genes, proteins, and pathways. On the one hand, autophagy prevents cancer by removing intracellular damaged organelles or toxic substances, which helps maintain the integrity of cells and genes[27,28]. On the other hand, autophagy can provide energy and rich nutrients for tumor cells to promote their proliferation and progression[28,29]. In this way, the impact of autophagy in different stages of CRC and the mechanisms of tumor initiation and progression vary[30]. Enhancing or inhibiting autophagy may result in different effects at different stages of CRC. We now briefly introduce the roles of autophagy and several key autophagy regulatory proteins in CRC (Table 1).

The mammalian target of rapamycin (mTOR) is a serine/threonine kinase that primarily regulates cell growth and proliferation and plays an anabolic role[31]. mTOR is recognized as the upstream negative regulator of the autophagy initiation stage. Under nutrient-rich conditions, high mTOR activity prevents ULK1 activation by phosphorylating ULK1 Ser 757, thereby inhibiting autophagy[32]. As early as 2012, aspirin was found to induce autophagy by reducing mTOR signaling in CRC cells through inhibition of the mTOR effector S6K1[33]. Moreover, oxiconazole (OXI) can downregulate the expression of the peroxiredoxin-2 (PRDX2) protein, extinguish mTOR, and initiate autophagy[34]. Moreover, OXI can block the fusion of autophagosomes with lysosomes, resulting in the extreme accumulation of autophagosomes and subsequent inhibition of CRC cell growth[34]. In addition, there are numerous compounds that target the mTOR pathway to regulate autophagy in CRC, all with promising antitumor effects[35,36]. Thus, mTOR may serve as an effective target for the treatment of CRC.

BECN1 is a core protein in autophagy nucleation. In one study, BECN1 expression was higher in CRC tissues than in normal colorectal tissues[37]. Patients with lower BECN1 expression had longer overall survival than those with high BECN1 expression[37]. ABHD5, an activator of cellular lipolysis, binds to BECN1, preventing its cleavage and consequently increasing autophagic flux, thus suppressing CRC tumorigenesis[38]. These pieces of evidence support the idea that BECN1 can inhibit the occurrence of CRC. However, more recent studies tend to focus on the tumor-promoting effect and chemical resistance of BECN1 in CRC[39,40]. For example, sex-determining region Y-box2 (SOX2) transcriptionally induces BECN1 expression, thus activating autophagy to increase CRC chemoresistance[41]. In another study, firre intergenic repeating RNA element (FIRRE) combines with the polypyridine binding protein to form an RNA protein complex, which interacts with the 3' end of BECN1 mRNA to enhance autophagy activity and promote the development of CRC[42]. Studies addressing the relationship between BECN1 and CRC have not yet yielded a broadly uniform result, possibly due to the different pathways of BECN1-mediated autophagy that are involved in different stages of CRC; this complexity could be a challenge *vs* an opportunity in CRC therapy.

Sequestosome 1 (SQSTM1/p62) is both a cargo receptor for autophagy and a substrate for selective autophagy. P62 has been identified as having multiple domains, including the Phox1 and Bem1p (PB1) domain, zinc finger (ZZ), tumor necrosis factor receptor-associated factor 6 (TRAF6) binding domain, LC3-interacting region (LIR), KEAP1-interacting region (KIR) and ubiquitin-associated (UBA) domain[43]. While p62 attaches to the autophagosome by binding with LC3 *via* the LIR, its other domains bind the corresponding proteins, and eventually, they are degraded together in the autolysosome[44,45]. Therefore, the accumulation of p62 represents a decrease in autophagic flux. One group has shown that the expression of p62 is associated with the prognosis of CRC[46,47]. Increased autophagy leads to decreased p62 expression, which enables GATA4 to evade autophagic degradation, enhance NF-κB function, and drive the antioxidant reaction to support CRC survival[48]. Toll-like receptor (TLR) signaling acts as an immunomodulator that regulates inflammatory responses and plays a critical role in colitis-associated CRC[49]. TLR4 mediates the formation of the TRAF6-BECN1 complex, which activates autophagy, facilitating the migration and invasion of cancer cells[50]. P62 negatively regulates TLR4-induced autophagy activation and inhibits cancer cell progression[50]; thus, p62 may become a therapeutic target for CRC.

FERROPTOSIS AND CRC

Mechanisms of ferroptosis

Ferroptosis is a form of cell death caused by iron-dependent lipid peroxidation. In general, the regulatory mechanism of ferroptosis can be divided into three main pathways: iron metabolism, lipid metabolism, and the antioxidant system. The three pathways are inseparable, and an imbalance in any one of the pathways drives ferroptosis. The mechanisms of ferroptosis and its effect on CRC are summarized in Figure 1 and Table 2.

Iron metabolism: Iron is an essential trace element in physiological metabolism, and an imbalance in iron homeostasis might lead to many pathological processes[51]. Iron mainly exists in the form of ferric ions (Fe^{3+}) outside the cell, which are transported by transferrin (Tf). Iron-laden Tf binds to the transferrin receptor (TfR1) on the cell membrane to

Table 1 The role of autophagy in colorectal cancer

Intervention	Target	Effects and mechanism	Ref.
Aspirin	mTOR↓, AMPK↑	Inhibits mTOR signal transduction and activates AMPK to induce autophagy of CRC	[33]
TBK1	mTORC1↓	TBK1 initiates mTORC1 inhibition and induces autophagy to promote CRC progression	[139]
ABHD5	BECN1↑	ABHD5 prevents CASP3 from cleaving BECN1 and enhances autophagy flux to inhibit CRC	[38]
SOX_2	BECN1↑	SOX2-β-catenin/Beclin1/autophagy signaling axis promotes chemoresistance of CRC	[41]
FIRRE	Stabilize BECN1	Stabilizes BECN1 and promotes autophagy in a PTBP1 mediated manner to stimulate the development of CRC	[42]
IL-6	BECN1↑	IL-6/BECN1 pathway activates autophagy and promotes chemotherapy resistance of CRC	[39]
Pelareorep	BECN1↑	Upregulates BECN1 expression and induces autophagy to enhance CRC proliferation	[140]
Fusobacterium nucleatum	BECN1↑, CARD3↑	Upregulates CARD3 expression and activates autophagy signal to promote CRC metastasis	[141]
DCZ5248	p62↑	Induces lysosomal acidification and weakens lysosomal cathepsin activity to inhibit autophagy	[142]
Claudin 1	p62↓	Reduces the level of p62 and stimulates autophagy to promote CRC progression	[143]
DBTTS	p62↑	Induces accumulation of p62 protein and inhibits autophagy to induce CRC cell death	[47]

mTOR: The mammalian target of rapamycin; AMPK: Adenosine monophosphate-activated protein kinase; TBK1: TANK-binding kinase 1; mTORC1: mTOR complex 1; ABHD5: Abhydrolase domain containing 5; BECN1: Beclin1; CASP3: Caspase 3; SOX2: Sex-determining region Y-box2; FIRRE: Firre intergenic repeating RNA element; PTBP1: Polypyrimidine tract-binding protein; CARD3: Caspase activation and recruitment domain 3; DCZ5248: A heat shock protein 90 inhibitor; p62: Sequestosome 1; DBTTS: Diallyl tetrasulfide and its derivative, dibenzyl tetrasulfide; CRC: Colorectal cancer.

transport iron into the cell[52]. Intracellular Fe^{3+} is reduced to ferrous ions (Fe^{2+}) by six-transmembrane epithelial antigen of prostate 3 (STEAP3), forming the labile iron pool (LIP), which is involved in various metabolic reactions[53]. In ferroptosis, the role of iron can be summarized into two crucial types as follows: (1) Iron that catalyzes the nonenzymatic lipid autoxidation chain *via* the Fenton reaction; and (2) iron acting as an enzyme cofactor in enzymatic reactions of lipid peroxidation (see Figure 1). Fe^{2+} in LIP reacts with hydrogen peroxide (H_2O_2) to generate hydroxyl radicals (HO•), Fe^{3+}, and hydroxide ions, in a process known as the Fenton reaction[54]. HO• is a highly oxidative species that reacts with phospholipids to generate the phospholipid radical (PL•), initiating a lipid autoxidation chain reaction[55,56]. Ferrostatin-1 (fer-1), a ferroptosis inhibitor, can form a complex with Fe^{2+} to reduce LIP and scavenge alkoxy radicals produced by the lipid autoxidation chain, thereby inhibiting lipid peroxidation[57].

Lipid peroxidation: In addition to the iron-dependent Fenton reaction, another pathway of lipid peroxide production is the enzymatic reaction dominated by lipoxygenases (LOXs)[55]. Polyunsaturated fatty acids (PUFAs) are highly prone to peroxidation because of their bis-allylic carbons, and PUFAs play a central role in ferroptosis[58,59]. Polyunsaturated-fatty-acid-containing phospholipids (PUFA-PLs) are oxidized to phospholipid hydroperoxides (PLOOH) under the catalysis of LOXs[60]. The constant accumulation of lipid peroxides can destabilize membranes (membrane thinning and increased curvature), leading to pore formation, micellization, and ultimately cell death[61]. Furthermore, oxidative lipidomic analysis revealed that after cells were treated with ferroptosis inducers, the major oxidized phospholipid was PE[62]. Intracellular free PUFAs, especially arachidonic acid (AA) and adrenic acid (AdA), can be esterified to PE under the action of acyl-CoA synthetase long-chain family member 4 (ACSL4) and lysophosphatidylcholine acyltransferase 3 (LPCAT3), providing fuel for ferroptosis[58,63]. First, ACSL4 catalyzes the combination of coenzyme A (CoA) and PUFA to form a PUFA-CoA intermediate[64]. Next, LPCAT3 incorporates PUFA-CoA into membrane phospholipids[65]. The ACSL4 inhibitor rosiglitazone or LPCAT3 inhibitors can prevent ferroptosis[66,67]. Thus, ACSL4 and LPCAT3 are also important parts of the enzymatic reaction in ferroptosis.

Antioxidant defense systems: After the discovery of ferroptosis, researchers found the following common mediator for 12 ferroptosis-inducing small molecule compounds: glutathione peroxidase 4 (GPX4)[68]. GPX4 can reduce intracellular PLOOH to harmless phosphatidyl alcohol (PLOH), preventing the accumulation of lipid peroxides. This reaction requires the consumption of two molecules of glutathione (GSH) each time[69]. GSH, an important reducing substance in the body, is composed of three amino acids (glutamate, cysteine and glycine)[70]. Upon cellular oxidative stress, system Xc−, a cystine-glutamate antiporter, transports cystine into cells to provide raw materials for GSH synthesis[71]. At present, system Xc−-GSH-GPX4 is recognized as the most critical pathway by which the body resists ferroptosis. Ferroptosis inducers such as erastin inhibit system Xc− to prevent cystine uptake, resulting in the inability to synthesize GSH. GSH

Table 2 The role of ferroptosis in colorectal cancer

Intervention	Target	Effects and mechanism	Ref.
SRSF9	GPX4↓	Inhibition of SRSF9 increases erastin-induced iron death by downregulation of GPX4 level	[74]
IMCA	SLC7A11↓	IMCA induces SLC7A11 mediated ferroptosis through AMPK/mTOR pathway	[77]
TalaA	ROS↑, SLC7A11↓	TalaA induces ferroptosis to kill CRC cells	[144]
Lipocalin 2	GPX4↑, system Xc−↑	Overexpression of Lipocalin 2 inhibits ferroptosis and promotes CRC progression	[75]
TIGAR	GSH↓, ROS↑	TIGAR induces ferroptosis resistance in CRC by ROS/AMPK/SCD1 signaling pathway	[145]
HIF-2α	Iron↑	HIF-2α activation potentiates oxidative cell death in CRCs by increasing cellular iron	[79]
TP53	Lipid peroxidation, ACSL4↑	Restricts ferroptosis by blocking DPP4 activity in a transcription independent manner TP53	[91]
Tagitinin C	NRF2/HO-1↑, lipid peroxidation	Tagitin C activates NRF2/HO-1 pathway to induce ferroptosis	[82]
Cetuximab	NRF2↓, ROS↑	Cetuximab inhibits Nrf2/HO-1 pathway to promote ferroptosis in CRC	[85]
Beta-elemene	GSH↓, GPX4↓	Combined treatment with beta-elemene and cetuximab induces ferroptosis in CRC	[96]
Vitamin C	Iron↑, ROS↑	Vitamin C limits CRC resistance to EGFR-targeted therapies	[97]
FeOOH NSs	H_2S↓	FeOOH NSs eliminate endogenous H_2S to induce ferroptosis	[99]

SRSF9: Serine and arginine rich splicing factor 9; GPX4: Glutathione peroxidase 4; IMCA: The benzopyran derivative 2-imino-6-methoxy-2H-chromene-3-carbothioamide; SLC7A11: Solute carrier family 7 member 11; TalaA: Talaroconvolutin A; ROS: Reactive oxygen species; TIGAR: TP53-induced glycolysis and apoptosis regulator; GSH: Glutathione; SCD1: Stearoyl-coenzyme A desaturase-1; HIF-2α: Hypoxia-inducible factor 2α; TP53: Tumor suppressor p53; ACSL4: Acyl-CoA synthetase long-chain family member 4; NRF2: Nuclear factor erythroid 2-related factor 2; HO-1: Haem oxygenase 1; DPP4: Dipeptidyl-peptidase-4; FeOOH NSs: Iron oxide-hydroxide nanospindles; CRC: Colorectal cancer.

depletion inactivates the GPX4 enzyme, eventually triggering ferroptosis[56,68]. Another inducer, RSL3, binds directly to GPX4 to inactivate it[68]. Recently, new research has identified a GSH-independent pathway to inhibit ferroptosis. Ferroptosis suppressor protein 1 (FSP1) expression positively correlates with ferroptosis resistance[72]. Its main mode of action is that the reduced form of ubiquinone (also known as CoQ10) consumes lipid peroxyl radicals, while FSP1 uses NAD(P)H to catalyze the regeneration of ubiquinone[73].

The role of ferroptosis in CRC

Targeting the three pathways of ferroptosis described above can effectively impact CRC. Currently, there are more studies targeting system Xc−-GSH-GPX4 (versus the other two pathways) to regulate ferroptosis in CRC. Serine- and arginine-rich splicing factor 9 (SFRS9) is considered to be a carcinogen of cervical and bladder cancer. However, one group revealed that the expression of SFRS9 mRNA and protein was significantly higher in CRC tissues than in adjacent tissues. SFRS9 can bind to GPX4 mRNA and upregulate the expression of GPX4. Knockdown of SFRS9 inhibits CRC progression by triggering GPX4 reduction-mediated ferroptosis[74]. Lipocalin 2 has also been reported to inhibit ferroptosis by stimulating the expression of GPX4 and system Xc−[75]. Moreover, researchers isolated and purified petunidin 3-O-[rhamnopyranosyl-(trans-p-coumaroyl)]-5-O-(β-D-glucopyranoside) (Pt3R5G) from Lycium ruthenicum Murray, which inhibits RKO cell proliferation by downregulating solute carrier family 7 member 11 (SLC7A11), a subunit of system Xc−, which reduces ferroptosis[76]. In HCT116 cells, the benzopyran derivative 2-imino-6-methoxy-2H-chromene-3-carbothioamide (IMCA) downregulated SLC7A11 expression and decreased the content of cysteine and glutathione, leading to ROS accumulation and ferroptosis[77]. Therefore, inducing ferroptosis by inhibiting the system Xc−-GSH-GPX4 pathway may be an effective way to treat CRC. In addition, alterations in intracellular iron levels affect the growth of CRC cells. HIF-2α is a critical transcriptional regulator of cellular iron levels[78]. Activation of HIF-2α can lead to an increase in cellular iron and ROS levels; when this process is coupled with lipid-ROS induction by ferroptosis inducers, CRC cell death occurs[79].

In addition to the canonical system Xc−-GSH-GPX4 pathway, the nuclear factor erythroid 2-related factor 2/heme oxygenase 1 (NRF2/HO-1) axis also plays a major role in ferroptosis. NRF2 is the master transcription factor responsible for endogenous antioxidative stress, and many of its downstream target genes are also involved in the regulation of iron metabolism, particularly HO-1[80]. HO-1 catalyzes the cleavage of heme to produce Fe^{2+}, which increases the LIP and thus promotes ferroptosis[80,81]. For example, the natural product tagitinin C (TC), a novel inducer of ferroptosis, can

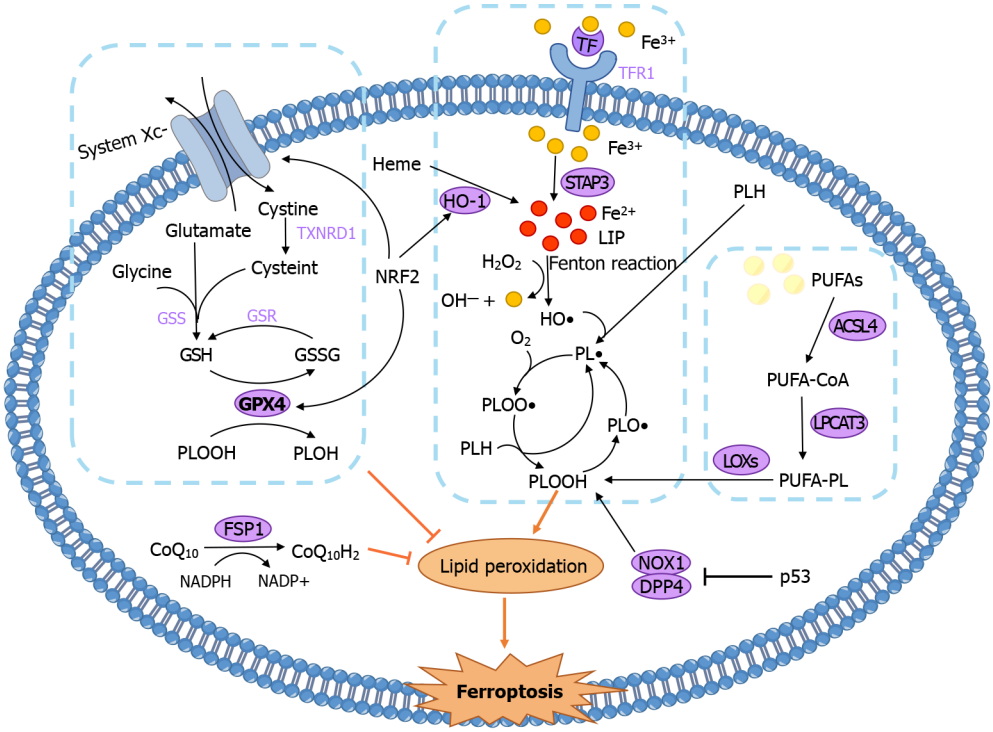

DOI: 10.4251/wjgo.v15.i7.1135 **Copyright** ©The Author(s) 2023.

Figure 1 Mechanisms of ferroptosis (created by Figdraw). TXNRD1: Thioredoxin reductase 1; GSS: Glutathione synthetase; GSH: Glutathione; GSSG: Oxidized glutathione; GSR: Glutathione-disulfide reductase; GPX4: Glutathione peroxidase 4; PLOOH: Phospholipid hydroperoxides; PLOH: Phosphatidyl alcohol; Fe^{3+}: Ferric ion; Fe^{2+}: Ferrous ion; TF: Transferrin; TfR1: Transferrin receptor 1; STEAP3: Six-transmembrane epithelial antigen of prostate 3; LIP: labile iron pool; H_2O_2: Hydrogen peroxide; HO•: Hydroxyl radicals; PL•: Phospholipid radical; PLH: Phospholipid; PLO•: Phospholipid alkoxyl radical; PLOO•: Phospholipid peroxyl radical; PUFAs: Polyunsaturated fatty acids; PUFA-PL: Polyunsaturated-fatty-acid-containing phospholipid; ACSL4: Acyl-CoA synthetase long-chain family member 4; LPCAT3: Lysophosphatidylcholine acyltransferase 3; LOXs: Lipoxygenases; NRF2: Nuclear factor erythroid 2-related factor 2; HO-1: Haem oxygenase 1; FSP1: Ferroptosis suppressor protein 1; CoQ_{10}: Ubiquinone; $CoQ_{10}H_2$: The reduced form of ubiquinone; p53: Tumor protein p53; DPP4: Dipeptidyl-peptidase-4; NOX1: A member of the NADPH oxidase protein family.

inhibit the growth of erastin-insensitive HCT116 cell lines[82]. Mechanistically, tagitinin C first induces oxidative stress, which activates the NRF2/HO-1 pathway and leads to the accumulation of iron, thus driving ferroptosis. Additionally, NRF2 is involved in the regulation of lipid metabolism. Another transcriptional target of NRF2 is GPX4, which allows NRF2 to exert anti-ferroptosis effects[83,84]. One group reported that cetuximab enhanced RSL3-induced lipid ROS accumulation by inhibiting the expression of NRF2 and HO-1 and ultimately promoted ferroptosis in KRAS-mutant CRC cells[85]. There is also research showing that lysionotin (Lys, a flavonoid) promotes the degradation of Nrf2, which leads to decreased expression of GPX4 and system Xc− and subsequently promotes ferroptosis[86]. Given the two different results of the above studies, further evidence is needed to clarify the relationship between NRF2, ferroptosis, and CRC. The balance between the driving effect and the suppressive effect is the key to treatment.

P53 is one of the most widely studied tumor suppressor genes, and it is mutated in almost all human cancers[87]. P53 is involved in a wide range of regulatory processes, including DNA repair, senescence, apoptosis, cell metabolism, ROS production, and ferroptosis[88]. P53 has a dual role in the regulation of ferroptosis[89]. The most classical pathway that promotes iron-mediated death involves p53-mediated repression of the transcription of the SLC7A11 gene, which decreases the expression of SLC7A11, affects the generation of GSH, and induces ferroptosis[90]. However, p53 has an antiferroptotic effect in CRC cells. Mechanistically, p53 binds with dipeptidyl peptidase 4 (DPP4) to block the formation of the DPP4-NOXI complex, leading to a decrease in DPP4-dependent lipid peroxidation, which suppresses ferroptosis [91]. In addition, TP53 target genes, such as cytochrome c oxidase 2 (SCO2), glutaminase 2 (GLS2), and spermidine/spermine N1 acetyltransferase 1 (SAT1), are also involved in the regulation of ferroptosis, but they have not been thoroughly studied in CRC[92,93].

Antitumor therapy based on ferroptosis in CRC

Cisplatin is one of the most widely used anticancer drugs in the clinic, and its most prominent mechanism of action is DNA damage and ultimately apoptosis. However, the chemotherapeutic efficacy of cisplatin has been greatly limited, as the attenuation of DNA damage-mediated apoptotic signaling leads to drug resistance[94]. However, recently, it was found that cisplatin could promote ferroptosis *via* GSH depletion and GPX inactivation in CRC and had a synergistic effect with erastin[95]. In addition, β-elemene, a compound isolated from the Chinese herb Curcumae Rhizoma, combined with cetuximab can induce ferroptosis in KRAS-mutant CRC cells by increasing cellular iron accumulation and lipid peroxidation, which inhibits CRC growth and metastasis[96]. Another study showed that combinatorial treatment with pharmacological doses of vitamin C and cetuximab can trigger ferroptosis, which ultimately prevents the emergence of

acquired resistance to anti-EGFR targeted therapy[97]. In addition to the drugs mentioned above, some novel compounds that inhibit CRC by inducing ferroptosis have also emerged with the rapid development of nanotechnology. For example, zinc oxide-coated virus-like silica nanoparticles (VZnO) can induce ferroptosis by scavenging H_2S and depleting GSH to inhibit CRC growth[98]. Additionally, iron oxide hydroxide nanospindles (FeOOH NSS) had similar effects and hold promise as therapeutic agents for CRC[99]. In summary, ferroptosis regulation has great potential for addressing the current problem of anticancer drug resistance and may provide a new strategy for the treatment of CRC.

THE INTERACTION BETWEEN AUTOPHAGY AND FERROPTOSIS

Autophagy and ferroptosis are two mechanistically distinct forms of cell death. Recent studies have revealed that autophagy inhibitors can prevent erastin-induced ferroptosis in cells and noted that ferroptosis is a form of autophagic cell death[9]. Although the interaction between autophagy and ferroptosis is not yet clear, several studies have noted the role of selective autophagy or certain autophagy factors in ferroptosis. For example, ferritinophagy, lipophagy, clockophagy, CMA and so on promote ferroptosis by inducing iron accumulation or lipid peroxidation[10,11,100]. Here, we summarize selective autophagy and possible regulatory pathways driving ferroptosis in the context of CRC (Figure 2).

Nuclear receptor coactivator 4-mediated ferritinophagy

Under normal physiological conditions, the LIP in cells maintains a dynamic balance, and excess Fe^{2+} is stored by ferritin [53]. Ferritin, composed of ferritin heavy chain 1 (FTH1) and ferritin light chain (FTL), protects against harmful oxidative stress under the condition of free iron overload. When cells are iron deficient, iron is released through an autophagy-related mechanism, known as "ferritinophagy"[101]. Nuclear receptor coactivator 4 (NCOA4), as a selective cargo receptor for ferritinophagy, transports ferritin for lysosomal degradation by binding to FTH1[102,103]. Ferritinophagy enhances cellular susceptibility to ferroptosis by controlling the size of the LIP[104,105]. New research has identified a novel ferroptosis inhibitor, 9a, that acts by disrupting the NCOA4-FTH1 interaction to reduce the amount of intracellular Fe^{2+}[106].

Immunohistochemistry of specimens from patients with colon adenocarcinoma showed that the expression of the NCOA4 protein in tumor tissues was lower than that in peritumoral neighboring tissues. Moreover, the NCOA4 expression level was highly correlated with overall survival, and patients with low protein expression had a worse prognosis[107]. One study showed that in CRC cells, inhibition of the GTP cyclohydrolase-1/tetrahydrobiopterin (GCH1/BH4) pathway resulted in increased levels of NCOA4 protein, decreased levels of FTH1, and the accumulation of free iron. This phenomenon can be reversed with the use of autophagy inhibitors. Altogether, inhibition of the GCH1/BH4 pathway promoted erastin-induced ferroptosis by activating ferritinophagy[108]. In contrast, another study showed that the knockdown of NCOA4 disrupted ferritinophagy and had no significant effect on erastin-induced ferroptosis in HCT116 cells[109]. We should consider whether there is another mechanism by which erastin-induced ferroptosis in CRC cells copes with iron reduction caused by decreased ferritinophagy. Therefore, we need more evidence to validate the role of ferritinophagy in CRC. Studies on ferritinophagy, which involves two major mechanisms, autophagy and ferroptosis, will provide new insights into the treatment of CRC.

BECN1-mediated system Xc− inhibition

BECN1 is a key factor in autophagy initiation, and its role in CRC is complex, as it can promote or inhibit autophagy. Thus far, in a variety of cancers, such as hepatocellular carcinoma, lung cancer, head and neck cancer, and others, there is substantial evidence that BECN1 regulates autophagy-dependent ferroptosis[110,111]. In several studies, BECN1 merely plays the classical role of activating autophagy, promoting the degradation of autophagic ferritin, which in turn leads to ferroptosis. For example, ELAV-like RNA binding protein 1 can bind to the 3'-untranslated region of BECN1, allow intracellular iron accumulation, and eventually lead to ferroptosis[112]. However, one study found that in CRC, BECN1 plays a direct role in regulating ferroptosis[113]. The transporter system Xc− in the anti-ferroptosis system is another agonist of this pathway. System Xc− consists of the following two core components: SLC7A11 and solute carrier family 3 member 2 (SLC3A2)[114]. BECN1 can block the activity of system Xc− by directly binding to SLC7A11, thereby promoting ferroptosis[113]. Adenosine monophosphate-activated protein kinase (AMPK) is upstream of this pathway, and its phosphorylation of BECN1 at Ser90/93/96 could promote the formation of a complex of BECN1 with system Xc− [113]. Taken together, these results indicate that BECN1 could be a regulatory target for ferroptosis, and its detailed regulatory pathways require further investigation.

P62-KEAP1-NRF2 pathway

NRF2 acts as an important defense factor against oxidative stress, and its negative regulator is Kelch-like ECH-associated protein 1 (KEAP1)[115]. Under normal physiological conditions, NRF2 binds to KEAP1, which is constantly ubiquitinated and degraded by the proteasome so that it has no function. When the organism undergoes oxidative stress, the site of KEAP1 binding to NRF2 changes so that NRF2 can translocate to the nucleus and activate the transcription of the antioxidant response element[116,117]. P62 is a selective cargo receptor for autophagy, and its regulation of NRF2-KEAP1 was revealed as early as 2010[118]. Upon autophagy deficiency and p62 accumulation, p62 competes with KEAP1 for the binding site of NRF2, exempting NRF2 from degradation and enabling the transcriptional activation of its target genes [119,120]. Recently, with the uncovering of new mechanistic insights into the regulation of ferroptosis by NRF2, a growing number of studies have demonstrated the role of the p62-KEAP1-NRF2 pathway in the regulation of ferroptosis [121,122]. A study showed that CRC cells could be treated with RH4 (the primary pharmacologically active component of

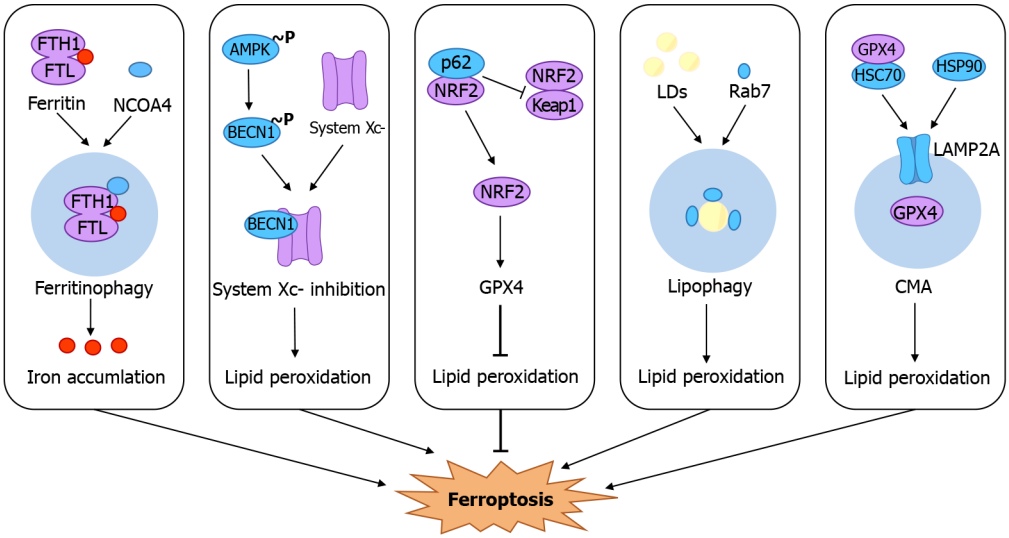

DOI: 10.4251/wjgo.v15.i7.1135 **Copyright** ©The Author(s) 2023.

Figure 2 The interaction mechanisms between autophagy and ferroptosis in colorectal cancer (created by Figdraw). Fe^{2+}: Ferrous ions; FTH1: Ferritin heavy chain 1; FTL: Ferritin light chain; NCOA4: Nuclear receptor coactivator 4; AMPK: Adenosine monophosphate-activated protein kinase; BECN1: Beclin1; p62: sequestosome 1; NRF2: Nuclear factor erythroid 2-related factor 2; KEAP1: Kelch-like ECH-associated protein 1; GPX4: Glutathione Peroxidase 4; LDs: Lipid droplets; Rab7: The small GTPase; HSC70: Heat shock cognate 71 kDa protein; HSP90: Heat shock protein 90; LAMP2A: Lysosome-associated membrane protein type 2A; CMA: Chaperone-mediated autophagy.

ginseng) and found an increase in Beclin1, LC3B, and NRF2 and a decrease in p62, which could ultimately induce ferroptosis. Treatment with the autophagy inhibitor 3-MA could reverse RH4-induced ferroptosis[123]. In another study, silencing NRF2 decreased the expression of p62, which improved the antitumor effects of tributyltin (IV) ferulate (TBT-F)[124]. These results establish a basis for the crosstalk between autophagy and ferroptosis and suggest that the p62-KEAP1-NRF2 pathway influences ferroptosis, which may be an important topic for future research.

Other potential pathways

In addition to the above, there are other potential mechanisms by which autophagy regulates ferroptosis in CRC. Lipophagy is a process in which intracellular lipid droplets (LDs) are targeted for transport into lysosomes for breakdown. LD is a dynamic organelle that stores neutral fatty acids and is involved in maintaining energy and redox homeostasis[125]. In hepatocytes, the small GTPase Rab7 recruits autophagosomes and lysosomes to the surface of LDs, resulting in lipophagy[126]. Tumor protein D52 (TPD52) or knockdown of Rab7 increased lipid storage, reduced lipid peroxidation, and suppressed RSL3-induced ferroptosis[127]. The results show that lipophagy is closely related to lipid peroxidation in ferroptosis. In addition, the accumulation of LDs contributes to chemoresistance in CRC[128]. Therefore, driving lipophagy, which leads to an increase in the occurrence of lipid peroxidation and promotes ferroptosis, may emerge as a novel treatment strategy for CRC. Most importantly, we must find the specific receptor of lipophagy in CRC.

CMA, unlike macroautophagy and microautophagy, is a type of selective autophagy that degrades only a specific subset of soluble proteins[129]. Heat shock cognate 71 kDa protein (HSC70) detects cytoplasmic proteins containing a KFERQ-like motif and then docks with lysosomes *via* lysosome-associated membrane protein type 2A (LAMP2A) to send the target proteins to lysosomes for degradation[130]. One research team found that GPX4 contains pentapeptide sequences (124 NVKFD 128, 169 LIDKN 173, and 187 QVIEK 191) consistent with a KFERQ-like motif, which is one of the substrates of CMA[131]. Heat shock protein 90 (HSP90) increases the levels of LAMP2A, mediating the degradation of GPX4 and leading to ferroptosis[131]. Antimony (sb) can upregulate the expression of HSP90, HSC70, and LAMP2A, which increases the rate of formation of the chaperone-GPX4 complex to mediate ferroptosis *via* CMA[132]. In addition, ACSL4 can also be recognized by HSC70 as a substrate for CMA-mediated ferroptosis[133]. In HCT116 cells, the lack of sorting nexin 10 (SNX10) promotes the proliferation of cancer cells by enhancing the degradation of the CMA substrate p21Cip1/WAF1[134]. The above studies laid the foundation for CMA-mediated ferroptosis of CRC cells. Future studies should focus on finding ferroptosis-related proteins containing a KFERQ-like motif and identifying the targets that drive CMA to degrade ferroptosis-related proteins.

Furthermore, hippocalcin-like 1 (HPCAL1), a neuronal calcium sensor, was identified as an important negative regulator of lipid synthesis and mTOR signaling activation, thereby blunting lipid metabolism to suppress tumorigenesis in the liver[135]. A recent study showed that HPCAL1 selectively degrades cadherin 2 and promotes lipid peroxidation to induce ferroptosis[136]. This phenomenon has been confirmed in a variety of cancer cells, including pancreatic cancer, non-small cell lung cancer, and bladder cancer cells, but this trend needs to be explored further in CRC.

CONCLUSION

In recent years, ferroptosis has consistently been under the spotlight in medical research. Ferroptosis can be used as a new treatment to clear cancer cells. For example, sorafenib itself is a ferroptosis inducer and ferroptosis inducers combined with chemotherapy drugs can overcome drug resistance; in addition, nanoparticulate anticancer drug delivery systems based on ferroptosis have emerged[137,138]. Although many studies are still in the experimental stage, these results have revealed the great potential of ferroptosis in cancer treatment. Furthermore, with a deeper understanding of the mechanisms of ferroptosis, an increasing number of studies have demonstrated crosstalk between ferroptosis and other types of RCD. Thus, autophagy-dependent ferroptosis takes the stage. Clarification of the crosstalk between autophagy and ferroptosis would not only provide a comprehensive understanding of the mechanisms of cell death but could also provide new insights for cancer treatment. Although much progress has been made, research on autophagy-dependent ferroptosis in CRC is still at an early stage. In this review, we summarized the mechanisms of autophagy and ferroptosis and their roles in CRC and focused on the possible pathways of crosstalk between them. While ferritinophagy, the BECN1–system Xc− pathway, and the p62-KEAP1-NRF2 pathway play a significant role in ferroptosis, the roles of lipophagy, CMA, or other regulators have not been validated in CRC. The mechanisms involved in the two different types of cell death are complex but also build a broader platform for subsequent research. Defining targets that regulate autophagy-dependent ferroptosis might lead to the discovery of novel therapeutic strategies for CRC.

ACKNOWLEDGEMENTS

We are very grateful to the other members of the research team for their careful review and suggestions.

FOOTNOTES

Author contributions: Zeng XY and Liu SQ designed the article framework; Zeng XY drafted the manuscript; Qiu XZ, Wu JN, Liang SM and Huang JA contributed to critical revision and supervised the manuscript; all authors have read and approved the final manuscript.

Supported by the National Natural Science Foundation of China, No. 82260579; the Natural Science Foundation of Guangxi, China, No. 2020GXNSFAA159056; and the Natural Science Foundation Fostering Science Foundation of the Second Affiliated Hospital of Guangxi Medical University, Guangxi, China, No. GJPY2018010.

Conflict-of-interest statement: The authors declare no conflicts of interest related to this article.

Country/Territory of origin: China

ORCID number: Xin-Ya Zeng 0000-0001-8312-8699; Xin-Ze Qiu 0000-0001-6373-3381; Jiang-Ni Wu 0000-0001-6514-226X; Sheng-Mei Liang 0000-0002-2930-7124; Jie-An Huang 0000-0003-0431-1888; Shi-Quan Liu 0000-0002-3552-8732.

S-Editor: Yan JP
L-Editor: A
P-Editor: Yuan YY

REFERENCES

1 **Siegel RL**, Miller KD, Fuchs HE, Jemal A. Cancer statistics, 2022. *CA Cancer J Clin* 2022; **72**: 7-33 [PMID: 35020204 DOI: 10.3322/caac.21708]
2 **Biller LH**, Schrag D. Diagnosis and Treatment of Metastatic Colorectal Cancer: A Review. *JAMA* 2021; **325**: 669-685 [PMID: 33591350 DOI: 10.1001/jama.2021.0106]
3 **Patankar JV**, Becker C. Cell death in the gut epithelium and implications for chronic inflammation. *Nat Rev Gastroenterol Hepatol* 2020; **17**: 543-556 [PMID: 32651553 DOI: 10.1038/s41575-020-0326-4]
4 **Choi AM**, Ryter SW, Levine B. Autophagy in human health and disease. *N Engl J Med* 2013; **368**: 651-662 [PMID: 23406030 DOI: 10.1056/NEJMra1205406]
5 **Dikic I**, Elazar Z. Mechanism and medical implications of mammalian autophagy. *Nat Rev Mol Cell Biol* 2018; **19**: 349-364 [PMID: 29618831 DOI: 10.1038/s41580-018-0003-4]
6 **Dixon SJ**, Lemberg KM, Lamprecht MR, Skouta R, Zaitsev EM, Gleason CE, Patel DN, Bauer AJ, Cantley AM, Yang WS, Morrison B 3rd, Stockwell BR. Ferroptosis: an iron-dependent form of nonapoptotic cell death. *Cell* 2012; **149**: 1060-1072 [PMID: 22632970 DOI: 10.1016/j.cell.2012.03.042]

7 **Li J**, Cao F, Yin HL, Huang ZJ, Lin ZT, Mao N, Sun B, Wang G. Ferroptosis: past, present and future. *Cell Death Dis* 2020; **11**: 88 [PMID: 32015325 DOI: 10.1038/s41419-020-2298-2]

8 **Yan HF**, Zou T, Tuo QZ, Xu S, Li H, Belaidi AA, Lei P. Ferroptosis: mechanisms and links with diseases. *Signal Transduct Target Ther* 2021; **6**: 49 [PMID: 33536413 DOI: 10.1038/s41392-020-00428-9]

9 **Gao M**, Monian P, Pan Q, Zhang W, Xiang J, Jiang X. Ferroptosis is an autophagic cell death process. *Cell Res* 2016; **26**: 1021-1032 [PMID: 27514700 DOI: 10.1038/cr.2016.95]

10 **Zhou B**, Liu J, Kang R, Klionsky DJ, Kroemer G, Tang D. Ferroptosis is a type of autophagy-dependent cell death. *Semin Cancer Biol* 2020; **66**: 89-100 [PMID: 30880243 DOI: 10.1016/j.semcancer.2019.03.002]

11 **Liu J**, Kuang F, Kroemer G, Klionsky DJ, Kang R, Tang D. Autophagy-Dependent Ferroptosis: Machinery and Regulation. *Cell Chem Biol* 2020; **27**: 420-435 [PMID: 32160513 DOI: 10.1016/j.chembiol.2020.02.005]

12 **Mizushima N**, Levine B, Cuervo AM, Klionsky DJ. Autophagy fights disease through cellular self-digestion. *Nature* 2008; **451**: 1069-1075 [PMID: 18305538 DOI: 10.1038/nature06639]

13 **Mijaljica D**, Prescott M, Devenish RJ. Microautophagy in mammalian cells: revisiting a 40-year-old conundrum. *Autophagy* 2011; **7**: 673-682 [PMID: 21646866 DOI: 10.4161/auto.7.7.14733]

14 **Shpilka T**, Elazar Z. Shedding light on mammalian microautophagy. *Dev Cell* 2011; **20**: 1-2 [PMID: 21238917 DOI: 10.1016/j.devcel.2010.12.010]

15 **Kaushik S**, Cuervo AM. Chaperone-mediated autophagy: a unique way to enter the lysosome world. *Trends Cell Biol* 2012; **22**: 407-417 [PMID: 22748206 DOI: 10.1016/j.tcb.2012.05.006]

16 **Mizushima N**, Levine B. Autophagy in Human Diseases. *N Engl J Med* 2020; **383**: 1564-1576 [PMID: 33053285 DOI: 10.1056/NEJMra2022774]

17 **Xie Y**, Kang R, Sun X, Zhong M, Huang J, Klionsky DJ, Tang D. Posttranslational modification of autophagy-related proteins in macroautophagy. *Autophagy* 2015; **11**: 28-45 [PMID: 25484070 DOI: 10.4161/15548627.2014.984267]

18 **Wong PM**, Puente C, Ganley IG, Jiang X. The ULK1 complex: sensing nutrient signals for autophagy activation. *Autophagy* 2013; **9**: 124-137 [PMID: 23295650 DOI: 10.4161/auto.23323]

19 **Hara T**, Takamura A, Kishi C, Iemura S, Natsume T, Guan JL, Mizushima N. FIP200, a ULK-interacting protein, is required for autophagosome formation in mammalian cells. *J Cell Biol* 2008; **181**: 497-510 [PMID: 18443221 DOI: 10.1083/jcb.200712064]

20 **Russell RC**, Tian Y, Yuan H, Park HW, Chang YY, Kim J, Kim H, Neufeld TP, Dillin A, Guan KL. ULK1 induces autophagy by phosphorylating Beclin-1 and activating VPS34 Lipid kinase. *Nat Cell Biol* 2013; **15**: 741-750 [PMID: 23685627 DOI: 10.1038/ncb2757]

21 **Wirth M**, Joachim J, Tooze SA. Autophagosome formation--the role of ULK1 and Beclin1-PI3KC3 complexes in setting the stage. *Semin Cancer Biol* 2013; **23**: 301-309 [PMID: 23727157 DOI: 10.1016/j.semcancer.2013.05.007]

22 **Kim KH**, Lee MS. Autophagy--a key player in cellular and body metabolism. *Nat Rev Endocrinol* 2014; **10**: 322-337 [PMID: 24663220 DOI: 10.1038/nrendo.2014.35]

23 **Kabeya Y**, Mizushima N, Ueno T, Yamamoto A, Kirisako T, Noda T, Kominami E, Ohsumi Y, Yoshimori T. LC3, a mammalian homologue of yeast Apg8p, is localized in autophagosome membranes after processing. *EMBO J* 2000; **19**: 5720-5728 [PMID: 11060023 DOI: 10.1093/emboj/19.21.5720]

24 **Satoo K**, Noda NN, Kumeta H, Fujioka Y, Mizushima N, Ohsumi Y, Inagaki F. The structure of Atg4B-LC3 complex reveals the mechanism of LC3 processing and delipidation during autophagy. *EMBO J* 2009; **28**: 1341-1350 [PMID: 19322194 DOI: 10.1038/emboj.2009.80]

25 **Don Wai Luu L**, Kaakoush NO, Castaño-Rodríguez N. The role of ATG16L2 in autophagy and disease. *Autophagy* 2022; **18**: 2537-2546 [PMID: 35239457 DOI: 10.1080/15548627.2022.2042783]

26 **Frudd K**, Burgoyne T, Burgoyne JR. Oxidation of Atg3 and Atg7 mediates inhibition of autophagy. *Nat Commun* 2018; **9**: 95 [PMID: 29311554 DOI: 10.1038/s41467-017-02352-z]

27 **Amaravadi R**, Kimmelman AC, White E. Recent insights into the function of autophagy in cancer. *Genes Dev* 2016; **30**: 1913-1930 [PMID: 27664235 DOI: 10.1101/gad.287524.116]

28 **Li X**, He S, Ma B. Autophagy and autophagy-related proteins in cancer. *Mol Cancer* 2020; **19**: 12 [PMID: 31969156 DOI: 10.1186/s12943-020-1138-4]

29 **Kimmelman AC**. The dynamic nature of autophagy in cancer. *Genes Dev* 2011; **25**: 1999-2010 [PMID: 21979913 DOI: 10.1101/gad.17558811]

30 **Wen X**, Klionsky DJ. At a glance: A history of autophagy and cancer. *Semin Cancer Biol* 2020; **66**: 3-11 [PMID: 31707087 DOI: 10.1016/j.semcancer.2019.11.005]

31 **Kim YC**, Guan KL. mTOR: a pharmacologic target for autophagy regulation. *J Clin Invest* 2015; **125**: 25-32 [PMID: 25654547 DOI: 10.1172/JCI73939]

32 **Kim J**, Kundu M, Viollet B, Guan KL. AMPK and mTOR regulate autophagy through direct phosphorylation of Ulk1. *Nat Cell Biol* 2011; **13**: 132-141 [PMID: 21258367 DOI: 10.1038/ncb2152]

33 **Din FV**, Valanciute A, Houde VP, Zibrova D, Green KA, Sakamoto K, Alessi DR, Dunlop MG. Aspirin inhibits mTOR signaling, activates AMP-activated protein kinase, and induces autophagy in colorectal cancer cells. *Gastroenterology* 2012; **142**: 1504-15.e3 [PMID: 22406476 DOI: 10.1053/j.gastro.2012.02.050]

34 **Shi J**, Zhou L, Huang HS, Peng L, Xie N, Nice E, Fu L, Jiang C, Huang C. Repurposing Oxiconazole against Colorectal Cancer *via* PRDX2-mediated Autophagy Arrest. *Int J Biol Sci* 2022; **18**: 3747-3761 [PMID: 35813474 DOI: 10.7150/ijbs.70679]

35 **Xiang X**, Tian Y, Hu J, Xiong R, Bautista M, Deng L, Yue Q, Li Y, Kuang W, Li J, Liu K, Yu C, Feng G. Fangchinoline exerts anticancer effects on colorectal cancer by inducing autophagy *via* regulation AMPK/mTOR/ULK1 pathway. *Biochem Pharmacol* 2021; **186**: 114475 [PMID: 33609560 DOI: 10.1016/j.bcp.2021.114475]

36 **Shen J**, Dong J, Shao F, Zhao J, Gong L, Wang H, Chen W, Zhang Y, Cai Y. Graphene oxide induces autophagy and apoptosis *via* the ROS-dependent AMPK/mTOR/ULK-1 pathway in colorectal cancer cells. *Nanomedicine (Lond)* 2022; **17**: 591-605 [PMID: 35394351 DOI: 10.2217/nnm-2022-0030]

37 **Yang Z**, Ghoorun RA, Fan X, Wu P, Bai Y, Li J, Chen H, Wang L, Wang J. High expression of Beclin-1 predicts favorable prognosis for patients with colorectal cancer. *Clin Res Hepatol Gastroenterol* 2015; **39**: 98-106 [PMID: 25130795 DOI: 10.1016/j.clinre.2014.06.014]

38 **Peng Y**, Miao H, Wu S, Yang W, Zhang Y, Xie G, Xie X, Li J, Shi C, Ye L, Sun W, Wang L, Liang H, Ou J. ABHD5 interacts with BECN1 to regulate autophagy and tumorigenesis of colon cancer independent of PNPLA2. *Autophagy* 2016; **12**: 2167-2182 [PMID: 27559856 DOI: 10.1080/15548627.2016.1217380]

39 **Hu F**, Song D, Yan Y, Huang C, Shen C, Lan J, Chen Y, Liu A, Wu Q, Sun L, Xu F, Hu F, Chen L, Luo X, Feng Y, Huang S, Hu J, Wang G. IL-6 regulates autophagy and chemotherapy resistance by promoting BECN1 phosphorylation. *Nat Commun* 2021; **12**: 3651 [PMID: 34131122 DOI: 10.1038/s41467-021-23923-1]

40 **Pan Y**, Zhao Z, Li J, Luo Y, Li W, You W, Zhang Y, Li Z, Yang J, Xiao ZJ, Wang Y. Nuclear Beclin 1 Destabilizes Retinoblastoma Protein to Promote Cell Cycle Progression and Colorectal Cancer Growth. *Cancers (Basel)* 2022; **14** [PMID: 36230664 DOI: 10.3390/cancers14194735]

41 **Zhu Y**, Huang S, Chen S, Chen J, Wang Z, Wang Y, Zheng H. SOX2 promotes chemoresistance, cancer stem cells properties, and epithelial-mesenchymal transition by β-catenin and Beclin1/autophagy signaling in colorectal cancer. *Cell Death Dis* 2021; **12**: 449 [PMID: 33953166 DOI: 10.1038/s41419-021-03733-5]

42 **Wang Y**, Li Z, Xu S, Li W, Chen M, Jiang M, Fan X. LncRNA FIRRE functions as a tumor promoter by interaction with PTBP1 to stabilize BECN1 mRNA and facilitate autophagy. *Cell Death Dis* 2022; **13**: 98 [PMID: 35110535 DOI: 10.1038/s41419-022-04509-1]

43 **Katsuragi Y**, Ichimura Y, Komatsu M. p62/SQSTM1 functions as a signaling hub and an autophagy adaptor. *FEBS J* 2015; **282**: 4672-4678 [PMID: 26432171 DOI: 10.1111/febs.13540]

44 **Pankiv S**, Clausen TH, Lamark T, Brech A, Bruun JA, Outzen H, Øvervatn A, Bjørkøy G, Johansen T. p62/SQSTM1 binds directly to Atg8/LC3 to facilitate degradation of ubiquitinated protein aggregates by autophagy. *J Biol Chem* 2007; **282**: 24131-24145 [PMID: 17580304 DOI: 10.1074/jbc.M702824200]

45 **Islam MA**, Sooro MA, Zhang P. Autophagic Regulation of p62 is Critical for Cancer Therapy. *Int J Mol Sci* 2018; **19** [PMID: 29738493 DOI: 10.3390/ijms19051405]

46 **Schmitz KJ**, Ademi C, Bertram S, Schmid KW, Baba HA. Prognostic relevance of autophagy-related markers LC3, p62/sequestosome 1, Beclin-1 and ULK1 in colorectal cancer patients with respect to KRAS mutational status. *World J Surg Oncol* 2016; **14**: 189 [PMID: 27444698 DOI: 10.1186/s12957-016-0946-x]

47 **Yagdi Efe E**, Mazumder A, Lee JY, Gaigneaux A, Radogna F, Nasim MJ, Christov C, Jacob C, Kim KW, Dicato M, Chaimbault P, Cerella C, Diederich M. Tubulin-binding anticancer polysulfides induce cell death *via* mitotic arrest and autophagic interference in colorectal cancer. *Cancer Lett* 2017; **410**: 139-157 [PMID: 28943451 DOI: 10.1016/j.canlet.2017.09.011]

48 **Liu X**, Zhao M, Sun X, Meng Z, Bai X, Gong Y, Xu L, Hao X, Yang T, Wei Z, Zhang X, Guo H, Li P, Liu Q, Shi Y, Shao C. Autophagic Flux Unleashes GATA4-NF-κB Axis to Promote Antioxidant Defense-Dependent Survival of Colorectal Cancer Cells under Chronic Acidosis. *Oxid Med Cell Longev* 2021; **2021**: 8189485 [PMID: 34987705 DOI: 10.1155/2021/8189485]

49 **Moradi-Marjaneh R**, Hassanian SM, Fiuji H, Soleimanpour S, Ferns GA, Avan A, Khazaei M. Toll like receptor signaling pathway as a potential therapeutic target in colorectal cancer. *J Cell Physiol* 2018; **233**: 5613-5622 [PMID: 29150944 DOI: 10.1002/jcp.26273]

50 **Kim MJ**, Min Y, Im JS, Son J, Lee JS, Lee KY. p62 is Negatively Implicated in the TRAF6-BECN1 Signaling Axis for Autophagy Activation and Cancer Progression by Toll-Like Receptor 4 (TLR4). *Cells* 2020; **9** [PMID: 32384667 DOI: 10.3390/cells9051142]

51 **Koleini N**, Shapiro JS, Geier J, Ardehali H. Ironing out mechanisms of iron homeostasis and disorders of iron deficiency. *J Clin Invest* 2021; **131** [PMID: 34060484 DOI: 10.1172/JCI148671]

52 **Gammella E**, Buratti P, Cairo G, Recalcati S. The transferrin receptor: the cellular iron gate. *Metallomics* 2017; **9**: 1367-1375 [PMID: 28671201 DOI: 10.1039/c7mt00143f]

53 **Lv H**, Shang P. The significance, trafficking and determination of labile iron in cytosol, mitochondria and lysosomes. *Metallomics* 2018; **10**: 899-916 [PMID: 29923582 DOI: 10.1039/c8mt00048d]

54 **Winterbourn CC**. Toxicity of iron and hydrogen peroxide: the Fenton reaction. *Toxicol Lett* 1995; **82-83**: 969-974 [PMID: 8597169 DOI: 10.1016/0378-4274(95)03532-x]

55 **Gaschler MM**, Stockwell BR. Lipid peroxidation in cell death. *Biochem Biophys Res Commun* 2017; **482**: 419-425 [PMID: 28212725 DOI: 10.1016/j.bbrc.2016.10.086]

56 **Zhang S**, Xin W, Anderson GJ, Li R, Gao L, Chen S, Zhao J, Liu S. Double-edge sword roles of iron in driving energy production *vs* instigating ferroptosis. *Cell Death Dis* 2022; **13**: 40 [PMID: 35013137 DOI: 10.1038/s41419-021-04490-1]

57 **Miotto G**, Rossetto M, Di Paolo ML, Orian L, Venerando R, Roveri A, Vučković AM, Bosello Travain V, Zaccarin M, Zennaro L, Maiorino M, Toppo S, Ursini F, Cozza G. Insight into the mechanism of ferroptosis inhibition by ferrostatin-1. *Redox Biol* 2020; **28**: 101328 [PMID: 31574461 DOI: 10.1016/j.redox.2019.101328]

58 **Yang WS**, Kim KJ, Gaschler MM, Patel M, Shchepinov MS, Stockwell BR. Peroxidation of polyunsaturated fatty acids by lipoxygenases drives ferroptosis. *Proc Natl Acad Sci U S A* 2016; **113**: E4966-E4975 [PMID: 27506793 DOI: 10.1073/pnas.1603244113]

59 **Feng H**, Stockwell BR. Unsolved mysteries: How does lipid peroxidation cause ferroptosis? *PLoS Biol* 2018; **16**: e2006203 [PMID: 29795546 DOI: 10.1371/journal.pbio.2006203]

60 **Shintoku R**, Takigawa Y, Yamada K, Kubota C, Yoshimoto Y, Takeuchi T, Koshiishi I, Torii S. Lipoxygenase-mediated generation of lipid peroxides enhances ferroptosis induced by erastin and RSL3. *Cancer Sci* 2017; **108**: 2187-2194 [PMID: 28837253 DOI: 10.1111/cas.13380]

61 **Agmon E**, Solon J, Bassereau P, Stockwell BR. Modeling the effects of lipid peroxidation during ferroptosis on membrane properties. *Sci Rep* 2018; **8**: 5155 [PMID: 29581451 DOI: 10.1038/s41598-018-23408-0]

62 **Wiernicki B**, Dubois H, Tyurina YY, Hassannia B, Bayir H, Kagan VE, Vandenabeele P, Wullaert A, Vanden Berghe T. Excessive phospholipid peroxidation distinguishes ferroptosis from other cell death modes including pyroptosis. *Cell Death Dis* 2020; **11**: 922 [PMID: 33110056 DOI: 10.1038/s41419-020-03118-0]

63 **Doll S**, Proneth B, Tyurina YY, Panzilius E, Kobayashi S, Ingold I, Irmler M, Beckers J, Aichler M, Walch A, Prokisch H, Trümbach D, Mao G, Qu F, Bayir H, Füllekrug J, Scheel CH, Wurst W, Schick JA, Kagan VE, Angeli JP, Conrad M. ACSL4 dictates ferroptosis sensitivity by shaping cellular lipid composition. *Nat Chem Biol* 2017; **13**: 91-98 [PMID: 27842070 DOI: 10.1038/nchembio.2239]

64 **Kuwata H**, Nakatani E, Shimbara-Matsubayashi S, Ishikawa F, Shibanuma M, Sasaki Y, Yoda E, Nakatani Y, Hara S. Long-chain acyl-CoA synthetase 4 participates in the formation of highly unsaturated fatty acid-containing phospholipids in murine macrophages. *Biochim Biophys Acta Mol Cell Biol Lipids* 2019; **1864**: 1606-1618 [PMID: 31376475 DOI: 10.1016/j.bbalip.2019.07.013]

65 **Jalil A**, Bourgeois T, Ménégaut L, Lagrost L, Thomas C, Masson D. Revisiting the Role of LXRs in PUFA Metabolism and Phospholipid Homeostasis. *Int J Mol Sci* 2019; **20** [PMID: 31382500 DOI: 10.3390/ijms20153787]

66 **Wang Y**, Zhang M, Bi R, Su Y, Quan F, Lin Y, Yue C, Cui X, Zhao Q, Liu S, Yang Y, Zhang D, Cao Q, Gao X. ACSL4 deficiency confers protection against ferroptosis-mediated acute kidney injury. *Redox Biol* 2022; **51**: 102262 [PMID: 35180475 DOI: 10.1016/j.redox.2022.102262]

67 **Reed A**, Ichu TA, Milosevich N, Melillo B, Schafroth MA, Otsuka Y, Scampavia L, Spicer TP, Cravatt BF. LPCAT3 Inhibitors Remodel the Polyunsaturated Phospholipid Content of Human Cells and Protect from Ferroptosis. *ACS Chem Biol* 2022; **17**: 1607-1618 [PMID: 35658397

DOI: 10.1021/acschembio.2c00317]
68 **Yang WS**, SriRamaratnam R, Welsch ME, Shimada K, Skouta R, Viswanathan VS, Cheah JH, Clemons PA, Shamji AF, Clish CB, Brown LM, Girotti AW, Cornish VW, Schreiber SL, Stockwell BR. Regulation of ferroptotic cancer cell death by GPX4. *Cell* 2014; **156**: 317-331 [PMID: 24439385 DOI: 10.1016/j.cell.2013.12.010]
69 **Forcina GC**, Dixon SJ. GPX4 at the Crossroads of Lipid Homeostasis and Ferroptosis. *Proteomics* 2019; **19**: e1800311 [PMID: 30888116 DOI: 10.1002/pmic.201800311]
70 **Wang L**, Ahn YJ, Asmis R. Sexual dimorphism in glutathione metabolism and glutathione-dependent responses. *Redox Biol* 2020; **31**: 101410 [PMID: 31883838 DOI: 10.1016/j.redox.2019.101410]
71 **Parker JL**, Deme JC, Kolokouris D, Kuteyi G, Biggin PC, Lea SM, Newstead S. Molecular basis for redox control by the human cystine/glutamate antiporter system xc(). *Nat Commun* 2021; **12**: 7147 [PMID: 34880232 DOI: 10.1038/s41467-021-27414-1]
72 **Bersuker K**, Hendricks JM, Li Z, Magtanong L, Ford B, Tang PH, Roberts MA, Tong B, Maimone TJ, Zoncu R, Bassik MC, Nomura DK, Dixon SJ, Olzmann JA. The CoQ oxidoreductase FSP1 acts parallel to GPX4 to inhibit ferroptosis. *Nature* 2019; **575**: 688-692 [PMID: 31634900 DOI: 10.1038/s41586-019-1705-2]
73 **Doll S**, Freitas FP, Shah R, Aldrovandi M, da Silva MC, Ingold I, Goya Grocin A, Xavier da Silva TN, Panzilius E, Scheel CH, Mourão A, Buday K, Sato M, Wanninger J, Vignane T, Mohana V, Rehberg M, Flatley A, Schepers A, Kurz A, White D, Sauer M, Sattler M, Tate EW, Schmitz W, Schulze A, O'Donnell V, Proneth B, Popowicz GM, Pratt DA, Angeli JPF, Conrad M. FSP1 is a glutathione-independent ferroptosis suppressor. *Nature* 2019; **575**: 693-698 [PMID: 31634899 DOI: 10.1038/s41586-019-1707-0]
74 **Wang R**, Xing R, Su Q, Yin H, Wu D, Lv C, Yan Z. Knockdown of SFRS9 Inhibits Progression of Colorectal Cancer Through Triggering Ferroptosis Mediated by GPX4 Reduction. *Front Oncol* 2021; **11**: 683589 [PMID: 34336668 DOI: 10.3389/fonc.2021.683589]
75 **Chaudhary N**, Choudhary BS, Shah SG, Khapare N, Dwivedi N, Gaikwad A, Joshi N, Raichanna J, Basu S, Gurjar M, P K S, Saklani A, Gera P, Ramadwar M, Patil P, Thorat R, Gota V, Dhar SK, Gupta S, Das M, Dalal SN. Lipocalin 2 expression promotes tumor progression and therapy resistance by inhibiting ferroptosis in colorectal cancer. *Int J Cancer* 2021; **149**: 1495-1511 [PMID: 34146401 DOI: 10.1002/ijc.33711]
76 **Han L**, Yan Y, Fan M, Gao S, Zhang L, Xiong X, Li R, Xiao X, Wang X, Ni L, Tong D, Huang C, Cao Y, Yang J. Pt3R5G inhibits colon cancer cell proliferation through inducing ferroptosis by down-regulating SLC7A11. *Life Sci* 2022; **306**: 120859 [PMID: 35931199 DOI: 10.1016/j.lfs.2022.120859]
77 **Zhang L**, Liu W, Liu F, Wang Q, Song M, Yu Q, Tang K, Teng T, Wu D, Wang X, Han W, Li Y. IMCA Induces Ferroptosis Mediated by SLC7A11 through the AMPK/mTOR Pathway in Colorectal Cancer. *Oxid Med Cell Longev* 2020; **2020**: 1675613 [PMID: 32322334 DOI: 10.1155/2020/1675613]
78 **Shah YM**, Matsubara T, Ito S, Yim SH, Gonzalez FJ. Intestinal hypoxia-inducible transcription factors are essential for iron absorption following iron deficiency. *Cell Metab* 2009; **9**: 152-164 [PMID: 19147412 DOI: 10.1016/j.cmet.2008.12.012]
79 **Singhal R**, Mitta SR, Das NK, Kerk SA, Sajjakulnukit P, Solanki S, Andren A, Kumar R, Olive KP, Banerjee R, Lyssiotis CA, Shah YM. HIF-2α activation potentiates oxidative cell death in colorectal cancers by increasing cellular iron. *J Clin Invest* 2021; **131** [PMID: 33914705 DOI: 10.1172/jci143691]
80 **Kerins MJ**, Ooi A. The Roles of NRF2 in Modulating Cellular Iron Homeostasis. *Antioxid Redox Signal* 2018; **29**: 1756-1773 [PMID: 28793787 DOI: 10.1089/ars.2017.7176]
81 **Anandhan A**, Dodson M, Schmidlin CJ, Liu P, Zhang DD. Breakdown of an Ironclad Defense System: The Critical Role of NRF2 in Mediating Ferroptosis. *Cell Chem Biol* 2020; **27**: 436-447 [PMID: 32275864 DOI: 10.1016/j.chembiol.2020.03.011]
82 **Wei R**, Zhao Y, Wang J, Yang X, Li S, Wang Y, Fei J, Hao X, Gui L, Ding X. Tagitinin C induces ferroptosis through PERK-Nrf2-HO-1 signaling pathway in colorectal cancer cells. *Int J Biol Sci* 2021; **17**: 2703-2717 [PMID: 34345202 DOI: 10.7150/ijbs.59404]
83 **Dodson M**, Castro-Portuguez R, Zhang DD. NRF2 plays a critical role in mitigating lipid peroxidation and ferroptosis. *Redox Biol* 2019; **23**: 101107 [PMID: 30692038 DOI: 10.1016/j.redox.2019.101107]
84 **Dong S**, Lu Y, Peng G, Li J, Li W, Li M, Wang H, Liu L, Zhao Q. Furin inhibits epithelial cell injury and alleviates experimental colitis by activating the Nrf2-Gpx4 signaling pathway. *Dig Liver Dis* 2021; **53**: 1276-1285 [PMID: 33640301 DOI: 10.1016/j.dld.2021.02.011]
85 **Yang J**, Mo J, Dai J, Ye C, Cen W, Zheng X, Jiang L, Ye L. Cetuximab promotes RSL3-induced ferroptosis by suppressing the Nrf2/HO-1 signalling pathway in KRAS mutant colorectal cancer. *Cell Death Dis* 2021; **12**: 1079 [PMID: 34775496 DOI: 10.1038/s41419-021-04367-3]
86 **Gao Z**, Jiang J, Hou L, Ji F. Lysionotin Induces Ferroptosis to Suppress Development of Colorectal Cancer *via* Promoting Nrf2 Degradation. *Oxid Med Cell Longev* 2022; **2022**: 1366957 [PMID: 35993016 DOI: 10.1155/2022/1366957]
87 **Machado-Silva A**, Perrier S, Bourdon JC. p53 family members in cancer diagnosis and treatment. *Semin Cancer Biol* 2010; **20**: 57-62 [PMID: 20206267 DOI: 10.1016/j.semcancer.2010.02.005]
88 **Hernández Borrero LJ**, El-Deiry WS. Tumor suppressor p53: Biology, signaling pathways, and therapeutic targeting. *Biochim Biophys Acta Rev Cancer* 2021; **1876**: 188556 [PMID: 33932560 DOI: 10.1016/j.bbcan.2021.188556]
89 **Ji H**, Wang W, Li X, Han X, Zhang X, Wang J, Liu C, Huang L, Gao W. p53: A double-edged sword in tumor ferroptosis. *Pharmacol Res* 2022; **177**: 106013 [PMID: 34856333 DOI: 10.1016/j.phrs.2021.106013]
90 **Jiang L**, Kon N, Li T, Wang SJ, Su T, Hibshoosh H, Baer R, Gu W. Ferroptosis as a p53-mediated activity during tumour suppression. *Nature* 2015; **520**: 57-62 [PMID: 25799988 DOI: 10.1038/nature14344]
91 **Xie Y**, Zhu S, Song X, Sun X, Fan Y, Liu J, Zhong M, Yuan H, Zhang L, Billiar TR, Lotze MT, Zeh HJ 3rd, Kang R, Kroemer G, Tang D. The Tumor Suppressor p53 Limits Ferroptosis by Blocking DPP4 Activity. *Cell Rep* 2017; **20**: 1692-1704 [PMID: 28813679 DOI: 10.1016/j.celrep.2017.07.055]
92 **Liu J**, Zhang C, Wang J, Hu W, Feng Z. The Regulation of Ferroptosis by Tumor Suppressor p53 and its Pathway. *Int J Mol Sci* 2020; **21** [PMID: 33182266 DOI: 10.3390/ijms21218387]
93 **Ou Y**, Wang SJ, Li D, Chu B, Gu W. Activation of SAT1 engages polyamine metabolism with p53-mediated ferroptotic responses. *Proc Natl Acad Sci U S A* 2016; **113**: E6806-E6812 [PMID: 27698118 DOI: 10.1073/pnas.1607152113]
94 **Siddik ZH**. Cisplatin: mode of cytotoxic action and molecular basis of resistance. *Oncogene* 2003; **22**: 7265-7279 [PMID: 14576837 DOI: 10.1038/sj.onc.1206933]
95 **Guo J**, Xu B, Han Q, Zhou H, Xia Y, Gong C, Dai X, Li Z, Wu G. Ferroptosis: A Novel Anti-tumor Action for Cisplatin. *Cancer Res Treat* 2018; **50**: 445-460 [PMID: 28494534 DOI: 10.4143/crt.2016.572]
96 **Chen P**, Li X, Zhang R, Liu S, Xiang Y, Zhang M, Chen X, Pan T, Yan L, Feng J, Duan T, Wang D, Chen B, Jin T, Wang W, Chen L, Huang X, Zhang W, Sun Y, Li G, Kong L, Li Y, Yang Z, Zhang Q, Zhuo L, Sui X, Xie T. Combinative treatment of β-elemene and cetuximab is

sensitive to KRAS mutant colorectal cancer cells by inducing ferroptosis and inhibiting epithelial-mesenchymal transformation. *Theranostics* 2020; **10**: 5107-5119 [PMID: 32308771 DOI: 10.7150/thno.44705]

97 **Lorenzato A**, Magrì A, Matafora V, Audrito V, Arcella P, Lazzari L, Montone M, Lamba S, Deaglio S, Siena S, Bertotti A, Trusolino L, Bachi A, Di Nicolantonio F, Bardelli A, Arena S. Vitamin C Restricts the Emergence of Acquired Resistance to EGFR-Targeted Therapies in Colorectal Cancer. *Cancers (Basel)* 2020; **12** [PMID: 32183295 DOI: 10.3390/cancers12030685]

98 **Pan X**, Qi Y, Du Z, He J, Yao S, Lu W, Ding K, Zhou M. Zinc oxide nanosphere for hydrogen sulfide scavenging and ferroptosis of colorectal cancer. *J Nanobiotechnology* 2021; **19**: 392 [PMID: 34838036 DOI: 10.1186/s12951-021-01069-y]

99 **Li Y**, Chen W, Qi Y, Wang S, Li L, Li W, Xie T, Zhu H, Tang Z, Zhou M. H(2) S-Scavenged and Activated Iron Oxide-Hydroxide Nanospindles for MRI-Guided Photothermal Therapy and Ferroptosis in Colon Cancer. *Small* 2020; **16**: e2001356 [PMID: 32789963 DOI: 10.1002/smll.202001356]

100 **Chen X**, Yu C, Kang R, Kroemer G, Tang D. Cellular degradation systems in ferroptosis. *Cell Death Differ* 2021; **28**: 1135-1148 [PMID: 33462411 DOI: 10.1038/s41418-020-00728-1]

101 **Arosio P**, Elia L, Poli M. Ferritin, cellular iron storage and regulation. *IUBMB Life* 2017; **69**: 414-422 [PMID: 28349628 DOI: 10.1002/iub.1621]

102 **Mancias JD**, Wang X, Gygi SP, Harper JW, Kimmelman AC. Quantitative proteomics identifies NCOA4 as the cargo receptor mediating ferritinophagy. *Nature* 2014; **509**: 105-109 [PMID: 24695223 DOI: 10.1038/nature13148]

103 **Dowdle WE**, Nyfeler B, Nagel J, Elling RA, Liu S, Triantafellow E, Menon S, Wang Z, Honda A, Pardee G, Cantwell J, Luu C, Cornella-Taracido I, Harrington E, Fekkes P, Lei H, Fang Q, Digan ME, Burdick D, Powers AF, Helliwell SB, D'Aquin S, Bastien J, Wang H, Wiederschain D, Kuerth J, Bergman P, Schwalb D, Thomas J, Ugwonali S, Harbinski F, Tallarico J, Wilson CJ, Myer VE, Porter JA, Bussiere DE, Finan PM, Labow MA, Mao X, Hamann LG, Manning BD, Valdez RA, Nicholson T, Schirle M, Knapp MS, Keaney EP, Murphy LO. Selective VPS34 inhibitor blocks autophagy and uncovers a role for NCOA4 in ferritin degradation and iron homeostasis in vivo. *Nat Cell Biol* 2014; **16**: 1069-1079 [PMID: 25327288 DOI: 10.1038/ncb3053]

104 **Hou W**, Xie Y, Song X, Sun X, Lotze MT, Zeh HJ 3rd, Kang R, Tang D. Autophagy promotes ferroptosis by degradation of ferritin. *Autophagy* 2016; **12**: 1425-1428 [PMID: 27245739 DOI: 10.1080/15548627.2016.1187366]

105 **Gryzik M**, Asperti M, Denardo A, Arosio P, Poli M. NCOA4-mediated ferritinophagy promotes ferroptosis induced by erastin, but not by RSL3 in HeLa cells. *Biochim Biophys Acta Mol Cell Res* 2021; **1868**: 118913 [PMID: 33245979 DOI: 10.1016/j.bbamcr.2020.118913]

106 **Fang Y**, Chen X, Tan Q, Zhou H, Xu J, Gu Q. Inhibiting Ferroptosis through Disrupting the NCOA4-FTH1 Interaction: A New Mechanism of Action. *ACS Cent Sci* 2021; **7**: 980-989 [PMID: 34235259 DOI: 10.1021/acscentsci.0c01592]

107 **Gu C**, Chang W, Wu J, Yao Y, Liu G, Yuan Y, Quan W, Sun Z, Shang A, Li D. NCOA4: An Immunomodulation-Related Prognostic Biomarker in Colon Adenocarcinoma and Pan-Cancer. *J Oncol* 2022; **2022**: 5242437 [PMID: 35756082 DOI: 10.1155/2022/5242437]

108 **Hu Q**, Wei W, Wu D, Huang F, Li M, Li W, Yin J, Peng Y, Lu Y, Zhao Q, Liu L. Blockade of GCH1/BH4 Axis Activates Ferritinophagy to Mitigate the Resistance of Colorectal Cancer to Erastin-Induced Ferroptosis. *Front Cell Dev Biol* 2022; **10**: 810327 [PMID: 35223839 DOI: 10.3389/fcell.2022.810327]

109 **Hasan M**, Reddy SM, Das NK. Ferritinophagy is not required for colon cancer cell growth. *Cell Biol Int* 2020; **44**: 2307-2314 [PMID: 32767706 DOI: 10.1002/cbin.11439]

110 **Li B**, Wei S, Yang L, Peng X, Ma Y, Wu B, Fan Q, Yang S, Li X, Jin H, Tang S, Huang M, Li H, Liu J. CISD2 Promotes Resistance to Sorafenib-Induced Ferroptosis by Regulating Autophagy in Hepatocellular Carcinoma. *Front Oncol* 2021; **11**: 657723 [PMID: 34485112 DOI: 10.3389/fonc.2021.657723]

111 **Li J**, Yuan J, Li Y, Wang J, Xie Q, Ma R, Ren M, Lu D, Xu Z. d-Borneol enhances cisplatin sensitivity *via* autophagy dependent EMT signaling and NCOA4-mediated ferritinophagy. *Phytomedicine* 2022; **106**: 154411 [PMID: 36030746 DOI: 10.1016/j.phymed.2022.154411]

112 **Zhang Z**, Yao Z, Wang L, Ding H, Shao J, Chen A, Zhang F, Zheng S. Activation of ferritinophagy is required for the RNA-binding protein ELAVL1/HuR to regulate ferroptosis in hepatic stellate cells. *Autophagy* 2018; **14**: 2083-2103 [PMID: 30081711 DOI: 10.1080/15548627.2018.1503146]

113 **Song X**, Zhu S, Chen P, Hou W, Wen Q, Liu J, Xie Y, Klionsky DJ, Kroemer G, Lotze MT, Zeh HJ, Kang R, Tang D. AMPK-Mediated BECN1 Phosphorylation Promotes Ferroptosis by Directly Blocking System X(c)(-) Activity. *Curr Biol* 2018; **28**: 2388-2399.e5 [PMID: 30057310 DOI: 10.1016/j.cub.2018.05.094]

114 **Koppula P**, Zhang Y, Zhuang L, Gan B. Amino acid transporter SLC7A11/xCT at the crossroads of regulating redox homeostasis and nutrient dependency of cancer. *Cancer Commun (Lond)* 2018; **38**: 12 [PMID: 29764521 DOI: 10.1186/s40880-018-0288-x]

115 **Baird L**, Swift S, Llères D, Dinkova-Kostova AT. Monitoring Keap1-Nrf2 interactions in single live cells. *Biotechnol Adv* 2014; **32**: 1133-1144 [PMID: 24681086 DOI: 10.1016/j.biotechadv.2014.03.004]

116 **Lu MC**, Ji JA, Jiang ZY, You QD. The Keap1-Nrf2-ARE Pathway As a Potential Preventive and Therapeutic Target: An Update. *Med Res Rev* 2016; **36**: 924-963 [PMID: 27192495 DOI: 10.1002/med.21396]

117 **Yamamoto M**, Kensler TW, Motohashi H. The KEAP1-NRF2 System: a Thiol-Based Sensor-Effector Apparatus for Maintaining Redox Homeostasis. *Physiol Rev* 2018; **98**: 1169-1203 [PMID: 29717933 DOI: 10.1152/physrev.00023.2017]

118 **Komatsu M**, Kurokawa H, Waguri S, Taguchi K, Kobayashi A, Ichimura Y, Sou YS, Ueno I, Sakamoto A, Tong KI, Kim M, Nishito Y, Iemura S, Natsume T, Ueno T, Kominami E, Motohashi H, Tanaka K, Yamamoto M. The selective autophagy substrate p62 activates the stress responsive transcription factor Nrf2 through inactivation of Keap1. *Nat Cell Biol* 2010; **12**: 213-223 [PMID: 20173742 DOI: 10.1038/ncb2021]

119 **Taguchi K**, Fujikawa N, Komatsu M, Ishii T, Unno M, Akaike T, Motohashi H, Yamamoto M. Keap1 degradation by autophagy for the maintenance of redox homeostasis. *Proc Natl Acad Sci U S A* 2012; **109**: 13561-13566 [PMID: 22872865 DOI: 10.1073/pnas.1121572109]

120 **Jiang T**, Harder B, Rojo de la Vega M, Wong PK, Chapman E, Zhang DD. p62 Links autophagy and Nrf2 signaling. *Free Radic Biol Med* 2015; **88**: 199-204 [PMID: 26117325 DOI: 10.1016/j.freeradbiomed.2015.06.014]

121 **Sun X**, Ou Z, Chen R, Niu X, Chen D, Kang R, Tang D. Activation of the p62-Keap1-NRF2 pathway protects against ferroptosis in hepatocellular carcinoma cells. *Hepatology* 2016; **63**: 173-184 [PMID: 26403645 DOI: 10.1002/hep.28251]

122 **Chen J**, Zhang J, Chen T, Bao S, Li J, Wei H, Hu X, Liang Y, Liu F, Yan S. Xiaojianzhong decoction attenuates gastric mucosal injury by activating the p62/Keap1/Nrf2 signaling pathway to inhibit ferroptosis. *Biomed Pharmacother* 2022; **155**: 113631 [PMID: 36122518 DOI: 10.1016/j.biopha.2022.113631]

123 **Wu Y**, Pi D, Chen Y, Zuo Q, Zhou S, Ouyang M. Ginsenoside Rh4 Inhibits Colorectal Cancer Cell Proliferation by Inducing Ferroptosis *via* Autophagy Activation. *Evid Based Complement Alternat Med* 2022; **2022**: 6177553 [PMID: 35677385 DOI: 10.1155/2022/6177553]

124 **Celesia A**, Morana O, Fiore T, Pellerito C, D'Anneo A, Lauricella M, Carlisi D, De Blasio A, Calvaruso G, Giuliano M, Emanuele S. ROS-

Dependent ER Stress and Autophagy Mediate the Anti-Tumor Effects of Tributyltin (IV) Ferulate in Colon Cancer Cells. *Int J Mol Sci* 2020; **21** [PMID: 33143349 DOI: 10.3390/ijms21218135]

125 **Jarc E**, Petan T. Lipid Droplets and the Management of Cellular Stress. *Yale J Biol Med* 2019; **92**: 435-452 [PMID: 31543707]

126 **Schroeder B**, Schulze RJ, Weller SG, Sletten AC, Casey CA, McNiven MA. The small GTPase Rab7 as a central regulator of hepatocellular lipophagy. *Hepatology* 2015; **61**: 1896-1907 [PMID: 25565581 DOI: 10.1002/hep.27667]

127 **Bai Y**, Meng L, Han L, Jia Y, Zhao Y, Gao H, Kang R, Wang X, Tang D, Dai E. Lipid storage and lipophagy regulates ferroptosis. *Biochem Biophys Res Commun* 2019; **508**: 997-1003 [PMID: 30545638 DOI: 10.1016/j.bbrc.2018.12.039]

128 **Jin L**, Zhu LY, Pan YL, Fu HQ, Zhang J. Prothymosin α promotes colorectal carcinoma chemoresistance through inducing lipid droplet accumulation. *Mitochondrion* 2021; **59**: 123-134 [PMID: 33872798 DOI: 10.1016/j.mito.2021.04.001]

129 **Bejarano E**, Cuervo AM. Chaperone-mediated autophagy. *Proc Am Thorac Soc* 2010; **7**: 29-39 [PMID: 20160146 DOI: 10.1513/pats.200909-102JS]

130 **Kaushik S**, Cuervo AM. The coming of age of chaperone-mediated autophagy. *Nat Rev Mol Cell Biol* 2018; **19**: 365-381 [PMID: 29626215 DOI: 10.1038/s41580-018-0001-6]

131 **Wu Z**, Geng Y, Lu X, Shi Y, Wu G, Zhang M, Shan B, Pan H, Yuan J. Chaperone-mediated autophagy is involved in the execution of ferroptosis. *Proc Natl Acad Sci U S A* 2019; **116**: 2996-3005 [PMID: 30718432 DOI: 10.1073/pnas.1819728116]

132 **Yu S**, Li Z, Zhang Q, Wang R, Zhao Z, Ding W, Wang F, Sun C, Tang J, Wang X, Zhang H, Huang R, Wu Q, Jiang J, Zhao X. GPX4 degradation *via* chaperone-mediated autophagy contributes to antimony-triggered neuronal ferroptosis. *Ecotoxicol Environ Saf* 2022; **234**: 113413 [PMID: 35305351 DOI: 10.1016/j.ecoenv.2022.113413]

133 **Liu C**, Sun W, Zhu T, Shi S, Zhang J, Wang J, Gao F, Ou Q, Jin C, Li J, Xu JY, Tian H, Xu GT, Lu L. Glia maturation factor-β induces ferroptosis by impairing chaperone-mediated autophagic degradation of ACSL4 in early diabetic retinopathy. *Redox Biol* 2022; **52**: 102292 [PMID: 35325805 DOI: 10.1016/j.redox.2022.102292]

134 **Zhang S**, Hu B, You Y, Yang Z, Liu L, Tang H, Bao W, Guan Y, Shen X. Sorting nexin 10 acts as a tumor suppressor in tumorigenesis and progression of colorectal cancer through regulating chaperone mediated autophagy degradation of p21(Cip1/WAF1). *Cancer Lett* 2018; **419**: 116-127 [PMID: 29355659 DOI: 10.1016/j.canlet.2018.01.045]

135 **Chen T**, Yuan Z, Lei Z, Duan J, Xue J, Lu T, Yan G, Zhang L, Liu Y, Li Q, Zhang Y. Hippocalcin-Like 1 blunts liver lipid metabolism to suppress tumorigenesis *via* directly targeting RUVBL1-mTOR signaling. *Theranostics* 2022; **12**: 7450-7464 [PMID: 36438486 DOI: 10.7150/thno.75936]

136 **Chen X**, Song X, Li J, Zhang R, Yu C, Zhou Z, Liu J, Liao S, Klionsky DJ, Kroemer G, Tang D, Kang R. Identification of HPCAL1 as a specific autophagy receptor involved in ferroptosis. *Autophagy* 2023; **19**: 54-74 [PMID: 35403545 DOI: 10.1080/15548627.2022.2059170]

137 **Chen F**, Cai X, Kang R, Liu J, Tang D. Autophagy-Dependent Ferroptosis in Cancer. *Antioxid Redox Signal* 2023 [PMID: 36734418 DOI: 10.1089/ars.2022.0202]

138 **Shan X**, Li S, Sun B, Chen Q, Sun J, He Z, Luo C. Ferroptosis-driven nanotherapeutics for cancer treatment. *J Control Release* 2020; **319**: 322-332 [PMID: 31917296 DOI: 10.1016/j.jconrel.2020.01.008]

139 **Zhou D**, Yao Y, Zong L, Zhou G, Feng M, Chen J, Liu G, Chen G, Sun K, Yao H, Liu Y, Shi X, Zhang W, Shi B, Tai Q, Wu G, Sun L, Hu W, Zhu X, He S. TBK1 Facilitates GLUT1-Dependent Glucose Consumption by suppressing mTORC1 Signaling in Colorectal Cancer Progression. *Int J Biol Sci* 2022; **18**: 3374-3389 [PMID: 35637944 DOI: 10.7150/ijbs.70742]

140 **Jiffry J**, Thavornwatanayong T, Rao D, Fogel EJ, Saytoo D, Nahata R, Guzik H, Chaudhary I, Augustine T, Goel S, Maitra R. Oncolytic Reovirus (pelareorep) Induces Autophagy in KRAS-mutated Colorectal Cancer. *Clin Cancer Res* 2021; **27**: 865-876 [PMID: 33168658 DOI: 10.1158/1078-0432.CCR-20-2385]

141 **Chen Y**, Chen Y, Zhang J, Cao P, Su W, Deng Y, Zhan N, Fu X, Huang Y, Dong W. Fusobacterium nucleatum Promotes Metastasis in Colorectal Cancer by Activating Autophagy Signaling *via* the Upregulation of CARD3 Expression. *Theranostics* 2020; **10**: 323-339 [PMID: 31903123 DOI: 10.7150/thno.38870]

142 **Chen XL**, Liu P, Zhu WL, Lou LG. DCZ5248, a novel dual inhibitor of Hsp90 and autophagy, exerts antitumor activity against colon cancer. *Acta Pharmacol Sin* 2021; **42**: 132-141 [PMID: 32404982 DOI: 10.1038/s41401-020-0398-2]

143 **Kim J**, Choi S, Kim JO, Kim KK. Autophagy-mediated upregulation of cytoplasmic claudin 1 stimulates the degradation of SQSTM1/p62 under starvation. *Biochem Biophys Res Commun* 2018; **496**: 159-166 [PMID: 29307823 DOI: 10.1016/j.bbrc.2018.01.017]

144 **Xia Y**, Liu S, Li C, Ai Z, Shen W, Ren W, Yang X. Discovery of a novel ferroptosis inducer-talaroconvolutin A-killing colorectal cancer cells *in vitro* and in vivo. *Cell Death Dis* 2020; **11**: 988 [PMID: 33203867 DOI: 10.1038/s41419-020-03194-2]

145 **Liu MY**, Li HM, Wang XY, Xia R, Li X, Ma YJ, Wang M, Zhang HS. TIGAR drives colorectal cancer ferroptosis resistance through ROS/AMPK/SCD1 pathway. *Free Radic Biol Med* 2022; **182**: 219-231 [PMID: 35271998 DOI: 10.1016/j.freeradbiomed.2022.03.002]

World Journal of Gastrointestinal Oncology

Submit a Manuscript: https://www.f6publishing.com

World J Gastrointest Oncol 2023 July 15; 15(7): 1149-1173

DOI: 10.4251/wjgo.v15.i7.1149

ISSN 1948-5204 (online)

REVIEW

Application of G-quadruplex targets in gastrointestinal cancers: Advancements, challenges and prospects

Zong-Qiang Han, Li-Na Wen

Specialty type: Oncology

Provenance and peer review: Invited article; Externally peer reviewed.

Peer-review model: Single blind

Peer-review report's scientific quality classification

Grade A (Excellent): 0
Grade B (Very good): B, B, B
Grade C (Good): 0
Grade D (Fair): 0
Grade E (Poor): 0

P-Reviewer: Jiang L, China; Uhlmann D, Germany; Wong WL, China

Received: February 11, 2023
Peer-review started: February 11, 2023
First decision: March 28, 2023
Revised: April 11, 2023
Accepted: May 8, 2023
Article in press: May 8, 2023
Published online: July 15, 2023

Zong-Qiang Han, Department of Laboratory Medicine, Beijing Xiaotangshan Hospital, Beijing 102211, China

Li-Na Wen, Department of Clinical Nutrition, Beijing Shijitan Hospital, Capital Medical University, Beijing 100038, China

Corresponding author: Li-Na Wen, Doctor, Research Associate, Department of Clinical Nutrition, Beijing Shijitan Hospital, Capital Medical University, No. 10 Tieyi Road, Yangfangdian Street, Haidian District, Beijing 100038, China. wenlina3074@bjsjth.cn

Abstract

Genomic instability and inflammation are considered to be two enabling characteristics that support cancer development and progression. G-quadruplex structure is a key element that contributes to genomic instability and inflammation. G-quadruplexes were once regarded as simply an obstacle that can block the transcription of oncogenes. A ligand targeting G-quadruplexes was found to have anticancer activity, making G-quadruplexes potential anticancer targets. However, further investigation has revealed that G-quadruplexes are widely distributed throughout the human genome and have many functions, such as regulating DNA replication, DNA repair, transcription, translation, epigenetics, and inflammatory response. G-quadruplexes play double regulatory roles in transcription and translation. In this review, we focus on G-quadruplexes as novel targets for the treatment of gastrointestinal cancers. We summarize the application basis of G-quadruplexes in gastrointestinal cancers, including their distribution sites, structural characteristics, and physiological functions. We describe the current status of applications for the treatment of esophageal cancer, pancreatic cancer, hepatocellular carcinoma, gastric cancer, colorectal cancer, and gastrointestinal stromal tumors, as well as the associated challenges. Finally, we review the prospective clinical applications of G-quadruplex targets, providing references for targeted treatment strategies in gastrointestinal cancers.

Key Words: G-quadruplex; Pancreatic cancer; Liver cancer; Gastric cancer; Colorectal cancer; Gastrointestinal stromal tumor

Core Tip: G-quadruplexes are widely distributed in the human genome and have many functions. G-quadruplexes play double regulatory roles in transcription and translation. We focus on G-quadruplexes as novel therapeutic targets for gastrointestinal cancers. We summarize the application basis of G-quadruplexes in gastrointestinal cancers, including their distribution sites, structural characteristics, and physiological functions. We describe the current status of applications for the treatment of esophageal cancer, pancreatic cancer, hepatocellular carcinoma, gastric cancer, colorectal cancer, and gastrointestinal stromal tumors, as well as the associated challenges. We review prospective clinical applications of G-quadruplex targets, providing references for targeted treatment in gastrointestinal cancers.

Citation: Han ZQ, Wen LN. Application of G-quadruplex targets in gastrointestinal cancers: Advancements, challenges and prospects. *World J Gastrointest Oncol* 2023; 15(7): 1149-1173
URL: https://www.wjgnet.com/1948-5204/full/v15/i7/1149.htm
DOI: https://dx.doi.org/10.4251/wjgo.v15.i7.1149

INTRODUCTION

Gastrointestinal cancers seriously affect the quality of life of patients and are among the cancers with the highest incidence and mortality worldwide. There currently remains a lack of effective therapeutic methods for these cancers, despite the development of many anticancer strategies. This is mainly because the etiology and molecular mechanisms associated with the occurrence and development of many cancer types are unclear, despite tumor immunotherapy and molecular targeted therapies having achieved promising results. In the multistep development of various human cancers, 14 characteristics were summarized as the latest hallmarks of cancer: Sustaining proliferative signaling, evading growth suppression signals, avoiding immune destruction, enabling replicative immortality, tumor-promoting inflammation, activating invasion and metastasis, inducing or accessing the vasculature, genomic instability and mutation, resisting cell death, deregulating cellular metabolism, unlocking phenotypic plasticity, nonmutational epigenetic reprogramming, polymorphic microbiomes, and senescent cells[1]. Genomic instability and inflammation have been considered as the two enabling characteristics that allow cancer to acquire these hallmarks[2]. Importantly, inflammation itself can induce genomic instability[3]. The role of inflammation in the transformation of gastrointestinal cancers, such as gastric, intestinal and liver cancers, should not be ignored. Hence, in the future, anticancer strategies targeting genomic instability may have potentially broad applications for the treatment of cancer. The molecular and cellular elements affecting genomic instability may become effective anticancer targets.

In 1962, the unusual four-stranded helix structures of guanine-rich DNA sequences with a high tendency to self-assemble into planar guanine quartets (G-quartets) were first reported and named as G-quadruplexes[4]. Afterwards, DNA G-quadruplexes were found in telomeres[5], oncogene promoters[6,7], microsatellite fragments[8], and additional regions. In 1992, tetraplex formation of nucleotide sequences in the 3′ terminus of the 5s RNA were found in *Escherichia coli* in the presence of K^+ solution[9]. Subsequently, > 3000 RNA G-quadruplex component elements in the mRNA 3′ and 5′ untranslated regions (UTRs)[10,11] and exons[12,13], as well as in other noncoding RNAs[14], were discovered in the human genome. As a nucleic acid secondary structure, a G-quadruplex differs from the typical A-, B-, C- or Z- of duplex DNA, conventional RNA, and was the supplement to nucleic acid structure type. The crystal or solution structures of various DNA or RNA G-quadruplexes have been increasingly resolved, with their physiological functions gradually clarified, especially their roles in various forms of cancers, such as breast cancer, osteosarcoma, and cervical carcinoma[3,15-19]. G-quadruplexes can regulate DNA replication[20,21], repair[22], methylation[23], and gene transcription and translation[24], and correlate with genomic instability[3,25]. In this review, we summarize the literature on G-quadruplexes and their ligands from 1962 to 2023 and describe G-quadruplex characteristics, including the existing sites, structural details, and physiological functions, and their potential applications in gastrointestinal cancer therapy. In addition, we summarize the challenges and prospects of targeting G-quadruplexes in digestive tumors to potentially prevent and treat gastrointestinal cancers.

BASIS OF THERAPEUTIC APPLICATIONS OF G-QUADRUPLEXES IN GASTROINTESTINAL CANCERS

The clinical application value of biological molecules is dependent upon their biological functions, which are affected by intracellular distribution, molecular structure and other properties. Therefore, such molecular characteristics form the basis for clinical application potential, as shown in Figure 1.

Potential G-quadruplex sites in humans

Potential G-quadruplex structures in the human genome can be predicted *via* computer analysis by retrieving the pattern sequences ($G_{\geq 3}N_{1\text{-}7}G_{\geq 3}N_{1\text{-}7}G_{\geq 3}N_{1\text{-}7}G_{\geq 3}$)[26]. They can also be formed with less than three guanines contrary to this dogma [27]. With the development of G-quadruplex-specific antibodies, fluorescent probes, sequencing technology, and genomic mapping, G-quadruplex structures are being increasingly detected and visualized in cells[28-33]. Currently, at least 700000 potential G-quadruplex structures have been inferred to exist in humans[34-36]. Telomeric DNA was the first

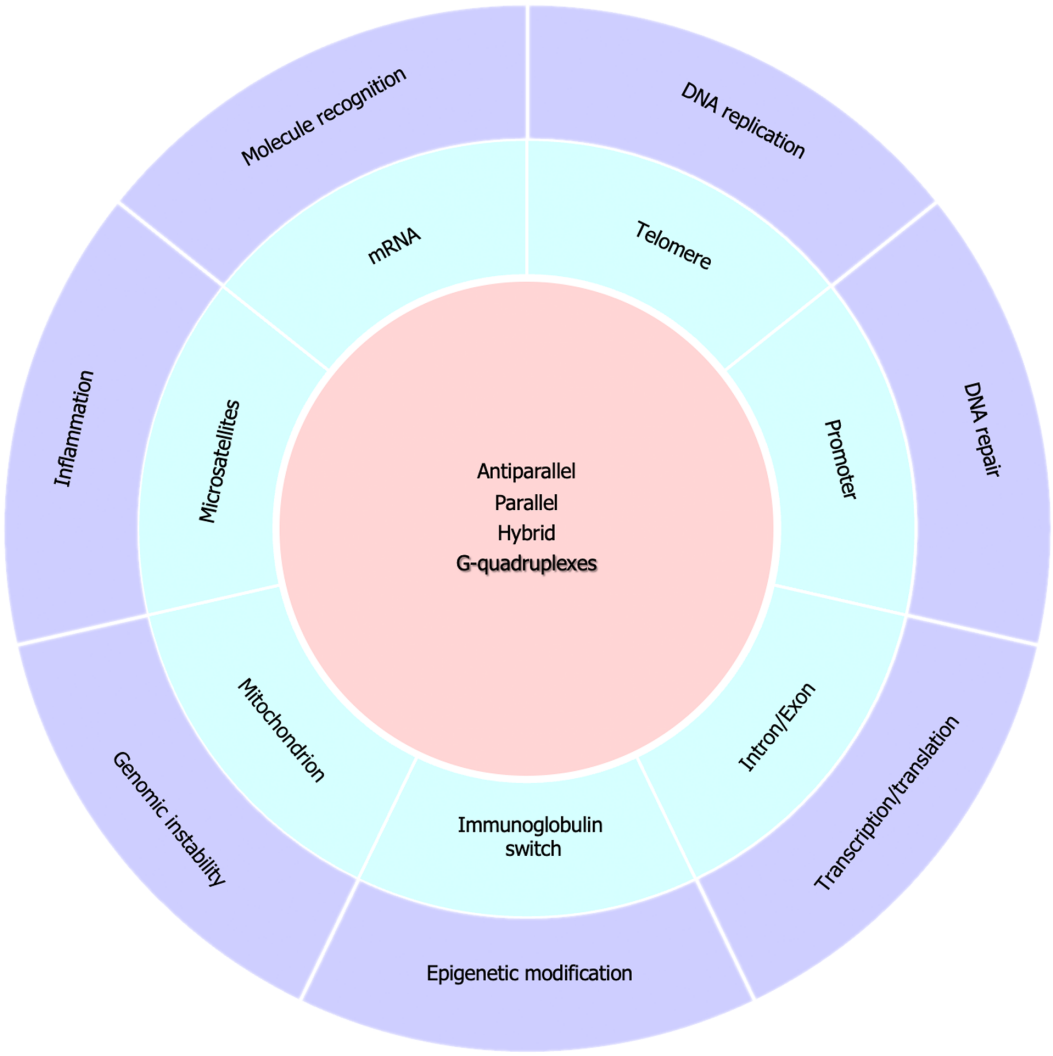

DOI: 10.4251/wjgo.v15.i7.1149

Figure 1 Application basis of G-quadruplex targets in gastrointestinal cancers: G-quadruplex characteristics. From the inner ring to the outer ring, there are basic structure types, distribution sites and physiological functions of G-quadruplexes.

biologically-related G-quadruplex target investigated in detail[37] and was considered to have the highest abundance of potential G-quadruplex structures. The 5000-10000 bp of tandemly repeated sequence (TTAGGG) contained in telomeres can fold into a G-quadruplex to regulate telomere maintenance[38,39]. Maintaining its structural stability can help inhibit the activity of telomerase and thus prevent the unlimited proliferation of tumor cells[40]. In addition to telomeres, genome-wide sequencing analyses have suggested that more than 8000 potential G-quadruplexes are likely enriched in promoter regions spanning 1 kb upstream of the transcription initiation sites in humans[41,42]. In the past, close attention was paid to proto-oncogene promoter G-quadruplexes, including Kirsten rat sarcoma viral oncogene homologue (*KRAS*)[43], *HRAS*[44], *c-MYC*[45], *c-KIT*[46], *RET*[47], *MST1R*[48], and others. G-quadruplexes in promoter regions of carcinoma-related genes were studied as well, such as B-cell lymphoma 2 (*BCL2*)[49], hypoxia inducible factor 1 subunit alpha (*HIF1a*)[50], vascular endothelial-derived growth factor (*VEGF*)[51], platelet-derived growth factor subunit A (*PDGFA*)[52], PDGF receptor-β (*PDGFR-β*)[53], human telomerase reverse transcriptase (*hTERT*)[54], nuclear factor (erythroid-derived 2)-like 2[55], *SMARCA4*[56], and multidrug resistance protein 1[57]. Recent studies have indicated that G-quadruplexes also exist in promoter regions of *MYH7β* gene and are associated with various myopathies[58], as well as in *CSTB* gene, and are related to progressive myoclonus epilepsy type 1[59]. Moreover, there were G-quadruplex-forming sequences (GGGGCC) in intron 1 of the *C9orf72* gene, which was the usual hereditary factor of amyotrophic lateral sclerosis and frontotemporal dementia[60]. Similar sequences were also found in other genes, for example, (GGCCT) in the first intron of *NOP56* relevant to spinocerebellar ataxia (SCA36)[61], (CCCCATGGTGGTGGCTGGGGACAG) in the coding exon of the *PRNP* gene indicating Creutzfeldt–Jakob disease[62], TAGGGCGGGAGGGAGGGAA in the first intron of the *N-myc* gene[63], and $(GGGT)_4$ in human microsatellites[8]. Additionally, abundant potential G-quadruplex formation sites exist in mRNAs (especially in the 5′ UTRs) or microRNAs. For instance, mRNA G-quadruplexes reportedly include *VEGF*[64], *FMR1*[65], *MMP16*[66], transforming growth factor-β (*TGFβ2*)[10], neuroblastoma RAS viral oncogene homolog (*NRAS*)[67], insulin-like growth factor 2[68], telomere repeat binding factor 2 (*TRF2*)[69], *PIM1*[70], beta-site amyloid precursor protein cleaving enzyme 1[71] and *YY1*[72]. G-quadruplex structures have recently been

explored in miR-92a[73], miR-1229[74] and miR-1587[75]. G-quadruplexes have also been discovered in immunoglobulin switches, microsatellites, and mitochondria genes. However, when and where the potential G-quadruplex structures can actually form and exert corresponding physiological functions *in vivo* depend on environmental conditions, which require further investigation.

Structural characteristics of G-quadruplexes

Different from the Watson-Crick base pairing regulation of double-stranded DNA, three to four guanines assemble into a G-quartet by Hoogsteen hydrogen-bonding in a square planar platform. The G-quartets then further stack on top of one another to form G-quadruplexes, which remain stable by monovalent cations in the central ion channel[76]. Because of the different number and spatial arrangement of bases, G-quadruplex structures have obvious polymorphisms. X-ray diffraction and high-field nuclear magnetic resonance spectroscopy are two effective methods for understanding the crystal and solution structures, which can be categorized as intramolecular or intermolecular G-quadruplexes. An intramolecular G-quadruplex is unimolecular and previous studies have confirmed that there are three basic types according to the orientation of the G-quartet: Parallel structure, antiparallel structure, and hybrid structure[77]. These different structures have varying levels of stability, which may affect their respective functions. Because of the restrictions of the external environment and central cation, a G-quadruplex sequence may present multiple configurations. For the human telomeric sequence, crystal or solution structural elucidation revealed that in the presence of K^+ solution, the G-quadruplex had parallel, antiparallel, hybrid-2, and hybrid-1 configurations, with an intermediate of two-tetrad[18,78-81]. However, in the presence of Na^+ solution, one unfolded state and three G-quadruplex-related configurations are observed, and the structure can interconvert between these forms[82]. *KRAS*, *c-MYC*, *VEGF*, *PDGFR-β* and *HIF1a* promoter G-quadruplexes take on parallel structures in K^+ solution[50,76], *BCL2* promoter G-quadruplexes adopt the hybrid-2 or parallel conformation in K^+ solution[76], and *c-KIT* promoter sequences can form a parallel or antiparallel G-quadruplex[83,84]. G-quadruplex structures present in other sites, such as in mRNAs, also conform to these three basic structural types. For intramolecular G-quadruplexes, more than two unimolecular G-quadruplex sequences can assemble into intermolecular parallel G-quadruplexes[18,58,75].

Physiological functions of G-quadruplexes

G-quadruplexes and DNA replication: Current research supports two seemingly opposing views on how G-quadruplexes can influence DNA replication: One view suggests that the G-quadruplex motif is necessary for replication initiation, while the other argues that a G-quadruplex is an obstacle to replication. Evidence supporting the former view is that 70%-90% of replication origins are preceded by a potential G-quadruplex-forming sequence, called the origin G-rich repeated element, which is 250-300 bp upstream of the replication initiation site in the non-nucleosome region[72,85]. Either deleting these elements in several model origins or introducing point mutations that affect G-quadruplex stability may reduce replication initiation activity in cells[86]. In addition, G-quadruplexes can recruit replication activators to play a role in DNA replication[87]. The latter view also has strong evidence, including that small molecular ligands targeting G-quadruplexes can result in DNA damage[88]. Additionally, it was demonstrated that the helicase, chromatin-remodeling protein ATRX, and human CTC1-STN1-TEN1 complex prevented replication defects by unwinding G-quadruplexes[89-92]. There were two possible conclusions regarding this argument. First, a G-quadruplex structure preferentially formed in the firing origin rather than the licensing origin[93,94]. Second, the negative regulation of DNA replication mediated by G-quadruplexes mostly occurred under pathological conditions, such as in the presence of G-quadruplex ligands or absence of ATRX. The negative effects of G-quadruplexes on DNA may be counteracted by unwinding proteins, such as helicase, in wild type cells under undisturbed situation[21].

G-quadruplexes and DNA repair: DNA damage can be triggered by exogenous stimuli, such as physical and chemical factors, or endogenous stress, which includes reactive oxygen species (ROS) production, replicative stress, and the formation of nucleic acid secondary structure. In addition to telomeres, promoters and transcriptional start sites, G-quadruplexes are enriched in DNA double-strand break (DSB) sites during mitosis and meiosis, and G-quadruplex formation may induce DNA damage and negatively impact effective DNA repair mechanisms[22,95]. However, G-quadruplexes can sometimes promote certain repair pathways under specific conditions. There are six main pathways involved with DSB repair over DNA replication: Homologous recombination (HR), nonhomologous end joining, base excision repair (BER), nucleotide excision repair (NER), mismatch repair (MMR), and translesion synthesis (TLS). One model suggested that stabilization of G-quadruplexes can active HR, leading to bypass/repair of G-quadruplex-mediated DNA damage[22]. As a sensor for endogenous oxidative damage of DNA, G-quadruplexes may provide feedback to drive BER to promote genomic stability under oxidative stress[96]. Zoo1 could assist NER function and regulate the selection of DNA repair pathways near G-quadruplex structures[97]. MMR activation was not restricted when G/T and G-quadruplex mismatch were in close proximity[98], and the stable G-quadruplex structure could inhibit the activity of endonuclease of MutL and indirectly interfere with the MMR process[99].

G-quadruplexes and transcription and translation: Potential G-quadruplex forming-sequences are frequently enriched in DNA promoter regions and the 3′ or 5′ UTRs, providing an opportunity for regulation of transcription or translation. For highly expressed cancer-related genes, proteins such as nucleolin and small molecular ligands that promote G-quadruplex formation can induce transcriptional repression. However, proteins that unwind G-quadruplexes such as the nucleoside diphosphate kinase NM23H2, poly ADP-ribose polymerase and RecQ family helicase can lead to transcriptional activation of target genes[100,101]. Moreover, putative G-quadruplex-forming sequences were also found at the docking sites of transcription factors SP1 and c-MYC associated zinc-finger protein (MAZ), which may help recruit SP1 and MAZ and facilitate transcription in cancer progression[102,103]. In noncancerous cells, studies have shown that G-

quadruplexes can directly interfere with mitochondrial genome replication, transcription, and respiratory function[104]. Therefore, a G-quadruplex is a key factor that can regulate gene transcription. Similarly, RNA G-quadruplexes can control translation. For instance, oxymatrine inhibited the translation of *VEGFA* mRNA in human cervical cancer cells by selectively binding to the G-quadruplex structure in *VEGFA* 5′ UTRs[105]. Additionally, DEAH box polypeptide 36 (DHX36) can bind to 5′ UTRs G-quadruplexes and control translation to promote muscle stem cell regeneration[106]. Thus, G-quadruplexes play significant roles in gene transcription and translation.

G-quadruplexes and epigenetic modifications: C-5 methylation of cytosine by DNA methyltransferase DNMT1, DNMT3A and DNMT3B is a key DNA epigenetic modification in mammalian development and disease. About 90% of CpGs can be highly methylated, but CpG islands (CGIs), found in dense guanine-cytosine-rich regions, largely lack methylation and are universally present in the promoter regions of genes[107]. CGIs can be progressively methylated during certain biological events, such as aging[108] and cancer[109], but the underlying regulatory mechanisms are not fully clear. Studies have shown that G-quadruplex structures are present in CGIs and are closely related to reduce levels of CGIs methylation in the human genome[110]. G4-chromatin immunoprecipitation sequencing (G4-ChIP-seq) analysis indicated that G-quadruplex structures were colocalized with DNMT1 and inhibited methylation by inhibiting activity of this enzyme[110]. Recent studies have shown that the methylation efficiency decreased with increasing G-quadruplex stability, and the degree of methylation can be controlled by adjusting the G-quadruplex topology[111].

In addition to DNA methylation, histone modification is also an important epigenetic regulation. The local conformations and biological functions of G-quadruplexes can be regulated by their specific binding proteins. For example, RNA G-quadruplexes and RNA-binding proteins participate in telomere maintenance and transcriptional regulation through histone modifications. G-quadruplex RNA-binding proteins, such as translocated in liposarcoma/fused in sarcoma and TRF2, can promote the trimethylation of histone H3 at lysine 9 in telomere histones through G-quadruplex telomeric repeat-containing RNA (TERRA)[112,113]. G-quadruplex TERRA possibly regulates methylation and demethylation of histones in telomeric DNA, and can act as a noncompetitive inhibitor to suppress lysine specific histone demethylase-mediated histone demethylation[114]. Polycomb repressive complex 2 (PRC2) interactions with TERRA can catalyze the trimethylation of histone H3 at lysine 27 (H3K27me3), and G-quadruplex RNA can specifically prevent PRC2 from interacting with genes in human and mouse cells to block methylation at H3K27[115]. These mechanisms work together to maintain telomere length and chromatin function.

G-quadruplexes and genomic instability: DNA is vulnerable to damage from various types of endogenous and exogenous stimuli. This can hinder DNA replication and induce genomic instability, which includes point mutations, insertions, deletions, inversions, translocations, expansions/contractions of repeated sequences, gross chromosomal rearrangements, aneuploidy and other characteristics. Such genomic instability is often observed in cancer and can be induced by G-quadruplexes. G-quadruplexes are enriched at regions of base substitutions, insertion-deletion mutations, and chromosome translocation breakpoints that are associated with a variety of human cancers, such as colon cancer, and is the main inducing factor of carcinogenic transformation[116-118]. The instability of potential G-quadruplex-forming sequences increases in a transcription-dependent manner, as transcription can provoke genomic instability of G-quadruplexes by releasing single-stranded DNA, which is easy to fold into secondary structures[117,119].

G-quadruplex and inflammation: G-quadruplexes are correlated with inflammation. Studies have shown that there was a high frequency of potential G-quadruplex formation sequences in the promoter regions of many inflammatory factors, such as tumor necrosis factor, TGF-β, interleukin (IL)-6, IL-12, IL-17, the XC and TAFA family chemokines, and β-chain family cytokines[120]. G-quadruplexes are also distributed in the binding sites of transcription factors involved in inflammatory and immune processes, including nuclear factor nuclear factor kappa B1, interferon regulatory factor 5, transcription factor p65, transcription factor RelB, and nuclear factor of activated T cells 5[120]. In addition, genes containing G-quadruplex structures that can regulate and participate in inflammatory-related processes have been identified through experimental studies[121]. G-quadruplexes can trigger inflammatory reactions by upregulating proinflammatory cytokines, making these structures a marker of increased inflammation and a contributor to inflammatory diseases development[121]. However, another study suggested that G-quadruplexes can interfere with switch-like recombination in B cells to alleviate allergic inflammation[122]. Collectively, this evidence suggests that G-quadruplexes may be a potential target for treating inflammation-related diseases.

Ion and molecule recognition functions of G-quadruplexes: The stability of G-quadruplex structure needs to be maintained by the monovalent cations located in the central ion channel, allowing the G-quadruplex sequence to specifically recognize monovalent cations such as K^+ and Na^+. In addition, because the specific G-quadruplex-forming sequence can fold into a special conformation and the fluorescence emission of some small molecules is significantly enhanced after binding with G-quadruplexes, G-quadruplexes could be used to identify small molecular ligands (berberine, porphyrin, and more) or proteins (thrombin, nucleolin, and more) that can specifically bind to them[16,57,123,124] or assist imaging. Therefore, G-quadruplexes have been widely used as recognition elements to construct biosensors for detecting targeting ions and molecules, such as tumor biomarkers, in tumor diagnosis, as well as targeting agents or drug carriers of anticancer drug delivery systems for tumor treatment[125,126]. In such applications, the G-quadruplex sequences are also called aptamers.

APPLICATION OF G-QUADRUPLEX TARGETS IN GASTROINTESTINAL CANCER THERAPIES

The above complex biological functions of G-quadruplexes imply that they have broad application prospects for the diagnosis and treatment of gastrointestinal cancers. The role of a G-quadruplex as a recognition element in the molecular diagnosis of gastrointestinal cancers will not be discussed in this review. The application of G-quadruplexes in therapy is mainly discussed from two perspectives: (1) The therapeutic effect of small molecule ligands and biomolecules targeting G-quadruplexes to regulate gene transcription; and (2) The therapeutic effect of G-quadruplex sequences for molecular recognition functions.

Application of small molecule ligands or biomolecules targeting G-quadruplexes in the treatment of gastrointestinal cancers

Esophageal cancer: Esophageal cancer (EC) is a gastrointestinal disease with high mortality rates. Surgery is the first choice of treatment for resectable EC cases, but neoadjuvant chemotherapy can improve the 5-year survival rate without increasing postoperative complications. Targeting G-quadruplexes may provide a new perspective for treating EC, although relevant research on this is currently limited. The telomere is an early G-quadruplex target. The G-quadruplex ligand 2,6-bis[3-(N-piperidino) propionamido] anthracene-9,10-dione, which is also considered to be a telomerase inhibitor, can shorten telomeres and exert antiproliferative and proapoptotic effects in both BIC-1 and SEG-1 EC cell lines [127]. A recent study found that zinc benzoate terpyridine complexes (1-6) in combination with G-quadruplex sequence (G2T4G2CAG2GT4G2T) resulted in various degrees of antiproliferative effects in the EC cell line Eca-109[128] (Table 1). Hence, further exploration of a G-quadruplex-related treatment strategy in EC is needed.

Pancreatic cancer: Pancreatic cancer (PC) is a refractory tumor disease with poor prognosis among cancers. About 97% of PC cases are accompanied by alterations of genes and 90% have *KRAS* oncogene mutations, which are essential for initiation of pancreatic ductal adenocarcinoma. Because *KRAS* can drive oncogene addiction, inhibiting gene mutation and downregulating gene expression are reasonable ways to block PC progression. Many attempts have been paid to target *KRAS* oncogenes, but clinically useful therapies are still limited. The mutant KRAS protein has attracted much attention, causing other approaches involving targeting *KRAS* transcription to not be fully explored. Additionally, telomere, heat shock protein 90 (*HSP90*), *c-MYC*, *Bcl-2* and others are important genes that affect cancer cell fate. Therefore, inhibiting the transcription of PC-related genes may be effective. There are G-quadruplex configurations in telomere and the promoter regions of *HSP90*, *KRAS*, *c-MYC* and *Bcl-2*, that are potential targets. Stable G-quadruplex structure usually acts as an obstacle to gene transcription. Small molecular ligands that stabilize G-quadruplex conformation can exhibit clear anticancer effects in PC.

Naphthalene diimide compounds are part of an important ligand set. A series of tetrasubstituted naphthalene diimide ligands tended to make telomeric G-quadruplexes fold into a parallel conformation, preventing binding of human protection of telomeres 1 and topoisomerase IIIα with telomeric DNA, triggering cytotoxicity in multiple PC cell lines [129]. Tetrasubstituted naphthalene diimide derivatives (compounds 3d) retain high affinity to human telomeric G-quadruplexes, upregulate DNA damage responsive genes such as *CDKN1A* and *DDIT3*, downregulate telomere maintenance genes such as *POT1* and *PARP1*, and induce cellular senescence[130]. Tetrasubstituted naphthalene diimide isomer ligands (compounds 2-5) are more inclined to stabilize telomeric G-quadruplex structure and improve antiproliferative potency[131]. Tetrasubstituted naphthalene diimide derivative (MM41) combines with and stabilizes G-quadruplex structure and downregulates expression levels of *BCL-2* and *KRAS* to promote apoptosis and decrease tumor growth of MIA-Pa-Ca2 xenografts[132,133]. Tetrasubstituted naphthalene diimide derivative (CM03) causes DNA damage and promotes the presence of nuclear G-quadruplexes in PANC-1 cells; inhibits expression of *GLI4*, *PLXNA1*, *PRKCZ* and *MAPK11*; partitions *PARD6A*, and *CBFA2T3* in MIA PaCa-2 and PANC-1 cells; and decreases tumor growth of MIA-Pa-Ca2 xenografts[133-135]. Tetrasubstituted naphthalene diimide derivative (SOP1812) was verified to have antiproliferative activity by combining with *hTERT* and telomere G-quadruplexes[135]. Another naphthalene diimide derivative (BMSG-SH3) decreases telomerase activity, inhibits *HSP90* expression, and reduces tumor growth of MIA-Pa-Ca2 xenografts by 50% through maintaining the stability of telomere and *HSP90* promoter G-quadruplex structures[136].

Porphyrin compounds are part of another important ligand set. A cationic alkyl-substituted porphyrin compound C14 binds to the *KRAS* promoter G-quadruplex, protoxidizes the guanines, suppresses gene expression and eventually leads to growth inhibition of PC cell line PANC-1 under photosensitive conditions[137]. Alkyl cationic porphyrins can promote apoptosis *in vitro* and restrict metabolism and tumor growth *in vivo* by targeting G-quadruplexes of *KRAS* and *NRAS* mRNAs[138]. Porphyrin derivative octaacetyl and tetrakis can both induce apoptosis and block metastasis by inhibiting epithelial to mesenchymal transition through stabilizing *KRAS* promoter G-quadruplexes and downregulating *KRAS* expression levels[139], while porphyrin derivative (5Me) may regulate cell proliferation and cell cycle progression by interacting with telomere, *Bcl-2*, *c-MYC* and *KRAS* G-quadruplexes[140]. Previous studies have shown that TMPyP4 can bind to intermolecular G-quadruplexes to arrest cell proliferation and induce both cellular senescence and apoptosis in MIA PaCa-2 cells[140].

Different from TMPyP4, telomestatin can bind to intramolecular G-quadruplexes and control cell proliferation, senescence and apoptosis in MIA PaCa-2 cells[141]. The benzophenanthridine alkaloid nitidine combines with the *KRAS* promoter G-quadruplex and stabilizes its structure, further downregulating *KRAS* expression levels and inducing cytotoxicity in AsPC-1, BxPC-3, MIA PaCa-2, and PANC-1 cells[142]. 4,11-bis(2-Aminoethy-llamino)anthra[2,3-b]furan-5,10-dione(2a),11-bis(2-aminoethylamino)anthra[2,3b]thiophene-5,10-dione (2b) stabilizes *KRAS* RNA G-quadruplexes, inhibits its translation, and induces apoptosis and growth inhibition of PANC-1 cells[143]. Unsymmetrical bisacridines derivatives can inhibit the proliferation of cancer cells *in vitro* and *in vivo* by increasing the stability of telomere, *c-MYC* and *KRAS* G-quadruplexes[144]. Copper(ii) l/d-valine-(1,10-phen) complexes (complex 1a, 1b) induce cytotoxicity of

Table 1 Overviews of investigations on the effects of small molecule ligands or biomolecules based on G-quadruplex targets in esophageal cancer

Ligands/biomolecules	Cell lines	Targeting gene/G-quadruplex	Effects on G-quadruplex	Effects on genes	Anticancer phenotypes	Ref.
2,6-bis[3-(N-Piperidino) propionamido] anthrace- ne-9,10-dione	BIC-1, SEG-1	Telomere	Not detected	Shortened telomeres	Inhibited telomerase activity, arrested cell proliferation, reduced colony number and size, and promoted cell apoptosis	[127]
Zinc benzoate erpyridine complexes (1-6)	Eca-109	G2T4G2CA, G2GT4G2T	Bound with G-quadruplex	Not detected	Inhibited cell proliferation	[128]

BxPC3 and AsPC1 cells from its affinity with telomeric G-quadruplexes[145]. CX-5461, the ligand of telomere, *c-MYC* and *c-kit* G-quadruplexes, also exhibits antiproliferative activity, and phase I/II clinical trials of CX-5461 as an anticancer drug have been launched[146,147]. A small molecular fluoroquinolone derivative CX-3543 (quarfloxin) can decrease tumor growth of MIA PaCa-2 xenografts by disrupting nucleolin/G-quadruplex complexes on rDNA and inhibiting rRNA synthesis[148,149]. FDA-approved antihelminthic pyrvinium pamoate inhibits mitochondrial RNA transcription and tumor growth by selectively binding to mitochondrial G-quadruplexes[150]. NSC 317605 and novel indoloquinolines derived from it show *KRAS* G-quadruplex-dependent cytotoxicity in PC cell lines[151]. Two sets of quinazoline-pyrimidine derivative ligands have been shown to prevent tumor growth *via* targeting telomere, *c-MYC*, *c-kit*, *KRAS* and *BCL-2* G-quadruplexes[152].

Some small molecules can play anticancer roles in PC mainly by stabilizing G-quadruplex structures to inhibit gene transcription. However, in addition, some proteins can promote PC progression by destabilizing G-quadruplexes to support gene transcription. For example, integrin linked kinase (ILK) can stimulate *KRAS* expression *via* destabilization of G-quadruplexes mediated by *hnRNPA1* in the promoter. This in turn affected ILK expression levels, with transcriptional activation mediated by E2F1. This has been called the KRAS-E2F1-ILK-hnRNPA1 regulatory loop, which can result in aggressive phenotypes in the tumor microenvironment[153-155]. Under oxidative stress conditions, poly (ADP-ribose) polymerase 1 (PARP-1) is recruited and binds to *KRAS* promoter G-quadruplexes, which favors the recruitment of MAZ and hnRNPA1 to the *KRAS* promoter by activating a ROS-G-quadruplex-PARP-1 axis. This ultimately results in stimulation of *KRAS* transcription[156]. Different from this mechanism, the G-quadruplex-binding protein apurinic/apyrimidinic endonuclease 1 can also bind to *KRAS* G-quadruplexes. However, it maintains the structural stability and recruits MAZ to promote *KRAS* upregulation *in vivo* and *in vitro*[157]. Moreover, polypurine reverse Hoogsteen hairpins (PPRHs) can suppress gene transcription and cell proliferation by promoting the formation of *KRAS* and *c-MYC* G-quadruplexes in PC cells[158,159].

In summary, the G-quadruplex targets of PC include *KRAS*, *KRAS* mRNA, telomere, *HSP90*, *hTERT*, *Bcl-2*, *c-MYC*, and mitochondrial G-quadruplexes, the regulatory functions of which involve transcription and translation. Proteins that can promote oncogene transcription through G-quadruplexes are also expected to become potential anticancer targets. All details are described in Table 2.

Hepatocellular carcinoma: Different from the genetic pathogenesis of PC, specific mutations in proto-oncogenes that can induce hepatocellular carcinoma (HCC) have not been identified. However, anticancer strategies for HCC involving oncogene G-quadruplexes are still being explored. At present, G-quadruplex ligands targeting *c-MYC*, *c-kit* and *HERC5* have been synthesized and verified for potential application in HCC treatment. Platinum (II) complexes with tridentate ligands, prolinamide derivatives containing triazole, a series of novel 9-O-substituted-13-octylberberine derivatives and novel 9-N-substituted-13-alkylberberine derivatives were all tested and found to have good antiproliferative activities in HepG2 cells, mainly from their good affinity with *c-MYC* promoter G-quadruplexes and their improved structural stability[160-163]. A series of thiazole orange derivatives were synthesized to effectively bind to telomeric G-quadruplexes, which can stabilize the structures and exhibit cytotoxicity in HCC cell lines[164]. The peptidomimetic ligands showed high affinity to *c-kit1* G-quadruplexes also exhibit antiproliferative and proapoptotic properties in HepG2 cells[165]. A 7,11-disubstituted quinazoline derivative HZ-6d targeting *HERC5* G-quadruplexes showed anticancer effects *in vivo* and *in vitro* through downregulation of *HERC5* expression[166].

Viral hepatitis is a primary cause of HCC. Hepatitis B virus (HBV) and hepatitis C virus (HCV) infections can develop into chronic hepatitis and then cirrhosis, eventually leading to HCC. Therefore, early intervention is an effective strategy for delaying HCC progression. In recent years, G-quadruplexes have become a potential target for antiviral therapy. RNA helicase dead box polypeptide 5 can facilitate mRNA translation of *STAT1* by unwinding the RNA G-quadruplex structure at the 5′ end of the 5′ UTR, subsequently stimulating the antiviral effects of interferon-α in HBV-infected hepatoma cells[167]. Additionally, cellular nucleolin can directly interact with viral core RNA G-quadruplexes, thereby suppressing the replication and expression of wild-type HCV[168]. All details are described in Table 3.

Gastric cancer: Gastric cancer (GC) ranked third worldwide in malignant tumor mortality rates in 2020. Most patients had late stage disease at diagnosis. For advanced GC, chemotherapy is the preferred option, but the associated adverse effects should not be ignored. It is necessary to seek new methods to treat GC, which could include targeted drug therapies based on G-quadruplexes. Small molecules selectively binding to *c-kit*, telomere and *BCL-2* G-quadruplexes have been found to antagonize GC. For example, benzo[a]phenoxazines and quinazolone derivatives display cytotoxicity

Table 2 Overviews of investigations on the effects of small molecule ligands or biomolecules based on G-quadruplex targets in pancreatic cancer

Ligands/biomolecules	Cell lines	Targeting gene/G-quadruplex	Effects on G-quadruplex	Effects on genes	Anticancer phenotypes	Ref.
Tetrasubstituted naphthalene diimide ligands	PANC-1, MIA PaCa-2, HPAC, BxPc-3	Telomere	Induced formation of a parallel G-quadruplex	Inhibited the binding of hPOT1 and topoisomerase IIIα to telomeric DNA	Cytotoxicity	[129]
Tetrasubstituted naphthalene diimide derivatives (compounds 3d)	MIA PaCa-2	Telomere	Retained high affinity to human telomeric G-quadruplex	Upregulated some DNA damage responsive genes, downregulated some telomere maintenance genes	Induced cellular senescence but did not inhibit telomerase activity	[130]
Naphthalene diimide isomer ligands (compounds 2-5)	MIA PaCa-2, PANC-1	*HSP90*	Stabilized G-quadruplex structure	Not detected	Inhibited cell proliferation	[131]
Tetrasubstituted naphthalene diimide derivative (MM41)	MIA PaCa-2	*BCL-2, K-RAS*	Bound and stabilized G-quadruplex structure	Downregulated expression of *BCL-2, K-RAS*	Promoted cell apoptosis, decreased tumor growth of MIA-Pa-Ca2 xenografts	[132]
Tetrasubstituted naphthalene diimide derivative (CM03)	MIA PaCa-2, PANC-1	Not detected	Increased presence of nuclear G-quadruplex	Induces DNA damage, downregulated expression of *Gli4, PLXNA1, PRKCZ, MAPK11, PARD6A, CBFA2T3*	Decreased tumor growth of MIA-Pa-Ca2 xenografts	[133-135]
Tetrasubstituted naphthalene diimide derivative (SOP1812)	MIA PaCa-2, PANC-1, Capan-1, BXPC-3	*hTERT*, telomere	Had affinity with G-quadruplex	Downregulated expression of *WNT5B, DVL1, AXIN1, APC2, GLI1, MAPK11, BCL-2, hTERT*	Inhibited cell proliferation, reduced MIA PaCa-2 xenograft growth	[135]
Tetrasubstituted naphthalene diimide derivative (BMSG-SH3)	MIA PaCa-2	*HSP90*	Stabilized G-quadruplex structure	Not detected	Reduced telomerase activity and HSP90 expression, 50% decreased tumor growth of MIA-Pa-Ca2 xenografts	[136]
Cationic alkyl-substituted porphyrin compound C14	PANC-1	*KRAS*	Bound with G-quadruplex and protoxidized the guanines	Downregulated expression of *KRAS*	Induced cell growth arrest	[137]
Alkyl cationic porphyrins	MIA PaCa-2, PANC-1	*KRAS* mRNA, *NRAS* mRNA	Bound G-quadruplex	Downregulated expression of *KRAS, NRAS* only if photoactivated	Activated apoptosis, reduced the metabolic activity of pancreatic cancer cells and the growth of a PANC-1 xenograft	[138]
Porphyrin derivative (Octaacetyl)	PANC-1, MIA PaCa-2	*KRAS*	Bound and stabilized G-quadruplex	Downregulated expression of *KRAS*	Cytotoxicity, induced apoptosis, blocked metastasis by inhibiting epithelial to mesenchymal transition	[139]
Porphyrin derivative (Tetrakis)	PANC-1, MIA PaCa-2	*KRAS*	Bound and stabilized G-quadruplex	Downregulated expression of *KRAS*	Cytotoxicity, induced apoptosis, blocked metastasis by inhibiting epithelial to messenchymal transition	[139]
Porphyrin derivative (5Me)	PANC-1	Telomere, *Bcl-2, c-MYC, KRAS*	Bound and stabilized G-quadruplex	Not detected	Inhibited cell proliferation, arrest G2/M phase cell cycle	[140]
TMPyP4	MIA PaCa-2	Intermolecular G-quadruplex	Not detected	Shortened telomeres	Cytotoxicity, arrested cell proliferation, induced anaphase bridges, cellular senescence and apoptosis	[141]

Telomestatin	MIA PaCa-2	Intramolecular G-quadruplex	Not detected	Shortened telomeres	Cytotoxicity, arrested cell proliferation, and induced cellular senescence and apoptosis	[141]
Nitidine	AsPC-1, BxPC-3, MIA PaCa-2, PANC-1	*KRAS*	Bound and stabilized G-quadruplex structure	Downregulated expression of *KRAS*	Cytotoxicity	[142]
4,11-bis(2-Aminoethy-llamino)anthra[2,3-b]furan-5,10-dione(2a),11-bis(2-aminoethylamino) anthra[2,3b]thiophene-5,10-dione (2b)	PANC-1	*KRAS* mRNA	Bound and stabilized G-quadruplex	Inhibited translation of *KRAS*	Induced apoptosis, inhibited cell growth and colony formation	[143]
Unsymmetrical bisacridines derivatives	PANC-1, MIA PaCa-2, BXpC-3, AsPC-1, Capan-2	Telomere, *c-MYC*, *KRAS*	Bound and stabilized G-quadruplex	Not detected	Inhibited cell proliferation, reduced PANC-1 and MIA PaCa-2 xenograft growth *in vivo*	[144]
Copper(ii) l/d-valine-(1,10-phen) complexes (complex 1a, 1b)	BxPC3, AsPC1	Telomere	Had affinity with G-quadruplex	Not detected	Cytotoxicity	[145]
CX-5461 (Pidnarulex)	MIA PaCa-2, PANC-1	Telomere, *c-MYC*, *c-kit*	Bound with G-quadruplex	Not detected	Inhibited cell proliferation	[146,147]
CX-3543 (Quarfloxin)	MIA PaCa-2	Nucleolin/ribosomal DNA G-quadruplex complexes	Disrupts nucleolin/G-quadruplex complexes on ribosomal DNA	Inhibited rRNA synthesis	Inhibited proliferation, inhibited Pol I transcription, induced apoptosis, decreased tumor growth of MIA PaCa-2 xenografts	[148,149]
Antihelminthic pyrvinium pamoate	PANC-1, Capan-1, HS766T, CFPAC, MIA PaCa-2	Mitochondrial DNA	Bound G-quadruplex	Inhibited transcription of mitochondrial RNA	Inhibited cell viability, mitochondrial pathways, tumor growth of MIA PaCa-2 xenografts	[150]
NSC 317605 and novel indolo-quinolines	AsPc1, PANC1, BxPc3, MIA PaCa-2	*c-MYC*, *KRAS*	Bound and stabilized G-quadruplex	Downregulated expression of *KRAS*	Cytotoxicity	[151]
Quinazoline-pyrimidine derivatives	Tumor-naïve pancreatic stellate cells	Telomere, *c-MYC*, *c-kit*, *KRAS*, *BCL-2*	Bound and stabilized G-quadruplex	Not detected	Inhibited tumor growth	[152]
hnRNPA1 and integrinlinked kinase	AsPC-1, PANC-1, MIA PaCa-2, Capan-2	*KRAS*	Destabilized G-quadruplex	Stimulated transcription of *KRAS*	Promoted KRAS-E2F1-ILK-hnRNPA1 circuitry, tumor growth and aggressive phenotypes	[153-155]
Poly [ADP-ribose] polymerase 1	PANC-1	*KRAS*	Destabilized G-quadruplex	Stimulated transcription of *KRAS*	Activated a ROS-G-quadruplex-PARP-1 axis	[156]
Apurinic/apyrimidinic endonuclease 1	PANC-1, BxPc3, MIA PaCa-2	*KRAS*	Bound and stabilized G-quadruplex	Upregulated expression of *KRAS*	Did not sensitize pancreatic cancer cells to chemotherapeutic drugs *in vitro* and *in vivo*	[157]
Polypurine reverse Hoogsteen hairpins	AsPc-1, MIA PaCa-2	*KRAS*, *c-MYC*	Bound and stabilized G-quadruplex	Inhibited transcription of *KRAS* and *c-MYC*	Inhibited cell proliferation	[158,159]

hPOT1: Human protection of telomeres 1; ILK: Integrinlinked kinase; BCL-2: B-cell lymphoma 2; KRAS: Kirsten rat sarcoma viral oncogene homologue; HSP90: Heat shock protein 90; hTERT: Human telomerase reverse transcriptase; NRAS: Neuroblastoma RAS viral oncogene homolog; ROS: Reactive oxygen species.

effects in HGC-27 cells by interacting with *c-kit* promoter G-quadruplexes and inhibiting gene transcription, while a 1,10-phenanthroline derivative causes DNA damage, telomere dysfunction, autophagy, and antitumor effects in AGS cells by stabilizing telomere, *c-kit* and *BCL-2* G-quadruplexes[169-171]. Use of G-quadruplex antibody confirmed that the targeting regulation could help suppress GC[172]. All details are described in Table 4.

Table 3 Overviews of investigations on the effects of small molecule ligands or biomolecules based on G-quadruplex targets in hepatocellular carcinoma

Ligands/biomolecules	Cell lines	Targeting gene/G-quadruplex	Effects on G-quadruplex	Effects on genes	Anticancer phenotypes	Ref.
Platinum(II) complexes with tridentate ligands	HepG2	*c-MYC*	Bound and stabilized G-quadruplex	Inhibited *c-MYC* expression	Cytotoxicity	[160]
Prolinamide derivatives containing triazole	HepG2	*c-MYC*	Bound and stabilized G-quadruplex	Inhibited *c-MYC* expression	Cytotoxicity	[161]
A series of novel 9-O-substituted-13-octylberberine derivatives	HepG2, Sk-Hep-1, Huh-7	*c-MYC*	Bound and stabilized G-quadruplex	Not detected	Cytotoxicity, blocked cell cycle, induced apoptosis, inhibited tumor growth of H22 xenografts	[162]
Series of novel 9-N-substituted-13-alkylberberine derivatives	HepG2, Sk-Hep-1, Huh-7, Hep3	*c-MYC*	Bound and stabilized G-quadruplex	Not detected	Cytotoxicity, blocked cell cycle, induced apoptosis, inhibited tumor growth of H22 xenografts	[163]
Thiazole orange derivatives	HepG2	Telomere	Bound and stabilized G-quadruplex	Not detected	Cytotoxicity	[164]
Peptidomimetic ligands	HepG2	*c-kit1*	Had high affinity with G-quadruplex	Not detected	Inhibited cell proliferation, induced apoptosis	[165]
A 7, 11-disubstituted quinazoline derivative HZ-6d	HepG2, SMMC-7721	*HERC5*	Bound and stabilized G-quadruplex	Inhibited *HERC5* expression	Inhibited cell growth, migration, induced apoptosis, suppressed tumor growth of SMMC-7721 xenografts	[166]
DDX5	HepG2, Huh7, Snu387, Snu423, HepaRG, HepAD38	*STAT1* mRNA	Unwound G-quadruplex	Promoted translation of *STAT1*	Upregulated expression of STAT1 and enhanced IFN-α mediated antiviral effects	[167]
Nucleolin	Huh7.5.1, Huh7.5	Viral core RNA, G-quadruplex	Directly interacted with G-quadruplex	Inhibited viral RNA replication	Suppressed wild-type viral replication and expression	[168]

IFN: Interferon.

Colorectal cancer: Colorectal cancer (CRC) is a digestive tract disease with high morbidity and mortality. *KRAS* mutations are present in about 50% of CRC patients. Gene-targeted therapy is a promising direction for treating CRC. Currently, the potential G-quadruplex gene targets being studied in CRC include telomere, *c-MYC*, *KRAS* and *c-kit*. For the telomeric G-quadruplex ligands, BRACO-19 leads to rapid growth inhibition of flavopiridol-resistant cells[173]; 3,11-difluoro-6,8,13-trimethyl-8H-quino[4,3,2-kl]-acridinium methosulfate (RHPS4), as well as RHPS4-derivatives, induces DNA damage and antiproliferative activity, stabilizes topoisomerase (TOPO) I, and displays cytotoxic and synergistic anticancer effects with TOPO1 inhibitors in CRC cell lines[174-177]. A series of anthracene derivatives substituted with one or two 4,5-dihydro-1H-imidazol-2-yl-hydrazonic groups stabilize G-quadruplexes to different degrees, inhibit telomerase activity, and mediate cytotoxicity[178]. EMICORON cause telomere damage and block cell proliferation and tumor growth of a patient-derived tumor xenograft model[179,180]. Chromene derivatives, the binders of TERRA G-quadruplexes, have cytotoxic effects in HT29 cells[181]. For the ligands targeting *c-MYC* G-quadruplexes, TMPyP4-mediated stabilization of the mutated G-quadruplex reinstate *c-MYC* G-quadruplex structure and inhibit its gene expression[182]. CX3543 (quarfoxin) exhibit proapoptotic and antiproliferative effects by downregulating *c-MYC* and *CCAT1* expression levels *in vivo* and *in vitro*[183]. CX-5461 (pidnarulex) induces DNA damage and inhibits tumor growth *in vivo* by binding to telomere, *c-MYC* and *c-kit* G-quadruplexes[184]. Dihydrochelerythrine and its derivatives improve the stability of *c-MYC* and *c-kit* G-quadruplexes and inhibit HCT116 cell proliferation[185]. Unsymmetrical bisacridines derivatives stabilize *c-MYC* and *KRAS* G-quadruplexes and induce cytotoxicity, apoptosis and senescence in HCT116 cells [144,186]. Additionally, the ligands 7-carboxylate indolo[3,2-b] quinoline tri-alkylamine derivatives targeting *KRAS* and *HSP90A* promoter G-quadruplexes also show anti-CRC activity by decreasing *KRAS* and *HSP90A* expression levels[187]. 3-[2-(Diethylamino)ethyl]-12-methyl-6-oxo-2,3,6,12-tetrahydro-1Hbenzo[4,5]imidazo [1,2-a] imidazo[1',2':1,6]pyrido[2,3-d]pyrimidin-14-ium bromide inhibits cell proliferation by interacting with *KRAS* G-quadruplexes[188]. In addition to those common cancer-related genes, G-quadruplexes of other functional genes have been shown on anticancer drug research and development. A naphthalene diimides compound T5 was shown to inhibit CRC cell growth by decreasing

Table 4 Overviews of investigations on the effects of small molecule ligands or biomolecules based on G-quadruplex targets in gastric cancer

Ligands/biomolecules	Cell lines	Targeting gene/G-quadruplex	Effects on G-quadruplex	Effects on genes	Anticancer phenotypes	Ref.
Benzo[a]phenoxazines	HGC-27	*c-kit*	Bound with G-quadruplex	Inhibited *c-MYC* transcription	Cytotoxicity	[169]
Quinazolone derivatives	HGC-27	*c-kit*	Stabilized G-quadruplex	Inhibited *c-kit* transcription	Cytotoxicity	[170]
3-(4-(1H-imidazo[4,5-f][1,10]phenanthrolin-2-yl)-3-(ptolyl)-1Hpyrazol-1-yl)-N,N-dimethylpropan-1-amine (13d)	AGS	Telomere, *c-kit*, *BCL-2*	Stabilized G-quadruplex	Induced telomere dysfunction, DNA damage response	Inhibited cell proliferation, migration, and invasion, promoted cell apoptosis and autophagy by blocking the Akt/mTOR pathway	[171]
G-quadruplex antibody	AGS	G-quadruplex	Not detected	Inhibited transcription of *hTERT* and *BCL-2*	Inhibited cell proliferation, migration, invasion and expression of hTERT and BCL-2, induced apoptosis, blocked cell cycle	[172]

BCL-2: B-cell lymphoma 2; hTERT: Human telomerase reverse transcriptase; mTOR: Mammalian/mechanistic target of rapamycin.

RNA polymerase I (Pol I)-mediated transcription by targeting ribosomal DNA G-quadruplexes[189]. Thiosugar naphthalene diimide conjugates exhibit cytotoxic effects by targeting telomere, *c-MYC* and *KRAS* G-quadruplexes[190]. The natural product gallic acid was found to selectively recognize and stabilize G-quadruplexes of rDNA and *c-MYC*, inhibit their associated mRNA expression, and subsequently suppress tumor growth *in vitro* and *in vivo*[191].

The functional protein or oligonucleotide molecules regulating CRC progression based on special G-quadruplexes have also been explored. For example, hnRNPA1 destabilizes *TRA2B* promoter G-quadruplexes and stimulates its mRNA and protein expression levels, which facilitates proliferation of HCT116 cells[192]. Small nuclear ribonucleoprotein polypeptide A consistently modulates translation of *BAG-1* and inhibits HCT116 cell proliferation[193,194]. PPRHs induces *c-MYC* G-quadruplexes and inhibits proliferation of SW480 cells[159].

The LMNAV6 promoter region forms multiple G-quadruplexes, which increases its transcriptional activity, promotes Lamin A/C protein expression, and induces CRC cell proliferation[195]. FLJ39051, a highly expressed long noncoding RNA in CRC, contains G-quadruplexes. It combines with the RNA helicase DHX36 and promotes CRC cell migration [196]. At present, small molecular ligands or proteins targeting LMNAV6 and FLJ39051 G-quadruplexes have not been reported. All details are described in Table 5.

Gastrointestinal stromal tumors: Gastrointestinal stromal tumors (GISTs) are soft tissue sarcomas originating from Cajal interstitial cells. They mostly frequently occur in the stomach, small intestine, and colorectum, but rarely occur in the esophagus, mesentery, omentum and retroperitoneum. GISTs are characterized by aberrant expression of *c-kit* oncogene, CD117 and CD34. The kinase inhibitor imatinib is an effective drug, but resistance to imatinib induced by active-site mutations has become a practical challenge that cannot be fully addressed by second and third-generation inhibitors. There are two G-quadruplex-forming sequences (*c-kit1* positioned between -12 and -33 bp, *c-kit2* positioned between -64 and -83 bp) upstream of the transcription initiation sites of the human *c-kit* promoter. There are also potential binding sites for transcription factors SP1 and AP2, providing an opportunity for *c-kit*-targeted therapy. A series of 6-substituted indenoisoquinolines and N,N′-Bis[2-(pyrrolidin-1-yl)ethylamino]-2,6-bis[2-(pyrrolidin-1-yl)ethylamino]-1,4,5,8-naphthalenetetracarboxylic acid diimide have been confirmed to stabilize *c-kit* promoter G-quadruplexes, mediate cytotoxicity, and downregulate c-kit protein expression levels in GIST cell lines[197,198]. The latter can also stabilize *BCL-2* promoter and mRNA G-quadruplexes to promote cytotoxicity and inhibit BCL-2 protein expression[198]. All details are described in Table 6.

In summary, targeting G-quadruplexes of cancer-related genes in cancer cells and inducing cytotoxic effects by regulating gene transcription may be an effective strategy for preventing and treating various gastrointestinal cancers. An overview of the advancement of potential drugs that target G-quadruplexes in gastrointestinal cancers is shown as Figure 2.

Application of G-quadruplex in the treatment of gastrointestinal cancers

As anticancer agents: In addition to acting as a target of ligands or proteins, G-quadruplexes can serve as anticancer agents. They can recognize specific biomacromolecules with a high degree of specificity, regulate their biological function, and interfere with cancer progression. The G-quadruplex formed by the G-rich sequence T-22AG can competitively bind to nuclear protein, inhibit its combination with *KRAS* G-quadruplex, and thus inhibit gene transcription and proliferation of Panc-1 cells[199]. AS1411 was an earlier discovered G-quadruplex sequence with antiproliferative activity by targeting nucleolin in a variety of cancer cells, such as PC, GC and CRC[200]. The sequences TBA and its derivatives exhibit antiproliferative effects in HCT 116p53$^{-/-}$ cells *via* the G-quadruplex structure; the target of which may be uL3

Table 5 Overviews of investigations on the effects of small molecule ligands or biomolecules based on G-quadruplex targets in colorectal cancer

Ligands/biomolecules	Cell lines	Targeting gene/G-quadruplex	Effects on G-quadruplex	Effects on genes	Anticancer phenotypes	Ref.
BRACO-19	HCT116, Flavopiridol-resistant HCT116	Telomere	Stabilized G-quadruplex	Not detected	Rapid inhibition of cell growth	[173]
RHPS4 (3,11-difluoro-6,8,13-trimethyl-8H-quino[4,3,2-kl]acridinium methosulfate) and RHPS4-derivatives	HT29, HCT116	Telomere	Bound with G-quadruplex	Induced DNA damage	Stabilized TOPO1, cytotoxicity, inhibited cell proliferation, had synergistic anticancer effects with TOPO1 inhibitors	[174-177]
A series of anthracene derivatives substituted with one or two 4,5-dihydro-1H-imidazol-2-yl-hydrazonic groups	LoVo	Telomere	Induced G-quadruplex structures, bound and stabilized G-quadruplex	Induced DNA damage	Cytotoxicity, telomerase inhibition	[178]
EMICORON	HT29, HCT116, A90 colon epithelial tumor cell line	Telomere	Bound with G-quadruplex	Increased telomere damage	Cytotoxicity, inhibited cell proliferation and tumor growth of patient-derived tumor xenograft	[179, 180]
Chromene derivatives	HT29	*Telomere* RNA	Bound with G-quadruplex	Not detected	Cytotoxicity	[181]
TMPyP4	SW480, SW620	*c-MYC*	Stabilized the mutated G-quadruplex structure	Inhibited *c-MYC* expression	Silenced *c-MYC* expression	[182]
CX-3543 (quarfloxin)	HT29	*c-MYC*	Not detected	Inhibited *c-MYC* expression	Reduced *CCAT1* expression, promoted cell apoptosis, inhibited cell proliferation and tumor growth of HT29 xenografts	[183]
CX-5461 (pidnarulex)	HT-29, DLD-1, CT26	Telomere, *c-MYC*, *c-kit*	Bound with G-quadruplex	Caused DNA damage	Inhibited tumor growth of CT26 xenografts	[184]
Dihydrochelerythrine and its derivatives	HCT116	*c-MYC*, *c-kit*	Stabilized G-quadruplex	Not detected	Inhibited cell proliferation	[185]
Unsymmetrical bisacridines derivatives	HCT116	*c-MYC*, *KRAS*	Bound and stabilized G-quadruplex	Not detected	Induced cytotoxicity, apoptosis and senescence	[144, 186]
7-carboxylate indolo[3,2-b] quinoline tri-alkylamine derivatives	HCT116, SW620	*KRAS*, *HSP90A*	Stabilized G-quadruplex	Decreased *KRAS* and *HSP90* mRNA expression, and *KRAS* transcription	Inhibited cell proliferation and protein expression of KRAS and HSP90A, promoted apoptosis	[187]
	HCT116	*KRAS*	Bound and stabilized G-quadruplex	Decreased *KRAS* mRNA expression	Inhibited cell proliferation	[188]
Naphthalene diimides compound T5	Colorectal cancer cell	rDNA	Had high affinity with G-quadruplex	Impaired RNA Pol I elongation, inhibited Pol I transcription	Inhibited cell growth by inducing a rapid inhibition of Pol I transcription, nucleolus disruption, proteasome-dependent Pol I catalytic subunit A degradation and autophagy	[189]
Thiosugar naphthalene diimide conjugates	HT29	Telomere, *c-MYC*, *KRAS*	Bound and stabilized G-quadruplex	Not detected	Cytotoxicity	[190]
Gallic acid		rDNA, *c-MYC*	Bound and stabilized G-quadruplex	Inhibited expression of rDNA and *c-MYC*	Cytotoxicity, inhibited tumor growth of SW480 xenografts	[191]
HnRNPA1	HCT116	*TRA2B* promoter	Destabilized G-quadruplex	Stimulated *TRA2B* transcription	Promoted cell proliferation and expression of TRA2B	[192]
SNRPA	HCT116	*BAG-1* mRNA	Bound with G-quadruplex	Inhibited translation of *BAG-*	Inhibited cell proliferation	[193, 194]

				1		
PPRHs	SW480	*c-MYC*	Bound and stabilized G-quadruplex	Inhibited transcription of *c-MYC*	Inhibited cell proliferation	[159]

PPRHs: Polypurine reverse Hoogsteen hairpins; TOPO: Topoisomerase; KRAS: Kirsten rat sarcoma viral oncogene homologue; HSP90: Heat shock protein 90.

Table 6 Overview of investigations on the effects of small molecule ligands based on G-quadruplex targets in gastrointestinal stromal tumor

Ligands/biomolecules	Cell lines	Targeting gene/G-quadruplex	Effects on G-quadruplex	Effects on genes	Anticancer phenotypes	Ref.
6-Substituted indenoisoquinolines	GIST882	*c-kit*	Stabilized G-quadruplex	Inhibited *c-kit* transcription	Cytotoxicity, inhibited expression of c-kit protein	[196]
N,N′-Bis(2-(pyrrolidin-1-yl)ethylamino)-2,6-bis(2-(pyrrolidin-1-yl)ethylamino)-1,4,5,8-naphthalen-etetracarboxylic acid diimide	GIST882, GIST48, GIST62	*c-kit*, *BCL-2*, *BCL-2* mRNA	Stabilized G-quadruplex	Not detected	Cytotoxicity, inhibited expression of c-kit and BCL-2 proteins	[197, 198]

BCL-2: B-cell lymphoma 2.

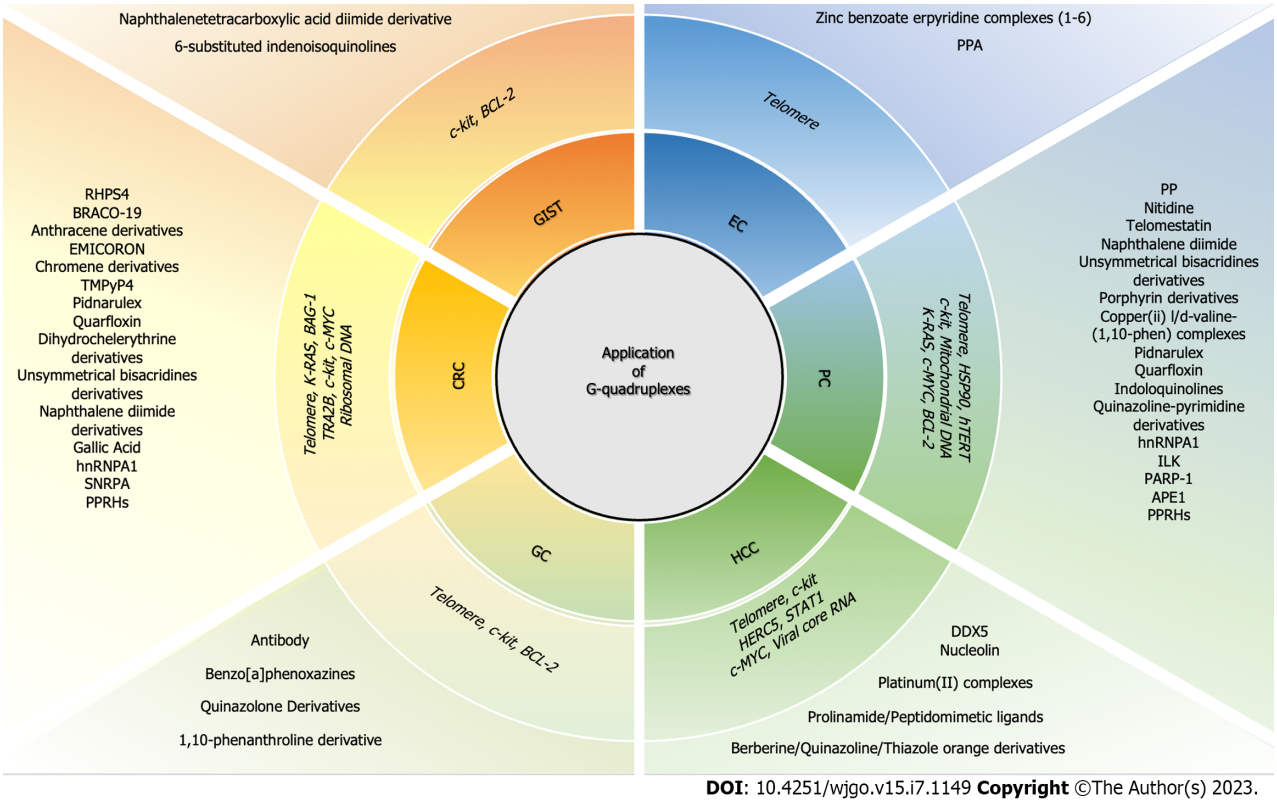

DOI: 10.4251/wjgo.v15.i7.1149

Figure 2 G-quadruplex targets and the targeting small molecule ligands and biomolecules in six gastrointestinal cancer types. EC: Esophageal cancer; PC: Pancreatic cancer; HCC: Hepatocellular carcinoma; GC: Gastric cancer; CRC: Colorectal cancer, GIST: Gastrointestinal stromal tumor; PPA: 2,6-bis[3-(N-Piperidino) propionamido] anthrace-ne-9,10-dione; PP: Antihelminthic pyrvinium pamoate; ILK: Integrinlinked kinase; PARP1: Poly (ADP-ribose) polymerase 1; APE1: Apurinic/apyrimidinic endonuclease 1; PPRHs: Polypurine reverse Hoogsteen hairpins; DDX5: Dead box polypeptide 5; RHPS4: (3,11-difluoro-6,8,13-trimethyl-8H-quino[4,3,2-kl]acridinium methosulfate) and RHPS4-derivatives; SNRPA: Nuclear ribonucleoprotein polypeptide A; BCL-2: B-cell lymphoma 2; TRA2B: Transformer-2 protein homolog beta; KRAS: Kirsten rat sarcoma viral oncogene homologue; HSP90: Heat shock protein 90; hTERT: Human telomerase reverse transcriptase.

[201]. Similarly, the G-quadruplex sequences INT-B (T30175) and its derivatives, along with d(GGGT)$_4$ and its analogs also inhibit HCT 116p53$^{-/-}$ cell proliferation, but the specific target remains unclear[202,203]. All details are described in Table 7.

As an assistant in anticancer agents: G-quadruplex sequences mainly have two functions. In the research and development of anticancer drugs, G-quadruplex sequences were often used as the carriers of drugs or targeted agents in delivery systems to improve the delivery efficiency and targeting of anticancer drugs[204]. The carried molecules have included such chemotherapeutic drugs as paclitaxel, docetaxel, doxorubicin, triptolide, epirubicin, gemcitabine, thymoquinone, TMPyP4 and 5-fluorouracil, targeting cancers like HCC, PC and CRC[205,206]. As an important component of anticancer agents, G-quadruplex sequences can also help produce or improve anticancer efficacy. For example, the G-quadruplex dependent intracellular self-assembly device can continuously produce ROS to enhance antitumor effects of 5-aminolevulinic-acid in EC cells[207]. The parallel G-quadruplex configurations boost the cellular uptake of 5-fluoro-20-deoxyuridine oligomers, which stimulate cytotoxicity in 5-fluorouracil resistant CRC cells[208].

CHALLENGES OF ANTICANCER STRATEGIES BASED ON G-QUADRUPLEX TARGETS

Although many small molecular ligands or biomolecules targeting G-quadruplexes have been found to have anticancer activity *in vitro* and *in vivo*, it is still uncertain whether they can achieve such effects in humans. Unfortunately, many promising drugs have not passed clinical trials in the past, as biological systems are complex and many internal and external factors can affect drug effectiveness. The application of G-quadruplex targets in the treatment of gastrointestinal cancers will also face some challenges.

Dual role of G-quadruplexes in transcriptional and translational regulations

At first, G-quadruplexes were simply described as an obstacle to the transcription of cancer-related genes, leading to increased efforts to design and develop small molecule ligands as anticancer drugs targeting G-quadruplex structure, which attracted widespread attention[209]. However, evidence has shown that G-quadruplexes can regulate gene transcription at multiple levels, including through epigenetic modification and chromatin structure[210]. Because of the complexity of gene expression regulation, G-quadruplexes can play dual roles in gene transcription: Blocking polymerase to inhibit gene transcription; and recruiting transcription factors to promote gene transcription[117]. Under certain conditions, G-quadruplexes can trigger opposing effects on the same target[211]. The regulation of translation by RNA G-quadruplexes also has two sides. G-quadruplexes can prevent ribosome entry under conditions of cap-dependent translation, but can also prompt ribosome entry under conditions of cap-independent translation[212]. With both DNA G-quadruplex-mediated regulation of transcription and RNA G-quadruplex-mediated regulation of translation, the final effects depend on the specific environment. Further research is required to investigate if ligands targeting G-quadruplexes in the tumor microenvironment can result in the predicted anticancer effects and if they can affect normal cells.

Biological factors affecting G-quadruplex formation

Chromatin and DNA modifications: The formation of G-quadruplexes *in vivo* is the result of the comprehensive action of various factors within its cell environment, including chromatin. Although a previous study indicated that transcriptional activation increased the instability of potential G-quadruplex-forming sequences, ChIP-seq research confirmed that promoter G-quadruplex formation preceded transcription rather than depending on transcription. Additionally, chromatin compaction led to a loss of RNA polymerase II (Pol II) and promoter G-quadruplexes[213]. Different types of DNA modifications can directly influence the formation of G-quadruplexes. For example, the stability and kinetic associations of G-quadruplex structures were increased by cytosine methylation (in addition with 5mC), which did not directly act on the Hoogsteen bonding[214]. Guanine bases in nucleic acids can be oxidized to 8-oxo-7,8-dihydroguanine (8-oxoguanine), which can destroy the G-quadruplex structure in cancers[215]. Oncogene promoter regions are prone to hypomethylation, while those of tumor suppressor genes are prone to hypermethylation. These factors may indirectly impact the formation of G-quadruplexes and the resulting regulatory effects.

G-quadruplex-binding proteins: G-quadruplexes play various regulatory functions by interacting with proteins. G-quadruplex-binding proteins indirectly participate in biological processes such as DNA replication, gene transcription and telomere maintenance *via* G-quadruplexes. The influence of binding proteins on the formation of G-quadruplexes mainly involves two aspects: Unfolding G-quadruplex structures and stabilizing G-quadruplex structures. Helicases are important binding proteins that can unwind G-quadruplexes and interfere with their regulatory functions. Such proteins are mainly classified as canonical helicases, including the RecQ-like and DEAD box or DEAH box helicase families. *In vitro*, these three helicases have been reported to bind to the 3′ tail of the DNA substrate and subsequently repetitively catalyze 3′-5′ unfolding of G-quadruplexes in an ATP-independent manner[216]. In addition, nonhelicase binding proteins, such as G-rich RNA sequence binding factor 1 and cellular nucleic acid-binding protein, can sequester the unfolded G-quadruplex form[216-218]. In contrast, there are also binding proteins that can support the G-quadruplex structure, such as nucleolin and RNA-binding protein 4[168,219]. Additionally, RNA-binding proteins are important influencing factors of RNA G-quadruplexes. G-quadruplex-binding proteins are also potential targets for cancer treatment because their effects contribute to G-quadruplex functions[220]. Significantly, the specific effects of these binding proteins on the targeted G-quadruplexes depend on their specific intracellular environments.

Table 7 G-quadruplexes as anticancer agents

Tumor model	G-quadruplex name	Sequence (5'-3')	Protein target	Cells	Anticancer phenotype	Ref.
Pancreatic cancer	*T-22AG*	GGAGGGGGAGAAGGGAGAAGGG	Nuclear protein	Panc-1	Reduces cell growth	[199]
	AS1411	GGTGGTGGTGGTTGTGGTGGTGGTGG	Nucleolin	PANC-1	Inhibited cell proliferation	[200]
Gastric cancer	*AS1411*	GGTGGTGGTGGTTGTGGTGGTGGTGG	Nucleolin	KATOIIIe, HGC27	Inhibited cell proliferation	[200]
Colorectal cancer	*AS1411*	GGTGGTGGTGGTTGTGGTGGTGGTGG	Nucleolin	HCC 2998, HT-29, KM12, HCT-116, SW620, HCT-15, LS174T	Inhibited cell proliferation	[200]
	TBA	GGTTGGTGTGGTTGG	uL3	HCT 116p53$^{-/-}$	Impaired ribosomal RNA processing, leading to the accumulation of pre-ribosomal RNAs, arrested cells in the G2/M phase and induced early apoptosis	[201]
	L-TBA	GGTTGGTGTGGTTGG				
	LQ1	GGTTGGTGTGGTTGG				
	LQ2	GGTTGGGTGTGGTTGG				
	LQ3	GGTTGGGTGTGGTTGG				
	INT-B (T30175)	GTGGTGGGTGGGTGGGT	Not detected	HCT 116p53$^{-/-}$	Inhibited cell proliferation	[202]
	INT-BS2	GSGGTGGGTGGGTGGGT				
	INT-BS5	GTGGSGGGTGGGTGGGT				
	INT-BS9	GTGGTGGGSGGGTGGGT				
	INT-BS13	GTGGTGGGTGGGSGGGT				
	INT-BS17	GTGGTGGGTGGGTGGGS				
	TT-INT-B	TTGTGGTGGGTGGGTGGGT				
	Qnat	GGGTGGGTGGGTGGGT	Not detected	HCT 116p53$^{-/-}$	Inhibited cell proliferation	[203]
	QS4	GGGSGGGTGGGTGGGT				
	QS8	GGGTGGGSGGGTGGGT				
	QS12	GGGTGGGTGGGSGGGT				
	QS16	GGGTGGGTGGGTGGGS				

Inflammatory cytokines: Inflammatory cytokines produced during inflammation reactions can support the production of ROS and nitrogen species (RONS), which may cause DNA damage. RONS can remove an electron from DNA bases and generate an electron hole, then transfer it to a base with a lower ionization potential. Guanine has the lowest ionization energy among the four DNA bases, making it particularly vulnerable to oxidative damage[221]. The most significant oxidative damage involves hydroxyl free radicals interacting with guanine to induce 8-oxoguanine, which can pair with adenine bases, and induce a G>T conversion during replication[3]. The degree of DNA damage depends on the position of the oxidized guanines and G-quartets.

Lack of selectivity of G-quadruplex ligands

At present, the design of small molecules is mainly based on the specific G-quadruplex configurations. As mentioned previously, there are three basic configurations for G-quadruplexes, and different nucleic acid sequences may form the same G-quadruplex configuration. Therefore, one small molecule ligand may have similar binding stabilities with the G-quadruplex structures of different genes, which may reduce the targeting of gene therapy. For example, berberine can combine with the parallel structures of the *KRAS* and *c-MYC* promoters[6,16]. This inhibits *KRAS* and *c-MYC* expression and induces cytotoxicity in various cancer cells that express these oncogenes. Further work is needed to determine if this drug can cause negative effects in normal cells.

PROSPECTS

G-quadruplexes are widely distributed throughout the human genome and are key aspects of gene transcription and translation regulation. Therefore, G-quadruplexes can be the drug targets against multiple human diseases, such as viral infection[222], bacterial infection[223], muscular atrophy[60] and cancer, especially gastrointestinal cancers. However, there are some uncertainties with this application that should be explored further. Firstly, G-quadruplex-mediated regulation of transcription and translation in gastrointestinal tissues require more investigation, especially during tumorigenesis. The development of high-throughput sequencing and single nucleotide polymorphism detection may provide new opportunities to establish specific gene therapy strategies for gastrointestinal cancers based on G-quadruplexes. Secondly, the transcriptional activation function of G-quadruplexes is needed in some normal physiological processes, raising the concern that anticancer therapies targeting G-quadruplexes may interfere with normal cellular activities. Fully understanding the roles of G-quadruplexes in different biological processes, especially in various diseases, is helpful for addressing this challenge. Thirdly, G-quadruplexes can both inhibit and promote gene transcription and translation, with the final effects depending on the intracellular environment. This ultimately directly affects the treatment outcome. With the progress of molecular diagnosis technology, it may be necessary to specifically evaluate the patient's internal environment before treatment. Fourthly, small molecule ligands and biomolecules may simultaneously target genes with the same G-quadruplex configurations, resulting in a need for improved selectivity or targeting. Fifthly, the formation of a G-quadruplex is affected by a variety of biological factors. Whether these factors can interfere with a G-quadruplex-targeted therapy requires further study. Sixthly, clinical trials are needed to verify the efficacy of such small molecule ligands and biomolecules.

CONCLUSION

In addition to telomeres, G-quadruplexes are widely present in the promoter regions of oncogenes as well as cancerous genes, and can regulate various biological processes, especially gene transcription and translation, laying a good foundation for G-quadruplexes to become anticancer targets from the perspective of gene regulation. Multiple genes regulating EC, PC, HCC, GC, CRC and GIST have been found to contain G-quadruplex structures, including the key regulatory gene *KRAS* for PC and CRC, and *c-kit* for GC and GIST. Many small molecular ligands or biomolecules based on the G-quadruplex of these genes have been designed, synthesized, or discovered, and preclinical studies have shown that these molecules have good anticancer effects. Therefore, G-quadruplexes as targets against gastrointestinal cancers have broad application prospects. However, due to the diversity of G-quadruplex functions and the complexity of the biological internal environment, the application of G-quadruplex as a target of anticancer drugs still faces some challenges, which requires further exploration and research. We hope this work will provide references for anticancer strategies based on G-quadruplex targets in gastrointestinal cancers.

FOOTNOTES

Author contributions: Wen LN conceived the study and performed the manuscript review; Han ZQ implemented document retrieval and manuscript editing; Wen LN and Han ZQ drafted the original manuscript.

Supported by the National Natural Science Foundation of China, No. 81803773.

Conflict-of-interest statement: All the authors report no relevant conflicts of interest for this article.

Country/Territory of origin: China

ORCID number: Li-Na Wen 0000-0001-6507-2978.

S-Editor: Wang JJ
L-Editor: A
P-Editor: Zhang XD

REFERENCES

1 **Hanahan D**. Hallmarks of Cancer: New Dimensions. *Cancer Discov* 2022; **12**: 31-46 [PMID: 35022204 DOI: 10.1158/2159-8290.CD-21-1059]
2 **Hanahan D**, Weinberg RA. Hallmarks of cancer: the next generation. *Cell* 2011; **144**: 646-674 [PMID: 21376230 DOI:

10.1016/j.cell.2011.02.013]
3 **Stein M**, Eckert KA. Impact of G-Quadruplexes and Chronic Inflammation on Genome Instability: Additive Effects during Carcinogenesis. *Genes (Basel)* 2021; **12** [PMID: 34828385 DOI: 10.3390/genes12111779]
4 **GELLERT M**, LIPSETT MN, DAVIES DR. Helix formation by guanylic acid. *Proc Natl Acad Sci U S A* 1962; **48**: 2013-2018 [PMID: 13947099 DOI: 10.1073/pnas.48.12.2013]
5 **Tan J**, Lan L. The DNA secondary structures at telomeres and genome instability. *Cell Biosci* 2020; **10**: 47 [PMID: 32257105 DOI: 10.1186/s13578-020-00409-z]
6 **Wang KB**, Liu Y, Li J, Xiao C, Wang Y, Gu W, Li Y, Xia YZ, Yan T, Yang MH, Kong LY. Structural insight into the bulge-containing KRAS oncogene promoter G-quadruplex bound to berberine and coptisine. *Nat Commun* 2022; **13**: 6016 [PMID: 36224201 DOI: 10.1038/s41467-022-33761-4]
7 **Monsen RC**, DeLeeuw LW, Dean WL, Gray RD, Chakravarthy S, Hopkins JB, Chaires JB, Trent JO. Long promoter sequences form higher-order G-quadruplexes: an integrative structural biology study of c-Myc, k-Ras and c-Kit promoter sequences. *Nucleic Acids Res* 2022; **50**: 4127-4147 [PMID: 35325198 DOI: 10.1093/nar/gkac182]
8 **Ogloblina AM**, Bannikova VA, Khristich AN, Oretskaya TS, Yakubovskaya MG, Dolinnaya NG. Parallel G-Quadruplexes Formed by Guanine-Rich Microsatellite Repeats Inhibit Human Topoisomerase I. *Biochemistry (Mosc)* 2015; **80**: 1026-1038 [PMID: 26547071 DOI: 10.1134/S0006297915080088]
9 **Cheong C**, Moore PB. Solution structure of an unusually stable RNA tetraplex containing G- and U-quartet structures. *Biochemistry* 1992; **31**: 8406-8414 [PMID: 1382577 DOI: 10.1021/bi00151a003]
10 **Agarwala P**, Pandey S, Ekka MK, Chakraborty D, Maiti S. Combinatorial role of two G-quadruplexes in 5' UTR of transforming growth factor β2 (TGFβ2). *Biochim Biophys Acta Gen Subj* 2019; **1863**: 129416 [PMID: 31425729 DOI: 10.1016/j.bbagen.2019.129416]
11 **Scionti F**, Juli G, Rocca R, Polerà N, Nadai M, Grillone K, Caracciolo D, Riillo C, Altomare E, Ascrizzi S, Caparello B, Cerra M, Arbitrio M, Richter SN, Artese A, Alcaro S, Tagliaferri P, Tassone P, Di Martino MT. TERRA G-quadruplex stabilization as a new therapeutic strategy for multiple myeloma. *J Exp Clin Cancer Res* 2023; **42**: 71 [PMID: 36967378 DOI: 10.1186/s13046-023-02633-0]
12 **Khan S**, Singh A, Nain N, Kukreti S. Alkali cation-mediated topology displayed by an exonic G-rich sequence of TRPA1 gene. *J Biomol Struct Dyn* 2022; 1-12 [PMID: 36458452 DOI: 10.1080/07391102.2022.2150686]
13 **Sugimoto W**, Kinoshita N, Nakata M, Ohyama T, Tateishi-Karimata H, Nishikata T, Sugimoto N, Miyoshi D, Kawauchi K. Intramolecular G-quadruplex-hairpin loop structure competition of a GC-rich exon region in the TMPRSS2 gene. *Chem Commun (Camb)* 2021; **58**: 48-51 [PMID: 34811561 DOI: 10.1039/d1cc05523b]
14 **Ghafouri-Fard S**, Abak A, Baniahmad A, Hussen BM, Taheri M, Jamali E, Dinger ME. Interaction between non-coding RNAs, mRNAs and G-quadruplexes. *Cancer Cell Int* 2022; **22**: 171 [PMID: 35488342 DOI: 10.1186/s12935-022-02601-2]
15 **Liu W**, Zhu BC, Liu LY, Xia XY, Mao ZW. G-quadruplex structural transition driven by a platinum compound. *Nucleic Acids Res* 2022; **50**: 7816-7828 [PMID: 35766415 DOI: 10.1093/nar/gkac572]
16 **Dickerhoff J**, Brundridge N, McLuckey SA, Yang D. Berberine Molecular Recognition of the Parallel MYC G-Quadruplex in Solution. *J Med Chem* 2021; **64**: 16205-16212 [PMID: 34677968 DOI: 10.1021/acs.jmedchem.1c01508]
17 **Beseiso D**, Chen EV, McCarthy SE, Martin KN, Gallagher EP, Miao J, Yatsunyk LA. The first crystal structures of hybrid and parallel four-tetrad intramolecular G-quadruplexes. *Nucleic Acids Res* 2022; **50**: 2959-2972 [PMID: 35212369 DOI: 10.1093/nar/gkac091]
18 **Criscuolo A**, Napolitano E, Riccardi C, Musumeci D, Platella C, Montesarchio D. Insights into the Small Molecule Targeting of Biologically Relevant G-Quadruplexes: An Overview of NMR and Crystal Structures. *Pharmaceutics* 2022; **14** [PMID: 36365179 DOI: 10.3390/pharmaceutics14112361]
19 **Kosiol N**, Juranek S, Brossart P, Heine A, Paeschke K. G-quadruplexes: a promising target for cancer therapy. *Mol Cancer* 2021; **20**: 40 [PMID: 33632214 DOI: 10.1186/s12943-021-01328-4]
20 **Mellor C**, Perez C, Sale JE. Creation and resolution of non-B-DNA structural impediments during replication. *Crit Rev Biochem Mol Biol* 2022; **57**: 412-442 [PMID: 36170051 DOI: 10.1080/10409238.2022.2121803]
21 **Bryan TM**. Mechanisms of DNA Replication and Repair: Insights from the Study of G-Quadruplexes. *Molecules* 2019; **24** [PMID: 31546714 DOI: 10.3390/molecules24193439]
22 **Linke R**, Limmer M, Juranek SA, Heine A, Paeschke K. The Relevance of G-Quadruplexes for DNA Repair. *Int J Mol Sci* 2021; **22** [PMID: 34830478 DOI: 10.3390/ijms222212599]
23 **Jansson-Fritzberg LI**, Sousa CI, Smallegan MJ, Song JJ, Gooding AR, Kasinath V, Rinn JL, Cech TR. DNMT1 inhibition by pUG-fold quadruplex RNA. *RNA* 2023; **29**: 346-360 [PMID: 36574982 DOI: 10.1261/rna.079479.122]
24 **Ogasawara S**. Transcription Driven by Reversible Photocontrol of Hyperstable G-Quadruplexes. *ACS Synth Biol* 2018; **7**: 2507-2513 [PMID: 30350586 DOI: 10.1021/acssynbio.8b00216]
25 **Wu CG**, Spies M. G-quadruplex recognition and remodeling by the FANCJ helicase. *Nucleic Acids Res* 2016; **44**: 8742-8753 [PMID: 27342280 DOI: 10.1093/nar/gkw574]
26 **Huppert JL**, Balasubramanian S. Prevalence of quadruplexes in the human genome. *Nucleic Acids Res* 2005; **33**: 2908-2916 [PMID: 15914667 DOI: 10.1093/nar/gki609]
27 **Asamitsu S**, Takeuchi M, Ikenoshita S, Imai Y, Kashiwagi H, Shioda N. Perspectives for Applying G-Quadruplex Structures in Neurobiology and Neuropharmacology. *Int J Mol Sci* 2019; **20** [PMID: 31200506 DOI: 10.3390/ijms20122884]
28 **Schaffitzel C**, Berger I, Postberg J, Hanes J, Lipps HJ, Plückthun A. In vitro generated antibodies specific for telomeric guanine-quadruplex DNA react with Stylonychia lemnae macronuclei. *Proc Natl Acad Sci U S A* 2001; **98**: 8572-8577 [PMID: 11438689 DOI: 10.1073/pnas.141229498]
29 **Oganesian L**, Bryan TM. Physiological relevance of telomeric G-quadruplex formation: a potential drug target. *Bioessays* 2007; **29**: 155-165 [PMID: 17226803 DOI: 10.1002/bies.20523]
30 **Biffi G**, Tannahill D, McCafferty J, Balasubramanian S. Quantitative visualization of DNA G-quadruplex structures in human cells. *Nat Chem* 2013; **5**: 182-186 [PMID: 23422559 DOI: 10.1038/nchem.1548]
31 **Di Antonio M**, Ponjavic A, Radzevičius A, Ranasinghe RT, Catalano M, Zhang X, Shen J, Needham LM, Lee SF, Klenerman D, Balasubramanian S. Single-molecule visualization of DNA G-quadruplex formation in live cells. *Nat Chem* 2020; **12**: 832-837 [PMID: 32690897 DOI: 10.1038/s41557-020-0506-4]
32 **Henderson A**, Wu Y, Huang YC, Chavez EA, Platt J, Johnson FB, Brosh RM Jr, Sen D, Lansdorp PM. Detection of G-quadruplex DNA in mammalian cells. *Nucleic Acids Res* 2017; **45**: 6252 [PMID: 28449109 DOI: 10.1093/nar/gkx300]

33 **Zhang S**, Sun H, Chen H, Li Q, Guan A, Wang L, Shi Y, Xu S, Liu M, Tang Y. Direct visualization of nucleolar G-quadruplexes in live cells by using a fluorescent light-up probe. *Biochim Biophys Acta Gen Subj* 2018; **1862**: 1101-1106 [PMID: 29410183 DOI: 10.1016/j.bbagen.2018.01.022]

34 **Todd AK**, Johnston M, Neidle S. Highly prevalent putative quadruplex sequence motifs in human DNA. *Nucleic Acids Res* 2005; **33**: 2901-2907 [PMID: 15914666 DOI: 10.1093/nar/gki553]

35 **Hänsel-Hertsch R**, Spiegel J, Marsico G, Tannahill D, Balasubramanian S. Genome-wide mapping of endogenous G-quadruplex DNA structures by chromatin immunoprecipitation and high-throughput sequencing. *Nat Protoc* 2018; **13**: 551-564 [PMID: 29470465 DOI: 10.1038/nprot.2017.150]

36 **Chambers VS**, Marsico G, Boutell JM, Di Antonio M, Smith GP, Balasubramanian S. High-throughput sequencing of DNA G-quadruplex structures in the human genome. *Nat Biotechnol* 2015; **33**: 877-881 [PMID: 26192317 DOI: 10.1038/nbt.3295]

37 **Henderson E**, Hardin CC, Walk SK, Tinoco I Jr, Blackburn EH. Telomeric DNA oligonucleotides form novel intramolecular structures containing guanine-guanine base pairs. *Cell* 1987; **51**: 899-908 [PMID: 3690664 DOI: 10.1016/0092-8674(87)90577-0]

38 **Rhodes D**, Lipps HJ. G-quadruplexes and their regulatory roles in biology. *Nucleic Acids Res* 2015; **43**: 8627-8637 [PMID: 26350216 DOI: 10.1093/nar/gkv862]

39 **Moye AL**, Porter KC, Cohen SB, Phan T, Zyner KG, Sasaki N, Lovrecz GO, Beck JL, Bryan TM. Telomeric G-quadruplexes are a substrate and site of localization for human telomerase. *Nat Commun* 2015; **6**: 7643 [PMID: 26158869 DOI: 10.1038/ncomms8643]

40 **Spiegel J**, Adhikari S, Balasubramanian S. The Structure and Function of DNA G-Quadruplexes. *Trends Chem* 2020; **2**: 123-136 [PMID: 32923997 DOI: 10.1016/j.trechm.2019.07.002]

41 **Huppert JL**, Balasubramanian S. G-quadruplexes in promoters throughout the human genome. *Nucleic Acids Res* 2007; **35**: 406-413 [PMID: 17169996 DOI: 10.1093/nar/gkl1057]

42 **Marsico G**, Chambers VS, Sahakyan AB, McCauley P, Boutell JM, Antonio MD, Balasubramanian S. Whole genome experimental maps of DNA G-quadruplexes in multiple species. *Nucleic Acids Res* 2019; **47**: 3862-3874 [PMID: 30892612 DOI: 10.1093/nar/gkz179]

43 **Marquevielle J**, Robert C, Lagrabette O, Wahid M, Bourdoncle A, Xodo LE, Mergny JL, Salgado GF. Structure of two G-quadruplexes in equilibrium in the KRAS promoter. *Nucleic Acids Res* 2020; **48**: 9336-9345 [PMID: 32432667 DOI: 10.1093/nar/gkaa387]

44 **Cogoi S**, Xodo LE. G4 DNA in ras genes and its potential in cancer therapy. *Biochim Biophys Acta* 2016; **1859**: 663-674 [PMID: 26855080 DOI: 10.1016/j.bbagrm.2016.02.002]

45 **Li ML**, Yuan JM, Yuan H, Wu BH, Huang SL, Li QJ, Ou TM, Wang HG, Tan JH, Li D, Chen SB, Huang ZS. Design, Synthesis, and Evaluation of New Sugar-Substituted Imidazole Derivatives as Selective c-MYC Transcription Repressors Targeting the Promoter G-Quadruplex. *J Med Chem* 2022; **65**: 12675-12700 [PMID: 36121464 DOI: 10.1021/acs.jmedchem.2c00467]

46 **Yang Y**, Yang Y, Wang S, Li H, Chen DDY. Detecting the formation of human c-KIT oncogene promoter G-Quadruplex by Taylor dispersion analysis. *Talanta* 2021; **233**: 122533 [PMID: 34215036 DOI: 10.1016/j.talanta.2021.122533]

47 **Tong X**, Lan W, Zhang X, Wu H, Liu M, Cao C. Solution structure of all parallel G-quadruplex formed by the oncogene RET promoter sequence. *Nucleic Acids Res* 2011; **39**: 6753-6763 [PMID: 21540209 DOI: 10.1093/nar/gkr233]

48 **Robert C**, Marquevielle J, Salgado GF. The Promoter Region of the Proto-Oncogene MST1R Contains the Main Features of G-Quadruplexes Formation. *Int J Mol Sci* 2022; **23** [PMID: 36361696 DOI: 10.3390/ijms232112905]

49 **Dai J**, Chen D, Jones RA, Hurley LH, Yang D. NMR solution structure of the major G-quadruplex structure formed in the human BCL2 promoter region. *Nucleic Acids Res* 2006; **34**: 5133-5144 [PMID: 16998187 DOI: 10.1093/nar/gkl610]

50 **Lombardo CM**, Welsh SJ, Strauss SJ, Dale AG, Todd AK, Nanjunda R, Wilson WD, Neidle S. A novel series of G-quadruplex ligands with selectivity for HIF-expressing osteosarcoma and renal cancer cell lines. *Bioorg Med Chem Lett* 2012; **22**: 5984-5988 [PMID: 22889802 DOI: 10.1016/j.bmcl.2012.07.009]

51 **Stein M**, Hile SE, Weissensteiner MH, Lee M, Zhang S, Kejnovský E, Kejnovská I, Makova KD, Eckert KA. Variation in G-quadruplex sequence and topology differentially impacts human DNA polymerase fidelity. *DNA Repair (Amst)* 2022; **119**: 103402 [PMID: 36116264 DOI: 10.1016/j.dnarep.2022.103402]

52 **Qin Y**, Rezler EM, Gokhale V, Sun D, Hurley LH. Characterization of the G-quadruplexes in the duplex nuclease hypersensitive element of the PDGF-A promoter and modulation of PDGF-A promoter activity by TMPyP4. *Nucleic Acids Res* 2007; **35**: 7698-7713 [PMID: 17984069 DOI: 10.1093/nar/gkm538]

53 **Chen JN**, He YD, Liang HT, Cai TT, Chen Q, Zheng KW. Regulation of PDGFR-β gene expression by targeting the G-vacancy bearing G-quadruplex in promoter. *Nucleic Acids Res* 2021; **49**: 12634-12643 [PMID: 34850916 DOI: 10.1093/nar/gkab1154]

54 **Monsen RC**, DeLeeuw L, Dean WL, Gray RD, Sabo TM, Chakravarthy S, Chaires JB, Trent JO. The hTERT core promoter forms three parallel G-quadruplexes. *Nucleic Acids Res* 2020; **48**: 5720-5734 [PMID: 32083666 DOI: 10.1093/nar/gkaa107]

55 **Waller ZA**, Howell LA, Macdonald CJ, O'Connell MA, Searcey M. Identification and characterisation of a G-quadruplex forming sequence in the promoter region of nuclear factor (erythroid-derived 2)-like 2 (Nrf2). *Biochem Biophys Res Commun* 2014; **447**: 128-132 [PMID: 24699415 DOI: 10.1016/j.bbrc.2014.03.117]

56 **Navarro A**, Benabou S, Eritja R, Gargallo R. Influence of pH and a porphyrin ligand on the stability of a G-quadruplex structure within a duplex segment near the promoter region of the SMARCA4 gene. *Int J Biol Macromol* 2020; **159**: 383-393 [PMID: 32416304 DOI: 10.1016/j.ijbiomac.2020.05.062]

57 **Joshi S**, Singh A, Kukreti S. Porphyrin induced structural destabilization of a parallel DNA G-quadruplex in human MRP1 gene promoter. *J Mol Recognit* 2022; **35**: e2950 [PMID: 34990028 DOI: 10.1002/jmr.2950]

58 **Singh A**, Joshi S, Kukreti S. Cationic porphyrins as destabilizer of a G-quadruplex located at the promoter of human MYH7 β gene. *J Biomol Struct Dyn* 2020; **38**: 4801-4816 [PMID: 31809672 DOI: 10.1080/07391102.2019.1689850]

59 **Borel C**, Migliavacca E, Letourneau A, Gagnebin M, Béna F, Sailani MR, Dermitzakis ET, Sharp AJ, Antonarakis SE. Tandem repeat sequence variation as causative cis-eQTLs for protein-coding gene expression variation: the case of CSTB. *Hum Mutat* 2012; **33**: 1302-1309 [PMID: 22573514 DOI: 10.1002/humu.22115]

60 **Geng Y**, Liu C, Cai Q, Luo Z, Miao H, Shi X, Xu N, Fung CP, Choy TT, Yan B, Li N, Qian P, Zhou B, Zhu G. Crystal structure of parallel G-quadruplex formed by the two-repeat ALS- and FTD-related GGGGCC sequence. *Nucleic Acids Res* 2021; **49**: 5881-5890 [PMID: 34048588 DOI: 10.1093/nar/gkab302]

61 **Kobayashi H**, Abe K, Matsuura T, Ikeda Y, Hitomi T, Akechi Y, Habu T, Liu W, Okuda H, Koizumi A. Expansion of intronic GGCCTG hexanucleotide repeat in NOP56 causes SCA36, a type of spinocerebellar ataxia accompanied by motor neuron involvement. *Am J Hum Genet* 2011; **89**: 121-130 [PMID: 21683323 DOI: 10.1016/j.ajhg.2011.05.015]

62 **Mead S**, Webb TE, Campbell TA, Beck J, Linehan JM, Rutherfoord S, Joiner S, Wadsworth JD, Heckmann J, Wroe S, Doey L, King A, Collinge J. Inherited prion disease with 5-OPRI: phenotype modification by repeat length and codon 129. *Neurology* 2007; **69**: 730-738 [PMID: 17709704 DOI: 10.1212/01.wnl.0000267642.41594.9d]

63 **Trajkovski M**, da Silva MW, Plavec J. Unique structural features of interconverting monomeric and dimeric G-quadruplexes adopted by a sequence from the intron of the N-myc gene. *J Am Chem Soc* 2012; **134**: 4132-4141 [PMID: 22303871 DOI: 10.1021/ja208483v]

64 **Bilgen E**, Persil Çetinkol Ö. Doxorubicin exhibits strong and selective association with VEGF Pu(22) G-quadruplex. *Biochim Biophys Acta Gen Subj* 2020; **1864**: 129720 [PMID: 32860839 DOI: 10.1016/j.bbagen.2020.129720]

65 **Blice-Baum AC**, Mihailescu MR. Biophysical characterization of G-quadruplex forming FMR1 mRNA and of its interactions with different fragile X mental retardation protein isoforms. *RNA* 2014; **20**: 103-114 [PMID: 24249225 DOI: 10.1261/rna.041442.113]

66 **Morris MJ**, Wingate KL, Silwal J, Leeper TC, Basu S. The porphyrin TmPyP4 unfolds the extremely stable G-quadruplex in MT3-MMP mRNA and alleviates its repressive effect to enhance translation in eukaryotic cells. *Nucleic Acids Res* 2012; **40**: 4137-4145 [PMID: 22266651 DOI: 10.1093/nar/gkr1308]

67 **Kumari S**, Bugaut A, Huppert JL, Balasubramanian S. An RNA G-quadruplex in the 5' UTR of the NRAS proto-oncogene modulates translation. *Nat Chem Biol* 2007; **3**: 218-221 [PMID: 17322877 DOI: 10.1038/nchembio864]

68 **Christiansen J**, Kofod M, Nielsen FC. A guanosine quadruplex and two stable hairpins flank a major cleavage site in insulin-like growth factor II mRNA. *Nucleic Acids Res* 1994; **22**: 5709-5716 [PMID: 7838726 DOI: 10.1093/nar/22.25.5709]

69 **Gomez D**, Guédin A, Mergny JL, Salles B, Riou JF, Teulade-Fichou MP, Calsou P. A G-quadruplex structure within the 5'-UTR of TRF2 mRNA represses translation in human cells. *Nucleic Acids Res* 2010; **38**: 7187-7198 [PMID: 20571083 DOI: 10.1093/nar/gkq563]

70 **Arora A**, Suess B. An RNA G-quadruplex in the 3' UTR of the proto-oncogene PIM1 represses translation. *RNA Biol* 2011; **8**: 802-805 [PMID: 21734463 DOI: 10.4161/rna.8.5.16038]

71 **Fisette JF**, Montagna DR, Mihailescu MR, Wolfe MS. A G-rich element forms a G-quadruplex and regulates BACE1 mRNA alternative splicing. *J Neurochem* 2012; **121**: 763-773 [PMID: 22303960 DOI: 10.1111/j.1471-4159.2012.07680.x]

72 **Huang W**, Smaldino PJ, Zhang Q, Miller LD, Cao P, Stadelman K, Wan M, Giri B, Lei M, Nagamine Y, Vaughn JP, Akman SA, Sui G. Yin Yang 1 contains G-quadruplex structures in its promoter and 5'-UTR and its expression is modulated by G4 resolvase 1. *Nucleic Acids Res* 2012; **40**: 1033-1049 [PMID: 21993297 DOI: 10.1093/nar/gkr849]

73 **Xi M**, Li Y, Zhou J. Exploration of the formation and structure characteristics of a miR-92a promoter G-quadruplex by ESI-MS and CD. *Talanta* 2020; **211**: 120708 [PMID: 32070614 DOI: 10.1016/j.talanta.2019.120708]

74 **Imperatore JA**, Then ML, McDougal KB, Mihailescu MR. Characterization of a G-Quadruplex Structure in Pre-miRNA-1229 and in Its Alzheimer's Disease-Associated Variant rs2291418: Implications for miRNA-1229 Maturation. *Int J Mol Sci* 2020; **21** [PMID: 31991575 DOI: 10.3390/ijms21030767]

75 **Li F**, Tan W, Chen H, Zhou J, Xu M, Yuan G. Up- and downregulation of mature miR-1587 function by modulating its G-quadruplex structure and using small molecules. *Int J Biol Macromol* 2019; **121**: 127-134 [PMID: 30290263 DOI: 10.1016/j.ijbiomac.2018.10.017]

76 **Chen L**, Dickerhoff J, Sakai S, Yang D. DNA G-Quadruplex in Human Telomeres and Oncogene Promoters: Structures, Functions, and Small Molecule Targeting. *Acc Chem Res* 2022; **55**: 2628-2646 [PMID: 36054116 DOI: 10.1021/acs.accounts.2c00337]

77 **Ma Y**, Iida K, Nagasawa K. Topologies of G-quadruplex: Biological functions and regulation by ligands. *Biochem Biophys Res Commun* 2020; **531**: 3-17 [PMID: 31948752 DOI: 10.1016/j.bbrc.2019.12.103]

78 **Liu Y**, Cheng D, Ge M, Lin W. The Truncated Human Telomeric Sequence forms a Hybrid-Type Intramolecular Mixed Parallel/antiparallel G-quadruplex Structure in K(+) Solution. *Chem Biol Drug Des* 2016; **88**: 122-128 [PMID: 26867976 DOI: 10.1111/cbdd.12740]

79 **Ambrus A**, Chen D, Dai J, Bialis T, Jones RA, Yang D. Human telomeric sequence forms a hybrid-type intramolecular G-quadruplex structure with mixed parallel/antiparallel strands in potassium solution. *Nucleic Acids Res* 2006; **34**: 2723-2735 [PMID: 16714449 DOI: 10.1093/nar/gkl348]

80 **Dai J**, Carver M, Punchihewa C, Jones RA, Yang D. Structure of the Hybrid-2 type intramolecular human telomeric G-quadruplex in K+ solution: insights into structure polymorphism of the human telomeric sequence. *Nucleic Acids Res* 2007; **35**: 4927-4940 [PMID: 17626043 DOI: 10.1093/nar/gkm522]

81 **Zhang Z**, Dai J, Veliath E, Jones RA, Yang D. Structure of a two-G-tetrad intramolecular G-quadruplex formed by a variant human telomeric sequence in K+ solution: insights into the interconversion of human telomeric G-quadruplex structures. *Nucleic Acids Res* 2010; **38**: 1009-1021 [PMID: 19946019 DOI: 10.1093/nar/gkp1029]

82 **Noer SL**, Preus S, Gudnason D, Aznauryan M, Mergny JL, Birkedal V. Folding dynamics and conformational heterogeneity of human telomeric G-quadruplex structures in Na+ solutions by single molecule FRET microscopy. *Nucleic Acids Res* 2016; **44**: 464-471 [PMID: 26615192 DOI: 10.1093/nar/gkv1320]

83 **Mazzini S**, Gargallo R, Musso L, De Santis F, Aviñó A, Scaglioni L, Eritja R, Di Nicola M, Zunino F, Amatulli A, Dallavalle S. Stabilization of c-KIT G-Quadruplex DNA Structures by the RNA Polymerase I Inhibitors BMH-21 and BA-41. *Int J Mol Sci* 2019; **20** [PMID: 31590335 DOI: 10.3390/ijms20194927]

84 **Kotar A**, Rigo R, Sissi C, Plavec J. Two-quartet kit* G-quadruplex is formed *via* double-stranded pre-folded structure. *Nucleic Acids Res* 2019; **47**: 2641-2653 [PMID: 30590801 DOI: 10.1093/nar/gky1269]

85 **Cayrou C**, Ballester B, Peiffer I, Fenouil R, Coulombe P, Andrau JC, van Helden J, Méchali M. The chromatin environment shapes DNA replication origin organization and defines origin classes. *Genome Res* 2015; **25**: 1873-1885 [PMID: 26560631 DOI: 10.1101/gr.192799.115]

86 **Valton AL**, Hassan-Zadeh V, Lema I, Boggetto N, Alberti P, Saintomé C, Riou JF, Prioleau MN. G4 motifs affect origin positioning and efficiency in two vertebrate replicators. *EMBO J* 2014; **33**: 732-746 [PMID: 24521668 DOI: 10.1002/embj.201387506]

87 **Prorok P**, Artufel M, Aze A, Coulombe P, Peiffer I, Lacroix L, Guédin A, Mergny JL, Damaschke J, Schepers A, Cayrou C, Teulade-Fichou MP, Ballester B, Méchali M. Involvement of G-quadruplex regions in mammalian replication origin activity. *Nat Commun* 2019; **10**: 3274 [PMID: 31332171 DOI: 10.1038/s41467-019-11104-0]

88 **Rodriguez R**, Miller KM, Forment JV, Bradshaw CR, Nikan M, Britton S, Oelschlaegel T, Xhemalce B, Balasubramanian S, Jackson SP. Small-molecule-induced DNA damage identifies alternative DNA structures in human genes. *Nat Chem Biol* 2012; **8**: 301-310 [PMID: 22306580 DOI: 10.1038/nchembio.780]

89 **Vannier JB**, Sandhu S, Petalcorin MI, Wu X, Nabi Z, Ding H, Boulton SJ. RTEL1 is a replisome-associated helicase that promotes telomere and genome-wide replication. *Science* 2013; **342**: 239-242 [PMID: 24115439 DOI: 10.1126/science.1241779]

90 **Drosopoulos WC**, Kosiyatrakul ST, Schildkraut CL. BLM helicase facilitates telomere replication during leading strand synthesis of

telomeres. *J Cell Biol* 2015; **210**: 191-208 [PMID: 26195664 DOI: 10.1083/jcb.201410061]
91 **Dyer MA**, Qadeer ZA, Valle-Garcia D, Bernstein E. ATRX and DAXX: Mechanisms and Mutations. *Cold Spring Harb Perspect Med* 2017; **7** [PMID: 28062559 DOI: 10.1101/cshperspect.a026567]
92 **Zhang M**, Wang B, Li T, Liu R, Xiao Y, Geng X, Li G, Liu Q, Price CM, Liu Y, Wang F. Mammalian CST averts replication failure by preventing G-quadruplex accumulation. *Nucleic Acids Res* 2019; **47**: 5243-5259 [PMID: 30976812 DOI: 10.1093/nar/gkz264]
93 **Bidula S**, Brázda V. Genomic Analysis of Non-B Nucleic Acids Structures in SARS-CoV-2: Potential Key Roles for These Structures in Mutability, Translation, and Replication? *Genes (Basel)* 2023; **14** [PMID: 36672896 DOI: 10.3390/genes14010157]
94 **Sugimoto N**, Maehara K, Yoshida K, Ohkawa Y, Fujita M. Genome-wide analysis of the spatiotemporal regulation of firing and dormant replication origins in human cells. *Nucleic Acids Res* 2018; **46**: 6683-6696 [PMID: 29893900 DOI: 10.1093/nar/gky476]
95 **Galati E**, Bosio MC, Novarina D, Chiara M, Bernini GM, Mozzarelli AM, García-Rubio ML, Gómez-González B, Aguilera A, Carzaniga T, Todisco M, Bellini T, Nava GM, Frigè G, Sertic S, Horner DS, Baryshnikova A, Manzari C, D'Erchia AM, Pesole G, Brown GW, Muzi-Falconi M, Lazzaro F. VID22 counteracts G-quadruplex-induced genome instability. *Nucleic Acids Res* 2021; **49**: 12785-12804 [PMID: 34871443 DOI: 10.1093/nar/gkab1156]
96 **Lee HT**, Bose A, Lee CY, Opresko PL, Myong S. Molecular mechanisms by which oxidative DNA damage promotes telomerase activity. *Nucleic Acids Res* 2017; **45**: 11752-11765 [PMID: 28981887 DOI: 10.1093/nar/gkx789]
97 **De Magis A**, Götz S, Hajikazemi M, Fekete-Szücs E, Caterino M, Juranek S, Paeschke K. Zuo1 supports G4 structure formation and directs repair toward nucleotide excision repair. *Nat Commun* 2020; **11**: 3907 [PMID: 32764578 DOI: 10.1038/s41467-020-17701-8]
98 **Pavlova AV**, Monakhova MV, Ogloblina AM, Andreeva NA, Laptev GY, Polshakov VI, Gromova ES, Zvereva MI, Yakubovskaya MG, Oretskaya TS, Kubareva EA, Dolinnaya NG. Responses of DNA Mismatch Repair Proteins to a Stable G-Quadruplex Embedded into a DNA Duplex Structure. *Int J Mol Sci* 2020; **21** [PMID: 33233554 DOI: 10.3390/ijms21228773]
99 **Pavlova AV**, Savitskaya VY, Dolinnaya NG, Monakhova MV, Litvinova AV, Kubareva EA, Zvereva MI. G-Quadruplex Formed by the Promoter Region of the hTERT Gene: Structure-Driven Effects on DNA Mismatch Repair Functions. *Biomedicines* 2022; **10** [PMID: 36009419 DOI: 10.3390/biomedicines10081871]
100 **Lejault P**, Mitteaux J, Sperti FR, Monchaud D. How to untie G-quadruplex knots and why? *Cell Chem Biol* 2021; **28**: 436-455 [PMID: 33596431 DOI: 10.1016/j.chembiol.2021.01.015]
101 **Voter AF**, Qiu Y, Tippana R, Myong S, Keck JL. A guanine-flipping and sequestration mechanism for G-quadruplex unwinding by RecQ helicases. *Nat Commun* 2018; **9**: 4201 [PMID: 30305632 DOI: 10.1038/s41467-018-06751-8]
102 **Da Ros S**, Nicoletto G, Rigo R, Ceschi S, Zorzan E, Dacasto M, Giantin M, Sissi C. G-Quadruplex Modulation of SP1 Functional Binding Sites at the KIT Proximal Promoter. *Int J Mol Sci* 2020; **22** [PMID: 33396937 DOI: 10.3390/ijms22010329]
103 **Cogoi S**, Paramasivam M, Membrino A, Yokoyama KK, Xodo LE. The KRAS promoter responds to Myc-associated zinc finger and poly(ADP-ribose) polymerase 1 proteins, which recognize a critical quadruplex-forming GA-element. *J Biol Chem* 2010; **285**: 22003-22016 [PMID: 20457603 DOI: 10.1074/jbc.M110.101923]
104 **Falabella M**, Kolesar JE, Wallace C, de Jesus D, Sun L, Taguchi YV, Wang C, Wang T, Xiang IM, Alder JK, Maheshan R, Horne W, Turek-Herman J, Pagano PJ, St Croix CM, Sondheimer N, Yatsunyk LA, Johnson FB, Kaufman BA. G-quadruplex dynamics contribute to regulation of mitochondrial gene expression. *Sci Rep* 2019; **9**: 5605 [PMID: 30944353 DOI: 10.1038/s41598-019-41464-y]
105 **Hu XX**, Wang SQ, Gan SQ, Liu L, Zhong MQ, Jia MH, Jiang F, Xu Y, Xiao CD, Shen XC. A Small Ligand That Selectively Binds to the G-quadruplex at the Human Vascular Endothelial Growth Factor Internal Ribosomal Entry Site and Represses the Translation. *Front Chem* 2021; **9**: 781198 [PMID: 34858949 DOI: 10.3389/fchem.2021.781198]
106 **Chen X**, Yuan J, Xue G, Campanario S, Wang D, Wang W, Mou X, Liew SW, Umar MI, Isern J, Zhao Y, He L, Li Y, Mann CJ, Yu X, Wang L, Perdiguero E, Chen W, Xue Y, Nagamine Y, Kwok CK, Sun H, Muñoz-Cánoves P, Wang H. Translational control by DHX36 binding to 5'UTR G-quadruplex is essential for muscle stem-cell regenerative functions. *Nat Commun* 2021; **12**: 5043 [PMID: 34413292 DOI: 10.1038/s41467-021-25170-w]
107 **Angeloni A**, Bogdanovic O. Sequence determinants, function, and evolution of CpG islands. *Biochem Soc Trans* 2021; **49**: 1109-1119 [PMID: 34156435 DOI: 10.1042/BST20200695]
108 **Xiao FH**, Wang HT, Kong QP. Dynamic DNA Methylation During Aging: A "Prophet" of Age-Related Outcomes. *Front Genet* 2019; **10**: 107 [PMID: 30833961 DOI: 10.3389/fgene.2019.00107]
109 **Zhao L**, Wu X, Zheng J, Dong D. DNA methylome profiling of circulating tumor cells in lung cancer at single base-pair resolution. *Oncogene* 2021; **40**: 1884-1895 [PMID: 33564067 DOI: 10.1038/s41388-021-01657-0]
110 **Mao SQ**, Ghanbarian AT, Spiegel J, Martínez Cuesta S, Beraldi D, Di Antonio M, Marsico G, Hänsel-Hertsch R, Tannahill D, Balasubramanian S. DNA G-quadruplex structures mold the DNA methylome. *Nat Struct Mol Biol* 2018; **25**: 951-957 [PMID: 30275516 DOI: 10.1038/s41594-018-0131-8]
111 **Matsumoto S**, Tateishi-Karimata H, Sugimoto N. DNA methylation is regulated by both the stability and topology of G-quadruplex. *Chem Commun (Camb)* 2022; **58**: 12459-12462 [PMID: 36263745 DOI: 10.1039/d2cc04383a]
112 **Takahama K**, Takada A, Tada S, Shimizu M, Sayama K, Kurokawa R, Oyoshi T. Regulation of telomere length by G-quadruplex telomere DNA- and TERRA-binding protein TLS/FUS. *Chem Biol* 2013; **20**: 341-350 [PMID: 23521792 DOI: 10.1016/j.chembiol.2013.02.013]
113 **Mei Y**, Deng Z, Vladimirova O, Gulve N, Johnson FB, Drosopoulos WC, Schildkraut CL, Lieberman PM. TERRA G-quadruplex RNA interaction with TRF2 GAR domain is required for telomere integrity. *Sci Rep* 2021; **11**: 3509 [PMID: 33568696 DOI: 10.1038/s41598-021-82406-x]
114 **Porro A**, Feuerhahn S, Lingner J. TERRA-reinforced association of LSD1 with MRE11 promotes processing of uncapped telomeres. *Cell Rep* 2014; **6**: 765-776 [PMID: 24529708 DOI: 10.1016/j.celrep.2014.01.022]
115 **Beltran M**, Tavares M, Justin N, Khandelwal G, Ambrose J, Foster BM, Worlock KB, Tvardovskiy A, Kunzelmann S, Herrero J, Bartke T, Gamblin SJ, Wilson JR, Jenner RG. G-tract RNA removes Polycomb repressive complex 2 from genes. *Nat Struct Mol Biol* 2019; **26**: 899-909 [PMID: 31548724 DOI: 10.1038/s41594-019-0293-z]
116 **Katapadi VK**, Nambiar M, Raghavan SC. Potential G-quadruplex formation at breakpoint regions of chromosomal translocations in cancer may explain their fragility. *Genomics* 2012; **100**: 72-80 [PMID: 22659239 DOI: 10.1016/j.ygeno.2012.05.008]
117 **Kim N**. The Interplay between G-quadruplex and Transcription. *Curr Med Chem* 2019; **26**: 2898-2917 [PMID: 29284393 DOI: 10.2174/0929867325666171229132619]
118 **Georgakopoulos-Soares I**, Morganella S, Jain N, Hemberg M, Nik-Zainal S. Noncanonical secondary structures arising from non-B DNA

motifs are determinants of mutagenesis. *Genome Res* 2018; **28**: 1264-1271 [PMID: 30104284 DOI: 10.1101/gr.231688.117]

119 **Williams JD**, Fleetwood S, Berroyer A, Kim N, Larson ED. Sites of instability in the human TCF3 (E2A) gene adopt G-quadruplex DNA structures in vitro. *Front Genet* 2015; **6**: 177 [PMID: 26029241 DOI: 10.3389/fgene.2015.00177]

120 **Bidula S**. Analysis of putative G-quadruplex forming sequences in inflammatory mediators and their potential as targets for treating inflammatory disorders. *Cytokine* 2021; **142**: 155493 [PMID: 33713881 DOI: 10.1016/j.cyto.2021.155493]

121 **Wang X**, Chen S, Zhao Z, Chen F, Huang Y, Guo X, Lei L, Wang W, Luo Y, Yu H, Wang J. Genomic G-quadruplex folding triggers a cytokine-mediated inflammatory feedback loop to aggravate inflammatory diseases. *iScience* 2022; **25**: 105312 [PMID: 36304116 DOI: 10.1016/j.isci.2022.105312]

122 **Dalloul Z**, Chenuet P, Dalloul I, Boyer F, Aldigier JC, Laffleur B, El Makhour Y, Ryffel B, Quesniaux VFJ, Togbé D, Mergny JL, Cook-Moreau J, Cogné M. G-quadruplex DNA targeting alters class-switch recombination in B cells and attenuates allergic inflammation. *J Allergy Clin Immunol* 2018; **142**: 1352-1355 [PMID: 29935221 DOI: 10.1016/j.jaci.2018.06.011]

123 **Zhu BC**, He J, Xia XY, Jiang J, Liu W, Liu LY, Liang BB, Yao HG, Ke Z, Xia W, Mao ZW. Solution structure of a thrombin binding aptamer complex with a non-planar platinum(ii) compound. *Chem Sci* 2022; **13**: 8371-8379 [PMID: 35919711 DOI: 10.1039/d2sc01196d]

124 **Santos T**, Salgado GF, Cabrita EJ, Cruz C. Nucleolin: a binding partner of G-quadruplex structures. *Trends Cell Biol* 2022; **32**: 561-564 [PMID: 35410819 DOI: 10.1016/j.tcb.2022.03.003]

125 **Liu J**, Yan L, He S, Hu J. Engineering DNA quadruplexes in DNA nanostructures for biosensor construction. *Nano Res* 2022; **15**: 3504-3513 [PMID: 35401944 DOI: 10.1007/s12274-021-3869-y]

126 **Zhang C**, Fu S, Zhang F, Han M, Wang X, Du J, Zhang H, Li W. Affibody Modified G-quadruplex DNA Micelles Incorporating Polymeric 5-Fluorodeoxyuridine for Targeted Delivery of Curcumin to Enhance Synergetic Therapy of HER2 Positive Gastric Cancer. *Nanomaterials (Basel)* 2022; **12** [PMID: 35215023 DOI: 10.3390/nano12040696]

127 **Shammas MA**, Koley H, Beer DG, Li C, Goyal RK, Munshi NC. Growth arrest, apoptosis, and telomere shortening of Barrett's-associated adenocarcinoma cells by a telomerase inhibitor. *Gastroenterology* 2004; **126**: 1337-1346 [PMID: 15131795 DOI: 10.1053/j.gastro.2004.01.026]

128 **Jiang J**, Li J, Liu C, Liu R, Liang X, Zhou Y, Pan L, Chen H, Ma Z. Study on the substitution effects of zinc benzoate terpyridine complexes on photoluminescence, antiproliferative potential and DNA binding properties. *J Biol Inorg Chem* 2020; **25**: 311-324 [PMID: 32112291 DOI: 10.1007/s00775-020-01763-6]

129 **Hampel SM**, Sidibe A, Gunaratnam M, Riou JF, Neidle S. Tetrasubstituted naphthalene diimide ligands with selectivity for telomeric G-quadruplexes and cancer cells. *Bioorg Med Chem Lett* 2010; **20**: 6459-6463 [PMID: 20932753 DOI: 10.1016/j.bmcl.2010.09.066]

130 **Micco M**, Collie GW, Dale AG, Ohnmacht SA, Pazitna I, Gunaratnam M, Reszka AP, Neidle S. Structure-based design and evaluation of naphthalene diimide G-quadruplex ligands as telomere targeting agents in pancreatic cancer cells. *J Med Chem* 2013; **56**: 2959-2974 [PMID: 23514618 DOI: 10.1021/jm301899y]

131 **Mpima S**, Ohnmacht SA, Barletta M, Husby J, Pett LC, Gunaratnam M, Hilton ST, Neidle S. The influence of positional isomerism on G-quadruplex binding and anti-proliferative activity of tetra-substituted naphthalene diimide compounds. *Bioorg Med Chem* 2013; **21**: 6162-6170 [PMID: 23769166 DOI: 10.1016/j.bmc.2013.05.027]

132 **Ohnmacht SA**, Marchetti C, Gunaratnam M, Besser RJ, Haider SM, Di Vita G, Lowe HL, Mellinas-Gomez M, Diocou S, Robson M, Šponer J, Islam B, Pedley RB, Hartley JA, Neidle S. A G-quadruplex-binding compound showing anti-tumour activity in an in vivo model for pancreatic cancer. *Sci Rep* 2015; **5**: 11385 [PMID: 26077929 DOI: 10.1038/srep11385]

133 **Marchetti C**, Zyner KG, Ohnmacht SA, Robson M, Haider SM, Morton JP, Marsico G, Vo T, Laughlin-Toth S, Ahmed AA, Di Vita G, Pazitna I, Gunaratnam M, Besser RJ, Andrade ACG, Diocou S, Pike JA, Tannahill D, Pedley RB, Evans TRJ, Wilson WD, Balasubramanian S, Neidle S. Targeting Multiple Effector Pathways in Pancreatic Ductal Adenocarcinoma with a G-Quadruplex-Binding Small Molecule. *J Med Chem* 2018; **61**: 2500-2517 [PMID: 29356532 DOI: 10.1021/acs.jmedchem.7b01781]

134 **Ahmed AA**, Marchetti C, Ohnmacht SA, Neidle S. A G-quadruplex-binding compound shows potent activity in human gemcitabine-resistant pancreatic cancer cells. *Sci Rep* 2020; **10**: 12192 [PMID: 32699225 DOI: 10.1038/s41598-020-68944-w]

135 **Ahmed AA**, Angell R, Oxenford S, Worthington J, Williams N, Barton N, Fowler TG, O'Flynn DE, Sunose M, McConville M, Vo T, Wilson WD, Karim SA, Morton JP, Neidle S. Asymmetrically Substituted Quadruplex-Binding Naphthalene Diimide Showing Potent Activity in Pancreatic Cancer Models. *ACS Med Chem Lett* 2020; **11**: 1634-1644 [PMID: 32832034 DOI: 10.1021/acsmedchemlett.0c00317]

136 **Gunaratnam M**, de la Fuente M, Hampel SM, Todd AK, Reszka AP, Schätzlein A, Neidle S. Targeting pancreatic cancer with a G-quadruplex ligand. *Bioorg Med Chem* 2011; **19**: 7151-7157 [PMID: 22041170 DOI: 10.1016/j.bmc.2011.09.055]

137 **Faudale M**, Cogoi S, Xodo LE. Photoactivated cationic alkyl-substituted porphyrin binding to g4-RNA in the 5'-UTR of KRAS oncogene represses translation. *Chem Commun (Camb)* 2012; **48**: 874-876 [PMID: 22127206 DOI: 10.1039/c1cc15850c]

138 **Ferino A**, Nicoletto G, D'Este F, Zorzet S, Lago S, Richter SN, Tikhomirov A, Shchekotikhin A, Xodo LE. Photodynamic Therapy for ras-Driven Cancers: Targeting G-Quadruplex RNA Structures with Bifunctional Alkyl-Modified Porphyrins. *J Med Chem* 2020; **63**: 1245-1260 [PMID: 31930916 DOI: 10.1021/acs.jmedchem.9b01577]

139 **Pattanayak R**, Barua A, Das A, Chatterjee T, Pathak A, Choudhury P, Sen S, Saha P, Bhattacharyya M. Porphyrins to restrict progression of pancreatic cancer by stabilizing KRAS G-quadruplex: In silico, in vitro and in vivo validation of anticancer strategy. *Eur J Pharm Sci* 2018; **125**: 39-53 [PMID: 30223034 DOI: 10.1016/j.ejps.2018.09.011]

140 **Chilakamarthi U**, Koteshwar D, Jinka S, Vamsi Krishna N, Sridharan K, Nagesh N, Giribabu L. Novel Amphiphilic G-Quadruplex Binding Synthetic Derivative of TMPyP4 and Its Effect on Cancer Cell Proliferation and Apoptosis Induction. *Biochemistry* 2018; **57**: 6514-6527 [PMID: 30369235 DOI: 10.1021/acs.biochem.8b00843]

141 **Liu W**, Sun D, Hurley LH. Binding of G-quadruplex-interactive agents to distinct G-quadruplexes induces different biological effects in MiaPaCa cells. *Nucleosides Nucleotides Nucleic Acids* 2005; **24**: 1801-1815 [PMID: 16438049 DOI: 10.1080/15257770500267238]

142 **Kaiser CE**, Van Ert NA, Agrawal P, Chawla R, Yang D, Hurley LH. Insight into the Complexity of the i-Motif and G-Quadruplex DNA Structures Formed in the KRAS Promoter and Subsequent Drug-Induced Gene Repression. *J Am Chem Soc* 2017; **139**: 8522-8536 [PMID: 28570076 DOI: 10.1021/jacs.7b02046]

143 **Miglietta G**, Cogoi S, Marinello J, Capranico G, Tikhomirov AS, Shchekotikhin A, Xodo LE. RNA G-Quadruplexes in Kirsten Ras (KRAS) Oncogene as Targets for Small Molecules Inhibiting Translation. *J Med Chem* 2017; **60**: 9448-9461 [PMID: 29140695 DOI: 10.1021/acs.jmedchem.7b00622]

144 **Paluszkiewicz E**, Horowska B, Borowa-Mazgaj B, Peszyńska-Sularz G, Paradziej-Łukowicz J, Augustin E, Konopa J, Mazerska Z. Design, synthesis and high antitumor potential of new unsymmetrical bisacridine derivatives towards human solid tumors, specifically pancreatic

cancers and their unique ability to stabilize DNA G-quadruplexes. *Eur J Med Chem* 2020; **204**: 112599 [PMID: 32736230 DOI: 10.1016/j.ejmech.2020.112599]

145 **Arjmand F**, Sharma S, Parveen S, Toupet L, Yu Z, Cowan JA. Copper(ii) l/d-valine-(1,10-phen) complexes target human telomeric G-quadruplex motifs and promote site-specific DNA cleavage and cellular cytotoxicity. *Dalton Trans* 2020; **49**: 9888-9899 [PMID: 32638779 DOI: 10.1039/d0dt01527j]

146 **Bossaert M**, Pipier A, Riou JF, Noirot C, Nguyên LT, Serre RF, Bouchez O, Defrancq E, Calsou P, Britton S, Gomez D. Transcription-associated topoisomerase 2α (TOP2A) activity is a major effector of cytotoxicity induced by G-quadruplex ligands. *Elife* 2021; **10** [PMID: 34180392 DOI: 10.7554/eLife.65184]

147 **Xu H**, Di Antonio M, McKinney S, Mathew V, Ho B, O'Neil NJ, Santos ND, Silvester J, Wei V, Garcia J, Kabeer F, Lai D, Soriano P, Banáth J, Chiu DS, Yap D, Le DD, Ye FB, Zhang A, Thu K, Soong J, Lin SC, Tsai AH, Osako T, Algara T, Saunders DN, Wong J, Xian J, Bally MB, Brenton JD, Brown GW, Shah SP, Cescon D, Mak TW, Caldas C, Stirling PC, Hieter P, Balasubramanian S, Aparicio S. CX-5461 is a DNA G-quadruplex stabilizer with selective lethality in BRCA1/2 deficient tumours. *Nat Commun* 2017; **8**: 14432 [PMID: 28211448 DOI: 10.1038/ncomms14432]

148 **Drygin D**, Siddiqui-Jain A, O'Brien S, Schwaebe M, Lin A, Bliesath J, Ho CB, Proffitt C, Trent K, Whitten JP, Lim JK, Von Hoff D, Anderes K, Rice WG. Anticancer activity of CX-3543: a direct inhibitor of rRNA biogenesis. *Cancer Res* 2009; **69**: 7653-7661 [PMID: 19738048 DOI: 10.1158/0008-5472.CAN-09-1304]

149 **Xu H**, Hurley LH. A first-in-class clinical G-quadruplex-targeting drug. The bench-to-bedside translation of the fluoroquinolone QQ58 to CX-5461 (Pidnarulex). *Bioorg Med Chem Lett* 2022; **77**: 129016 [PMID: 36195286 DOI: 10.1016/j.bmcl.2022.129016]

150 **Schultz CW**, McCarthy GA, Nerwal T, Nevler A, DuHadaway JB, McCoy MD, Jiang W, Brown SZ, Goetz A, Jain A, Calvert VS, Vishwakarma V, Wang D, Preet R, Cassel J, Summer R, Shaghaghi H, Pommier Y, Baechler SA, Pishvaian MJ, Golan T, Yeo CJ, Petricoin EF, Prendergast GC, Salvino J, Singh PK, Dixon DA, Brody JR. The FDA-Approved Anthelmintic Pyrvinium Pamoate Inhibits Pancreatic Cancer Cells in Nutrient-Depleted Conditions by Targeting the Mitochondria. *Mol Cancer Ther* 2021; **20**: 2166-2176 [PMID: 34413127 DOI: 10.1158/1535-7163.MCT-20-0652]

151 **Psaras AM**, Carty RK, Miller JT, Tumey LN, Brooks TA. Indoloquinoline-Mediated Targeted Downregulation of KRAS through Selective Stabilization of the Mid-Promoter G-Quadruplex Structure. *Genes (Basel)* 2022; **13** [PMID: 36011352 DOI: 10.3390/genes13081440]

152 **Bhuma N**, Chand K, Andréasson M, Mason J, Das RN, Patel AK, Öhlund D, Chorell E. The effect of side chain variations on quinazoline-pyrimidine G-quadruplex DNA ligands. *Eur J Med Chem* 2023; **248**: 115103 [PMID: 36645982 DOI: 10.1016/j.ejmech.2023.115103]

153 **Chu PC**, Yang MC, Kulp SK, Salunke SB, Himmel LE, Fang CS, Jadhav AM, Shan YS, Lee CT, Lai MD, Shirley LA, Bekaii-Saab T, Chen CS. Regulation of oncogenic KRAS signaling *via* a novel KRAS-integrin-linked kinase-hnRNPA1 regulatory loop in human pancreatic cancer cells. *Oncogene* 2016; **35**: 3897-3908 [PMID: 26616862 DOI: 10.1038/onc.2015.458]

154 **Cogoi S**, Rapozzi V, Cauci S, Xodo LE. Critical role of hnRNP A1 in activating KRAS transcription in pancreatic cancer cells: A molecular mechanism involving G4 DNA. *Biochim Biophys Acta Gen Subj* 2017; **1861**: 1389-1398 [PMID: 27888145 DOI: 10.1016/j.bbagen.2016.11.031]

155 **Chu PC**, Kulp SK, Bekaii-Saab T, Chen CS. Targeting integrin-linked kinase to suppress oncogenic KRAS signaling in pancreatic cancer. *Small GTPases* 2018; **9**: 452-456 [PMID: 27936345 DOI: 10.1080/21541248.2016.1251383]

156 **Cinque G**, Ferino A, Pedersen EB, Xodo LE. Role of Poly [ADP-ribose] Polymerase 1 in Activating the Kirsten ras (KRAS) Gene in Response to Oxidative Stress. *Int J Mol Sci* 2020; **21** [PMID: 32872305 DOI: 10.3390/ijms21176237]

157 **Pramanik S**, Chen Y, Song H, Khutsishvili I, Marky LA, Ray S, Natarajan A, Singh PK, Bhakat KK. The human AP-endonuclease 1 (APE1) is a DNA G-quadruplex structure binding protein and regulates KRAS expression in pancreatic ductal adenocarcinoma cells. *Nucleic Acids Res* 2022; **50**: 3394-3412 [PMID: 35286386 DOI: 10.1093/nar/gkac172]

158 **Psaras AM**, Valiuska S, Noé V, Ciudad CJ, Brooks TA. Targeting KRAS Regulation with PolyPurine Reverse Hoogsteen Oligonucleotides. *Int J Mol Sci* 2022; **23** [PMID: 35216221 DOI: 10.3390/ijms23042097]

159 **Valiuska S**, Psaras AM, Noé V, Brooks TA, Ciudad CJ. Targeting MYC Regulation with Polypurine Reverse Hoogsteen Oligonucleotides. *Int J Mol Sci* 2022; **24** [PMID: 36613820 DOI: 10.3390/ijms24010378]

160 **Wang P**, Leung CH, Ma DL, Yan SC, Che CM. Structure-based design of platinum(II) complexes as c-myc oncogene down-regulators and luminescent probes for G-quadruplex DNA. *Chemistry* 2010; **16**: 6900-6911 [PMID: 20437426 DOI: 10.1002/chem.201000167]

161 **Chauhan A**, Paladhi S, Debnath M, Dash J. Selective recognition of c-MYC G-quadruplex DNA using prolinamide derivatives. *Org Biomol Chem* 2016; **14**: 5761-5767 [PMID: 26963597 DOI: 10.1039/c6ob00177g]

162 **Chen J**, Duan Y, Yu X, Zhong J, Bai J, Li NG, Zhu Z, Xu J. Development of novel 9-O-substituted-13-octylberberine derivatives as potential anti-hepatocellular carcinoma agents. *J Enzyme Inhib Med Chem* 2022; **37**: 2423-2433 [PMID: 36065941 DOI: 10.1080/14756366.2022.2118268]

163 **Chen J**, Duan Y, Yang K, Wang J, Yan J, Gu C, Wang S, Zhu Z, Liu EH, Xu J. Design, synthesis and biological evaluation of novel 9-N-substituted-13-alkylberberine derivatives from Chinese medicine as anti-hepatocellular carcinoma agents. *Bioorg Med Chem* 2023; **79**: 117156 [PMID: 36640595 DOI: 10.1016/j.bmc.2023.117156]

164 **Jin J**, Hou J, Long W, Zhang X, Lu YJ, Li D, Zhang K, Wong WL. Synthesis of fluorescent G-quadruplex DNA binding ligands for the comparison of terminal group effects in molecular interaction: Phenol versus methoxybenzene. *Bioorg Chem* 2020; **99**: 103821 [PMID: 32279036 DOI: 10.1016/j.bioorg.2020.103821]

165 **Chauhan A**, Paladhi S, Debnath M, Mandal S, Das RN, Bhowmik S, Dash J. A small molecule peptidomimetic that binds to c-KIT1 G-quadruplex and exhibits antiproliferative properties in cancer cells. *Bioorg Med Chem* 2014; **22**: 4422-4429 [PMID: 24961873 DOI: 10.1016/j.bmc.2014.05.060]

166 **Wang Y**, Ding Q, Xu T, Li CY, Zhou DD, Zhang L. HZ-6d targeted HERC5 to regulate p53 ISGylation in human hepatocellular carcinoma. *Toxicol Appl Pharmacol* 2017; **334**: 180-191 [PMID: 28919514 DOI: 10.1016/j.taap.2017.09.011]

167 **Sun J**, Wu G, Pastor F, Rahman N, Wang WH, Zhang Z, Merle P, Hui L, Salvetti A, Durantel D, Yang D, Andrisani O. RNA helicase DDX5 enables STAT1 mRNA translation and interferon signalling in hepatitis B virus replicating hepatocytes. *Gut* 2022; **71**: 991-1005 [PMID: 34021034 DOI: 10.1136/gutjnl-2020-323126]

168 **Bian WX**, Xie Y, Wang XN, Xu GH, Fu BS, Li S, Long G, Zhou X, Zhang XL. Binding of cellular nucleolin with the viral core RNA G-quadruplex structure suppresses HCV replication. *Nucleic Acids Res* 2019; **47**: 56-68 [PMID: 30462330 DOI: 10.1093/nar/gky1177]

169 **McLuckie KI**, Waller ZA, Sanders DA, Alves D, Rodriguez R, Dash J, McKenzie GJ, Venkitaraman AR, Balasubramanian S. G-quadruplex-binding benzo[a]phenoxazines down-regulate c-KIT expression in human gastric carcinoma cells. *J Am Chem Soc* 2011; **133**: 2658-2663

[PMID: 21294544 DOI: 10.1021/ja109474c]

170 **Ma X**, Awadasseid A, Zhou K, Wang X, Shen C, Zhao X, Cheng M, Zhang W. A 1,10-phenanthroline derivative selectively targeting telomeric G-quadruplex induces cytoprotective autophagy, causing apoptosis of gastric cancer cells. *Life Sci* 2021; **287**: 120095 [PMID: 34715135 DOI: 10.1016/j.lfs.2021.120095]

171 **Wang X**, Zhou CX, Yan JW, Hou JQ, Chen SB, Ou TM, Gu LQ, Huang ZS, Tan JH. Synthesis and Evaluation of Quinazolone Derivatives as a New Class of c-KIT G-Quadruplex Binding Ligands. *ACS Med Chem Lett* 2013; **4**: 909-914 [PMID: 24900584 DOI: 10.1021/ml400271y]

172 **Zhang YQ**, Pei JH, Shi SS, Zheng J, Wang JM, Guo XS, Cui GY, Wang XY, Zhang HP, Hu WQ. G-quadruplex antibody attenuates human gastric cancer cell proliferation and promotes apoptosis through hTERT/telomerase pathway. *Eur Rev Med Pharmacol Sci* 2018; **22**: 2614-2623 [PMID: 29771410 DOI: 10.26355/eurrev_201805_14955]

173 **Incles CM**, Schultes CM, Kelland LR, Neidle S. Acquired cellular resistance to flavopiridol in a human colon carcinoma cell line involves up-regulation of the telomerase catalytic subunit and telomere elongation. Sensitivity of resistant cells to combination treatment with a telomerase inhibitor. *Mol Pharmacol* 2003; **64**: 1101-1108 [PMID: 14573759 DOI: 10.1124/mol.64.5.1101]

174 **Salvati E**, Leonetti C, Rizzo A, Scarsella M, Mottolese M, Galati R, Sperduti I, Stevens MF, D'Incalci M, Blasco M, Chiorino G, Bauwens S, Horard B, Gilson E, Stoppacciaro A, Zupi G, Biroccio A. Telomere damage induced by the G-quadruplex ligand RHPS4 has an antitumor effect. *J Clin Invest* 2007; **117**: 3236-3247 [PMID: 17932567 DOI: 10.1172/JCI32461]

175 **Rizzo A**, Salvati E, Porru M, D'Angelo C, Stevens MF, D'Incalci M, Leonetti C, Gilson E, Zupi G, Biroccio A. Stabilization of quadruplex DNA perturbs telomere replication leading to the activation of an ATR-dependent ATM signaling pathway. *Nucleic Acids Res* 2009; **37**: 5353-5364 [PMID: 19596811 DOI: 10.1093/nar/gkp582]

176 **Biroccio A**, Porru M, Rizzo A, Salvati E, D'Angelo C, Orlandi A, Passeri D, Franceschin M, Stevens MF, Gilson E, Beretta G, Zupi G, Pisano C, Zunino F, Leonetti C. DNA damage persistence as determinant of tumor sensitivity to the combination of Topo I inhibitors and telomere-targeting agents. *Clin Cancer Res* 2011; **17**: 2227-2236 [PMID: 21355072 DOI: 10.1158/1078-0432.CCR-10-3033]

177 **Rizzo A**, Iachettini S, Zizza P, Cingolani C, Porru M, Artuso S, Stevens M, Hummersone M, Biroccio A, Salvati E, Leonetti C. Identification of novel RHPS4-derivative ligands with improved toxicological profiles and telomere-targeting activities. *J Exp Clin Cancer Res* 2014; **33**: 81 [PMID: 25288403 DOI: 10.1186/s13046-014-0081-x]

178 **Folini M**, Pivetta C, Zagotto G, De Marco C, Palumbo M, Zaffaroni N, Sissi C. Remarkable interference with telomeric function by a G-quadruplex selective bisantrene regioisomer. *Biochem Pharmacol* 2010; **79**: 1781-1790 [PMID: 20206144 DOI: 10.1016/j.bcp.2010.02.018]

179 **Franceschin M**, Rizzo A, Casagrande V, Salvati E, Alvino A, Altieri A, Ciammaichella A, Iachettini S, Leonetti C, Ortaggi G, Porru M, Bianco A, Biroccio A. Aromatic core extension in the series of N-cyclic bay-substituted perylene G-quadruplex ligands: increased telomere damage, antitumor activity, and strong selectivity for neoplastic over healthy cells. *ChemMedChem* 2012; **7**: 2144-2154 [PMID: 23097341 DOI: 10.1002/cmdc.201200348]

180 **Porru M**, Artuso S, Salvati E, Bianco A, Franceschin M, Diodoro MG, Passeri D, Orlandi A, Savorani F, D'Incalci M, Biroccio A, Leonetti C. Targeting G-Quadruplex DNA Structures by EMICORON Has a Strong Antitumor Efficacy against Advanced Models of Human Colon Cancer. *Mol Cancer Ther* 2015; **14**: 2541-2551 [PMID: 26304235 DOI: 10.1158/1535-7163.MCT-15-0253]

181 **Rocca R**, Scionti F, Nadai M, Moraca F, Maruca A, Costa G, Catalano R, Juli G, Di Martino MT, Ortuso F, Alcaro S, Tagliaferri P, Tassone P, Richter SN, Artese A. Chromene Derivatives as Selective TERRA G-Quadruplex RNA Binders with Antiproliferative Properties. *Pharmaceuticals (Basel)* 2022; **15** [PMID: 35631373 DOI: 10.3390/ph15050548]

182 **Thakur RK**, Kumar P, Halder K, Verma A, Kar A, Parent JL, Basundra R, Kumar A, Chowdhury S. Metastases suppressor NM23-H2 interaction with G-quadruplex DNA within c-MYC promoter nuclease hypersensitive element induces c-MYC expression. *Nucleic Acids Res* 2009; **37**: 172-183 [PMID: 19033359 DOI: 10.1093/nar/gkn919]

183 **Yao YX**, Xu BH, Zhang Y. CX-3543 Promotes Cell Apoptosis through Downregulation of CCAT1 in Colon Cancer Cells. *Biomed Res Int* 2018; **2018**: 9701957 [PMID: 30519593 DOI: 10.1155/2018/9701957]

184 **Chung SY**, Chang YC, Hsu DS, Hung YC, Lu ML, Hung YP, Chiang NJ, Yeh CN, Hsiao M, Soong J, Su Y, Chen MH. A G-quadruplex stabilizer, CX-5461 combined with two immune checkpoint inhibitors enhances in vivo therapeutic efficacy by increasing PD-L1 expression in colorectal cancer. *Neoplasia* 2023; **35**: 100856 [PMID: 36442297 DOI: 10.1016/j.neo.2022.100856]

185 **Malhotra R**, Rarhi C, Diveshkumar KV, Barik R, D'cunha R, Dhar P, Kundu M, Chattopadhyay S, Roy S, Basu S, Pradeepkumar PI, Hajra S. Dihydrochelerythrine and its derivatives: Synthesis and their application as potential G-quadruplex DNA stabilizing agents. *Bioorg Med Chem* 2016; **24**: 2887-2896 [PMID: 27234888 DOI: 10.1016/j.bmc.2016.04.059]

186 **Pawłowska M**, Kulesza J, Augustin E. c-Myc Protein Level Affected by Unsymmetrical Bisacridines Influences Apoptosis and Senescence Induced in HCT116 Colorectal and H460 Lung Cancer Cells. *Int J Mol Sci* 2022; **23** [PMID: 35328482 DOI: 10.3390/ijms23063061]

187 **Brito H**, Martins AC, Lavrado J, Mendes E, Francisco AP, Santos SA, Ohnmacht SA, Kim NS, Rodrigues CM, Moreira R, Neidle S, Borralho PM, Paulo A. Targeting KRAS Oncogene in Colon Cancer Cells with 7-Carboxylate Indolo[3,2-b]quinoline Tri-Alkylamine Derivatives. *PLoS One* 2015; **10**: e0126891 [PMID: 26024321 DOI: 10.1371/journal.pone.0126891]

188 **D'Aria F**, D'Amore VM, Di Leva FS, Amato J, Caterino M, Russomanno P, Salerno S, Barresi E, De Leo M, Marini AM, Taliani S, Da Settimo F, Salgado GF, Pompili L, Zizza P, Shirasawa S, Novellino E, Biroccio A, Marinelli L, Giancola C. Targeting the KRAS oncogene: Synthesis, physicochemical and biological evaluation of novel G-Quadruplex DNA binders. *Eur J Pharm Sci* 2020; **149**: 105337 [PMID: 32311457 DOI: 10.1016/j.ejps.2020.105337]

189 **Sanchez-Martin V**, Schneider DA, Ortiz-Gonzalez M, Soriano-Lerma A, Linde-Rodriguez A, Perez-Carrasco V, Gutierrez-Fernandez J, Cuadros M, González C, Soriano M, Garcia-Salcedo JA. Targeting ribosomal G-quadruplexes with naphthalene-diimides as RNA polymerase I inhibitors for colorectal cancer treatment. *Cell Chem Biol* 2021; **28**: 1590-1601.e4 [PMID: 34166611 DOI: 10.1016/j.chembiol.2021.05.021]

190 **Belmonte-Reche E**, Benassi A, Peñalver P, Cucchiarini A, Guédin A, Mergny JL, Rosu F, Gabelica V, Freccero M, Doria F, Morales JC. Thiosugar naphthalene diimide conjugates: G-quadruplex ligands with antiparasitic and anticancer activity. *Eur J Med Chem* 2022; **232**: 114183 [PMID: 35168151 DOI: 10.1016/j.ejmech.2022.114183]

191 **Sanchez-Martin V**, Plaza-Calonge MDC, Soriano-Lerma A, Ortiz-Gonzalez M, Linde-Rodriguez A, Perez-Carrasco V, Ramirez-Macias I, Cuadros M, Gutierrez-Fernandez J, Murciano-Calles J, Rodríguez-Manzaneque JC, Soriano M, Garcia-Salcedo JA. Gallic Acid: A Natural Phenolic Compound Exerting Antitumoral Activities in Colorectal Cancer *via* Interaction with G-Quadruplexes. *Cancers (Basel)* 2022; **14** [PMID: 35681628 DOI: 10.3390/cancers14112648]

192 **Nishikawa T**, Kuwano Y, Takahara Y, Nishida K, Rokutan K. HnRNPA1 interacts with G-quadruplex in the TRA2B promoter and stimulates its transcription in human colon cancer cells. *Sci Rep* 2019; **9**: 10276 [PMID: 31311954 DOI: 10.1038/s41598-019-46659-x]

193 **Bolduc F**, Turcotte MA, Perreault JP. The Small Nuclear Ribonucleoprotein Polypeptide A (SNRPA) binds to the G-quadruplex of the BAG-1 5'UTR. *Biochimie* 2020; **176**: 122-127 [PMID: 32629040 DOI: 10.1016/j.biochi.2020.06.013]

194 **Jodoin R**, Carrier JC, Rivard N, Bisaillon M, Perreault JP. G-quadruplex located in the 5'UTR of the BAG-1 mRNA affects both its cap-dependent and cap-independent translation through global secondary structure maintenance. *Nucleic Acids Res* 2019; **47**: 10247-10266 [PMID: 31504805 DOI: 10.1093/nar/gkz777]

195 **Nishikawa T**, Kuwano Y, Nakata M, Rokutan K, Nishida K. Multiple G-quadruplexes in the LMNA promoter regulate LMNA variant 6 transcription and promote colon cancer cell growth. *Biochim Biophys Acta Gene Regul Mech* 2021; **1864**: 194746 [PMID: 34419630 DOI: 10.1016/j.bbagrm.2021.194746]

196 **Matsumura K**, Kawasaki Y, Miyamoto M, Kamoshida Y, Nakamura J, Negishi L, Suda S, Akiyama T. The novel G-quadruplex-containing long non-coding RNA GSEC antagonizes DHX36 and modulates colon cancer cell migration. *Oncogene* 2017; **36**: 1191-1199 [PMID: 27797375 DOI: 10.1038/onc.2016.282]

197 **Bejugam M**, Gunaratnam M, Müller S, Sanders DA, Sewitz S, Fletcher JA, Neidle S, Balasubramanian S. Targeting the c-Kit Promoter G-quadruplexes with 6-Substituted Indenoisoquinolines. *ACS Med Chem Lett* 2010; **1**: 306-310 [PMID: 24900212 DOI: 10.1021/ml100062z]

198 **Gunaratnam M**, Collie GW, Reszka AP, Todd AK, Parkinson GN, Neidle S. A naphthalene diimide G-quadruplex ligand inhibits cell growth and down-regulates BCL-2 expression in an imatinib-resistant gastrointestinal cancer cell line. *Bioorg Med Chem* 2018; **26**: 2958-2964 [PMID: 29724653 DOI: 10.1016/j.bmc.2018.04.050]

199 **Cogoi S**, Quadrifoglio F, Xodo LE. G-rich oligonucleotide inhibits the binding of a nuclear protein to the Ki-ras promoter and strongly reduces cell growth in human carcinoma pancreatic cells. *Biochemistry* 2004; **43**: 2512-2523 [PMID: 14992588 DOI: 10.1021/bi035754f]

200 **Bates PJ**, Laber DA, Miller DM, Thomas SD, Trent JO. Discovery and development of the G-rich oligonucleotide AS1411 as a novel treatment for cancer. *Exp Mol Pathol* 2009; **86**: 151-164 [PMID: 19454272 DOI: 10.1016/j.yexmp.2009.01.004]

201 **Pecoraro A**, Virgilio A, Esposito V, Galeone A, Russo G, Russo A. uL3 Mediated Nucleolar Stress Pathway as a New Mechanism of Action of Antiproliferative G-quadruplex TBA Derivatives in Colon Cancer Cells. *Biomolecules* 2020; **10** [PMID: 32290083 DOI: 10.3390/biom10040583]

202 **Virgilio A**, Benigno D, Pecoraro A, Russo A, Russo G, Esposito V, Galeone A. Exploring New Potential Anticancer Activities of the G-Quadruplexes Formed by [(GTG(2)T(G(3)T)(3)] and Its Derivatives with an Abasic Site Replacing Single Thymidine. *Int J Mol Sci* 2021; **22** [PMID: 34208896 DOI: 10.3390/ijms22137040]

203 **Virgilio A**, Pecoraro A, Benigno D, Russo A, Russo G, Esposito V, Galeone A. Antiproliferative Effects of the Aptamer d(GGGT)(4) and Its Analogues with an Abasic-Site Mimic Loop on Different Cancer Cells. *Int J Mol Sci* 2022; **23** [PMID: 35682635 DOI: 10.3390/ijms23115952]

204 **Lopes-Nunes J**, Oliveira PA, Cruz C. G-Quadruplex-Based Drug Delivery Systems for Cancer Therapy. *Pharmaceuticals (Basel)* 2021; **14** [PMID: 34358097 DOI: 10.3390/ph14070671]

205 **Bates PJ**, Reyes-Reyes EM, Malik MT, Murphy EM, O'Toole MG, Trent JO. G-quadruplex oligonucleotide AS1411 as a cancer-targeting agent: Uses and mechanisms. *Biochim Biophys Acta Gen Subj* 2017; **1861**: 1414-1428 [PMID: 28007579 DOI: 10.1016/j.bbagen.2016.12.015]

206 **Park JY**, Cho YL, Chae JR, Moon SH, Cho WG, Choi YJ, Lee SJ, Kang WJ. Gemcitabine-Incorporated G-Quadruplex Aptamer for Targeted Drug Delivery into Pancreas Cancer. *Mol Ther Nucleic Acids* 2018; **12**: 543-553 [PMID: 30195790 DOI: 10.1016/j.omtn.2018.06.003]

207 **Shi J**, Nie W, Zhao X, Yang X, Cheng H, Zhou T, Zhang Y, Zhang K, Liu J. An Intracellular Self-Assembly-Driven Uninterrupted ROS Generator Augments 5-Aminolevulinic-Acid-Based Tumor Therapy. *Adv Mater* 2022; **34**: e2201049 [PMID: 35488781 DOI: 10.1002/adma.202201049]

208 **Clua A**, Fàbrega C, García-Chica J, Grijalvo S, Eritja R. Parallel G-quadruplex Structures Increase Cellular Uptake and Cytotoxicity of 5-Fluoro-2'-deoxyuridine Oligomers in 5-Fluorouracil Resistant Cells. *Molecules* 2021; **26** [PMID: 33804620 DOI: 10.3390/molecules26061741]

209 **Awadasseid A**, Ma X, Wu Y, Zhang W. G-quadruplex stabilization *via* small-molecules as a potential anti-cancer strategy. *Biomed Pharmacother* 2021; **139**: 111550 [PMID: 33831835 DOI: 10.1016/j.biopha.2021.111550]

210 **Robinson J**, Raguseo F, Nuccio SP, Liano D, Di Antonio M. DNA G-quadruplex structures: more than simple roadblocks to transcription? *Nucleic Acids Res* 2021; **49**: 8419-8431 [PMID: 34255847 DOI: 10.1093/nar/gkab609]

211 **Rigo R**, Palumbo M, Sissi C. G-quadruplexes in human promoters: A challenge for therapeutic applications. *Biochim Biophys Acta Gen Subj* 2017; **1861**: 1399-1413 [PMID: 28025083 DOI: 10.1016/j.bbagen.2016.12.024]

212 **Kharel P**, Becker G, Tsvetkov V, Ivanov P. Properties and biological impact of RNA G-quadruplexes: from order to turmoil and back. *Nucleic Acids Res* 2020; **48**: 12534-12555 [PMID: 33264409 DOI: 10.1093/nar/gkaa1126]

213 **Shen J**, Varshney D, Simeone A, Zhang X, Adhikari S, Tannahill D, Balasubramanian S. Promoter G-quadruplex folding precedes transcription and is controlled by chromatin. *Genome Biol* 2021; **22**: 143 [PMID: 33962653 DOI: 10.1186/s13059-021-02346-7]

214 **Stevens AJ**, de Jong L, Kennedy MA. The Dynamic Regulation of G-Quadruplex DNA Structures by Cytosine Methylation. *Int J Mol Sci* 2022; **23** [PMID: 35269551 DOI: 10.3390/ijms23052407]

215 **Hahm JY**, Park J, Jang ES, Chi SW. 8-Oxoguanine: from oxidative damage to epigenetic and epitranscriptional modification. *Exp Mol Med* 2022; **54**: 1626-1642 [PMID: 36266447 DOI: 10.1038/s12276-022-00822-z]

216 **Varshney D**, Spiegel J, Zyner K, Tannahill D, Balasubramanian S. The regulation and functions of DNA and RNA G-quadruplexes. *Nat Rev Mol Cell Biol* 2020; **21**: 459-474 [PMID: 32313204 DOI: 10.1038/s41580-020-0236-x]

217 **Hensen F**, Potter A, van Esveld SL, Tarrés-Solé A, Chakraborty A, Solà M, Spelbrink JN. Mitochondrial RNA granules are critically dependent on mtDNA replication factors Twinkle and mtSSB. *Nucleic Acids Res* 2019; **47**: 3680-3698 [PMID: 30715486 DOI: 10.1093/nar/gkz047]

218 **David AP**, Pipier A, Pascutti F, Binolfi A, Weiner AMJ, Challier E, Heckel S, Calsou P, Gomez D, Calcaterra NB, Armas P. CNBP controls transcription by unfolding DNA G-quadruplex structures. *Nucleic Acids Res* 2019; **47**: 7901-7913 [PMID: 31219592 DOI: 10.1093/nar/gkz527]

219 **Niu K**, Zhang X, Song Q, Feng Q. G-Quadruplex Regulation of VEGFA mRNA Translation by RBM4. *Int J Mol Sci* 2022; **23** [PMID: 35054929 DOI: 10.3390/ijms23020743]

220 **Shu H**, Zhang R, Xiao K, Yang J, Sun X. G-Quadruplex-Binding Proteins: Promising Targets for Drug Design. *Biomolecules* 2022; **12** [PMID: 35625576 DOI: 10.3390/biom12050648]

221 **Fleming AM**, Burrows CJ. Interplay of Guanine Oxidation and G-Quadruplex Folding in Gene Promoters. *J Am Chem Soc* 2020; **142**: 1115-1136 [PMID: 31880930 DOI: 10.1021/jacs.9b11050]

222 **Ruggiero E**, Richter SN. Viral G-quadruplexes: New frontiers in virus pathogenesis and antiviral therapy. *Annu Rep Med Chem* 2020; **54**: 101-

131 [PMID: 32427223 DOI: 10.1016/bs.armc.2020.04.001]

223 **Zheng BX**, Yu J, Long W, Chan KH, Leung AS, Wong WL. Structurally diverse G-quadruplexes as the noncanonical nucleic acid drug target for live cell imaging and antibacterial study. *Chem Commun (Camb)* 2023; **59**: 1415-1433 [PMID: 36636928 DOI: 10.1039/d2cc05945b]

World Journal of Gastrointestinal Oncology

Submit a Manuscript: https://www.f6publishing.com

World J Gastrointest Oncol 2023 July 15; 15(7): 1174-1181

DOI: 10.4251/wjgo.v15.i7.1174

ISSN 1948-5204 (online)

MINIREVIEWS

Clinical value of serum pepsinogen in the diagnosis and treatment of gastric diseases

Yuan Qin, Jia-Xin Geng, Biao Huang

Specialty type: Medicine, research and experimental

Provenance and peer review: Invited article; Externally peer reviewed.

Peer-review model: Single blind

Peer-review report's scientific quality classification

Grade A (Excellent): A
Grade B (Very good): B
Grade C (Good): 0
Grade D (Fair): D
Grade E (Poor): 0

P-Reviewer: Caboclo JLF, Brazil; Haruma K, Japan; Kishikawa H, Japan

Received: March 28, 2023
Peer-review started: March 28, 2023
First decision: May 12, 2023
Revised: May 28, 2023
Accepted: June 14, 2023
Article in press: June 14, 2023
Published online: July 15, 2023

Yuan Qin, Jia-Xin Geng, Biao Huang, College of Life Sciences and Medicine, Zhejiang Sci-Tech University, Hangzhou 310018, Zhejiang Province, China

Corresponding author: Biao Huang, PhD, Professor, College of Life Sciences and Medicine, Zhejiang Sci-Tech University, No. 928, No. 2 Street, Qiantang District, Hangzhou 310018, Zhejiang Province, China. jswxhb@163.com

Abstract

Pepsinogen, secreted from the gastric mucosa, is the precursor of pepsin. It is categorized as pepsinogen 1 and pepsinogen 2 based on its immunogenicity. The pepsinogen content that can enter the blood circulation through the capillaries of the gastric mucosa is approximately 1% and remains stable all the time. The pepsinogen content in serum will change with the pathological changes of gastric mucosa. Therefore, the level of pepsinogen in serum can play a role in serologic biopsy to reflect the function and morphology of different regions of gastric mucosa and serve as an indicator of gastric disease. This study conducts relevant research on serum pepsinogen 1, pepsinogen 2, and the ratio of pepsinogen 1 to pepsinogen 2, and reviews their important value in clinical diagnosis of *Helicobacter pylori* infection, gastric ulcer, and even gastric carcinoma, providing ideas for other researchers.

Key Words: Pepsinogen 1; Pepsinogen 2; Gastric diseases; Serological marker; Serological biopsy

Core Tip: Pepsinogen is the precursor of pepsin, including pepsinogen 1 and pepsinogen 2. Serum pepsinogen has certain clinical value in determining *Helicobacter pylori* (*H. pylori*) infection and its treatment monitoring, in identifying the location and extent of gastric mucosal lesions, and in diagnosing and screening ongoing gastric cancer and precancerous lesions. This work summarizes the clinical value of serum pepsinogen 1, pepsinogen 2, and the ratio of pepsinogen 1 to pepsinogen 2 in the diagnosis of *H. pylori* infection, atrophic gastritis, and gastric cancer to provide readers with research ideas.

Citation: Qin Y, Geng JX, Huang B. Clinical value of serum pepsinogen in the diagnosis and treatment of gastric diseases. *World J Gastrointest Oncol* 2023; 15(7): 1174-1181
URL: https://www.wjgnet.com/1948-5204/full/v15/i7/1174.htm
DOI: https://dx.doi.org/10.4251/wjgo.v15.i7.1174

INTRODUCTION

Pepsinogen is an inactive precursor of pepsin, a specific functional enzyme in gastric mucosa, which was initially reported in duodenal ulcer[1,2]. It is secreted by gastric mucosal cells. According to immunogenicity, it can be classified into two types: Pepsinogen 1 and pepsinogen 2. Pepsinogen 1 mainly comes from the secretion of the chief cells of the gastric fundus gland, which is the cervical mucus cells. Pepsinogen 2 can originate from the mucous cells of the cardiac and pyloric glands in the gastric antrum, as well as from the duodenal gland in the upper part of the duodenum. Please refer to Figure 1[3,4] for details. Pepsin is mainly stored in glandular cells as a proenzyme particle synthesized by the main cell and has no activity[5,6]. Under external or physiological chemical stimuli, these particles are secreted into the stomach[7]. Under acidic conditions in the stomach, pepsinogen can be hydrolyzed into active pepsin[8]. pepsinogen also can interact with existing active gastric proteases[8]. Pepsin can decompose most proteins in the human body, thereby completing food digestion[8]. Most of pepsinogen is secreted into the stomach, and a small portion is also secreted into the bloodstream[9]. When cells are stimulated, most pepsinogen is released into the glandular cavity under exocytosis. The pepsinogen that can enter the blood circulation is approximately 1%, and the content is always stable[10]. They participate in the circulation through the capillaries of gastric mucosa[10]. After blood circulation, about two-thirds of pepsinogen 1 is metabolized by the kidneys, whereas pepsinogen 2 is reabsorbed and completely metabolized by the kidneys[6]. The number of cells in gastric mucosa and the glands in it could be reflected by the level of pepsinogen 1/2 in the serum, not only that, but also the morphology of different regions of gastric mucosa and whether its secretion function is normal can be indirectly reflected by the level of pepsinogen 1/2[11,12]. If the patient's gastric mucosa is diseased, the pepsinogen content in the serum will also be affected. One indicator of the function of gastric acid secreting gland cells is pepsinogen 1[13]. When gastric acid secretion increases, pepsinogen I increases and vice versa[1]. The secretory sites of pepsinogen II and its influencing factors are relatively numerous, and its rise is related to the atrophy of fundus gland, epithelial metaplasia, dysplasia, and various conditions[3]. Therefore, in order to detect the status of gastric mucosa, joint monitoring of pepsinogen 1 and pepsinogen 2 can be carried out. The relevant monitoring data of pepsinogen 1/pepsinogen 2 is also of significance for serological biopsy of gastric fundus gland mucosa. This study aims to investigate the clinical value of serum pepsinogen in the diagnosis and treatment of gastric diseases, with the hope of providing valuable insights for researchers.

PEPSINOGEN AND *HELICOBACTER PYLORI* INFECTION

Helicobacter pylori (*H. Pylori*) infection is a contributing factor to the development of gastric cancer[14,15]. In addition, it can induce atrophic gastritis in the antrum of the stomach[16,17]. Atrophic gastritis is widely acknowledged as a premalignant lesion of gastric cancer[18]. Lipopolysaccharides produced after *H. pylori* infection stimulate the chief cells of gastric mucosa, leading to increased pepsinogen 1 content in the serum[15]. It can also cause the release of INF-α, INF-γ, and other factors that promote cell apoptosis, thereby resulting in gastric gland atrophy and decreased gastric acid secretion[19,20]. *H. pylori* can promote the release of NF-κB and other cytokines, as well as gene transcription. Therefore, it will affect the chief cells and pepsinogen secretion. Some scholars believe that the increase of pepsinogen 2 content in serum is directly related to the changes of gastric mucosa caused by *H. pylori* infection, which is important in distinguishing normal gastric mucosa from abnormal gastric mucosa[3]. The pepsinogen contents of *H. pylori*-infected patients before and after sterilization treatment have been compared in some studies. The pepsinogen 1 content in the successful sterilization group is significantly lower than that prior to treatment, and the pepsinogen 2 content decreases more significantly. Accordingly, pepsinogen 1/pepsinogen 2 increases significantly. In the nonsterilization group, the pepsinogen content in serum does not significantly differ from that prior to treatment. Detecting the pepsinogen content has certain clinical value in evaluating whether *H. pylori* is eradicated. The development process from *H. pylori* infection to atrophic gastritis to gastric cancer is accompanied by changes in pepsinogen[21]. Extensive clinical research data have shown that *H. pylori* infection is very important in inducing gastric cancer. The World Health Origination classifies *H. pylori* infection as Class I carcinogen. Some studies have shown that *H. pylori* can promote AE1/p16 interaction by upregulating p16, thereby inducing gastric cancer. As shown in Figure 2, if *H. pylori* eradication treatment can be completed prior to "the point of no return" of gastric cancer, it can more effectively reduce the incidence rate of cancer. It can even prevent the occurrence of intestinal cancer. Until now, there have been main methods for eradicating *H. pylori*: Proton pump inhibitor (PPI) based triple therapy and PPI dual therapy administered through high-dose amoxicillin[22,23]. PPI has been approved by FDA and can be used for the treatment of *H. pylori* infection or other diseases, as it can effectively reduce the production of acids in the upper digestive system[7,24,25]. But new research suggests that if patients use PPI for a long time, it is likely to cause adverse reactions to the body[26,27]. Patients who receive long-term PPI treatment also have an increased risk of death[28]. Therefore, in the clinical practice of *H. pylori* eradication treatment, PPI drugs use should be used closely monitored, especially long-term medication.

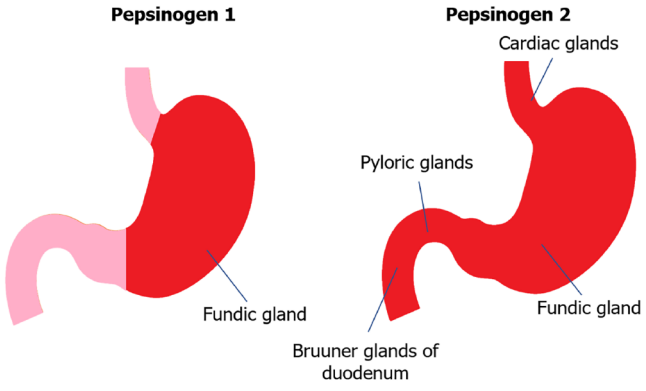

DOI: 10.4251/wjgo.v15.i7.1174 **Copyright** ©The Author(s) 2023.

Figure 1 Expression of pepsinogen 1 and pepsinogen 2 in gastric mucosa.

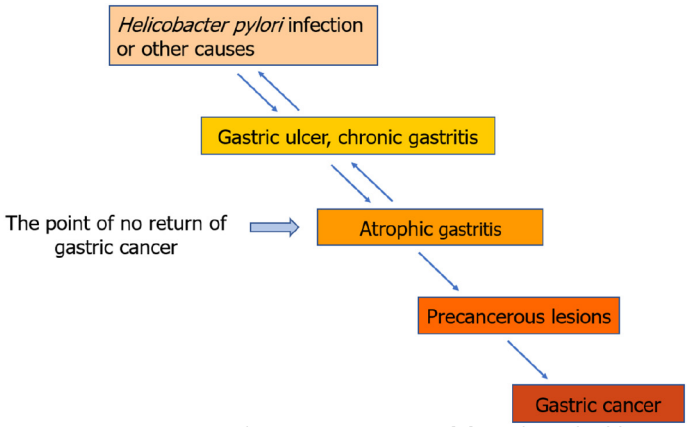

DOI: 10.4251/wjgo.v15.i7.1174 **Copyright** ©The Author(s) 2023.

Figure 2 Development of gastric mucosal lesion.

In common cases, after *H. pylori* eradication, plasma pepsinogen 1 and pepsinogen 2 levels decrease and pepsinogen 2 decreases more significantly than pepsinogen 1[29]. Therefore, pepsinogen 1/pepsinogen 2 levels increase. Generally, pepsinogen 2 decreases after one month of *H. pylori* eradication, and the pepsinogen 1 level decreases within six months [30,31]. Currently, no unified view on whether pepsinogen can be used as a noninvasive serological indicator to evaluate the efficacy of *H. pylori* eradication. Gatta *et al*[32] suggested that the pepsinogen 2 level after eight weeks of *H. pylori* eradication is a reliable indicator of a successful procedure. The sensitivity and specificity of the optimum cutoff values (< 22.7 ng/mL) used to detect the complete eradication of *H. pylori* are 100.0% and 96.6%, respectively. No acceptable results are found with regard to other factors (pepsinogen 1 and gastrin-17) evaluated. However, according to Di Mario *et al*[3], pepsinogen 2 cannot be used as a successful marker for eradicating *H. pylori*. The biomarkers used to determine gastritis and *H. pylori* infection should be pepsinogen 2 serum level, pepsinogen 1 serum level, and pepsinogen 1/pepsinogen 2 ratio.

PEPSINOGEN, GASTRIC ULCER AND ATROPHIC GASTRITIS

Current research results on the relationship between gastric ulcer lesions and serum pepsinogen levels, there are differences in current research results. The differences would be related to the population, and also be affected by detection methods, and interference from dietary factors. In those patients who had gastric ulcer, the increase of pepsinogen 1 and pepsinogen 2 is related to the increase in gastric acid secretion, leading to an increase in serum pepsinogen secretion, and an increase in gastric mucosal permeability, with a large amount of pepsinogen entering the blood. Therefore, in clinical diagnosis, the serum level of pepsinogen can serve as a reliable biomarker for the diagnosis of gastric ulcers in patients. Atrophic gastritis is the first step in the reaction cascade leading to gastric adenocarcinoma, and it is an important precancerous lesion[33,34]. The gold standard for diagnosing atrophic gastritis remains gastroscopy and histological examination of biopsy specimens[35]. However, because the latter is conducted randomly and atrophic gastritis is distributed patchily, histological examination reflects only the state of mucosa, and the related detection is limited. Normal mucosa and gastric glands can secrete pepsinogen and gastric acid as required[36]. Pepsinogen can be activated to produce biologically active pepsin under acidic conditions, playing its physiological role[36]. When mucosal

atrophy occurs, patients experience various degrees of atrophy of gastric glands[37]. Consequently, the gastric juice changes pH and the gastric juice decreases volume affecting the pepsinogen activity. The cells secreting pepsinogen 1 and pepsinogen 2 differ. When gastric mucosa atrophy occurs, the number of glandular cells and chief cells decreases, resulting in different changes in serum pepsinogen 1 and pepsinogen 2 contents[38,39]. Many studies have shown that the pepsinogen 1/pepsinogen 2 in serum and the pepsinogen 1 in it at low levels are indicators of atrophic gastritis[40]. Atrophic gastritis of the stomach is defined as serum pepsinogen 1/pepsinogen 2 < 3 and serum pepsinogen 1 level < 70 ng/mL[41]. Although a good correlation exists among endoscopy, histology, serology, and atrophic gastritis, the gastric atrophy presence is not always consistent with endoscopic findings[42]. The levels of pepsinogen 1 and the ratio of pepsinogen 1 to pepsinogen 2 in serum will decrease with the histological progression of atrophic gastritis. Moreover, when the stomach is severely atrophic, serum pepsinogen 1/pepsinogen 2 will also decrease accordingly[43,44]. For patients who was suffered severe atrophic gastritis, the levels of pepsinogen 1/pepsinogen 2 in their bodies would be lower than those mild atrophic gastritis patients[43,45].

The cutoff value of atrophic gastritis diagnosis and the diagnostic efficiency also vary due to different regions, genetic backgrounds of populations, and test kits[46]. Cha *et al*[47] used pepsinogen 1/ pepsinogen 2 = 4 as the cutoff value, and the sensitivity and specificity of detecting atrophic gastritis are 82.6% and 91.7%, respectively. According to Zoalfaghari A's research, the specificity and sensitivity of pepsinogen 1/pepsinogen 2 in the diagnosis of atrophic gastritis were 71%, 71%, with the receiver operating characteristic curve area 0.639 (cut-off value = 8). Nguyen *et al*[48] conducted relevant studies on the Vietnamese population and found that serum pepsinogen 1 and pepsinogen 1/pepsinogen 2 ratios have diagnostic value for patients with moderate and severe atrophic gastritis. The specificity demonstrated by the research institute is 83.9%, the detection sensitivity is 73.0%, and the optimal critical value is pepsinogen 1/pepsinogen 2 ≤ 4.6; pepsinogen 1 ≤ 69.0[48]. Therefore, it is necessary to ensure the diagnosis of atrophic gastritis through serum pepsinogen testing, based on the premise of determining reasonable diagnostic parameters according to the actual situation.

PEPSINOGEN AND GASTRIC CANCER

The occurrence of gastric cancer is a multistep, multifactor, interactive process[49,50]. Gastric cancer develops from precancerous diseases, including atrophic gastritis, dysplasia and intestinal metaplasia[51,52]. In recent years, with the continuous deepening of clinical research, the status and function of gastric mucosa can be reflected effectively based on the serum pepsinogen level detection[16]. It can be used as a serological reference index for screening high-risk groups with precancerous lesions and early gastric cancer[53]. The significance of serum pepsinogen level change in the clinical screening of high-risk population with gastric cancer and the relationship between serum pepsinogen content and gastric cancer gradually become the research focus of scholars from various countries[6]. Persistent progression of precancerous lesions can lead to gastric cancer[54]. Therefore, the factors associated with the onset of gastric cancer are also related to the progression of precancerous lesions. The stomach is the only source of pepsinogen. Thus, the change in pepsinogen level can effectively reflect functional changes in the gastric mucosa[10]. Atrophic gastritis is an important background for mucosal gastric cancer, and pepsinogen 1/pepsinogen 2 levels continuously decrease with the continuous progression of gastric mucosal atrophy[14,55]. The atrophic degree of gastric mucosa of patients can be evaluated and judged through the detection of pepsinogen 1/pepsinogen 2 level[54].

According to existing research, there is a good correlation between changes in the morphology and function of the gastric mucosa in patients and serum levels of pepsinogen 1 and the ratio of pepsinogen 1 to pepsinogen 2. In the process of cancer screening, serum pepsinogen measurement is of great significance. According to research conducted by researchers on cancer patients and control groups, pepsinogen 1 ≤ 50 ng/mL and pepsinogen 1/pepsinogen 2 < 3 can be used for clinical diagnosis of cancer. The sensitivity, specificity, and accuracy values are 55%, 75%, and 72% respectively [11]. A 14-year cohort study based on a Japanese population shows that 97 of 2742 residents aged 40 and above develop symptomatic cancer. Among patients with early symptoms, approximately 62.8% (61 patients) showed pepsinogen 1/ pepsinogen 2 levels < 3, while pepsinogen 1 levels < 70 ng/mL[56]. According to Mansour-Ghanaei *et al*[57], pepsinogen 1 serum levels and pepsinogen 1/pepsinogen 2 ratios can be used as screening serum biomarkers for gastric cancer screening. If the critical value of pepsinogen 1 is 70.95 μg/L, and the critical value of pepsinogen 1/pepsinogen 2 is 2.99, indicating excellent sensitivity and specificity in patients[57]. Therefore, it can be concluded that serum pepsinogen can be used to predict gastric cancer. However, this does not mean that large-scale cancer risk screening can be conducted through serum pepsinogen level detection, as there is a high likelihood of pepsinogen negative cancers represented by diffuse cancers[58-60]. Miki *et al*[58] created a set of "ABC classification" detection methods in 2011. This detection method can detect pepsinogen negative cancers[58,59]. Assess the cancer risk of patients by measuring their *H. pylori* antibody titers and serum pepsinogen levels, and then divide them into four groups: Group 1 [*H. pylori* antibody (-) pepsinogen (-)], Group 2 [*H. pylori* antibody (+) pepsinogen (-)], group 3 [*H. pylori* antibody (+) pepsinogen (+)], and group 4 [*H. pylori* antibody (-) pepsinogen (+)]. The risk of cancer gradually increases from group 1 to group 4[61-63]. In theory, the risk of cancer in Group 1 is the lowest. However, 2% to 10% of cancer patients are classified as Group 1[64]. Some patients were inaccurately classified as Group 1 due to receiving antibiotics to eradicate *H. pylori* and showing negative *H. pylori* antibodies[65]. From this perspective, when conducting risk assessment for gastric cancer, patients with high negative *H. pylori* antibodies should be distinguished and evaluated through other tests.

In addition, the joint detection of serum pepsinogen 1 and other gastric cancer-related tumor markers have very important diagnostic value. For the early diagnosis of gastric cancer, the joint detection of serum pepsinogen and serum tumor markers (such as CA125, CA199, CA242, CA724, and CEA) can play an important role. The research team led by the author of this article conducted joint testing on pepsinogen and serum soluble Tim-3[66]. The test results obtained

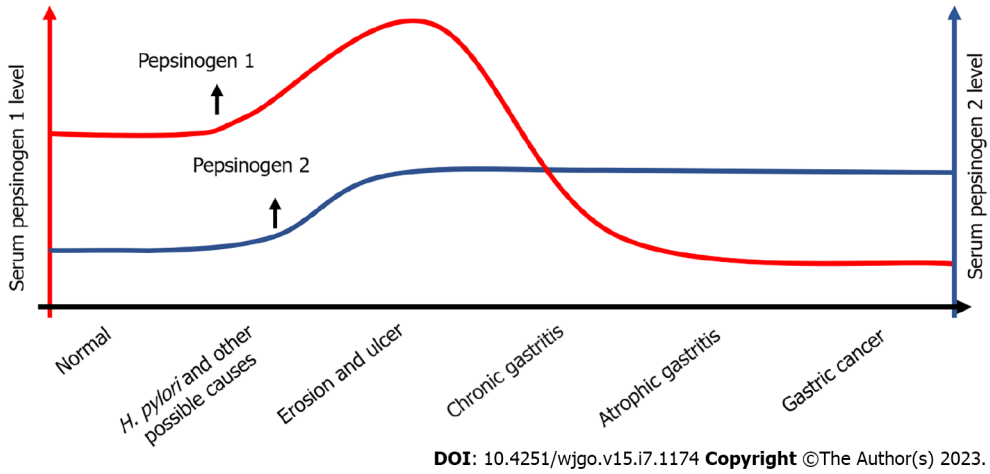

DOI: 10.4251/wjgo.v15.i7.1174

Figure 3 Relationship between serum pepsinogen level and gastric diseases. *H. pylori*: *Helicobacter pylori*.

indicate that the sensitivity for detecting cancer is 86.44%, while the specificity is 91.78%, significantly higher than those obtained by single detection[66]. For patients whose detection results indicate gradually decreased pepsinogen 1 and pepsinogen 1/ pepsinogen 2 levels, relevant endoscopic techniques can be used jointly. Some studies show that the joint detection of serum pepsinogen 1 and staining endoscopy improves the diagnostic rate of early gastric cancer, and the sensitivity of the joint detection is significantly higher than that of the individual approach[67].

CONCLUSION

Pepsinogen is a serological marker whose subtypes are closely related to *H. pylori* and various gastrointestinal diseases [11]. Serum pepsinogen has certain clinical value in determining *H. pylori* infection and its treatment monitoring, in identifying the location and extent of gastric mucosal lesions, and in diagnosing and screening ongoing gastric cancer and precancerous lesions (Figure 3)[68]. Pepsinogen 1, pepsinogen 2, and pepsinogen 1/pepsinogen 2 are serum indicators of a certain gastric disease, and the changes in their levels in serum occur continuously throughout the process from inflammation to carcinogenesis in gastric tissue. Compared with the gastroscopy, serum pepsinogen detection is inexpensive, non-invasive, and simple. Thus, it is suitable for screening gastric diseases in large populations. The current research results on the diagnostic and therapeutic value of serum pepsinogen detection for gastric cancer are inconsistent, some shortcomings remain, and unified diagnostic standards cannot be used. However, with the establishment of screening strategies applicable to different populations and the deepening of related research, pepsinogen plays an important role in the prevention, screening, and diagnosis of cancer and atrophic gastritis. Moreover, it also performs well in predicting postoperative recurrence and metastasis of cancer. Moreover, developing novel sensitive and convenient detection methods is greatly important in further exerting the clinical value of serum pepsinogen detection.

FOOTNOTES

Author contributions: Huang B and Qin Y designed this study; Qin Y and Geng JX conducted the reference analyses, drafted the initial version of the paper, and received contributions from all authors.

Supported by the National Natural Science Foundation of China, No. 82172336; "Pioneer" and "Leading Goose" R&D Program of Zhejiang, No. 2022C03118 and No. 2023C03075; Natural Science Foundation of Zhejiang Province, No. LQ23H050005; and Scientific Research Project of Zhejiang Provincial Education Department, No. Y202250731.

Conflict-of-interest statement: Authors declare no conflict of interests for this article.

Country/Territory of origin: China

ORCID number: Yuan Qin 0000-0002-5651-8293; Biao Huang 0000-0003-1883-0670.

S-Editor: Chen YL

L-Editor: A
P-Editor: Yu HG

REFERENCES

1 **Kageyama T**. Pepsinogens, progastricsins, and prochymosins: structure, function, evolution, and development. *Cell Mol Life Sci* 2002; **59**: 288-306 [PMID: 11915945 DOI: 10.1007/s00018-002-8423-9]
2 **Rotter JI**, Sones JQ, Samloff IM, Richardson CT, Gursky JM, Walsh JH, Rimoin DL. Duodenal-ulcer disease associated with elevated serum pepsinogen I: an inherited autosomal dominant disorder. *N Engl J Med* 1979; **300**: 63-66 [PMID: 758579 DOI: 10.1056/NEJM197901113000203]
3 **Di Mario F**, Crafa P, Barchi A, Franzoni L, Franceschi M, Russo M, Bricca L, Brozzi L, Rodriguez Castro K, Rugge M. Pepsinogen II in gastritis and Helicobacter pylori infection. *Helicobacter* 2022; **27**: e12872 [PMID: 34997989 DOI: 10.1111/hel.12872]
4 **Hamashima C**. Forthcoming Step in Gastric Cancer Prevention: How Can Risk Stratification Be Combined with Endoscopic Screening for Gastric Cancer? *Gut Liver* 2022; **16**: 811-824 [PMID: 35314519 DOI: 10.5009/gnl210313]
5 **Wang Y**, Zhu Z, Liu Z, Zhao Z, Xue X, Li X, Li P, Rong G, Ma Y. Diagnostic value of serum pepsinogen I, pepsinogen II, and gastrin-17 levels for population-based screening for early-stage gastric cancer. *J Int Med Res* 2020; **48**: 300060520914826 [PMID: 32228342 DOI: 10.1177/0300060520914826]
6 **Trivanovic D**, Plestina S, Honovic L, Dobrila-Dintinjana R, Vlasic Tanaskovic J, Vrbanec D. Gastric cancer detection using the serum pepsinogen test method. *Tumori* 2022; **108**: 386-391 [PMID: 33993805 DOI: 10.1177/03008916211014961]
7 **Gritti I**, Banfi G, Roi GS. Pepsinogens: physiology, pharmacology pathophysiology and exercise. *Pharmacol Res* 2000; **41**: 265-281 [PMID: 10675278 DOI: 10.1006/phrs.1999.0586]
8 **Muller MJ**, Defize J, Hunt RH. Control of pepsinogen synthesis and secretion. *Gastroenterol Clin North Am* 1990; **19**: 27-40 [PMID: 2184130]
9 **Zhou MJ**, Huang RJ. Catching Up with the World: Pepsinogen Screening for Gastric Cancer in the United States. *Cancer Epidemiol Biomarkers Prev* 2022; **31**: 1257-1258 [PMID: 35775231 DOI: 10.1158/1055-9965.EPI-22-0372]
10 **Juan Cai W**, Yin L, Kang Q, Chen Zeng Z, Liang Wang S, Cheng J. The Serum Pepsinogen Test as a Predictor of Kazakh Gastric Cancer. *Sci Rep* 2017; **7**: 43536 [PMID: 28251999 DOI: 10.1038/srep43536]
11 **Massarrat S**, Haj-Sheykholeslami A. Increased Serum Pepsinogen II Level as a Marker of Pangastritis and Corpus-Predominant Gastritis in Gastric Cancer Prevention. *Arch Iran Med* 2016; **19**: 137-140 [PMID: 26838085]
12 **Zhang J**, Guo JZ, Xiao HL, Zhu L, Liu HY, Zhang Y, Huang B. Simultaneous detection of different serum pepsinogens and its primary application. *World J Gastroenterol* 2010; **16**: 3072-3077 [PMID: 20572312 DOI: 10.3748/wjg.v16.i24.3072]
13 **Mabe K**, Inoue K, Kamada T, Kato K, Kato M, Haruma K. Endoscopic screening for gastric cancer in Japan: Current status and future perspectives. *Dig Endosc* 2022; **34**: 412-419 [PMID: 34143908 DOI: 10.1111/den.14063]
14 **Lahner E**, Carabotti M, Annibale B. Treatment of Helicobacter pylori infection in atrophic gastritis. *World J Gastroenterol* 2018; **24**: 2373-2380 [PMID: 29904244 DOI: 10.3748/wjg.v24.i22.2373]
15 **Wang F**, Meng W, Wang B, Qiao L. Helicobacter pylori-induced gastric inflammation and gastric cancer. *Cancer Lett* 2014; **345**: 196-202 [PMID: 23981572 DOI: 10.1016/j.canlet.2013.08.016]
16 **Selgrad M**, Bornschein J, Rokkas T, Malfertheiner P. Helicobacter pylori: gastric cancer and extragastric intestinal malignancies. *Helicobacter* 2012; **17** Suppl 1: 30-35 [PMID: 22958153 DOI: 10.1111/j.1523-5378.2012.00980.x]
17 **Cheung KS**, Leung WK. Risk of gastric cancer development after eradication of Helicobacter pylori. *World J Gastrointest Oncol* 2018; **10**: 115-123 [PMID: 29770171 DOI: 10.4251/wjgo.v10.i5.115]
18 **Cave TR**, Cave DR. Helicobacter pylori stimulates pepsin secretion from isolated rabbit gastric glands. *Scand J Gastroenterol Suppl* 1991; **181**: 9-14 [PMID: 1866598 DOI: 10.3109/00365529109093202]
19 **Codolo G**, Coletta S, D'Elios MM, de Bernard M. HP-NAP of Helicobacter pylori: The Power of the Immunomodulation. *Front Immunol* 2022; **13**: 944139 [PMID: 35844568 DOI: 10.3389/fimmu.2022.944139]
20 **Li W**, Chen T. An Insight into the Clinical Application of Gut Microbiota during Anticancer Therapy. *Adv Gut & Microbiome Res* 2022; **2022**: 8183993 [DOI: 10.1155/2022/8183993]
21 **Ohkusa T**, Takashimizu I, Fujiki K, Araki A, Honda K, Shimoi K, Sakurazawa T, Horiuchi T, Suzuki S, Ariake K, Ishii K. Changes in serum pepsinogen, gastrin, and immunoglobulin G antibody titers in helicobacter pylori-positive gastric ulcer after eradication of infection. *J Clin Gastroenterol* 1997; **25**: 317-322 [PMID: 9412911 DOI: 10.1097/00004836-199707000-00004]
22 **Yun J**, Wu Z, Qi G, Han T, Zhang D. The high-dose amoxicillin-proton pump inhibitor dual therapy in eradication of Helicobacter pylori infection. *Expert Rev Gastroenterol Hepatol* 2021; **15**: 149-157 [PMID: 32960107 DOI: 10.1080/17474124.2021.1826306]
23 **Liu C**, Wang Y, Shi J, Zhang C, Nie J, Li S, Zheng T. The status and progress of first-line treatment against Helicobacter pylori infection: a review. *Therap Adv Gastroenterol* 2021; **14**: 1756284821989177 [PMID: 34262609 DOI: 10.1177/1756284821989177]
24 **Vaezi MF**, Yang YX, Howden CW. Complications of Proton Pump Inhibitor Therapy. *Gastroenterology* 2017; **153**: 35-48 [PMID: 28528705 DOI: 10.1053/j.gastro.2017.04.047]
25 **Edinoff AN**, Wu NW, Parker K, Dudossat E, Linquest L, Flanagan CJ, Dharani A, Patel H, Willett O, Cornett EM, Kaye AM, Kaye AD. Proton Pump Inhibitors, Kidney Damage, and Mortality: An Updated Narrative Review. *Adv Ther* 2023; **40**: 2693-2709 [PMID: 37140707 DOI: 10.1007/s12325-023-02476-3]
26 **Lespessailles E**, Toumi H. Proton Pump Inhibitors and Bone Health: An Update Narrative Review. *Int J Mol Sci* 2022; **23** [PMID: 36142643 DOI: 10.3390/ijms231810733]
27 **Castellana C**, Pecere S, Furnari M, Telese A, Matteo MV, Haidry R, Eusebi LH. Side effects of long-term use of proton pump inhibitors: practical considerations. *Pol Arch Intern Med* 2021; **131**: 541-549 [PMID: 33982542 DOI: 10.20452/pamw.15997]
28 **Chinzon D**, Domingues G, Tosetto N, Perrotti M. SAFETY OF LONG-TERM PROTON PUMP INHIBITORS: FACTS AND MYTHS. *Arq Gastroenterol* 2022; **59**: 219-225 [PMID: 35830032 DOI: 10.1590/S0004-2803.202202000-40]

29 **Daugule I**, Ruskule A, Moisejevs G, Rudzite D, Jonaitis L, Janciauskas D, Kiudelis G, Kupcinskas L, Leja M. Long-term dynamics of gastric biomarkers after eradication of Helicobacter pylori infection. *Eur J Gastroenterol Hepatol* 2015; **27**: 501-505 [PMID: 25822857 DOI: 10.1097/MEG.0000000000000308]

30 **Pérez-Paramo M**, Albillos A, Calleja JL, Salas C, Marín MC, Marcos ML, Cacho G, Escartín P, Ortiz-Berrocal J. Changes in gastrin and serum pepsinogens in monitoring of Helicobacter pylori response to therapy. *Dig Dis Sci* 1997; **42**: 1734-1740 [PMID: 9286242 DOI: 10.1023/a:1018873717985]

31 **Leja M**, Lapina S, Polaka I, Rudzite D, Vilkoite I, Daugule I, Belkovets A, Pimanov S, Makarenko J, Tolmanis I, Lejnieks A, Boka V, Rumba-Rozenfelde I, Vikmanis U. Pepsinogen testing for evaluation of the success of Helicobacter pylori eradication at 4 weeks after completion of therapy. *Medicina (Kaunas)* 2014; **50**: 8-13 [PMID: 25060199 DOI: 10.1016/j.medici.2014.05.001]

32 **Gatta L**, Di Mario F, Vaira D, Rugge M, Franzè A, Plebani M, Cavestro GM, Lucarini P, Lera M, Scarpignato C. Quantification of serum levels of pepsinogens and gastrin to assess eradication of Helicobacter pylori. *Clin Gastroenterol Hepatol* 2011; **9**: 440-442 [PMID: 21172454 DOI: 10.1016/j.cgh.2010.12.009]

33 **Komoto K**, Haruma K, Kamada T, Tanaka S, Yoshihara M, Sumii K, Kajiyama G, Talley NJ. Helicobacter pylori infection and gastric neoplasia: correlations with histological gastritis and tumor histology. *Am J Gastroenterol* 1998; **93**: 1271-1276 [PMID: 9707050 DOI: 10.1111/j.1572-0241.1998.00408.x]

34 **Huang YK**, Yu JC, Kang WM, Ma ZQ, Ye X, Tian SB, Yan C. Significance of Serum Pepsinogens as a Biomarker for Gastric Cancer and Atrophic Gastritis Screening: A Systematic Review and Meta-Analysis. *PLoS One* 2015; **10**: e0142080 [PMID: 26556485 DOI: 10.1371/journal.pone.0142080]

35 **Dinis-Ribeiro M**, Areia M, de Vries AC, Marcos-Pinto R, Monteiro-Soares M, O'Connor A, Pereira C, Pimentel-Nunes P, Correia R, Ensari A, Dumonceau JM, Machado JC, Macedo G, Malfertheiner P, Matysiak-Budnik T, Megraud F, Miki K, O'Morain C, Peek RM, Ponchon T, Ristimaki A, Rembacken B, Carneiro F, Kuipers EJ; MAPS Participants; European Society of Gastrointestinal Endoscopy; European Helicobacter Study Group; European Society of Pathology; Sociedade Portuguesa de Endoscopia Digestiva. Management of precancerous conditions and lesions in the stomach (MAPS): guideline from the European Society of Gastrointestinal Endoscopy (ESGE), European Helicobacter Study Group (EHSG), European Society of Pathology (ESP), and the Sociedade Portuguesa de Endoscopia Digestiva (SPED). *Virchows Arch* 2012; **460**: 19-46 [PMID: 22190006 DOI: 10.1007/s00428-011-1177-8]

36 **Dooley CP**, Cohen H, Fitzgibbons PL, Bauer M, Appleman MD, Perez-Perez GI, Blaser MJ. Prevalence of Helicobacter pylori infection and histologic gastritis in asymptomatic persons. *N Engl J Med* 1989; **321**: 1562-1566 [PMID: 2586553 DOI: 10.1056/NEJM198912073212302]

37 **Zagari RM**, Rabitti S, Greenwood DC, Eusebi LH, Vestito A, Bazzoli F. Systematic review with meta-analysis: diagnostic performance of the combination of pepsinogen, gastrin-17 and anti-Helicobacter pylori antibodies serum assays for the diagnosis of atrophic gastritis. *Aliment Pharmacol Ther* 2017; **46**: 657-667 [PMID: 28782119 DOI: 10.1111/apt.14248]

38 **Lee SY**. Endoscopic gastritis, serum pepsinogen assay, and Helicobacter pylori infection. *Korean J Intern Med* 2016; **31**: 835-844 [PMID: 27604795 DOI: 10.3904/kjim.2016.166]

39 **Kiyohira K**, Yoshihara M, Ito M, Haruma K, Tanaka S, Chayama K. Serum pepsinogen concentration as a marker of Helicobacter pyloriinfection and the histologic grade of gastritis; evaluation of gastric mucosa by serum pepsinogen levels. *J Gastroenterol* 2003; **38**: 332-338 [PMID: 12743772 DOI: 10.1007/s005350300060]

40 **Leung WK**, Wu MS, Kakugawa Y, Kim JJ, Yeoh KG, Goh KL, Wu KC, Wu DC, Sollano J, Kachintorn U, Gotoda T, Lin JT, You WC, Ng EK, Sung JJ; Asia Pacific Working Group on Gastric Cancer. Screening for gastric cancer in Asia: current evidence and practice. *Lancet Oncol* 2008; **9**: 279-287 [PMID: 18308253 DOI: 10.1016/S1470-2045(08)70072-X]

41 **Kato M**, Asaka M. Recent development of gastric cancer prevention. *Jpn J Clin Oncol* 2012; **42**: 987-994 [PMID: 23018579 DOI: 10.1093/jjco/hys151]

42 **Kishikawa H**, Nakamura K, Ojiro K, Katayama T, Arahata K, Takarabe S, Sasaki A, Miura S, Hayashi Y, Hoshi H, Kanai T, Nishida J. Relevance of pepsinogen, gastrin, and endoscopic atrophy in the diagnosis of autoimmune gastritis. *Sci Rep* 2022; **12**: 4202 [PMID: 35273265 DOI: 10.1038/s41598-022-07947-1]

43 **Yamada S**, Matsuhisa T, Makonkawkeyoon L, Chaidatch S, Kato S, Matsukura N. Helicobacter pylori infection in combination with the serum pepsinogen I/II ratio and interleukin-1beta-511 polymorphisms are independent risk factors for gastric cancer in Thais. *J Gastroenterol* 2006; **41**: 1169-1177 [PMID: 17287896 DOI: 10.1007/s00535-006-1951-6]

44 **Samloff IM**, Varis K, Ihamaki T, Siurala M, Rotter JI. Relationships among serum pepsinogen I, serum pepsinogen II, and gastric mucosal histology. A study in relatives of patients with pernicious anemia. *Gastroenterology* 1982; **83**: 204-209 [PMID: 7084603]

45 **Sitas F**, Smallwood R, Jewell D, Millard PR, Newell DG, Meuwissen SG, Moses S, Zwiers A, Forman D. Serum anti-Helicobacter pylori IgG antibodies and pepsinogens A and C as serological markers of chronic atrophic gastritis. *Cancer Epidemiol Biomarkers Prev* 1993; **2**: 119-123 [PMID: 8467246]

46 **Brenner H**, Rothenbacher D, Weck MN. Epidemiologic findings on serologically defined chronic atrophic gastritis strongly depend on the choice of the cutoff-value. *Int J Cancer* 2007; **121**: 2782-2786 [PMID: 17691112 DOI: 10.1002/ijc.22992]

47 **Cha JH**, Jang JS. Clinical correlation between serum pepsinogen level and gastric atrophy in gastric neoplasm. *Korean J Intern Med* 2020; **35**: 550-558 [PMID: 30400679 DOI: 10.3904/kjim.2018.282]

48 **Nguyen CL**, Dao TT, Phi TN, Nguyen TP, Pham VT, Vu TK. Serum pepsinogen: A potential non-invasive screening method for moderate and severe atrophic gastritis among an asian population. *Ann Med Surg (Lond)* 2022; **78**: 103844 [PMID: 35734694 DOI: 10.1016/j.amsu.2022.103844]

49 **Zhang P**, Yang M, Zhang Y, Xiao S, Lai X, Tan A, Du S, Li S. Dissecting the Single-Cell Transcriptome Network Underlying Gastric Premalignant Lesions and Early Gastric Cancer. *Cell Rep* 2019; **27**: 1934-1947.e5 [PMID: 31067475 DOI: 10.1016/j.celrep.2019.04.052]

50 **Venerito M**, Vasapolli R, Rokkas T, Malfertheiner P. Gastric cancer: epidemiology, prevention, and therapy. *Helicobacter* 2018; **23** Suppl 1: e12518 [PMID: 30203589 DOI: 10.1111/hel.12518]

51 **Smyth EC**, Nilsson M, Grabsch HI, van Grieken NC, Lordick F. Gastric cancer. *Lancet* 2020; **396**: 635-648 [PMID: 32861308 DOI: 10.1016/S0140-6736(20)31288-5]

52 **Iijima K**, Abe Y, Kikuchi R, Koike T, Ohara S, Sipponen P, Shimosegawa T. Serum biomarker tests are useful in delineating between patients with gastric atrophy and normal, healthy stomach. *World J Gastroenterol* 2009; **15**: 853-859 [PMID: 19230047 DOI: 10.3748/wjg.15.853]

53 **Chen XZ**, Huang CZ, Hu WX, Liu Y, Yao XQ. Gastric Cancer Screening by Combined Determination of Serum Helicobacter pylori Antibody and Pepsinogen Concentrations: ABC Method for Gastric Cancer Screening. *Chin Med J (Engl)* 2018; **131**: 1232-1239 [PMID: 29722342 DOI: 10.4103/0366-6999.231512]

54 **Cho JH**, Jin SY, Park S. Scoring model for discriminating gastric cancer risk in patients with negative serum pepsinogen and anti-Helicobacter pylori antibody results. *J Gastroenterol Hepatol* 2021; **36**: 3345-3353 [PMID: 34328237 DOI: 10.1111/jgh.15630]

55 **Magris R**, De Re V, Maiero S, Fornasarig M, Guarnieri G, Caggiari L, Mazzon C, Zanette G, Steffan A, Canzonieri V, Cannizzaro R. Low Pepsinogen I/II Ratio and High Gastrin-17 Levels Typify Chronic Atrophic Autoimmune Gastritis Patients With Gastric Neuroendocrine Tumors. *Clin Transl Gastroenterol* 2020; **11**: e00238 [PMID: 33094954 DOI: 10.14309/ctg.0000000000000238]

56 **Oishi Y**, Kiyohara Y, Kubo M, Tanaka K, Tanizaki Y, Ninomiya T, Doi Y, Shikata K, Yonemoto K, Shirota T, Matsumoto T, Iida M. The serum pepsinogen test as a predictor of gastric cancer: the Hisayama study. *Am J Epidemiol* 2006; **163**: 629-637 [PMID: 16443800 DOI: 10.1093/aje/kwj088]

57 **Mansour-Ghanaei F**, Joukar F, Baghaee M, Sepehrimanesh M, Hojati A. Only serum pepsinogen I and pepsinogen I/II ratio are specific and sensitive biomarkers for screening of gastric cancer. *Biomol Concepts* 2019; **10**: 82-90 [PMID: 31188744 DOI: 10.1515/bmc-2019-0010]

58 **Miki K**. Gastric cancer screening by combined assay for serum anti-Helicobacter pylori IgG antibody and serum pepsinogen levels - "ABC method". *Proc Jpn Acad Ser B Phys Biol Sci* 2011; **87**: 405-414 [PMID: 21785258 DOI: 10.2183/pjab.87.405]

59 **Furihata C**. Human gastric cancer risk screening: From rat pepsinogen studies to the ABC method. *Proc Jpn Acad Ser B Phys Biol Sci* 2021; **97**: 462-478 [PMID: 34629355 DOI: 10.2183/pjab.97.023]

60 **Leja M**, Linē A. Early detection of gastric cancer beyond endoscopy - new methods. *Best Pract Res Clin Gastroenterol* 2021; **50-51**: 101731 [PMID: 33975677 DOI: 10.1016/j.bpg.2021.101731]

61 **Park CH**, Kim EH, Jung DH, Chung H, Park JC, Shin SK, Lee SK, Lee YC. The new modified ABCD method for gastric neoplasm screening. *Gastric Cancer* 2016; **19**: 128-135 [PMID: 25663259 DOI: 10.1007/s10120-015-0473-4]

62 **Kishikawa H**, Kimura K, Takarabe S, Kaida S, Nishida J. Helicobacter pylori Antibody Titer and Gastric Cancer Screening. *Dis Markers* 2015; **2015**: 156719 [PMID: 26494936 DOI: 10.1155/2015/156719]

63 **Mizutani S**, Takahashi Y, Shimamoto T, Nakagawa H, Hisada H, Oshio K, Kubota D, Mizutani H, Ohki D, Sakaguchi Y, Yakabi S, Niimi K, Kakushima N, Tsuji Y, Wada R, Yamamichi N, Fujishiro M. Performing the ABC Method Twice for Gastric Cancer Risk Stratification: A Retrospective Study Based on Data from a Large-Scale Screening Facility. *Diagnostics (Basel)* 2023; **13** [PMID: 37046502 DOI: 10.3390/diagnostics13071284]

64 **Tsai KF**, Liou JM, Chen MJ, Chen CC, Kuo SH, Lai IR, Yeh KH, Lin MT, Wang HP, Cheng AL, Lin JT, Shun CT, Wu MS; Taiwan Gastrointestinal Disease and Helicobacter Consortium. Distinct Clinicopathological Features and Prognosis of Helicobacter pylori Negative Gastric Cancer. *PLoS One* 2017; **12**: e0170942 [PMID: 28152027 DOI: 10.1371/journal.pone.0170942]

65 **Osborn JF**, Cattaruzza MS, Ferri AM, De Angelis F, Renzi D, Marani A, Vaira D. How long will it take to reduce gastric cancer incidence by eradicating Helicobacter pylori infection? *Cancer Prev Res (Phila)* 2013; **6**: 695-700 [PMID: 23682077 DOI: 10.1158/1940-6207.CAPR-12-0428]

66 **Chen L**, Hong J, Hu R, Yu X, Chen X, Zheng S, Qin Y, Zhou X, Wang Y, Zheng L, Fang H, Liu P, Huang B. Clinical Value of Combined Detection of Serum sTim-3 and Pepsinogen for Gastric Cancer Diagnosis. *Cancer Manag Res* 2021; **13**: 7759-7769 [PMID: 34675671 DOI: 10.2147/CMAR.S328312]

67 **Kamei M**, Yamashita S, Tokuishi K, Hashioto T, Moroga T, Suehiro S, Ono K, Miyawaki M, Takeno S, Yamamoto S, Kawahara K. HE4 expression can be associated with lymph node metastases and disease-free survival in breast cancer. *Anticancer Res* 2010; **30**: 4779-4783 [PMID: 21115941]

68 **In H**, Sarkar S, Ward J, Friedmann P, Parides M, Yang J, Epplein M. Serum Pepsinogen as a Biomarker for Gastric Cancer in the United States: A Nested Case-Control Study Using the PLCO Cancer Screening Trial Data. *Cancer Epidemiol Biomarkers Prev* 2022; **31**: 1426-1432 [PMID: 35534235 DOI: 10.1158/1055-9965.EPI-21-1328]

World Journal of Gastrointestinal Oncology

Submit a Manuscript: https://www.f6publishing.com

World J Gastrointest Oncol 2023 July 15; 15(7): 1182-1199

DOI: 10.4251/wjgo.v15.i7.1182

ISSN 1948-5204 (online)

ORIGINAL ARTICLE

Basic Study

ENTPD1-AS1–miR-144-3p-mediated high expression of *COL5A2* correlates with poor prognosis and macrophage infiltration in gastric cancer

Han-Mei Yuan, Xiao-Feng Pu, Hui Wu, Chao Wu

Specialty type: Oncology

Provenance and peer review: Unsolicited article; Externally peer reviewed.

Peer-review model: Single blind

Peer-review report's scientific quality classification

Grade A (Excellent): 0
Grade B (Very good): B, B
Grade C (Good): C
Grade D (Fair): 0
Grade E (Poor): 0

P-Reviewer: de Melo FF, Brazil; Li DH, China; Liu YQ, United States

Received: December 7, 2022
Peer-review started: December 7, 2022
First decision: January 18, 2023
Revised: March 30, 2023
Accepted: April 30, 2023
Article in press: April 30, 2023
Published online: July 15, 2023

Han-Mei Yuan, Hui Wu, Chao Wu, Department of Laboratory Medicine, The Eighth Affiliated Hospital, Sun Yat-sen University, Shenzhen 518033, Guangdong Province, China

Xiao-Feng Pu, Department of Clinical Laboratory, The General Hospital of Western Theater Command, Chengdu 610000, Sichuan Province, China

Corresponding author: Chao Wu, PhD, Professor, Department of Laboratory Medicine, The Eighth Affiliated Hospital, Sun Yat-sen University, No. 3025 Shennan Zhong Lu, Shenzhen 518033, Guangdong Province, China. chaowu261@163.com

Abstract

BACKGROUND

Gastric cancer (GC) is a malignant tumor with high morbidity and mortality. Expression of *COL5A2* is significantly elevated in GC. Abnormal expression of noncoding RNAs (ncRNAs) have been found in GC, including microRNA (miRNA) and long noncoding RNA (lncRNA). Competing endogenous RNA network plays an important regulatory role in GC. However, its specific regulatory mechanism has not been elucidated.

AIM

To gain insight into the ncRNA regulatory mechanism and immune microenvironment related to *COL5A2* in GC.

METHODS

RNA sequencing data and clinical information from The Cancer Genome Atlas data portal were used to analyze the expressions of *COL5A2*, miRNA and lncRNA related to the prognosis of GC. Cox regression analysis and Kyoto Encyclopedia of Genes and Genomes analysis were performed to assess the risk factors and relevant function of *COL5A2*. StarBase was used to predict the interaction of miRNA–lncRNA or miRNA–mRNA in GC. The relationship between *COL5A2*, miR-144-3p and ENTPD1-AS1 were verified by dual luciferase reporter assay. The association of *COL5A2* with immune cell infiltration were analyzed using the Tumor Immune Estimation Resource database and single sample gene set enrichment analysis. The expression of *COL5A2* and macrophages in paired GC tissues were detected by immunohistochemical staining.

RESULTS

We verified that the upregulation of *COL5A2* expression was associated with the prognosis of GC and was an independent risk factor for GC. miR-144-3p was downregulated and correlated with the prognosis of GC. miR-144-3p regulated the expression of *COL5A2* through direct interaction with *COL5A2*. ENTPD1-AS1 was elevated in GC and competitively bound to miR-144-3p, thus inhibiting the expression of miR-144-3p. ENTPD1-AS1 enhanced the expression of *COL5A2* through sponging miR-144-3p. Compared to paired normal tissue, *COL5A2* expression was upregulated at the protein level, especially in the middle and late stages of GC. The high expression of *COL5A2* was positively linked to macrophage infiltration in GC.

CONCLUSION

COL5A2 regulated by ENTPD1-AS1–miR-144-3p was associated with poor prognosis and macrophage infiltration in GC. This could be a new biomarker and therapeutic target in GC.

Key Words: *COL5A2*; Noncoding RNAs; Macrophage infiltration; Prognosis; Gastric cancer

Core Tip: Gastric cancer (GC) is a malignant tumor with high fatality rate. Competing endogenous RNA network and infiltration of immune cells play an important role in the development of GC. In this study, we verified that high expression of *COL5A2* was closely related to poor prognosis and was an independent risk factor for GC. We predicted and validated that long noncoding RNA ENTPD1-AS1 regulated the expression of *COL5A2* through sponging miR-144-3p. Additionally, we confirmed that upregulation of *COL5A2* expression strongly correlated with immune infiltration of macrophages. ENTPD1-AS1-miR-144-3p-*COL5A2* might be a new therapeutic target for GC.

Citation: Yuan HM, Pu XF, Wu H, Wu C. ENTPD1-AS1–miR-144-3p-mediated high expression of *COL5A2* correlates with poor prognosis and macrophage infiltration in gastric cancer. *World J Gastrointest Oncol* 2023; 15(7): 1182-1199
URL: https://www.wjgnet.com/1948-5204/full/v15/i7/1182.htm
DOI: https://dx.doi.org/10.4251/wjgo.v15.i7.1182

INTRODUCTION

Gastric cancer (GC) remains the fourth leading cause of cancer death worldwide. About 95% of cases are gastric adenocarcinoma (GAD) subtype[1]. The survival rate of GC has improved with medical advances. However, the median survival time for advanced GC is < 12 mo[2]. Accordingly, exploring the molecular mechanism of GC is of great significance for finding better therapeutic targets and better treatment.

The extracellular matrix is mainly composed of collagen and is related to proliferation, differentiation, migration, and metabolism of cancer[3]. Recent studies have shown that *COL5A2*, one of the collagen genes, is upregulated in several types of cancer and associated with immune cells infiltration[4,5]. Traditionally, *COL5A2* is considered tightly related to the occurrence of classical Ehlers–Danlos syndrome[6,7]. However, high expression of *COL5A2* is found to be associated with worse prognosis and drug resistance[8-10]. *COL5A* is also found closely associated with immune cell infiltration, which may be related to the inhibitory effect of collagen on the production of CCL2[5]. In proliferative diabetic retinopathy, *COL5A2* is closely related to the infiltration of M2 macrophages[11].

Noncoding RNAs (ncRNAs), such as microRNAs (miRNAs), long noncoding RNAs (lncRNAs) and circular RNAs (circRNAs), are critically involved in GC development[12]. ncRNAs could affect the proliferation, invasion, migration and metastasis of GC by regulating target miRNA genes[13]. Studies have revealed that miR-144-3p can affect the occurrence, development, and prognosis of cancer by inhibiting the expression of target genes[14,15]. ncRNAs can upregulate the expression of cancer-promoting genes by inhibiting the expression of miR-144-3p[16,17]. ENTPD1-AS1 is an antisense lncRNA that may be associated with short stature[18]. Recently, ENTPD1-AS1 is considered to be a new ncRNA that regulates the proliferation and apoptosis of cancer cells and also serves as a prognostic marker in glioblastoma multiforme[19,20]. However, the ncRNA regulatory mechanism and immune infiltration of *COL5A2* are still unclear in GC.

In this study, we verified that high expression of *COL5A2* in GC was closely related to poor prognosis and was an independent risk factor. We predicted and verified a new competing endogenous RNA (ceRNA) network, namely, ENTPD1-AS1 regulated *COL5A2* expression through sponging miR-144-3p. We confirmed that upregulation of *COL5A2* expression strongly correlated with immune infiltration of macrophages. ENTPD1-AS1–miR-144-3p regulation of *COL5A2* correlated with poor prognosis and macrophage infiltration in GC.

MATERIALS AND METHODS

Sample collection

We collected 40 paired GC and normal specimens from the Eighth Affiliated Hospital of Sun Yat-Sen University. These tissues were obtained from the patients undergoing GC surgery. All the patients signed informed consent forms. This research was approved by the Ethics Committee of the Eighth Affiliated Hospital of the Sun Yat-Sen University.

Cell culture

Human Embryonic Kidney cells (293T) and human GAD cell line (AGS) were cultured in dulbecco's modified eagle medium (GIBCO, Invitrogen, Carlsbad, CA, United States) containing 10% FBS (GIBCO) and 100 U/mL penicillin, and 0.1 mg/mL streptomycin (Invitrogen, Carlsbad, CA, United States).

Expression and prognostic analysis of COL5A2 in GC

The Gene Expression Profiling Interactive Analysis (GEPIA; http://gepia.cancer-pku.cn/) database was utilized for the expression and prognostic analysis of *COL5A2* in numerous cancers.

Clinical information and data acquisition of patients with GAD

The mRNA expression data of GAD in tumor and normal tissues (446 cases of tumor, and 45 cases of normal tissue) and clinical material were obtained from The Cancer Genome Atlas (TCGA) public database (https://portal.gdc.cancer.gov). The basic information of human miRNA was downloaded from http://www.mirbase.org. We conducted a differential analysis and survival analysis on the expression of *COL5A2* in normal tissues and GC tissues. Data transformation was achieved using Perl script. R version 4.1.2 was used in several analyses.

Cox regression analysis

We organized the clinical data of GAD and matched the expression of *COL5A2* in the corresponding samples. Samples with incomplete or missing data were excluded from this analysis, and finally 322 specimens were obtained. Univariate and multivariate Cox proportional hazards regression models were used to assess *COL5A2* for prediction of overall survival (OS).

Functional enrichment analysis of COL5A2

We analyzed Kyoto Encyclopedia of Genes and Genomes (KEGG) signaling pathway enrichment of *COL5A2* by gene set enrichment analysis (GSEA). We found gene markers corresponding to 22 immune cells and extracted the expression of these gene markers from the TCGA data. Using single sample GSEA (ssGSEA), we determined the infiltration of these immune cells in *COL5A2* high expression and low expression groups.

Prediction and analysis of the interaction between mRNA and miRNA or miRNA and lncRNA

We used starBase (http://starbase.sysu.edu.cn/) to predict the interaction of miRNA–mRNA or miRNA–lncRNA. StarBase is a powerful target gene prediction software, and it includes 7 functional domains for prediction. We set the screening conditions for at least two sites that considered the gene to be the target gene of *COL5A2*, and the gene was retained. The expression data of miR-144-3p and ENTPD1-AS1 came from the TCGA database. We conducted the expression analysis, correlation analysis, and survival analysis using R version 4.1.2.

Dual-luciferase reporter assay

The sequences of *COL5A2* or ENTPD1-AS1 that may bind to miR-144-3p were cloned into the pmirGLO vector (Sangon Biotech Co., Ltd. Shanghai, China). We constructed four kinds of double luciferase report plasmids: *COL5A2* 3′UTR-wt, *COL5A2* 3′UTR-mut, ENTPD1-AS1-wt and ENTPD1-AS1-mut.

SiRNAs and miRNA mimics

siRNAs, miRNA mimics and their corresponding negative controls (NC) were designed by GenePharma Co., Ltd., (Shanghai, China). The sequence was as follows: MiR-144-3p mimics: (UACAGUAUAGAUGAUGUACU), mimics NC: (UUGUACUACACAAAAGUACUG), si-ENTPD1-AS1: (GGCCCGUAAUGGAGAUCGATT, UCGAUCUCCAUUACGGGCCTT), si-NC: (UUCUCCGAACGUGUCACGUTT, ACGUGACACGUUCGGAGAATT).

Cell transfection

We seeded cells into 24-well plates at a density of 1.5 × 10^5 cells per well. When the cells reached 60% to 70%, dual luciferase reporter vector and miR-144-3p mimics or NC mimics were transfection into 293T cells and AGS cells in the presence of Lipofectamine™ and P3000™ (L3000001, Invitrogen, United States). In some experiments, mixture of Lipofectamine™ and miR-144-3p or si-ENTPD1-AS1 was transfection into AGS cells. After 6 h, fresh medium was replaced. 48 h later, Fluorescence intensity was detected by Dual-Luciferase® Reporter Assay System (E1910, Promega, United States).

Quantitative reverse transcriptase polymerase chain reaction

RNAs were extracted by Trizol from AGS cells. RNA was reversely transcribed into cDNA with Evo M-MLV RT Premix (AG11701, Accurate Biotechnology, Hunan, China) and then detected gene expression with SYBR® Green Premix Pro Taq

HS quantitative polymerase chain reaction (qPCR) Kit for qPCR (AG1170, Accurate Biotechnology, Hunan, China). The primers were synthesized by Sangon Biotech Co., Ltd (Shanghai, China). *COL5A2*: (Forward: GGATCACAGGGACCAAGAGGAGAG, Reverse: GCACCAGGTTGACCAGGAACAC), ENTP1-AS1 (Forward: CCTGCCTCTGCCTCCAAGTAG, Reverse: TTCGAGACCAGCCTGACCAAC), hsa-miR-144-3p (RT Primer: GTCGTATCCAGTGCAGGGTCCGAGGTATTCGCACTGGATACGACAGTACA, Forward: GCGCGCGTACAGTATAGATGA, Reverse: ATCCAGTGCAGGGTCCGAGG). U6 (Forward: GGAACGATACAGAGAAGATTAGC, Reverse: TGGAACGCTTCACGAATTTGCG), GAPDH (Forward: TGTGTCCGTCGTGGATCTGA, Reverse: GCAGCTGTGACACACAGTA). miRNA was detected by stem-loop. U6 or GAPDH as internal control. The relative expression of genes was calculated by $2^{-\Delta\Delta Ct}$.

Correlation analysis of COL5A2 and immunological checkpoints

Tumor IMmune Estimation Resource (TIMER) database (https://cistrome.shinyapps.io/timer/) integrated the results of multiple algorithms based on the sequencing results of TCGA. We used the TIMER and GEPIA database to analyze the correlation between *COL5A2* and immune cells or immune checkpoints.

Immunohistochemistry

All tissue slides were dewaxed, hydrated, and antigen was retrieved. We inactivated endogenous enzymatic activity and blocked nonspecific sites. Primary and secondary antibodies were incubated and rendered with Diaminobenzidine (DAB). The concentration of primary antibodies was anti-*COL5A2* (1:100, Thermo Fisher, PA5-38880, United States), anti-CD68 (1:2000, Abcam, ab955, United Kingdom). We selected the corresponding secondary antibody according to the primary antibody (1:100, Santa Cruz Biotechnology, sc-2357/sc-516102); DAB detection kit (50:1, Servicebio, G1212, China). All slides were observed and counted by a Carl Zeiss microscope (Axio Imager A2, Germany). The $CD68^+$ cell counts were conducted by taking the average value of three high power fields (HP). Based on the number of $CD68^+$ cells, the macrophage infiltration was categorized into weak (30–60/HP), moderate (60–90/HP), and strong (> 90/HP) subgroups.

Statistical analysis

R with the survminer, survival, Ggforest and limma packages was used for analysis. GraphPad 8 with unpaired *t*-test and Spearman correlations was used for some analyses. $^aP < 0.05$ was considered statistically significant.

RESULTS

Expression and prognostic analysis of COL5A2 in pan-cancer

To identify the differential expression of *COL5A2* in pan-cancer, the expression of *COL5A2* was assessed in 18 types of cancer by GEPIA. The expression of *COL5A2* was significantly increased in nine cancers compared with the normal group (Figure 1A, $P < 0.05$). There was no significant difference in the other nine cancers (Supplementary Figure 1). Among the cancers with significant differences in *COL5A2* expression, OS analysis was conducted using GEPIA database. No significant prognostic difference in 8 out of 9 cancers was observed (Figure 1B–I). Only in GC, high expression of *COL5A2* was associated with poorer prognosis (Figure 1J, $P = 0.01$).

Cox regression analysis and KEGG enrichment analysis of COL5A2 in GC

To verify the results obtained from the GEPIA database, we analyzed the expression and survival prognosis of *COL5A2* using RNA-sequencing data from TCGA. In line with previous studies[21], significantly high expression of *COL5A2* was found in TCGA data and 27 paired specimens (Figure 2A and B). We performed survival analysis and found a significant difference in OS between high and low *COL5A2* expression groups (Figure 2C, $P = 0.018$).

Excluding patients with missing or incomplete information, 322 of the 433 patients were included in the cox regression analysis. From clinical information, it suggested that patients with GC were mainly in the middle and late stages, with a high rate of lymph node metastasis, less distant metastasis, and a high mortality rate (Supplementary Table 1). Cancer stage, especially N stage, was the most important prognostic indicator. Age, T stage, and *COL5A2* expression were risk factors for GC (Table 1). To determine whether these risk factors were independent of other factors, multivariate Cox regression was conducted. Only age [1.03 (1.01-1.1), $P = 0.002$] and expression of *COL5A2* [1.23 (1.05-1.5), $P = 0.013$] were independent prognostic factors (Figure 2D).

Dividing GCs into *COL5A2* high- and low-expression groups, we used KEGG enrichment to analyze which signaling pathways were associated with differential genes between the two groups. According to normalized enrichment score, nominal *P* value, the 10 most enriched signaling pathways in KEGG were shown in Supplementary Table 2). To be more concise, we integrated these signaling pathways into one diagram (Figure 2E). The most significantly enriched signaling pathways in the *COL5A2* high expression group were the interaction between extracellular matrix and receptors, focal adhesion, and some classic cancer-related signaling pathways such as the transforming growth factor-β signaling pathway.

miRNAs that interact with COL5A2 in GC

To investigate whether *COL5A2* was regulated by miRNAs in GC, we used starBase to predict which miRNAs would bind to *COL5A2*. There were 69 miRNAs with the potential to bind to *COL5A2*, and it was visualized by cytoscape (Supplementary Figure 2). According to the principle of gene regulation, miRNA should negatively correlate with

Table 1 Univariate analysis and multivariate analysis of correlation of *COL5A2* expression among gastric cancer patients

Parameter	Univariate analysis		*P* value	Multivariate analysis		*P* value
	HR	95%CI		HR	95%CI	
Age	1.022	1.004-1.039	0.014[a]	1.030	1.011-1.049	0.002[b]
Gender	1.372	0.941-2.001	0.100	1.289	0.873-1.903	0.202
Grade	1.364	0.963-1.930	0.080	1.397	0.974-2.005	0.069
Stae	1.576	1.268-1.959	< 0.001[c]	1.446	0.956-2.187	0.081
T	1.276	1.022-1.593	0.032[a]	0.954	0.702-1.295	0.761
M	1.809	0.973-3.364	0.061	1.475	0.677-3.214	0.328
N	1.343	1.147-1.573	< 0.001[c]	1.119	0.891-1.405	0.334
COL5A2	1.278	1.096-1.489	0.002[b]	2.321	1.215-4.434	0.011[a]

[a]$P < 0.05$.
[b]$P < 0.01$.
[c]$P < 0.001$.

COL5A2. Thus, we set the screening condition that miRNA was negatively correlated with *COL5A2* and $P < 0.001$. For *COL5A2* was upregulated in GC, so the target miRNA was downregulaed in GC compared with normal tissues. miR-29c-3p and miR-144-3p were negatively correlated with *COL5A2* [Figure 3A (r = -0.27, P = 2.1e-07) and Figure 3B (r = -0.16, P = 0.0017)] and markedly downregulated in GC [Figure 3C (P = 1.4e-09) and Figure 3D (P = 0.013)]. We analyzed the prognostic impact of miR-29c-3p and miR-144-3p. Only low expression of miR-144-3p had a significant effect on survival [Figure 3E (P = 0.058) and Figure 3F (P = 0.041)]. All these findings meant that miR-144-3p was the most likely upstream miRNA to regulate *COL5A2* in GC.

Prediction and analysis of upstream lncRNAs of miR-144-3p

lncRNAs can competitively bind to miRNAs, which leads to upregulation of oncogenes. We predicted using starBase which lncRNAs would interact with miR-144-3p. We examined the correlation between lncRNAs, *COL5A2* and miR-144-3p (Table 2). For downregulated miR-144-3p, expression of lncRNAs should be upregulated in GC. Among all lncRNAs, ENTPD1-AS1, NORAD, and ZNF460-AS1 were negatively correlated with miR-144-3p [Figure 4A (r = -0.32, P = 1.6e-10), Figure 4B (r = -0.21, P = 3e-05) and Figure 4C (r = -0.24, P = 2.1e-6)]. ENTPD1-AS1 and NORAD were positively correlated with *COL5A2*. ZNF460-AS1 had a negative correlation with *COL5A2* [Figure 4D (r = 0.11, P = 0.036), Figure 4E (r = 0.14, P = 0.0067) and Figure 4F (r = -0.042, P = 0.42)]. We analyzed the expression of lncRNA in GC, and three lncRNAs were significantly upregulated in GC [Figure 4G (P = 3.6e-06), Figure 4H (P = 1e-10) and Figure 4I (P = 0.011)]. Kaplan–Meier analysis revealed that the higher the ENTPD1-AS1 expression, the better the OS [Figure 4J (P = 0.002), Figure 4K (P = 0.229) and Figure 4L (P = 0.351)]. By taking into account expression and prognostic analysis, our data suggested that ENTPD1-AS1 was the most likely lncRNA to regulate the miR-144-3p/*COL5A2* axis in GC.

LncRNA ENTPD1-AS1 enhances the expression of COL5A2 through sponging miR-144-3p

In order to verify the interaction of ENTPD1-AS1, miR-144-3p and *COL5A2*, we constructed dual luciferase reporter vector (Figure 5A). The results showed that in the presence of miR-144-3p mimics, the luciferase activity of *COL5A2* 3′UTR-wt group was significantly reduced compared to *COL5A2* 3′UTR-mut group in both 293T cells and AGS cells. However, when transfected with NC mimics, there was no difference in fluorescence intensity between *COL5A2* 3′UTR-wt group and *COL5A2* 3′UTR-mut group (Figure 5B and C). Similarly, the luciferase activity was reduced when miR-144-3p mimics interacted with ENTPD1-AS1-wt instead of ENTPD1-AS1-mut. When transfected with NC mimics, the change of fluorescence intensity disappeared (Figure 5D and E). Additionally, when miR-144-3p enrichment was present, the expression of *COL5A2* was decreased in AGS cells (Figure 5F and G). Compared to si-NC, si-ENTPD1-AS1 led to a decrease of miR-144-3p (Figure 5H and I). All these results suggested that ENTPD1-AS1 might promote the expression of *COL5A2* by suppressing the expression of miR-144-3p.

COL5A2 has a correlation with immune checkpoints in GC

For immunotherapy having a low response in many cancers, there is a pressing need to find new target genes that could improve the efficacy of immunotherapy. Considering the cancer-promoting role of *COL5A2*, we analyzed the association of *COL5A2* with checkpoints using the TIMER database. Our analyses revealed a high correlation between *COL5A2* and CD274 and a lower correlation between *COL5A2* and CTLA4 or PDCD1 (Figure 6A). We observed similar results in the GEPIA database (Figure 6B–D). These results suggested that *COL5A2* mediated immune escape in GC.

COL5A2 is associated with immune cell infiltration in GC

To explore the link between *COL5A2* and immune cells, we determined the relationship between *COL5A2* and immune

Table 2 Correlation analysis between long noncoding RNA and *COL5A2* or long noncoding RNA and miR-144-3p in gastric cancer

lncRNA	miRNA/mRNA	*R* value	*P* value
ENTPD1-AS1	miR-144-3p	-0.324	1.6E-10[c]
ZNF460-AS1	miR-144-3p	-0.243	2.1E-06[c]
NORAD	miR-144-3p	-0.215	3.0E-05[c]
ENTPD1-AS1	COL5A2	0.109	3.6E-02[a]
ZNF460-AS1	COL5A2	-0.042	4.2E-01
NORAD	COL5A2	0.140	6.7E-03[b]

[a]$P < 0.05$.
[b]$P < 0.01$.
[c]$P < 0.001$. lncRNA: Long noncoding RNA.

cell biomarkers. We found a significant and positive association with *COL5A2* and M2 macrophage biomarkers (CD163, VSIG4 and MS4A4A). The other immune cells biomarkers had a lower correlation or only some of the markers had a correlation with *COL5A2* (Table 3). The TIMER database indicated that *COL5A2* was significantly associated with infiltration of various immune cells, including neutrophils, macrophages and dendritic cells, but most correlated with macrophage infiltration (Figure 7A). We used ssGSEA to analyze the enrichment of 22 types of immune cells in groups with high and low *COL5A2* expression. We discovered a significant difference in immune infiltration of macrophages, neutrophils and B memory cells between *COL5A2* high and low expression groups. In line with our previous results, macrophage infiltration was most correlated with *COL5A2* (Figure 7B, $P < 0.001$). These results indicated that *COL5A2* was significantly positively linked to macrophage infiltration.

Expression of COL5A2 and its correlation with macrophages in GC

To verify the correlation between *COL5A2* and macrophage infiltration in GC, we detected expression of *COL5A2* and macrophages ($CD68^+$) by immunohistochemistry in GC and paired normal tissues. According to the stain density, we divided the expression of *COL5A2* into three levels, including weak, moderate, and strong staining, with corresponding scores of 1–3. According to the number of $CD68^+$ cells, we divided macrophage infiltration into three groups: Weak (30–60/HP), moderate (60–90/HP), and strong (> 90/HP) (Figure 8A). The expression of *COL5A2* at the protein level was clearly higher than in the paired peritumor tissues (Figure 8B, $P = 0.025$). Expression of *COL5A2* between low stage GC (I and II) and high stage GC (III and IV) was assessed to determine whether *COL5A2* was related to GC stage. Compared with low stage GC, the level of *COL5A2* was significantly higher in high stage GC (Figure 8C, $P = 0.0106$). Pearson correlation analysis was performed to determine the relation between *COL5A2* expression and macrophage infiltration in GC. Clearly, macrophage infiltration was consistent with *COL5A2* staining intensity (Figure 8D, $r = 0.7459$, $P < 0.0001$). These results demonstrated that high expression of *COL5A2* was observed in GC and *COL5A2* was strongly positively correlated with macrophage infiltration.

DISCUSSION

GC is one of the tumors with high morbidity and mortality. Collagen is upregulated in advanced GC, and some collagen genes can be used as cancer biomarkers and can distinguish precancerous from cancerous lesions[22,23]. Several studies have shown that *COL5A2* is upregulated in various cancers and can be used as a prognostic marker[24,25]. Here, we explored the upstream regulatory molecular mechanisms and immune function of *COL5A2* in GC. We confirmed that *COL5A2* was enriched and can predict poor prognosis in GC. We verified that *COL5A2* was closely related to macrophage infiltration in GC. A new ceRNA network, ENTPD1-AS1–miR-144-3p–*COL5A2* was identified, which may partially explain the upstream regulatory mechanism of *COL5A2* in GC.

We confirmed that *COL5A2* was increased in a number of tumors, but it was associated with worse survival only in GC. Cox regression analysis found that *COL5A2* could be an independent prognostic factor for GC. KEGG enrichment analysis found that high expression of *COL5A2* was associated with multiple signal transduction pathways. All these results revealed that *COL5A2* was strongly associated with worse prognosis and has a crucial role in the development of GC. ceRNA plays a critical role in the regulation of gene expression in GC[26,27]. The mechanism of ceRNA mainly refers to that lncRNAs inhibit the negative regulation of miRNAs. For example, upregulation of circRNA *KIF4A* expression in GC can regulate the miRNA-144-3p–EZH2 axis to facilitate cell migration and invasion[28]. To investigate whether *COL5A2* was regulated by the ceRNA network, we predicted by starBase which miRNAs could bind to *COL5A2*. We discovered that miR-29c-3p and miR-144-3p were most likely to regulate *COL5A2* in GC. Although miR-29c reduced in GC and associated with tumor aggressiveness had been reported, our findings suggest that miR-29c-3p plays a role in GC by regulating *COL5A2*. Some studies have demonstrated that miR-144-3p inhibited cancer proliferation and migration, potentially serving as a biomarker in GC[16,29], which was consistent with our results that miR-144-3p was downreg-

Table 3 Correlation analysis between *COL5A2* and biomarkers of immune cells in gastric cancer

Immune cell	Biomarker	*R* value	*P* value
B cell	*CD19*	-0.053	3.1×10^{-1}
	CD79A	0.008	8.8×10^{-1}
CD8+ T cell	*CD8A*	0.078	1.3×10^{-1}
	CD8B	-0.066	2.0×10^{-1}
CD4+ T cell	*CD4*	0.312	8.4×10^{-10}[c]
M1 macrophage	*NOS2*	0.146	4.6×10^{-3}[b]
	IRF5	0.154	2.7×10^{-3}[b]
	PTGS2	0.373	1.1×10^{-13}[c]
M2 macrophage	*CD163*	0.466	$< 2.2 \times 10^{-16}$[c]
	VSIG4	0.454	$< 2.2 \times 10^{-16}$[c]
	MS4A4A	0.400	$< 2.2 \times 10^{-16}$[c]
Neutrophil	*CEACAM8*	0.018	7.3×10^{-1}
	ITGAM	0.443	$< 2.2 \times 10^{-16}$[c]
	CCR7	0.072	1.7×10^{-1}
Dendritic cell	*HLA-DPB1*	0.100	5.4×10^{-2}
	HLA-DQB1	0.103	4.7×10^{-2}[a]
	HLA-DRA	0.118	2.3×10^{-2}
	HLA-DPA1	0.096	6.2×10^{-2}
	CD1C	0.064	2.2×10^{-1}
	NRP1	0.568	$< 2.2 \times 10^{-16}$[c]
	ITGAX	0.470	$< 2.2 \times 10^{-16}$[c]

[a]$P < 0.05$.
[b]$P < 0.01$.
[c]$P < 0.001$.

ulated and closely related to prognosis in GC. Considering correlation analysis and expression analysis, ENTPD1-AS1, NORAD, and ZNF460–AS1 might regulate *COL5A2* through a ceRNA network in GC. Three lncRNAs were negatively correlated with miR-144-3p, but only ENTPD1-AS1 and NORAD were positively correlated with *COL5A2*. Therefore, we focused on ENTPD1-AS1 and NORAD. Survival analysis suggested that ENTPD1-AS1 was significantly associated with GC survival. The most potentially upregulated lncRNAs was ENTPD1-AS1. Many lncRNAs have been identified as ceRNAs in GC, such as HOTAIR, MALAT1, NORAD and H19[30]. Some studies reported that lncRNA NORAD promoted GC cell growth by inhibiting expression of miR-608 or miR-433-3p[31,32]. Here, we revealed that NORAD promoted the development of GC by inhibiting expression of miR-144-3p. ENTPD1-AS1 is an antisense transcription lncRNA, which can be used as a prognostic marker in glioblastoma multiforme[19]. We confirmed that the most probable ceRNA regulatory network for *COL5A2* in GC was NTPD1-AS1–miR-144-3p–*COL5A2* through dual luciferase assay.

Recent studies have shown that fibrillar collagen can facilitate immune cell infiltration with bioinformatics analysis [33]. Genes associated with M2 infiltration of GC have been described in some previous studies, including COL1A1, COL4A1, COL12A1 and PDGFRB[34,35]. Wei *et al*[36] identified that stromal-relevant gene clusters could be used as prognostic genes and were associated with macrophage infiltration in GC. However, most of the results were obtained through database analysis and lacked experimental validation. Similar to previous studies, we found that *COL5A2* was markedly positively associated with macrophage infiltration, using the TIMER database and ssGSEA. We confirmed by immunohistochemical staining that *COL5A2* was significantly highly expressed, especially in the high stage of GC and was significantly positively correlated with macrophage infiltration at the protein level by IHC staining. These results give us a more complete view that macrophage infiltration may partially explain the carcinogenesis mediated by *COL5A2* in GC.

There are some limitations to this study. First, although we proved the direct interaction of miR-144-3p and *COL5A2* or miR-144-3p and ENTPD1-AS1 by Dual-Luciferase Reporter Assay and siRNA transfection, further experimental verification and confirmation were needed, such as RNA Binding Protein Immunoprecipitation (RIP) and *in vivo* experiments. Second, *COL5A2* was found to be associated with poor prognosis of GC and macrophage infiltration by *in vitro* experiments, the sample size was small, these results thus should be verified in *COL5A2* knockout mice, and tested

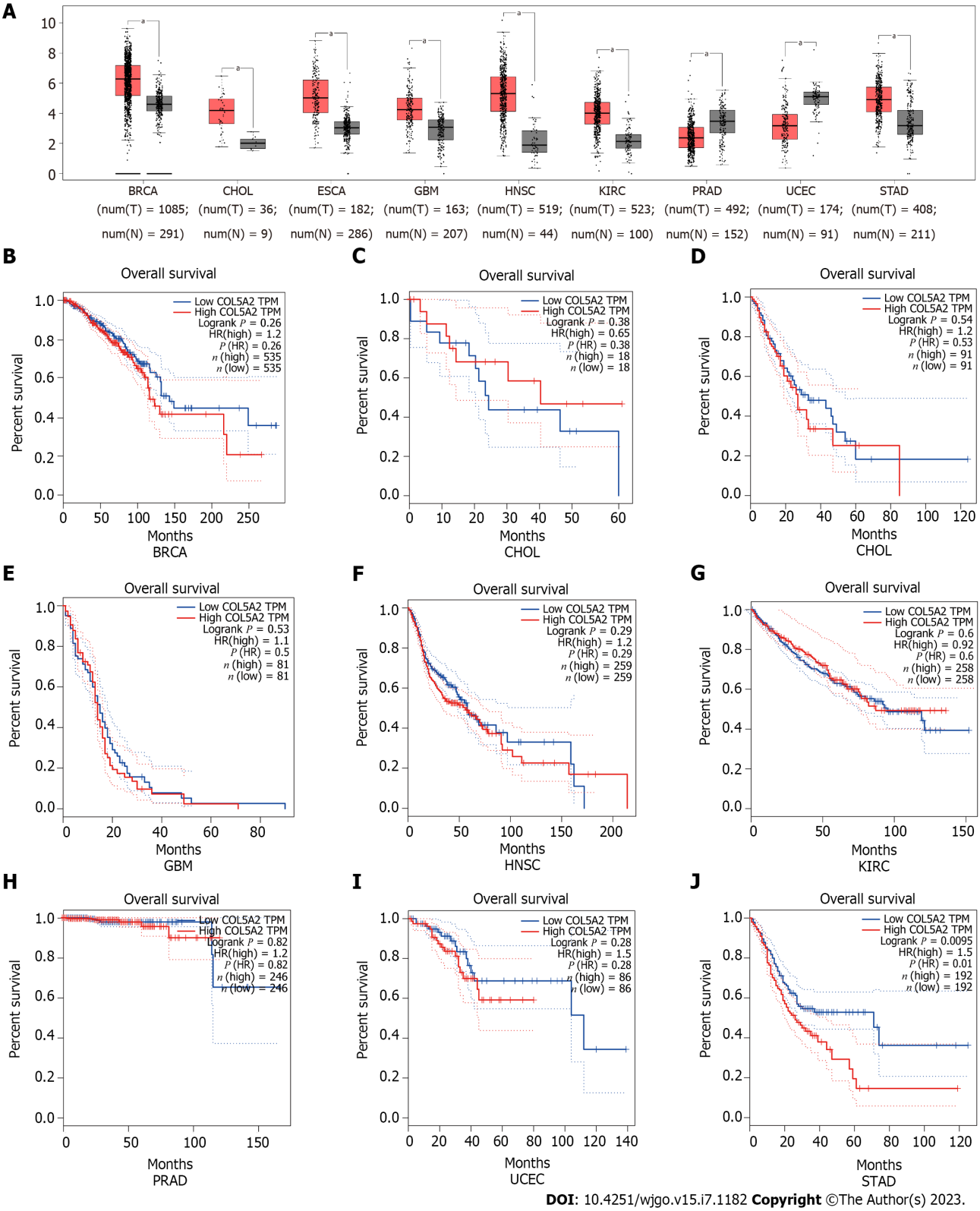

DOI: 10.4251/wjgo.v15.i7.1182

Figure 1 *COL5A2* was upregulated in pan cancer and associated with the overall survival of gastric cancer. A: Analysis of *COL5A2* expression in 9 types of cancer by Gene Expression Profiling Interactive Analysis database; B: Associations of *COL5A2* expression with the overall survival (OS) in Breast invasive carcinoma; C: Associations of *COL5A2* expression with the OS in Cholangio carcinoma; D: Associations of *COL5A2* expression with the OS in esophageal carcinoma; E: Associations of *COL5A2* expression with the OS in Glioblastoma multiforme; F: Associations of *COL5A2* expression with the OS in head and neck squamous cell carcinoma; G: Associations of *COL5A2* expression with the OS in kidney renal clear cell carcinoma; H: Associations of *COL5A2* expression with the OS in prostate adenocarcinoma; I: Associations of *COL5A2* expression with the OS in Uterine Corpus Endometrial Carcinoma; J: Associations of *COL5A2* expression with the OS in stomach adenocarcinoma. $^{a}P < 0.05$. BRCA: Breast invasive carcinoma; CHOL: Cholangio carcinoma; ESCA: Esophageal carcinoma; GBM: Glioblastoma multiforme; HNSC: Head and Neck squamous cell carcinoma; KIRC: kidney renal clear cell carcinoma; PRAD: Prostate adenocarcinoma; UCEC: Uterine Corpus Endometrial Carcinoma; STAD: Stomach adenocarcinoma.

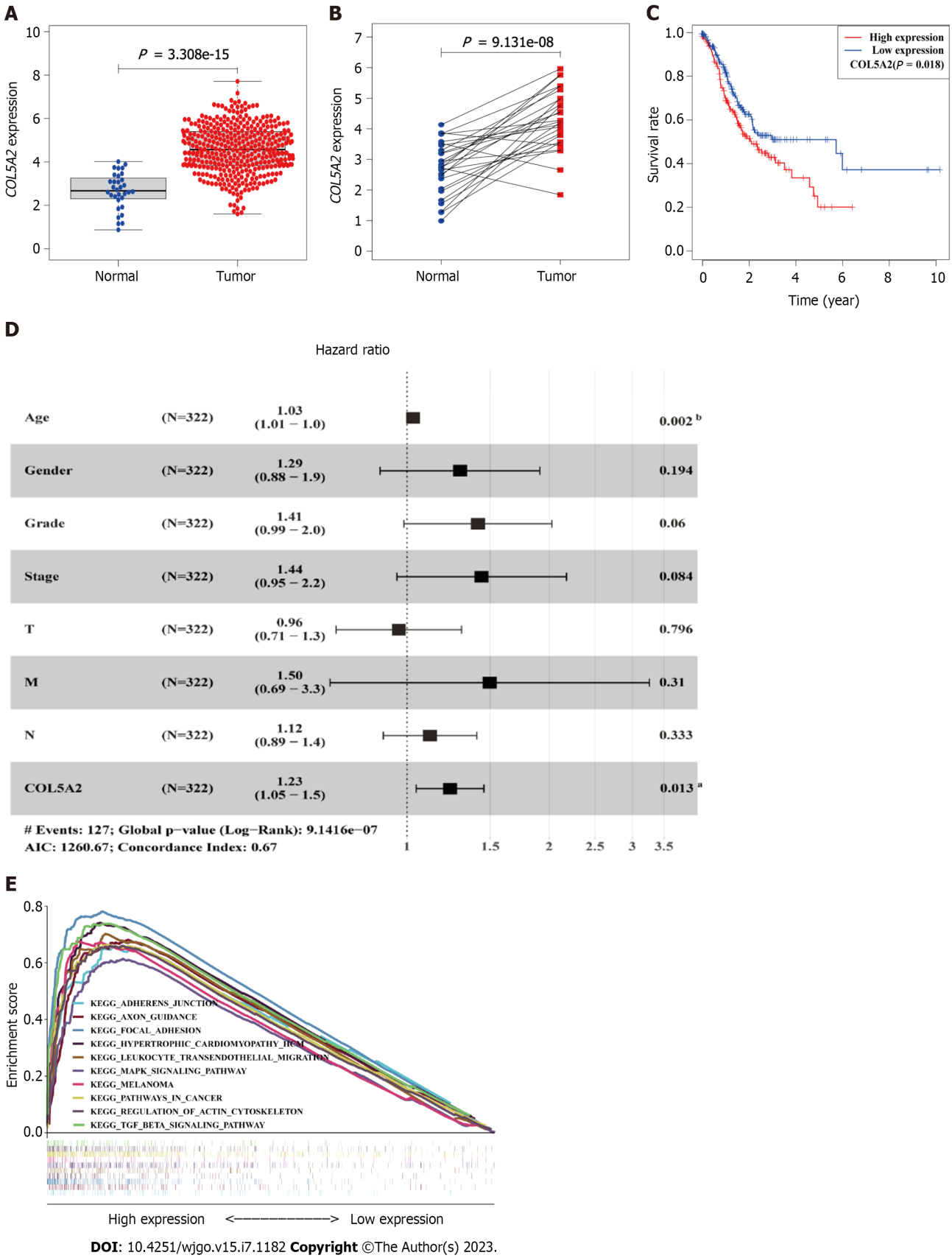

DOI: 10.4251/wjgo.v15.i7.1182 **Copyright** ©The Author(s) 2023.

Figure 2 Expression, prognostic value, and enriched function of *COL5A2* in gastric cancer from The Cancer Genome Atlas data. A: Expression of *COL5A2* in gastric cancer (GC), normal (n = 45), tumor (n = 446); B: *COL5A2* expression in 27 paired normal and tumor tissues; C: Overall survival of GC patients grouped by *COL5A2* median cutoff; D: Forest plots depicting the results of multivariate Cox regression analysis. Age and high expression of *COL5A2* predicted a low survival rate independently, n = 322. Error bars represent 95% confidence intervals; E: Gene set enrichment analysis illustrating the key pathways enriched in *COL5A2* high expression group. $^{a}P < 0.05$, $^{b}P < 0.01$.

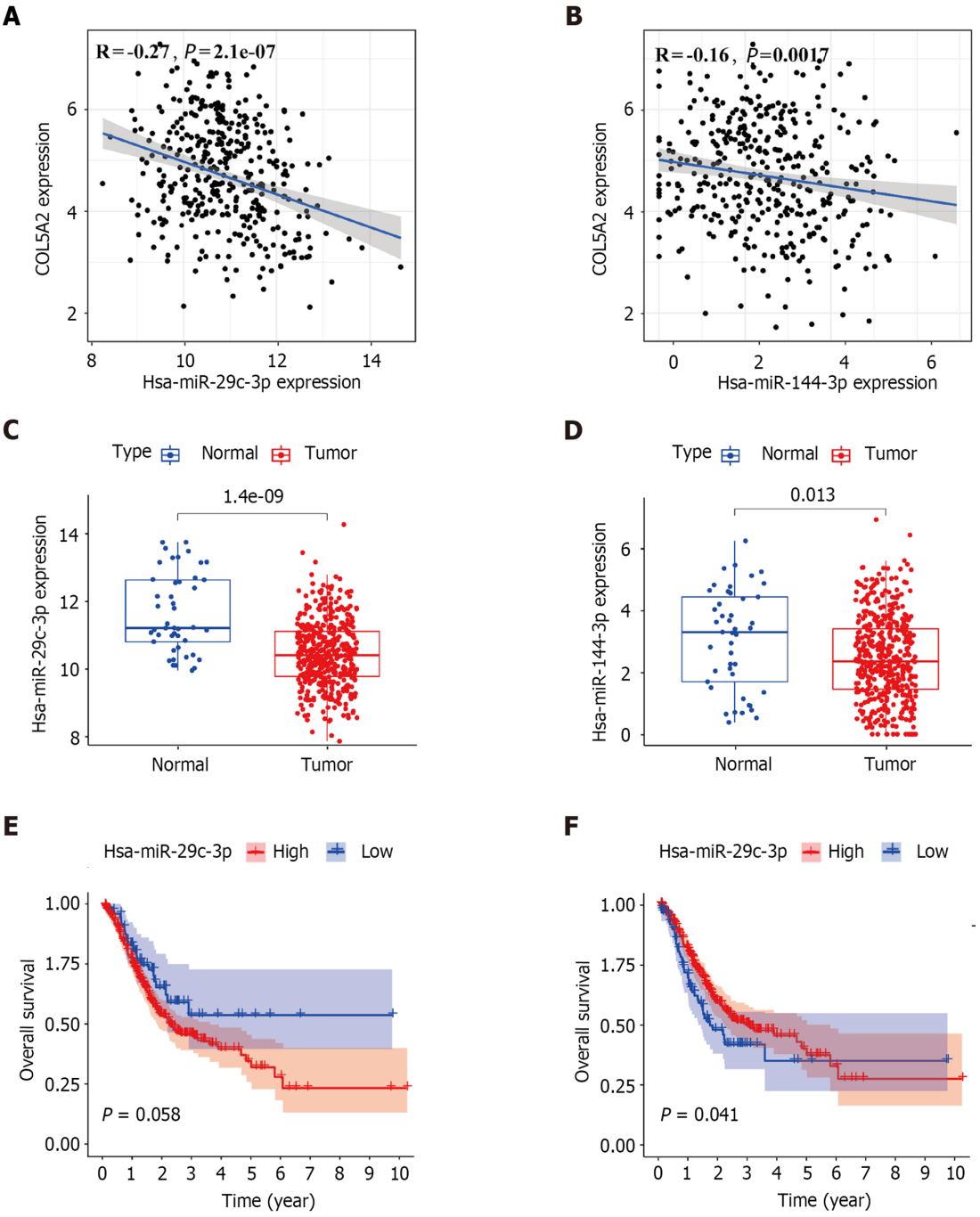

DOI: 10.4251/wjgo.v15.i7.1182

Figure 3 miR-29c-3p and miR-144-3p may bind to *COL5A2*. A: Expression correlation between miR-29c-3p and *COL5A2* in gastric cancer (GC) based on The Cancer Genome Atlas (TCGA) data; B: Expression correlation between miR-144-3p and *COL5A2* in GC based on TCGA data; C: Expression of miR-29c-3p in GC and control samples; D: Expression of miR-144-3p in GC and control samples; E: Prognostic value of miR-29c-3p in GC; F: Prognostic value of miR-144-3p in GC. Normal: n = 45, tumor: n = 446.

in big samples.

CONCLUSION

We verify that *COL5A2* is an independent risk factor and can be as a biomarker for GC. Our results demonstrate that *COL5A2* exerts a tumor-promoting effect by promoting immune cell infiltration, especially macrophage infiltration. We have identified a novel ceRNA network that facilitates *COL5A2* expression in GC, namely, lncRNA ENTPD1-AS1 upregulates the expression of *COL5A2* by inhibiting the expression of miR-144-3p. These results partly explained the upstream regulatory mechanism and immune mechanism of *COL5A2* in GC. *COL5A2*–miR-144-3p–ENTPD1-AS1 has the potential to be a novel therapeutic target for GC.

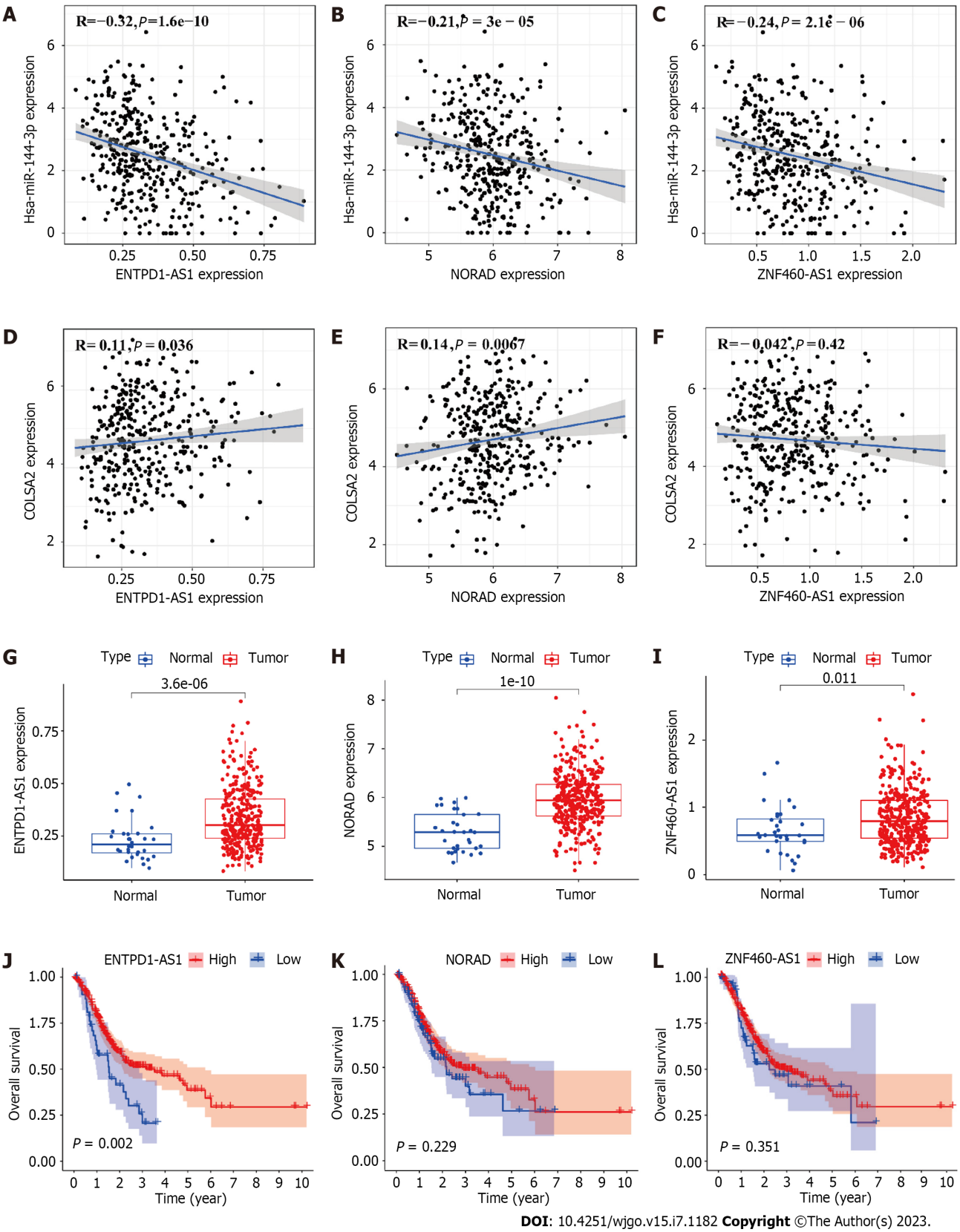

DOI: 10.4251/wjgo.v15.i7.1182 **Copyright** ©The Author(s) 2023.

Figure 4 ENTPD1-AS1, NORAD and ZNF460-AS1 may interact with miR-144-3p in gastric cancer. A: Correlation analysis between miR-144-3p and ENTPD1-AS1; B: Correlation analysis between miR-144-3p and NORAD; C: Correlation analysis between miR-144-3p and ZNF460-AS1; D: Correlation analysis between ENTPD1-AS1 and *COL5A2*; E: Correlation analysis between NORAD and *COL5A2*; F: Correlation analysis between ZNF460-AS1 and *COL5A2*; G: Expression of ENTPD1-AS1 in tumor and normal tissues; H: Expression of NORAD in tumor and normal tissues; I: Expression of ZNF460-AS1 in tumor and normal tissues; J: Overall survival (OS) analysis for ENTPD1-AS1 in gastric cancer (GC); K: OS analysis for NORAD in GC; L: OS analysis for ZNF460-AS1 in GC. Normal: n = 45, tumor: n = 446. $P < 0.05$ means a significant difference.

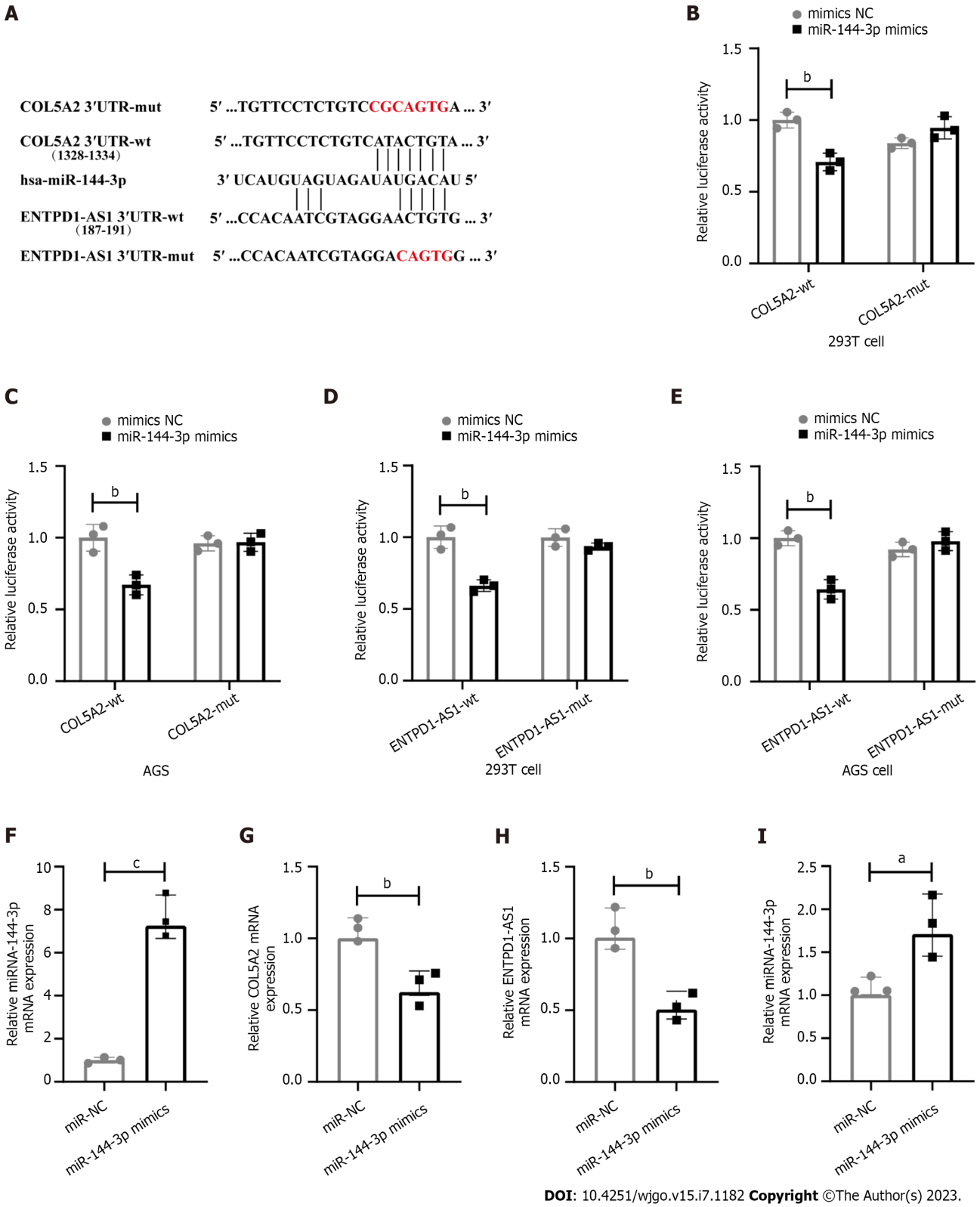

DOI: 10.4251/wjgo.v15.i7.1182 **Copyright** ©The Author(s) 2023.

Figure 5 Long noncoding RNA ENTPD1-AS1 regulated the expression of *COL5A2* through sponging miR-144-3p. A: Construction of dual luciferase reporter plasmids, including wild type (wt) and mutant (mut) of 3'UTR *COL5A2* and ENTPD1-AS1; B: dual luciferase reporter assay to evaluate the direct interaction of *COL5A2* and miR-144-3p in 293T; C: Dual luciferase reporter assay to evaluate the direct interaction of *COL5A2* and miR-144-3p in human gastric adenocarcinoma cell line (AGS); D: dual luciferase reporter assay to detect the interaction of ENTPD1-AS1 and miR-144-3p in 293T; E: dual luciferase reporter assay to detect the interaction of ENTPD1-AS1 and miR-144-3p in AGS; F: The Transfection efficiency of miR-144-3p in AGS was evaluated; G: Effect of miR-144-3p on the expression of *COL5A2*, detected by quantitative reverse transcriptase polymerase chain reaction (qRT-PCR); H: The Transfection efficiency of ENTPD1-AS1 in AGS was evaluated; I: Effect of ENTPD1-AS1 on the expression of miR-144-3p in AGS, detected by qRT-PCR. $^{a}P < 0.05$, $^{b}P < 0.01$, $^{c}P < 0.001$. AGS: Human gastric adenocarcinoma cell line; NC: Negative controls.

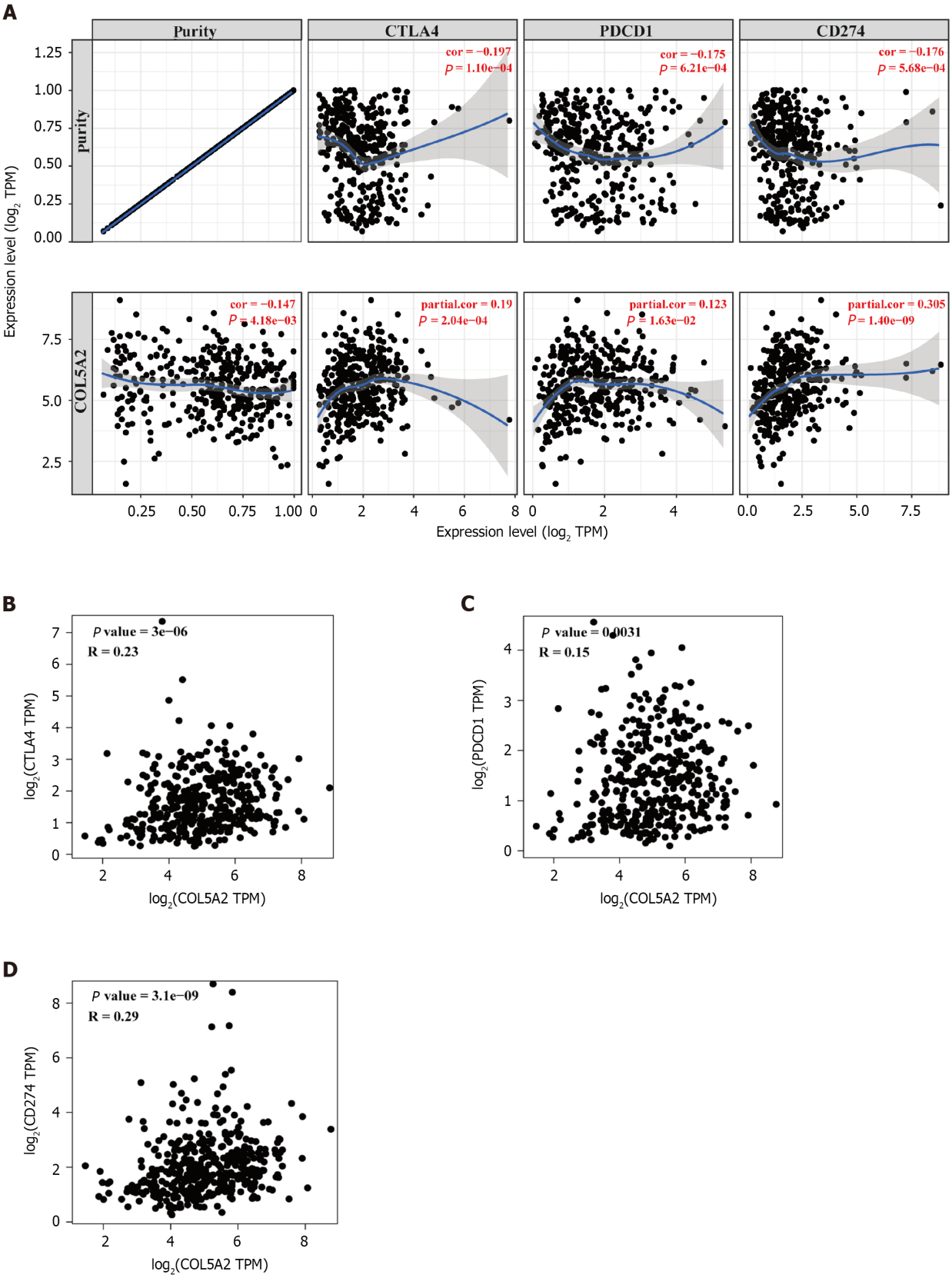

DOI: 10.4251/wjgo.v15.i7.1182 **Copyright** ©The Author(s) 2023.

Figure 6 Association of *COL5A2* and checkpoints. A: Correlation analysis between *COL5A2* and immune checkpoints in Tumor Immune Estimation Resource database; B: Correlation analysis between *COL5A2* and CTLA4 by Gene Expression Profiling Interactive Analysis database; C: Correlation analysis between *COL5A2* and PDCD1; D: Correlation analysis between *COL5A2* and CD274.

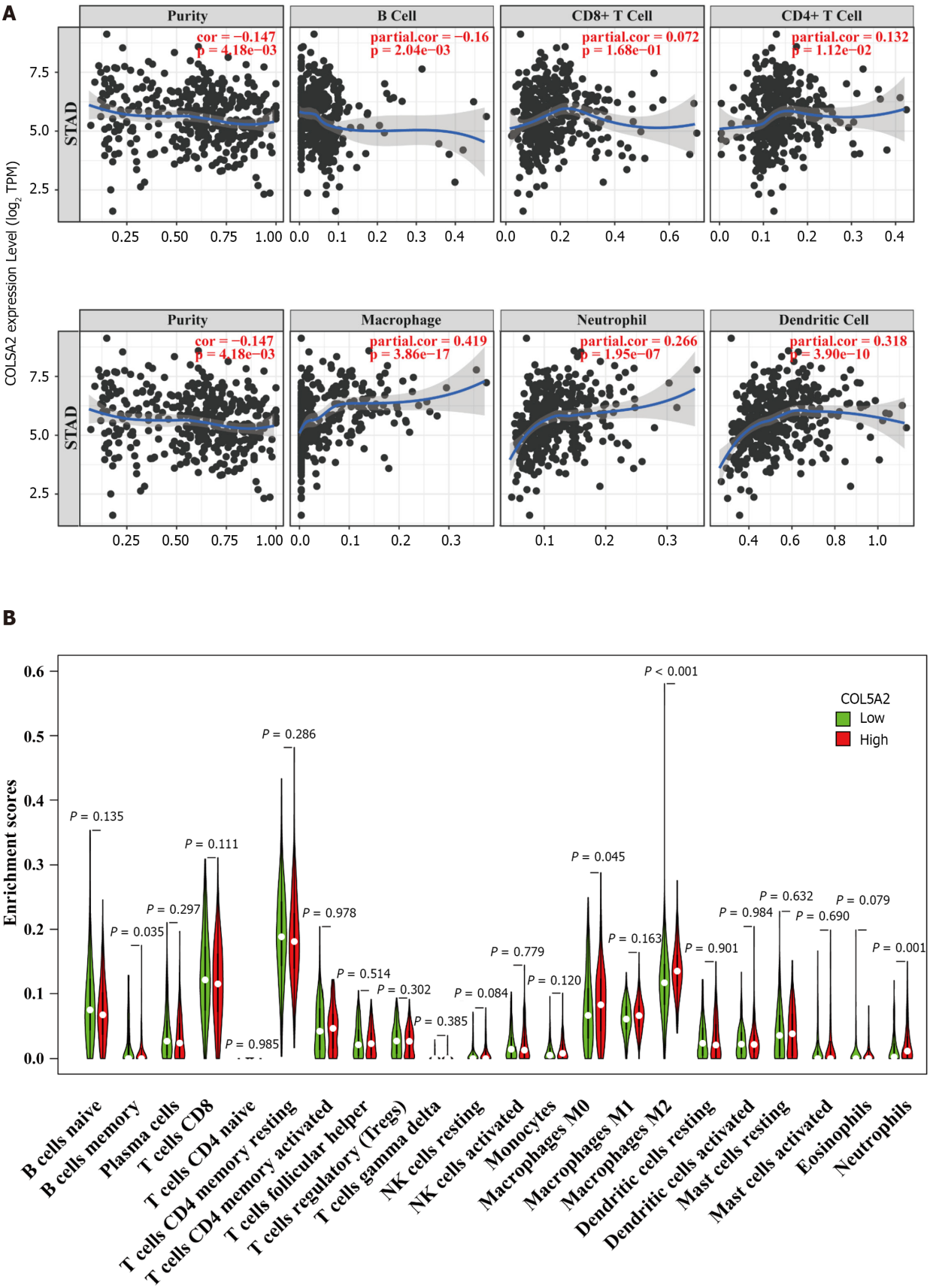

DOI: 10.4251/wjgo.v15.i7.1182

Figure 7 *COL5A2* was associated with immune cell infiltration. A: Tumor Immune Estimation Resource database to analyze the correlation between *COL5A2* and immune cells adjusted by tumor purity; B: Enrichment of 22 kinds of immune cells in the *COL5A2* high and low expression group, *n* = 376.

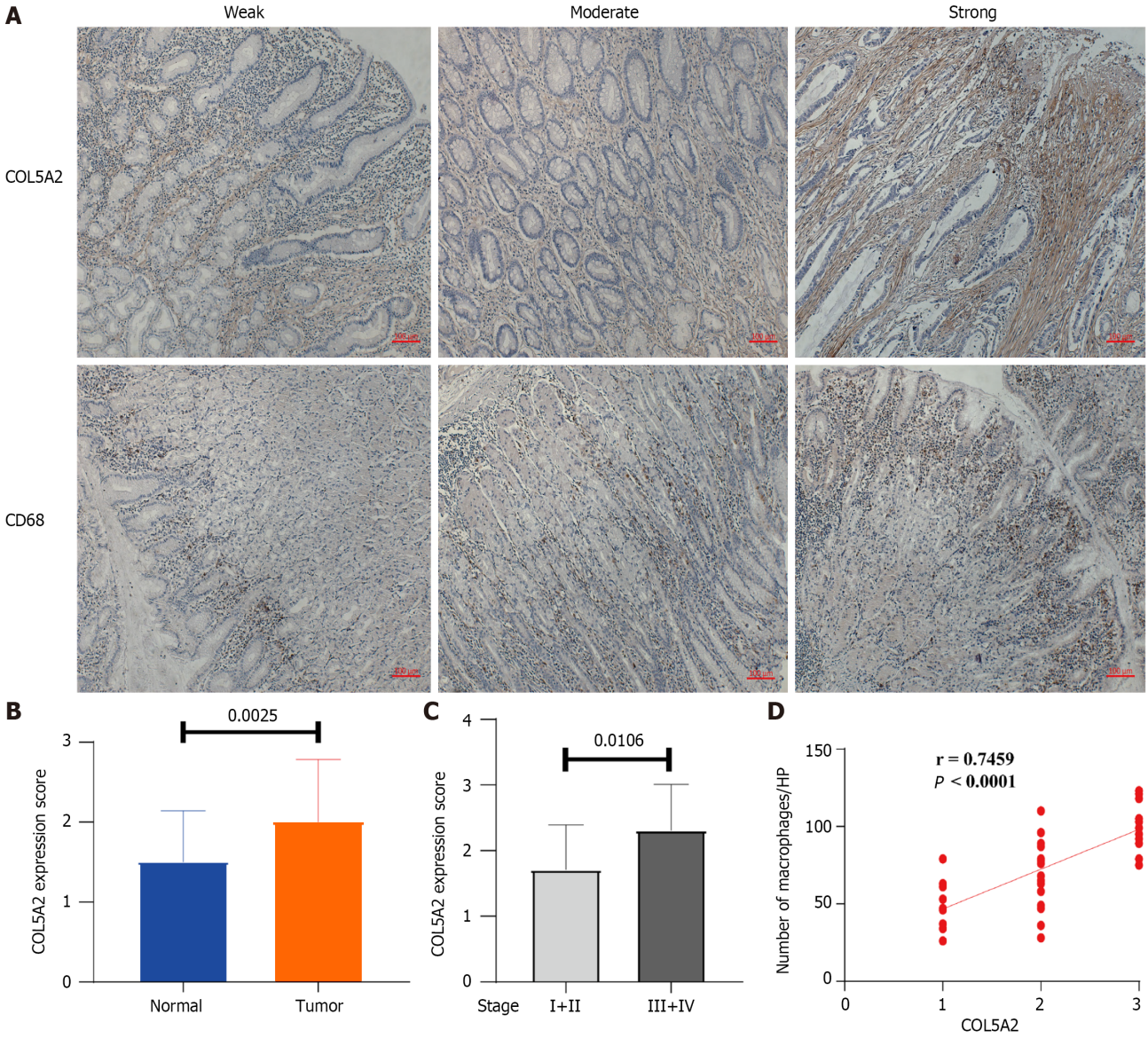

DOI: 10.4251/wjgo.v15.i7.1182 **Copyright** ©The Author(s) 2023.

Figure 8 *COL5A2* was upregulated in gastric cancer and closely related to macrophage infiltration. A: Expression of *COL5A2* and macrophages ($CD68^+$) in gastric cancer (GC) and normal tissues by immunohistochemistry. Weak, moderate and strong were assessed by scoring staining intensity or average number of $CD68^+$ cells/high power field, respectively; B: Protein expression of *COL5A2* in paired tumor and nontumor tissues, $n = 40$; C: Expression of *COL5A2* in low stage (I and II) and high stage (III and IV) GC, $n = 40$; D: Correlation between *COL5A2* and macrophages in GC tissue was analyzed with Spearman correlation, $n = 40$. HP: High power field.

ARTICLE HIGHLIGHTS

Research background

Gastric cancer (GC) is a malignant tumor with high morbidity and mortality. Expression of *COL5A2* is significantly elevated in GC. However, its specific regulatory mechanism has not been elucidated.

Research motivation

Abnormal expression of noncoding RNAs (ncRNAs) has been found in GC, including microRNA (miRNA) and long noncoding RNA (lncRNA). The ncRNA regulatory mechanism and immune microenvironment related to *COL5A2* in GC are not well understand.

Research objectives

To explore the competing endogenous RNA regulatory mechanism and immune mechanism of *COL5A2* in GC.

Research methods

StarBase was used to predict the interaction of miRNA–lncRNA or miRNA–mRNA in GC. The direct interaction between

COL5A2, miR-144-3p and ENTPD1-AS1 were verified by dual luciferase reporter assay. The correlation between of *COL5A2* and macrophages infiltration was analyzed through bioinformatics and validated in paired GC tissues by immunohistochemical staining.

Research results

miR-144-3p interacted directly with *COL5A2* and negatively regulated the expression of *COL5A2*. ENTPD1-AS1 was elevated in GC and competitively bound to miR-144-3p, thus inhibiting the expression of miR-144-3p. Compared to paired normal tissue, *COL5A2* expression was upregulated at the protein level, especially in the middle and late stages of GC. The high expression of *COL5A2* was positively linked to macrophage infiltration in GC.

Research conclusions

COL5A2 regulated by ENTPD1-AS1–miR-144-3p is associated with poor prognosis and macrophage infiltration in GC.

Research perspectives

ENTPD1-AS1-miR-144-3p-*COL5A2* might be a new therapeutic target for GC.

FOOTNOTES

Author contributions: Yuan HM designed the experiments and wrote the manuscript; Pu XF and Wu H collected clinical specimens and completed the related experiments; Wu C reviewed and edited the manuscript; All authors contributed to the article and approved the submitted version.

Supported by National Natural Science Foundation of China, No. 81971489; and Natural Science Foundation of Guangdong Province, No. 2022A1515011122.

Institutional review board statement: The study was reviewed and approved by the Medical Research Ethics Committee of the Eighth Affiliated Hospital of Sun Yat-sen University, No. ZB-KYIRB-AF/SC-08/01.0.

Informed consent statement: All study participants or their legal guardian provided informed written consent about personal and medical data collection prior to study enrolment.

Conflict-of-interest statement: All the authors report no relevant conflicts of interest for this article.

Data sharing statement: The original contributions presented in the study are included in the article/Supplementary material, further inquiries can be directed to the corresponding author.

Country/Territory of origin: China

ORCID number: Chao Wu 0000-0002-1331-2746.

S-Editor: Fan JR
L-Editor: A
P-Editor: Zhang XD

REFERENCES

1 **Smyth EC**, Nilsson M, Grabsch HI, van Grieken NC, Lordick F. Gastric cancer. *Lancet* 2020; **396**: 635-648 [PMID: 32861308 DOI: 10.1016/S0140-6736(20)31288-5]
2 **Sexton RE**, Al Hallak MN, Diab M, Azmi AS. Gastric cancer: a comprehensive review of current and future treatment strategies. *Cancer Metastasis Rev* 2020; **39**: 1179-1203 [PMID: 32894370 DOI: 10.1007/s10555-020-09925-3]
3 **Fischer H**, Stenling R, Rubio C, Lindblom A. Colorectal carcinogenesis is associated with stromal expression of COL11A1 and COL5A2. *Carcinogenesis* 2001; **22**: 875-878 [PMID: 11375892 DOI: 10.1093/carcin/22.6.875]
4 **Lü XZ**, Chen WT, Zhang CP. [Investigation of mRNA expression of collagen genes in oral squamous cell carcinoma and paired normal tissue]. *Nan Fang Yi Ke Da Xue Xue Bao* 2011; **31**: 1197-1199 [PMID: 21764694]
5 **Mohan H**, Krumbholz M, Sharma R, Eisele S, Junker A, Sixt M, Newcombe J, Wekerle H, Hohlfeld R, Lassmann H, Meinl E. Extracellular matrix in multiple sclerosis lesions: Fibrillar collagens, biglycan and decorin are upregulated and associated with infiltrating immune cells. *Brain Pathol* 2010; **20**: 966-975 [PMID: 20456365 DOI: 10.1111/j.1750-3639.2010.00399.x]
6 **Ma N**, Zhu Z, Liu J, Peng Y, Zhao X, Tang W, Jia Z, Xi H, Gao B, Wang H, Du J. Clinical and genetic analysis of classical Ehlers-Danlos

syndrome patient caused by synonymous mutation in COL5A2. *Mol Genet Genomic Med* 2021; **9**: e1632 [PMID: 33834621 DOI: 10.1002/mgg3.1632]

7 **Jacinto JGP**, Häfliger IM, Veiga IMB, Letko A, Benazzi C, Bolcato M, Drögemüller C. A Heterozygous Missense Variant in the COL5A2 in Holstein Cattle Resembling the Classical Ehlers-Danlos Syndrome. *Animals (Basel)* 2020; **10** [PMID: 33143196 DOI: 10.3390/ani10112002]

8 **Januchowski R**, Zawierucha P, Ruciński M, Zabel M. Microarray-based detection and expression analysis of extracellular matrix proteins in drugresistant ovarian cancer cell lines. *Oncol Rep* 2014; **32**: 1981-1990 [PMID: 25199881 DOI: 10.3892/or.2014.3468]

9 **Cao L**, Chen Y, Zhang M, Xu DQ, Liu Y, Liu T, Liu SX, Wang P. Identification of hub genes and potential molecular mechanisms in gastric cancer by integrated bioinformatics analysis. *PeerJ* 2018; **6**: e5180 [PMID: 30002985 DOI: 10.7717/peerj.5180]

10 **Meng XY**, Shi MJ, Zeng ZH, Chen C, Liu TZ, Wu QJ, Li S. The Role of COL5A2 in Patients With Muscle-Invasive Bladder Cancer: A Bioinformatics Analysis of Public Datasets Involving 787 Subjects and 29 Cell Lines. *Front Oncol* 2018; **8**: 659 [PMID: 30697528 DOI: 10.3389/fonc.2018.00659]

11 **Meng Z**, Chen Y, Wu W, Yan B, Meng Y, Liang Y, Yao X, Luo J. Exploring the Immune Infiltration Landscape and M2 Macrophage-Related Biomarkers of Proliferative Diabetic Retinopathy. *Front Endocrinol (Lausanne)* 2022; **13**: 841813 [PMID: 35692390 DOI: 10.3389/fendo.2022.841813]

12 **Wei L**, Sun J, Zhang N, Zheng Y, Wang X, Lv L, Liu J, Xu Y, Shen Y, Yang M. Noncoding RNAs in gastric cancer: implications for drug resistance. *Mol Cancer* 2020; **19**: 62 [PMID: 32192494 DOI: 10.1186/s12943-020-01185-7]

13 **Shin VY**, Chu KM. MiRNA as potential biomarkers and therapeutic targets for gastric cancer. *World J Gastroenterol* 2014; **20**: 10432-10439 [PMID: 25132759 DOI: 10.3748/wjg.v20.i30.10432]

14 **Xue X**, Pan J, Zhang H, Lu Y, Mao Q, Ma K. Baihe Dihuang (Lilium Henryi Baker and Rehmannia Glutinosa) decoction attenuates somatostatin interneurons deficits in prefrontal cortex of depression *via* miRNA-144-3p mediated GABA synthesis and release. *J Ethnopharmacol* 2022; **292**: 115218 [PMID: 35337919 DOI: 10.1016/j.jep.2022.115218]

15 **Xing B**, Shen C, Yang Q, Wang Z, Tan W. miR-144-3p represses hepatocellular carcinoma progression by affecting cell aerobic glycolysis *via* FOXK1. *Int J Exp Pathol* 2023 [PMID: 36806218 DOI: 10.1111/iep.12468]

16 **Wang B**, Xu L, Zhang J, Cheng X, Xu Q, Wang J, Mao F. LncRNA NORAD accelerates the progression and doxorubicin resistance of neuroblastoma through up-regulating HDAC8 *via* sponging miR-144-3p. *Biomed Pharmacother* 2020; **129**: 110268 [PMID: 32563146 DOI: 10.1016/j.biopha.2020.110268]

17 **Cao H**, Xu X, Wang K, Li C. Circ_0047835 Combines with miR-144-3p to Promote the Proliferation, Invasion, Migration, and Fibrosis of TGF-β1-Treated Human Tenon's Capsule Fibroblasts by Upregulating SP1. *Curr Eye Res* 2023; **48**: 371-381 [PMID: 36524862 DOI: 10.1080/02713683.2022.2159980]

18 **Zhang X**, Liu Q, Zhang H, Zhao S, Huang J, Sovannary T, Bunnath L, Aun HS, Samnom H, Su B, Chen H. The distinct morphological phenotypes of Southeast Asian aborigines are shaped by novel mechanisms for adaptation to tropical rainforests. *Natl Sci Rev* 2022; **9**: nwab072 [PMID: 35371514 DOI: 10.1093/nsr/nwab072]

19 **Zhou M**, Zhang Z, Zhao H, Bao S, Cheng L, Sun J. An Immune-Related Six-lncRNA Signature to Improve Prognosis Prediction of Glioblastoma Multiforme. *Mol Neurobiol* 2018; **55**: 3684-3697 [PMID: 28527107 DOI: 10.1007/s12035-017-0572-9]

20 **Tonge DP**, Darling D, Farzaneh F, Williams GT. Whole-genome-scale identification of novel non-protein-coding RNAs controlling cell proliferation and survival through a functional forward genetics strategy. *Sci Rep* 2022; **12**: 182 [PMID: 34997014 DOI: 10.1038/s41598-021-03983-5]

21 **Li Z**, Liu Z, Shao Z, Li C, Li Y, Liu Q, Zhang Y, Tan B, Liu Y. Identifying multiple collagen gene family members as potential gastric cancer biomarkers using integrated bioinformatics analysis. *PeerJ* 2020; **8**: e9123 [PMID: 32509452 DOI: 10.7717/peerj.9123]

22 **Januchowski R**, Świerczewska M, Sterzyńska K, Wojtowicz K, Nowicki M, Zabel M. Increased Expression of Several Collagen Genes is Associated with Drug Resistance in Ovarian Cancer Cell Lines. *J Cancer* 2016; **7**: 1295-1310 [PMID: 27390605 DOI: 10.7150/jca.15371]

23 **Weng K**, Huang Y, Deng H, Wang R, Luo S, Wu H, Chen J, Long M, Hao W. Collagen family genes and related genes might be associated with prognosis of patients with gastric cancer: an integrated bioinformatics analysis and experimental validation. *Transl Cancer Res* 2020; **9**: 6246-6262 [PMID: 35117235 DOI: 10.21037/tcr-20-1726]

24 **Ren X**, Chen X, Fang K, Zhang X, Wei X, Zhang T, Li G, Lu Z, Song N, Wang S, Qin C. COL5A2 Promotes Proliferation and Invasion in Prostate Cancer and Is One of Seven Gleason-Related Genes That Predict Recurrence-Free Survival. *Front Oncol* 2021; **11**: 583083 [PMID: 33816226 DOI: 10.3389/fonc.2021.583083]

25 **Yin W**, Zhu H, Tan J, Xin Z, Zhou Q, Cao Y, Wu Z, Wang L, Zhao M, Jiang X, Ren C, Tang G. Identification of collagen genes related to immune infiltration and epithelial-mesenchymal transition in glioma. *Cancer Cell Int* 2021; **21**: 276 [PMID: 34034744 DOI: 10.1186/s12935-021-01982-0]

26 **Ghafouri-Fard S**, Vafaee R, Shoorei H, Taheri M. MicroRNAs in gastric cancer: Biomarkers and therapeutic targets. *Gene* 2020; **757**: 144937 [PMID: 32640300 DOI: 10.1016/j.gene.2020.144937]

27 **Bure IV**, Nemtsova MV. Methylation and Noncoding RNAs in Gastric Cancer: Everything Is Connected. *Int J Mol Sci* 2021; **22** [PMID: 34073603 DOI: 10.3390/ijms22115683]

28 **Yan H**, Han L, He N, Li R, He S. Upregulated Circular RNA KIF4A Promotes Cell Migration and Invasion by Regulating MicroRNA-144-3p/EZH2 Axis in Gastric Cancer. *J Oncol* 2022; **2022**: 3985621 [PMID: 35466313 DOI: 10.1155/2022/3985621]

29 **Lario S**, Brunet-Vega A, Quílez ME, Ramírez-Lázaro MJ, Lozano JJ, García-Martínez L, Pericay C, Miquel M, Junquera F, Campo R, Calvet X. Expression profile of circulating microRNAs in the Correa pathway of progression to gastric cancer. *United European Gastroenterol J* 2018; **6**: 691-701 [PMID: 30083331 DOI: 10.1177/2050640618759433]

30 **Zhao Z**, Liu H, Zhou X, Fang D, Ou X, Ye J, Peng J, Xu J. Necroptosis-Related lncRNAs: Predicting Prognosis and the Distinction between the Cold and Hot Tumors in Gastric Cancer. *J Oncol* 2021; **2021**: 6718443 [PMID: 34790235 DOI: 10.1155/2021/6718443]

31 **Miao Z**, Guo X, Tian L. The long noncoding RNA NORAD promotes the growth of gastric cancer cells by sponging miR-608. *Gene* 2019; **687**: 116-124 [PMID: 30453063 DOI: 10.1016/j.gene.2018.11.052]

32 **Wang J**, Sun Y, Zhang X, Cai H, Zhang C, Qu H, Liu L, Zhang M, Fu J, Zhang J, Wang J, Zhang G. Oxidative stress activates NORAD expression by H3K27ac and promotes oxaliplatin resistance in gastric cancer by enhancing autophagy flux *via* targeting the miR-433-3p. *Cell Death Dis* 2021; **12**: 90 [PMID: 33462197 DOI: 10.1038/s41419-020-03368-y]

33 **Zhang H**, Ding C, Li Y, Xing C, Wang S, Yu Z, Chen L, Li P, Dai M. Data mining-based study of collagen type III alpha 1 (COL3A1) prognostic value and immune exploration in pan-cancer. *Bioengineered* 2021; **12**: 3634-3646 [PMID: 34252356 DOI: 10.1080/21655979.2021.1949838]

34 **Liu B**, Ma X, Ha W. Identification of Potential Prognostic Biomarkers Associated With Macrophage M2 Infiltration in Gastric Cancer. *Front Genet* 2021; **12**: 827444 [PMID: 35111208 DOI: 10.3389/fgene.2021.827444]

35 **Chivu-Economescu M**, Necula LG, Matei L, Dragu D, Bleotu C, Sorop A, Herlea V, Dima S, Popescu I, Diaconu CC. Collagen Family and Other Matrix Remodeling Proteins Identified by Bioinformatics Analysis as Hub Genes Involved in Gastric Cancer Progression and Prognosis. *Int J Mol Sci* 2022; **23** [PMID: 35328635 DOI: 10.3390/ijms23063214]

36 **Wei S**, Lu J, Lou J, Shi C, Mo S, Shao Y, Ni J, Zhang W, Cheng X. Gastric Cancer Tumor Microenvironment Characterization Reveals Stromal-Related Gene Signatures Associated With Macrophage Infiltration. *Front Genet* 2020; **11**: 663 [PMID: 32695142 DOI: 10.3389/fgene.2020.00663]

World Journal of Gastrointestinal Oncology

Submit a Manuscript: https://www.f6publishing.com

World J Gastrointest Oncol 2023 July 15; 15(7): 1200-1214

DOI: 10.4251/wjgo.v15.i7.1200

ISSN 1948-5204 (online)

ORIGINAL ARTICLE

Basic Study

Clinical significance and potential application of cuproptosis-related genes in gastric cancer

Jia-Ning Yan, Li-Hua Guo, Dan-Ping Zhu, Guo-Liang Ye, Yong-Fu Shao, Han-Xuan Zhou

Specialty type: Oncology

Provenance and peer review: Unsolicited article; Externally peer reviewed.

Peer-review model: Single blind

Peer-review report's scientific quality classification

Grade A (Excellent): 0
Grade B (Very good): 0
Grade C (Good): C
Grade D (Fair): D
Grade E (Poor): 0

P-Reviewer: Casella C, Italy; Wang CY, Taiwan

Received: February 4, 2023
Peer-review started: February 4, 2023
First decision: March 21, 2023
Revised: March 28, 2023
Accepted: May 6, 2023
Article in press: May 6, 2023
Published online: July 15, 2023

Jia-Ning Yan, Li-Hua Guo, Dan-Ping Zhu, Guo-Liang Ye, Yong-Fu Shao, Department of Gastroenterology, The First Affiliated Hospital of Ningbo University, Ningbo 315000, Zhejiang Province, China

Han-Xuan Zhou, Department of Pharmacy, Yinzhou Integrated TCM and Western Medicine Hospital, Ningbo 315000, Zhejiang Province, China

Corresponding author: Yong-Fu Shao, MD, PhD, Doctor, Department of Gastroenterology, The First Affiliated Hospital of Ningbo University, No. 247 Renmin Road, Ningbo 315000, Zhejiang Province, China. fyshaoyongfu@nbu.edu.cn

Abstract

BACKGROUND

Worldwide, gastric cancer (GC) is a common lethal solid malignancy with a poor prognosis. Cuproptosis is a novel type of cell death mediated by protein lipoylation and may be related to GC prognosis.

AIM

To offer new insights to predict GC prognosis and provide multiple therapeutic targets related to cuproptosis-related genes (CRGs) for future therapy.

METHODS

We collected data from several public data portals, systematically estimated the expression level and prognostic values of CRGs in GC samples, and investigated related mechanisms using public databases and bioinformatics.

RESULTS

Our results revealed that *FDX1*, *LIAS*, and *MTF1* were differentially expressed in GC samples and exhibited important prognostic significance in The Cancer Genome Atlas (TCGA) cohort. We constructed a nomogram model for overall survival and disease-specific survival prediction and validated it *via* calibration plots. Mecha-nistically, immune cell infiltration and DNA methylation prominently affected the survival time of GC patients. Moreover, protein-protein interaction network, KEGG pathway and gene ontology enrichment analyses demonstrated that *FDX1*, *LIAS*, *MTF1* and related proteins play key roles in the tricarboxylic acid cycle and cuproptosis. Gene Expression Omnibus database validation showed that the expression levels of *FDX1*, *LIAS*, and *MTF1* were consistent with those in the TCGA cohort. Top 10 perturbagens has been filtered

by Connectivity Map.

CONCLUSION

In conclusion, *FDX1*, *LIAS*, and *MTF1* could serve as potential prognostic biomarkers for GC patients and provide novel targets for immunotarget therapy.

Key Words: Cuproptosis; Prognosis; Gastric cancer; Biomarker; Nomogram; Bioinformatics

Core Tip: In this study, the molecular biological mechanisms of cuproptosis-related genes (CRGs) were explored in gastric cancer, and clinical prognostic models for gastric cancer treatment were constructed by interactively analysing the links among CRGs and clinical information using bioinformatics. We constructed a significant prognostic nomogram model for gastric cancer and found that *FDX1*, *LIAS*, and *MTF1* could serve as potential prognostic biomarkers for gastric cancer patients and provide novel targets for immunotarget therapy.

Citation: Yan JN, Guo LH, Zhu DP, Ye GL, Shao YF, Zhou HX. Clinical significance and potential application of cuproptosis-related genes in gastric cancer. *World J Gastrointest Oncol* 2023; 15(7): 1200-1214
URL: https://www.wjgnet.com/1948-5204/full/v15/i7/1200.htm
DOI: https://dx.doi.org/10.4251/wjgo.v15.i7.1200

INTRODUCTION

Currently, gastric cancer (GC) is a common malignant tumour with a high incidence and mortality rate worldwide, imposing a substantial economic burden on society[1]. The detailed pathogenesis of GC is currently unclear, and more than 35% of patients are initially diagnosed with distant metastasis and poor prognosis[2]. Although novel treatments, such as chemotherapy, surgery, radiotherapy and combination therapy, are constantly being updated, the prognosis of GC patients remains suboptimal[3]. Hence, it is urgent to understand the molecular mechanisms of GC and establish an effective prognostic model for clinical application.

Copper is an important cofactor for essential enzymes, and dysregulation of copper homeostasis can trigger cytotoxicity. Recent research points out that copper ionophores induce a distinct form of regulated cell death mediated by protein lipoylation of the tricarboxylic acid (TCA) cycle[4]. This special process is also called cuproptosis. Moreover, lipoylated proteins are tightly associated with a variety of human tumours, and cells with high levels of lipoylated proteins are sensitive to cuproptosis, which suggests that cuproptosis is strongly correlated with the biological behaviour of malignant tumour cells[4]. Additionally, it has been confirmed that abnormalities in intermediates in the TCA cycle are related to mitochondrial functions and GC morbidity[5]. All of this evidence suggests that cuproptosis influences the development and distal survival time of GC patients.

In our study, we systematically analysed the molecular alterations in cuproptosis-related genes (CRGs) and constructed a novel prognostic nomogram model in GC using bioinformatics technology. Our findings offer new insights into predicting GC prognosis and provide multiple therapeutic targets for future therapy.

MATERIALS AND METHODS

Data source retrieval and processing

We chose several open-source databases to retrieve the expression profiles, clinical information and survival data of GC and normal tissues, such as The Cancer Genome Atlas (TCGA) database (https://genome-cancer.ucsc.edu/) and the Genotype-Tissue Expression (GTEx) project. A total of 414 GC samples, 36 adjunct nontumor samples and 174 normal tissues were analysed in this study. All data were available in public open-access databases, and additional approval from the local ethics committee was not needed.

Analysis of differentially expressed and prognosis-related CRGs

After a literature search, we selected 19 genes (*ATP7A*, *ATP7B*, *CDKN2A*, *DBT*, *DLAT*, *DLD*, *DLST*, *FDX1*, *GCSH*, *GLS*, *LIAS*, *LIPT1*, *LIPT2*, *MTF1*, *NFE2L2*, *NLRP3*, *PDHA1*, *PDHB*, *SLC31A1*) that function closely with cuproptosis[4]. We first compared the differentially expressed CRGs in GC from the TCGA cohort and in normal tissues in the GTEx cohort using the R statistical computing environment (3.6.3; R Foundation for Statistical Computing). $P < 0.05$ was considered statistically significant. We logged into the cBioPortal website (https://www.cbioportal.org/) and surveyed the mutation information for differentially expressed CRGs in GC[6].

Cox proportional hazards regression was performed to filter the prognosis-related genes, and $P < 0.2$ was considered statistically significant in the multivariate Cox proportional hazards regression model.

Survival analysis and nomogram construction using prognosis-related CRGs

We first calculated the risk score for each sample using regression coefficients to identify the prognostic signature of CRGs for overall survival (OS) and disease-specific survival (DSS). The patients were further divided into high-risk and low-risk groups according to the median risk score. Subsequently, we analysed the survival data for each prognosis-related CRG in the high-risk and low-risk groups using the Kaplan-Meier method *via* the R package survival v 3.2-10.

Moreover, we established an OS and DSS nomogram model based on these prognosis-related CRGs. The concordance index (C-index) was used to obtain the discrimination of the nomogram, and calibration plots were generated to display the association between the predicted and observed risk results.

Methylation analysis of prognosis-related CRGs

Methylation analysis of prognosis-related CRGs was performed *via* Methsurv (https://biit.cs.ut.ee/methsurv/), a web tool to perform multivariable survival analysis using DNA methylation data[7-9].

Analysis of the association between prognosis-related CRGs and immune infiltration

We determined the survival significance of prognosis-related CRGs and the immune infiltration levels of several immune cell types. Survival Genie is a web tool used to perform survival analysis of single-cell RNA-seq data and a variety of other molecular inputs for several cancer types[10]. We first applied Survival Genie to investigate correlations between prognosis-related CRGs and immune infiltration levels. Then, we detected the immune infiltration level of multifarious immune cells in the TCGA cohort using the R package "GSVA"[11]. TIMER, an online portal for systematic analysis of immune infiltrates across diverse cancer types (http://timer.cistrome.org), was used to validate the results[12-14]. Spearman's correlation analysis was performed to determine the association between quantitative variables.

Functional analysis of prognosis-related CRGs

The GeneMANIA prediction server is a web interface for generating hypotheses about biological network integration for gene prioritization and predicting gene function[15]. We input the prognosis-related CRGs and output the nearest gene for each locus. The Search Tool for the Retrieval of Interacting Genes/Proteins (STRING) website (https://string-db.org/) contains various protein-protein correlation data, which were used to build a prognosis-related CRG interacting protein-protein interaction (PPI) network. A confidence score > 0.7 was considered significant[16]. We input the genes preserved from GeneMANIA and output the networks. The nodes in the PPI network were further used to perform KEGG pathway enrichment analysis and gene ontology (GO) classification *via* the R packages "clusterProfiler" and "ggplot2". A P value < 0.05, min enrichment > 3, and min overlap > 3 were considered significant[17]. Connectivity Map (https://clue.io/, CMap) is a systematic tool to discover functional connections among diseases and was utilized to find perturbagens to the expression of CRGs[18-20]. We selected the "Query" module and further filtered the top 10 perturbagens of "FDR_q_nlog 10" with an explicit "moa".

Differential expression validation of prognosis-related CRGs

The TNM plot is a web tool from the National Center for Biotechnology Information (www.tnmplot.com) used for comparison of gene expression in various tumours[21]. We chose the "compare Tumour and Normal" and "Gene chip data" modules for validation using Gene Expression Omnibus (GEO) samples. $P < 0.05$ was deemed statistically significant.

RESULTS

Differential expression and genetic alterations of CRGs in GC

As previously mentioned, we contrasted the expression levels of CRGs in the GC cohort displayed in Figure 1A. We found that *ATP7A*, *ATP7B*, *CDKN2A*, *DLAT*, *DLD*, *FDX1*, *GCSH*, *GLS*, *LIAS*, *LIPT1*, *LIPT2*, *MTF1*, *NFE2L2*, *NLRP3*, *PDHA1*, *PDHB*, and *SLC31A1* were differentially expressed in GC ($P < 0.05$). Then, we performed coexpression analysis of these CRGs and visualized them *via* a heatmap, which showed a high correlation (Figure 1B). For example, *FDX1* was significantly positively associated with *LIAS* and negatively associated with *MTF1*.

Furthermore, we determined the gene mutation patterns of these CRGs in GC. The overall mutation landscape is shown in Figure 1C, and we list the particular patterns of each gene mutation in Figure 1D.

Identification of prognosis-related CRGs and survival analysis

We further investigated the relationship between the expression of CRGs and prognosis in GC samples. We first constructed a multivariable Cox regression model to estimate the roles of CRGs in OS and DSS in the TCGA cohort. Our results showed that *FDX1* ($P = 0.059$) and *MTF1* ($P = 0.088$) were remarkably associated with OS in GC samples, as shown in Table 1. Similarly, *FDX1* ($P = 0.181$), *LIAS* ($P = 0.045$), and *MTF1* ($P = 0.117$) were remarkably associated with DSS in GC samples, as shown in Table 2. Hence, we selected *FDX1*, *LIAS*, and *MTF1* as prognosis-related CRGs. The clinical information for *FDX1*, *LIAS*, and *MTF1* in the TCGA cohort is shown in Supplementary Tables 1-3.

Table 1 Univariate and multivariate analysis of the correlation of differentially expressed cuproptosis-related gene expression with overall survival among gastric cancer patients

Gene	Total, *n*	Univariate analysis		Multivariate analysis	
		Hazard ratio (95%CI)	*P* value	Hazard ratio (95%CI)	*P* value
ATP7A	370	1.037 (0.725-1.483)	0.842		
ATP7B	370	0.922 (0.781-1.088)	0.334		
CDKN2A	370	0.985 (0.887-1.094)	0.782		
DLAT	370	0.785 (0.577-1.069)	0.124		
DLD	370	0.961 (0.678-1.363)	0.825		
FDX1	370	0.737 (0.533-1.018)	0.064	0.735 (0.534-1.011)	0.059
GCSH	370	1.054 (0.769-1.446)	0.744		
GLS	370	1.052 (0.845-1.310)	0.650		
LIAS	370	0.730 (0.498-1.068)	0.105		
LIPT1	370	1.168 (0.713-1.916)	0.537		
LIPT2	370	1.014 (0.794-1.294)	0.912		
MTF1	370	0.642 (0.410-1.006)	0.053	0.661 (0.411-1.064)	0.088
NFE2L2	370	0.701 (0.477-1.031)	0.071	0.809 (0.534-1.225)	0.317
NLRP3	370	1.279 (0.946-1.729)	0.110		
PDHA1	370	0.873 (0.632-1.206)	0.409		
PDHB	370	1.051 (0.686-1.611)	0.818		
SLC31A1	370	0.834 (0.653-1.065)	0.146		

CI: Confidence interval.

According to the outcomes of the Cox regression model, we used regression coefficients to build the OS/DSS risk score model. Risk score OS = -0.308 × *FDX1* - 0.413 × *MTF1* + 2.812. Risk score DSS = -0.373 × *FDX1* - 0.601 × *LIAS* - 0.413 × *MTF1* + 3.534. We separated the samples into high- and low-risk groups in terms of the risk score displayed in Figure 2A and B. Then, we built a survival curve *via* the Kaplan-Meier method to evaluate the prognostic value for each CRG. Our results suggested that all of these CRGs were prominently associated with OS and DSS in GC (Figure 2C and D), which was in keeping with the previous results.

Construction of the nomogram and validation in GC

To better guide clinical application, we generated nomograms from the prognosis-related CRGs and the observed OS and DSS at 1, 3 and 5 years of survival (Figure 3A and B). The C-index was calculated to be 0.673 for OS and 0.623 for DSS. The nomogram calibration curves demonstrated ideal agreement between prediction and observation at 1, 3 and 5 years (Figure 3C and D), indicating that our nomogram models are worthy of a multicentre, prospective clinical study.

Exploration of the mechanism of CRGs in distal prognosis determination in GC

The dynamic relationship between malignant tumours and immune cells in the microenvironment plays important roles in cancer development[22]. We evaluated the correlations between *FDX1*, *LIAS*, *MTF1* and distal survival probability from single-cell RNA-seq (scRNA-seq) data using Survival Genie. We found that *FDX1*, *LIAS*, and *MTF1* were remarkably related to survival time, as shown in Figure 4A-C. Then, we investigated the immune cell infiltration level using scRNA-seq data, and our results showed that the expression of *FDX1* was correlated with CD4 T+ memory cells, monocytes, and naive B cells, as shown in Figure 4D. *LIAS* was associated with CD4 T+ memory cells, Tregs, mast cells, NK cells, gamma delta T cells, eosinophils, and naive B cells, as shown in Figure 4E. *MTF1* was significantly related to NK cells, Tregs, neutrophils, monocytes, and activated dendritic cells, as shown in Figure 4E. On this basis, we detected the immune cell infiltration level in GC tissues and visualized the results as lollipop plots in Figure 4F-I. The length of the bars in the lollipop plots is relative to the correlation levels, and the colour of the cycles is relative to the *P* value. Subsequently, we used TIMER to validate our results and found that the expression of *FDX1*, *LIAS*, and *MTF1* and immune infiltration of macrophages were prominently correlated with the OS time of GC patients, which was consistent with our results (Supplementary Figure 1). Meanwhile, higher levels of methylation in *MTF1* and lower levels of methylation in *FDX1*, *LIAS* were associated with poor prognosis in GC patients (Figure 4J-L). All of the evidence suggests that the prognosis-related CRGs can regulate immune cell infiltration and the tumour microenvironment to influence the survival times of GC patients.

Table 2 Univariate and multivariate analysis of the correlation of differentially expressed cuproptosis-related gene expression with disease-specific survival among gastric cancer patients

Gene	Total, *n*	Univariate analysis		Multivariate analysis	
		Hazard ratio (95%CI)	*P* value	Hazard ratio (95%CI)	*P* value
ATP7A	349	1.032 (0.656-1.625)	0.891		
ATP7B	349	0.957 (0.776-1.180)	0.680		
CDKN2A	349	1.019 (0.894-1.162)	0.774		
DLAT	349	0.701 (0.471-1.043)	0.080	1.185 (0.708-1.982)	0.518
DLD	349	0.657 (0.415-1.039)	0.072	0.926 (0.529-1.622)	0.788
FDX1	349	0.668 (0.441-1.013)	0.057	0.722 (0.448-1.164)	0.181
GCSH	349	1.280 (0.863-1.900)	0.220		
GLS	349	1.041 (0.788-1.376)	0.778		
LIAS	349	0.509 (0.310-0.836)	0.008	0.578 (0.338-0.989)	0.045
LIPT1	349	1.117 (0.594-2.101)	0.731		
LIPT2	349	1.014 (0.745-1.381)	0.928		
MTF1	349	0.581 (0.329-1.023)	0.060	0.604 (0.321-1.135)	0.117
NFE2L2	349	0.584 (0.360-0.947)	0.029	0.709 (0.414-1.215)	0.211
NLRP3	349	1.082 (0.716-1.634)	0.710		
PDHA1	349	0.676 (0.441-1.036)	0.072	0.780 (0.469-1.297)	0.338
PDHB	349	0.809 (0.465-1.408)	0.454		
SLC31A1	349	0.768 (0.564-1.046)	0.094	1.029 (0.717-1.476)	0.878

CI: Confidence interval.

Biofunction analysis of prognosis-related CRGs in GC

To explore the biofunction of prognosis-related CRGs, we input *FDX1*, *LIAS*, and *MTF1* into GeneMANIA to test their interactions and gathered 23 genes in the network (Figure 5A). Then, we inputted these genes into STRING to investigate the functions of their coding proteins, which were visualized as a PPI network (Figure 5B). Moreover, we performed KEGG pathway enrichment analysis and gene ontology classification to understand the related signalling pathways and biological functions in the PPI network. The results in Figure 5C show that *FDX1*, *LIAS*, and *MTF1* play key roles in prognosis and immune cell infiltration by mediating iron ion binding and mitochondrial metabolism, which are closely associated with the TCA cycle and necroptosis. Furthermore, we performed CMap to explore the top 10 perturbagens to the expression of genes in the PPI network. We compared the expression levels of the genes in the PPI network using the TCGA cohort shown in Supplementary Figure 2 and identified upregulated genes in CMap. Our results revealed that fluconazole, KD-025, and clofarabine may be potential perturbagens of prognostic CRGs (Table 3).

Validation of FDX1, LIAS, and MTF1 differential expression in GC

To identify promising prognosis-related CRGs, we validated the expression level using the GEO database for preliminary verification. In the GEO dataset, *FDX1* was remarkably higher in GC patients ($P = 3.67 \times 10^{-2}$), and *MTF1* was significantly overexpressed in the GC group ($P = 7.04 \times 10^{-3}$). *LIAS* was prominently downregulated in GC samples ($P < 0.001$), which was in line with the TCGA cohort data and revealed the role of *LIAS* as a tumour suppressor gene and the role of *FDX1* and *MTF1* as cancer promotors (Figure 6).

DISCUSSION

Despite aggressive multimodal therapy, GC is still a devastating disease with a very poor prognosis[23]. The pathogenesis of GC is complicated, and the in-depth mechanisms and molecular signalling pathways remain to be elucidated. Luckily, the development of bioinformatics can help to open different perspectives on analysing clinical samples from multiple dimensions and improve the efficiency and accuracy of studies focusing on several genes and cancer[24]. Cuproptosis is an unusual mechanism of cell death that is helpful in explaining the pathological mechanisms related to copper overload disease and suggests a new method of treating cancer with copper toxicity[4]. To the best of our knowledge, no previous studies have estimated the relationship between CRGs and the progression of GC. Hence,

Table 3 Potential perturbagens of interactive prognostic cuproptosis-related genes

Perturbagen	Moa	Raw_cs	FDR_q_nlog 10
Fluconazole	Sterol demethylase inhibitor	0.79	1.03
KD-025	Rho associated kinase inhibitor	0.77	0.95
Clofarabine	Ribonucleoside reductase inhibitor	0.76	0.89
Tramadol	Opioid receptor agonist, Norepinephrine reuptake inhibitor, Serotonin reuptake inhibitor	0.76	0.89
Doxorubicin	Topoisomerase inhibitor	0.75	0.88
AXD-5438	CDK inhibitor	0.73	0.80
BRD-K67174965	Mucolytic	0.73	0.79
Faropenem	Lactamase inhibitor	0.72	0.76
Clocortolone-pivalate	Steroid	0.72	0.68
Ganglioside	Src activator	0.71	0.46

our study focused on the prognostic signature and explored the biofunction and oncological mechanism of CRGs in GC *via* bioinformatics.

There are distinct advantages in our research. We first filtered the differentially expressed CRGs in the TCGA cohort and defined their prognostic significance *via* multivariable Cox regression and Kaplan-Meier methods. Then, we constructed and validated a nomogram model for clinical application. Moreover, we explored the mechanisms of how prognosis-related CRGs influence distal prognosis at the DNA methylation level and immune cell infiltration level. Finally, we discovered the functions of *FDX1*, *LIAS*, and *MTF1* and validated their differential expression *via* the GEO database.

The prognostic models constructed in our study consist of three CRGs (*FDX1*, *LIAS*, and *MTF1*). *FDX1* has been confirmed to encode a reductase that decreases Cu2+ to its more toxic form, Cu1+. *LIAS* encodes lipoyl synthase, a critical component of the lipoic acid pathway. Deletion of *FDX1* and *LIAS* can confer resistance to copper-induced cell death[4]. Existing studies have revealed that *FDX1* plays a key role in steroidogenesis and mediates ageing and tumour suppression *via* the FDXR-p73 axis[25]. Furthermore, downregulated expression of *FDX1* is correlated with more advanced tumour-node-metastasis stages and poor prognosis in clear cell renal cell carcinoma[26]. Burr *et al*[27] noted that *LIAS* was an important regulator controlling the stability of HIFα and that disruption of *LIAS* decreased the activity of HIFα, which may further facilitate tumour formation[27]. Higher *LIAS* expression was also considered a prognostic biomarker indicating better distant metastasis-free survival time in breast cancer[28]. *MTF1* is a key transcription factor in charge of intracellular zinc efflux associated with the TCA cycle, is overexpressed in glioma and regulates malignant biological behaviours by modulating the TAF15/LINC00665/*MTF1* (YY2)/GTSE1 axis[29]. Similarly, it has been demonstrated that elevated *MTF1* is important for hepatocellular carcinoma tumour growth and migration and is regulated by the METTL3-METTL14-WTAP axis[30]. However, there are few studies on these genes in GC. Our study identified differentially expressed CRGs in GC and assessed their prognostic value and their biofunctions. Additionally, our prognostic model focusing on CRG expression displayed a fantastic performance in survival prediction, which warrants larger sample sizes and longitudinal research.

We further explored the potential mechanisms associated with prognosis in GC. Infiltration of immune cells within the tumour is typically related to distal prognosis and response to immunotherapy[31]. We delineated 22 unique clusters of immune cells in GC *via* scRNA-seq and examination of tissue samples. Our results showed that *FDX1*, *LIAS*, and *MTF1* in scRNA-seq samples affected multiple types of immune cells, such as CD4 T+ memory cells, monocytes, naive B cells, NK cells, and Tregs. Similarly, in GC tissues, these genes impacted Th2 cells, T helper cells, DCs, iDCs, pDCs, B cells, T cells, Tgd cells, and NK cells and thus are important prognostic factors and could be promising targets for conventional immunosuppressant therapy or combination immunosuppression. Likewise, analysis of the levels of DNA methylation also suggested the prognostic significance of *FDX1*, *LIAS* and *MTF1*. The existing results indicate intrinsic connections between DNA methylation and prognosis, which are worthy of further validation.

Moreover, we performed functional analysis of *FDX1*, *LIAS*, and *MTF1* using GeneMANIA, STRING, KEGG pathway enrichment analysis and GO classification. Functional analysis showed that the proteins associated with *FDX1*, *LIAS*, and *MTF1* are involved in the TCA cycle, cuproptosis and several signalling pathways. *FDX1*, *LIAS*, *MTF1* and related genes can modulate the progression of iron ion binding and mitochondrial metabolism to influence the survival time and immune cell infiltration. In addition, it is important to explore biological targets to develop novel drugs, and perturbagens are indispensable mediators in these efforts to discover biological connections[32]. We found 16 upregulated and only 4 downregulated genes detected in the TCGA GC cohort and GTEx cohort; thus, we imported only the overexpressed genes into the CMap tool, which still provided potential opportunities to directly build connections between targets and drugs at the gene transcriptional level.

Finally, we validated the differential expression of *FDX1*, *LIAS*, and *MTF1* in the GEO database to make our results more robust. Interestingly, the expression levels of *FDX1*, *LIAS*, and *MTF1* in the GEO database were in line with those in the TCGA cohort, which further supports the merits of application and warrants attention in future research.

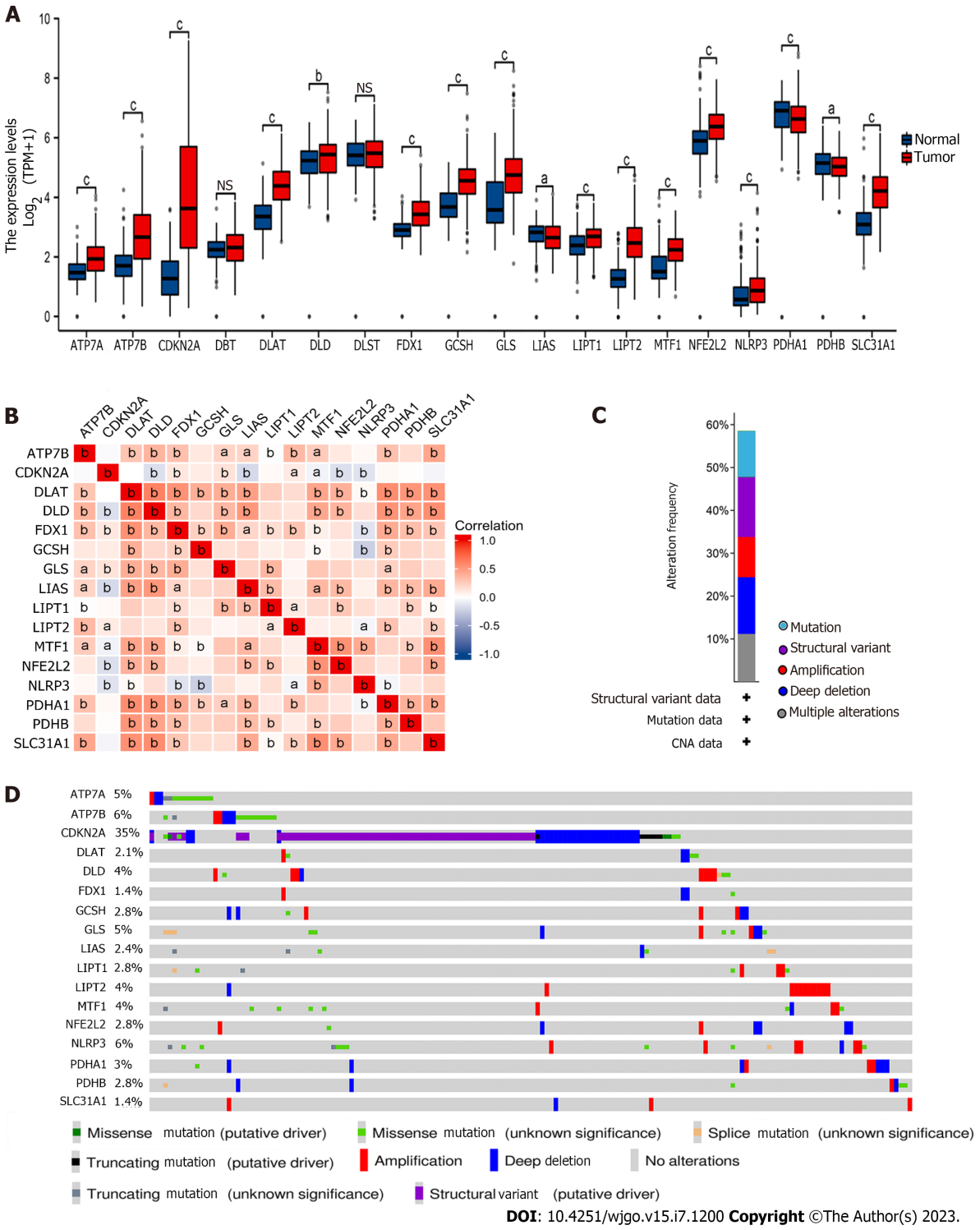

DOI: 10.4251/wjgo.v15.i7.1200 **Copyright** ©The Author(s) 2023.

Figure 1 Cuproptosis-related gene expression status in gastric cancer. A: Expression levels of 19 human cuproptosis-related genes (CRGs) in gastric cancer tissues and corresponding normal tissues in the Cancer Genome Atlas database; B: Correlations between the expression of 16 differential CRGs in gastric cancer; C: Overall landscape of gene mutations of differential CRGs in gastric cancer; D: Patterns of gene mutation of differentially expressed CRGs in gastric cancer ($^aP < 0.05$, $^bP < 0.01$, $^cP < 0.001$). NS: Not significant.

CONCLUSION

In conclusion, our study systematically analysed the prognostic significance and interactive landscapes of CRGs in GC samples using bioinformatics. The prognostic risk score based on the expression signature of *FDX1*, *LIAS*, and *MTF1* had important implications in the prediction of OS and DSS in GC patients, and these CRGs were associated with infiltration of various immune cell types, providing novel insights into therapeutic strategies for GC patients.

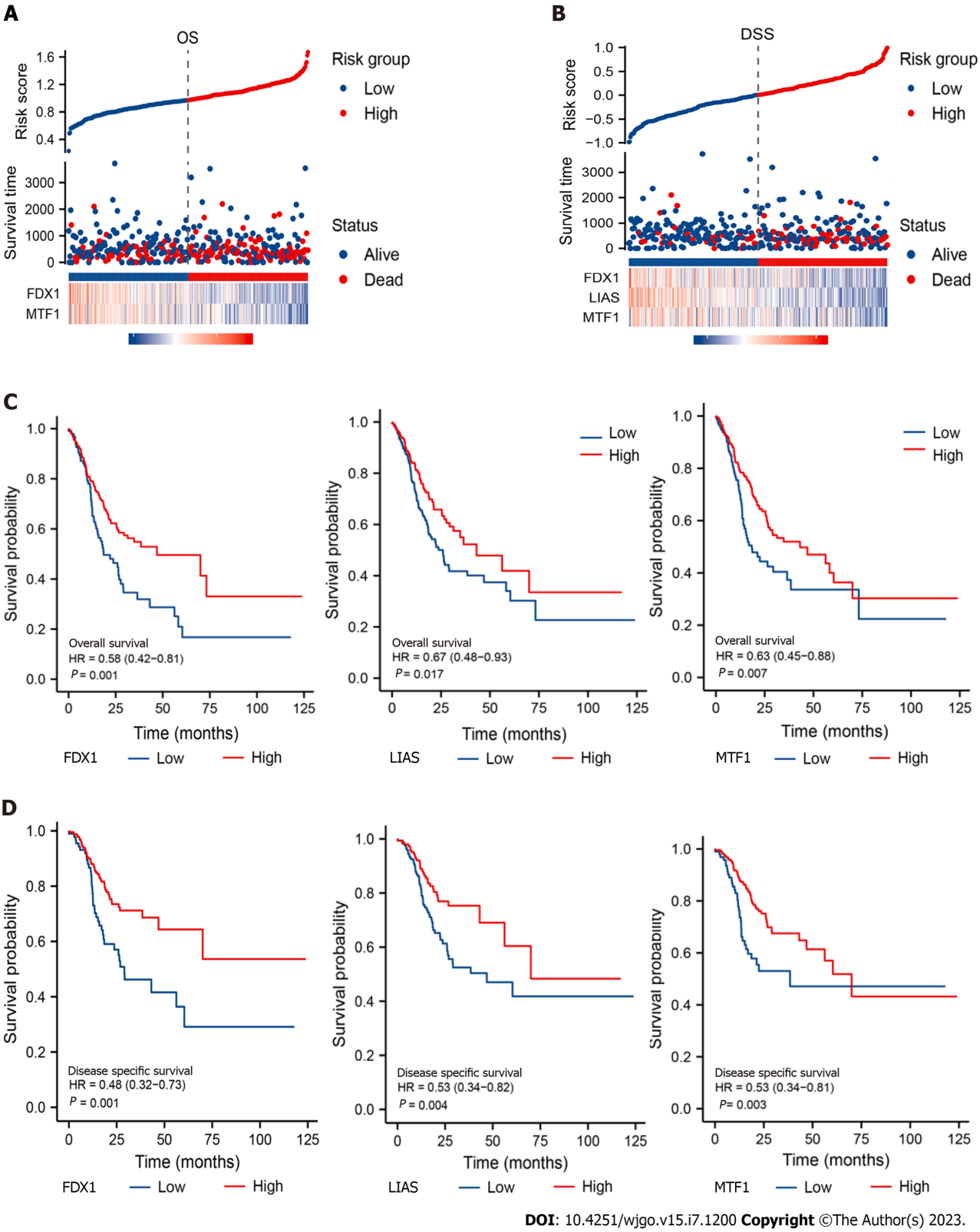

DOI: 10.4251/wjgo.v15.i7.1200 **Copyright** ©The Author(s) 2023.

Figure 2 Clinical significance of prognostic cuproptosis-related genes in gastric cancer in the Cancer Genome Atlas cohort. A: Distribution of risk score, overall survival (OS) status and the expression of *FDX1* and *MTF1* in gastric cancer (GC) patients; B: Distribution of risk score, disease-specific survival (DSS) status and the expression of *FDX1* and *MTF1* in GC patients; C: Kaplan-Meier curves of the expression of *FDX1*, *LIAS*, *MTF1* and OS time; D: Kaplan-Meier curves of the expression of *FDX1*, *LIAS*, and *MTF1* and DSS time.

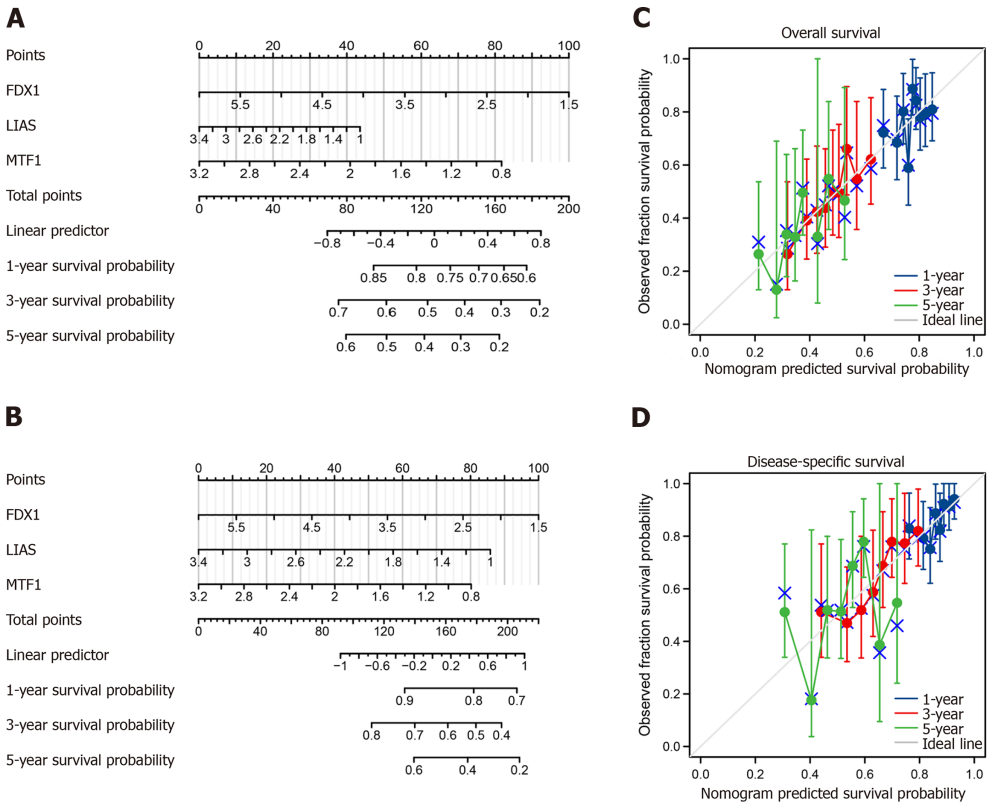

DOI: 10.4251/wjgo.v15.i7.1200

Figure 3 Overall survival nomogram model and calibration plots. A: Prognostic nomogram plot constructed to predict the 1-, 3-, and 5-year overall survival (OS) times of gastric cancer patients in The Cancer Genome Atlas (TCGA) cohort; B: Prognostic nomogram plot constructed to predict the 1-, 3-, and 5-year disease-specific survival (DSS) times of gastric cancer patients in the TCGA cohort; C: Calibration plot of the nomogram for 1-, 3-, and 5-year OS time; D: Calibration plot of the nomogram for 1-, 3-, and 5-year DSS time.

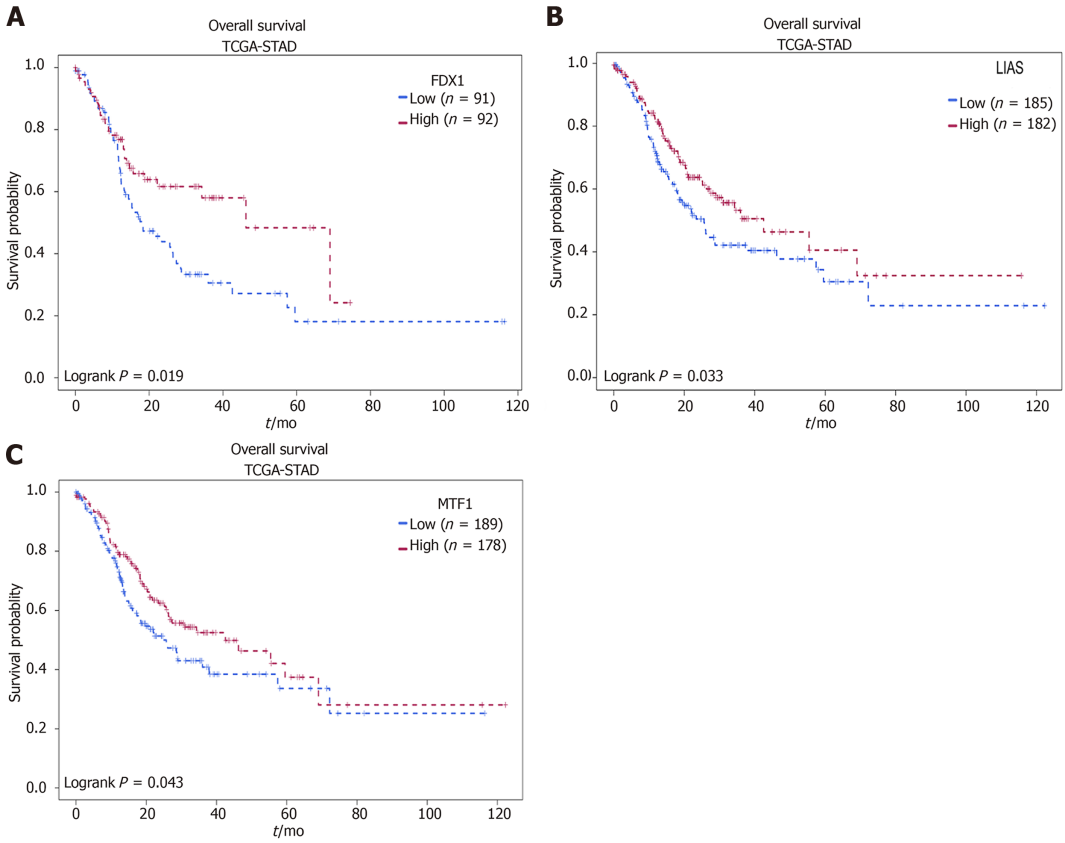

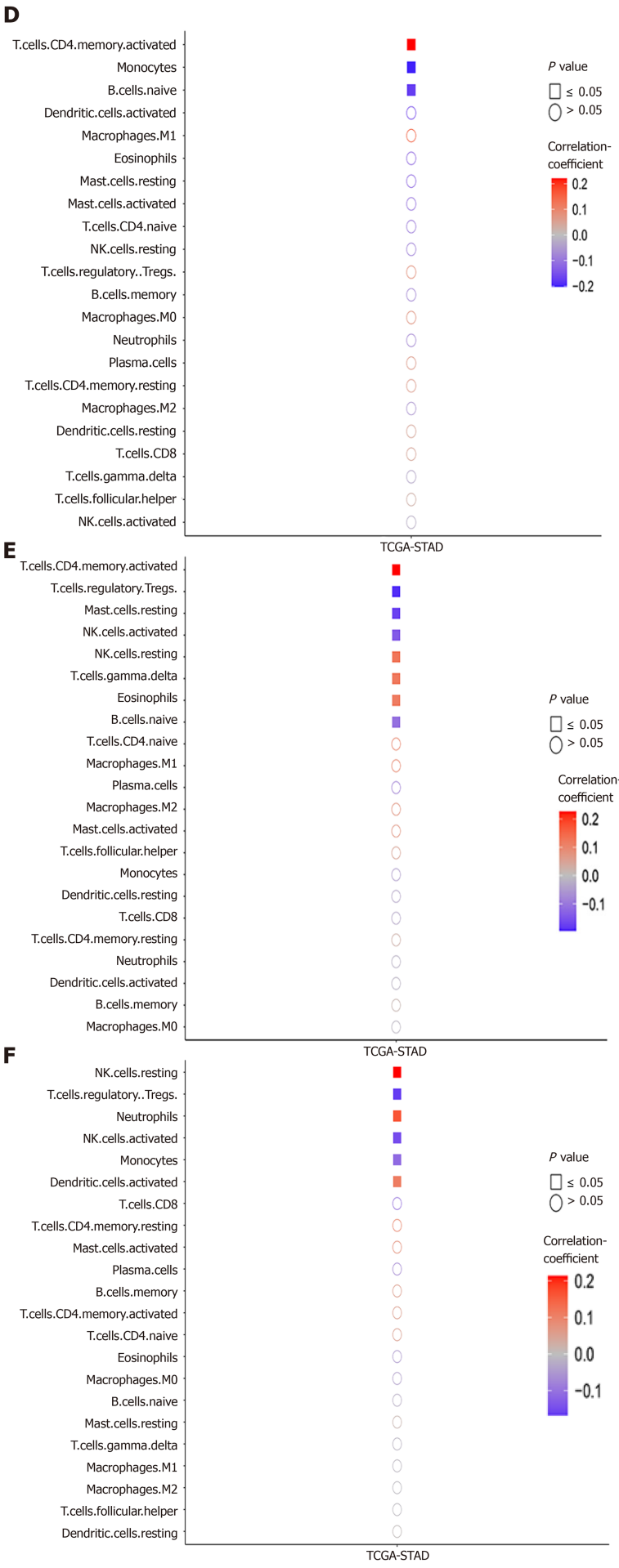
D
T.cells.CD4.memory.activated
Monocytes
B.cells.naive
Dendritic.cells.activated
Macrophages.M1
Eosinophils
Mast.cells.resting
Mast.cells.activated
T.cells.CD4.naive
NK.cells.resting
T.cells.regulatory..Tregs.
B.cells.memory
Macrophages.M0
Neutrophils
Plasma.cells
T.cells.CD4.memory.resting
Macrophages.M2
Dendritic.cells.resting
T.cells.CD8
T.cells.gamma.delta
T.cells.follicular.helper
NK.cells.activated
TCGA-STAD
P value
≤ 0.05
> 0.05
Correlation-coefficient
0.2
0.1
0.0
-0.1
-0.2
E
T.cells.CD4.memory.activated
T.cells.regulatory.Tregs.
Mast.cells.resting
NK.cells.activated
NK.cells.resting
T.cells.gamma.delta
Eosinophils
B.cells.naive
T.cells.CD4.naive
Macrophages.M1
Plasma.cells
Macrophages.M2
Mast.cells.activated
T.cells.follicular.helper
Monocytes
Dendritic.cells.resting
T.cells.CD8
T.cells.CD4.memory.resting
Neutrophils
Dendritic.cells.activated
B.cells.memory
Macrophages.M0
TCGA-STAD
P value
≤ 0.05
> 0.05
Correlation-coefficient
0.2
0.1
0.0
-0.1
F
NK.cells.resting
T.cells.regulatory..Tregs.
Neutrophils
NK.cells.activated
Monocytes
Dendritic.cells.activated
T.cells.CD8
T.cells.CD4.memory.resting
Mast.cells.activated
Plasma.cells
B.cells.memory
T.cells.CD4.memory.activated
T.cells.CD4.naive
Eosinophils
Macrophages.M0
B.cells.naive
Mast.cells.resting
T.cells.gamma.delta
Macrophages.M1
Macrophages.M2
T.cells.follicular.helper
Dendritic.cells.resting
TCGA-STAD
P value
≤ 0.05
> 0.05
Correlation-coefficient
0.2
0.1
0.0
-0.1

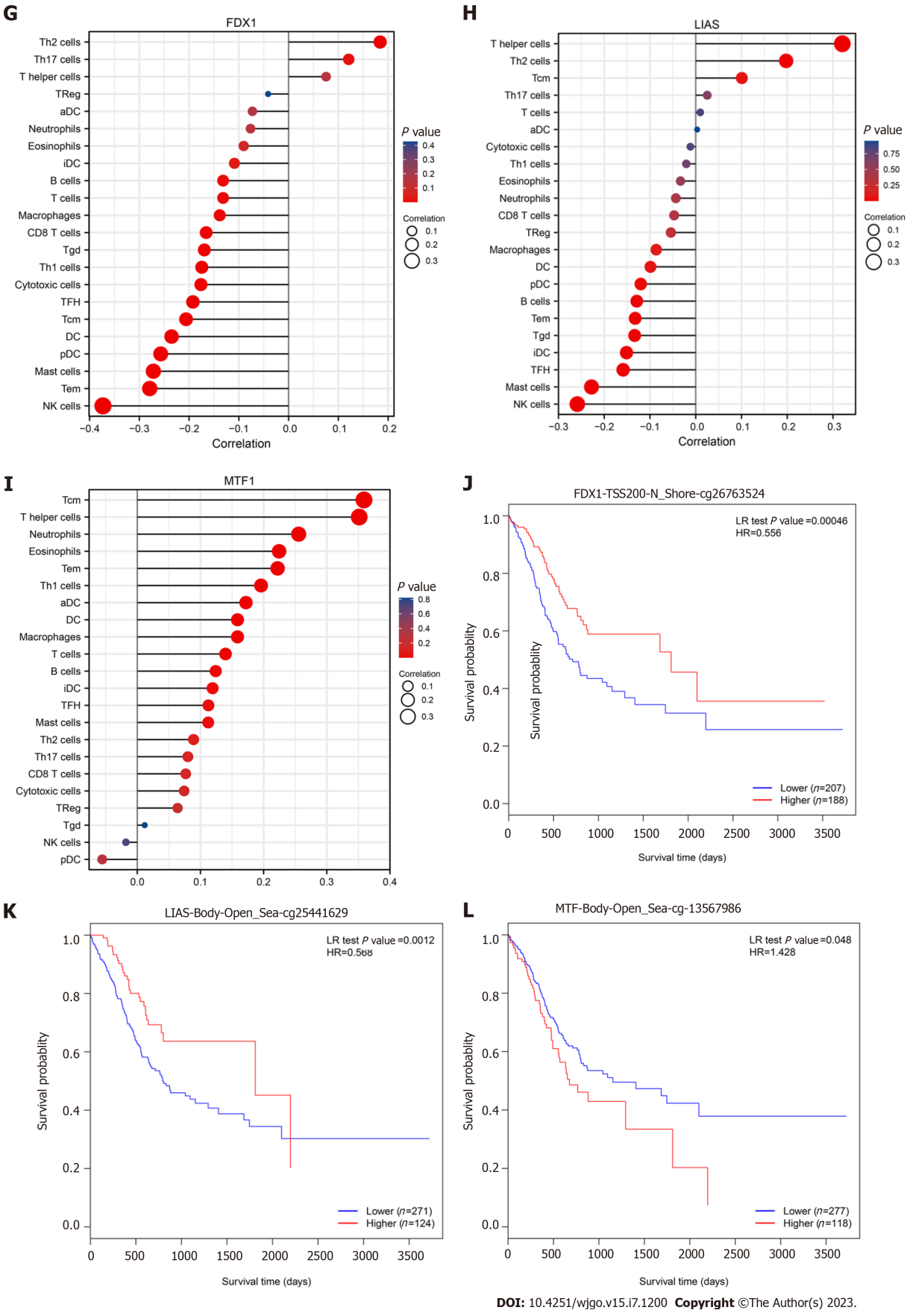

DOI: 10.4251/wjgo.v15.i7.1200

Figure 4 Relationship between the expression of prognostic cuproptosis-related genes and immune cell infiltration levels in gastric cancer. A-C: Kaplan-Meier curves of the expression of *FDX1* (A), *LIAS* (B), *MTF1* (C) in scRNA-seq samples and immune cell infiltration level groups. All of these genes were correlated with the overall survival time of gastric cancer patients; D-F: The correlation of different immune cell infiltration levels and the expression of FDX (D), *LIAS* (E), and *MTF1* (F) in scRNA-seq samples; G-I: Lollipop plots of different immune cell infiltration levels and the expression of FDX (G), *LIAS* (H), and

MTF1 (I). The length of the bars in the lollipop plots is relative to the correlation levels, and the color of the cycles is relative to the *P* value; J-L: Lower levels of methylation in *FDX1* (J) and higher levels of methylation in *LIAS* (K), *MTF1* (L) are associated with poor prognosis. HR: Hazard ratio; STAD: Stomach adenocarcinoma; TCGA: The Cancer Genome Atlas.

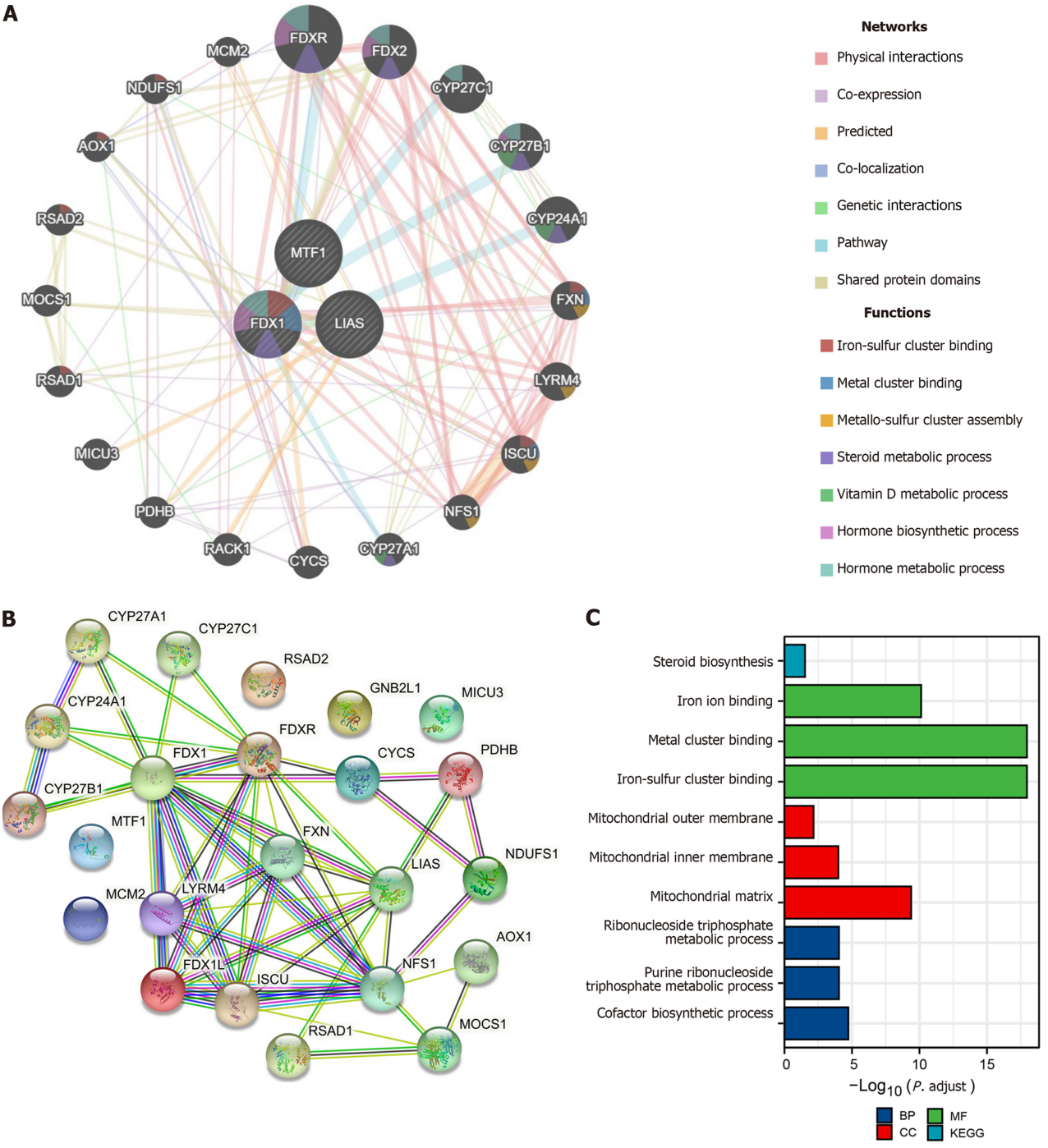

DOI: 10.4251/wjgo.v15.i7.1200

Figure 5 Analysis of the biological functions of prognostic cuproptosis-related genes. A: Gene network associated with *FDX1*, *LIAS*, and *MTF1* containing 23 related genes, constructed using GeneMANIA. The different colors of the lines are associated with the different functions; B: Protein-protein interaction network diagram of interactions between proteins encoded by genes related to *FDX1*, *LIAS*, and *MTF1* constructed using GeneMANIA and STRING; C: KEGG pathway enrichment analysis and gene ontology classification of several targets from STRING. BP: Biological process; CC: Cellular component; MF: Molecular function.

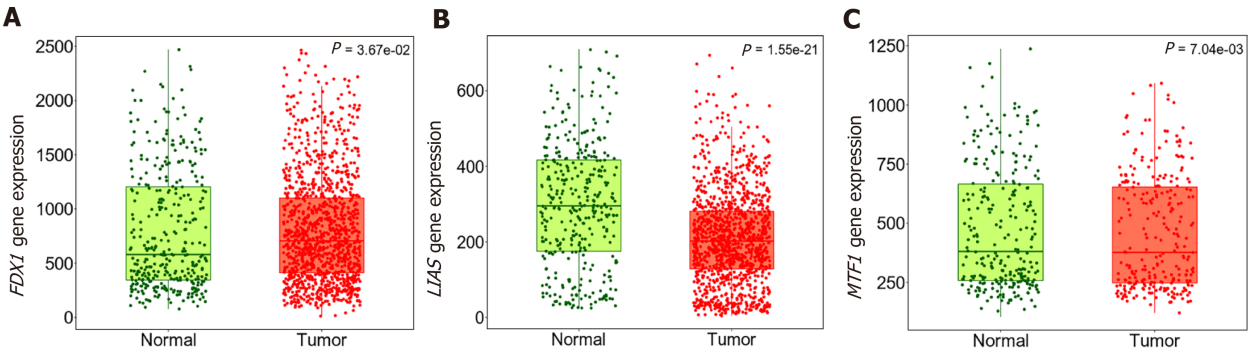

DOI: 10.4251/wjgo.v15.i7.1200

Figure 6 Differential expression analysis and validation of prognostic cuproptosis-related genes in the TNM plot database. A: *FDX1* was remarkably overexpressed in gastric cancer (GC) cancer samples in the Gene Expression Omnibus (GEO) in the TNM plot database; B: *LIAS* was remarkably downregulated in GC cancer samples in GEO in the TNM plot database; C: *MTF1* was remarkably overexpressed in GC cancer samples in GEO in the TNM plot database.

ARTICLE HIGHLIGHTS

Research background

Gastric cancer (GC) is one of the most common digestive system cancers with high mortality rates worldwide.

Research motivation

Cuproptosis is strongly correlated with the biological behaviour of malignant tumour cells and no previous studies have estimated the relationship between cuproptosis related genes (CRGs) and the progression of GC.

Research objectives

Our study aims to offer new insights to predict GC prognosis and provide multiple therapeutic targets for future therapy about CRGs.

Research methods

We collected data from several public data portals and systematically estimated the expression level and prognostic values of CRGs in GC samples and related mechanisms using public databases and bioinformatics.

Research results

We found that *FDX1*, *LIAS*, and *MTF1* were differentially expressed in GC samples and exhibited important prognostic significance. We constructed a nomogram model for overall survival and disease-specific survival prediction and validated it *via* calibration plots. Mechanistically, immune cell infiltration and DNA methylation prominently affected the survival time of GC patients. Moreover, protein-protein interaction network, KEGG pathway and gene ontology enrichment analyses demonstrated that *FDX1*, *LIAS*, *MTF1* and related proteins played key roles in the tricarboxylic acid cycle and cuprotosis. Top 10 perturbagens were filtered as well.

Research conclusions

Our findings suggested that *FDX1*, *LIAS*, and *MTF1* had important implications for the prediction of OS and DSS in GC patients, which were associated with various immune cell infiltrations, providing novel insights into therapeutic strategies for GC patients.

Research perspectives

Considerable effort needs to be expended in exploring the therapeutic strategies *via* CRGs in GC.

FOOTNOTES

Author contributions: Yan JN designed and performed the research and wrote the paper; Shao YF and Ye GL designed the research and supervised the report; Zhou HX and Guo LH designed the research and contributed to the analysis; Shao YF and Zhu DP were responsible for the revision of the manuscript for important intellectual content; All authors expressed approval of the final version to be submitted.

Supported by The Key Scientific and Technological Projects of Ningbo, No. 2021Z133.

Institutional review board statement: Our research is based on the Cancer Genome Atlas (TCGA, https://tega-data.nci.nih.gov/)

database, the Genotype-Tissue Expression (GTEx) data portal (https://www.gtexportal.org/home/index.html) and the Gene Expression Omnibus (GEO, https://www.nebi.nlm.nih.gov/gds) database. All of these are open-access public databases. Thus, no institutional review board approval was required.

Conflict-of-interest statement: All the authors report having no relevant conflicts of interest for this article.

Data sharing statement: The technical appendix, statistical code, and datasets are available from the corresponding author at fyshaoyongfu@nbu.edu.cn.

Country/Territory of origin: China

ORCID number: Jia-Ning Yan 0000-0002-8781-9021; Guo-Liang Ye 0000-0003-0600-9981; Yong-Fu Shao 0000-0001-6256-1426.

S-Editor: Li L
L-Editor: Filipodia
P-Editor: Ji MX

REFERENCES

1 **Sung H**, Ferlay J, Siegel RL, Laversanne M, Soerjomataram I, Jemal A, Bray F. Global Cancer Statistics 2020: GLOBOCAN Estimates of Incidence and Mortality Worldwide for 36 Cancers in 185 Countries. *CA Cancer J Clin* 2021; **71**: 209-249 [PMID: 33538338 DOI: 10.3322/caac.21660]
2 **Ding XQ**, Wang ZY, Xia D, Wang RX, Pan XR, Tong JH. Proteomic Profiling of Serum Exosomes From Patients With Metastatic Gastric Cancer. *Front Oncol* 2020; **10**: 1113 [PMID: 32754443 DOI: 10.3389/fonc.2020.01113]
3 **Wang P**, Zhang W, Wang L, Liang W, Cai A, Gao Y, Chen L. RCC2 Interacts with Small GTPase RalA and Regulates Cell Proliferation and Motility in Gastric Cancer. *Onco Targets Ther* 2020; **13**: 3093-3103 [PMID: 32341655 DOI: 10.2147/OTT.S228914]
4 **Tsvetkov P**, Coy S, Petrova B, Dreishpoon M, Verma A, Abdusamad M, Rossen J, Joesch-Cohen L, Humeidi R, Spangler RD, Eaton JK, Frenkel E, Kocak M, Corsello SM, Lutsenko S, Kanarek N, Santagata S, Golub TR. Copper induces cell death by targeting lipoylated TCA cycle proteins. *Science* 2022; **375**: 1254-1261 [PMID: 35298263 DOI: 10.1126/science.abf0529]
5 **Hu JD**, Tang HQ, Zhang Q, Fan J, Hong J, Gu JZ, Chen JL. Prediction of gastric cancer metastasis through urinary metabolomic investigation using GC/MS. *World J Gastroenterol* 2011; **17**: 727-734 [PMID: 21390142 DOI: 10.3748/wjg.v17.i6.727]
6 **Cerami E**, Gao J, Dogrusoz U, Gross BE, Sumer SO, Aksoy BA, Jacobsen A, Byrne CJ, Heuer ML, Larsson E, Antipin Y, Reva B, Goldberg AP, Sander C, Schultz N. The cBio cancer genomics portal: an open platform for exploring multidimensional cancer genomics data. *Cancer Discov* 2012; **2**: 401-404 [PMID: 22588877 DOI: 10.1158/2159-8290.CD-12-0095]
7 **Modhukur V**, Iljasenko T, Metsalu T, Lokk K, Laisk-Podar T, Vilo J. MethSurv: a web tool to perform multivariable survival analysis using DNA methylation data. *Epigenomics* 2018; **10**: 277-288 [PMID: 29264942 DOI: 10.2217/epi-2017-0118]
8 **Anuraga G**, Wang WJ, Phan NN, An Ton NT, Ta HDK, Berenice Prayugo F, Minh Xuan DT, Ku SC, Wu YF, Andriani V, Athoillah M, Lee KH, Wang CY. Potential Prognostic Biomarkers of NIMA (Never in Mitosis, Gene A)-Related Kinase (NEK) Family Members in Breast Cancer. *J Pers Med* 2021; **11** [PMID: 34834441 DOI: 10.3390/jpm11111089]
9 **Xing C**, Wang Z, Zhu Y, Zhang C, Liu M, Hu X, Chen W, Du Y. Integrate analysis of the promote function of Cell division cycle-associated protein family to pancreatic adenocarcinoma. *Int J Med Sci* 2021; **18**: 672-684 [PMID: 33437202 DOI: 10.7150/ijms.53243]
10 **Dwivedi B**, Mumme H, Satpathy S, Bhasin SS, Bhasin M. Survival Genie, a web platform for survival analysis across pediatric and adult cancers. *Sci Rep* 2022; **12**: 3069 [PMID: 35197510 DOI: 10.1038/s41598-022-06841-0]
11 **Hänzelmann S**, Castelo R, Guinney J. GSVA: gene set variation analysis for microarray and RNA-seq data. *BMC Bioinformatics* 2013; **14**: 7 [PMID: 23323831 DOI: 10.1186/1471-2105-14-7]
12 **Li T**, Fu J, Zeng Z, Cohen D, Li J, Chen Q, Li B, Liu XS. TIMER2.0 for analysis of tumor-infiltrating immune cells. *Nucleic Acids Res* 2020; **48**: W509-W514 [PMID: 32442275 DOI: 10.1093/nar/gkaa407]
13 **Kao TJ**, Wu CC, Phan NN, Liu YH, Ta HDK, Anuraga G, Wu YF, Lee KH, Chuang JY, Wang CY. Prognoses and genomic analyses of proteasome 26S subunit, ATPase (PSMC) family genes in clinical breast cancer. *Aging (Albany NY)* 2021; **13**: 17970 [PMID: 34329194 DOI: 10.18632/aging.203345]
14 **Laham AJ**, El-Awady R, Lebrun JJ, Ayad MS. A Bioinformatics Evaluation of the Role of Dual-Specificity Tyrosine-Regulated Kinases in Colorectal Cancer. *Cancers (Basel)* 2022; **14** [PMID: 35454940 DOI: 10.3390/cancers14082034]
15 **Warde-Farley D**, Donaldson SL, Comes O, Zuberi K, Badrawi R, Chao P, Franz M, Grouios C, Kazi F, Lopes CT, Maitland A, Mostafavi S, Montojo J, Shao Q, Wright G, Bader GD, Morris Q. The GeneMANIA prediction server: biological network integration for gene prioritization and predicting gene function. *Nucleic Acids Res* 2010; **38**: W214-W220 [PMID: 20576703 DOI: 10.1093/nar/gkq537]
16 **Szklarczyk D**, Gable AL, Nastou KC, Lyon D, Kirsch R, Pyysalo S, Doncheva NT, Legeay M, Fang T, Bork P, Jensen LJ, von Mering C. The STRING database in 2021: customizable protein-protein networks, and functional characterization of user-uploaded gene/measurement sets. *Nucleic Acids Res* 2021; **49**: D605-D612 [PMID: 33237311 DOI: 10.1093/nar/gkaa1074]
17 **Yu G**, Wang LG, Han Y, He QY. clusterProfiler: an R package for comparing biological themes among gene clusters. *OMICS* 2012; **16**: 284-287 [PMID: 22455463 DOI: 10.1089/omi.2011.0118]

18 **Lamb J**, Crawford ED, Peck D, Modell JW, Blat IC, Wrobel MJ, Lerner J, Brunet JP, Subramanian A, Ross KN, Reich M, Hieronymus H, Wei G, Armstrong SA, Haggarty SJ, Clemons PA, Wei R, Carr SA, Lander ES, Golub TR. The Connectivity Map: using gene-expression signatures to connect small molecules, genes, and disease. *Science* 2006; **313**: 1929-1935 [PMID: 17008526 DOI: 10.1126/science.1132939]

19 **Subramanian A**, Narayan R, Corsello SM, Peck DD, Natoli TE, Lu X, Gould J, Davis JF, Tubelli AA, Asiedu JK, Lahr DL, Hirschman JE, Liu Z, Donahue M, Julian B, Khan M, Wadden D, Smith IC, Lam D, Liberzon A, Toder C, Bagul M, Orzechowski M, Enache OM, Piccioni F, Johnson SA, Lyons NJ, Berger AH, Shamji AF, Brooks AN, Vrcic A, Flynn C, Rosains J, Takeda DY, Hu R, Davison D, Lamb J, Ardlie K, Hogstrom L, Greenside P, Gray NS, Clemons PA, Silver S, Wu X, Zhao WN, Read-Button W, Haggarty SJ, Ronco LV, Boehm JS, Schreiber SL, Doench JG, Bittker JA, Root DE, Wong B, Golub TR. A Next Generation Connectivity Map: L1000 Platform and the First 1,000,000 Profiles. *Cell* 2017; **171**: 1437-1452.e17 [PMID: 29195078 DOI: 10.1016/j.cell.2017.10.049]

20 **Wang CY**, Chiao CC, Phan NN, Li CY, Sun ZD, Jiang JZ, Hung JH, Chen YL, Yen MC, Weng TY, Chen WC, Hsu HP, Lai MD. Gene signatures and potential therapeutic targets of amino acid metabolism in estrogen receptor-positive breast cancer. *Am J Cancer Res* 2020; **10**: 95-113 [PMID: 32064155]

21 **Bartha Á**, Győrffy B. TNMplot.com: A Web Tool for the Comparison of Gene Expression in Normal, Tumor and Metastatic Tissues. *Int J Mol Sci* 2021; **22** [PMID: 33807717 DOI: 10.3390/ijms22052622]

22 **Acs B**, Ahmed FS, Gupta S, Wong PF, Gartrell RD, Sarin Pradhan J, Rizk EM, Gould Rothberg B, Saenger YM, Rimm DL. An open source automated tumor infiltrating lymphocyte algorithm for prognosis in melanoma. *Nat Commun* 2019; **10**: 5440 [PMID: 31784511 DOI: 10.1038/s41467-019-13043-2]

23 **Zhang K**, Zhang L, Mi Y, Tang Y, Ren F, Liu B, Zhang Y, Zheng P. A ceRNA network and a potential regulatory axis in gastric cancer with different degrees of immune cell infiltration. *Cancer Sci* 2020; **111**: 4041-4050 [PMID: 32860283 DOI: 10.1111/cas.14634]

24 **Zhang Y**, Ma S, Wang M, Shi W, Hu Y. Comprehensive Analysis of Prognostic Markers for Acute Myeloid Leukemia Based on Four Metabolic Genes. *Front Oncol* 2020; **10**: 578933 [PMID: 33117716 DOI: 10.3389/fonc.2020.578933]

25 **Zhang J**, Kong X, Zhang Y, Sun W, Wang J, Chen M, Chen X. FDXR regulates TP73 tumor suppressor *via* IRP2 to modulate aging and tumor suppression. *J Pathol* 2020; **251**: 284-296 [PMID: 32304229 DOI: 10.1002/path.5451]

26 **Wang T**, Liu Y, Li Q, Luo Y, Liu D, Li B. Cuproptosis-related gene *FDX1* expression correlates with the prognosis and tumor immune microenvironment in clear cell renal cell carcinoma. *Front Immunol* 2022; **13**: 999823 [PMID: 36225932 DOI: 10.3389/fimmu.2022.999823]

27 **Burr SP**, Costa AS, Grice GL, Timms RT, Lobb IT, Freisinger P, Dodd RB, Dougan G, Lehner PJ, Frezza C, Nathan JA. Mitochondrial Protein Lipoylation and the 2-Oxoglutarate Dehydrogenase Complex Controls HIF1α Stability in Aerobic Conditions. *Cell Metab* 2016; **24**: 740-752 [PMID: 27923773 DOI: 10.1016/j.cmet.2016.09.015]

28 **Cai Y**, He Q, Liu W, Liang Q, Peng B, Li J, Zhang W, Kang F, Hong Q, Yan Y, Peng J, Xu Z, Bai N. Comprehensive analysis of the potential cuproptosis-related biomarker *LIAS* that regulates prognosis and immunotherapy of pan-cancers. *Front Oncol* 2022; **12**: 952129 [PMID: 35982953 DOI: 10.3389/fonc.2022.952129]

29 **Ruan X**, Zheng J, Liu X, Liu Y, Liu L, Ma J, He Q, Yang C, Wang D, Cai H, Li Z, Liu J, Xue Y. lncRNA LINC00665 Stabilized by TAF15 Impeded the Malignant Biological Behaviors of Glioma Cells *via* STAU1-Mediated mRNA Degradation. *Mol Ther Nucleic Acids* 2020; **20**: 823-840 [PMID: 32464546 DOI: 10.1016/j.omtn.2020.05.003]

30 **Yang Y**, Qian Cai Q, Sheng Fu L, Wei Dong Y, Fan F, Zhong Wu X. Reduced N6-Methyladenosine Mediated by METTL3 Acetylation Promotes *MTF1* Expression and Hepatocellular Carcinoma Cell Growth. *Chem Biodivers* 2022; **19**: e202200333 [PMID: 36149370 DOI: 10.1002/cbdv.202200333]

31 **Wu L**, Shi W, Long J, Guo X, Michailidou K, Beesley J, Bolla MK, Shu XO, Lu Y, Cai Q, Al-Ejeh F, Rozali E, Wang Q, Dennis J, Li B, Zeng C, Feng H, Gusev A, Barfield RT, Andrulis IL, Anton-Culver H, Arndt V, Aronson KJ, Auer PL, Barrdahl M, Baynes C, Beckmann MW, Benitez J, Bermisheva M, Blomqvist C, Bogdanova NV, Bojesen SE, Brauch H, Brenner H, Brinton L, Broberg P, Brucker SY, Burwinkel B, Caldés T, Canzian F, Carter BD, Castelao JE, Chang-Claude J, Chen X, Cheng TD, Christiansen H, Clarke CL; NBCS Collaborators, Collée M, Cornelissen S, Couch FJ, Cox D, Cox A, Cross SS, Cunningham JM, Czene K, Daly MB, Devilee P, Doheny KF, Dörk T, Dos-Santos-Silva I, Dumont M, Dwek M, Eccles DM, Eilber U, Eliassen AH, Engel C, Eriksson M, Fachal L, Fasching PA, Figueroa J, Flesch-Janys D, Fletcher O, Flyger H, Fritschi L, Gabrielson M, Gago-Dominguez M, Gapstur SM, García-Closas M, Gaudet MM, Ghoussaini M, Giles GG, Goldberg MS, Goldgar DE, González-Neira A, Guénel P, Hahnen E, Haiman CA, Håkansson N, Hall P, Hallberg E, Hamann U, Harrington P, Hein A, Hicks B, Hillemanns P, Hollestelle A, Hoover RN, Hopper JL, Huang G, Humphreys K, Hunter DJ, Jakubowska A, Janni W, John EM, Johnson N, Jones K, Jones ME, Jung A, Kaaks R, Kerin MJ, Khusnutdinova E, Kosma VM, Kristensen VN, Lambrechts D, Le Marchand L, Li J, Lindström S, Lissowska J, Lo WY, Loibl S, Lubinski J, Luccarini C, Lux MP, MacInnis RJ, Maishman T, Kostovska IM, Mannermaa A, Manson JE, Margolin S, Mavroudis D, Meijers-Heijboer H, Meindl A, Menon U, Meyer J, Mulligan AM, Neuhausen SL, Nevanlinna H, Neven P, Nielsen SF, Nordestgaard BG, Olopade OI, Olson JE, Olsson H, Peterlongo P, Peto J, Plaseska-Karanfilska D, Prentice R, Presneau N, Pylkäs K, Rack B, Radice P, Rahman N, Rennert G, Rennert HS, Rhenius V, Romero A, Romm J, Rudolph A, Saloustros E, Sandler DP, Sawyer EJ, Schmidt MK, Schmutzler RK, Schneeweiss A, Scott RJ, Scott CG, Seal S, Shah M, Shrubsole MJ, Smeets A, Southey MC, Spinelli JJ, Stone J, Surowy H, Swerdlow AJ, Tamimi RM, Tapper W, Taylor JA, Terry MB, Tessier DC, Thomas A, Thöne K, Tollenaar RAEM, Torres D, Truong T, Untch M, Vachon C, Van Den Berg D, Vincent D, Waisfisz Q, Weinberg CR, Wendt C, Whittemore AS, Wildiers H, Willett WC, Winqvist R, Wolk A, Xia L, Yang XR, Ziogas A, Ziv E; kConFab/AOCS Investigators, Dunning AM, Pharoah PDP, Simard J, Milne RL, Edwards SL, Kraft P, Easton DF, Chenevix-Trench G, Zheng W. A transcriptome-wide association study of 229,000 women identifies new candidate susceptibility genes for breast cancer. *Nat Genet* 2018; **50**: 968-978 [PMID: 29915430 DOI: 10.1038/s41588-018-0132-x]

32 **Li P**, Bai C, Zhan L, Zhang H, Zhang Y, Zhang W, Wang Y, Zhao J. Specific gene module pair-based target identification and drug discovery. *Front Pharmacol* 2022; **13**: 1089217 [PMID: 36726786 DOI: 10.3389/fphar.2022.1089217]

World Journal of Gastrointestinal Oncology

Submit a Manuscript: https://www.f6publishing.com

World J Gastrointest Oncol 2023 July 15; 15(7): 1215-1226

DOI: 10.4251/wjgo.v15.i7.1215

ISSN 1948-5204 (online)

ORIGINAL ARTICLE

Clinical and Translational Research

Integrated analysis of single-cell and bulk RNA-seq establishes a novel signature for prediction in gastric cancer

Fei Wen, Xin Guan, Hai-Xia Qu, Xiang-Jun Jiang

Specialty type: Oncology

Provenance and peer review: Unsolicited article; Externally peer reviewed.

Peer-review model: Single blind

Peer-review report's scientific quality classification

Grade A (Excellent): 0
Grade B (Very good): B, B, B, B
Grade C (Good): C, C, C
Grade D (Fair): 0
Grade E (Poor): 0

P-Reviewer: Cheng YH, United States; El-Arabey AA, Egypt; Emran TB, Bangladesh; Li Q, China

Received: February 1, 2023
Peer-review started: February 1, 2023
First decision: March 21, 2023
Revised: March 31, 2023
Accepted: May 8, 2023
Article in press: May 8, 2023
Published online: July 15, 2023

Fei Wen, Qingdao University, Medical College, Qingdao 266000, Shandong Province, China

Xin Guan, Hai-Xia Qu, Xiang-Jun Jiang, Department of Gastroenterology, Qingdao Municipal Hospital, Qingdao 266071, Shandong Province, China

Corresponding author: Xiang-Jun Jiang, PhD, Doctor, Department of Gastroenterology, Qingdao Municipal Hospital, No. 1 Jiaozhou Road, Qingdao 266071, Shandong Province, China. drjxj@163.com

Abstract

BACKGROUND

Single-cell sequencing technology provides the capability to analyze changes in specific cell types during the progression of disease. However, previous single-cell sequencing studies on gastric cancer (GC) have largely focused on immune cells and stromal cells, and further elucidation is required regarding the alterations that occur in gastric epithelial cells during the development of GC.

AIM

To create a GC prediction model based on single-cell and bulk RNA sequencing (bulk RNA-seq) data.

METHODS

In this study, we conducted a comprehensive analysis by integrating three single-cell RNA sequencing (scRNA-seq) datasets and ten bulk RNA-seq datasets. Our analysis mainly focused on determining cell proportions and identifying differentially expressed genes (DEGs). Specifically, we performed differential expression analysis among epithelial cells in GC tissues and normal gastric tissues (NAGs) and utilized both single-cell and bulk RNA-seq data to establish a prediction model for GC. We further validated the accuracy of the GC prediction model in bulk RNA-seq data. We also used Kaplan–Meier plots to verify the correlation between genes in the prediction model and the prognosis of GC.

RESULTS

By analyzing scRNA-seq data from a total of 70707 cells from GC tissue, NAG, and chronic gastric tissue, 10 cell types were identified, and DEGs in GC and normal epithelial cells were screened. After determining the DEGs in GC and normal gastric samples identified by bulk RNA-seq data, a GC predictive classifier was constructed using the Least absolute shrinkage and selection

operator (LASSO) and random forest methods. The LASSO classifier showed good performance in both validation and model verification using The Cancer Genome Atlas and Genotype-Tissue Expression (GTEx) datasets [area under the curve (AUC)_min = 0.988, AUC_1se = 0.994], and the random forest model also achieved good results with the validation set (AUC = 0.92). Genes *TIMP1*, *PLOD3*, *CKS2*, *TYMP*, *TNFRSF10B*, *CPNE1*, *GDF15*, *BCAP31*, and *CLDN7* were identified to have high importance values in multiple GC predictive models, and KM-PLOTTER analysis showed their relevance to GC prognosis, suggesting their potential for use in GC diagnosis and treatment.

CONCLUSION

A predictive classifier was established based on the analysis of RNA-seq data, and the genes in it are expected to serve as auxiliary markers in the clinical diagnosis of GC.

Key Words: Gastric cancer; Single-cell RNA sequencing; Prediction model; Least absolute shrinkage and selection operator; Random forest

Core Tip: In this study, we integrated and analyzed three single-cell RNA sequencing datasets and 10 bulk RNA sequencing datasets of gastric cancer (GC) from the Gene Expression Omnibus database. We conducted a differential expression analysis of epithelial cell subpopulations from GC tissue and normal gastric mucosa tissue and constructed GC prediction classifiers using the Least absolute shrinkage and selection operator (LASSO) method and random forest method. The LASSO prediction model was further validated in the Cancer Genome Atlas stomach adenocarcinoma dataset. *TIMP1*, *PLOD3*, *CKS2*, *TYMP*, *TNFRSF10B*, *CPNE1*, *GDF15*, *BCAP31*, and *CLDN7* were selected as the predictive genes for GC. This study provides a new approach for constructing prediction models based on single-cell sequencing data and offers new reference targets for the clinical diagnosis and treatment of GC.

Citation: Wen F, Guan X, Qu HX, Jiang XJ. Integrated analysis of single-cell and bulk RNA-seq establishes a novel signature for prediction in gastric cancer. *World J Gastrointest Oncol* 2023; 15(7): 1215-1226
URL: https://www.wjgnet.com/1948-5204/full/v15/i7/1215.htm
DOI: https://dx.doi.org/10.4251/wjgo.v15.i7.1215

INTRODUCTION

Gastric cancer (GC) is the second leading cause of cancer-related mortality globally[1-3]. Endoscopy remains the most prevalent and reliable method for GC diagnosis[3]. Nevertheless, due to the invasiveness of the procedure and the often asymptomatic nature of early-stage GC, patients are frequently diagnosed in advanced stages, resulting in poor survival and prognosis rates. Thus, the development of effective diagnostic methods and specific biomarkers for GC is urgently needed.

Serological markers and liquid biopsies (circulating tumor cells, circulating tumor DNA or RNA, microRNA, exosomes) are used to diagnose GC[2,4,5]. However, due to the small amount of circulating tumor cells and tumor DNA and the uneven distribution in the peripheral circulation, the repeatability of liquid biopsy is greatly limited[2,6]. Serological markers such as carcinoembryonic antigen (CEA), carbohydrate antigen 19-9 and carbohydrate antigen 72-4 are not sensitive enough to diagnose GC and have little importance in the diagnosis of early GC[6,7].

The tumor microenvironment (TME) consists of tumor cells and stromal cells, including fibroblasts, pericytes, mesenchymal stem cells, and various types of immune cells[8,9]. Tumorigenesis and progression result from the collective action of multiple cells[10]. Single-cell RNA sequencing (scRNA-seq) provides a promising avenue for understanding the cellular composition of tumors at a single-cell level and obtaining complete RNA transcripts of individual cells[11,12]. Conventional bulk RNA sequencing (bulk RNA-seq) of average signals from a group of different cells obscures the recognition of specific cell types and states. ScRNA-seq enables objective genome-wide analysis of many cells at the single-cell level in a single run, helping to characterize cellular heterogeneity in each sample. ScRNA-seq can be used to study gene expression, cell interactions, cell differentiation and the development of different cell types in TME.

Based on the scRNA-seq data, we identified genes that were differentially expressed in epithelial cell populations between normal gastric tissue (NAG) and GC tissue. Subsequently, using bulk RNA-seq data, we developed a predictive classifier. Our findings suggest that developing a prediction model for GC based on epithelial cells is a viable approach and that the results could serve as promising biomarkers for the diagnosis and prognosis of this disease.

MATERIALS AND METHODS

Dataset collection

We utilized three scRNA-seq datasets (GSE134520, GSE183904, GSE150290) and ten bulk RNA-seq datasets (GSE79973, GSE66229, GSE64951, GSE57303, GSE38749, GSE35809, GSE34942, GSE19826, GSE13911, GSE15459) that were obtained from the Gene Expression Omnibus (GEO) website (https://www.ncbi.nlm.nih.gov/geo/). We used the stomach adenocarcinoma (STAD) dataset and Genotype-Tissue Expression (GTEx) dataset obtained from the University of California at Santa Cruz website (https://xenabrowser.net/datapages/). The study did not require ethical approval because the data we used came from a publicly accessible database. The workflow of this study is shown in Figure 1.

Single-cell sequencing data analysis

Cells with fewer than 7000 and more than 400 genes possessing less than 10% mitochondria and less than 20% ribosomes were retained. To ensure adequate data quality, samples with fewer than 800 cells were removed before data integration. Ultimately, a total of 34 samples from three datasets were used for data integration and subsequent analysis, including 2 cases of NAG, 3 cases of chronic atrophic gastritis (CAG), 7 cases of intestinal metaplasia (IM) and 22 cases of GC (13 cases of intestinal GC, 6 cases of diffuse GC and 3 cases of mixed GC) (Supplementary Table 1). For scRNA-seq data analysis, we utilized the Seurat package[13] (https://satijalab.org/seurat/; 4.3.0) and its related functions. We employed the *RunUMAP* function for dimensionality reduction (using the first 20 PCs), the *FindClusters* function for cell clustering (resolution = 1.2), and the *FindAllMarkers* function for differential gene expression analysis. Default parameter values were used for all other functions.

Bulk sequencing data analysis

Ten GC chip sequencing datasets based on GPL570 were included in this study, including 834 GC samples and 187 NAG samples. The samples were processed using the robust multichip average algorithm to perform background correction and standardization. To mitigate the effects of batch variation, the COMBAT algorithm was utilized.

This paper includes the STAD data and the GTEx data. For both datasets, 'log2 (fpkm + 1)' data were used for subsequent analysis, and the *normalizeBetweenArrays* function was used to remove batch effects. The STAD dataset contained 375 GC samples and 32 paracancerous samples. The GTEx contains 174 samples of normal stomach tissue.

Differential expression and functional enrichment analysis

The *FindMarkers* function and the scCODE package[14] (https://github.com/XZouProjects/scCODE; version 1.0.1.0) were used to identify differentially expressed genes (DEGs) in scRNA-seq. The *lmfit* function was used to identify DEGs in the bulk RNA-seq data. Genes with a P value > 0.05 and an absolute logFC value greater than 0.5 were considered DEGs and subjected to functional enrichment analysis. The clusterProfiler package (version 4.2.0) was used to functionally annotate DEGs to identify significantly enriched Gene Ontology (GO) and Kyoto Encyclopedia of Genes and Genomes (KEGG) pathways.

Protein interaction analysis

We conducted molecular interaction analysis utilizing the STRING database (https://cn.string-db.org/). To present the results, we utilized Cytoscape (https://cytoscape.org/).

Prediction model construction

We screened DEGs in epithelial cells obtained from GC and normal adjacent gastric tissue (NAG), preserving genes with logFC > 0.5 and detected-times = 5. These genes were then compared with DEGs identified in bulk RNA-seq data between GC and NAG (logFC > 0.5 and P value < 0.05) to obtain an overlapping set. Subsequently, we used these genes to build a LASSO regression model and random forest model in the GEO training set and verified them in the GEO test set and The Cancer Genome Atlas (TCGA)-GTEx dataset. The GEO data were randomly divided into a training set and test set in a 6:4 ratio. The LASSO model was established using the *glmnet* function (version 4.1-6). The *randomForest* function (version 4.7-1.1) was used to build the random forest model. Finally, we evaluated the relationship between the gene and GC survival rates using Kaplan–Meier plotter (http://kmplot.com/analysis/).

Data visualization

The molecular interactions were illustrated using Cytoscape software, while all other visualizations were created using ggplot2.

RESULTS

Ten cell types in the gastric microenvironment were identified by scRNA-seq data

After applying quality control criteria, our analysis included 70707 cells that were classified into 43 clusters (Figure 2A). We assigned each cluster to a specific cell type based on cluster-specific genes and DEGs (Figure 2B-D): T cells (*CD3D* and *CD3E*), myeloid cells (*C1QA*, *S100A8*), mast cells (*KIT*, *TPSAB1*), B cells (*CD79A*), endothelial cells (*VWF*, *PLVAP*), epithelial cells (*MUC5AC*, *EPCAM*), chief cells (*PGC*, *PGA3*), endocrine cells (*CHGA*, *GAST*), fibroblasts (*ACTA2*, *DCN*), and SMCs (*RGS5*) (Figure 2B).

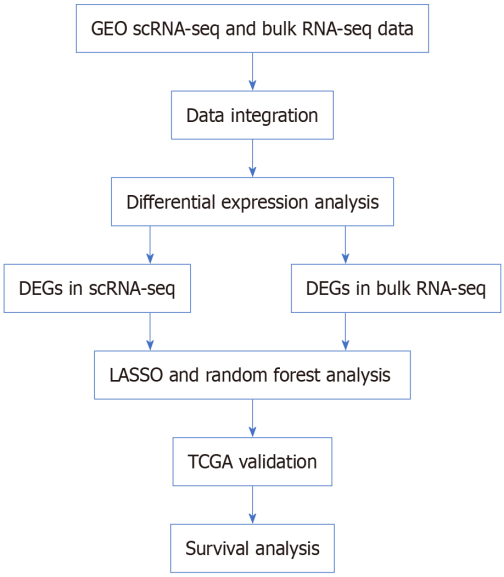

DOI: 10.4251/wjgo.v15.i7.1215

Figure 1 Workflow of the study. Bulk RNA-seq: Bulk RNA sequencing; DEGs: Differentially expressed genes; LASSO: Least absolute shrinkage and selection operator; scRNA-seq: Single-cell RNA sequencing; GEO: Gene Expression Omnibus.

Analysis of cell composition revealed that the proportions of T cells, myeloid cells, fibroblasts, endothelial cells, and SMCs increased during the progression from nonatrophic gastritis to atrophic gastritis, intestinal metaplasia, and GC (Figure 2E and F). Both nonatrophic gastritis and atrophic gastritis without intestinal metaplasia exhibited a high proportion of epithelial cells (Figure 2F). There was no significant difference in cell composition among different Lauren subtypes of GC (Figure 2F).

Bulk RNA-seq data analysis was performed to identify DEGs

We performed an analysis of bulk RNA-seq data to identify genes that were differentially expressed. Our analysis involved the integration of 10 bulk RNA-seq datasets, and the principal component analysis (PCA) results before and after using COMBAT indicated that the batch effect was successfully eliminated (Figure 3A-C). Our differential expression analysis between GC and NAGs identified 757 genes that were highly expressed in GC tissues ($P < 0.05$, logFC > 0.5). We sorted the DEGs by '-log10 (P value)' and displayed the top 20 genes in the volcano plot (Figure 3D). Enrichment analyses of highly expressed genes in GC tissues using GO and KEGG pathway databases showed that pathways related to cell proliferation, such as nuclear division and DNA replication, were enriched (Figure 3E). Additionally, we observed enrichment of pathways related to tumorigenesis, such as the p53 signaling pathway and IL17 signaling pathway (Figure 3E).

Prediction model construction and verification

We screened for DEGs in epithelial cells obtained from GC and NAG, retaining 934 genes with logFC > 0.5 and detected-times = 5. Then, these genes were compared to the 757 DEGs identified between GC and NAG (logFC > 0.5 and P value < 0.05), resulting in an overlapping set of 69 genes. Among the 69 genes, *EPCAM*, *CLDN7*, *CLDN3*, and *CLDN4*, essential components of gastrointestinal tract, were found (Figure 4, Supplementary Table 2). Additionally, we identified immune-related genes, such as *CEACAM6*, *MIF*, *C1QBP*, *EPCAM*, *TNFRSF10B*, *CXCL16* (Figure 4, Supplementary Table 2).

Using LASSO regression analysis, we selected "prob_min" and "prob_1se" to calculate the prediction model (Figure 5A). The "prob_min" model consisted of 22 genes, including *CLDN7*, *TFF3*, *TYMP*, *PLOD3*, *NOP58*, *CCL20*, *IFI6*, *LACTB2*, *TNFRSF10B*, *CPNE1*, *PKM*, *EFNA1*, *GDF15*, *UPP1*, *MISP*, *TIMP1*, *EPCAM*, *CXCL3*, *MIF*, *MDK*, *CKS2*, and *BCAP31* (Supplementary Table 3). The "prob_1se" model included 12 genes, such as *CLDN7*, *TYMP*, *PLOD3*, *TNFRSF10B*, *CPNE1*, *PKM*, *GDF15*, *UPP1*, *TIMP1*, *CKS2*, *BCAP31*, and *SNRPB* (Supplementary Table 4). Notably, the *CLDN7*, *TYMP*, *PLOD3*, *TNFRSF10B*, *CPNE1*, *PKM*, *GDF15*, *UPP1*, *TIMP1*, *CKS2*, and *BCAP31* genes were present in both models. We validated the performance of the model, and in the validation set, the model could effectively distinguish between tumor tissue and NAG ($P < 0.01$) (Figure 5B). We ranked the importance values of the feature genes in the model. In the "prob_min" model, *TIMP1*, *GDF15*, *CPNE1*, *CKS2*, and *MIF* had the highest importance values (Figure 5C); in the "prob_1se" model, *TIMP1*, *BCAP31*, *CKS2*, *GDF15*, and *CLDN7* had the highest importance values (Figure 5D). Using the TCGA and GTEx datasets for validation, the "prob_min" model had an AUC of 0.988, and the "prob_1se" model had an AUC of 0.994 (Figure 5E). These results suggest that both LASSO models have good predictive performance.

We first applied the *Boruta* function to further screen the feature genes and sorted them based on their importance values (Importance) (Figure 6A). A total of 57 genes were defined as 'confirmed' and entered the next step of constructing the random forest model as the feature set. We used Caret for hyperparameter tuning and chose mtry = 9 (Figure 6B) to build the final model. The contribution values of each feature in the final model are shown in Figure 6C, where *SNRBP*, *TIMP1*, *GDF15*, *PLOD3*, and *CKS2* had the highest contribution values. Compared with the LASSO model, *TIMP1*,

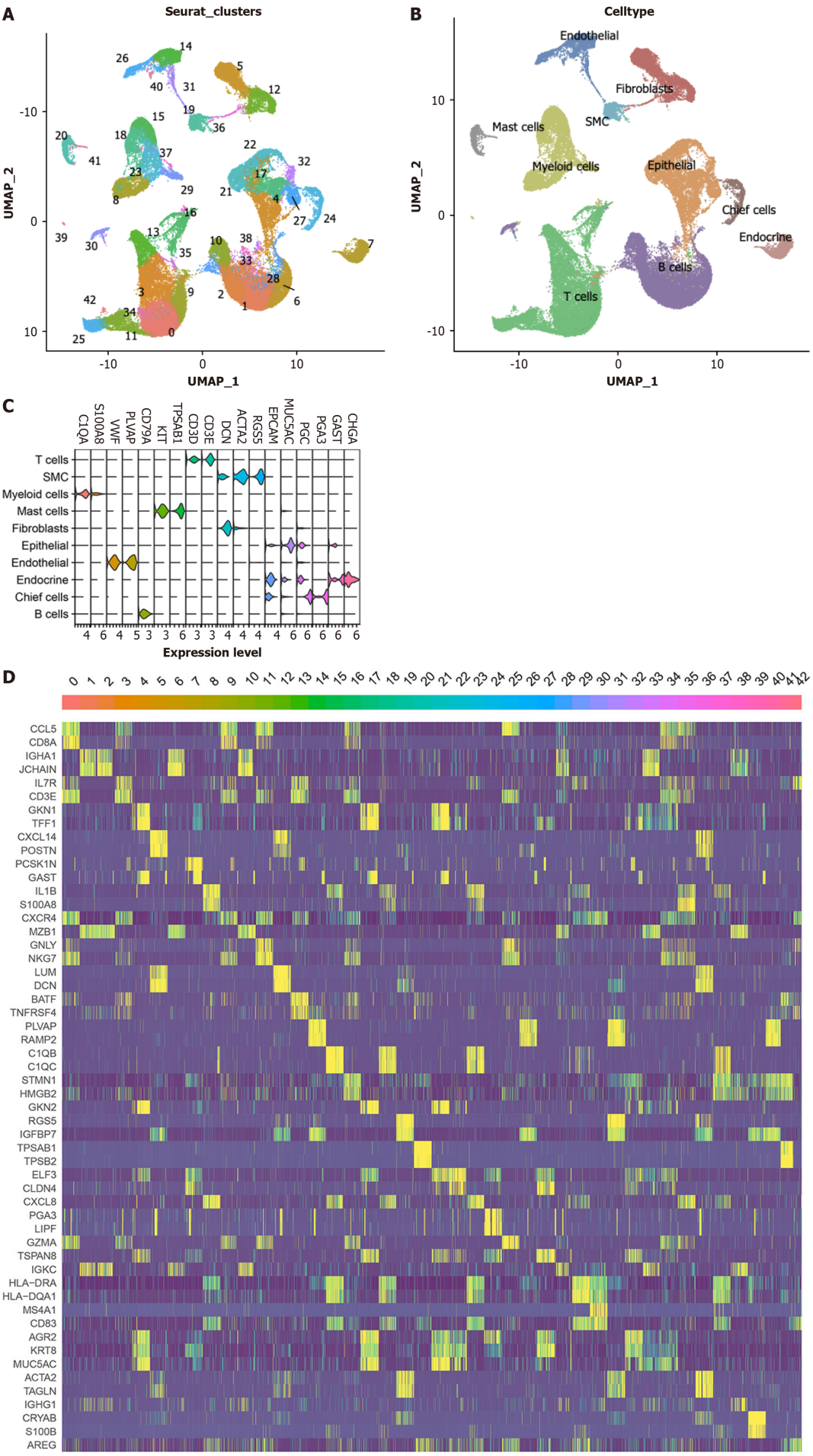
A
Seurat_clusters
UMAP_2
UMAP_1
B
Celltype
Endothelial
Fibroblasts
SMC
Mast cells
Myeloid cells
Epithelial
Chief cells
Endocrine
B cells
T cells
C
C1QA S100A8 VWF PLVAP CD79A KIT TPSAB1 CD3D CD3E DCN ACTA2 RGS5 EPCAM MUC5AC PGC PGA3 GAST CHGA
T cells
SMC
Myeloid cells
Mast cells
Fibroblasts
Epithelial
Endothelial
Endocrine
Chief cells
B cells
Expression level
D
CCL5 CD8A IGHA1 JCHAIN IL7R CD3E GKN1 TFF1 CXCL14 POSTN PCSK1N GAST IL1B S100A8 CXCR4 MZB1 GNLY NKG7 LUM DCN BATF TNFRSF4 PLVAP RAMP2 C1QB C1QC STMN1 HMGB2 GKN2 RGS5 IGFBP7 TPSAB1 TPSB2 ELF3 CLDN4 CXCL8 PGA3 LIPF GZMA TSPAN8 IGKC HLA-DRA HLA-DQA1 MS4A1 CD83 AGR2 KRT8 MUC5AC ACTA2 TAGLN IGHG1 CRYAB S100B AREG

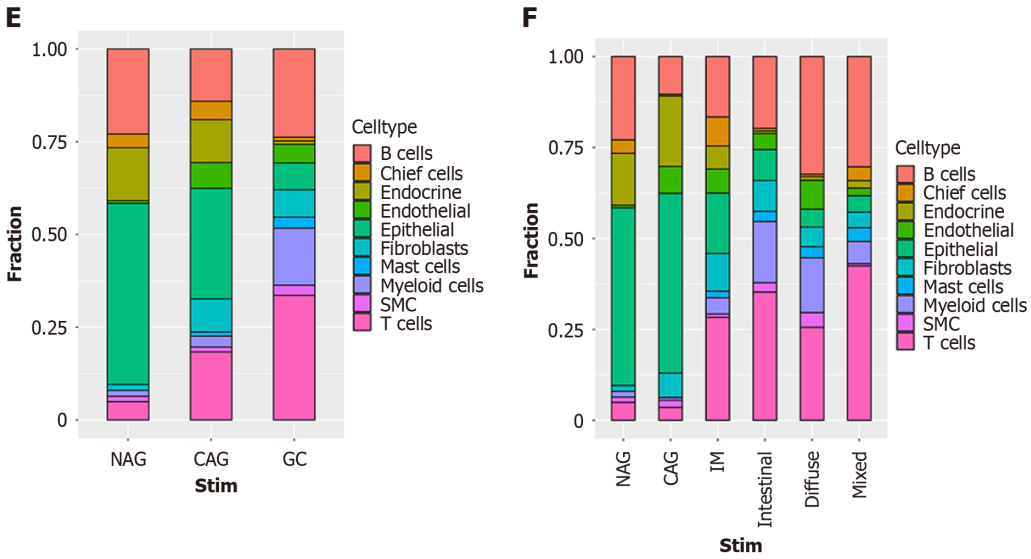

DOI: 10.4251/wjgo.v15.i7.1215

Figure 2 Analysis results of single-cell sequencing. A: UMAP of integrated samples, color-coded by cell clusters; B: UMAP of integrated samples, color-coded by cell types; C: Violin plot of expression of typical marker genes in different cell types; D: Heatmap of expression of typical marker genes in different cell clusters; E: Bar plot showing the proportion of each cell type in different tissues [normal gastric tissue (NAG), chronic atrophic gastritis (CAG), gastric cancer (GC)]; F: Bar plot showing the proportion of each cell type in different tissues [NAG, CAG, intestinal metaplasia (IM), intestinal GC, mixed GC, diffuse GC].

GDF15, and *CKS2* had high contribution values in all three models. The AUC value of the random forest model for predicting the validation set was 0.92 (Figure 6D), indicating good predictive performance.

We analyzed the important genes in the model using KM-PLOTTER (Figure 7) and found that several GC-related genes, such as *TIMP1*, *PLOD3*, *CKS2*, *TYMP*, *TNFRSF10B*, *CPNE1*, *GDF15*, *BCAP31*, and *CLDN7*, were associated with the prognosis of GC. Among them, *CKS2*, *CLDN7*, and *GDF15* were positively correlated with the survival time of GC patients, while the other genes were negatively correlated.

DISCUSSION

This study combined single-cell sequencing data and bulk RNA-seq data to identify GC-specific genes and construct a GC prediction model.

Our study combined single-cell sequencing data and bulk RNA-seq data to identify GC-specific genes and construct a GC prediction model. Our GC prediction model suggests that genes such as *TIMP1*, *CKS2*, and *GDF15* have potential for the clinical diagnosis of GC. *TIMP1* belongs to the *TIMP* gene family and encodes a natural inhibitor of matrix metalloproteinases, which can promote tumor cell proliferation and may also have antiapoptotic functions[15,16]. Studies have shown that *TIMP6* and *TIMP8* can be used as diagnostic markers for colorectal cancer, while the significance of other members of the *TIMP* family in cancer diagnosis remains unclear[17]. Our study proposes for the first time that *TIMP1* may be a diagnostic marker for GC. *TYMP* is highly expressed in various solid tumors compared to adjacent noncancerous tissues, and research has found it to be related to tumor angiogenesis and immune regulation[18,19], but its importance in cancer diagnosis is not yet clear. *GDF15* controls hematopoietic growth, energy homeostasis, adipose tissue metabolism, organismal growth, bone remodeling, and response to stress signals, and its role in cancer development and progression is complex[20]. Studies have shown that *GDF15* can be used as a diagnostic marker for early-stage liver cancer[21,22]. *BCAP31* is associated with the proliferation and metastasis of breast cancer, lung cancer and other tumors [23,24]. Based on our study, using the above genes as markers for predicting or diagnosing GC has potential feasibility, but further validation is required through experimental and clinical exploration.

The rapid development of scRNA-seq technology has enabled researchers to explore the molecular characteristics of cells in TME. However, most of this work has focused on immune cells and mesenchymal cells[25,26], and the study of epithelial cells has not received enough attention. Our study analyzed the DEGs of GC from the perspective of epithelial cells for the first time and identified GC-specific genes. However, our study did not carry out cytological and histological verifications, and the clinical guidance significance of the above feature genes needs further exploration.

Our study confirmed that combining single-cell sequencing technology with bulk RNA-seq technology to analyze GC-related marker genes from the perspective of cell subpopulations is feasible. However, during the study, we observed that technical noise and batch effects from single-cell sequencing affected the results (such as a small number of cells from the epithelial cell subpopulation mixing into the T/B-cell group). We also observed that the sequencing results were more enriched in immune cells, while the loss of epithelial cells was significant, especially in tumor tissues. The reasons for these limitations are related to many factors, such as the high sequencing depth of single-cell sequencing introducing technical noise, mechanical damage to cells during sample processing, and differences in cell size and morphology.

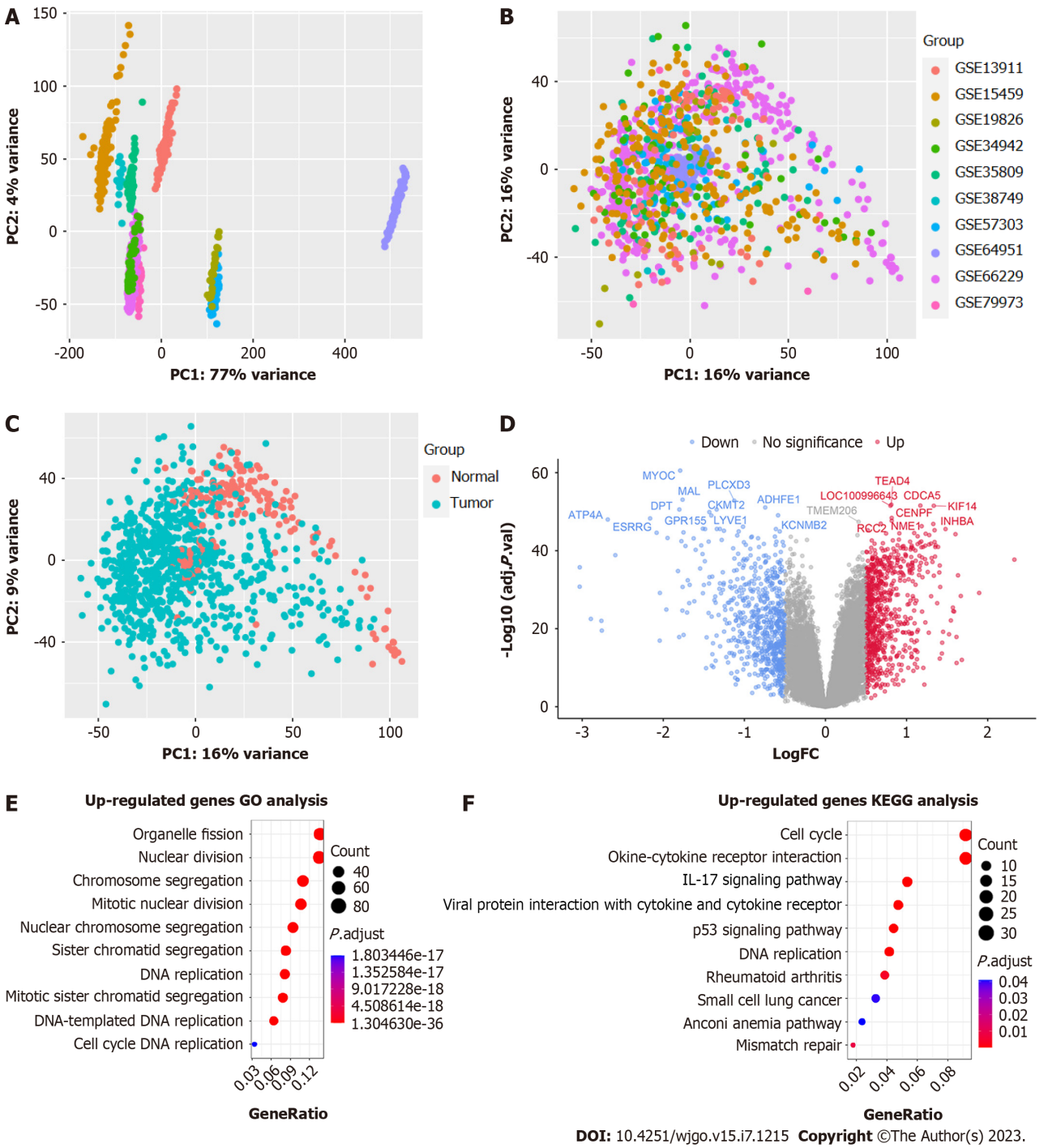

DOI: 10.4251/wjgo.v15.i7.1215

Figure 3 Analysis results of bulk RNA sequencing. A: Principal component analysis (PCA) before COMBAT (presented by dataset); B: PCA after COMBAT (presented by dataset); C: PCA after COMBAT (by pathology type); D: Volcano plot showing differentially expressed genes with top 20 genes labeled according to '-log10 (*P* value)'; E: Gene Ontology (GO) and Kyoto Encyclopedia of Genes and Genomes (KEGG) enrichment analysis of highly expressed genes in gastric cancer tissues.

Studies have shown that single-nucleus RNA sequencing (snRNA-seq) has a significant advantage over single-cell sequencing in identifying epithelial cells[27,28]. On the basis of existing studies, the inclusion of snRNA-seq results may supplement the findings of this study and provide better clinical guidance.

CONCLUSION

In summary, we have successfully established a predictive classifier based on the analysis of RNA-seq data, and the genes included in it are expected to serve as auxiliary markers in the clinical diagnosis of GC. This research achievement provides valuable references and guidance for the early diagnosis and treatment of GC.

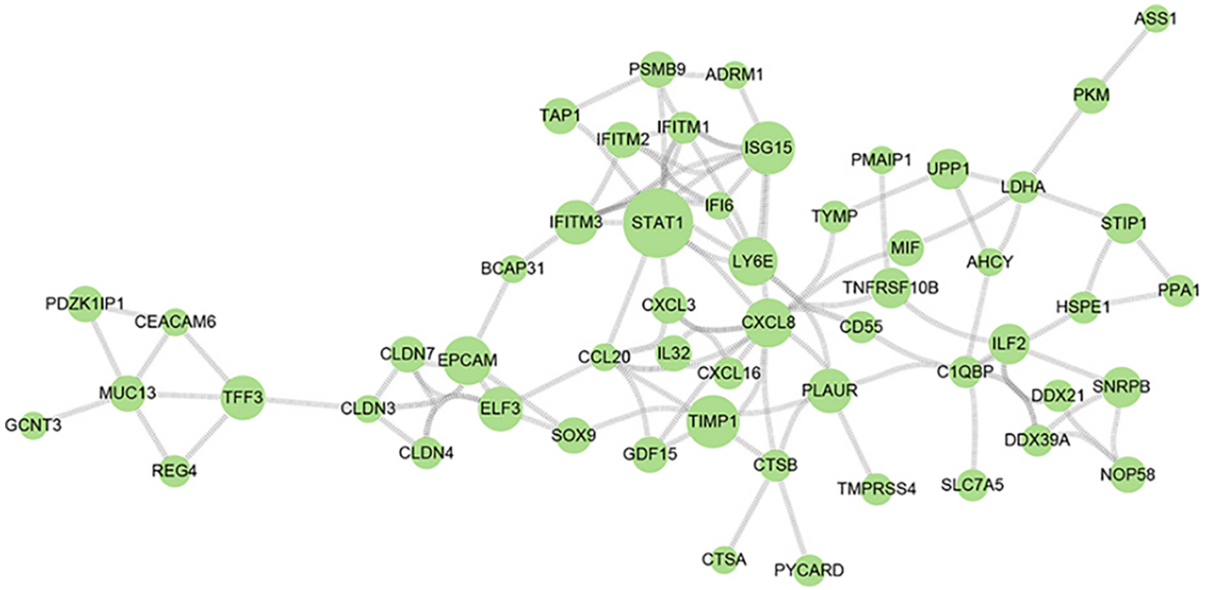

DOI: 10.4251/wjgo.v15.i6.1215

Figure 4 Protein interaction analysis of the differentially expressed genes.

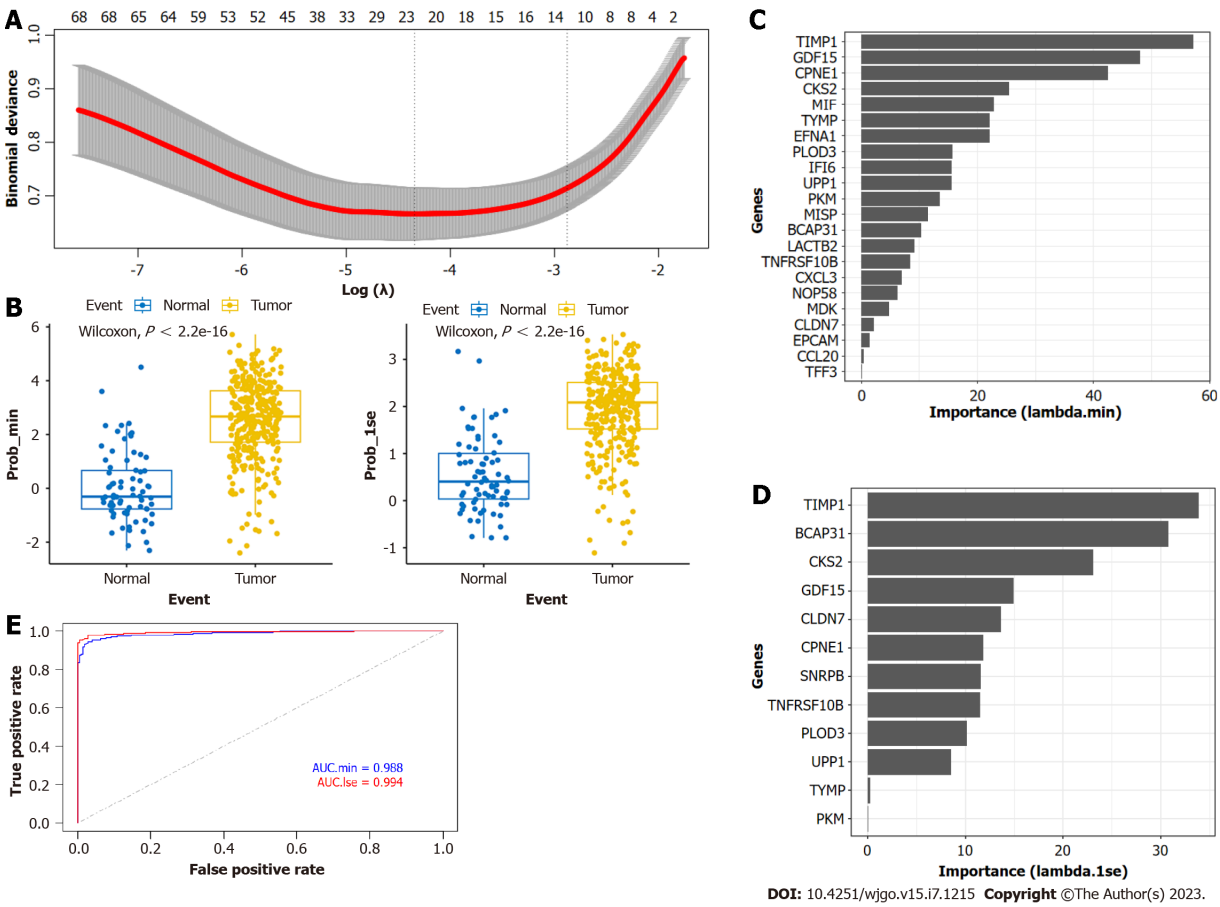

DOI: 10.4251/wjgo.v15.i7.1215

Figure 5 Gastric cancer prediction model constructed by Least absolute shrinkage and selection operator. A: Plot showing 'prob_min' and 'prob_1se' selected to construct the Least absolute shrinkage and selection operator (LASSO) model; B: Plot showing the predictive efficiency of the LASSO model; C: Importance values of genes in the 'prob_min' model; D: Importance values of genes in the 'prob_1se' model; E: Area under the curve (AUC) analyses depicting the predictive efficiency of the LASSO model in the The Cancer Genome Atlas and Genotype-Tissue Expression datasets.

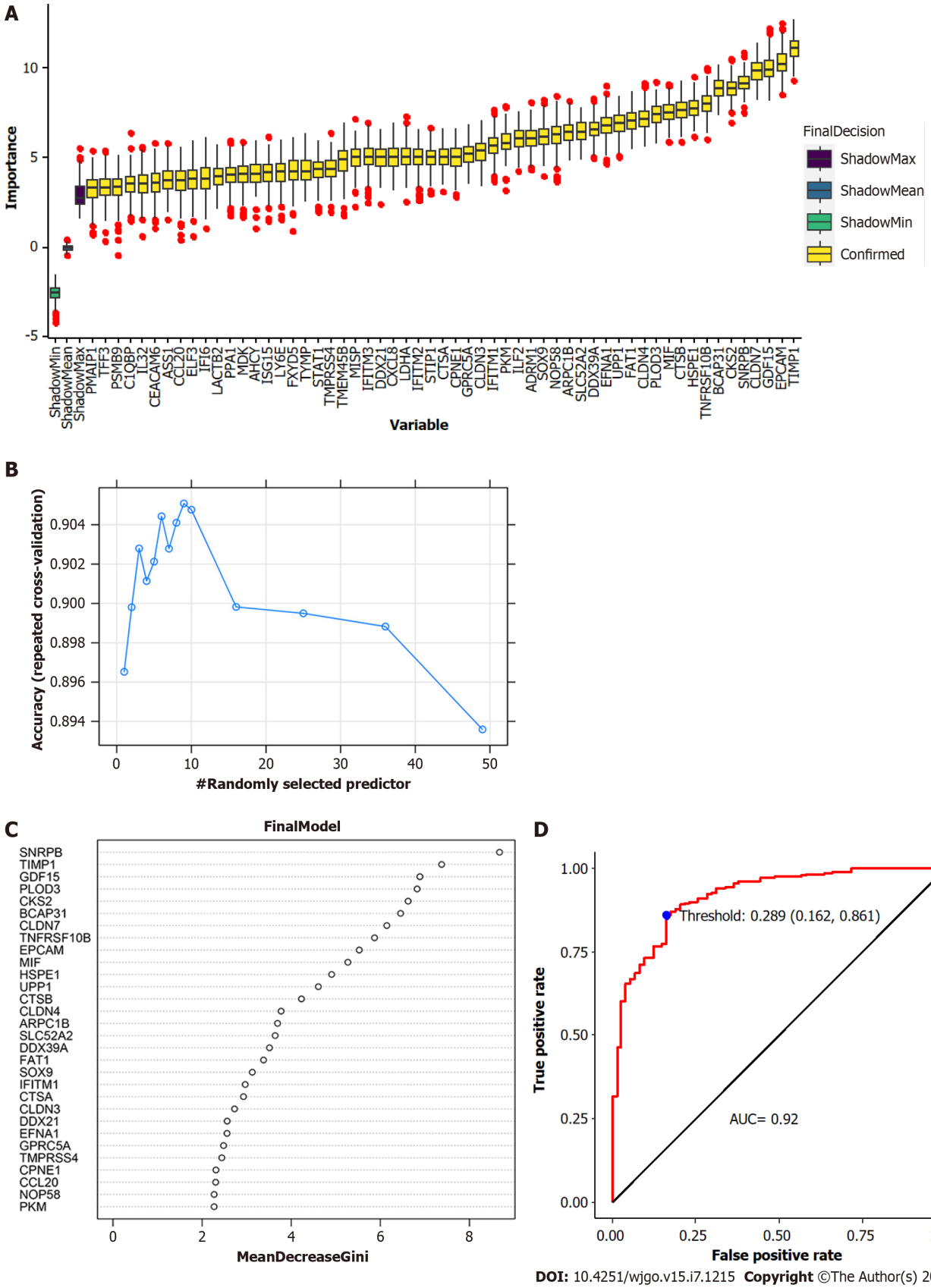

DOI: 10.4251/wjgo.v15.i7.1215

Figure 6 Gastric cancer prediction model constructed by random forest. A: Feature selection of the gastric cancer prediction model based on random forest; B: Accuracy of randomly selected predictors across repeated cross validation; C: Importance values of genes in the random forest model; D: Area under curve value of the random forest prediction model.

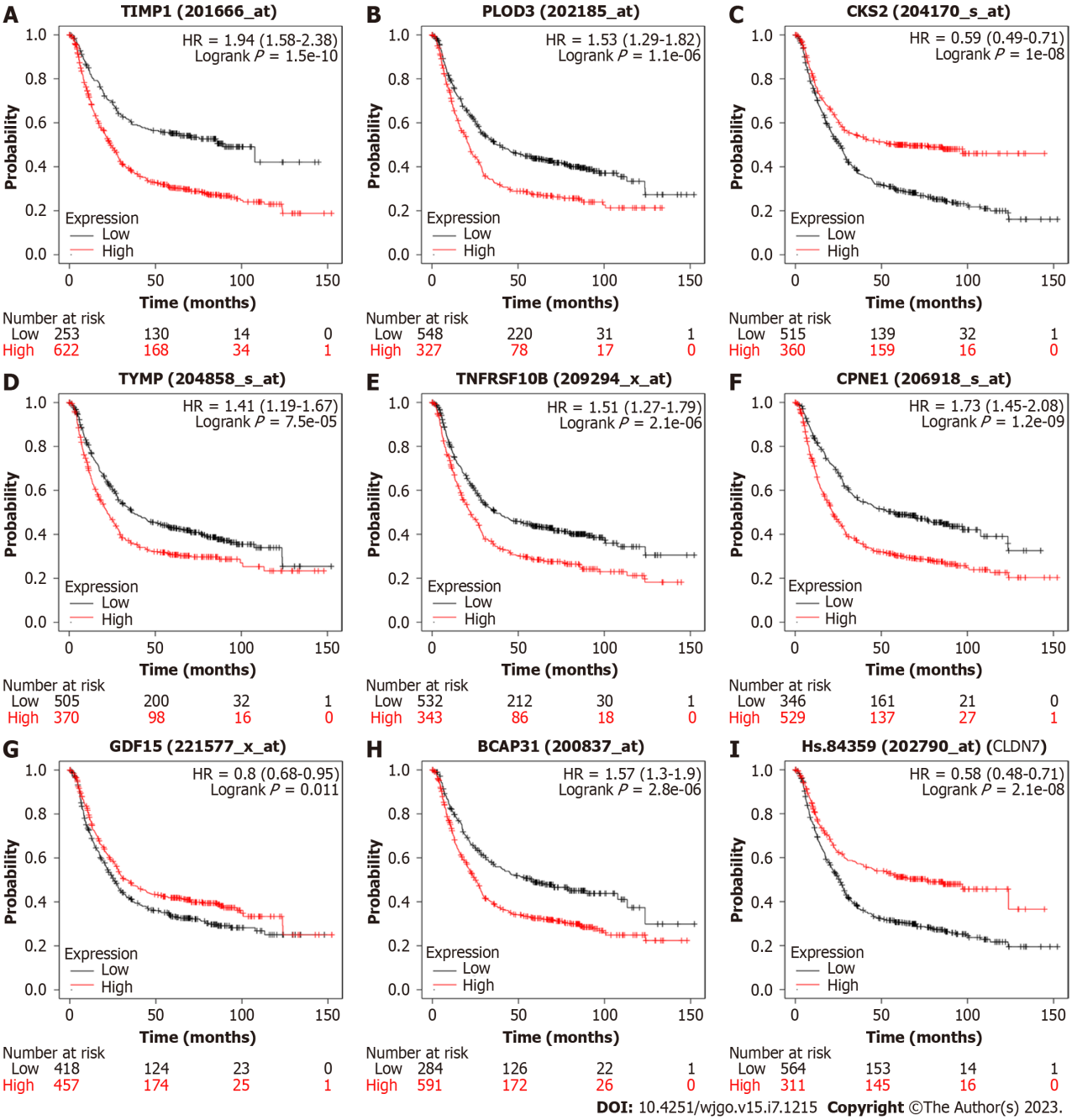

DOI: 10.4251/wjgo.v15.i7.1215

Figure 7 Kaplan–Meier plots evaluating the association between gene expression and gastric cancer survival. A: *TIMP1*; B: *PLOD3*; C: *CSK2*; D: *TYMP*; E: *TNFRSF10B*; F: *CPNE1*; G: *GDF15*; H: *BCAP31*; I: *CLDN7*. HR: Hazard ratio.

ARTICLE HIGHLIGHTS

Research background

Improving early diagnosis rates of gastric cancer (GC) is of great importance for reducing GC-related deaths. This study aimed to construct a predictive model for GC by integrating single-cell sequencing data and bulk RNA sequencing (bulk RNA-seq) data to identify potential targets for GC prediction.

Research motivation

Identifying predictive targets for GC is an important approach to reduce GC-related deaths, which is the driving force behind this study.

Research objectives

The objective of this study was to develop a predictive model for GC by combining single-cell sequencing data and bulk RNA-seq data and to identify potential targets for predicting GC.

Research methods

We downloaded GC single-cell sequencing and bulk RNA-seq datasets from the Gene Expression Omnibus and University of California at Santa Cruz databases. The single-cell sequencing data were analyzed using the Seurat package, and the bulk RNA-seq data were analyzed using the limma package. The construction of the GC prediction model was based on the Least absolute shrinkage and selection operator (LASSO) and random forest methods. Survival analysis was conducted using the KM-PLOTTER online database.

Research results

By analyzing single-cell RNA sequencing data from 70707 cells from GC tissue, normal gastric tissue, and chronic gastric tissue, we identified 10 different cell types and screened for genes differentially expressed between GC and normal epithelial cells. After determining differentially expressed genes identified from batch RNA sequencing data of GC and normal gastric samples, we constructed a GC prediction classifier using LASSO and random forest methods. The LASSO classifier performed well when validated and when the model was verified using The Cancer Genome Atlas and Genotype-Tissue Expression datasets [area under the curve (AUC)_min = 0.988, AUC_1se = 0.994], and the random forest model also achieved good results with the validation set (AUC = 0.92). We identified genes such as *TIMP1*, *PLOD3*, *CKS2*, *TYMP*, *TNFRSF10B*, *CPNE1*, *GDF15*, *BCAP31*, and *CLDN7* with significant importance in multiple GC prediction models, and KM-PLOTTER analysis showed their relevance to GC prognosis, indicating their potential value in GC diagnosis and treatment. However, the limitation of our study is the lack of clinical sample validation for the GC prediction models.

Research conclusions

This study demonstrates that the combination of single-cell sequencing data and bulk RNA-seq data is feasible for constructing a GC prediction model.

Research perspectives

Using single-nucleus sequencing to assist in constructing GC prediction models may lead to more reliable results, as it has advantages in identifying epithelial cells.

FOOTNOTES

Author contributions: Jiang XJ designed and coordinated the study; Wen F, Qu HX, and Guan X performed data collection and analysis; Wen F interpreted the data and wrote the manuscript; All authors approved the final version of the article.

Institutional review board statement: Given that our article is based on a study of sequencing data in the public database, GEO, there are no ethical issues involved, so the institutional review board approval form or document and institutional animal care and use committee approval form or document are not applicable.

Conflict-of-interest statement: All the authors report having no relevant conflicts of interest for this article.

Data sharing statement: No additional data are available.

Country/Territory of origin: China

ORCID number: Hai-Xia Qu 0000-0001-8593-1629; Xiang-Jun Jiang 0000-0001-8786-9654.

S-Editor: Li L
L-Editor: Filipodia
P-Editor: Ju JL

REFERENCES

1 **Siegel RL**, Miller KD, Fuchs HE, Jemal A. Cancer statistics, 2022. *CA Cancer J Clin* 2022; **72**: 7-33 [PMID: 35020204 DOI: 10.3322/caac.21708]
2 **Ma S**, Zhou M, Xu Y, Gu X, Zou M, Abudushalamu G, Yao Y, Fan X, Wu G. Clinical application and detection techniques of liquid biopsy in gastric cancer. *Mol Cancer* 2023; **22**: 7 [PMID: 36627698 DOI: 10.1186/s12943-023-01715-z]
3 **Joshi SS**, Badgwell BD. Current treatment and recent progress in gastric cancer. *CA Cancer J Clin* 2021; **71**: 264-279 [PMID: 33592120 DOI: 10.3322/caac.21657]
4 **Izumi D**, Zhu Z, Chen Y, Toden S, Huo X, Kanda M, Ishimoto T, Gu D, Tan M, Kodera Y, Baba H, Li W, Chen J, Wang X, Goel A. Assessment of the Diagnostic Efficiency of a Liquid Biopsy Assay for Early Detection of Gastric Cancer. *JAMA Netw Open* 2021; **4**: e2121129

[PMID: 34427680 DOI: 10.1001/jamanetworkopen.2021.21129]

5 **Chen H**, Huang C, Wu Y, Sun N, Deng C. Exosome Metabolic Patterns on Aptamer-Coupled Polymorphic Carbon for Precise Detection of Early Gastric Cancer. *ACS Nano* 2022; **16**: 12952-12963 [PMID: 35946596 DOI: 10.1021/acsnano.2c05355]

6 **Ma X**, Ou K, Liu X, Yang L. Application progress of liquid biopsy in gastric cancer. *Front Oncol* 2022; **12**: 969866 [PMID: 36185234 DOI: 10.3389/fonc.2022.969866]

7 **Xu Y**, Zhang P, Zhang K, Huang C. The application of CA72-4 in the diagnosis, prognosis, and treatment of gastric cancer. *Biochim Biophys Acta Rev Cancer* 2021; **1876**: 188634 [PMID: 34656687 DOI: 10.1016/j.bbcan.2021.188634]

8 **Nallasamy P**, Nimmakayala RK, Parte S, Are AC, Batra SK, Ponnusamy MP. Tumor microenvironment enriches the stemness features: the architectural event of therapy resistance and metastasis. *Mol Cancer* 2022; **21**: 225 [PMID: 36550571 DOI: 10.1186/s12943-022-01682-x]

9 **Sherman MH**, Beatty GL. Tumor Microenvironment in Pancreatic Cancer Pathogenesis and Therapeutic Resistance. *Annu Rev Pathol* 2023; **18**: 123-148 [PMID: 36130070 DOI: 10.1146/annurev-pathmechdis-031621-024600]

10 **El-Arabey AA**, Abdalla M, Abd-Allah AR. SnapShot: TP53 status and macrophages infiltration in TCGA-analyzed tumors. *Int Immunopharmacol* 2020; **86**: 106758 [PMID: 32663767 DOI: 10.1016/j.intimp.2020.106758]

11 **Bridges K**, Miller-Jensen K. Mapping and Validation of scRNA-Seq-Derived Cell-Cell Communication Networks in the Tumor Microenvironment. *Front Immunol* 2022; **13**: 885267 [PMID: 35572582 DOI: 10.3389/fimmu.2022.885267]

12 **Liu Z**, Li H, Dang Q, Weng S, Duo M, Lv J, Han X. Integrative insights and clinical applications of single-cell sequencing in cancer immunotherapy. *Cell Mol Life Sci* 2022; **79**: 577 [PMID: 36316529 DOI: 10.1007/s00018-022-04608-4]

13 **Hao Y**, Hao S, Andersen-Nissen E, Mauck WM 3rd, Zheng S, Butler A, Lee MJ, Wilk AJ, Darby C, Zager M, Hoffman P, Stoeckius M, Papalexi E, Mimitou EP, Jain J, Srivastava A, Stuart T, Fleming LM, Yeung B, Rogers AJ, McElrath JM, Blish CA, Gottardo R, Smibert P, Satija R. Integrated analysis of multimodal single-cell data. *Cell* 2021; **184**: 3573-3587.e29 [PMID: 34062119 DOI: 10.1016/j.cell.2021.04.048]

14 **Zou J**, Deng F, Wang M, Zhang Z, Liu Z, Zhang X, Hua R, Chen K, Zou X, Hao J. scCODE: an R package for data-specific differentially expressed gene detection on single-cell RNA-sequencing data. *Brief Bioinform* 2022; **23** [PMID: 35598331 DOI: 10.1093/bib/bbac180]

15 **Jackson HW**, Defamie V, Waterhouse P, Khokha R. TIMPs: versatile extracellular regulators in cancer. *Nat Rev Cancer* 2017; **17**: 38-53 [PMID: 27932800 DOI: 10.1038/nrc.2016.115]

16 **Grünwald B**, Schoeps B, Krüger A. Recognizing the Molecular Multifunctionality and Interactome of TIMP-1. *Trends Cell Biol* 2019; **29**: 6-19 [PMID: 30243515 DOI: 10.1016/j.tcb.2018.08.006]

17 **Łukaszewicz-Zając M**, Mroczko B. Circulating Biomarkers of Colorectal Cancer (CRC)-Their Utility in Diagnosis and Prognosis. *J Clin Med* 2021; **10** [PMID: 34071492 DOI: 10.3390/jcm10112391]

18 **Paladhi A**, Daripa S, Mondal I, Hira SK. Targeting thymidine phosphorylase alleviates resistance to dendritic cell immunotherapy in colorectal cancer and promotes antitumor immunity. *Front Immunol* 2022; **13**: 988071 [PMID: 36090972 DOI: 10.3389/fimmu.2022.988071]

19 **Gu Y**, Guo Y, Gao N, Fang Y, Xu C, Hu G, Guo M, Ma Y, Zhang Y, Zhou J, Luo Y, Zhang H, Wen Q, Qiao H. The proteomic characterization of the peritumor microenvironment in human hepatocellular carcinoma. *Oncogene* 2022; **41**: 2480-2491 [PMID: 35314790 DOI: 10.1038/s41388-022-02264-3]

20 **Siddiqui JA**, Pothuraju R, Khan P, Sharma G, Muniyan S, Seshacharyulu P, Jain M, Nasser MW, Batra SK. Pathophysiological role of growth differentiation factor 15 (GDF15) in obesity, cancer, and cachexia. *Cytokine Growth Factor Rev* 2022; **64**: 71-83 [PMID: 34836750 DOI: 10.1016/j.cytogfr.2021.11.002]

21 **Zhang S**, Gao C, Zhou Q, Chen L, Huang GF, Tang H, Song X, Zhang Z, Whittaker K, Chen X, Huang RP. Identification and validation of circulating biomarkers for detection of liver cancer with antibody array. *Neoplasma* 2023; **70**: 36-45 [PMID: 36620875 DOI: 10.4149/neo_2022_220606N600]

22 **Guo H**, Liu Q. Clinical Value of Growth Differentiation Factor 15 Detection in the Diagnosis of Early Liver Cancer Based on Data Mining. *Biomed Res Int* 2022; **2022**: 4448075 [PMID: 36440365 DOI: 10.1155/2022/4448075]

23 **Fu W**, Sun H, Zhao Y, Chen M, Yang X, Liu Y, Jin W. BCAP31 drives TNBC development by modulating ligand-independent EGFR trafficking and spontaneous EGFR phosphorylation. *Theranostics* 2019; **9**: 6468-6484 [PMID: 31588230 DOI: 10.7150/thno.35383]

24 **Wang J**, Jiang D, Li Z, Yang S, Zhou J, Zhang G, Zhang Z, Sun Y, Li X, Tao L, Shi J, Lu Y, Zheng L, Song C, Yang K. BCAP31, a cancer/testis antigen-like protein, can act as a probe for non-small-cell lung cancer metastasis. *Sci Rep* 2020; **10**: 4025 [PMID: 32132574 DOI: 10.1038/s41598-020-60905-7]

25 **Yu L**, Shen N, Shi Y, Shi X, Fu X, Li S, Zhu B, Yu W, Zhang Y. Characterization of cancer-related fibroblasts (CAF) in hepatocellular carcinoma and construction of CAF-based risk signature based on single-cell RNA-seq and bulk RNA-seq data. *Front Immunol* 2022; **13**: 1009789 [PMID: 36211448 DOI: 10.3389/fimmu.2022.1009789]

26 **Yang J**, Zhang J, Na S, Wang Z, Li H, Su Y, Ji L, Tang X, Yang J, Xu L. Integration of single-cell RNA sequencing and bulk RNA sequencing to reveal an immunogenic cell death-related 5-gene panel as a prognostic model for osteosarcoma. *Front Immunol* 2022; **13**: 994034 [PMID: 36225939 DOI: 10.3389/fimmu.2022.994034]

27 **Cuevas-Diaz Duran R**, González-Orozco JC, Velasco I, Wu JQ. Single-cell and single-nuclei RNA sequencing as powerful tools to decipher cellular heterogeneity and dysregulation in neurodegenerative diseases. *Front Cell Dev Biol* 2022; **10**: 884748 [PMID: 36353512 DOI: 10.3389/fcell.2022.884748]

28 **Kim N**, Kang H, Jo A, Yoo SA, Lee HO. Perspectives on single-nucleus RNA sequencing in different cell types and tissues. *J Pathol Transl Med* 2023; **57**: 52-59 [PMID: 36623812 DOI: 10.4132/jptm.2022.12.19]

World Journal of Gastrointestinal Oncology

Submit a Manuscript: https://www.f6publishing.com

World J Gastrointest Oncol 2023 July 15; 15(7): 1227-1240

DOI: 10.4251/wjgo.v15.i7.1227

ISSN 1948-5204 (online)

ORIGINAL ARTICLE

Case Control Study

Proteomics-based identification of proteins in tumor-derived exosomes as candidate biomarkers for colorectal cancer

Ge-Yu-Jia Zhou, Dong-Yan Zhao, Teng-Fei Yin, Qian-Qian Wang, Yuan-Chen Zhou, Shu-Kun Yao

Specialty type: Oncology

Provenance and peer review: Unsolicited article; Externally peer reviewed.

Peer-review model: Single blind

Peer-review report's scientific quality classification

Grade A (Excellent): 0
Grade B (Very good): 0
Grade C (Good): C
Grade D (Fair): 0
Grade E (Poor): 0

P-Reviewer: Belder N, Turkey

Received: March 26, 2023
Peer-review started: March 26, 2023
First decision: April 18, 2023
Revised: April 28, 2023
Accepted: May 25, 2023
Article in press: May 25, 2023
Published online: July 15, 2023

Ge-Yu-Jia Zhou, Department of Gastroenterology, China-Japan Friendship Hospital (Institute of Clinical Medical Sciences), Beijing 100029, China

Ge-Yu-Jia Zhou, Dong-Yan Zhao, Shu-Kun Yao, Graduate School, Chinese Academy of Medical Sciences & Peking Union Medical College, Beijing 100730, China

Teng-Fei Yin, Qian-Qian Wang, Yuan-Chen Zhou, Graduate School, Peking University China-Japan Friendship School of Clinical Medicine, Beijing 100029, China

Shu-Kun Yao, Department of Gastroenterology, China-Japan Friendship Hospital, Beijing 100029, China

Corresponding author: Shu-Kun Yao, Doctor, MD, PhD, Chief Physician, Professor, Department of Gastroenterology, China-Japan Friendship Hospital, No. 2 Yinghua East Road, Chaoyang District, Beijing 100029, China. shukunyao@126.com

Abstract

BACKGROUND

Colorectal cancer (CRC) is the second leading cause of cancer-related death, with high morbidity worldwide. There is an urgent need to find reliable diagnostic biomarkers of CRC and explore the underlying molecular mechanisms. Exosomes are involved in intercellular communication and participate in multiple pathological processes, serving as an important part of the tumor microenvironment.

AIM

To investigate the proteomic characteristics of CRC tumor-derived exosomes and to identify candidate exosomal protein markers for CRC.

METHODS

In this study, 10 patients over 50 years old who were diagnosed with moderately differentiated adenocarcinoma were recruited. We paired CRC tissues and adjacent normal intestinal tissues (> 5 cm) to form the experimental and control groups. Purified exosomes were extracted separately from each tissue sample. Data-independent acquisition mass spectrometry was implemented in 8 matched samples of exosomes to explore the proteomic expression profiles, and differentially expressed proteins (DEPs) were screened by bioinformatics analysis. Promising exosomal proteins were verified using parallel reaction monitoring

(PRM) analysis in 10 matched exosome samples.

RESULTS

A total of 1393 proteins were identified in the CRC tissue group, 1304 proteins were identified in the adjacent tissue group, and 283 proteins were significantly differentially expressed between them. Enrichment analysis revealed that DEPs were involved in multiple biological processes related to cytoskeleton construction, cell movement and migration, immune response, tumor growth and telomere metabolism, as well as ECM-receptor interaction, focal adhesion and mTOR signaling pathways. Six differentially expressed exosomal proteins (NHP2, OLFM4, TOP1, SAMP, TAGL and TRIM28) were validated by PRM analysis and evaluated by receiver operating characteristic curve (ROC) analysis. The area under the ROC curve was 0.93, 0.96, 0.97, 0.78, 0.75, and 0.88 ($P < 0.05$) for NHP2, OLFM4, TOP1, SAMP, TAGL, and TRIM28, respectively, indicating their good ability to distinguish CRC tissues from adjacent intestinal tissues.

CONCLUSION

In our study, comprehensive proteomic profiles were obtained for CRC tissue exosomes. Six exosomal proteins, NHP2, OLFM4, TOP1, SAMP, TAGL and TRIM28, may be promising diagnostic markers and effective therapeutic targets for CRC, but further experimental investigation is needed.

Key Words: Exosomes; Colorectal cancer; Data-independent acquisition; Parallel reaction monitoring; Biomarker

Core Tip: We innovatively combined high-throughput quantitative proteomics analysis with colorectal cancer (CRC) tissue-originated exosomes. The comprehensive proteomic signature of CRC tissue exosomes was described using data-independent acquisition mass spectrometry, which revealed a mass of differentially expressed exosomal proteins. Six promising exosomal proteins, NHP2, OLFM4, TOP1, SAMP, TAGL and TRIM28, were verified by parallel reaction monitoring analysis and receiver operating characteristic curve analysis. The results indicated that these exosomal proteins could become potential diagnostic markers and effective therapeutic targets for CRC.

Citation: Zhou GYJ, Zhao DY, Yin TF, Wang QQ, Zhou YC, Yao SK. Proteomics-based identification of proteins in tumor-derived exosomes as candidate biomarkers for colorectal cancer. *World J Gastrointest Oncol* 2023; 15(7): 1227-1240
URL: https://www.wjgnet.com/1948-5204/full/v15/i7/1227.htm
DOI: https://dx.doi.org/10.4251/wjgo.v15.i7.1227

INTRODUCTION

Malignant tumors have become the leading cause of death in China[1], and over 4.8 million new cancer cases and approximately 3.2 million cancer deaths occurred in 2022[2]. Colorectal cancer (CRC) is among the most common malignant tumors and is a serious threat to human health[3]. In China, CRC is common among both sexes and has caused a great burden, with the incidence rate and mortality rate showing significant upward trends in recent years[4,5]. Statistics from 2020 revealed that the number of CRC cases in China accounted for 28.8% of the total newly diagnosed CRC cases and 30.6% of CRC-related deaths worldwide. The 5-year survival rate for CRC patients is closely associated with the stage of the tumor at initial diagnosis, more than 90% for patients diagnosed in the early stage and lower than 10% for patients diagnosed in the advanced stage[6]. Early detection of CRC is critical. The earlier the diagnosis is, the greater the treatment benefits for the patient. Moreover, it is essential to thoroughly elucidate the malignant biological mechanism of CRC so that novel therapeutic targets for individualized treatment can be identified.

Liquid biopsy is an emerging and booming technology that has been applied for early cancer screening, stratified therapy and posttreatment recurrence monitoring and can broadly be categorized by the ability to analyze circulating tumor cells, circulating tumor DNA, or extracellular vesicles (EVs)[7]. Exosomes are a subclass of extracellular vesicles with a relatively small size (30-150 nm in diameter) that are rich in a variety of nucleic acids (RNA, DNA), proteins and lipids[8]. In contrast to the other two types, exosomes can be actively released into body fluids by tumor cells at any stage of tumor development. Exosomes were initially recognized as cellular waste expelled outside the cell. With the rapid development of exosome extraction technology and in-depth research, researchers have found that exosomes are an important component of the tumor microenvironment. Exosomes play a critical role in intercellular communication and widely participate in the pathological processes of tumors, including the induction of proliferation, stimulation of angiogenesis, promotion of migration, and suppression of apoptosis and immune escape. Therefore, exosomes could be further developed as promising biomarkers for tumor diagnosis, treatment and prognostic assessment[9].

Based on a search of domestic and international literature, among the contents of exosomes, researchers have shown great interest in proteins and miRNAs. Proteins are the basis of life activity, and various pathological states of the body are often accompanied by protein dysfunction. Benefitting from the advancement in high-throughput liquid chromato-

graphy coupled with tandem mass spectrometry (LC-MS/MS) and the construction of related instruments to measure proteins, proteomics has become an indispensable and important tool for studying biological processes at the protein level[10]. In this study, we aimed to find potential novel biomarkers for the diagnosis and treatment of CRC. A total of 10 CRC patients were recruited, and exosomes from CRC tissues and paired healthy tissues adjacent to CRC tumors were isolated. We implemented data-independent acquisition (DIA) MS to obtain quantitative data, screened for significant differential proteins using bioinformatics analysis, and utilized parallel reaction monitoring (PRM) for further validation. In summary, our research comprehensively compared the protein profiles of exosomes from CRC tissues and adjacent normal tissues and identified differentially expressed exosomal proteins that might contribute to the further development of diagnostic and therapeutic strategies for CRC in the future.

MATERIALS AND METHODS

Ethics and clinical sample collection

This research was approved by the Clinical Research Ethics Committee of China-Japan Friendship Hospital. Written informed consent forms were signed by all patients. Patients over 50 years old who were pathologically diagnosed with moderately differentiated adenocarcinoma at the Department of General Surgery, China-Japan Friendship Hospital from January 2021 to October 2021 were recruited; five male patients and five female patients were eventually selected. Primary CRC tumor tissues and healthy tissues 5 cm adjacent to the cancer foci were collected simultaneously; the former was defined as group CT, and the latter was defined as group NT. All tissue specimens were rapidly frozen in liquid nitrogen after removal and stored at -80 °C for subsequent study. The patient information is summarized in Supplementary Table 1.

Exosome isolation by size-exclusion chromatography

The protocols for exosome extraction from tissues were modified and optimized based on the methodology by Vella *et al* [11]. Tissues were sectioned into small slices, dissociated and then filtered through a 70 μm filter to remove the residues, producing original tissue homogenates. Next, we performed differential centrifugation to isolate EVs. In brief, tissue homogenates were centrifuged at 4 °C at 300 × g for 10 min, 2000 × g for 10 min, and 10000 × g for 20 min in sequence. The collected supernatants were filtered slowly and gently through a 0.22 μm filter to further remove cell debris before centrifugation at 4 °C at 150000 × g for 2 h. The exosome pellet was resuspended in PBS and further purified with Exosupur columns (Echobiotech, China). Fractions were concentrated using Amicon 100 kDa ultrafiltration tubes (Merck, Germany) to obtain purified exosomes, which were stored at -80 °C.

Nanoparticle tracking analysis

The nanoparticle size and exosome concentration were measured with a ZetaView PMX 110 (Particle Metrix, Germany). A video was recorded with time duration of 90 s, and the rate of frames per second was 30. A laser source with a wavelength of 405 nm was used to irradiate the exosome suspension at 25 °C. The scattered light of the nanoparticles was detected, and the concentration was calculated by counting the scattered nanoparticles. Moreover, by tracking the Brownian motion trajectory of the nanoparticles, the mean-square displacement of the nanoparticles per unit time was acquired; as a result, the nanoparticle size distribution could be determined.

Transmission electron microscopy

Purified exosomes (10 μL) were placed onto carbon-coated copper grids, incubated at room temperature for 10 min, washed with sterile distilled water and then negatively stained with 10 μL of 2% uranyl acetate for 1 min. Samples were observed and imaged under an H-7650 electron microscope (Hitachi, Japan).

Western blot analysis

Proteins were extracted from the exosomes, and the protein concentration was determined using a Pierce BCA protein assay kit (Thermo Scientific, United States). Next, we denatured the proteins by adding 5 × SDS loading buffer to the protein solution. For Western blotting, the protein samples were loaded into 10% SDS-PAGE gels for electrophoretic protein separation and then transferred to a nitrocellulose (NC) membrane at 300 mA for 2 h. Cell lysate was set as the positive control, and 10 μg of total protein from the control was used to detect each signature marker. For exosome samples, 30 μg of total protein was loaded to detect each signature marker. The membrane was blocked in 3% BSA-TBST at room temperature for 30 min and further incubated overnight at 4 °C with the following primary antibodies: anti-mouse CD9 (1:1000), anti-mouse CD63 (1:200), anti-rabbit HSP70 (1:1000), anti-rabbit TSG101 (1:1000) and anti-rabbit calnexin (1:500). We then incubated the membrane with the following secondary antibodies: anti-rabbit HRP-conjugated (1:10000) or anti-mouse HRP-conjugated (1:10000) for 40 min at room temperature. The protein immunolabels were visualized and captured with a Tanon4600 automated chemiluminescence image analysis system (Tanon, China).

Peptide preparation for mass spectrometry

The purified exosome samples were ground into powders with liquid nitrogen and lysed in lysis buffer, followed by intermittent sonication with a metal probe on ice. After sufficient lysis, the lysate mixture was centrifuged at 12000 × g for 15 min at 4 °C. We collected the supernatant and quantified the protein concentration using a BCA protein assay kit according to the manufacturer's instructions.

Protein samples were reduced with 5 mmol/L DTT at 37 °C for 1 h and then alkylated with 10 mmol/L iodoacetamide at room temperature in the dark for 45 min. The protein samples were diluted with 25 mmol/L NH_4HCO_3 and then treated with trypsin at a ratio of 1:50 (trypsin:protein) overnight at 37 °C. The enzymatic digestion reaction was terminated by adding formic acid to adjust the pH to less than 3.0. We desalinated the digested peptides with C18 desalting columns, which were activated by 100% acetonitrile and equilibrated with 0.1% formic acid. The samples were loaded onto the desalting columns, washed with 0.1% formic acid to remove impurities, and eluted with 70% acetonitrile. Finally, we collected the eluates and freeze-dried the desalted samples for storage.

LC-MS/MS analysis

Equal amounts of peptides were taken from each sample and mixed. The mixed sample was fractionated on a Rigol L3000 HPLC system using a C18 column and monitored at a UV wavelength of 214 nm. Buffer A (2% acetonitrile, ammonium hydroxide, pH 10.0) and buffer B (98% acetonitrile, ammonium hydroxide, pH 10.0) were used as mobile phases with gradient elution at a flow rate of 0.7 mL/min. The eluates were collected in tubes at one-minute intervals and combined into 6 fractions, which were then vacuum dried and stored for further analysis.

LC-MS/MS analysis was performed using the EASY-nLC 1200 Liquid chromatography system (Thermo Scientific, United States) coupled with the Orbitrap Eclipse mass spectrometer (Thermo Scientific, United States) and a Nanospray Flex ion source. Buffer A (0.1% formic acid in water) and buffer B (80% acetonitrile, 0.1% formic acid) were used as mobile phases. The dried fraction samples and peptide samples were redissolved in 10 μL of buffer A, mixed with 0.2 μL of standard peptides (iRT kit, Biognosys, Switzerland), and then loaded onto a C18 nanotrap column. Peptide separation was performed with an analytical column eluted with the following gradient program: the starting conditions (6% buffer B) were held for 8 min. Then, the content of buffer B was increased from 6%-12% in 8 min, 12%-30% in 55 min, 30%-40% in 12 min, and 40%-95% in 1 min, then held at 95% buffer B for 10 min. Lastly, the concentration of buffer B was decreased from 95%-6% in 1 min.

Data-dependent acquisition (DDA) mode was used to build a spectral library. The MS full scan ranged from m/z 350 to 1500 at a resolution of 120000. Automatic gain control (AGC) was set to $4e^5$, and the maximum injection time was 50 ms. Precursor ions were fragmented using high-energy collision cleavage (HCD). MS/MS scans were conducted in top speed mode with an AGC of $5e^4$, a maximum injection time of 22 ms and a normalized collision energy of 30%. For DIA acquisition, the MS full scan ranged from m/z 350 to 1500 at a resolution of 120000. The maximum injection time was set to 50 ms. The MS/MS scan was conducted in top speed mode with AGC in standard mode and the maximum injection time set in auto mode. The normalized collision energy was 30%[12,13].

The DDA and DIA raw data files were imported directly into Spectronaut software for spectral library construction and subsequent data extraction. The search parameters were set as follows: trypsin/P was used as the cleavage enzyme, the maximum number of missed cleavage sites was set as 2, carbamidomethyl on cysteine was selected as the fixed modification, and oxidation on methionine and acetyl was selected as the variable modification. Identified proteins were filtered with a false discovery rate (FDR) < 1%.

Bioinformatics analysis

Data visualization was achieved based on R software (version 3.6). A Venn diagram was constructed using VennDiagram. Principal component analysis (PCA) was performed to assess the distribution and variation of the samples, generated using ggbiplot. Differentially expressed proteins (DEPs) were visualized with a column chart and volcano map using ggplot2. The clustering heatmap of DEPs was generated using pheatmap. The Clusters of Orthologous Groups (COG) database was used for protein classification. Gene Ontology (GO) and Kyoto Encyclopedia of Genes and Genomes (KEGG) pathway enrichment was performed for protein functional annotation and analysis. COG and enrichment analyses were visualized with ggplot2. Receiver operating characteristic curves (ROC) and the area under the ROC curve (AUC) were used to assess and measure the diagnostic power of the candidate proteins in distinguishing CRC tissues from normal intestinal tissues, and plots were created using pROC.

PRM

The DEPs screened from the previous LC-MS/MS analysis were further validated using PRM analysis to eliminate false-positive proteins[14]. The procedures of protein extraction, enzymatic digestion and desalination were the same as those for DDA/DIA. Gradient elution was performed at a flow rate of 0.7 mL/min, then fractions were collected and combined into three fractions. PRM analysis was performed using an Orbitrap Q Exactive HFX mass spectrometer (Thermo Scientific, United States) at a flow rate of 600 nL/min. The gradient was 8%-12% buffer B in 5 min, 12%-30% in 30 min, 30%-40% in 9 min, and 40%-95% in 1 min and holding at 95% buffer B for 15 min. The MS full scan ranged from m/z 350 to 1500 at a resolution of 120000 with an AGC of $3e^6$ and a maximum injection time of 80 ms. The MS/MS scan was conducted at a resolution of 15000 with an AGC of $5e^4$ and a maximum injection time of 45 ms. The normalized collision energy of fragmentation was set to 27%. The raw data were assessed by Skyline software for the qualitative and quantitative analysis of candidate peptides.

Statistical analysis

The data obtained from LC-MS/MS analysis were processed by median normalization (MDN). A paired *t* test was used to compare the data and identify DEPs between the CRC group and the control group. Fold change (FC) cutoffs > 1.2 or < 1/1.2 were applied for screening. A two-sided *P* value < 0.05 was defined as statistically significant. Statistical analysis was processed by SPSS software (Version 26.0).

Survival analysis

GEPIA2 (http://gepia2.cancer-pku.cn/#index) was applied to analyze patient survival based on gene expression. The median gene expression was selected as the group cutoff to separate the high expression cohort and low expression cohort. The log-rank test was used to compare survival times between the two cohorts mentioned above, and Kaplan–Meier plots were applied to show the differences in overall survival (OS) and disease free survival (DFS) between the cohorts.

RESULTS

Study strategy

We performed DIA analysis to explore promising biomarkers and PRM analysis to verify candidate proteins. Due to the limitation of tissue sampling, a total of 10 patients were recruited for the research. We paired CRC tissues (n = 10) and corresponding normal tissues 5 cm apart (n = 10), forming the experimental and control groups. General information and detailed clinical data, including the TNM stage, are listed in Supplementary Table 1. DIA analysis was performed for 8 of the 10 patients, and data from all 10 were used for PRM validation. Exosomes from both groups were isolated and enriched. Then, after exosome lysis and protein digestion, peptides were obtained and analyzed using DIA mass spectrometry. Following bioinformatics analysis of the proteomic data, the screened DEPs between the CRC group and control group were further validated by PRM.

Characterization of the tissue exosomes

Exosomes were isolated from paired CRC tissues and adjacent healthy intestinal tissues. We determined the size distribution and particle concentration by nanoparticle tracking analysis (NTA) analysis. The particle concentrations of the exosomes from the cancer tissues and adjacent tissues were 1.0E+11/mL and 1.1E+11/mL, respectively, with a very slight difference, as shown in Figure 1A. The results showed that exosomes derived from CRC tissues exhibited a mean size of 144.5 nm, and the mean size of the exosomes from the adjacent tissues was 148.3 nm (Figure 1A), which is consistent with the exosome size distribution. The morphology of the exosomes was visualized by transmission electron microscopy (TEM, Figure 1B). The exosomes appeared cup- or round-like in shape by TEM, in accordance with typical exosome structures. Then, we detected the exosome-specific marker proteins TSG101, HSP70, CD9, CD63 and calnexin by Western blot analysis. A mixed cell lysate was used as a positive control. Figure 1C indicates that TSG101, HSP70, CD9 and CD63 exhibit high expression and that calnexin is absent, verifying the exosome isolation and concentration procedures. Characterization by NTA, TEM and Western blot analysis validated that the materials we extracted from the cancer tissues and adjacent tissues were of exosomal origin.

Proteomic features of CRC tissue exosomes

We performed label-free quantitative proteomics analysis with 8 paired samples to measure protein abundance and quantify protein expression. A total of 8425 peptides and 1565 proteins were initially screened in 8 CRC tissues and 8 paired normal intestinal tissues, and 1437 proteins were finally quantitatively detected. A total of 1393 proteins were identified in the CRC tissue group, 1304 proteins were identified in the adjacent healthy tissue group, and 1260 proteins were shared (Figure 2A). To better determine the connections and distinctions in all tissue samples, we performed global cluster analysis and PCA, as shown in Figure 2B. The protein expression profile of group CT was clearly distinguished from that of group NT. These results suggested that CRC tissue exosomes exhibit unique proteomic characteristics.

To compare the DEPs between the CRC tissue group and adjacent normal intestinal tissue group, the screening criteria were set as follows: cutoff value of FC value larger than 1.2 or less than 1/1.2 and t test P value < 0.05. There were 283 proteins significantly differentially expressed in group CT samples compared to group NT samples, with 128 proteins significantly upregulated and 155 significantly downregulated (Figure 2C). The volcano plot in Figure 2D shows the overall differential exosomal protein expression profile between the CT samples and NT samples (FC > 1.2 or FC < 1/1.2, P value < 0.05). The 283 DEPs obtained from the two groups were subjected to cluster analysis (Figure 2E).

The COG database identified vertical homologous proteins and divided numerous proteins into a total of 26 different categories according to the similarity of the protein sequences. Each COG category represents a class of homologous proteins that descend from an ancestor and carry out the same function. In the current study, all the detected exosomal proteins constituted 25 COG categories, illustrated in detail with a bar chart in Figure 2F. Among all basic functions, posttranslational modification, protein turnover, chaperones, signal transduction mechanisms, intracellular trafficking, secretion, and vesicular transport occupy a large proportion.

To further clarify the biological functions of the DEPs between CRC tissue exosomes and normal intestinal exosomes, GO annotation and enrichment analysis were performed at three levels, including molecular function (MF), cellular component (CC), and biological process (BP), for all 283 DEPs. Bubble diagrams were used to display partial significantly enriched pathways for the exosomal DEPs (P < 0.05, Figure 2G). Among them, the significantly enriched biological processes of the DEPs were extracellular matrix organization, angiogenesis, rRNA processing, platelet activation, tissue development, positive regulation of telomerase RNA localization to Cajal body, positive regulation of epithelial cell migration, basement membrane assembly, positive regulation of actin filament bundle assembly, and T cell costimulation. The clustered BP terms were principally related to the processes of cytoskeleton construction, cell movement and migration, immune response, tumor growth and telomere metabolism.

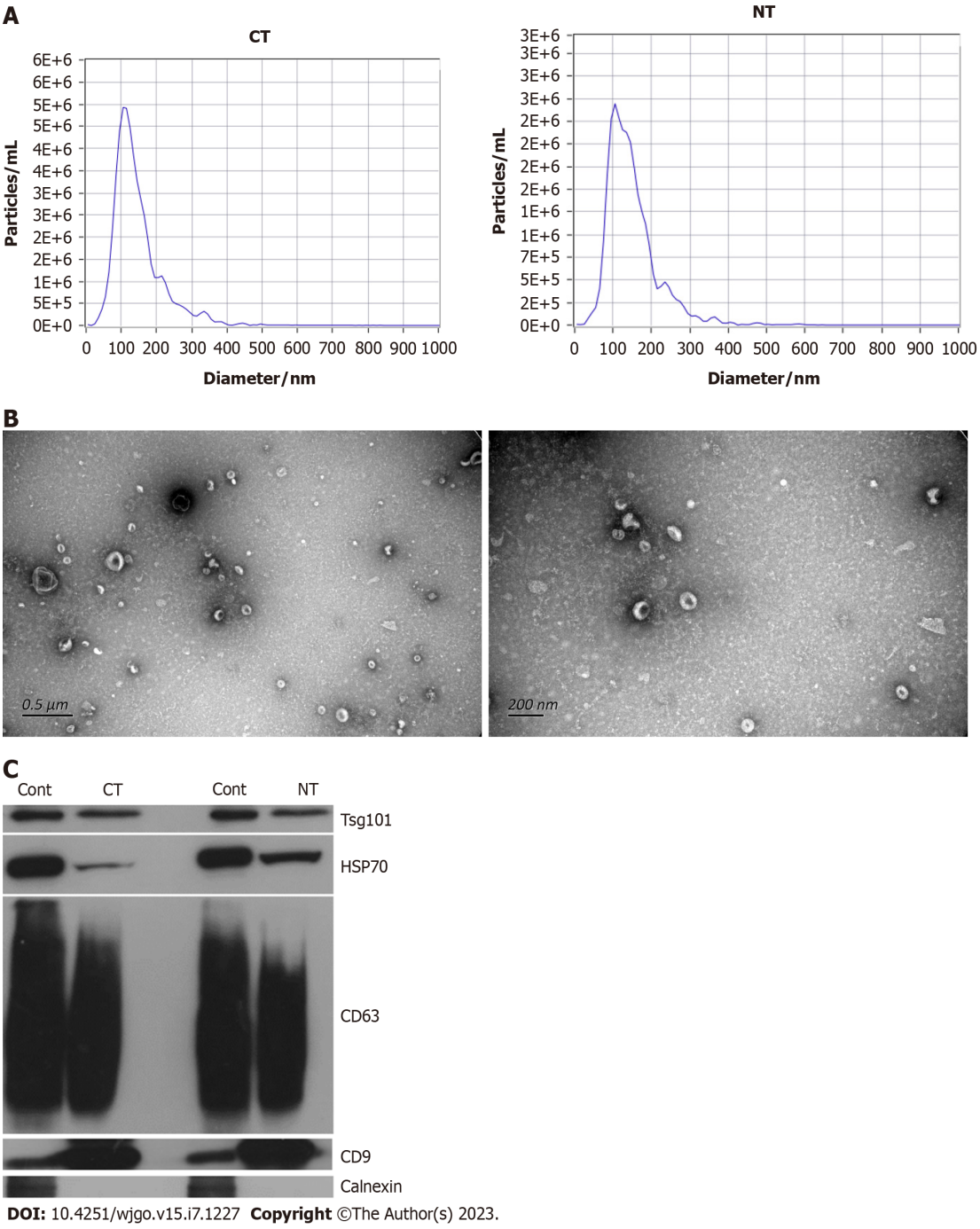

DOI: 10.4251/wjgo.v15.i7.1227

Figure 1 Characteristics of tissue exosomes. A: Nanoparticle tracking analysis of colorectal cancer tissue exosomes and normal intestinal tissue exosomes; B: Transmission electron microscopy of normal intestinal exosomes observed at the scales of 0.5 μm and 200 μm; C: Western blot analysis of colorectal cancer tissue exosomes and normal intestinal tissue exosomes, compared with the positive control. CT: Colorectal cancer tissues; NT: Normal intestinal tissues; Cont: Control.

KEGG pathway enrichment analysis was then performed to further characterize the functional enrichment of DEPs. The results revealed that the pathways in which the DEPs between group CT and group NT were significantly enriched included those of ECM-receptor interaction, focal adhesion, mTOR signaling pathway, proteoglycans in cancer, ribosome, pancreatic secretion, gap junctions, renin secretion, aldosterone synthesis and secretion, and metabolism of xenobiotics by cytochrome P450. The pathway of ECM-receptor interactions is of particular interest to our research, given the nature of exosomes in the tumor microenvironment[15]. Additionally, other pathways[16,17] that were found to be significant in our analysis are also relevant to the initiation and progression of CRC tumors.

PRM validation of candidate proteins

To evaluate the authenticity of the DIA MS data, PRM was carried out with ten paired samples of CRC tissue and normal intestinal tissue (8 of which were identical to the DIA samples with an additional 2 new pairs). To screen candidate proteins for PRM validation, the filtration strategy was set as follows: the P value was screened from small to large; ROC analysis of DEPs was performed in 8 paired samples, and the AUC value needed to be greater than 80% (ROC analysis of

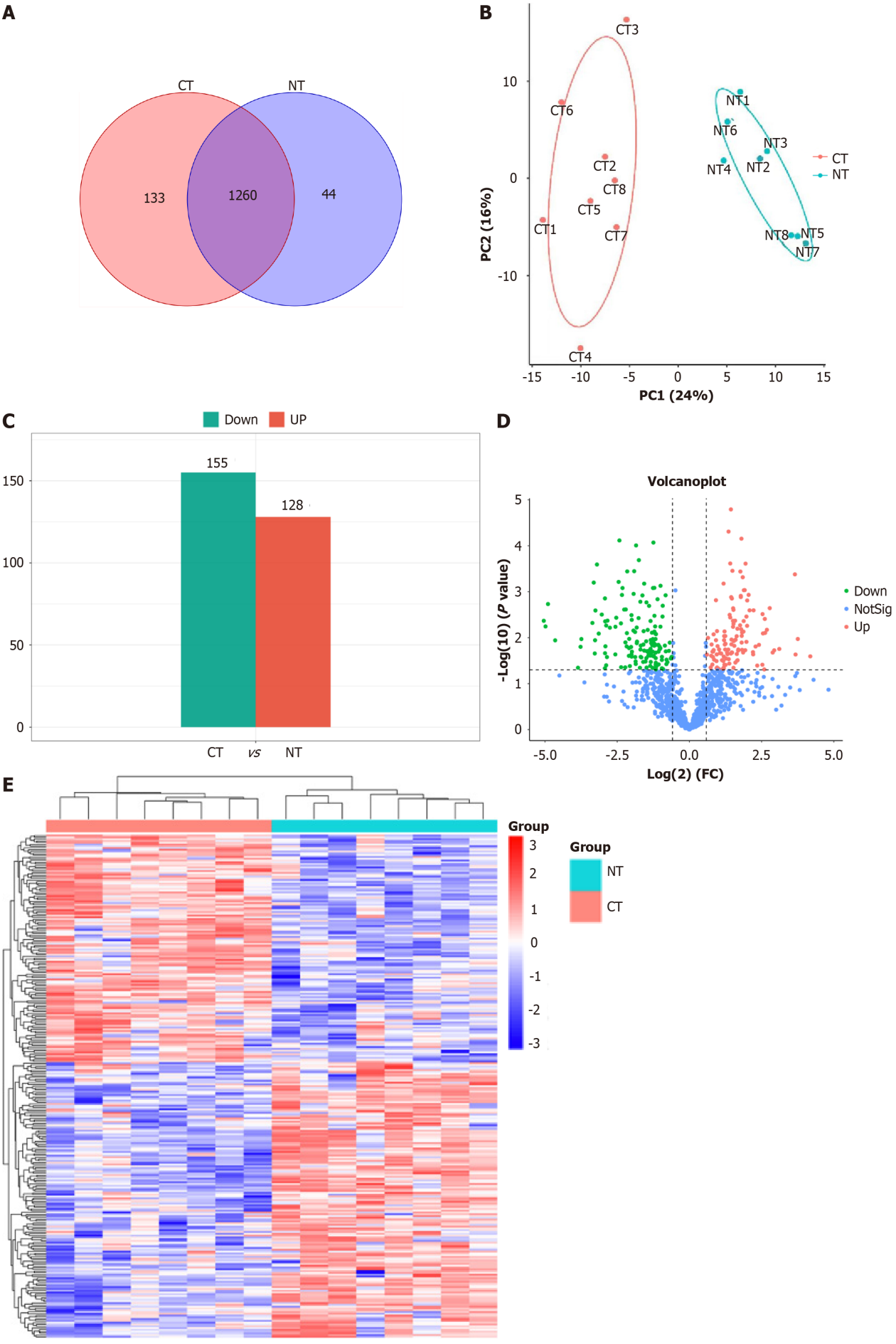
A
CT
NT
133
1260
44
B
CT3
CT6
CT2
CT8
CT5
CT1
CT7
CT4
NT1
NT6
NT3
NT4
NT2
NT8
NT5
NT7
CT
NT
PC2 (16%)
PC1 (24%)
C
Down
UP
155
128
CT
vs
NT
D
Volcanoplot
-Log(10) (P value)
Log(2) (FC)
Down
NotSig
Up
E
Group
NT
CT

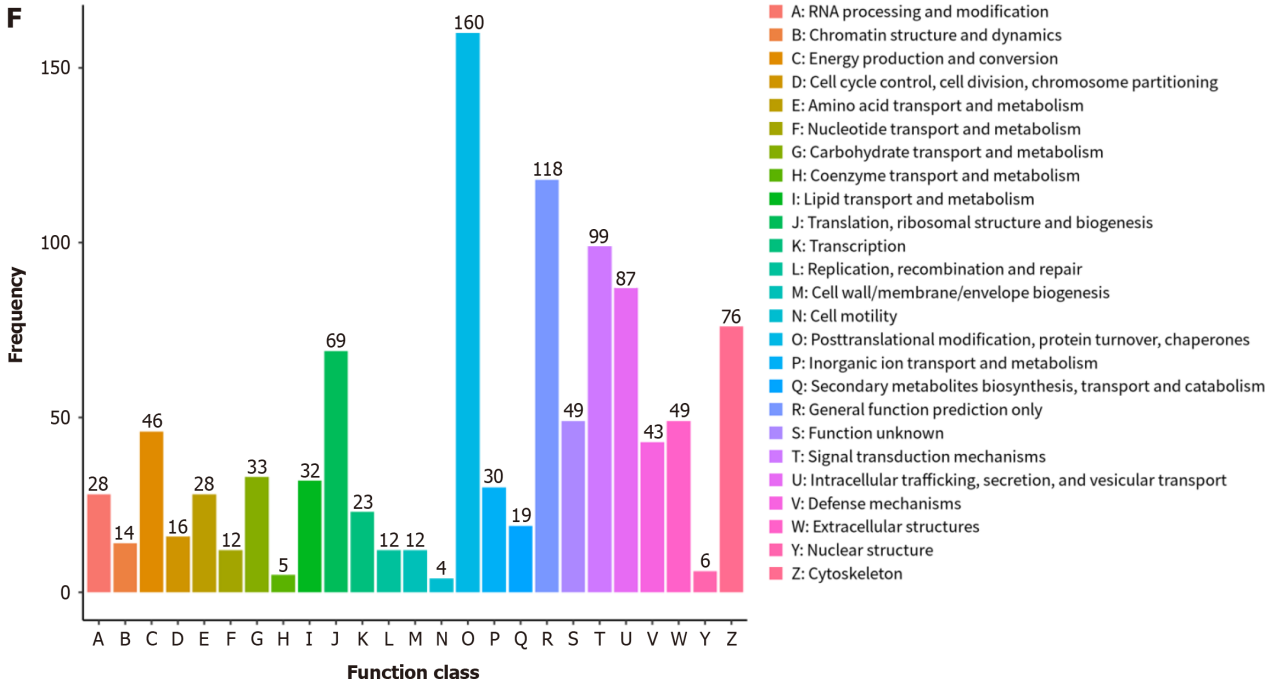
F
Frequency
150
100
50
0
28
14
46
16
28
12
33
5
32
69
23
12
12
4
160
30
19
118
49
99
87
43
49
6
76
A B C D E F G H I J K L M N O P Q R S T U V W Y Z
Function class
A: RNA processing and modification
B: Chromatin structure and dynamics
C: Energy production and conversion
D: Cell cycle control, cell division, chromosome partitioning
E: Amino acid transport and metabolism
F: Nucleotide transport and metabolism
G: Carbohydrate transport and metabolism
H: Coenzyme transport and metabolism
I: Lipid transport and metabolism
J: Translation, ribosomal structure and biogenesis
K: Transcription
L: Replication, recombination and repair
M: Cell wall/membrane/envelope biogenesis
N: Cell motility
O: Posttranslational modification, protein turnover, chaperones
P: Inorganic ion transport and metabolism
Q: Secondary metabolites biosynthesis, transport and catabolism
R: General function prediction only
S: Function unknown
T: Signal transduction mechanisms
U: Intracellular trafficking, secretion, and vesicular transport
V: Defense mechanisms
W: Extracellular structures
Y: Nuclear structure
Z: Cytoskeleton

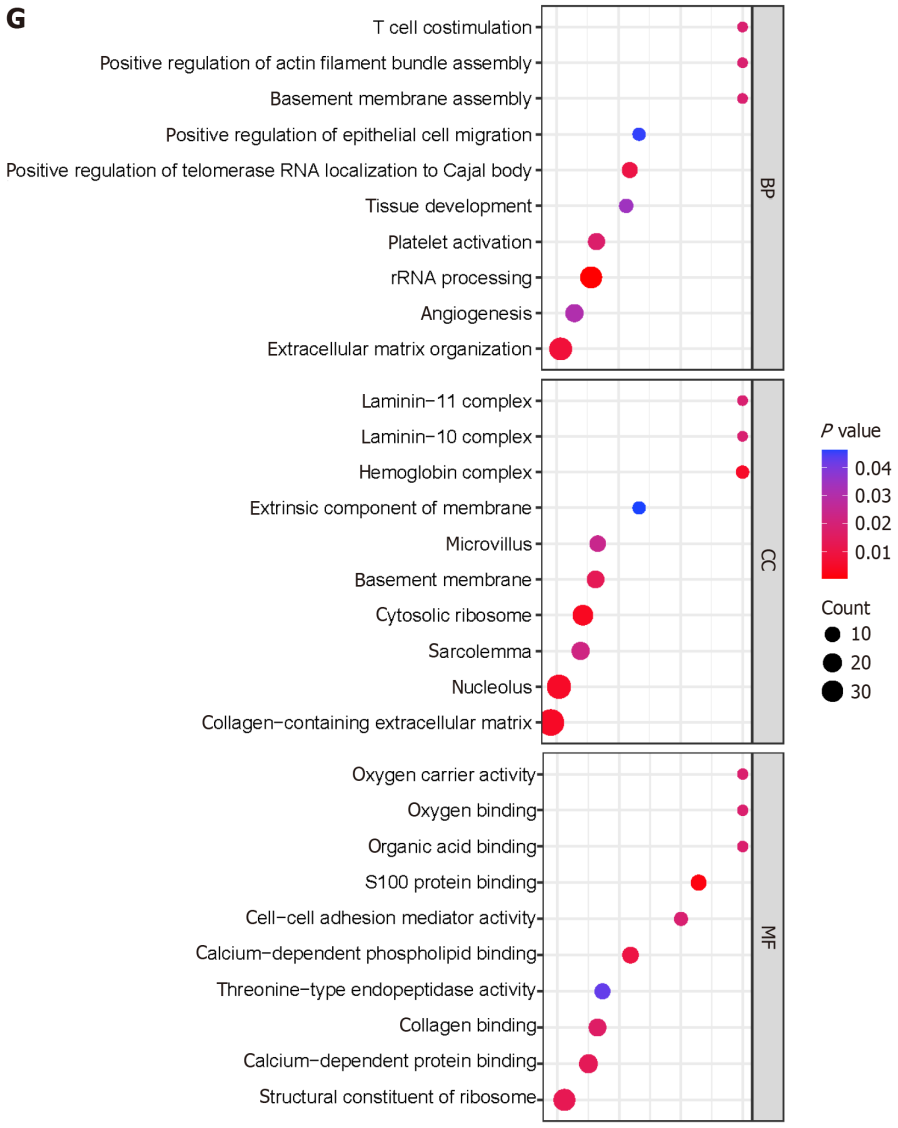
G
T cell costimulation
Positive regulation of actin filament bundle assembly
Basement membrane assembly
Positive regulation of epithelial cell migration
Positive regulation of telomerase RNA localization to Cajal body
Tissue development
Platelet activation
rRNA processing
Angiogenesis
Extracellular matrix organization
BP
Laminin−11 complex
Laminin−10 complex
Hemoglobin complex
Extrinsic component of membrane
Microvillus
Basement membrane
Cytosolic ribosome
Sarcolemma
Nucleolus
Collagen−containing extracellular matrix
CC
Oxygen carrier activity
Oxygen binding
Organic acid binding
S100 protein binding
Cell−cell adhesion mediator activity
Calcium−dependent phospholipid binding
Threonine−type endopeptidase activity
Collagen binding
Calcium−dependent protein binding
Structural constituent of ribosome
MF
P value
0.04
0.03
0.02
0.01
Count
10
20
30

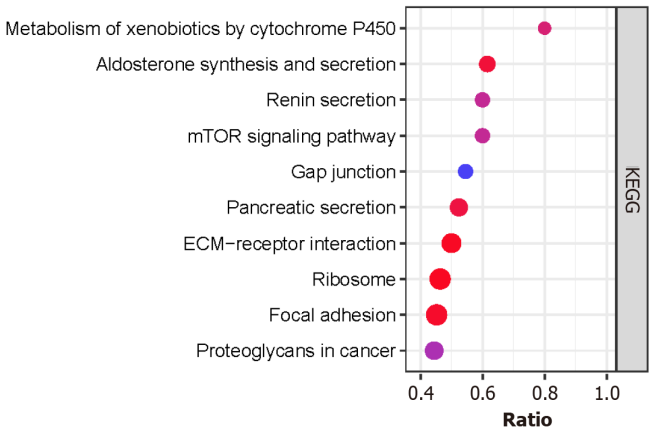

DOI: 10.4251/wjgo.v15.i7.1227

Figure 2 Quantitative proteomic signature and bioinformatic analysis of colorectal cancer. A: The Venn diagram shows detected proteins in colorectal cancer tissue exosomes and normal intestinal tissue exosomes; B: Principal component analysis of colorectal cancer tissue exosomes and normal intestinal tissue exosomes; C: The bar chart shows 128 significantly upregulated proteins and 155 significantly downregulated proteins between colorectal cancer tissue exosomes and normal intestinal tissue exosomes; D: The volcano plot shows differentially expressed proteins between colorectal cancer tissue exosomes and normal intestinal tissue exosomes; E: The heat map shows differentially expressed proteins between colorectal cancer tissue exosomes and normal intestinal tissue exosomes; F: Clusters of Orthologous Groups analysis shows 25 categories constituted by all the detected exosomal proteins; G: Gene ontology analysis shows that differentially expressed proteins are involved in biological processes, cellular components, and molecular functions; Kyoto encyclopedia of genes and genomes analysis shows that differentially expressed proteins are clustered in multiple pathways. CT: Colorectal cancer tissues; NT: Normal intestinal tissues; PC: Principal component; NotSig: COG: Clusters of Orthologous Groups; GO: Gene ontology; KEGG: Kyoto encyclopedia of genes and genomes; ECM: Extracellular matrix.

candidates seen in Supplementary Figure 1). In addition, tumor-related literature in recent years was reviewed. Based on the above strategy and a brief literature review[18-20], we selected six DEPs of interest for qualification and validation. These proteins were as follows: H/ACA ribonucleoprotein complex subunit 2 (NHP2), olfactomedin-4 (OLFM4), DNA topoisomerase 1 (TOP1), serum amyloid P-component (SAMP), transgelin (TAGL), and tripartite motif-containing protein 28 (TRIM28). The expression levels of these proteins showed significant differences by PRM analysis, and the differential expression results from PRM were consistent with those from DIA. These data revealed that the following proteins were significantly upregulated in group CT compared to group NT: NHP2 (P = 0.007), OLFM4 (P = 0.034), TOP1 (P = 0.007), and TRIM28 (P = 0.007). In addition, the following proteins were significantly downregulated: SAMP (P = 0.006) and TAGL (P = 0.04) (Figure 3A).

Subsequently, we assessed the diagnostic power of these candidate proteins using ROC curves for all 10 paired samples. The AUC values of the six candidate proteins were NHP2 (AUC = 0.93), OLFM4 (AUC = 0.96), TOP1 (AUC = 0.97), SAMP (AUC = 0.78), TAGL (AUC = 0.75), and TRIM28 (AUC = 0.88). This result indicated that all candidates could easily distinguish CRC tissues from healthy tissues (Figure 3B).

Survival analysis

To investigate the relationship between candidate proteins and patient prognosis, OS and DFS were analyzed in the expression of genes corresponding to candidate proteins using GEPIA2. Except for the SAMP gene, prognosis-related data for the other five genes were found in the TCGA and GTEx databases. Survival analysis was carried out in the cohorts of a total of 270 CRC patients (Supplementary Figures 2-11). The analysis revealed that patients with high TAGL gene expression exhibited significantly decreased OS (P = 0.014) and significantly decreased DFS (P = 0.046), while patients with low TAGL gene expression showed a relatively good prognosis. The results for OS and DFS for the NHP2, OLFM4, TOP1 and TRIM28 genes showed no statistical significance (P > 0.05).

DISCUSSION

The high morbidity and mortality of CRC are of concern. Early diagnosis of CRC can significantly improve patient prognosis and prolong survival time. Although there have been a number of studies focused on CRC, the exact molecular mechanisms remain elusive. Recently, the search for cancer biomarkers and exploration of pathogenesis have entered the era of multiomics, including genomics, transcriptomics, metabolomics and proteomics[21]. Benefitting from objective and unbiased biomarker screening, high-throughput omics technologies provide a new perspective on the diagnosis, treatment and prognosis of CRC. Proteomics is the best way to determine the physiological state of an organism. Through comprehensive protein and related functional profiling, proteomics clearly presents epigenetic information on and posttranslational modifications in CRC[22] and provides highly sensitive approaches for early tumor detection. Hundreds of clinical cohorts[23,24] have detected different proteomic signatures of CRC at different stages. With the support of the LC-MS/MS technique, DEPs are easy to identify and can serve as promising biomarkers for in-depth study as well as clinical application.

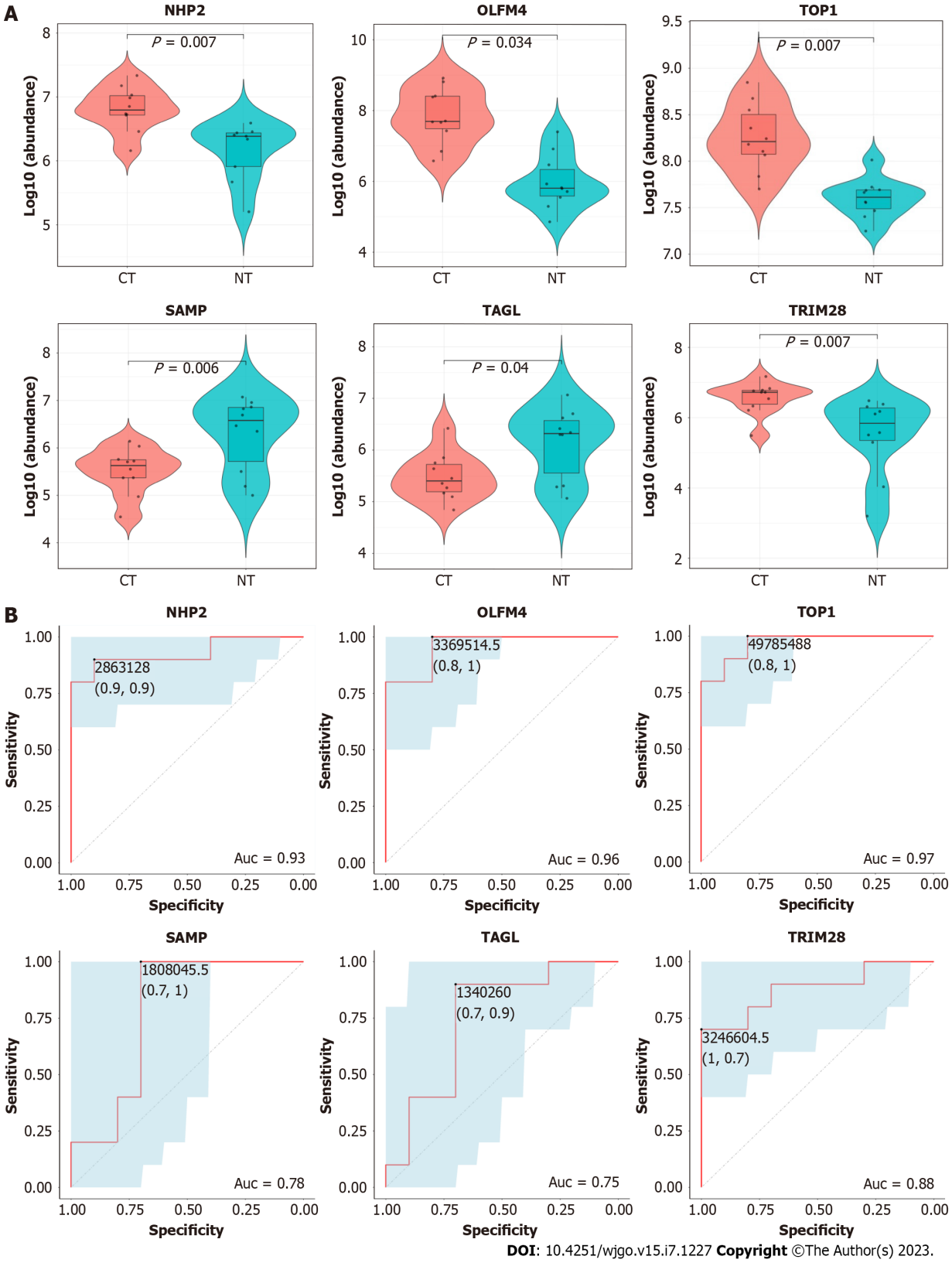

DOI: 10.4251/wjgo.v15.i7.1227

Figure 3 Verification of candidate exosomal proteins. A: Parallel reaction monitoring analysis shows the upregulation of NHP2 (P = 0.007), OLFM4 (P = 0.034), TOP1 (P = 0.007), TRIM28 (P = 0.007), and the downregulation of SAMP (P = 0.006), TAGL(p=0.04) between colorectal cancer tissue exosomes and normal intestinal tissue exosomes; B: Receiver operating characteristic curve analysis shows that the area under curve of NHP2, OLFM4, TOP1, SAMP, TAGL, and TRIM28 are 0.93, 0.96, 0.97, 0.78, 0.75, 0.88, respectively (P < 0.05). CT: Colorectal cancer tissues; NT: Normal intestinal tissues; ROC: Receiver operating characteristic curve; AUC: Area under ROC curve; NHP2: H/ACA ribonucleoprotein complex subunit 2; OLFM4: Olfactomedin-4; TOP1: DNA topoisomerase 1; SAMP: Serum amyloid P-component; TAGL: Transgelin; TRIM28: Tripartite motif-containing protein 28.

Proteomics has been carried out in different kinds of biological samples, such as serum, plasma, tissue, and feces; however, only a few studies have concentrated on the exosome level. Multiple studies have suggested that exosomes are closely related to the occurrence and development of tumors and play an important role in the tumor microenvironment. Tumor-derived exosomes can escape immune surveillance and mediate immune suppression[25], such as by carrying and releasing PD-L1 into the lymphatic system[26]. In addition, exosomes participate in cancer metastasis by regulating epithelial–mesenchymal transition (EMT), tumor angiogenesis and extracellular matrix (ECM) remodeling[27,28]. The contents and biological functions of exosomes remain to be explored, revealing a new direction to search for novel biomarkers and mechanisms of CRC at the exosome level. The strategy in our study was to directly obtain tissue specimens of CRC, rather than serum or plasma specimens, to acquire exosomes of definite tumor origin. Further experiments and analysis of CRC tissue-derived exosomes may provide a clearer understanding of CRC tumors.

In the present study, we identified 283 DEPs in CRC tissue exosomes compared to normal tissue exosomes and found that quite a few DEPs were involved in extracellular matrix organization. Moreover, focal adhesion and ECM-receptor interaction pathways were activated. These results suggest that exosomes may play a crucial role through the extracellular matrix. The ECM participates in the formation of the tumor microenvironment and regulates the processes of cell proliferation, differentiation, migration and invasion, as well as tissue morphogenesis[29]. As described in the results, the enrichment of DEPs involved in angiogenesis and tissue development apparently promoted tumor progression. The mTOR signaling pathway has been regarded as a significant regulatory mechanism of CRC. Other significantly enriched functions and pathways shown in this study are responsible for tumor development to a certain extent, which was consistent with what others have reported. Overexpression or activation of telomerase gives most cancer cells the ability to proliferate indefinitely, and telomerase activity is a key indicator for the early diagnosis of CRC and prognosis assessment[30]. Regulation of the abnormal immune response in CRC may become a potential target for immunotherapy[31]. In addition, we noticed that renin secretion as well as aldosterone synthesis and secretion were clustered in KEGG, which might be a clue regarding the activation of the renin-angiotensin system. Disorder of the latter is associated with poor prognosis of CRC, and accumulating evidence has demonstrated the therapeutic potential of these inhibitors in CRC[32].

Based on quantitative LC-MS/MS analysis, subsequent PRM verification and ROC measurements, NHP2, OLFM4, TOP1, SAMP, TAGL and TRIM28 were recognized as critical cancer-promoting factors or cancer-suppressing factors with excellent diagnostic performance, making them promising diagnostic biomarkers and therapeutic targets of CRC. TRIM28, which is also known as KRAB-associated protein 1 (KAP1) or transcription intermediary factor 1-beta (TIF1B), is a member of the tripartite motif (TRIM) family. TRIM28 has been reported to be aberrantly expressed in multiple types of cancer, such as lung, prostate, ovarian, breast, gastric and liver cancers, with its elevation in expression level typically correlated with aggressive clinical manifestation and poor OS[33-35]. Considered an oncogenic factor, TRIM28 plays an important role in tumorigenesis and progression[36]. Nevertheless, its expression level and pathogenesis in CRC remain unclear. In our study, TRIM28 was overexpressed in CRC tissue exosomes compared to adjacent healthy tissue exosomes. However, unfortunately, the expression level of the TRIM28 gene did not show prognostic relevance. Therefore, TRIM28 could be a potential target, although further experiments and perhaps larger samples are needed to explore its role in CRC. NHP2 is an indispensable component of the telomerase complex[37]. A previous study on CRC[18] reported that NHP2 expression was significantly associated with age, with high expression suggesting poor prognosis, and downregulating NHP2 inhibited the proliferation of CRC cells. OLFM4, also called GW112 or hGC-1, is highly expressed in the gastrointestinal tract as a marker of intestinal stem cells. Previous studies have revealed that OLFM4 is upregulated in inflammatory bowel disease, gastric cancer, CRC, pancreatic cancer and gallbladder cancer[38]. This result suggested that OLFM4 is involved in anti-inflammation, cell adhesion, proliferation and apoptosis. TOP1 is a subclass of DNA topoisomerase enzymes that play a role in tumor pathogenesis by promoting DNA replication and cell division. TOP1 serves as an important target for anticancer therapy[39]. The TOP1 inhibitor irinotecan was developed years ago and has been among the first-line drugs in the treatment of advanced CRC. In addition to the above 4 upregulated proteins, there were two downregulated proteins in group CT *vs* group NT in the present study, namely, SAMP and TAGL. SAMP belongs to the pentraxin protein family and has been applied as a marker for the diagnosis of inflammatory bowel diseases. Recent research has implicated its good diagnostic efficacy in distinguishing Crohn's disease from ulcerative colitis[40]. A preceding proteomic analysis[20] revealed that TAGL is downregulated in colon cancer tissues, similar to our results. However, other studies[41,42] have revealed that TAGL promotes tumor progression and invasion and is closely connected to a worse prognosis in advanced CRC, which is consistent with the present study. There is no definite evidence regarding TAGL at the exosome level, so its role in CRC tumorigenesis and development remains unclear, which provides a new area for further exploration.

In our study, high-throughput quantitative proteomics analysis and tissue-originated exosomes were innovatively combined. We comprehensively supplied valuable information on the proteomic characteristics of CRC tissue exosomes. The results provide a new and feasible perspective for future research on tissue exosomes. *In vitro* and *in vivo* experiments should be carried out to verify and further explore the definite mechanisms of tumor exosomal proteins that can be gradually translated to clinical applications from these laboratory data. Due to limitations caused by technical complexity and high costs, only 10 pairs of tissues were analyzed in this study. In the future, more matched samples and even single-cell omics could be included to reduce the impact of tumor heterogeneity and obtain more precise and valuable protein information.

CONCLUSION

In summary, comprehensive proteomic profiles of CRC tissues were described compared to normal tissues. The study provided proteomic evidence at the level of tissue exosomes as well as a foundation and direction for future research. Six exosomal proteins, NHP2, OLFM4, TOP1, SAMP, TAGL and TRIM28, were screened and identified and may be promising diagnostic biomarkers and effective therapeutic targets for CRC.

ARTICLE HIGHLIGHTS

Research background

Colorectal cancer (CRC) is the third most common malignancy in the world and has the second highest mortality rate. Early diagnosis can improve the prognosis of patients, so the search for biomarkers for CRC diagnosis is of clinical importance. Oncology research has entered the era of omics, in which proteomics is closely linked to the pathophysiological state of the human body, providing clear epigenetic information.

Research motivation

Although many studies have focused on CRC, the means of diagnosis and treatment have not improved significantly, and the specific molecular mechanisms of CRC remain unclear. Exploring the proteomic profile of CRC and searching for potential diagnostic biomarkers and therapeutic targets is essential.

Research objectives

To comprehensively characterize the exosomal proteomic profile of CRC tissue and to search for promising exosomal proteins as diagnostic biomarkers for CRC.

Research methods

Exosomes were extracted from paired CRC tissues and paracancerous tissues for data-independent acquisition mass spectrometry. Differentially expressed exosomal proteins were screened by bioinformatics analysis and validated by parallel reaction monitoring analysis. Receiver operating characteristic analysis and survival analysis were performed to detect the diagnostic ability and prognostic relevance of the candidate exosomal proteins.

Research results

The study identified 128 upregulated proteins and 155 downregulated proteins between CRC tissue exosomes and paracancerous tissue exosomes. Functional enrichment of proteins is closely associated with the extracellular matrix. The candidate exosomal proteins TRIM28, NHP2, OLFM4, TOP1, SAMP and TAGL could distinguish CRC tissues well from paracancerous tissues and are potential diagnostic biomarkers for CRC.

Research conclusions

This study provides a comprehensive exosomal proteomic characterization of CRC. The exosomal proteins TRIM28, NHP2, OLFM4, TOP1, SAMP and TAGL have the potential to be diagnostic biomarkers for CRC.

Research perspectives

Mining novel diagnostic biomarkers for CRC at the level of exosomes and proteomics to improve the detection rate of CRC.

FOOTNOTES

Author contributions: Zhou GYJ designed the study, analyzed the data, and drafted the manuscript; Zhao DY and Yin TF provided guidance on experimental procedures; Wang Q and Zhou YC collected the samples and the clinical data; Yao SK supervised the study, revised the manuscript, and obtained the funding; all authors read and approved the final manuscript.

Supported by National Key Development Plan for Precision Medicine Research, No. 2017YFC0910002.

Institutional review board statement: This study was approved by the Ethics Committee of China-Japan Friendship Hospital (No. 2018-116-K85).

Informed consent statement: All study participants, or their legal guardian, provided informed written consent prior to study enrollment.

Conflict-of-interest statement: All authors declare no conflicts of interest for this article.

Data sharing statement: No additional data are available.

STROBE statement: The authors have read the STROBE Statement—checklist of items, and the manuscript was prepared and revised according to the STROBE Statement—checklist of items.

Country/Territory of origin: China

ORCID number: Ge-Yu-Jia Zhou 0000-0002-4196-1436; Dong-Yan Zhao 0000-0002-7026-068X; Teng-Fei Yin 0000-0003-1140-8637; Qian-Qian Wang 0000-0002-7709-2121; Yuan-Chen Zhou 0000-0001-6024-6246; Shu-Kun Yao 0000-0002-8512-2589.

S-Editor: Yan JP
L-Editor: A
P-Editor: Ju JL

REFERENCES

1 **Zou H**, Li Z, Tian X, Ren Y. The top 5 causes of death in China from 2000 to 2017. *Sci Rep* 2022; **12**: 8119 [PMID: 35581260 DOI: 10.1038/s41598-022-12256-8]
2 **Xia C**, Dong X, Li H, Cao M, Sun D, He S, Yang F, Yan X, Zhang S, Li N, Chen W. Cancer statistics in China and United States, 2022: profiles, trends, and determinants. *Chin Med J (Engl)* 2022; **135**: 584-590 [PMID: 35143424 DOI: 10.1097/CM9.0000000000002108]
3 **Siegel RL**, Miller KD, Fuchs HE, Jemal A. Cancer statistics, 2022. *CA Cancer J Clin* 2022; **72**: 7-33 [PMID: 35020204 DOI: 10.3322/caac.21708]
4 **Wei W**, Zeng H, Zheng R, Zhang S, An L, Chen R, Wang S, Sun K, Matsuda T, Bray F, He J. Cancer registration in China and its role in cancer prevention and control. *Lancet Oncol* 2020; **21**: e342-e349 [PMID: 32615118 DOI: 10.1016/S1470-2045(20)30073-5]
5 **Cao W**, Chen HD, Yu YW, Li N, Chen WQ. Changing profiles of cancer burden worldwide and in China: a secondary analysis of the global cancer statistics 2020. *Chin Med J (Engl)* 2021; **134**: 783-791 [PMID: 33734139 DOI: 10.1097/CM9.0000000000001474]
6 **Li N**, Lu B, Luo C, Cai J, Lu M, Zhang Y, Chen H, Dai M. Incidence, mortality, survival, risk factor and screening of colorectal cancer: A comparison among China, Europe, and northern America. *Cancer Lett* 2021; **522**: 255-268 [PMID: 34563640 DOI: 10.1016/j.canlet.2021.09.034]
7 **Yu W**, Hurley J, Roberts D, Chakrabortty SK, Enderle D, Noerholm M, Breakefield XO, Skog JK. Exosome-based liquid biopsies in cancer: opportunities and challenges. *Ann Oncol* 2021; **32**: 466-477 [PMID: 33548389 DOI: 10.1016/j.annonc.2021.01.074]
8 **Zhou B**, Xu K, Zheng X, Chen T, Wang J, Song Y, Shao Y, Zheng S. Application of exosomes as liquid biopsy in clinical diagnosis. *Signal Transduct Target Ther* 2020; **5**: 144 [PMID: 32747657 DOI: 10.1038/s41392-020-00258-9]
9 **He C**, Zheng S, Luo Y, Wang B. Exosome Theranostics: Biology and Translational Medicine. *Theranostics* 2018; **8**: 237-255 [PMID: 29290805 DOI: 10.7150/thno.21945]
10 **Li X**, Wang W, Chen J. Recent progress in mass spectrometry proteomics for biomedical research. *Sci China Life Sci* 2017; **60**: 1093-1113 [PMID: 29039124 DOI: 10.1007/s11427-017-9175-2]
11 **Vella LJ**, Scicluna BJ, Cheng L, Bawden EG, Masters CL, Ang CS, Willamson N, McLean C, Barnham KJ, Hill AF. A rigorous method to enrich for exosomes from brain tissue. *J Extracell Vesicles* 2017; **6**: 1348885 [PMID: 28804598 DOI: 10.1080/20013078.2017.1348885]
12 **Gillet LC**, Navarro P, Tate S, Röst H, Selevsek N, Reiter L, Bonner R, Aebersold R. Targeted data extraction of the MS/MS spectra generated by data-independent acquisition: a new concept for consistent and accurate proteome analysis. *Mol Cell Proteomics* 2012; **11**: O111.016717 [PMID: 22261725 DOI: 10.1074/mcp.O111.016717]
13 **Dyring-Andersen B**, Løvendorf MB, Coscia F, Santos A, Møller LBP, Colaço AR, Niu L, Bzorek M, Doll S, Andersen JL, Clark RA, Skov L, Teunissen MBM, Mann M. Spatially and cell-type resolved quantitative proteomic atlas of healthy human skin. *Nat Commun* 2020; **11**: 5587 [PMID: 33154365 DOI: 10.1038/s41467-020-19383-8]
14 **Bourmaud A**, Gallien S, Domon B. Parallel reaction monitoring using quadrupole-Orbitrap mass spectrometer: Principle and applications. *Proteomics* 2016; **16**: 2146-2159 [PMID: 27145088 DOI: 10.1002/pmic.201500543]
15 **Liu J**, Ren L, Li S, Li W, Zheng X, Yang Y, Fu W, Yi J, Wang J, Du G. The biology, function, and applications of exosomes in cancer. *Acta Pharm Sin B* 2021; **11**: 2783-2797 [PMID: 34589397 DOI: 10.1016/j.apsb.2021.01.001]
16 **Afzal O**, Altamimi ASA, Mubeen B, Alzarea SI, Almalki WH, Al-Qahtani SD, Atiya EM, Al-Abbasi FA, Ali F, Ullah I, Nadeem MS, Kazmi I. mTOR as a Potential Target for the Treatment of Microbial Infections, Inflammatory Bowel Diseases, and Colorectal Cancer. *Int J Mol Sci* 2022; **23** [PMID: 36293326 DOI: 10.3390/ijms232012470]
17 **Wang C**, Chen J, Kuang Y, Cheng X, Deng M, Jiang Z, Hu X. A novel methylated cation channel TRPM4 inhibited colorectal cancer metastasis through Ca(2+)/Calpain-mediated proteolysis of FAK and suppression of PI3K/Akt/mTOR signaling pathway. *Int J Biol Sci* 2022; **18**: 5575-5590 [PMID: 36147460 DOI: 10.7150/ijbs.70504]
18 **Gong Y**, Liu Y, Wang T, Li Z, Gao L, Chen H, Shu Y, Li Y, Xu H, Zhou Z, Dai L. Age-Associated Proteomic Signatures and Potential Clinically Actionable Targets of Colorectal Cancer. *Mol Cell Proteomics* 2021; **20**: 100115 [PMID: 34129943 DOI: 10.1016/j.mcpro.2021.100115]
19 **Praus F**, Künstner A, Sauer T, Kohl M, Kern K, Deichmann S, Végvári Á, Keck T, Busch H, Habermann JK, Gemoll T. Panomics reveals patient individuality as the major driver of colorectal cancer progression. *J Transl Med* 2023; **21**: 41 [PMID: 36691026 DOI: 10.1186/s12967-022-03855-0]
20 **Buttacavoli M**, Albanese NN, Roz E, Pucci-Minafra I, Feo S, Cancemi P. Proteomic Profiling of Colon Cancer Tissues: Discovery of New

Candidate Biomarkers. *Int J Mol Sci* 2020; **21** [PMID: 32353950 DOI: 10.3390/ijms21093096]

21 **Ullah I**, Yang L, Yin FT, Sun Y, Li XH, Li J, Wang XJ. Multi-Omics Approaches in Colorectal Cancer Screening and Diagnosis, Recent Updates and Future Perspectives. *Cancers (Basel)* 2022; **14** [PMID: 36428637 DOI: 10.3390/cancers14225545]

22 **Dalal N**, Jalandra R, Sharma M, Prakash H, Makharia GK, Solanki PR, Singh R, Kumar A. Omics technologies for improved diagnosis and treatment of colorectal cancer: Technical advancement and major perspectives. *Biomed Pharmacother* 2020; **131**: 110648 [PMID: 33152902 DOI: 10.1016/j.biopha.2020.110648]

23 **Bhardwaj M**, Weigl K, Tikk K, Holland-Letz T, Schrotz-King P, Borchers CH, Brenner H. Multiplex quantitation of 270 plasma protein markers to identify a signature for early detection of colorectal cancer. *Eur J Cancer* 2020; **127**: 30-40 [PMID: 31972396 DOI: 10.1016/j.ejca.2019.11.021]

24 **Ghazanfar S**, Fatima I, Aslam M, Musharraf SG, Sherman NE, Moskaluk C, Fox JW, Akhtar MW, Sadaf S. Identification of actin beta-like 2 (ACTBL2) as novel, upregulated protein in colorectal cancer. *J Proteomics* 2017; **152**: 33-40 [PMID: 27989943 DOI: 10.1016/j.jprot.2016.10.011]

25 **Whiteside TL**. Exosomes and tumor-mediated immune suppression. *J Clin Invest* 2016; **126**: 1216-1223 [PMID: 26927673 DOI: 10.1172/JCI81136]

26 **Poggio M**, Hu T, Pai CC, Chu B, Belair CD, Chang A, Montabana E, Lang UE, Fu Q, Fong L, Blelloch R. Suppression of Exosomal PD-L1 Induces Systemic Anti-tumor Immunity and Memory. *Cell* 2019; **177**: 414-427.e13 [PMID: 30951669 DOI: 10.1016/j.cell.2019.02.016]

27 **Zhang X**, Sai B, Wang F, Wang L, Wang Y, Zheng L, Li G, Tang J, Xiang J. Hypoxic BMSC-derived exosomal miRNAs promote metastasis of lung cancer cells *via* STAT3-induced EMT. *Mol Cancer* 2019; **18**: 40 [PMID: 30866952 DOI: 10.1186/s12943-019-0959-5]

28 **Ludwig N**, Yerneni SS, Razzo BM, Whiteside TL. Exosomes from HNSCC Promote Angiogenesis through Reprogramming of Endothelial Cells. *Mol Cancer Res* 2018; **16**: 1798-1808 [PMID: 30042174 DOI: 10.1158/1541-7786.MCR-18-0358]

29 **Guo Y**, Wang M, Zou Y, Jin L, Zhao Z, Liu Q, Wang S, Li J. Mechanisms of chemotherapeutic resistance and the application of targeted nanoparticles for enhanced chemotherapy in colorectal cancer. *J Nanobiotechnology* 2022; **20**: 371 [PMID: 35953863 DOI: 10.1186/s12951-022-01586-4]

30 **Tao HY**, He SM, Zhao CY, Wang Y, Sheng WJ, Zhen YS. Antitumor efficacy of a recombinant EGFR-targeted fusion protein conjugate that induces telomere shortening and telomerase downregulation. *Int J Biol Macromol* 2023; **226**: 1088-1099 [PMID: 36435475 DOI: 10.1016/j.ijbiomac.2022.11.225]

31 **Xia X**, Mao Z, Wang W, Ma J, Tian J, Wang S, Yin K. Netrin-1 Promotes the Immunosuppressive Activity of MDSCs in Colorectal Cancer. *Cancer Immunol Res* 2023; **11**: 600-613 [PMID: 36812256 DOI: 10.1158/2326-6066.CIR-22-0658]

32 **Tabatabai E**, Khazaei M, Parizadeh MR, Nouri M, Hassanian SM, Ferns GA, Rahmati M, Avan A. The Potential Therapeutic Value of Renin-Angiotensin System Inhibitors in the Treatment of Colorectal Cancer. *Curr Pharm Des* 2022; **28**: 71-76 [PMID: 34635038 DOI: 10.2174/1381612827666211011113308]

33 **Jin JO**, Lee GD, Nam SH, Lee TH, Kang DH, Yun JK, Lee PC. Sequential ubiquitination of p53 by TRIM28, RLIM, and MDM2 in lung tumorigenesis. *Cell Death Differ* 2021; **28**: 1790-1803 [PMID: 33328571 DOI: 10.1038/s41418-020-00701-y]

34 **Fong KW**, Zhao JC, Song B, Zheng B, Yu J. TRIM28 protects TRIM24 from SPOP-mediated degradation and promotes prostate cancer progression. *Nat Commun* 2018; **9**: 5007 [PMID: 30479348 DOI: 10.1038/s41467-018-07475-5]

35 **McAvera RM**, Crawford LJ. TIF1 Proteins in Genome Stability and Cancer. *Cancers (Basel)* 2020; **12** [PMID: 32731534 DOI: 10.3390/cancers12082094]

36 **Yang Y**, Tan S, Han Y, Huang L, Yang R, Hu Z, Tao Y, Oyang L, Lin J, Peng Q, Jiang X, Xu X, Xia L, Peng M, Wu N, Tang Y, Li X, Liao Q, Zhou Y. The role of tripartite motif-containing 28 in cancer progression and its therapeutic potentials. *Front Oncol* 2023; **13**: 1100134 [PMID: 36756159 DOI: 10.3389/fonc.2023.1100134]

37 **Shay JW**, Wright WE. Telomeres and telomerase: three decades of progress. *Nat Rev Genet* 2019; **20**: 299-309 [PMID: 30760854 DOI: 10.1038/s41576-019-0099-1]

38 **Wang XY**, Chen SH, Zhang YN, Xu CF. Olfactomedin-4 in digestive diseases: A mini-review. *World J Gastroenterol* 2018; **24**: 1881-1887 [PMID: 29740203 DOI: 10.3748/wjg.v24.i17.1881]

39 **Talukdar A**, Kundu B, Sarkar D, Goon S, Mondal MA. Topoisomerase I inhibitors: Challenges, progress and the road ahead. *Eur J Med Chem* 2022; **236**: 114304 [PMID: 35413618 DOI: 10.1016/j.ejmech.2022.114304]

40 **Wang W**, Wu L, Wu X, Li K, Li T, Xu B, Liu W. Combined analysis of serum SAP and PRSS2 for the differential diagnosis of CD and UC. *Clin Chim Acta* 2021; **514**: 8-14 [PMID: 33333044 DOI: 10.1016/j.cca.2020.12.014]

41 **Liu J**, Zhang Y, Li Q, Wang Y. Transgelins: Cytoskeletal Associated Proteins Implicated in the Metastasis of Colorectal Cancer. *Front Cell Dev Biol* 2020; **8**: 573859 [PMID: 33117801 DOI: 10.3389/fcell.2020.573859]

42 **Elsafadi M**, Manikandan M, Almalki S, Mahmood A, Shinwari T, Vishnubalaji R, Mobarak M, Alfayez M, Aldahmash A, Kassem M, Alajez NM. Transgelin is a poor prognostic factor associated with advanced colorectal cancer (CRC) stage promoting tumor growth and migration in a TGFβ-dependent manner. *Cell Death Dis* 2020; **11**: 341 [PMID: 32393769 DOI: 10.1038/s41419-020-2529-6]

World Journal of Gastrointestinal Oncology

Submit a Manuscript: https://www.f6publishing.com

World J Gastrointest Oncol 2023 July 15; 15(7): 1241-1252

DOI: 10.4251/wjgo.v15.i7.1241

ISSN 1948-5204 (online)

ORIGINAL ARTICLE

Retrospective Cohort Study

Development and validation of a postoperative pulmonary infection prediction model for patients with primary hepatic carcinoma

Chao Lu, Zhi-Xiang Xing, Xi-Gang Xia, Zhi-Da Long, Bo Chen, Peng Zhou, Rui Wang

Specialty type: Gastroenterology and hepatology

Provenance and peer review: Unsolicited article; Externally peer reviewed.

Peer-review model: Single blind

Peer-review report's scientific quality classification

Grade A (Excellent): 0
Grade B (Very good): B
Grade C (Good): C, C
Grade D (Fair): D
Grade E (Poor): 0

P-Reviewer: Lee KS, South Korea; Lin HH, China; Patel J, United States

Received: May 1, 2023
Peer-review started: May 1, 2023
First decision: May 11, 2023
Revised: May 14, 2023
Accepted: June 12, 2023
Article in press: June 12, 2023
Published online: July 15, 2023

Chao Lu, Zhi-Xiang Xing, Xi-Gang Xia, Zhi-Da Long, Bo Chen, Peng Zhou, Rui Wang, Department of Hepatobiliary & Pancreaticospleen Surgery, Yangtze University, Jing Zhou hospital, Jingzhou 434020, Hubei Province, China

Corresponding author: Rui Wang, MD, Surgical Oncologist, Department of Hepatobiliary & Pancreaticospleen Surgery, Yangtze University, Jing Zhou hospital, No. 26 Chuyuan Road, Jingzhou District, Jingzhou 434020, Hubei Province, China. wangrui_20222022@163.com

Abstract

BACKGROUND

There are factors that significantly increase the risk of postoperative pulmonary infections in patients with primary hepatic carcinoma (PHC). Previous reports have shown that over 10% of patients with PHC experience postoperative pulmonary infections. Thus, it is crucial to prioritize the prevention and treatment of postoperative pulmonary infections in patients with PHC.

AIM

To identify the risk factors for postoperative pulmonary infection in patients with PHC and develop a prediction model to aid in postoperative management.

METHODS

We retrospectively collected data from 505 patients who underwent hepatobiliary surgery between January 2015 and February 2023 in the Department of Hepatobiliary and Pancreaticospleen Surgery. Radiomics data were selected for statistical analysis, and clinical pathological parameters and imaging data were included in the screening database as candidate predictive variables. We then developed a pulmonary infection prediction model using three different models: An artificial neural network model; a random forest model; and a generalized linear regression model. Finally, we evaluated the accuracy and robustness of the prediction model using the receiver operating characteristic curve and decision curve analyses.

RESULTS

Among the 505 patients, 86 developed a postoperative pulmonary infection, resulting in an incidence rate of 17.03%. Based on the gray-level co-occurrence matrix, we identified 14 categories of radiomic data for variable screening of pulmonary infection prediction models. Among these, energy, contrast, the sum of squares (SOS), the inverse difference (IND), mean sum (MES), sum variance (SUV), sum entropy (SUE), and entropy were independent risk factors for

pulmonary infection after hepatectomy and were listed as candidate variables of machine learning prediction models. The random forest model algorithm, in combination with IND, SOS, MES, SUE, SUV, and entropy, demonstrated the highest prediction efficiency in both the training and internal verification sets, with areas under the curve of 0.823 and 0.801 and a 95% confidence interval of 0.766-0.880 and 0.744-0.858, respectively. The other two types of prediction models had prediction efficiencies between areas under the curve of 0.734 and 0.815 and 95% confidence intervals of 0.677-0.791 and 0.766-0.864, respectively.

CONCLUSION

Postoperative pulmonary infection in patients undergoing hepatectomy may be related to risk factors such as IND, SOS, MES, SUE, SUV, energy, and entropy. The prediction model in this study based on diffusion-weighted images, especially the random forest model algorithm, can better predict and estimate the risk of pulmonary infection in patients undergoing hepatectomy, providing valuable guidance for postoperative management.

Key Words: Primary hepatic carcinoma; Pulmonary infection; Gray-level co-occurrence matrix; Machine learning; Prediction

Core Tip: Identifying risk factors for postoperative pulmonary infection in patients with primary hepatic carcinoma can improve the level of prevention and clinical treatment, ultimately reducing or even avoiding the occurrence of postoperative infection complications, reducing treatment time and costs, and improving patient efficacy and prognosis. The prediction model developed in our study provides valuable guidance for clinicians in predicting the risk of pulmonary infection and effectively preventing, diagnosing, and treating postoperative infection in patients with primary hepatic carcinoma, leading to an improved patient prognosis.

Citation: Lu C, Xing ZX, Xia XG, Long ZD, Chen B, Zhou P, Wang R. Development and validation of a postoperative pulmonary infection prediction model for patients with primary hepatic carcinoma. *World J Gastrointest Oncol* 2023; 15(7): 1241-1252
URL: https://www.wjgnet.com/1948-5204/full/v15/i7/1241.htm
DOI: https://dx.doi.org/10.4251/wjgo.v15.i7.1241

INTRODUCTION

Primary hepatic carcinoma (PHC) is a widespread malignant tumor with high incidence and mortality rates that poses a serious threat to human health worldwide. Surgical treatment remains the most effective treatment option for PHC[1]. However, postoperative infections, including surgical site and pulmonary infections, are among the main complications following surgery[2,3]. Patients with PHC are often accompanied by malnutrition, weakened immunity, and sputum accumulation in the respiratory tract due to prolonged bed rest and increased chronic consumption after surgery[4]. These factors significantly increase the risk of postoperative pulmonary infections in patients with PHC. Previous reports have shown that over 10% of patients with PHC experience postoperative pulmonary infections[5]. Thus, it is crucial to prioritize the prevention and treatment of postoperative pulmonary infections in patients with PHC.

Previous studies have shown that the causes of postoperative pulmonary infection in patients with PHC are related to the condition, respiratory microbiota, anesthesia-related factors, intraoperative procedures, and postoperative care of the patients. Of these factors, intraoperative procedures and the condition of the patients are considered the main triggers[2,6]. However, preoperative indicators that could be effective in preventing postoperative pulmonary infections and predictive models for such infections are still lacking. With the vigorous popularization of information technology in clinical practice, vast amounts of patient imaging data are now available, providing doctors with crucial objective data for clinical diagnosis, disease tracking, and surgical planning[7,8].

In this context, this study aimed to extract the texture features of radiomics of patients with PHC using a gray-level co-occurrence matrix (GLCM) to develop a predictive model to aid doctors in clinical decision-making and medical resource allocation for early interventions and treatments.

MATERIALS AND METHODS

Study population

We conducted a retrospective study on 505 patients with PHC who underwent surgical treatment at Jing Zhou Hospital between January 2015 and February 2023. The study included patients who met the following criteria: (1) Patients who met the diagnostic criteria for PHC (2011 version); (2) Patients with no distant liver cancer metastasis and feasible liver cancer radical surgery; (3) Patients who were confirmed by preoperative imaging to have no pulmonary infection; and (4) Patients whose postoperative adjuvant treatment and follow-up examinations were conducted in the same hospital.

Exclusion criteria included: (1) Patients with Child-Pugh grade C; (2) Patients with preoperative pulmonary disease; (3) Patients with other malignant tumors who have a history of chest trauma, surgery, and radiation chemotherapy; (4) Patients with a history of chronic respiratory diseases in the past; and (5) Patients who had not undergone liver and abdominal magnetic resonance imaging (MRI) examinations or whose imaging data collection was incomplete upon admission. As this was a retrospective chart review, informed written consent was not required in accordance with institutional review board policy, and the research scheme was implemented following the artificial intelligence model training specifications of the unit. All personal information of the patients was encrypted to prevent leakage and exempted from informed consent by the above ethics committee. The process of patient selection and development of the prediction model is shown in Figure 1.

Diagnostic criteria for postoperative pulmonary infection

In this study, postoperative pulmonary infection was diagnosed based on the following criteria: (1) Positive sputum culture after surgery; and (2) Identification of abnormal lung inflammatory rales upon lung auscultation. Both criteria need to be met in order for the diagnosis to be made.

Acquisition of MRI-based radiomics parameters

A GE Signa HD (3.0T) MR scanner was used in this study. The scanning sequence and parameter settings were as follows: Transverse fast spin echo T1-weighted imaging (repetition time, 400-620 ms, echo time, 10-16 ms); transverse, coronal, and sagittal plane fluid-sensitive proton density-weighted imaging (repetition time, 1800-3400 ms, echo time, 24-34 ms); layer thickness of 3-5 mm, layer spacing of 2 mm, matrix of 320 × (192-320) × 256, and field of view of 16 cm × (16-22) cm × 22 cm. We exported the MRI data of all patients in bitmap image file format from the picture archiving and communication system workstation for analysis. To ensure the reliability of the research results, we unified the window width or window level of T1-weighted imaging and fluid-sensitive proton density-weighted images at 1240/460 and 1050/340, respectively, when exporting the imaging data. Two experienced MRI diagnostic physicians selected a total of three layers of images to display the characteristics of the lesion, including the largest and consecutive layers, for measurement and analysis. We selected a sequence that displayed clear lesion boundaries to determine the lesion range as a reference standard and kept the region of interest (ROI) of other sequences consistent with it.

Training and verification of the segmentation model

With the guidance of two senior physicians, one physician manually delineated the ROI along the lesion boundary, covering the maximum layer of the lesion and one layer before and after the lesion. A total of three layers of images were used for calculating texture parameters. The average value was taken, and subsequent analysis was performed using MaZda software (available from: http://www.ele-tel.p.lodz.pl/mazda). To reduce bias caused by changes in brightness and contrast during result analysis, the grayscale of the image was standardized before extracting texture features. The MaZda software was used to calculate histogram and GLCM parameters within the ROI, including energy, contrast, correlation, the sum of squares (SOS), an inverse difference (IND), mean sum (MES), sum variance (SUV), sum entropy (SUE), entropy, and difference variance and entropy.

Analysis and evaluation of the pulmonary infection prediction model

All patients included in this study were randomly assigned to a model training set and an internal validation set at a 7:3 ratio. In the early stages of candidate variable selection, least absolute shrinkage and selection operator (LASSO) regression with minimum penalty coefficient and Pearson correlation coefficient were used to select variables that could ultimately be used to develop pulmonary infection prediction models. Three prediction models with different algorithms were developed, namely the artificial neural network model (ANNM), the random forest model (RFM), and the generalized linear regression model (GLRM)[9-12]. Additionally, LASSO was selected to develop a classification model for predicting pulmonary infection based on MRI images[13]. The effectiveness evaluation of each model mainly included decision curve analysis (DCA)[14], area under the receiver operating characteristic curve, and clinical influence curve[15].

Statistical analysis

The Wilcoxon rank-sum test or *t*-test was used to compare continuous variables, while the χ^2 test was used to compare categorical variables. Pearson's correlation coefficients were used to assess the correlation between two continuous variables[16]. The charts in this study were analyzed visually using R Studio software (available from: https://www.r-project.org/). Statistical significance was defined as a two-tailed P value of < 0.05.

RESULTS

Clinical characteristics of patients with PHC with or without pulmonary infection

In the study, a total of 505 patients with PHC were included in the development of the pulmonary infection prediction models. Of these, 86 patients developed postoperative pulmonary infections and were categorized as the infected group, while 419 patients who did not have postoperative infections were included in the non-infected group. The incidence rates of postoperative pulmonary infection in the training and validation sets were 17.28% (61/353) and 16.45% (25/152), respectively. The specific surgical procedures performed included left hepatectomy, left hepatectomy and cholecystectomy, right hepatectomy, right hepatectomy and cholecystectomy, left hepatectomy and biliary drainage, right

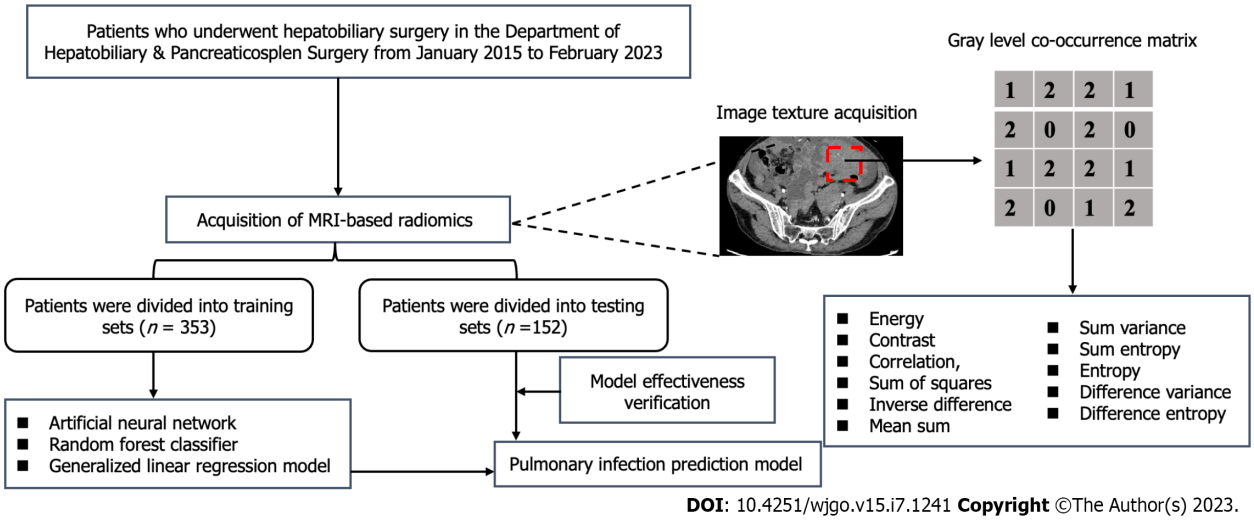

DOI: 10.4251/wjgo.v15.i7.1241

Figure 1 Flow chart of patient selection and data process. MRI: Magnetic resonance imaging.

hepatectomy, intraoperative radiofrequency therapy, and left hepatectomy. All patients with pulmonary infections improved after receiving treatment such as anti-inflammatory drugs and thoracic puncture drainage, and no other pulmonary complications occurred. The baseline data and radiomics-related extracted variables of the two groups of patients with PHC were summarized in Table 1 and Supplementary Table 1.

Features selected by LASSO regression analysis

As the included candidate variables were inevitably biased and had a non-normal distribution, we added penalty terms to the loss function (*i.e.*, optimization goal) during the training and parameter-solving processes. This allowed the size of the coefficient to be considered. By setting a reduction coefficient (penalty coefficient), the coefficient of features with less impact was reduced to zero, retaining only important features, which is known as LASSO regression. Specifically, cross-validation was performed on all candidate parameters, and a dashed line was drawn at the optimal parameter (*i.e.*, nine for non-zero parameters) to indicate the best-fit LASSO regression model. In the subsequent prediction model analysis, the optimal lambda value selected was substituted into the LASSO coefficient curve containing 18 variables, including 11 independent variables. This was used to develop an independent variable for predicting the risk propensity of postoperative pulmonary infection (Figure 2).

Development of a nomogram using GLRM analysis

As shown in Supplementary Table 2, we conducted a multivariate logistic regression analysis on all included candidate variables and found that seven variables were independent risk factors for postoperative pulmonary infection, including IND, SOS, MES, SUE, SUV, energy, and entropy. Based on the Akaike information criterion, we developed a predictive model for postoperative pulmonary infection and a nomogram (Figure 3). The nomogram showed the overall variables included in the prediction model on the left side, and each variable was assigned a scale value. The total score can be obtained by assigning scores to each variable for the included patients. Finally, the probability of pulmonary infection in patients can be evaluated based on the corresponding risk scale value of the total score. Moreover, the C-index value, which was verified internally by the bootstrap method, was 0.785, indicating good clinical applicability.

Development of the machine learning-based pulmonary infection prediction model

RFM and ANNM are the most widely used machine learning algorithms in various fields, including healthcare[9]. In this study, four supervised learning algorithms were used to develop the pulmonary infection model. As shown in Supplementary Table 3, top-ranking weight values in the RFM prediction model were obtained for energy, entropy, and variance, indicating their potential as candidate variables for RFM-based prediction of pulmonary infection (Figure 4A). Consequently, in ANNM, energy, entropy, SUV, SUE, IND, MES, contrast, and SOS also served as candidate variables for predicting pulmonary infection, and their assignments in the two different algorithm prediction models were inconsistent (Figure 4B, Supplementary Table 4).

Performance of pulmonary infection prediction models

The receiver operating characteristic curves were drawn to evaluate the predictive efficacy of each risk factor and the nomogram model. The receiver operating characteristic curve showed that the RFM model had higher predictive efficacy in both training and verification sets than the ANNM model, with areas under the curve of 0.823 and 0.801 and a 95% confidence interval (CI) of 0.766-0.880 and 0.744-0.858, respectively, compared to areas under the curve 0.815 and 0.787 and 95%CIs of 0.766-0.864 and 0.738-0.836, respectively, for the ANNM model. The predictive performance of preoperative GLCM-based radiomics for pulmonary infection was provided in Table 2. The prediction efficiency of the pulmonary infection prediction model for patients with PHC developed by a machine learning (ML)-based algorithm was

Table 1 Baseline demographic and radiomics of patients with primary hepatic carcinoma

Variables	Training cohort			*P* value	Testing cohort			*P* value
	Overall, *n* = 353	Infection, *n* = 61	Non-infection, *n* = 292		Overall, *n* = 152	Infection, *n* = 25	Non-infection, *n* = 127	
Age in yr								
> 60	240 (68.0)	37 (60.7)	203 (69.5)	0.231	109 (71.7)	16 (64.0)	93 (73.2)	0.488
≤ 60	113 (32.0)	24 (39.3)	89 (30.5)		43 (28.3)	9 (36.0)	34 (26.8)	
Sex								
Male	234 (66.3)	39 (63.9)	195 (66.8)	0.78	106 (69.7)	18 (72.0)	88 (69.3)	0.975
Female	119 (33.7)	22 (36.1)	97 (33.2)		46 (30.3)	7 (28.0)	39 (30.7)	
BMI								
≤ 18.5	47 (13.3)	10 (16.4)	37 (12.7)	0.877	20 (13.2)	4 (16.0)	16 (12.6)	0.627
18.5-23.9	121 (34.3)	21 (34.4)	100 (34.2)		54 (35.5)	6 (24.0)	48 (37.8)	
24.0-27.9	97 (27.5)	16 (26.2)	81 (27.7)		47 (30.9)	9 (36.0)	38 (29.9)	
≥ 28.0	88 (24.9)	14 (23.0)	74 (25.3)		31 (20.4)	6 (24.0)	25 (19.7)	
Smoking								
Yes	114 (32.3)	19 (31.1)	95 (32.5)	0.952	63 (41.4)	14 (56.0)	49 (38.6)	0.163
No	239 (67.7)	42 (68.9)	197 (67.5)		89 (58.6)	11 (44.0)	78 (61.4)	
Drinking								
Yes	100 (28.3)	18 (29.5)	82 (28.1)	0.945	56 (36.8)	8 (32.0)	48 (37.8)	0.747
No	253 (71.7)	43 (70.5)	210 (71.9)		96 (63.2)	17 (68.0)	79 (62.2)	
History of hepatitis B								
Yes	134 (38.0)	27 (44.3)	107 (36.6)	0.332	58 (38.2)	10 (40.0)	48 (37.8)	1.000
No	219 (62.0)	34 (55.7)	185 (63.4)		94 (61.8)	15 (60.0)	79 (62.2)	
History of hepatitis C								
Yes	129 (36.5)	22 (36.1)	107 (36.6)	1	50 (32.9)	9 (36.0)	41 (32.3)	0.898
No	224 (63.5)	39 (63.9)	185 (63.4)		102 (67.1)	16 (64.0)	86 (67.7)	
Hypertension								
Yes	110 (31.2)	19 (31.1)	91 (31.2)	1	57 (37.5)	11 (44.0)	46 (36.2)	0.611
No	243 (68.8)	42 (68.9)	201 (68.8)		95 (62.5)	14 (56.0)	81 (63.8)	
Diabetes								
Yes	119 (33.7)	21 (34.4)	98 (33.6)	1	52 (34.2)	9 (36.0)	43 (33.9)	1.000
No	234 (66.3)	40 (65.6)	194 (66.4)		100 (65.8)	16 (64.0)	84 (66.1)	
Cirrhosis								
Yes	176 (49.9)	32 (52.5)	144 (49.3)	0.76	68 (44.7)	7 (28.0)	61 (48.0)	0.105
No	177 (50.1)	29 (47.5)	148 (50.7)		84 (55.3)	18 (72.0)	66 (52.0)	
Child-Pugh								
A	253 (71.7)	39 (63.9)	214 (73.3)	0.187	102 (67.1)	14 (56.0)	88 (69.3)	0.289
B	100 (28.3)	22 (36.1)	78 (26.7)		50 (32.9)	11 (44.0)	39 (30.7)	
AFP in mg/L								
≤ 100	206 (58.4)	27 (44.3)	179 (61.3)	0.021	89 (58.6)	11 (44.0)	78 (61.4)	0.163
> 100	147 (41.6)	34 (55.7)	113 (38.7)		63 (41.4)	14 (56.0)	49 (38.6)	

HBV DNA								
Negative	233 (66.0)	41 (67.2)	192 (65.8)	0.944	106 (69.7)	15 (60.0)	91 (71.7)	0.357
Positive	120 (34.0)	20 (32.8)	100 (34.2)		46 (30.3)	10 (40.0)	36 (28.3)	
Tumor size in cm								
≤ 4	203 (57.5)	24 (39.3)	179 (61.3)	0.003	83 (54.6)	6 (24.0)	77 (60.6)	0.002
> 4	150 (42.5)	37 (60.7)	113 (38.7)		69 (45.4)	19 (76.0)	50 (39.4)	
Treatment								
Laparoscopic	95 (26.9)	17 (27.9)	78 (26.7)	0.979	45 (29.6)	8 (32.0)	37 (29.1)	0.962
Open	258 (73.1)	44 (72.1)	214 (73.3)		107 (70.4)	17 (68.0)	90 (70.9)	
LNM								
Yes	108 (30.6)	17 (27.9)	91 (31.2)	0.722	48 (31.6)	7 (28.0)	41 (32.3)	0.853
No	245 (69.4)	44 (72.1)	201 (68.8)		104 (68.4)	18 (72.0)	86 (67.7)	
Energy	4.48 (2.97, 5.91)	9.05 (7.07, 10.30)	4.02 (2.62, 5.26)	< 0.001	4.52 (2.74, 6.02)	8.82 (6.99, 10.91)	4.01 (2.45, 5.38)	< 0.001
Contrast	351.00 (316.00, 384.00)	289.00 (275.00, 301.00)	360.00 (334.00, 391.75)	< 0.001	347.00 (319.50, 381.00)	306.00 (275.00, 317.00)	355.00 (331.00, 388.00)	< 0.001
Correlation	16.39 (12.49, 20.01)	13.77 (11.43, 19.07)	16.70 (13.04, 20.11)	0.006	16.63 (12.02, 20.33)	18.08 (14.70, 21.30)	16.07 (11.96, 20.02)	0.093
SOS	0.89 (0.71, 1.08)	2.38 (2.01, 2.97)	0.83 (0.69, 0.97)	< 0.001	0.86 (0.73, 1.06)	2.61 (2.11, 3.06)	0.84 (0.69, 0.96)	< 0.001
IND	1.46 (1.17, 1.85)	3.43 (2.83, 4.07)	1.38 (1.12, 1.67)	< 0.001	1.52 (1.15, 1.90)	3.73 (3.11, 4.11)	1.44 (1.12, 1.69)	< 0.001
MES	2.77 (1.95, 3.47)	5.24 (4.60, 5.92)	2.50 (1.86, 3.12)	< 0.001	2.55 (1.96, 3.47)	4.90 (4.21, 5.93)	2.38 (1.89, 3.04)	< 0.001
SUV	20.10 (15.70, 25.60)	56.00 (39.50, 72.00)	18.60 (15.20, 22.83)	< 0.001	21.60 (16.67, 25.22)	61.80 (39.00, 70.10)	19.50 (15.70, 23.65)	< 0.001
SUE	21.80 (16.60, 27.00)	45.30 (37.20, 55.10)	19.85 (16.10, 24.00)	< 0.001	21.40 (15.97, 26.40)	46.60 (35.20, 53.30)	20.00 (15.45, 24.35)	< 0.001
Entropy	0.84 (0.62, 1.07)	2.07 (1.51, 2.44)	0.76 (0.58, 0.94)	< 0.001	0.82 (0.60, 1.10)	1.84 (1.45, 2.03)	0.73 (0.56, 0.94)	< 0.001
DIV	316.00 (210.00, 404.00)	295.00 (193.00, 402.00)	318.50 (224.50, 404.00)	0.411	296.50 (196.50, 391.75)	300.00 (191.00, 362.00)	296.00 (207.50, 400.50)	0.800
DIE	234.00 (188.00, 274.00)	244.00 (181.00, 274.00)	229.00 (188.00, 274.00)	0.774	232.50 (189.75, 274.50)	245.00 (204.00, 283.00)	231.00 (188.50, 271.50)	0.571

Data are presented as *n* (%) or median (interquartile range). AFP: Alpha-fetoprotein; BMI: Body mass index; DIE: Difference entropy; DIV: Difference variance; HBV: Hepatitis B virus; IND: Inverse difference; LNM: Lymph node metastasis; MES: Mean sum; SOS: Sum of squares; SUE: Sum entropy; SUV: Sum variance.

Table 2 Comparison of predictive efficacy of pulmonary infection prediction models *via* receiver operating characteristic curves

Model	Training set			Internal validation set		
	AUC mean	AUC 95%CI	Variables[1]	AUC mean	AUC 95%CI	Variables[1]
RFM	0.823	0.766-0.880	7	0.801	0.744-0.858	7
ANNM	0.815	0.766-0.864	8	0.787	0.738-0.836	8
GLRM	0.766	0.717-0.815	6	0.734	0.677-0.791	6

[1]Variables included in the model.

ANNM: Artificial neural network model; AUC: Area under the curve; CI: Confidence interval; GLRM: Generalized linear regression model; RFM: Random forest model.

better than that of the GLRM.

Furthermore, Figure 5 shows the DCA curve, with the abscissa indicating the threshold probability and the ordinate indicating the net benefit. The black horizontal line indicates a net benefit of zero, indicating that all patients were free of postoperative pulmonary infections. The gray diagonal line represents a scenario where all patients had a postoperative pulmonary infection and received treatment. DCA addresses the practical needs for clinical decision-making by

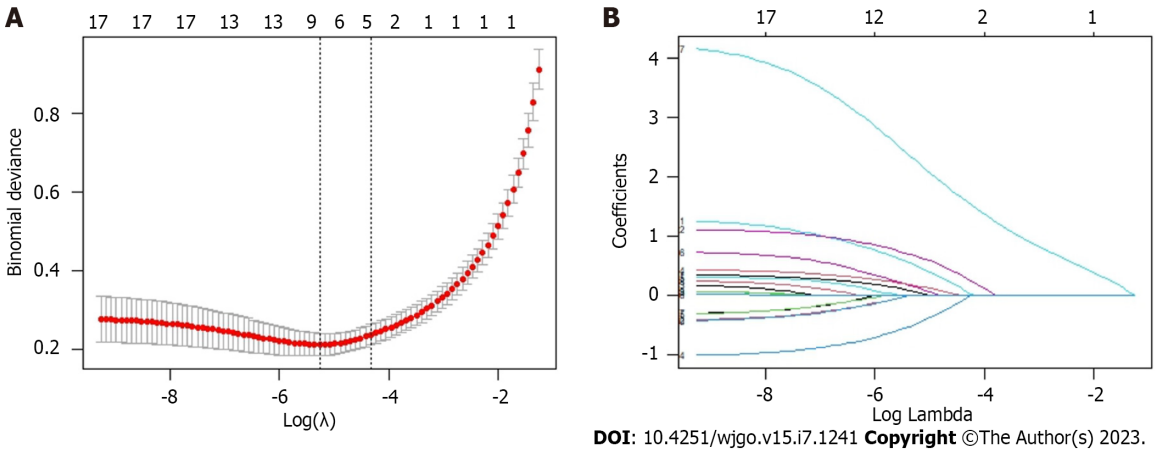

DOI: 10.4251/wjgo.v15.i7.1241

Figure 2 Predictor variable selection based on the least absolute shrinkage and selection operator regression method. A: Optimal parameter (lambda) selection in the least absolute shrinkage and selection operator (least absolute shrinkage and selection operator) model; B: Least absolute shrinkage and selection operator coefficient profiles of the candidate features.

incorporating patient or decision-maker preferences in the analysis. The DCA curve shows that the nomogram is more effective in predicting post-hepatectomy pulmonary infection than administering all or no postoperative treatment to patients.

Predictive value of an ML-based pulmonary infection prediction model

After developing three predictive models for pulmonary infection based on candidate predictive factors from preoperative MRI findings, we evaluated the optimal predictive performance of the RFM model. To further evaluate the differentiation efficiency of RFM, we used the clinical influence curve to assess the "classification accuracy" in the training set and internal verification set. As shown in Supplementary Figure 1, RFM effectively distinguished patients with pulmonary infection from those without pulmonary infection, which was consistent with the results of the postoperative pathological examination. Our study suggested that RFM is a reliable tool for the preoperative evaluation of pulmonary infection in patients with PHC and may become a powerful guiding tool for determining postoperative prevention of pulmonary infection. This also demonstrated that RFM was suitable for the preoperative assessment of the risk stratification of pulmonary infection.

DISCUSSION

The advancement in surgical technology has significantly reduced the preoperative mortality rate among patients with PHC. However, postoperative pulmonary infection has become a common and prominent complication, and its incidence rate has not shown significant improvement. Previous studies have reported postoperative pulmonary infection rates ranging from 9.60% to 22.38%[4,17]. The results of this study showed that the incidence rate of pulmonary infection after liver cancer surgery was 17.03%, consistent with previous studies[5,18,19]. The difference in the incidence rate of pulmonary infection can be attributed to the diagnostic criteria used by various diagnosis and treatment centers and the specific types of surgery for distinct populations. Furthermore, anti-infection and expectorant therapies are the main treatment measures for postoperative pulmonary infections in patients with PHC[5,20]. The reasonable selection of antibacterial and expectorant drugs, promotion of sputum excretion, prevention of respiratory difficulties caused by sputum stasis in pulmonary infections, and reduction of the induction of bronchial obstruction and atelectasis are all essential determinants of the incidence of postoperative pulmonary infections. Additionally, preoperative warning and evaluation for patients with primary liver cancer are crucial in reducing the occurrence of postoperative pulmonary infections[21,22]. In this context, our study employed advanced algorithms to explore the risk factors associated with postoperative infection, especially the predictive model developed using preoperative imaging parameters. This model can improve the level of prevention, clinical diagnosis, and treatment, reduce or avoid the occurrence of postoperative infection complications, and decrease treatment time and cost, thereby enhancing patient efficacy and prognosis.

This study used MRI, which has good soft tissue resolution and can perform multiplane and multisequence imaging. Its most significant advantage is its ability to achieve high spatial resolution and large-field scanning, making it the preferred imaging modality for preoperative MRI staging of cervical cancer. A non-inhibitory high-resolution MRI T2-weighted imaging sequence was used, and sagittal and short-axis scans (*i.e.*, perpendicular to the long axis of the liver) were performed to fully display the cross-sectional area of the tumor. Moreover, the higher spatial resolution of MRI was utilized to leverage the natural contrast of pelvic fat and clearly display the depth and extent of invasion of PHC. However, it is important to note that the infiltration of the PHC in T2-weighted imaging may show uneven signal intensity, and most enhancement scans show uneven enhancement. In contrast, inflammatory lesions in the parenchymatous organ show uniform enhancement. Previous studies have highlighted the abundant venous plexus

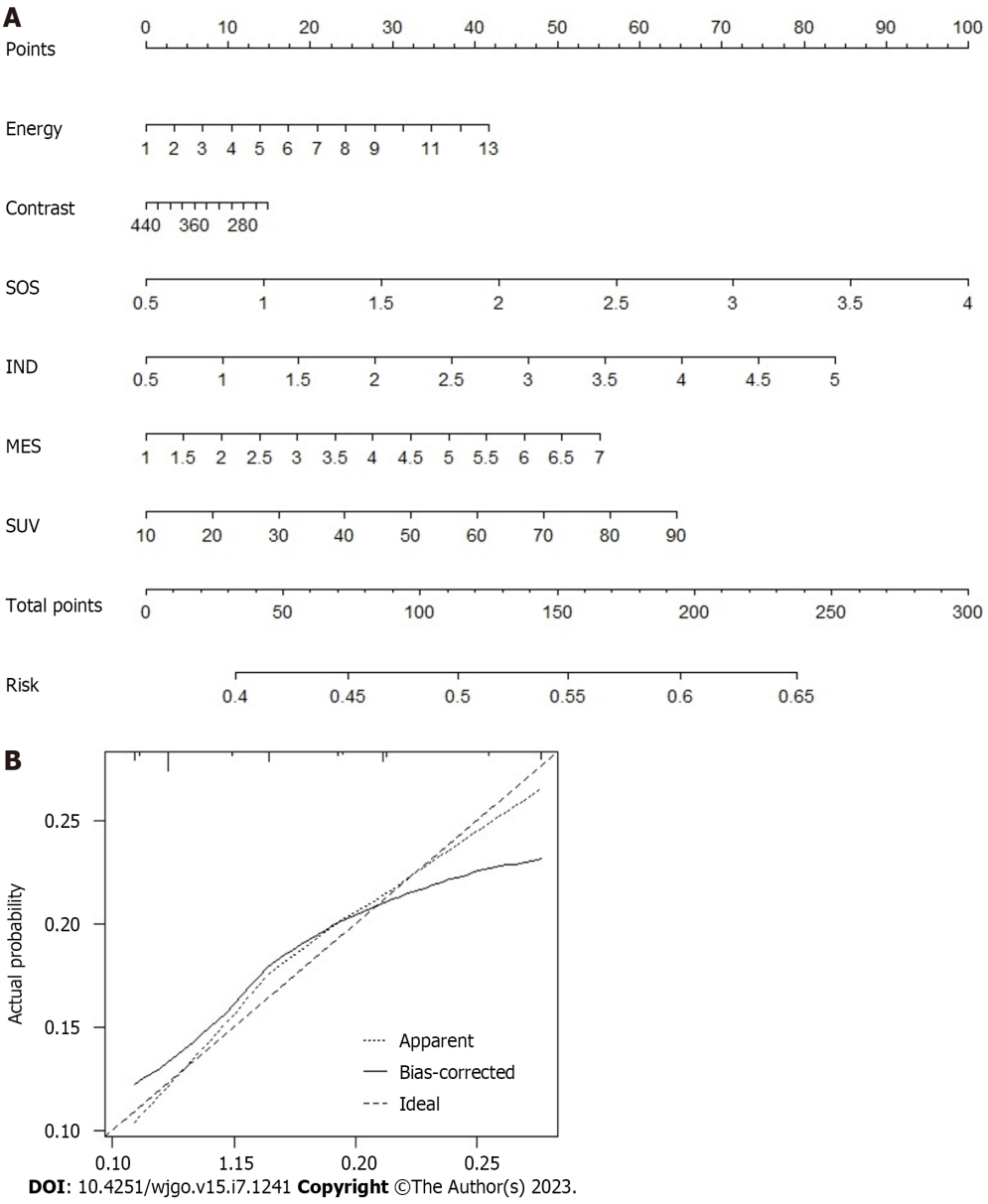

DOI: 10.4251/wjgo.v15.i7.1241

Figure 3 Nomogram prediction model for predicting pulmonary infection in patients with primary hepatic carcinoma undergoing hepatectomy. A: Nomogram predicts risk of pulmonary infection; B: Calibration curves for the nomogram. SOS: Sum of squares; IND: Inverse difference; MES: Mean sum; SUV: Sum variance.

around the liver, which can create an atypical enhancement of high signal intensity on MRI, leading to texture analysis errors[23-25]. Additionally, tumors with a larger volume, worsening inflammation and edema, and an abundant venous plexus around the uterus can also become key factors affecting the preoperative evaluation of pulmonary infection.

Currently, image texture analysis is increasingly widely used in various research fields, including tumor diagnosis, efficacy evaluation, and prognosis[26,27]. Our study showed that the texture feature parameters in various sequences of patients with pulmonary and non-pulmonary infection had certain predictive values in texture analysis. It is speculated that the neovascularization, tumor necrosis, and invasive growth patterns in malignant tumors can contribute to complex internal structures that can be perceived and quantified through image texture analysis. Additionally, the heterogeneity of lesions measured by texture analysis feature parameters can precisely reflect the different texture compositions of different tumors, including their potential invasiveness[28]. Through image texture features, we quantitatively described the spatial distribution of pixels in MRI images. Our results indicated that the parameters based on GLCM showed significant statistical differences, making them potential predictive variables for pulmonary infection. For example, this study found a significant positive correlation between entropy differences and pulmonary infections. Previous studies have shown that entropy difference, a characteristic parameter used to measure structural disorder or complexity of images, is higher in tumors with higher malignancy levels[29,30]. Similarly, this study found that patients with pulmonary infections had a higher entropy value. We also included candidate variables with predictive value in the ML-based algorithm model. The results demonstrated that without distinguishing the predictive variables, the GLCM-based prediction efficiency reached its highest value of 0.823. This suggests that MRI examination before hepatectomy and texture analysis using sequence images have significant potential for predicting the risk stratification of pulmonary

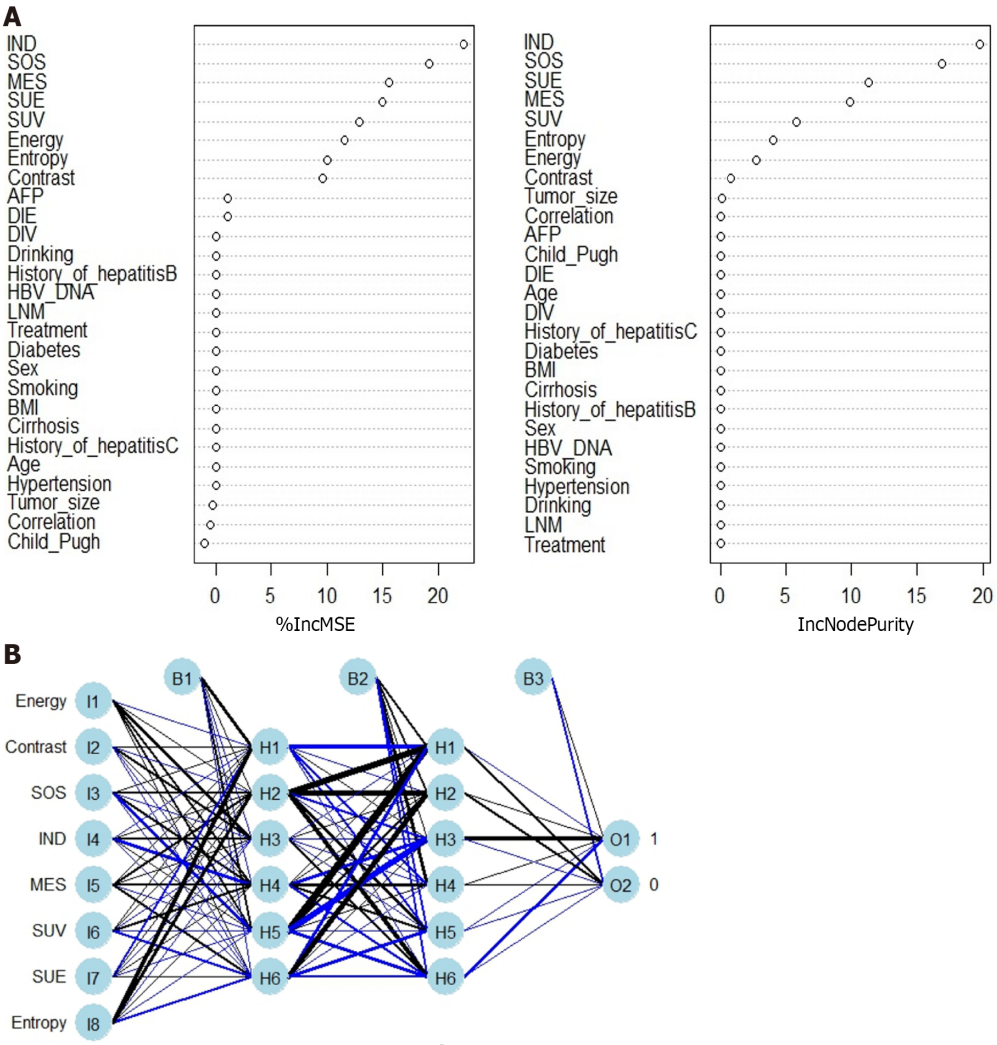

DOI: 10.4251/wjgo.v15.i7.1241

Figure 4 Construction of pulmonary infection prediction model *via* the random forest model and artificial neural network model. A: Random forest model. The application prediction model formula of the random forest model is as follows: C = argmax (∑(Ci)), where Ci represents the type of in prediction for the i-th tree, C is the final classification result, and I is the number of trees; B: Artificial neural network model. The formula of the artificial neural network model is as follows: θ = θ−η × ▽ (θ). J (θ) among them η is the learning rate, so (θ). J (θ) represents the gradient change of the loss function [*i.e.*, J(θ)]. AFP: Alpha-fetoprotein; BMI: Body mass index; DIE: Difference entropy; DIV: Difference variance; HBV: Hepatitis B virus; IND: Inverse difference; LNM: Lymph node metastasis; MES: Mean sum; SOS: Sum of squares; SUE: Sum entropy; SUV: Sum variance.

infection.

This study inevitably has the following limitations. First, the sample size was relatively small and from a single center, as we had strict requirements for MRI scanning parameters and equipment of the included patients. To overcome this, future studies should expand the sample size and conduct a prospective cohort study across multiple centers. Second, as a retrospective study, selection bias may have influenced the inclusion of the study population, leading to potential bias errors caused by the researcher's personal experience or subjective judgment. Third, although we extracted GLCM-related parameters from MRI, higher-order textures were not included in the analysis. Thus, future studies should focus on expanding the extraction of higher-order texture parameters and exploring more predictive texture features for pulmonary infection prediction. Nevertheless, our pulmonary infection prediction model based on GLCM still has great development value for future clinical practice.

CONCLUSION

In summary, incorporating ML-based algorithms and GLCM radiomics features can facilitate timely and accurate risk stratification of pulmonary infection in patients with PHC before hepatectomy. Specifically, the RFM based on a random forest algorithm can aid clinicians in identifying high-risk patients with pulmonary infections and determining an appropriate surgical scope in a timely manner. This approach has promising applications for improving clinical outcomes and enhancing patient care.

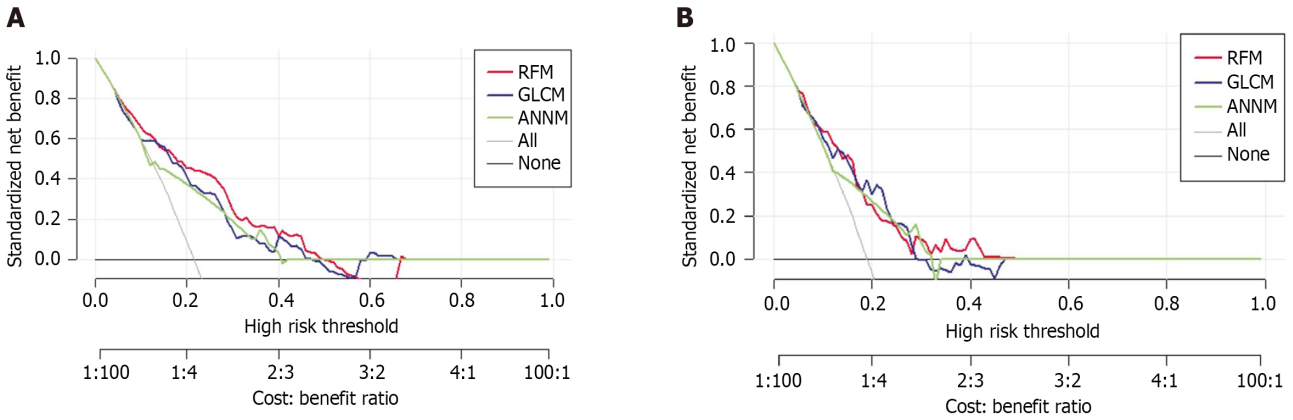

DOI: 10.4251/wjgo.v15.i7.1241

Figure 5 Prediction performance of pulmonary infection risk based on different supervised algorithm. A: Decision curve analysis for three prediction models in the training set; B: Decision curve analysis for three prediction models in the testing set. ANNM: Artificial neural network model; GLRM: Generalized linear regression model; RFM: Random forest model.

ARTICLE HIGHLIGHTS

Research background

Primary hepatic carcinoma (PHC) is a widespread malignant tumor with high incidence and mortality rates that poses a serious threat to human health worldwide. Surgical treatment remains the most effective treatment option for PHC. However, postoperative infections, including surgical site and pulmonary infections, are among the main complications following surgery.

Research motivation

To extract the texture features of radiomics of patients with PHC using a gray-level co-occurrence matrix to develop a predictive model to aid doctors in clinical decision-making and medical resource allocation for early interventions and treatments.

Research objectives

To identify the risk factors for postoperative pulmonary infection in patients with PHC and develop a prediction model to aid in postoperative management.

Research methods

Radiomics data were selected for statistical analysis, and clinical pathological parameters and imaging data were included in the screening database as candidate predictive variables. We then developed a pulmonary infection prediction model using three different models: An artificial neural network model; a random forest model (RFM); and a generalized linear regression model. Finally, we evaluated the accuracy and robustness of the prediction model using the receiver operating characteristic curve and decision curve analyses.

Research results

The RFM algorithm, in combination with sum of squares, inverse difference, mean sum, sum variance, sum entropy, and entropy, demonstrated the highest prediction efficiency in both the training and internal verification sets, with areas under the curve of 0.823 and 0.801 and 95% confidence intervals of 0.766-0.880 and 0.744-0.858, respectively. The artificial neural network model and generalized linear regression model had prediction efficiency areas under the curve of 0.734 and 0.815 and 95% confidence intervals of 0.677-0.791 and 0.766-0.864, respectively.

Research conclusions

Postoperative pulmonary infection in patients undergoing hepatectomy may be related to risk factors such as sum of squares, inverse difference, mean sum, sum variance, sum entropy, energy, and entropy. The RFM prediction model in this study based on diffusion-weighted images can better predict and estimate the risk of pulmonary infection in patients undergoing hepatectomy, providing valuable guidance for postoperative management.

Research perspectives

Identifying risk factors for postoperative pulmonary infection in patients with PHC can improve the level of prevention and clinical treatment, ultimately reducing or even avoiding the occurrence of postoperative infection complications, reducing treatment time and costs, and improving patient efficacy and prognosis. The prediction model developed in our study provides valuable guidance for clinicians in predicting the risk of pulmonary infection and effectively preventing, diagnosing, and treating postoperative infection in patients with PHC, leading to an improved patient prognosis.

ACKNOWLEDGEMENTS

We thank all R language and R package developers for their assistance as well as all R package selfless contributors used for statistical analysis and visualization in this study.

FOOTNOTES

Author contributions: Lu C and Xing ZX contributed equally to this research; Wang R was the guarantor and designed the study; Lu C, Xing ZX, Xia XG, Long ZD, Chen B, and Zhou P participated in the acquisition, analysis, and interpretation of the data and drafted the initial manuscript; Lu C, Xing ZX, and Wang R revised the article critically for important intellectual content.

Institutional review board statement: The study was reviewed and approved by the Institutional Review Board of Jingzhou Hospital (Approval No. 2023-JH019).

Informed consent statement: All personal information of the patients was encrypted to prevent leakage and exempted from informed consent by the above ethics committee.

Conflict-of-interest statement: The authors declare that they have no conflicts of interest.

Data sharing statement: No additional data are available.

STROBE statement: The authors have read the STROBE Statement—checklist of items, and the manuscript was prepared and revised according to the STROBE Statement—checklist of items.

Country/Territory of origin: China

ORCID number: Lu Chao 0000-0002-6236-1550; Rui Wang 0000-0002-6992-2287.

S-Editor: Chen YL
L-Editor: Filipodia
P-Editor: Zhang XD

REFERENCES

1 **Grandhi MS**, Kim AK, Ronnekleiv-Kelly SM, Kamel IR, Ghasebeh MA, Pawlik TM. Hepatocellular carcinoma: From diagnosis to treatment. *Surg Oncol* 2016; **25**: 74-85 [PMID: 27312032 DOI: 10.1016/j.suronc.2016.03.002]
2 **Ma Y**, Tan B, Wang S, Ren C, Zhang J, Gao Y. Influencing factors and predictive model of postoperative infection in patients with primary hepatic carcinoma. *BMC Gastroenterol* 2023; **23**: 123 [PMID: 37046206 DOI: 10.1186/s12876-023-02713-7]
3 **Endo S**, Watanabe Y, Abe Y, Shinkawa T, Tamiya S, Nishihara K, Nakano T. Hepatic inflammatory pseudotumor associated with primary biliary cholangitis and elevated alpha-fetoprotein lectin 3 fraction mimicking hepatocellular carcinoma. *Surg Case Rep* 2018; **4**: 114 [PMID: 30203247 DOI: 10.1186/s40792-018-0523-3]
4 **Chacon E**, Eman P, Dugan A, Davenport D, Marti F, Ancheta A, Gupta M, Shah M, Gedaly R. Effect of operative duration on infectious complications and mortality following hepatectomy. *HPB (Oxford)* 2019; **21**: 1727-1733 [PMID: 31229489 DOI: 10.1016/j.hpb.2019.05.001]
5 **Loncar Y**, Tartrat N, Lastennet D, Lemoine L, Vaillant JC, Savier E, Scatton O, Granger B, Eyraud D. Pulmonary infection after hepatic resection: Associated factors and impact on outcomes. *Clin Res Hepatol Gastroenterol* 2022; **46**: 101733 [PMID: 34146724 DOI: 10.1016/j.clinre.2021.101733]
6 **Wei T**, Zhang XF, Bagante F, Ratti F, Marques HP, Silva S, Soubrane O, Lam V, Poultsides GA, Popescu I, Grigorie R, Alexandrescu S, Martel G, Workneh A, Guglielmi A, Hugh T, Aldrighetti L, Endo I, Pawlik TM. Postoperative Infectious Complications Worsen Long-Term Survival After Curative-Intent Resection for Hepatocellular Carcinoma. *Ann Surg Oncol* 2022; **29**: 315-324 [PMID: 34378089 DOI: 10.1245/s10434-021-10565-2]
7 **Roth CG**, Mitchell DG. Hepatocellular carcinoma and other hepatic malignancies: MR imaging. *Radiol Clin North Am* 2014; **52**: 683-707 [PMID: 24889167 DOI: 10.1016/j.rcl.2014.02.015]
8 **Kabir T**, Syn NL, Tan ZZX, Tan HJ, Yen C, Koh YX, Kam JH, Teo JY, Lee SY, Cheow PC, Chow PKH, Chung AYF, Ooi LL, Chan CY, Goh BKP. Predictors of post-operative complications after surgical resection of hepatocellular carcinoma and their prognostic effects on outcome and survival: A propensity-score matched and structural equation modelling study. *Eur J Surg Oncol* 2020; **46**: 1756-1765 [PMID: 32345496 DOI: 10.1016/j.ejso.2020.03.219]
9 **Uddin S**, Khan A, Hossain ME, Moni MA. Comparing different supervised machine learning algorithms for disease prediction. *BMC Med Inform Decis Mak* 2019; **19**: 281 [PMID: 31864346 DOI: 10.1186/s12911-019-1004-8]
10 **Choi RY**, Coyner AS, Kalpathy-Cramer J, Chiang MF, Campbell JP. Introduction to Machine Learning, Neural Networks, and Deep Learning. *Transl Vis Sci Technol* 2020; **9**: 14 [PMID: 32704420 DOI: 10.1167/tvst.9.2.14]

11 **Ghiasi MM**, Zendehboudi S, Mohsenipour AA. Decision tree-based diagnosis of coronary artery disease: CART model. *Comput Methods Programs Biomed* 2020; **192**: 105400 [PMID: 32179311 DOI: 10.1016/j.cmpb.2020.105400]

12 **Huang S**, Cai N, Pacheco PP, Narrandes S, Wang Y, Xu W. Applications of Support Vector Machine (SVM) Learning in Cancer Genomics. *Cancer Genomics Proteomics* 2018; **15**: 41-51 [PMID: 29275361 DOI: 10.21873/cgp.20063]

13 **Alhamzawi R**, Ali HTM. The Bayesian adaptive lasso regression. *Math Biosci* 2018; **303**: 75-82 [PMID: 29920251 DOI: 10.1016/j.mbs.2018.06.004]

14 **Van Calster B**, Wynants L, Verbeek JFM, Verbakel JY, Christodoulou E, Vickers AJ, Roobol MJ, Steyerberg EW. Reporting and Interpreting Decision Curve Analysis: A Guide for Investigators. *Eur Urol* 2018; **74**: 796-804 [PMID: 30241973 DOI: 10.1016/j.eururo.2018.08.038]

15 **Hou N**, Li M, He L, Xie B, Wang L, Zhang R, Yu Y, Sun X, Pan Z, Wang K. Predicting 30-days mortality for MIMIC-III patients with sepsis-3: a machine learning approach using XGboost. *J Transl Med* 2020; **18**: 462 [PMID: 33287854 DOI: 10.1186/s12967-020-02620-5]

16 **Fay MP**, Malinovsky Y. Confidence intervals of the Mann-Whitney parameter that are compatible with the Wilcoxon-Mann-Whitney test. *Stat Med* 2018; **37**: 3991-4006 [PMID: 29984411 DOI: 10.1002/sim.7890]

17 **Vibert E**, Schwartz M, Olthoff KM. Advances in resection and transplantation for hepatocellular carcinoma. *J Hepatol* 2020; **72**: 262-276 [PMID: 31954491 DOI: 10.1016/j.jhep.2019.11.017]

18 **Hu Q**, Sun YS, Zhu KF. Minimally invasive *vs* open primary liver resections for hepatocellular carcinoma. *J Surg Oncol* 2021; **124**: 910-912 [PMID: 34216388 DOI: 10.1002/jso.26592]

19 **Kaibori M**, Ishizaki M, Matsui K, Kwon AH. Postoperative infectious and non-infectious complications after hepatectomy for hepatocellular carcinoma. *Hepatogastroenterology* 2011; **58**: 1747-1756 [PMID: 22086698 DOI: 10.5754/hge10533]

20 **Kwon JB**, Park K, Kim YD, Seo JH, Moon SW, Cho DG, Kim YW, Kim DG, Yoon SK, Lim HW. Clinical outcome after pulmonary metastasectomy from primary hepatocellular carcinoma: analysis of prognostic factors. *World J Gastroenterol* 2008; **14**: 5717-5722 [PMID: 18837090 DOI: 10.3748/wjg.14.5717]

21 **Zhao Y**, Jin Y, Wu Y. Postoperative infectious complications after liver resection for hepatocellular carcinoma. *J Cancer Res Ther* 2016; **12**: C268-C270 [PMID: 28230033 DOI: 10.4103/0973-1482.200754]

22 **Ruan DY**, Lin ZX, Li Y, Jiang N, Li X, Wu DH, Wang TT, Chen J, Lin Q, Wu XY. Poor oncologic outcomes of hepatocellular carcinoma patients with intra-abdominal infection after hepatectomy. *World J Gastroenterol* 2015; **21**: 5598-5606 [PMID: 25987785 DOI: 10.3748/wjg.v21.i18.5598]

23 **Schaapman JJ**, Tushuizen ME, Coenraad MJ, Lamb HJ. Multiparametric MRI in Patients With Nonalcoholic Fatty Liver Disease. *J Magn Reson Imaging* 2021; **53**: 1623-1631 [PMID: 32822095 DOI: 10.1002/jmri.27292]

24 **Donato H**, França M, Candelária I, Caseiro-Alves F. Liver MRI: From basic protocol to advanced techniques. *Eur J Radiol* 2017; **93**: 30-39 [PMID: 28668428 DOI: 10.1016/j.ejrad.2017.05.028]

25 **Zerunian M**, Pucciarelli F, Masci B, Siciliano F, Polici M, Bracci B, Guido G, Polidori T, De Santis D, Laghi A, Caruso D. Updates on Quantitative MRI of Diffuse Liver Disease: A Narrative Review. *Biomed Res Int* 2022; **2022**: 1147111 [PMID: 36619303 DOI: 10.1155/2022/1147111]

26 **Shamsil A**, Naish MD, Patel RV. Texture-based Intraoperative Image Guidance for Tumor Localization in Minimally Invasive Surgery. *Annu Int Conf IEEE Eng Med Biol Soc* 2021; **2021**: 3526-3530 [PMID: 34892000 DOI: 10.1109/EMBC46164.2021.9629758]

27 **Litvin AA**, Burkin DA, Kropinov AA, Paramzin FN. Radiomics and Digital Image Texture Analysis in Oncology (Review). *Sovrem Tekhnologii Med* 2021; **13**: 97-104 [PMID: 34513082 DOI: 10.17691/stm2021.13.2.11]

28 **Marusyk A**, Polyak K. Tumor heterogeneity: causes and consequences. *Biochim Biophys Acta* 2010; **1805**: 105-117 [PMID: 19931353 DOI: 10.1016/j.bbcan.2009.11.002]

29 **de Oliveira ME**, Neto LM. Directional entropy based model for diffusivity-driven tumor growth. *Math Biosci Eng* 2016; **13**: 333-341 [PMID: 27105991 DOI: 10.3934/mbe.2015005]

30 **Dercle L**, Ammari S, Bateson M, Durand PB, Haspinger E, Massard C, Jaudet C, Varga A, Deutsch E, Soria JC, Ferté C. Limits of radiomic-based entropy as a surrogate of tumor heterogeneity: ROI-area, acquisition protocol and tissue site exert substantial influence. *Sci Rep* 2017; **7**: 7952 [PMID: 28801575 DOI: 10.1038/s41598-017-08310-5]

World Journal of Gastrointestinal Oncology

Submit a Manuscript: https://www.f6publishing.com

World J Gastrointest Oncol 2023 July 15; 15(7): 1253-1261

DOI: 10.4251/wjgo.v15.i7.1253

ISSN 1948-5204 (online)

ORIGINAL ARTICLE

Retrospective Study

Clinical association between coagulation indicators and bone metastasis in patients with gastric cancer

Xuan Wang, Jing-Ya Wang, Min Chen, Juan Ren, Xin Zhang

Specialty type: Oncology

Provenance and peer review: Unsolicited article; Externally peer reviewed.

Peer-review model: Single blind

Peer-review report's scientific quality classification

Grade A (Excellent): 0
Grade B (Very good): B
Grade C (Good): C
Grade D (Fair): 0
Grade E (Poor): 0

P-Reviewer: Seretis C, Greece; Tanabe S, Japan

Received: February 6, 2023
Peer-review started: February 6, 2023
First decision: March 15, 2023
Revised: March 16, 2023
Accepted: May 6, 2023
Article in press: May 6, 2023
Published online: July 15, 2023

Xuan Wang, Min Chen, Juan Ren, Department of Radiotherapy and Oncology, The First Affiliated Hospital of Xi'an Jiaotong University, Xi'an 710061, Shaanxi Province, China

Jing-Ya Wang, Department of Gastroenterology, Xi'an Children's Hospital, Shaanxi Research Institute for Pediatric Diseases, The Affiliated Children's Hospital of Xi'an Jiaotong University and National Regional Medical Center for Children (Northwest), Xi'an 710003, Shaanxi Province, China

Xin Zhang, Department of Surgical Oncology, The First Affiliated Hospital of Xi'an Jiaotong University, Xi'an 710061, Shaanxi Province, China

Corresponding author: Xin Zhang, MD, Doctor, Department of Surgical Oncology, The First Affiliated Hospital of Xi'an Jiaotong University, No. 277 West Yanta Road, Xi'an 710061, Shaanxi Province, China. zhangxinzh@stu.xjtu.edu.cn

Abstract

BACKGROUND

Bones are one of the most common target organs for cancer metastasis. Early evaluation of bone metastasis (BM) status is clinically significant. Cancer patients often experience a hypercoagulable state.

AIM

To evaluate the correlation between coagulation indicators and the burden of BM in gastric cancer (GC).

METHODS

We conducted a single-center retrospective study and enrolled 454 patients. Clinical information including routine blood examination and coagulation markers were collected before any treatment. Patients were grouped according to the status of BM. Receiver operating characteristic curves were used to assess diagnostic performance and determine the optimal cutoff values of the above indicators. Cutoff values, sensitivity and specificity were based on the maximum Youden index. Univariate and multivariate logistic regression analyses were used to evaluate the relationships between biomarkers and BM.

RESULTS

Of the 454 enrolled patients, 191 patients were diagnosed with BM. The receiver operating characteristic curve analysis suggested that prothrombin time (PT)

[cutoff: 13.25; sensitivity: 0.651; specificity: 0.709; area under receiver operating characteristic curve (AUC) = 0.738], activated partial thromboplastin time (aPTT) (cutoff: 35.15; sensitivity: 0.640; specificity: 0.640; AUC = 0.678) and fibrin degradation products (FDP) (cutoff: 2.75; sensitivity: 0.668; specificity: 0.801; AUC = 0.768) act as novel predictors for BM. Based on multivariate logistic regression analysis, the results showed the independent correlation between PT [odds ratio (OR): 3.16; 95% confidence interval (CI): 1.612-6.194; P = 0.001], aPTT (OR: 2.234; 95%CI: 1.157-4.313; P = 0.017) and FDP (OR: 3.17; 95%CI: 1.637-6.139; P = 0.001) and BM in patients with GC. Moreover, age, carcinoembryonic antigen, erythrocyte and globulin were found to be significantly associated with BM.

CONCLUSION

Coagulation markers, namely PT, aPTT and FDP, might be potential predictors for screening BM in patients with GC.

Key Words: Gastric cancer; Bone metastasis; Coagulation markers; Risk factor; Activated partial thromboplastin time; Prothrombin time; Fibrin degradation products

Core Tip: Bones are one of the most common organs involved in cancer metastasis. Early evaluation of bone metastasis (BM) status is clinically significant. In this study, we confirmed that coagulation markers (prothrombin time, activated partial thromboplastin time and fibrin degradation products), carcinoembryonic antigen and globulin are independent risk factors for BM in patients with gastric cancer. Patients with these risk factors should be screened early for BM, which may significantly decrease mortality rates related to BM in patients with gastric cancer.

Citation: Wang X, Wang JY, Chen M, Ren J, Zhang X. Clinical association between coagulation indicators and bone metastasis in patients with gastric cancer. *World J Gastrointest Oncol* 2023; 15(7): 1253-1261
URL: https://www.wjgnet.com/1948-5204/full/v15/i7/1253.htm
DOI: https://dx.doi.org/10.4251/wjgo.v15.i7.1253

INTRODUCTION

Gastric cancer (GC) is one of the most malignant neoplasms worldwide. According to GLOBOCAN's 2020 statistics, there were approximately 1.089 million new GC cases and 769000 GC deaths worldwide. GC has the fifth highest incidence rate and the fourth highest mortality rate of all cancers[1].

Common metastatic sites of GC are the liver, lungs, and peritoneum. Bone metastasis (BM) is relatively rare, ranging from 0.9% to 3.8%[2,3]. However, this incidence has been as high as 13.4% in autopsies[4]. The majority of patients with BM have several symptoms including bone pain, mobility disorders, hypercalcemia, pathological fractures and spinal cord compression, which seriously affects their quality of life. Unfortunately, BM is often underdiagnosed because sensitive diagnostic tests are recommended only after the onset of clinical symptoms. In addition, the median survival time for patients with GC-related BM is only 3-6 mo[3,5].

Imaging is currently the most important diagnostic method for BM. Elevated serum tumor markers such as carcinoembryonic antigen (CEA), carbohydrate antigen 19-9 (CA19-9) and bone-associated alkaline phosphatase (ALP) provide additional diagnostic significance[6,7]. Computed tomography (CT) or enhanced CT is not a routine test for BM screening. It is only recommended when the patient is symptomatic, which leads to asymptomatic BM in patients with GC being largely undetected[4]. Previous studies have found that fibrinogen, activated partial thromboplastin time (aPTT) and D-dimer are independent risk factors for BM in non-small cell lung cancer[8]. However, there has been little research on multiple risk factors, such as a combination of clinical data and laboratory indicators, for BM in patients with GC. This study explored risk factors for BM from GC through multivariate analysis based on laboratory tests.

MATERIALS AND METHODS

Patients

We retrospectively collected data on patients diagnosed with GC at the First Affiliated Hospital of Xi'an Jiaotong University from January 2014 to January 2019. The inclusion criteria were no distant metastases or BM. Exclusion criteria included: (1) A history of thrombotic disease, anticoagulant therapy or antiplatelet therapy; (2) Acute infection or disseminated intravascular coagulation; and (3) Lack of pretreatment laboratory data. In total, 454 patients were enrolled in this study. Data evaluated included sex, age at diagnosis, preoperative routine blood examination (erythrocyte, hemoglobin, leukocyte, neutrophil, lymphocyte, monocyte and platelet), glucose, albumin, globulin, CEA, CA19-9, CA72-4 and

coagulation markers including prothrombin time (PT), prothrombin ratio (PTR), international normalized ratio (INR), aPTT, thrombin time (TT), fibrinogen, D-dimer and fibrin degradation products (FDP). Laboratory indicators were collected before any treatment. Blood parameters were those closest to the time of treatment. This study was approved by the Ethics Committee of First Affiliated Hospital of Xi'an Jiaotong University.

Statistical analysis

Cases were grouped according to BM status. Categorical variables were expressed as frequency (percentage) and compared using the χ^2 test. Continuous variables were expressed as mean and standard deviation or median and interquartile range depending on whether they were normally distributed. Normally distributed continuous variables were compared using the Student's *t*-test. Continuous variables that were not normally distributed were compared using the Mann-Whitney *U* test. The parameters with significant differences between the control group and the BM group were selected for receiver operating characteristic (ROC) analysis. The optimal cutoff values for parameters were obtained by ROC analyses based on the Youden index. The prediction probability (PP) of combined ROC curve was obtained by binary logistic regression. Multivariate logistic regression was performed to assess the relationship between laboratory variables and BM status. Statistical analyses and data plotting were performed with SPSS Statistics (version 20.0; IBM Corp., Armonk, NY, United States). A two-sided *P* value < 0.05 was considered statistically significant.

RESULTS

Patient characteristics

We collected data from 454 patients with GC and grouped them according to the method described previously. As shown in Table 1, there were 191 cases in the BM group. The median age of patients was 61 years, and males comprised the majority of patients (73.8%). Patients with BM had higher levels of GC markers (CEA, CA19-9 and CA72-4), neutrophils, glucose, globulin and most coagulation parameters (PT, PTR, INR, aPTT, fibrinogen, D-dimer and FDP) (all $P < 0.001$). Moreover, erythrocyte, lymphocyte and platelet levels were significantly lower in the BM group (all $P < 0.05$) (Table 1).

BM in patients with GC can be predicted by novel tumor markers PT, aPTT and FDP

We performed ROC analysis to assess the efficacy of parameters to predict BM in patients with GC and obtained a series of cutoff values. The optimal cutoff values (sensitivity and specificity) were: age, 59.5 (54.6% and 58.3%); CEA, 3.97 (64.9% and 71.1%); CA19-9, 12.81 (65.5% and 64.9%); CA72-4, 6.71 (51.8% and 74.7%); erythrocyte level, 4.43 (42.3% and 79.7%); hemoglobin, 133.5 (42.7% and 75.9%); leukocyte level, 6.28 (49.2% and 68.5%); neutrophil level, 4.23 (48.4% and 74.9%); lymphocyte level, 1.43 (55.2% and 64.2%); platelet level, 167.5 (73.1% and 44.9%); glucose, 4.82 (52.4% and 74.8%); globulin, 28.75 (50.0% and 81.4%); PT, 13.25 (65.1% and 70.9%); PTR, 1.09 (40.7% and 78.5%); INR, 1.1 (37.6% and 81.9%); aPTT, 35.15 (64.0% and 64.0%); TT, 15.95 (69.7% and 48.7%); fibrinogen, 4.06 (42.3% and 82.0%); D-dimer, 1.03 (69.0% and 72.8%); FDP, 2.75 (66.8% and 80.1%) (Figure 1, Supplementary Figures 1 and 2). The area under ROC curves and 95% confidence intervals (CI) were: CEA, 0.694 (0.639-0.748); CA19-9, 0.673 (0.617-0.729); CA72-4, 0.624 (0.560-0.688); PT, 0.738 (0.692-0.784); aPTT, 0.678 (0.629-0.727); and FDP, 0.768 (0.722-0.814) (Table 2, Figure 1).

Parameters were grouped by aforementioned cutoff values. Multivariate logistic regression analysis showed that higher PT [odds ratio (OR): 3.16; 95%CI: 1.612-6.194; $P = 0.001$), higher aPTT (OR: 2.234; 95%CI: 1.157-4.313; $P = 0.017$) and elevated FDP (OR: 3.17; 95%CI: 1.637-6.139; $P = 0.001$) were independent risk factors for BM in patients with GC. In addition, higher CEA and globulin as well as lower age and red blood cell count were also independent risk factors for BM with an OR (95%CI) of 2.847 (1.496-5.418), 4.253 (2.114-8.558), 0.392 (0.203-0.756), and 0.482 (0.24-0.966), respectively (all $P < 0.05$) (Table 3). The area under ROC curve (95%CI) of PP was 0.879 (0.841-0.917) with a sensitivity of 0.831 and a specificity of 0.806 (Table 2, Figure 1).

DISCUSSION

BM is a common complication of certain cancers, including breast cancer and prostate cancer[9], whereas BM due to GC is less frequent[10]. The common metastatic sites of GC are the liver, lungs and peritoneum. Most patients with BM due to GC have multiple metastases, and most metastases are difficult to resect surgically[11]. Once tumors have metastasized to the bone, they are virtually incurable and cause severe morbidity before the patient dies. BM leads to pain, pathological fractures, nerve compression syndrome and hypercalcemia. According to relevant research reports, the proportion of patients suspected of BM due to GC found by bone scan screening was as high as 25.0%-45.3%[12].

Several factors have been shown to have predictive value for BM due to GC. BM is a dynamic process of osteolytic and osteogenesis mediated by osteoclasts that disrupts normal bone homeostasis. Bone ALP is an indicator of osteoblast metabolism and a relatively specific osteogenic marker, which has predictive value in patients with BM due to GC[6]. Bone screening is recommended for cancer types with a high incidence of BM, such as prostate cancer, breast cancer, small cell lung cancer and renal cell carcinoma. A variety of imaging studies are available, including plain X-rays, bone scintigraphy, CT scans, magnetic resonance imaging, positron emission tomography and positron emission tomography/CT, to assess bone involvement. However, bone screening has not been routinely recommended by the Chinese Society of Clinical Oncology for patients with GC[13]. Excessive X-rays and CT imaging are expensive and put patients at risk of unnecessary radiation exposure and/or invasive procedures due to false positive results. Therefore, it is necessary to

Table 1 Demographic and baseline characteristics of patients

Characteristic	Overall, *n* = 454	No bone metastasis, *n* = 263	Bone metastasis, *n* = 191	*P* value
Male sex	335 (73.8)	196 (74.5)	139 (72.8)	0.676
Age, yr	59 (50-67)	61 (51-67)	57 (49-66)	0.046
CEA, ng/mL	3.53 (1.73-14.65)	2.43 (1.35-4.89)	5.29 (2.90-38.31)	< 0.001
CA19-9, U/mL	12.25 (6.30-46.88)	9.89 (4.92-20.20)	22.62 (9.73-113.35)	< 0.001
CA72-4, U/mL	3.39 (1.60-12.00)	2.58 (1.57-6.78)	7.09 (1.96-21.68)	< 0.001
Erythrocyte, × 10^{12}/L	4.14 (3.65-4.57)	4.27 (3.78-4.68)	4.00 (3.50-4.39)	< 0.001
Hemoglobin, g/L	124 (106-139)	127 (109-143)	119 (103-133)	< 0.001
Leukocyte, × 10^{9}/L	5.69 (4.51-7.12)	5.51 (4.43-6.76)	6.20 (4.69-7.86)	0.002
Neutrophil, × 10^{9}/L	3.54 (2.64-4.88)	3.23 (2.51-4.33)	4.04 (2.83-5.97)	< 0.001
Lymphocyte, × 10^{9}/L	1.37 (1.08-1.81)	1.48 (1.12-1.95)	1.30 (1.02-1.63)	0.001
Platelet, × 10^{9}/L	196 (150-253)	204 (160-260)	180 (140-235)	0.001
Monocyte, × 10^{9}/L	0.41 (0.30-0.54)	0.42 (0.31-0.54)	0.40 (0.30-0.55)	0.713
Glucose, mmol/L	4.54 (4.17-5.07)	4.40 (4.04-4.83)	4.84 (4.39-5.55)	< 0.001
Albumin, g/L	38.11 ± 4.96	37.80 ± 4.71	38.55 ± 5.26	0.113
Globulin, g/L	26.4 (23.7-29.8)	25.5 (22.8-28.2)	28.8 (25.1-31.6)	< 0.001
PT, s	13.1 (12.5-13.8)	12.8 (12.3-13.4)	13.5 (13.0-14.4)	< 0.001
PTR	1.05 (0.99-1.10)	1.03 (0.98-1.08)	1.06 (1.01-1.12)	< 0.001
INR	1.05 (0.99-1.10)	1.03 (0.98-1.08)	1.07 (1.01-1.13)	< 0.001
aPTT, s	35.0 (31.5-38.1)	33.5 (30.8-36.8)	36.3 (33.7-39.1)	< 0.001
TT, s	16.3 (15.6-16.9)	16.4 (15.7-17.0)	16.0 (15.3-16.8)	< 0.001
FIB, g/L	3.32 (2.76-4.16)	3.21 (2.62-3.82)	3.63 (2.93-4.59)	< 0.001
D-dimer, mg/L	0.9 (0.3-2.5)	0.5 (0.1-1.1)	2.0 (0.8-6.6)	< 0.001
FDP, mg/L	1.9 (0.9-4.9)	1.2 (0.7-2.5)	4.5 (1.7-16.2)	< 0.001

Data are shown as number of cases and percentage or median and interquartile range. aPTT: Activated partial prothrombin time; CA19-9: Carbohydrate antigen 19-9; CA72-4: Carbohydrate antigen 72-4; CEA: Carcinoembryonic antigen; FDP: Fibrin degradation products; FIB: Fibrinogen; INR: International normalized ratio; PT: Prothrombin time; PTR: Prothrombin ratio; TT: Thrombin time.

evaluate BM through a combination of imaging and analyzing hematological parameters and patient symptoms.

In this study, we screened possible risk factors for BM by comparing baseline data between the control group and the BM group. Through multivariate logistic regression analysis of candidate tumor markers, routine blood counts, coagulation indicators, albumin and globulin, we found that elevated CEA, globulin, PT, aPTT and FDP and younger age and lower red blood cells were independent risk factors for BM due to GC. CEA is a classic GC marker and has been shown to be a risk factor for distant metastasis and lymph node metastasis[14,15]. Globulin was identified as an independent predictor of occult metastasis in the neck of oral squamous cell carcinoma[16]. In GC, a high level of globulin is a valuable predictor of tumor progression[17].

Tumors are often accompanied by a state of coagulation activation[18]. Fibrinogen, aPTT and D-dimer were found to be risk factors for BM in non-small cell lung carcinoma patients[19]. Our study confirmed that PT, aPTT and FDP, as coagulation indicators, are independent predictors of BM in GC patients. In fact, tumor cells often express tissue factor or other procoagulants that can initiate coagulation[20]. There is considerable evidence that inhibiting coagulation can inhibit tumor metastasis[21,22]. BM due to GC can develop regardless of the tumor stage, although the proportion of patients with stage IV GC with BM exceeds the proportion of patients with stages I-III combined. It was found that even after radical gastrectomy, BM recurred in 1.8% of patients[23]. This indicates that the risk of BM should be considered when these indicators are abnormally elevated in patients with GC, especially when they are higher than the cutoff values in Table 2. Furthermore, the cutoff values of the BM risk factors indicated in this study are different from their respective upper limits of clinical normality. In other words, elevated coagulation indicators may indicate BM risk even within the range of clinically normal reference values.

A hypercoagulable state represents a heterogeneous group of disorders that cover a variety of risk factors such as thrombosis, obesity, pregnancy, cancer and its treatment, antiphospholipid antibody syndrome, heparin-induced thrombocytopenia and myeloproliferative disorders[24]. This suggests that in order to improve the specificity of

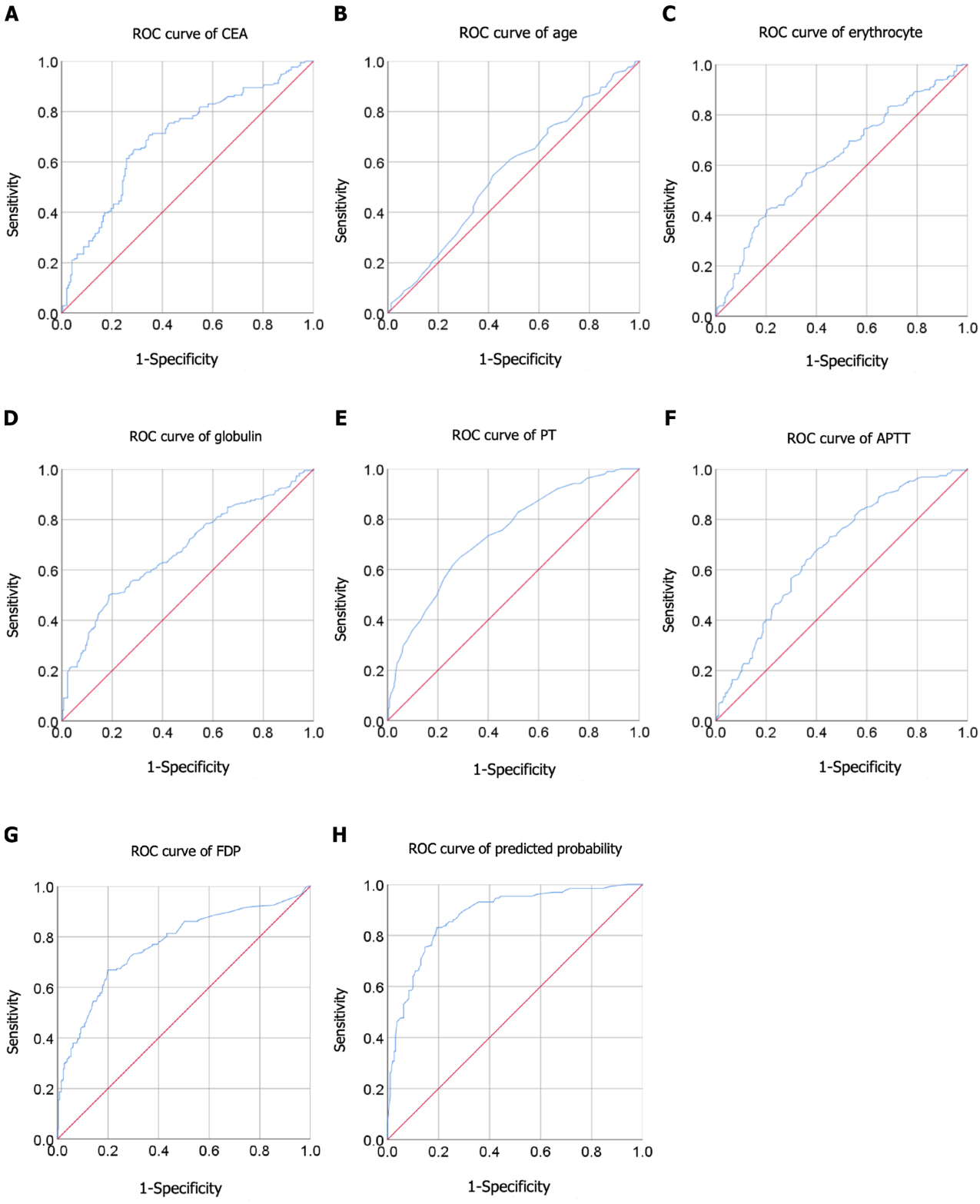

DOI: 10.4251/wjgo.v15.i7.1253

Figure 1 Receiver operating characteristic analysis for the prediction of bone metastasis. A-H: Area under the receiver operating characteristic (ROC) curve analysis indicated the diagnostic power of carcinoembryonic antigen (CEA) (A), age (B), erythrocyte level (C), globulin (D), prothrombin time (PT) (E), activated partial thromboplastin time (APTT) (F), fibrin degradation product (FDP) (G) and prediction probability (H) for bone metastasis. Prediction probability was obtained by binary logistic regression of CEA, age, erythrocyte level, globulin, PT, APTT and FDP. The area under the ROC curve of the prediction probability was 0.879 with a 95% confidence interval of 0.841-0.917. ROC: Receiver operating characteristic; FDP: Fibrin degradation product; PT: Prothrombin time; APTT: Activated partial thromboplastin time; CEA: Carcinoembryonic antigen.

coagulation factors in assessing BM due to GC, other factors that may affect their levels need to be excluded. Although we discovered independent risk factors for BM due to GC, we did not explore whether they were specific to BM or due to other metastatic sites' GC.

Table 2 Area under the receiver operating characteristic curves and cutoff values of diagnostic indicators at the maximum Youden index for bone metastasis

Parameter	AUC	95%CI	Cutoff	Sen	Spe	Youden index	PPV	NPV	*P* value
Age	0.558	0.501-0.616	59.5	0.546	0.583	0.129	0.433	0.546	0.046
CEA	0.694	0.639-0.748	3.97	0.649	0.711	0.36	0.665	0.711	< 0.001
CA19-9	0.673	0.617-0.729	12.81	0.655	0.649	0.304	0.614	0.649	< 0.001
CA72-4	0.624	0.560-0.688	6.71	0.518	0.747	0.265	0.603	0.747	< 0.001
Erythrocyte	0.623	0.571-0.675	4.43	0.423	0.797	0.220	0.498	0.423	< 0.001
Hemoglobin	0.599	0.547-0.651	133.50	0.427	0.759	0.186	0.488	0.427	< 0.001
Leukocyte	0.587	0.532-0.641	6.28	0.492	0.685	0.177	0.529	0.685	0.002
Neutrophil	0.63	0.576-0.683	4.23	0.484	0.749	0.233	0.581	0.749	< 0.001
Lymphocyte	0.591	0.539-0.644	1.43	0.552	0.642	0.194	0.508	0.552	0.001
Platelet	0.591	0.538-0.645	167.50	0.731	0.449	0.180	0.545	0.731	0.001
Glucose	0.664	0.613-0.716	4.82	0.524	0.748	0.272	0.595	0.748	< 0.001
Globulin	0.675	0.624-0.726	28.75	0.500	0.814	0.314	0.655	0.814	< 0.001
PT	0.738	0.692-0.784	13.25	0.651	0.709	0.360	0.618	0.709	< 0.001
PTR	0.622	0.570-0.675	1.09	0.407	0.785	0.193	0.579	0.785	< 0.001
INR	0.627	0.574-0.680	1.10	0.376	0.819	0.195	0.602	0.819	< 0.001
aPTT	0.678	0.629-0.727	35.15	0.640	0.640	0.280	0.563	0.640	< 0.001
TT	0.598	0.545-0.652	15.95	0.697	0.487	0.184	0.538	0.816	< 0.001
FIB	0.616	0.562-0.669	4.06	0.423	0.820	0.243	0.630	0.820	< 0.001
D-dimer	0.756	0.710-0.801	1.03	0.690	0.728	0.418	0.645	0.728	< 0.001
FDP	0.768	0.722-0.814	2.75	0.668	0.801	0.469	0.706	0.801	< 0.001
PP	0.879	0.841-0.917	0.364	0.831	0.806	0.637	0.745	0.806	< 0.001

aPTT: Activated partial prothrombin time; AUC: Area under receiver operating characteristic curve; CA19-9: Carbohydrate antigen 19-9; CA72-4: Carbohydrate antigen 72-4; CEA: Carcinoembryonic antigen; CI: Confidence interval; FDP: Fibrin degradation products; FIB: Fibrinogen; INR: International normalized ratio; NPV: Negative predictive value; PP: Prediction probability; PPV: Positive predictive value; PT: Prothrombin time; PTR: Prothrombin ratio; Sen: Sensitivity; Spe: Specificity; TT: Thrombin time.

Because we retrospectively collected data from patients with GC, bone-associated ALP was not routinely tested and was not included in the analysis. There is evidence that tumor-induced hypercoagulability and fibrin formation are required for tumor angiogenesis, metastasis and invasion because cross-linked fibrin in the extracellular matrix may be the framework for tumor cell migration during invasion. Based on this, circulating tumor cells and micrometastases are considered early events in the process of tumor cell metastasis[25]. Bone ALP is a specific marker of osteoblast metabolism and is significantly associated with the presence and degree of bone involvement in metastatic tumors. Bone-associated ALP has been shown to be an important predictor of BM in patients with breast and prostate cancer[26]. More than half of patients with BM due to GC have elevated ALP and tumor markers[3,6]. Coagulation indexes and bone ALP reflect the two stages of tumor hematogenous metastasis and BM, respectively. In this study, we demonstrated that the PP obtained by combination ROC had a higher diagnostic efficacy than any single risk factor. The combination of coagulation indexes, globulins, tumor markers and bone ALP may greatly improve the diagnostic efficiency of BM due to GC.

CONCLUSION

Overall, coagulation markers (PT, aPTT and FDP), CEA and globulin are independent risk factors for BM due to GC. Patients with these risk factors should be screened for BM early, which could lead to significantly decreased mortality in patients with GC and BM.

Table 3 Univariate and multivariate binary logistic regression analyses of variables for bone metastasis

	Univariate analysis			Multivariate analysis		
Parameter	Odds ratio	95%CI	*P* value	Odds ratio	95%CI	*P* value
Age	0.594	0.398-0.887	0.011	0.392	0.203-0.756	0.005
CEA	4.559	2.931-7.090	< 0.001	2.847	1.496-5.418	0.001
CA19-9	3.511	2.271-5.429	< 0.001			0.352
CA72-4	3.176	1.995-5.056	< 0.001			0.086
Erythrocyte	0.348	0.226-0.536	< 0.001	0.482	0.240-0.966	0.040
Hemoglobin	0.425	0.281-0.645	< 0.001			0.852
Leukocyte	2.102	1.426-3.099	< 0.001			0.693
Neutrophil	2.798	1.872-4.183	< 0.001			0.601
Lymphocyte	0.453	0.308-0.667	< 0.001			0.575
Platelet	0.452	0.304-0.672	< 0.001			0.066
Glucose	3.273	2.191-4.890	< 0.001			0.087
Globulin	4.367	2.861-6.667	< 0.001	4.253	2.114-8.558	< 0.001
PT	4.536	3.038-6.774	< 0.001	3.16	1.612-6.194	0.001
PTR	2.517	1.663-3.808	< 0.001			0.145
INR	2.727	1.771-4.199	< 0.001			0.072
aPTT	3.161	2.140-4.669	< 0.001	2.234	1.157-4.313	0.017
TT	0.535	0.344-0.833	0.006			0.842
FIB	3.342	2.179-5.125	< 0.001			0.193
D-dimer	5.952	3.939-8.993	< 0.001			0.956
FDP	8.103	5.271-12.457	< 0.001	3.17	1.637-6.139	0.001

The reference of parameters was set to be less than their cutoff values. aPTT: Activated partial prothrombin time; CA19-9: Carbohydrate antigen 19-9; CA72-4: Carbohydrate antigen 72-4; CEA: Carcinoembryonic antigen; CI: Confidence interval; FDP: Fibrin degradation products; FIB: Fibrinogen; INR: International normalized ratio; PT: Prothrombin time; PTR: Prothrombin ratio; TT: Thrombin time.

ARTICLE HIGHLIGHTS

Research background

Bones are one of the most common targets for cancer metastasis. However, bone metastasis (BM) is often underdiagnosed because sensitive diagnostic imaging methods are recommended only after the onset of clinical symptoms. Patients with gastric cancer (GC), especially in advanced stages, are often in a hypercoagulable state.

Research motivation

The purpose of this study was to explore the predictive value of blood indicators on the risk of BM due to GC and to improve the diagnostic efficacy of BM due to GC by screening effective risk factors.

Research objectives

The purpose of this study was to explore whether coagulation indicators can be used as independent risk factors for predicting BM due to GC, thus promoting the early diagnosis and treatment of BM.

Research methods

We conducted a retrospective study and enrolled 454 patients in this study. Receiver operating characteristic (ROC) curves were used to assess diagnostic performance. Univariate and multivariate logistic regression analyses were used to evaluate the relationship between biomarkers and BM.

Research results

ROC curve analysis indicated that coagulation markers have similar or better diagnostic efficacy than traditional GC markers. Based on multivariate logistic regression analysis, prothrombin time, activated partial thromboplastin time and fibrin degradation products were independently associated with BM due to GC. Moreover, age, carcinoembryonic

antigen, erythrocyte level and globulin were found to be risk factors of BM. Combining these indicators could improve the effectiveness of diagnosing BM.

Research conclusions

Coagulation markers (prothrombin time, activated partial thromboplastin time and fibrin degradation products), carcinoembryonic antigen and globulin were independent risk factors for BM due to GC. Patients with these risk factors should be screened early to detect BM due to GC and prevent bone-related events.

Research perspectives

Future research will explore the relationship and molecular mechanism between coagulation and tumor metastasis and explore new targets to block the process of tumor metastasis.

FOOTNOTES

Author contributions: Wang X, Ren J and Zhang X designed the research study; Wang X, Wang JY and Chen M performed the research; Wang X analyzed the data and wrote the manuscript; all authors read and approve the final manuscript.

Institutional review board statement: This study was approved by the Ethics Committee of First Affiliated Hospital of Xi'an Jiaotong University (Approval No. 2015-046).

Informed consent statement: Patients were not required to give informed consent to the study because the analysis used anonymous clinical data that were obtained after each patient agreed to treatment by written consent.

Conflict-of-interest statement: The authors declare that no competing interests exist.

Data sharing statement: Dataset available from the corresponding author at zhangxinzh@stu.xjtu.edu.cn

Country/Territory of origin: China

ORCID number: Xin Zhang 0000-0002-6206-4152.

S-Editor: Yan JP
L-Editor: A
P-Editor: Zhang XD

REFERENCES

1 **Sung H**, Ferlay J, Siegel RL, Laversanne M, Soerjomataram I, Jemal A, Bray F. Global Cancer Statistics 2020: GLOBOCAN Estimates of Incidence and Mortality Worldwide for 36 Cancers in 185 Countries. *CA Cancer J Clin* 2021; **71**: 209-249 [PMID: 33538338 DOI: 10.3322/caac.21660]

2 **Mikami J**, Kimura Y, Makari Y, Fujita J, Kishimoto T, Sawada G, Nakahira S, Nakata K, Tsujie M, Ohzato H. Clinical outcomes and prognostic factors for gastric cancer patients with bone metastasis. *World J Surg Oncol* 2017; **15**: 8 [PMID: 28061855 DOI: 10.1186/s12957-016-1091-2]

3 **Imura Y**, Tateiwa D, Sugimoto N, Inoue A, Wakamatsu T, Outani H, Tanaka T, Tamiya H, Yagi T, Naka N, Okawa S, Tabuchi T, Takenaka S. Prognostic factors and skeletal-related events in patients with bone metastasis from gastric cancer. *Mol Clin Oncol* 2020; **13**: 31 [PMID: 32765878 DOI: 10.3892/mco.2020.2101]

4 **Turkoz FP**, Solak M, Kilickap S, Ulas A, Esbah O, Oksuzoglu B, Yalcin S. Bone metastasis from gastric cancer: the incidence, clinicopathological features, and influence on survival. *J Gastric Cancer* 2014; **14**: 164-172 [PMID: 25328761 DOI: 10.5230/jgc.2014.14.3.164]

5 **Qiu MZ**, Shi SM, Chen ZH, Yu HE, Sheng H, Jin Y, Wang DS, Wang FH, Li YH, Xie D, Zhou ZW, Yang DJ, Xu RH. Frequency and clinicopathological features of metastasis to liver, lung, bone, and brain from gastric cancer: A SEER-based study. *Cancer Med* 2018; **7**: 3662-3672 [PMID: 29984918 DOI: 10.1002/cam4.1661]

6 **Lim SM**, Kim YN, Park KH, Kang B, Chon HJ, Kim C, Kim JH, Rha SY. Bone alkaline phosphatase as a surrogate marker of bone metastasis in gastric cancer patients. *BMC Cancer* 2016; **16**: 385 [PMID: 27377907 DOI: 10.1186/s12885-016-2415-x]

7 **Wu C**, Lin X, Li Z, Chen Z, Xie W, Zhang X, Wang X. A Diagnostic Nomogram Based on (18)F-FDG PET/CT for Bone Metastasis of Gastric Cancer. *Front Cell Dev Biol* 2021; **9**: 783466 [PMID: 34970546 DOI: 10.3389/fcell.2021.783466]

8 **Li Y**, Xu C, Yu Q. Risk factor analysis of bone metastasis in patients with non-small cell lung cancer. *Am J Transl Res* 2022; **14**: 6696-6702 [PMID: 36247263]

9 **Yin JJ**, Pollock CB, Kelly K. Mechanisms of cancer metastasis to the bone. *Cell Res* 2005; **15**: 57-62 [PMID: 15686629 DOI:

10.1038/sj.cr.7290266]

10 **Xiaobin C**, Zhaojun X, Tao L, Tianzeng D, Xuemei H, Fan Z, Chunyin H, Jianqiang H, Chen L. Analysis of Related Risk Factors and Prognostic Factors of Gastric Cancer with Bone Metastasis: A SEER-Based Study. *J Immunol Res* 2022; **2022**: 3251051 [PMID: 35211630 DOI: 10.1155/2022/3251051]

11 **Nakanishi H**, Araki N, Kuratsu S, Narahara H, Ishikawa O, Yoshikawa H. Skeletal metastasis in patients with gastric cancer. *Clin Orthop Relat Res* 2004; 208-212 [PMID: 15232450 DOI: 10.1097/01.blo.0000129159.65684.b3]

12 **Choi CW**, Lee DS, Chung JK, Lee MC, Kim NK, Choi KW, Koh CS. Evaluation of bone metastases by Tc-99m MDP imaging in patients with stomach cancer. *Clin Nucl Med* 1995; **20**: 310-314 [PMID: 7788986 DOI: 10.1097/00003072-199504000-00005]

13 **Wen L**, Li YZ, Zhang J, Zhou C, Yang HN, Chen XZ, Xu LW, Kong SN, Wang XW, Zhang HM. Clinical analysis of bone metastasis of gastric cancer: incidence, clinicopathological features and survival. *Future Oncol* 2019; **15**: 2241-2249 [PMID: 31215231 DOI: 10.2217/fon-2019-0039]

14 **Wang K**, Jiang X, Ren Y, Ma Z, Cheng X, Li F, Xiao J, Yu Z, Jiao Z. The significance of preoperative serum carcinoembryonic antigen levels in the prediction of lymph node metastasis and prognosis in locally advanced gastric cancer: a retrospective analysis. *BMC Gastroenterol* 2020; **20**: 100 [PMID: 32276616 DOI: 10.1186/s12876-020-01255-6]

15 **Ikeda Y**, Mori M, Adachi Y, Matsushima T, Sugimachi K, Saku M. Carcinoembryonic antigen (CEA) in stage IV gastric cancer as a risk factor for liver metastasis: a univariate and multivariate analysis. *J Surg Oncol* 1993; **53**: 235-238 [PMID: 8341054 DOI: 10.1002/jso.2930530409]

16 **Jin W**, Zhu M, Zheng Y, Wu Y, Ding X, Wu H, Ye J, Zhu Z, Song X. Perineural invasion, lactate dehydrogenase, globulin, and serum sodium predicting occult metastasis in oral cancer. *Oral Dis* 2022; **28**: 132-141 [PMID: 33289935 DOI: 10.1111/odi.13750]

17 **Chen J**, Zhou Y, Xu Y, Zhu HY, Shi YQ. Low pretreatment serum globulin may predict favorable prognosis for gastric cancer patients. *Tumour Biol* 2016; **37**: 3905-3911 [PMID: 26476541 DOI: 10.1007/s13277-015-3778-3]

18 **Falanga A**, Schieppati F, Russo D. Cancer Tissue Procoagulant Mechanisms and the Hypercoagulable State of Patients with Cancer. *Semin Thromb Hemost* 2015; **41**: 756-764 [PMID: 26408922 DOI: 10.1055/s-0035-1564040]

19 **Yao Y**, Zhou Y, Yang Z, Shen H. [Risk Factors of Non-small Cell Lung Cancer with Bone Metastasis after Therapy]. *Zhongguo Fei Ai Za Zhi* 2018; **21**: 476-480 [PMID: 29945707 DOI: 10.3779/j.issn.1009-3419.2018.06.09]

20 **Gale AJ**, Gordon SG. Update on tumor cell procoagulant factors. *Acta Haematol* 2001; **106**: 25-32 [PMID: 11549774 DOI: 10.1159/000046586]

21 **Gil-Bernabé AM**, Lucotti S, Muschel RJ. Coagulation and metastasis: what does the experimental literature tell us? *Br J Haematol* 2013; **162**: 433-441 [PMID: 23691951 DOI: 10.1111/bjh.12381]

22 **Palumbo JS**, Degen JL. Mechanisms linking tumor cell-associated procoagulant function to tumor metastasis. *Thromb Res* 2007; **120** Suppl 2: S22-S28 [PMID: 18023710 DOI: 10.1016/S0049-3848(07)70127-5]

23 **Park JM**, Song KY, O JH, Kim WC, Choi MG, Park CH. Bone recurrence after curative resection of gastric cancer. *Gastric Cancer* 2013; **16**: 362-369 [PMID: 22961057 DOI: 10.1007/s10120-012-0193-y]

24 **Anderson JA**, Weitz JI. Hypercoagulable states. *Crit Care Clin* 2011; **27**: 933-952, vii [PMID: 22082521 DOI: 10.1016/j.ccc.2011.09.007]

25 **Jiang HG**, Li J, Shi SB, Chen P, Ge LP, Jiang Q, Tang XP. Value of fibrinogen and D-dimer in predicting recurrence and metastasis after radical surgery for non-small cell lung cancer. *Med Oncol* 2014; **31**: 22 [PMID: 24861920 DOI: 10.1007/s12032-014-0022-8]

26 **Tankó LB**, Karsdal MA, Christiansen C, Leeming DJ. Biochemical approach to the detection and monitoring of metastatic bone disease: What do we know and what questions need answers? *Cancer Metastasis Rev* 2006; **25**: 659-668 [PMID: 17160557 DOI: 10.1007/s10555-006-9024-0]

World Journal of Gastrointestinal Oncology

Submit a Manuscript: https://www.f6publishing.com

World J Gastrointest Oncol 2023 July 15; 15(7): 1262-1270

DOI: 10.4251/wjgo.v15.i7.1262

ISSN 1948-5204 (online)

ORIGINAL ARTICLE

Retrospective Study

Efficacy of concurrent chemoradiotherapy with thalidomide and S-1 for esophageal carcinoma and its influence on serum tumor markers

Tian-Wei Zhang, Peng Zhang, Dong Nie, Xin-Yu Che, Tian-Tai Fu, Yan Zhang

Specialty type: Oncology

Provenance and peer review: Unsolicited article; Externally peer reviewed.

Peer-review model: Single blind

Peer-review report's scientific quality classification

Grade A (Excellent): 0
Grade B (Very good): B, B
Grade C (Good): 0
Grade D (Fair): 0
Grade E (Poor): 0

P-Reviewer: Brethauer SA, United States; Terashima M, Japan

Received: March 28, 2023
Peer-review started: March 28, 2023
First decision: April 10, 2023
Revised: May 2, 2023
Accepted: June 13, 2023
Article in press: June 13, 2023
Published online: July 15, 2023

Tian-Wei Zhang, Peng Zhang, Dong Nie, Xin-Yu Che, Tian-Tai Fu, Yan Zhang, Department of Hematology and Radiotherapy, Zibo 148 Hospital, Zibo 255300, Shandong Province, China

Corresponding author: Yan Zhang, MS, Doctor, Department of Hematology and Radiotherapy, Zibo 148 Hospital, No. 20 Zhanbei Road, Zhoucun District, Zibo 255300, Shandong Province, China. zhangyan100862023@163.com

Abstract

BACKGROUND

Although the current conventional treatment strategies for esophageal carcinoma (EC) have been proven effective, they are often accompanied by serious adverse events. Therefore, it is still necessary to continue to explore new therapeutic strategies for EC to improve the clinical outcome of patients.

AIM

To elucidate the clinical efficacy of concurrent chemoradiotherapy (CCRT) with thalidomide (THAL) and S-1 (tegafur, gimeracil, and oteracil potassium capsules) in the treatment of EC as well as its influence on serum tumor markers (STMs).

METHODS

First, 62 patients with EC treated at the Zibo 148 Hospital between November 2019 and November 2022 were selected and grouped according to the received treatment. Among these, 30 patients undergoing CCRT with cis-platinum and 5-fluorouracil were assigned to the control group (Con), and 32 patients receiving CCRT with THAL and S-1 were assigned to the research group (Res). Second, inter-group comparisons were carried out with respect to curative efficacy, incidence of drug toxicities, STMs [carbohydrate antigen 125 (CA125) and macrophage inflammatory protein-3α (MIP-3α)], angiogenesis-related indicators [vascular endothelial growth factor (VEGF); VEGF receptor-1 (VEGFR-1); basic fibroblast growth factor (bFGF); angiogenin-2 (Ang-2)], and quality of life (QoL) [QoL core 30 (QLQ-C30)] after one month of treatment.

RESULTS

The analysis showed no statistical difference in the overall response rate and disease control rate between the two patient cohorts; however, the incidences of grade I–II myelosuppression and gastrointestinal reactions were significantly lower in the Res than in the Con. Besides, the post-treatment CA125, MIP-3α, VEGF, VEGFR-1, bFGF, and Ang-2 Levels in the Res were markedly lower

compared with the pre-treatment levels and the corresponding post-treatment levels in the Con. Furthermore, more evident improvements in QLQ-C30 scores from the dimensions of physical, role, emotional, and social functions were determined in the Res.

CONCLUSION

The above results demonstrate the effectiveness of THAL + S-1 CCRT for EC, which contributes to mild side effects and significant reduction of CA125, MIP-3α, VEGF, VEGFR-1, bFGF, and Ang-2 Levels, thus inhibiting tumors from malignant progression and enhancing patients' QoL.

Key Words: Thalidomide; Concurrent chemoradiotherapy; Esophageal carcinoma; Therapeutic effect; Serum tumor markers

Core Tip: Esophageal carcinoma (EC) is a common and fatal digestive tract tumor, and the current therapeutic methods such as surgical resection, radiotherapy and chemotherapy have limited effects and are accompanied by relatively serious adverse events. Therefore, clinical exploration of new treatment strategies for esophageal cancer should be continued to optimize the management of EC patients.

Citation: Zhang TW, Zhang P, Nie D, Che XY, Fu TT, Zhang Y. Efficacy of concurrent chemoradiotherapy with thalidomide and S-1 for esophageal carcinoma and its influence on serum tumor markers. *World J Gastrointest Oncol* 2023; 15(7): 1262-1270
URL: https://www.wjgnet.com/1948-5204/full/v15/i7/1262.htm
DOI: https://dx.doi.org/10.4251/wjgo.v15.i7.1262

INTRODUCTION

Esophageal carcinoma (EC) is a common fatal gastrointestinal (GI) tumor with a five-year survival rate of only 15%–25%. It is characterized by high malignancy, invasiveness, and easy metastasis[1]. According to global statistics, EC is broadly pathologically classified into esophageal squamous cell carcinoma and esophageal adenocarcinoma; the former is primarily distributed in Southeast Asia and Africa and the latter in Europe and North America[2,3]. Onco-pathologically, EC is shown to be associated with the abnormal proliferation of esophageal epithelial cells that induces invasive cancer or invasive adenocarcinoma; meanwhile, the etiology is related to factors such as esophageal mucosa contact with carcinogens and mechanical damage[4,5]. Moreover, the disease is mainly presented clinically as dysphagia and unexpected weight loss but usually with no specific early symptoms[6]. At the present stage, EC is mainly treated with surgical resection, radiotherapy, and chemotherapy. Despite the confirmed effectiveness of these conventional treatments, they are accompanied by serious adverse events, resulting in unsatisfactory clinical outcomes[7]. Therefore, there is an urgent need to explore new strategies for treating EC and optimizing the treatment options for patients with EC; this can be of great value for improving treatment efficacy as well as patient prognosis and symptoms.

Thalidomide (THAL), which was originally used as a sedative for the relief of vomiting and nausea during pregnancy, has been used to treat solid tumors because of its anti-angiogenesis effects[8]. Its anti-tumor mechanism is reported to be linked to the regulation of the secretion of vascular endothelial growth factor (VEGF) and basic fibroblast growth factor (bFGF)[9]. Another molecular study shows that THAL exerts immunomodulatory actions by altering the expression of tumor necrosis factor receptor superfamilies in T cell subsets[10]. The fluorouracil drug S-1 consists of tegafur, gimeracil, and oteracil potassium. It can be used to treat gastric, pancreatic, gallbladder, colorectal, and esophageal cancers[11,12] and has been shown to not only exert better anticancer performance than 5-fluorouracil (5-FU) but also reduce cancer cells' resistance to chemotherapy[13]. In the analysis by Wang *et al*[14], definitive concurrent chemoradiotherapy (CCRT) with S-1 and cisplatin significantly improved the survival outcomes of older adults (≥ 60 years old) with EC.

The present study attempts to analyze the effectiveness of CCRT with THAL + S-1 for EC and its influence on serum tumor markers (STMs) in order to provide a new feasible scheme for improving the survival outcome of patients with EC.

MATERIALS AND METHODS

Patient information

The study population comprised 62 patients with EC treated at the Zibo 148 Hospital between November 2019 and November 2022. The patients were grouped according to the received treatment. A total of 30 patients undergoing CCRT with cis-platinum (DDP) and 5-FU were assigned to the control group (Con), and 32 patients receiving CCRT with THAL and S-1 were assigned to the research group (Res). The Con consisted of 17 males and 13 females with a mean age of 61.03 ± 6.91 years, and the Res consisted of 19 males and 13 females with a mean age of 61.44 ± 10.61 years. The present study is retrospective.

Criteria for patient enrollment and exclusion

Inclusion criteria: (1) Patients gastroscopically and pathologically diagnosed with EC and meeting the American Joint Committee on Cancer clinical staging criteria for EC; (2) patients with a life expectancy of three or more months; (3) patients with a Karnovsky Performance Scale score of ≥70 points; (4) patients capable of eating semi-liquid food; and (5) patients with normal hepatorenal function and blood routines.

Exclusion criteria: (1) Patients with an intolerance to the treatment scheme of the present study; (2) patients with other malignancies; (3) patients with hepatic fibrosis, (4) patients with renal fibrosis and other systemic fibrosis; (5) patients undergoing chemotherapy or other adjuvant treatment programs; and (6) patients with distant metastasis of the tumor.

Methods

All patients received three-dimensional intensity modulated radiation therapy. Gross tumor volume and organs at risk were delineated according to the pathology and imaging findings, and treatment schemes were specified based on patients' conditions. The prescribed dose was 56–70 Gy, with a single dose of 2 Gy administered five times a week for four weeks. Of these, 95% of the planned target area was irradiated with a prescription dose of at least 100% for the whole lung, no more than 25%–30% for V20, and no more than 18% for V30; the upper limits were set at 30 Gy and 45 Gy for the heart and the spinal cord, respectively.

The Con was treated with CCRT using DDP + FU. Cisplatin 20 mg/(m^2·d) and 5-FU 500 mg/(m^2·d) were given intravenously for 5 consecutive days; patients received two cycles of CCRT, which were performed at week 1 and week 4 of radiotherapy, respectively.

The Res received CCRT using THAL + S-1. Patients were given S-1 capsules, 40 mg/time, twice a day from day 1 to day 14; this was repeated every 21 days simultaneously with radiotherapy. The THAL was administered at a dose of 100 mg/d before bedtime in the first week and gradually increased to 200 mg/d in the second week until the end of radiotherapy. Patients in both groups were given symptomatic treatments, such as antiemesis, stomach protection, and nutritional support during chemotherapy, with their blood routines and hepatorenal function monitored weekly and biweekly, respectively.

Outcome measures

Short-term efficacy: The clinical efficacy, which was evaluated with reference to the Response Evaluation Criteria in Solid Tumors, was determined as complete response (CR; the tumor disappeared completely, with smooth margins shown by the barium meal test, smooth passage of the barium agent, slightly rigid tube wall, no narrowing or slight narrowing of the lumen, and basically recovered or thickened mucosa), partial response (PR; most of the lesions disappeared without obvious distortion, angulation, or extraluminal ulcer; the barium passed smoothly, but the edges were not smooth, with small filling defects or niches, or the lumen was obviously narrowed, although the edges were smooth), stable disease (SD; the lesion had residual or no obvious improvement at the end of radiotherapy, with obvious filling defects or niches), or progressive disease (worsened niche or stenosis). The overall response rate (ORR) is the sum of patients with CR and patients with PR as a percentage of the total number of cases. The disease control rate (DCR) is the sum of the percentages of CR, PR, and SD. The short-term efficacy was evaluated after radiotherapy in both groups.

Incidence of drug toxicities: The adverse reactions of anticancer drugs were classified into grades I–II or III–IV according to the WHO classification of adverse drug reactions, and the number of cases of myelosuppression (MS), GI reactions, and radiation esophagitis (RE) as well as the percentages of the corresponding side effect grades were recorded.

Serum tumor markers and angiogenesis-related indicators: Before and after treatment, 5 mL of venous blood was collected on an empty stomach during the morning hours and sent to the laboratory for examination after centrifugation. The levels of carbohydrate antigen 125 (CA125), macrophage inflammatory protein-3α (MIP-3α), VEGF, VEGF receptor-1 (VEGFR-1), bFGF, and angiogenin-2 (Ang-2) were determined by the enzyme-linked immunosorbent assay (ELISA).

Quality of life (QoL): Patients' QoL was assessed and compared at one month after treatment, using the QoL Questionnaire core 30. The scale includes five functional dimensions: body, role, emotion, cognition, and social function. A higher score suggests a better QoL.

Statistical analysis

In the present study, the SPSS 22.0 software was used for data analysis, and GraphPad Prism 7.0 was used for image rendering and export. The significance threshold was $P < 0.05$. mean ± SEM was used for statistical description of continuous variables (*e.g.*, age, tumor diameter, and CA125 expression), and the *t*-test and paired *t*-test were used for inter-group and intra-group comparisons (before and after treatment), respectively. Categorical variables (*e.g.*, sex, clinical staging, and history of alcoholism) were described by frequencies (percentages), and the comparison between groups was made using the χ^2 test.

RESULTS

Baseline data

As indicated by Table 1, the two patient cohorts have no evident differences in age, sex, clinical staging, tumor diameter,

Table 1 Baseline information

Indicators	Control group (*n* = 30)	Research group (*n* = 32)	χ^2/t	*P* value
Age (years old)	61.03 ± 6.91	61.44 ± 10.61	0.179	0.859
Gender (male/female)	17/13	19/13	0.047	0.829
Clinical staging (II/III)	18/12	16/16	0.625	0.429
Tumor diameter (cm)	5.68 ± 1.29	5.80 ± 1.50	0.337	0.738
History of alcoholism (with/without)	11/19	8/24	0.992	0.319
History of smoking (with/without)	8/22	7/25	0.194	0.660
Family medical history (yes/no)	5/25	9/23	1.163	0.281

Table 2 Short-term efficacy of two groups of esophageal carcinoma patients, *n* (%)

Indicators	Control group (*n* = 30)	Research group (*n* = 32)	χ^2	*P* value
Complete response	6 (20.00)	7 (21.88)	-	-
Partial response	12 (40.00)	13 (40.63)	-	-
Stable disease	7 (23.33)	8 (25.00)	-	-
Progressive disease	5 (16.67)	4 (12.50)	-	-
Overall response rate	18 (60.00)	20 (62.50)	0.041	0.840
Disease control rate	25 (83.33)	28 (87.50)	0.217	0.642

Table 3 Incidence of drug toxicities in two groups of esophageal carcinoma patients, *n* (%)

Indicators	Control group (*n* = 30)	Research group (*n* = 32)	χ^2	*P* value
Myelosuppression				
I-II	13 (43.33)	6 (18.75)	4.403	0.036
III-IV	6 (20.00)	2 (6.25)	2.605	0.107
Gastrointestinal reactions				
I-II	15 (50.00)	8 (25.00)	4.147	0.042
III-IV	7 (23.33)	3 (9.38)	2.230	0.135
Radiation esophagitis				
I-II	14 (46.67)	13 (40.63)	0.230	0.632
III-IV	7 (23.33)	6 (18.75)	0.196	0.658

alcoholism history, smoking history, and family history ($P > 0.05$).

Short-term efficacy in the two patient groups

The short-term curative effects between the Res and the Con at one month after treatment were analyzed and compared (Table 2). The ORRs of the Res and the Con were determined as 62.50% and 60.00%, respectively, while the DCRs were determined as 87.50% and 83.33%, respectively, showing no significant inter-group differences in both indicators ($P > 0.05$).

Incidence of drug toxicities in the two patient groups

The main drug toxicities were MS, GI reactions, and RE, with the incidence of grade I–II MS and grade I–II GI reactions markedly lower in the Res compared with the Con ($P < 0.05$; Table 3).

Serum tumor markers in the two patient groups

Two STMSs, CA125 and MIP-3α, were measured; no statistical differences were found in the corresponding pre-treatment levels between the Res and the Con ($P > 0.05$); a marked reduction in both indexes was determined in the two patient cohorts, especially in the Res ($P < 0.05$; Figure 1).

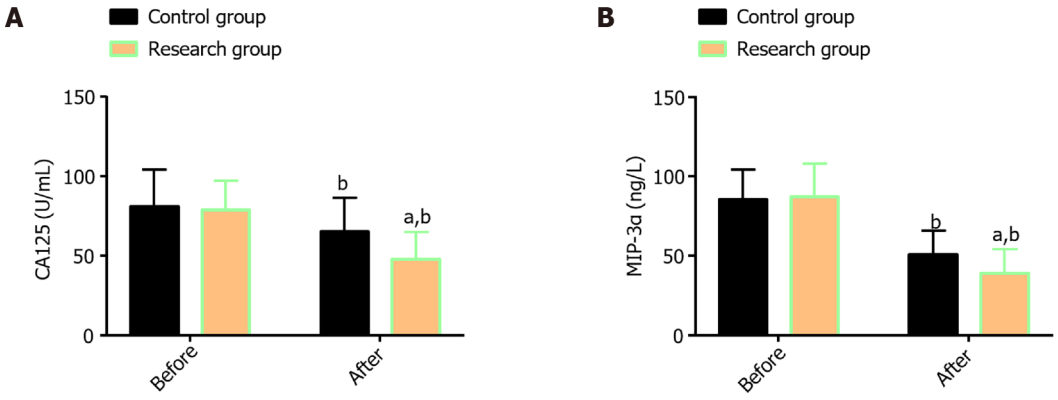

DOI: 10.4251/wjgo.v15.i7.1262 **Copyright** ©The Author(s) 2023.

Figure 1 Serum tumor markers in two groups of esophageal cancer patients. A: The research group had markedly lower CA125 levels than the control group after treatment; B: The research group had markedly lower MIP-3α levels than the control group after treatment. [a]*P* < 0.05 *vs* control; [b]*P* < 0.01, *vs* before treatment. CA125: Carbohydrate antigen 125; MIP-3α: Macrophage inflammatory protein-3α.

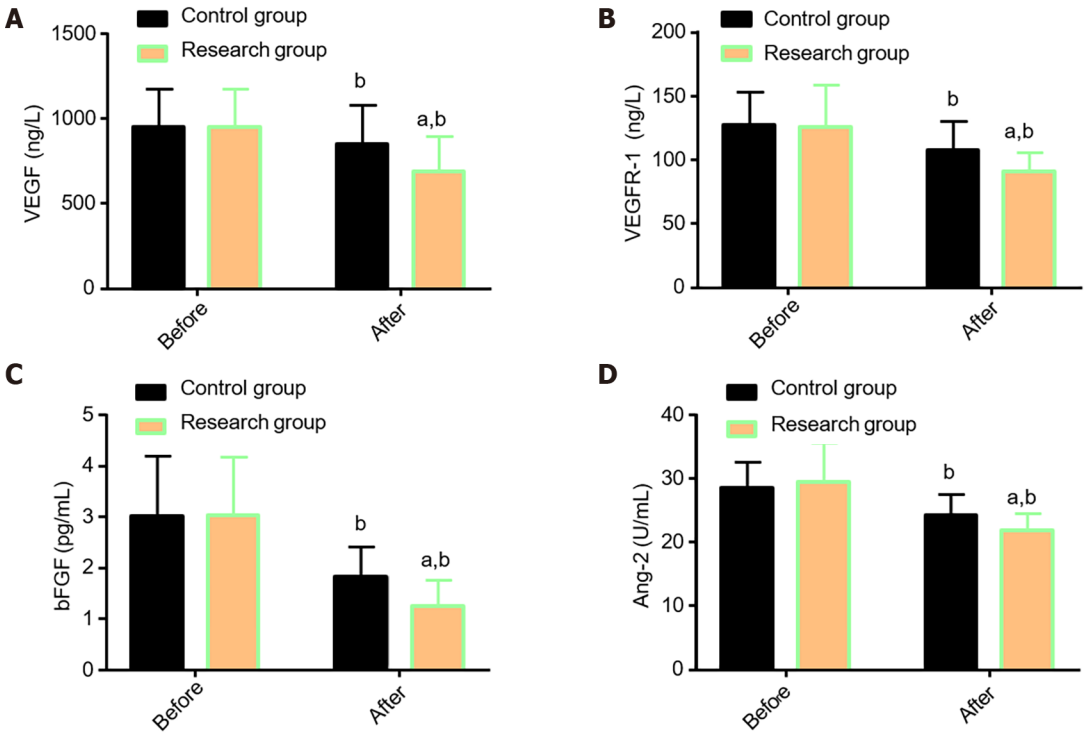

DOI: 10.4251/wjgo.v15.i7.1262 **Copyright** ©The Author(s) 2023.

Figure 2 Angiogenesis-related indexes in two groups of esophageal cancer patients. A: The research group had markedly lower VEGF levels than the control group after treatment; B: The research group had markedly lower VEGFR-1 Levels than the control group after treatment; C: The research group had markedly lower bFGF levels than the control group after treatment; D: The research group had markedly lower Ang-2 levels than the control group after treatment. [a]*P* < 0.05 *vs* control; [b]*P* < 0.01, *vs* before treatment. VEGF: Vascular endothelial growth factor; VEGFR-1: Vascular endothelial growth factor receptor-1; bFGF: Basic fibroblast growth factor; Ang-2: Angiogenin-2.

Angiogenesis-related indexes in the two patient groups

The angiogenesis-related indexes VEGF, VEGFR-1, bFGF, and Ang-2, were determined in both groups for comparative analysis (Figure 2). The VEGF, VEGFR-1, bFGF, and Ang-2 Levels were similar in the two cohorts before treatment ($P > 0.05$), but their levels reduced significantly after treatment ($P < 0.05$), with even lower levels in the Res ($P < 0.05$).

Quality of life in the two patient groups

The QoL of the two groups was compared and evaluated from five aspects: physical, role, emotional, social, and cognitive function (Figure 3). The data showed that with the exception of cognitive function, the aspect scores in the two groups increased significantly after treatment ($P < 0.05$), with more marked increases in the Res when compared with the Con ($P < 0.05$).

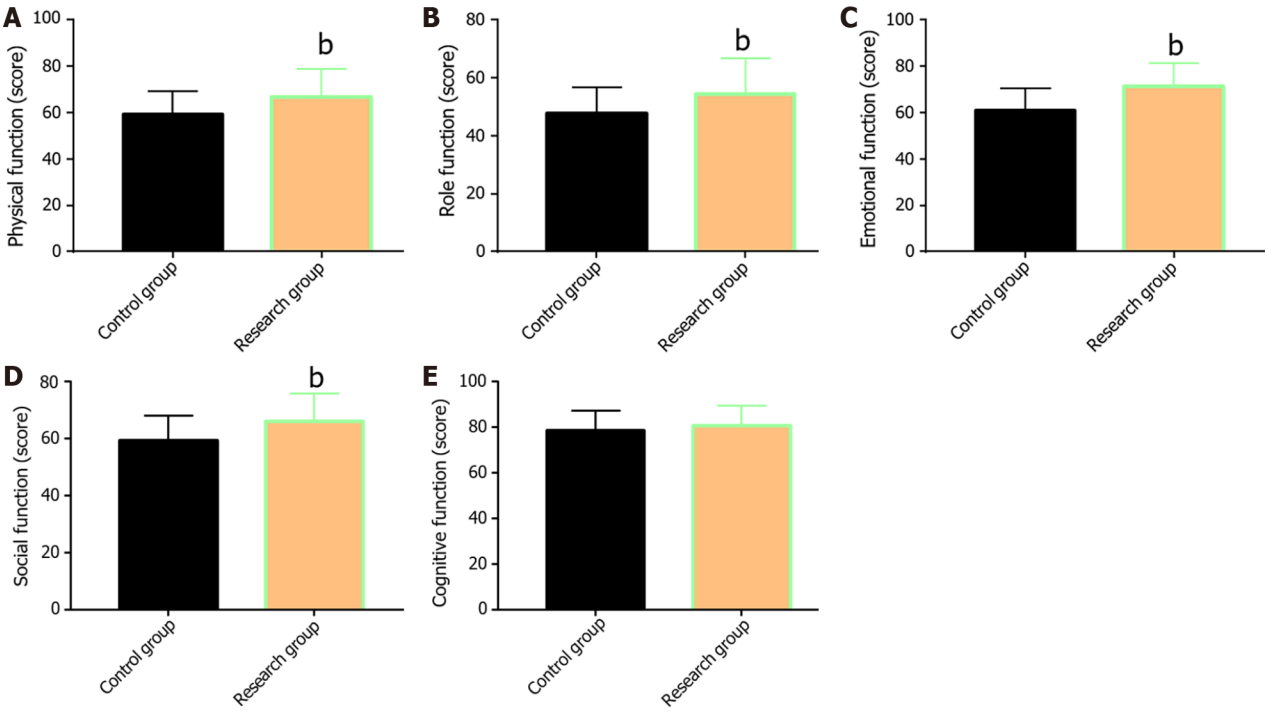

DOI: 10.4251/wjgo.v15.i7.1262

Figure 3 Quality of life of esophageal cancer patients. A: The research group had markedly higher physical function scores than the control group after treatment; B: The research group had markedly higher role function scores than the control group after treatment; C: The research group had statistically higher emotional function scores than the control group after treatment; D: The research group had markedly higher social function scores than the control group after treatment; E: The research group had obviously higher cognitive function scores than the control group after treatment. $^{b}P < 0.01$, *vs* before treatment.

DISCUSSION

The present study focuses on the efficacy of CCRT with THAL + S-1 for EC and its influence on patient STMs. Given the current scanty of research in this field, the present analysis is helpful in gaining a new understanding of the effectiveness of this CCRT protocol for patients with EC.

Many researchers have provided clinical references for EC treatment by analyzing relevant treatment strategies. For example, Song *et al*[15] showed that CCRT with S-1 effectively enhanced the curative effect and survival of elderly patients with non-metastatic esophageal squamous cell carcinoma compared with radiotherapy alone without increasing acute adverse reactions. As reported by McDowell *et al*[16], intensity-modulated radiotherapy combined with chemotherapy is conducive to improving the prognosis of patients with cervical EC. Ma *et al*[17] also pointed out that three-dimensional conformal radiotherapy was helpful in controlling mediastinal lymph node metastasis and recurrence after EC surgery, in addition to significantly improving the local tumor control rate and long-term survival rate. In the present study, the effectiveness of DDP + 5-FU *vs* THAL + S-1 were analyzed. The standard CCRT scheme for EC (DDP + 5-FU) still causes local failures in 46% of patients and fatal threats in 20%[18]. Hence, introducing new CCRT schemes is critical. Thalidomide can exert anti-inflammatory and immunosuppressive actions by inhibiting inflammatory factors and regulating key immunoregulatory molecules, thus exerting anti-tumor activity[19]. Among the S-1 components, tegafur is a prodrug of 5-Fu, and gimeracil can prolong the effective drug properties of 5-Fu in the blood by reducing dihydropyrimidine dehydrogenase[20].

In the present study, the Res was administered with THAL + S-1 and the Con was administered with DDP + 5-FU. The ORR and DCR of the Res were determined as 62.50% and 87.50%, respectively (slightly higher than but not significantly different from those in the Con); these results suggest equivalent curative efficacy of THAL + S-1 to that of DDP + 5-FU. Furthermore, according to the investigation of drug toxicities, the incidences of grade I–II MS and grade I–II GI reactions were identified as notably lower in the Res than in the Con, while the incidence of RE was similar, indicating the safety profile of THAL + S-1. This may be related to the inhibition of FU-related GI toxicity by oteracil potassium, one of the S-1 components[20].

Previous literature has shown a correlation of CA125 with lymph node metastasis and blood-borne metastasis of EC, as well as an association between MIP-3α (also known as CCL20) and the occurrence, development, and metastasis of EC[21,22]. While VEGF and VEGFR-1 are both significantly related to the poor prognosis of patients with EC[23], previous studies have also shown that abnormal overexpression of bFGF in advanced esophageal squamous cell carcinoma is closely associated with the development of invasive carcinoma. As a key regulator of tumor angiogenesis, Ang-2 also mediates the malignant procession of esophageal squamous cell carcinoma[24,25].

By further quantifying STMs (CA125 and MIP-3α) and angiogenesis-related indicators (VEGF, VEGFR-1, bFGF, and Ang-2) using ELISA, it was found that the post-treatment CA125, MIP-3α, VEGF, VEGFR-1, bFGF, and Ang-2 Levels in the Res were evidently lower than those before treatment and the Con levels. This suggests that CCRT with THAL + S-1

has a significant inhibitory effect on STMs and angiogenesis-related indicators in patients with EC.

In the research of Wang *et al*[26], THAL validly suppressed the increase of the serum VEGF level in patients with EC during treatment; this is similar to our research results. Tsuji *et al*[27] also reported the inhibitory action of S-1 against VEGF levels in patients with metastatic breast cancer, indicating certain anti-angiogenesis activity of S-1. Finally, the QoL of the two groups after treatment was evaluated and compared regarding five aspects: physical, role, emotional, social, and cognitive function. The Res was found to have higher scores in all the other four dimensions after treatment except the cognitive function, suggesting that THAL + S-1 is more effective than DDP + 5-FU in enhancing QoL in patients with EC.

CONCLUSION

Taken together, CCRT with THAL + S-1 is effective in the treatment of EC, with certain safety. This CCRT protocol has a significant inhibitory effect on STMs (CA125 and MIP-3α) and angiogenesis-related indicators (VEGF, VEGFR-1, bFGF, and Ang-2) and is conducive to improving patients' QoL, providing a new choice for clinical treatment of patients with EC. In addition, since the sample size included in the present study is limited, increasing the sample size in the future will be conducive to enhancing the credibility of the experimental results.

ARTICLE HIGHLIGHTS

Research background

Treatment strategies for esophageal carcinoma (EC) still need to be explored and optimized to improve patient symptoms, efficacy and prognosis.

Research motivation

This study provided a novel and feasible scheme to improve the survival outcome of EC patients.

Research objectives

This research intends to elucidate the clinical efficacy of concurrent chemoradiotherapy (CCRT) with thalidomide (THAL) and S-1 (tegafur, gimeracil and oteracil potassium capsules) for EC and its influence on serum tumor markers (STMs).

Research methods

Thirty cases of EC undergoing CCRT with cis-platinum and 5-fluorouracil were assigned to the control group (Con) and 32 cases receiving CCRT with THAL and S-1 were included in the research group (Res). The efficacy, incidence of drug toxicities, STMs [carbohydrate antigen 125 (CA125), macrophage inflammatory protein-3α (MIP-3α)], angiogenesis-related indicators [vascular endothelial growth factor (VEGF), vascular endothelial growth factor receptor-1 (VEGFR-1), basic fibroblast growth factor, (bFGF), angiogenin-2 (Ang-2)], and quality of life [Quality of Life Questionnaire core 30, (QLQ-C30)] of the two groups were collected for comparative analysis.

Research results

The overall response rate and disease control rate were not statistically different between the two patient cohorts, but the incidence of grade I-II myelosuppression and gastrointestinal reactions was significantly lower in the Res. In addition, the Res showed markedly reduced CA125, MIP-3α, VEGF, VEGFR-1, bFGF, and Ang-2 Levels after treatment, lower than those in the Con. Moreover, a better quality of life was determined in the Res, which was supported by more significant improvements in QLQ-C30 scores from physical, role, emotional and social function dimensions.

Research conclusions

CCRT with THAL and S-1 has a definite efficacy in the treatment of EC, which can significantly reduce CA125, MIP-3α, VEGF, VEGFR-1, bFGF and Ang-2 Levels while contributing to mild toxicities, thereby inhibiting tumor malignant progression and helping to improve the quality of life of patients.

Research perspectives

Although this study provides a new choice for the clinical treatment of EC patients by demonstrating the clinical efficacy and safety of CCRT with THAL and S-1, the credibility of our findings needs to be validated by increasing the sample size in the future due to the limited cases included in this research.

FOOTNOTES

Author contributions: Zhang TW and Zhang Y analyzed the data and wrote the manuscript; Zhang TW, Zhang P, Nie D, Che XY and Fu TT designed the research; Zhang TW modified the manuscript; and all authors read and approved the final manuscript.

Institutional review board statement: The study was conducted according to the guidelines of the Declaration of Helsinki, and approved by Medical Ethics Committee of Zibo 148 Hospital.

Informed consent statement: The informed consent was not required as the research was conducted on anonymized data for which consent from the volunteers have already been obtained.

Conflict-of-interest statement: The authors have no conflicts of interest to declare.

Data sharing statement: No additional data are available.

Country/Territory of origin: China

ORCID number: Yan Zhang 0009-0009-2897-3975.

S-Editor: Wang JL
L-Editor: A
P-Editor: Yu HG

REFERENCES

1 **Yu G**, Yu W, Xu X, Ye B, Yao L. Neoadjuvant immunotherapy for resectable esophageal cancer: A protocol of meta-analysis. *PLoS One* 2021; **16**: e0252829 [PMID: 34086821 DOI: 10.1371/journal.pone.0252829]
2 **Yang YM**, Hong P, Xu WW, He QY, Li B. Advances in targeted therapy for esophageal cancer. *Signal Transduct Target Ther* 2020; **5**: 229 [PMID: 33028804 DOI: 10.1038/s41392-020-00323-3]
3 **Watanabe M**, Otake R, Kozuki R, Toihata T, Takahashi K, Okamura A, Imamura Y. Recent progress in multidisciplinary treatment for patients with esophageal cancer. *Surg Today* 2020; **50**: 12-20 [PMID: 31535225 DOI: 10.1007/s00595-019-01878-7]
4 **Smyth EC**, Lagergren J, Fitzgerald RC, Lordick F, Shah MA, Lagergren P, Cunningham D. Oesophageal cancer. *Nat Rev Dis Primers* 2017; **3**: 17048 [PMID: 28748917 DOI: 10.1038/nrdp.2017.48]
5 **Uhlenhopp DJ**, Then EO, Sunkara T, Gaduputi V. Epidemiology of esophageal cancer: update in global trends, etiology and risk factors. *Clin J Gastroenterol* 2020; **13**: 1010-1021 [PMID: 32965635 DOI: 10.1007/s12328-020-01237-x]
6 **Short MW**, Burgers KG, Fry VT. Esophageal Cancer. *Am Fam Physician* 2017; **95**: 22-28 [PMID: 28075104]
7 **Bollschweiler E**, Plum P, Mönig SP, Hölscher AH. Current and future treatment options for esophageal cancer in the elderly. *Expert Opin Pharmacother* 2017; **18**: 1001-1010 [PMID: 28540761 DOI: 10.1080/14656566.2017.1334764]
8 **Ito T**, Handa H. Cereblon and its downstream substrates as molecular targets of immunomodulatory drugs. *Int J Hematol* 2016; **104**: 293-299 [PMID: 27460676 DOI: 10.1007/s12185-016-2073-4]
9 **Medinger M**, Halter J, Heim D, Buser A, Gerull S, Stern M, Passweg J. Angiogenic markers in plasma cell myeloma patients treated with novel agents. *Anticancer Res* 2015; **35**: 1085-1090 [PMID: 25667497]
10 **Kim BS**, Kim JY, Kim EJ, Lee JG, Joo DJ, Huh KH, Kim MS, Kim YS. Role of Thalidomide on the Expression of OX40, 4-1BB, and GITR in T Cell Subsets. *Transplant Proc* 2016; **48**: 1270-1274 [PMID: 27320601 DOI: 10.1016/j.transproceed.2015.12.088]
11 **Yasui H**, Kawakami T, Kashiwagi H, Mori K, Omae K, Kasai J, Yoshisue K, Kawahira M, Tsushima T, Machida N, Fukutomi A, Yamaguchi K. Pharmacokinetics of S-1 monotherapy in plasma and in tears for gastric cancer patients. *Int J Clin Oncol* 2019; **24**: 660-665 [PMID: 31011915 DOI: 10.1007/s10147-018-01387-6]
12 **Hiratsuka T**, Etoh T, Hara T, Akagi T, Tahara K, Matsumoto T, Ogawa T, Fujii K, Shiromizu A, Shiroshita H, Inomata M. Long-term outcomes of neoadjuvant-synchronous S-1 plus radiotherapy for locally advanced rectal cancer: a multi-institutional prospective phase II study. *J Anus Rectum Colon* 2018; **2**: 168-175 [PMID: 31559360 DOI: 10.23922/jarc.2018-011]
13 **Fukushima M**, Sakamoto K, Sakata M, Nakagawa F, Saito H, Sakata Y. Gimeracil, a component of S-1, may enhance the antitumor activity of X-ray irradiation in human cancer xenograft models in vivo. *Oncol Rep* 2010; **24**: 1307-1313 [PMID: 20878125 DOI: 10.3892/or_00000987]
14 **Wang H**, Li G, Chen L, Duan Y, Zou C, Hu C. Definitive concurrent chemoradiotherapy with S-1 and cisplatin in elderly esophageal squamous cell carcinoma patients. *J Thorac Dis* 2017; **9**: 646-654 [PMID: 28449472 DOI: 10.21037/jtd.2017.03.105]
15 **Song GM**, Tian X, Liu XL, Chen H, Zhou JG, Bian W, Chen WQ. Concurrent chemo-radiotherapy with S-1 as an alternative therapy for elderly Chinese patients with non-metastatic esophageal squamous cancer: evidence based on a systematic review and meta-analysis. *Oncotarget* 2017; **8**: 37963-37973 [PMID: 28415814 DOI: 10.18632/oncotarget.16302]
16 **McDowell LJ**, Huang SH, Xu W, Che J, Wong RKS, Brierley J, Kim J, Cummings B, Waldron J, Bayley A, Hansen A, Witterick I, Ringash J. Effect of Intensity Modulated Radiation Therapy With Concurrent Chemotherapy on Survival for Patients With Cervical Esophageal Carcinoma. *Int J Radiat Oncol Biol Phys* 2017; **98**: 186-195 [PMID: 28258892 DOI: 10.1016/j.ijrobp.2017.01.003]
17 **Ma DY**, Tan BX, Liu M, Li XF, Zhou YQ, Lu Y. Concurrent three-dimensional conformal radiotherapy and chemotherapy for postoperative recurrence of mediastinal lymph node metastases in patients with esophageal squamous cell carcinoma: a phase 2 single-institution study. *Radiat Oncol* 2014; **9**: 28 [PMID: 24438695 DOI: 10.1186/1748-717X-9-28]
18 **Yoshii T**, Hara H, Asayama M, Kumekawa Y, Miyazawa S, Takahashi N, Matsushima T, Shimizu S, Saito Y. Chemoradiotherapy with FOLFOX for esophageal squamous cell cancer with synchronous rectal cancer: Four case reports and a literature review. *Mol Clin Oncol* 2020;

12: 23-30 [PMID: 31814973 DOI: 10.3892/mco.2019.1945]

19 **Kim EJ**, Lee JG, Kim JY, Song SH, Joo DJ, Huh KH, Kim MS, Kim BS, Kim YS. Enhanced immune-modulatory effects of thalidomide and dexamethasone co-treatment on T cell subsets. *Immunology* 2017; **152**: 628-637 [PMID: 28758197 DOI: 10.1111/imm.12804]

20 **Zhao J**, Lei J, Yu J, Zhang C, Song X, Zhang N, Wang Y, Zhang S. Clinical efficacy and safety of apatinib combined with S-1 in advanced esophageal squamous cell carcinoma. *Invest New Drugs* 2020; **38**: 500-506 [PMID: 31650447 DOI: 10.1007/s10637-019-00866-5]

21 **Zhao H**, Chen W, Wu J, Wang L, Mao W. Clinical significance of preoperative serum tumor markers in esophageal squamous cell carcinoma. *J Cancer Res Ther* 2014; **10** Suppl: C179-C185 [PMID: 25450279 DOI: 10.4103/0973-1482.145863]

22 **Li Z**, Qian J, Li J, Zhu C. Clinical Significance of Serum Chemokines in Esophageal Cancer. *Med Sci Monit* 2019; **25**: 5850-5855 [PMID: 31385574 DOI: 10.12659/MSM.916846]

23 **Kilic E**, Schild SE, Thorns C, Bajrovic A, Rades D. Prognostic role of vascular endothelial growth factor and its receptor-1 in patients with esophageal cancer. *Anticancer Res* 2014; **34**: 5221-5226 [PMID: 25202119]

24 **Kitadai Y**, Onogawa S, Kuwai T, Matsumura S, Hamada H, Ito M, Tanaka S, Yoshihara M, Chayama K. Angiogenic switch occurs during the precancerous stage of human esophageal squamous cell carcinoma. *Oncol Rep* 2004; **11**: 315-319 [PMID: 14719061]

25 **Zhou YZ**, Fang XQ, Li H, Diao YT, Yang YF, Zhao DL, Wu K, Li HQ. Role of serum angiopoietin-2 level in screening for esophageal squamous cell cancer and its precursors. *Chin Med J (Engl)* 2007; **120**: 1216-1219 [PMID: 17697570]

26 **Wang J**, Yu J, Wang J, Ni X, Sun Z, Sun W, Sun S, Lu Y. Thalidomide combined with chemo-radiotherapy for treating esophageal cancer: A randomized controlled study. *Oncol Lett* 2019; **18**: 804-813 [PMID: 31289557 DOI: 10.3892/ol.2019.10354]

27 **Tsuji W**, Ishiguro H, Tanaka S, Takeuchi M, Ueno T, Toi M. Orally administered S-1 suppresses circulating endothelial cell counts in metastatic breast cancer patients. *Int J Clin Oncol* 2014; **19**: 452-459 [PMID: 23739924 DOI: 10.1007/s10147-013-0570-5]

World Journal of Gastrointestinal Oncology

Submit a Manuscript: https://www.f6publishing.com

World J Gastrointest Oncol 2023 July 15; 15(7): 1271-1282

DOI: 10.4251/wjgo.v15.i7.1271

ISSN 1948-5204 (online)

ORIGINAL ARTICLE

Retrospective Study

Development and validation of an online calculator to predict the pathological nature of colorectal tumors

Ya-Dan Wang, Jing Wu, Bo-Yang Huang, Chun-Mei Guo, Cang-Hai Wang, Hui Su, Hong Liu, Miao-Miao Wang, Jing Wang, Li Li, Peng-Peng Ding, Ming-Ming Meng

Specialty type: Oncology

Provenance and peer review: Unsolicited article; Externally peer reviewed.

Peer-review model: Single blind

Peer-review report's scientific quality classification

Grade A (Excellent): 0
Grade B (Very good): B, B
Grade C (Good): 0
Grade D (Fair): 0
Grade E (Poor): 0

P-Reviewer: Maher CA, United States; Rumpold H, Austria

Received: April 1, 2023
Peer-review started: April 1, 2023
First decision: April 19, 2023
Revised: April 27, 2023
Accepted: May 22, 2023
Article in press: May 22, 2023
Published online: July 15, 2023

Ya-Dan Wang, Chun-Mei Guo, Cang-Hai Wang, Hui Su, Hong Liu, Miao-Miao Wang, Jing Wang, Li Li, Peng-Peng Ding, Ming-Ming Meng, Department of Gastroenterology, Beijing Shijitan Hospital, Capital Medical University, Beijing 100038, China

Jing Wu, Department of Gastroenterology, Beijing Friendship Hospital, Capital Medical University, National Clinical Research Center for Digestive Diseases, Beijing Digestive Disease Center, Beijing Key Laboratory for Precancerous Lesion of Digestive Diseases, Beijing 100050, China

Bo-Yang Huang, Department of Gastroenterology, Beijing Shijitan Hospital, the Ninth Clinical Medicine Peking University, Beijing 100038, China

Corresponding author: Jing Wu, DO, MD, PhD, Dean, Doctor, Professor, Department of Gastroenterology, Beijing Friendship Hospital, Capital Medical University, National Clinical Research Center for Digestive Diseases, Beijing Digestive Disease Center, Beijing Key Laboratory for Precancerous Lesion of Digestive Diseases, No. 59 Yong'an Road, Xicheng District, Beijing 100050, China. wujing36youyi@ccmu.edu.cn

Abstract

BACKGROUND

No single endoscopic feature can reliably predict the pathological nature of colorectal tumors (CRTs).

AIM

To establish and validate a simple online calculator to predict the pathological nature of CRTs based on white-light endoscopy.

METHODS

This was a single-center study. During the identification stage, 530 consecutive patients with CRTs were enrolled from January 2015 to December 2021 as the derivation group. Logistic regression analysis was performed. A novel online calculator to predict the pathological nature of CRTs based on white-light images was established and verified internally. During the validation stage, two series of 110 images obtained using white-light endoscopy were distributed to 10 endoscopists [five highly experienced endoscopists and five less experienced endoscopists (LEEs)] for external validation before and after systematic training.

RESULTS
A total of 750 patients were included, with an average age of 63.6 ± 10.4 years. Early colorectal cancer (ECRC) was detected in 351 (46.8%) patients. Tumor size, left semicolon site, rectal site, acanthosis, depression and an uneven surface were independent risk factors for ECRC. The C-index of the ECRC calculator prediction model was 0.906 (P = 0.225, Hosmer–Lemeshow test). For the LEEs, significant improvement was made in the sensitivity, specificity and accuracy (57.6% *vs* 75.5%; 72.3% *vs* 82.4%; 64.2% *vs* 80.2%; $P < 0.05$), respectively, after training with the ECRC online calculator prediction model.

CONCLUSION
A novel online calculator including tumor size, location, acanthosis, depression, and uneven surface can accurately predict the pathological nature of ECRC.

Key Words: Pathological nature; Colorectal tumors; White-light endoscopy; Online calculator; Early colorectal cancer

Core Tip: White light endoscopy remains the most basic and indispensable tool in diagnosing colorectal tumors (CRTs). No single endoscopic feature can reliably predict the pathological nature of CRTs. Here, we investigated the endoscopic findings of CRTs, including lobulation, erosion, expansion, depression, acanthosis, lifting sign, stiffness, nodules larger than 10 mm, and so on. A logistic regression analysis was performed, and a novel online calculator for predicting the pathological nature of CRTs based on white-light imaging was established and verified.

Citation: Wang YD, Wu J, Huang BY, Guo CM, Wang CH, Su H, Liu H, Wang MM, Wang J, Li L, Ding PP, Meng MM. Development and validation of an online calculator to predict the pathological nature of colorectal tumors. *World J Gastrointest Oncol* 2023; 15(7): 1271-1282
URL: https://www.wjgnet.com/1948-5204/full/v15/i7/1271.htm
DOI: https://dx.doi.org/10.4251/wjgo.v15.i7.1271

INTRODUCTION

According to the latest global cancer statistics[1], there were more than 1.9 million new cases of colorectal cancer (CRC) and more than 930000 deaths worldwide in 2020. CRC ranks third in terms of incidence and second in terms of mortality among all malignancies. In China, the incidence of CRC has been increasing yearly, partially attributed to lifestyle changes and a westernized dietary pattern[2]. CRC is generally defined as malignant progression from adenomas through an adenoma–carcinoma sequence[3,4]. Early detection and removal of adenomas will provide an opportunity for screening and preventing the development of early CRC (ECRC). This strategy can substantially reduce the incidence and mortality of CRC[5,6].

Colorectal adenoma (CRA) and ECRC (including high-grade intraepithelial neoplasia and intramucosal cancer) are absolute indications for endoscopic treatment. superficial Submucosal invasion (SMI) corresponding to submucosal invasion < 1000 μm) stage CRC with superficial infiltration is a relative indication for endoscopic treatment. This approach requires strict pathological evaluation of resected specimens to determine the presence of lymphatic and vascular infiltration and the necessity for extensive surgery[7]. Therefore, it is important to differentiate colorectal neoplastic from nonneoplastic lesions and to determine the depth of invasion of colorectal neoplastic lesions based on endoscopic features. At present, Kudo's pit, capillary, and surface vascular patterns are widely applied to assess the risk of CRC[8-10]. However, these staging systems require staining endoscopy, magnification endoscopy (ME), narrow-band imaging (NBI), and experienced endoscopists who can perform NBI and ME. However, ordinary hospitals lack experienced endoscopists and top-tier endoscopic equipment, so the above staging systems are not applicable. In this study, we aimed to establish a simple, practical and stable online calculator to predict the nature of colorectal tumors (CRTs) based on white-light imaging (WLI). This calculator can assist endoscopists in diagnosing ECRC, improving the detection rate, and selecting treatment protocols.

MATERIALS AND METHODS

Participants

We carefully reviewed two datasets: One for the development and internal validation of a calculator and another for the external validation of the calculator. Patients who met the following inclusion criteria were recruited: (1) ECRC or CRA detected by colonoscopy; (2) Accurate pathological diagnosis; and (3) High-quality endoscopic images. The histological diagnosis was based on the World Health Organization criteria. Exclusion criteria included the following: (1) ECRC or

CRA not treated with endoscopy or surgery; (2) Patients with familial adenomatous polyposis, Lynch syndrome or Peutz–Jeghers syndrome, inflammatory bowel disease, intestinal tuberculosis; (3) Patients who underwent colectomy for other diseases; (4) Poor intestinal preparation; and (5) Patients with incomplete medical records. Patient demographics (age and sex) and clinicopathological characteristics (tumor location, size, differentiation, gross type, depth of invasion), as well as endoscopic features (redness, erosion, expansion, depression, uneven surface, lobulation, acanthosis, and nodules larger than 10 mm), were independently evaluated by three experienced endoscopists.

A total of 10 endoscopists with varying levels of experience participated in the present study. The endoscopists were divided into two groups: A group of less experienced endoscopists (LEEs) who had performed fewer than 1000 colonoscopies and a group of highly experienced endoscopists (HEEs) who had performed more than 3000 colonoscopies[11].

Study design

The present study consisted of two phases. During the identification phase, we retrospectively reviewed 530 patients who underwent surgery or endoscopic treatment for ECRC or CRA between January 2015 and December 2021 at Beijing Shijitan Hospital, Capital Medical University. Baseline information on demographic, clinicopathological and endoscopic characteristics of all patients was collected. Then, logistic regression analysis was performed, and a novel online calculator to predict the pathological nature of CRTs based on WLI was developed and verified internally.

During the validation phase, external validation of the calculator was performed. Ten endoscopists were required to independently evaluate a series of 110 images of CRTs according to WLI. Then, a systematic training program on this online calculator was conducted. During the training process, a schematic representation of the calculator was posted on the wall of each endoscopic room, and the images (Figure 1) used to educate the participants were presented in PowerPoint (Microsoft Corp.) by the leading investigator who was not involved in this study. Afterward, the participants were immediately asked to score another series of 110 images of CRTs by using the calculator (posttest). These images were retrospectively collected from 220 CRT patients who had undergone colonoscopy between January 2015 and December 2021 by the leading investigator.

Evaluation of endoscopic findings

All endoscopic images were taken using an endoscope (PCF-H260, PCF-Q260, CF-H260, CF-HQ290 and PCF-H290; Olympus, Tokyo, Japan) during preoperative diagnosis based on WLI. Generally, NBI + ME, stained endoscopy and ultrasound endoscopic evaluation were performed when carcinoma or submucosal carcinoma was suspected. The location, diameter, color, substrate, surface and morphology of the tumors were noted. Tumor location was divided into the right colon (including the cecum, ascending colon, transverse colon, and splenic flexure), left colon (including the descending colon and sigmoid colon) and rectum. Lesion size was estimated using 7 mm diameter open-biopsy forceps. Paris staging[12] was used to classify and describe the morphology, while tumors larger than 10 mm growing superficially along the intestinal lumen were defined as the laterally spreading tumor (LST) type.

We investigated endoscopic findings of the CRTs, including lobulation, erosion, expansion, depression, acanthosis, lifting sign, stiffness, and nodules larger than 10 mm. The definitions of the eight endoscopic findings were as follows (Figure 1): (1) Hyperemia: Redness and hyperemia on the surface of a tumor; (2) Erosion: Erosion and hyperemia on the surface of a tumor; (3) Acanthosis: Chicken skin mucosa beside the tumor; (4) Lobulation: Multiple nodules on the surface of a tumor; (5) Depression: Depressed demarcation on the surface of a tumor; (6) Expansion: A bursting appearance due to the expansive growth of a tumor; (7) Large nodule: Nodules larger than 10 mm; and (8) Uneven surface: Surface with bulges and depressions.

This study was approved by the Ethics Committee of Beijing Shijitan Hospital, Capital Medical University, No. sjtkyll-lx-2020 (19). The requirement to obtain informed consent was waived owing to the retrospective-design portion of the study. In the prospective-design portion of the study, informed consent was obtained from patients before endoscopy.

Statistical analysis

All statistical analyses were conducted using SPSS version 21.0 for Windows (SPSS, Chicago, IL, United States). Baseline information on demographic, endoscopic and clinicopathological characteristics was collected as candidate risk variables. The nature of CRTs was defined as a dependent variable. Continuous variables are presented as the mean ± SD, whereas categorical variables are presented as percentages. For comparisons of categorical and continuous variables, chi-square tests or individual sample t tests were applied, as appropriate. Univariate logistic regression analyses were performed on the derivation dataset to identify risk factors for ECRC. Multivariable logistic regression analyses were conducted on variables with a $P < 0.05$ for univariate analysis. The multivariate logistic regression model was built from the set of candidate variables by removing predictors based on P values in a stepwise manner. Model discrimination was assessed by calculating the area under the receiver operator characteristic (AUROC) curve (or C-index), whereas model calibration was determined by the Hosmer–Lemeshow (H-L) test. The nomogram was formulated based on multivariate analysis by using the RMS package (R software 4.1.3). The performance of the nomogram model was examined by calibration (calibration curves), discrimination (AUC) and clinical usefulness (decision curves), which was validated in the validation cohort. The "shiny: Web Application Framework for R" package was used to develop an online tool (https://nomogram7474.shinyapps.io/DynNomapp/).

The performance of the calculator in the histological prediction of CRTs included sensitivity, specificity, predictive values, and accuracy. All these indicators were calculated in 2 phases, with the histopathological diagnosis as the gold standard. Estimation of diagnostic accuracy was based on average values and 95%CI. Sensitivity, specificity, and accuracy were compared between the two phases and between the two groups by using the paired-samples Student's t-test and independent-samples Student's-test, respectively. A $P < 0.05$ was considered statistically significant.

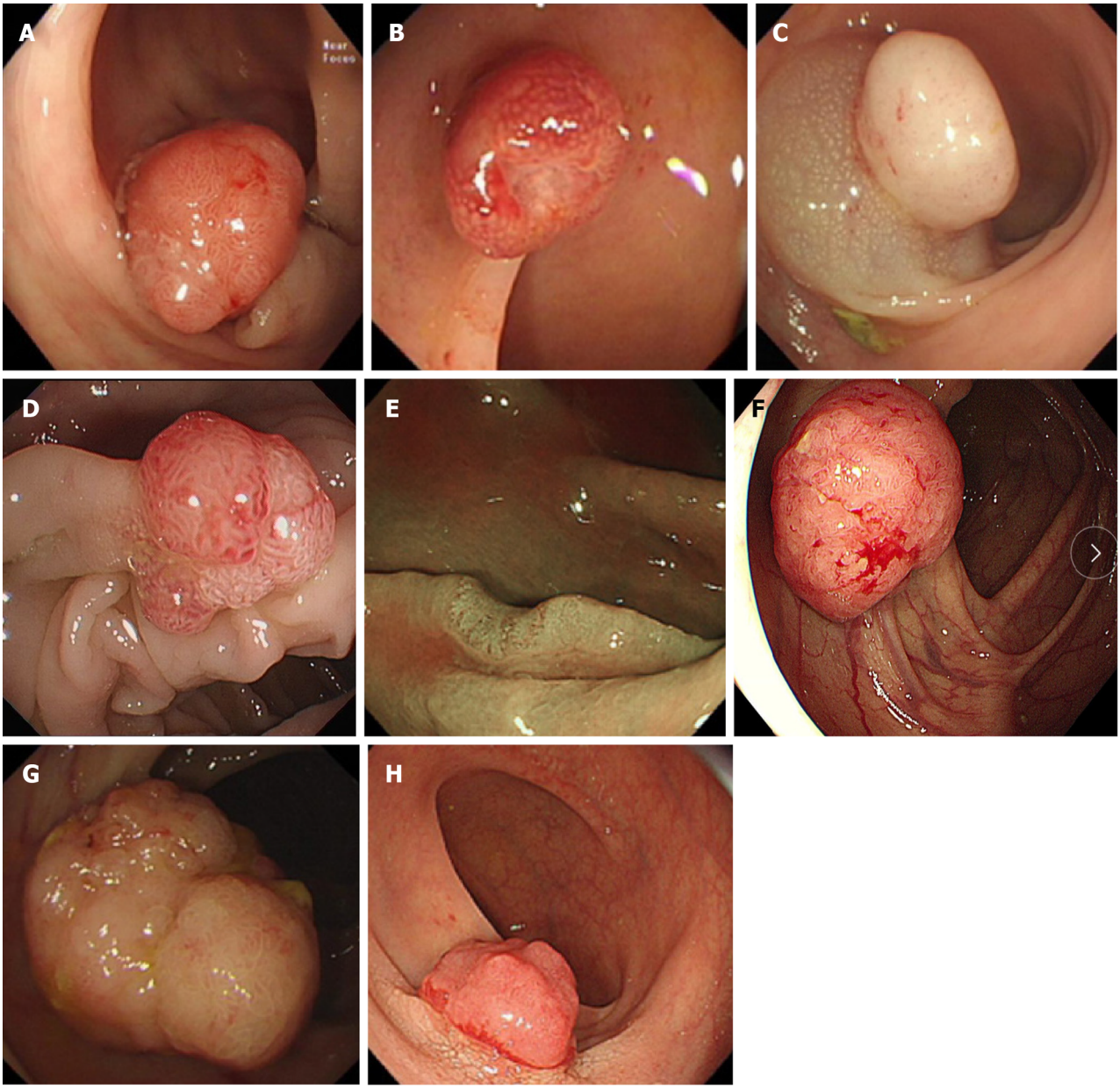

DOI: 10.4251/wjgo.v15.i7.1271 **Copyright** ©The Author(s) 2023.

Figure 1 The definitions of the eight endoscopic findings. A: Hyperemia: redness on the surface of a tumor; B: Erosion: erosion and hyperemia on the surface of a tumor; C: Acanthosis: chicken skin mucosa beside the tumor; D: Lobulation: multiple nodules on the surface of a tumor; E: Depression: depressed demarcation on the surface of a tumor; F: Expansive appearance: a bursting appearance due to the expansive growth of a tumor; G: Larger nodule: nodules larger than 10 mm; H: Uneven surface: surface with bulges and depressions.

RESULTS

Patient characteristics

A total of 750 patients were enrolled in this study, with 530 cases in the derivation group and 220 cases in the validation group. The mean age was 63.6 ± 10.4 years, and 499 patients (66.5%) were male. ECRC was detected in 351 (46.8%) patients, including 243 (45.8%; 243/530) in the derivation group and 108 (49.1%; 108/220) in the validation group. The incidence of ECRC was not significantly different between the derivation group and the validation group ($P > 0.05$). The mean size of the lesion was 15.32 ± 9.68 mm. Lesions were located in the right semicolon ($n = 358$), left semicolon ($n = 266$), and rectum ($n = 126$). The size and location of the lesions were not significantly different between the derivation group and the validation group ($P > 0.05$).

Risk factors for ECRC

In univariate models, location, size, hyperemia, erosion, acanthosis, lobulation, depression, expansive appearance, a large nodule and an uneven surface were associated with the development of ECRC ($P < 0.05$) (Table 1).

Table 1 Clinical and endoscopic characteristics of patients with colorectal adenoma and early colorectal cancer in model cohorts

Variables	CRA (*n* = 287)	ECRC (*n* = 243)	*P* value
Sex			0.296
Male (*n*, %)	191 (66.6)	172 (70.8)	
Female (*n*, %)	96 (33.4)	71 (29.2)	
Age (yr) (mean ± SD)	60.86 ± 10.37	64.65 ± 9.91	0.146
Type			0.086
0-I (*n*, %)	210 (73.2)	180 (74.1)	
0-II (*n*, %)	45 (15.7)	25 (10.3)	
LST (*n*, %)	32 (11.1)	38 (15.6)	
Location			0
Rectum (*n*, %)	26 (9.1)	54 (22.2)	
Left semicolon (*n*, %)	140 (48.8)	136 (56.0)	
Right semicolon (*n*, %)	121 (42.2)	53 (21.8)	
Size (mm, mean ± SD)	10.36 ± 5.61	19.28 ± 11.36	0
Size (mm)			0
< 10 (*n*, %)	147 (51.2)	25 (10.3)	
≥ 10 (*n*, %)	140 (48.8)	218 (89.7)	
Size (mm)			0
≤ 20 (*n*, %)	257 (89.5)	129 (53.1)	
> 20 (*n*, %)	30 (10.5)	114 (46.9)	
White-light endoscopy			
Hyperemia (*n*, %)	76 (26.5)	160 (65.8)	0
Erosion (*n*, %)	3 (1.0)	38 (15.6)	0
Acanthosis (*n*, %)	57 (19.9)	166 (68.3)	0
Lobulation (*n*, %)	66 (23.0)	100 (41.2)	0
Depression (*n*, %)	12 (4.2)	74 (30.5)	0
Expansive appearance (*n*, %)	37 (12.9)	63 (25.9)	0
Large nodule (*n*, %)	15 (5.2)	44 (18.1)	0
Uneven surface (*n*, %)	24 (8.4)	125 (51.4)	0

LST: Laterally spreading tumor; CRA: Colorectal adenoma; ECRC: Early colorectal cancer.

In multivariate models, size [odds ratio (OR), 5.233; 95%CI, 2.008-13.636], left semicolon site (OR, 2.338; 95%CI, 1.329-4.111), rectal site (OR, 3.715; 95%CI, 1.692-8.160), acanthosis (OR, 5.199; 95%CI, 3.057-8.842), depression (OR, 5.162; 95%CI, 2.216-12.021) and an uneven surface (OR, 5.583; 95%CI, 3.030-10.286) were independent risk factors for ECRC (Table 2).

Development of the nomogram and the calculator

An online calculator to predict the pathological nature of CRTs was established according to the above six independent risk factors (size, left semicolon site, rectal site, acanthosis, depression and uneven surface). A nomogram was constructed with point scales of these variables (Figure 2). The sum of each variable point was plotted on the total point axis. The probability rate of ECRC was obtained by drawing a vertical line from the plotted total point axis straight down to the outcome axis. Based on these nomogram models, online web-based calculators were developed to assess the probability of ECRC among patients with CRTs. The calculator is available at https://nomogram7474.shinyapps.io/DynNomapp/. When users simply input the requested information, the probability of ECRC can be derived (Figure 3).

Validation of the prediction calculator

After performing the internal validation by generating 1000 bootstrap replications, the calculator remained highly accurate, with a resulting AUROC (C-index) of 0.906 (95%CI, 0.880-0.932) (Figure 4). Moreover, the calibration plot of the

Table 2 Risk factors for early colorectal cancer in the multivariable logistic regression model

Variable	Univariate Model	Multivariate Model		
	P value	OR (95%CI)	β	*P* value
Size	< 0.001	5.233 (2.008-13.636)	1.655	0.001
Left semicolon	< 0.001	2.338 (1.329-4.111)	0.849	0.003
Rectum	< 0.001	3.715 (1.692-8.160)	1.312	0.001
Hyperemia	< 0.001	1.305 (0.756-2.251)	0.266	0.339
Erosion	< 0.001	3.848 (0.820-18.052)	1.348	0.088
Acanthosis	< 0.001	5.199 (3.057-8.842)	1.648	0
Lobulation	< 0.001	1.276 (0.729-2.233)	0.243	0.394
Depression	< 0.001	5.162 (2.216-12.021)	1.641	0
Expansive appearance	< 0.001	0.910 (0.471-1.756)	-0.095	0.778
Large nodule	< 0.001	1.146 (0.480-2.732)	0.136	0.759
Uneven surface	< 0.001	5.583 (3.030-10.286)	1.72	0

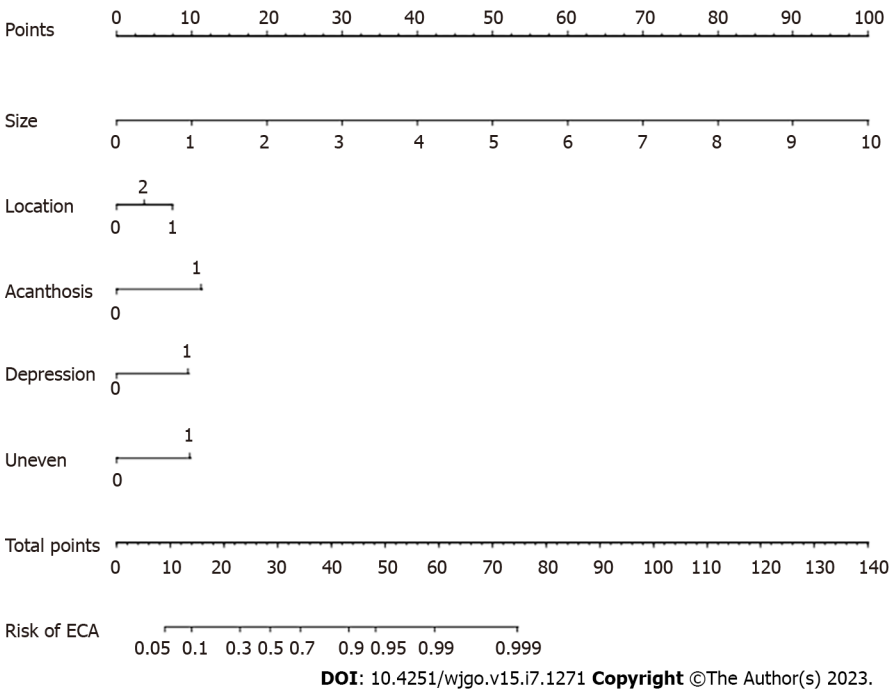

DOI: 10.4251/wjgo.v15.i7.1271

Figure 2 Nomogram for predicting the pathological nature of colorectal tumors. ECA: Early colorectal adenocarcinoma.

internal validation demonstrated good calibration (χ^2 = 10.614; P = 0.225) with the Hosmer-Lemeshow (H–L) test (Figure 5). Decision Curve Analysis was performed to ascertain its clinical usefulness (Figure 6). These results indicated good clinical applicability of the calculator in predicting the pathological nature of CRT according to good net benefit with wide and practical ranges of threshold probabilities.

To explore whether the calculator would be applicable to endoscopists, we conducted an external validation study among 10 endoscopists with varying levels of experience. Comparisons of performance for diagnosing CRT histology between the pretraining test and posttraining test (Table 3) were as follows: LEEs made significant improvements in the sensitivity, specificity and accuracy in the posttraining test compared with the pretraining test. The LEEs' performance characteristics in the pretraining test *vs* posttraining test were as follows: Sensitivity 57.6% *vs* 75.5% (P = 0.004), specificity 72.3% *vs* 82.4% (P = 0.023), and accuracy 64.2% *vs* 80.2% (P < 0.001). The κ-values of the LEEs in the pretraining test and posttraining test were 0.72 and 0.83, respectively, indicating good (> 0.60) to excellent (> 0.80) agreement. The HEEs made significant improvement in sensitivity in the posttraining test compared with the pretraining test but not in specificity or accuracy. The HEEs' performance in the pretraining test *vs* posttraining test were as follows: Sensitivity 71.2% *vs* 80.4% (P = 0.043), specificity 82.1% *vs* 88.2% (P = 0.223), and accuracy 76.5% *vs* 86.0% (P = 0.071). The κ-values of the HEEs in the pretraining test and posttraining test were 0.81 and 0.89, respectively. The κ-values were improved in both groups,

Table 3 Sensitivity, specificity, and accuracy in histology prediction during the pretraining test and posttraining test

Group	Pretraining test (95%CI)	Posttraining test (95%CI)	*P* value
LEE			
Sensitivity	57.6 (48.5-66.4)	75.5 (67.0-82.4)	0.004
Specificity	72.3 (61.8-80.5)	82.4 (74.2-88.5)	0.032
Accuracy	64.2 (56.4-70.3)	80.2 (71.3-87.6)	< 0.001
HEE			
Sensitivity	71.2 (60.4-80.1)	80.4 (71.6-88.1)	0.043
Specificity	82.1 (73.8-88.2)	88.2 (81.5-95.3)	0.223
Accuracy	76.5 (69.3-83.6)	86.0 (80.2-91.7)	0.071

LEE: Less-experienced endoscopists; HEE: Highly experienced endoscopists.

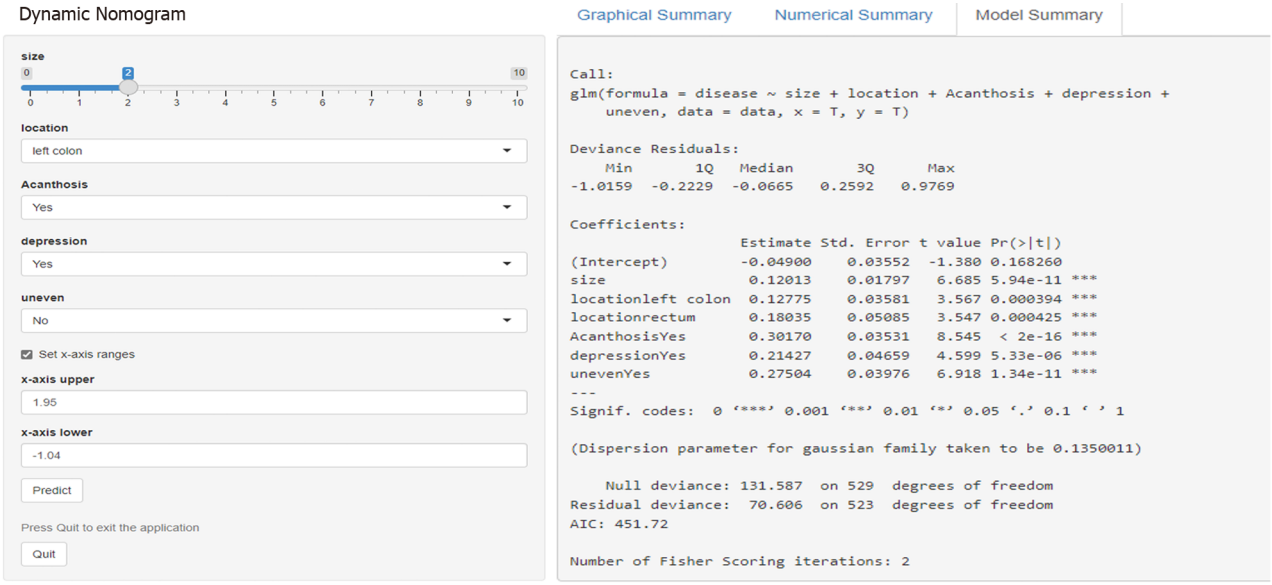

DOI: 10.4251/wjgo.v15.i7.1271

Figure 3 Internet browser-based online calculator. The online tool: (https://nomogram7474.shinyapps.io/DynNomapp/).

especially in the LEEs, suggesting that the LEEs benefited more from this predicting calculator.

DISCUSSION

CRA is a precancerous lesion of CRC, since most CRCs develop from CRAs through the adenoma-carcinoma pathway. Without timely intervention, precancerous lesions will progress to CRC within 10 to 15 years[13]. Notably, if the lesions are detected in the early stages of CRC and treated in a timely manner, the 5-year survival rate of these patients can reach as high as 90%[14]. In contrast, if the lesions are detected in the late stages of CRC, the 5-year survival rate will be reduced to less than 10%. Colonic endoscopy can be used for direct observation of intestinal lesions, which is irreplaceable in the examination of intestinal diseases, especially CRC. To improve the detection rate of precancerous lesions and early-stage CRC, assistive techniques, such as chromoendoscopy, magnifying endoscopy, fluorescence endoscopy, confocal laser endoscopy, and electronic staining endoscopy, have been introduced into clinical practice. However, the process of chromoendoscopy is complicated, time-consuming, labor-intensive, and requires magnification endoscopes. In addition, fluorescence endoscopy and confocal laser endoscopy are expensive. These disadvantages limit the application of the above techniques. Moreover, in clinical practice, the experience and the degree of image interpretation can vary greatly between endoscopists, which results in different judgments being made for the same lesion and thus a decrease in the accuracy of colonoscopy. To solve this problem, many endoscopists with extensive experience have defined and standardized the characteristics of CRTs, and several staging systems have been established and promoted in an attempt to improve the diagnostic accuracy and to reduce the possibility of missed diagnoses. With the advent of magnifying

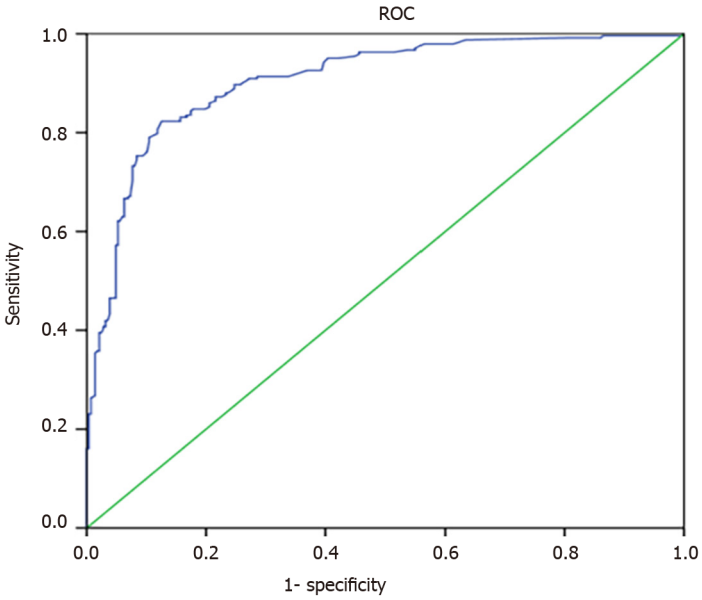

DOI: 10.4251/wjgo.v15.i7.1271 **Copyright** ©The Author(s) 2023.

Figure 4 Receiver operator characteristic curve in the validation cohort. ROC: The receiver operator characteristic curve.

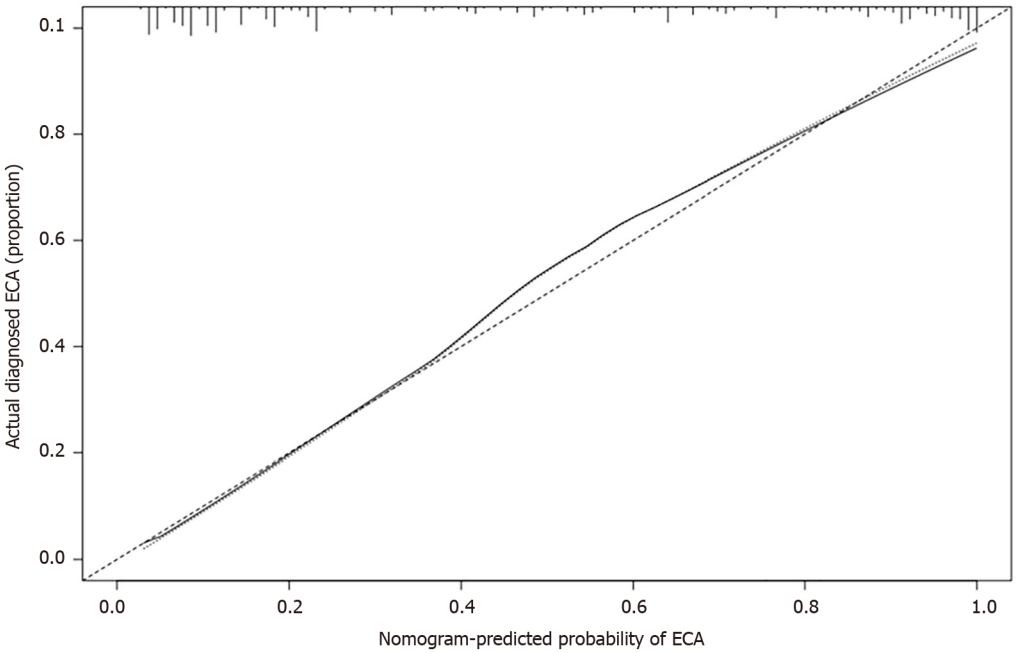

DOI: 10.4251/wjgo.v15.i7.1271 **Copyright** ©The Author(s) 2023.

Figure 5 Calibration plot of the prediction. The calibration curve shows good consistency between the predicted risk of early colorectal adenocarcinoma and the actual risk of pathological assessment using nomogram. ECA: Early colorectal adenocarcinoma.

endoscopy, the resolution of imaging has substantially improved. Currently, endoscopists can clearly observe the morphology of glandular duct openings and microvasculature on the mucosal surface of CRTs. Kudo's pit pattern classification[15] under magnifying chromoendoscopy was proposed in 1994. Later, a microvessel pattern under magnifying NBI was proposed by Sano *et al*[16] in 2006. These staging systems have been highly effective in predicting the histology of CRTs. Subsequently, JNET typing[17], Hiroshima typing[18], and Jikei typing[19] emerged based on mucosal microvascular morphology and surface structure. These typing systems have better performance in differentiating colorectal neoplastic and nonneoplastic lesions by combining the endoscopic features of lesions. Accordingly, the accuracy of differentiating benign from malignant lesions can be improved by providing appropriate training to primary endoscopists. However, the above typing systems require time-consuming, labor-intensive, and magnification endoscopes. Unfortunately, magnification endoscopes are not widely applied in the majority of primary-level hospitals, and LEE lacks experience in NBI + ME. These conditions limit the promotion of staging systems such as Kudo' pit pattern classification, NICE, and JNET in primary-level hospitals. Therefore, in this study, we established an online calculator to

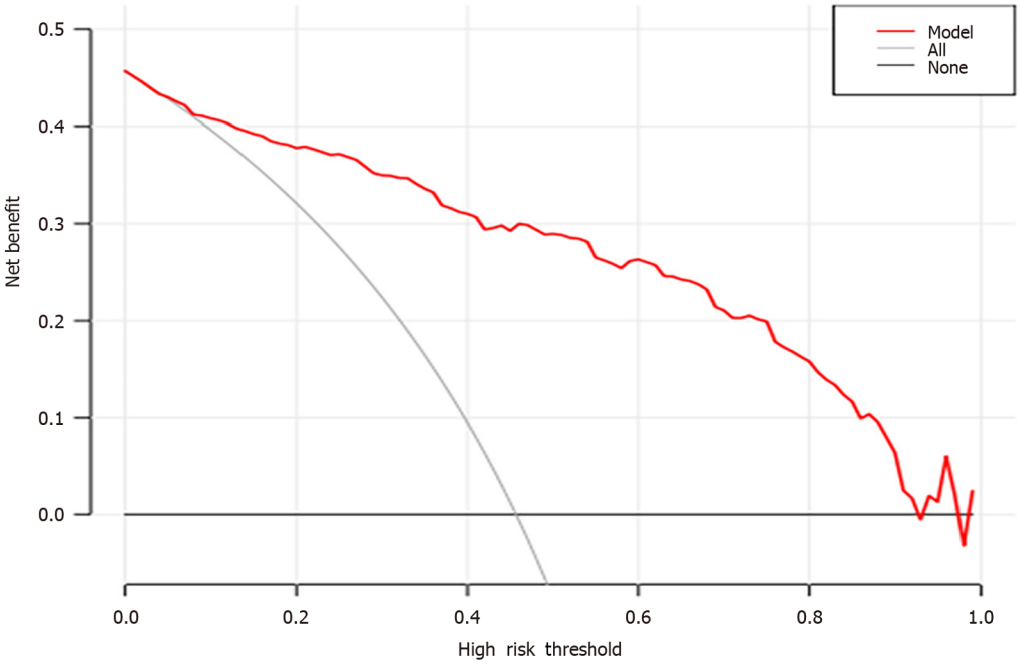

DOI: 10.4251/wjgo.v15.i7.1271

Figure 6 Decision curve analysis curve for the prediction model. The Decision Curve Analysis curve indicated good clinical applicability of the calculator in predicting the pathological nature of colorectal tumor.

predict the pathological nature of CRTs based on white-light endoscopy. The model consists of five variables: Location of the lesion, size of the lesion, acanthosis, depression, and an uneven surface. The AUC of the scoring system in our modeling cohort was 0.906 (> 0.80), indicating a good degree of differentiation. Based on the Hosmer-Lemeshow goodness-of-fit test (P = 0.225, > 0.1), our prediction model has value for risk stratification among patients with CRTs of unknown nature, which can provide a preliminary basis for the differential diagnosis of CRT. External verification identified significant improvement in the sensitivity and specificity in the posttraining test compared with the pretraining test, especially in the LEEs. Thus, this calculator may be applicable in primary-level hospitals. Our model and its scoring system may have good clinical credibility. First, the methods used for establishing and verifying the models are widely accepted, with external validation among endoscopists with different levels of experience. Second, all of the potential predictors were included, and there were no obvious missing items. Third, five variables (location, size, acanthosis, depression, and uneven surface) associated with CRC were obtained by logistic regression models.

The incidence of left-sided CRC (LCRC) is higher than that of right-sided CRC (RCRC). The American Cancer Society confirms a higher proportion of LCRC (51%) than RCRC (42%) in the United States[20]. Patients with RCRC present with more advanced tumor stages than those with LCRC[21]. Furthermore, higher TNM stages, larger tumors, increased frequency of vascular invasion, mucinous type, high grades and invasive tumor borders were more common in RCRC, whereas annular and polypoid tumors were more common in LCRC[21,22]. In our study, more patients were diagnosed with LCRC than RCRC, which was similar to previous studies.

CRC originates from a CRA, which slowly increases in size, followed by dysplasia and malignant transformation[23]. The size of a CRA is predictive for CRC diagnosis, which underscores the significance of this factor, especially considering its association with a less favorable histology and increased long-term risk of CRC[24]. The 10 mm cutoff represents a critical factor, since a small percentage of larger polyps contain cancerous cells[25,26]. Of the 530 Lesions with CRTs, 243 were diagnosed as ECRC. The mean size of the lesions was 19.28 ± 11.36 mm, of which 89.7% were ≥ 10 mm, consistent with previous studies.

It was reported that demarcated depression, fullness, and stalk swelling were typical findings of ECRC. Notably, 2.0% of the tumors were carcinoma, especially depressed tumors, which had a significantly higher frequency of carcinoma and submucosal invasion regardless of tumor size[27]. The Japanese Guideline for CRC has listed the following endoscopic findings as diagnostic indicators of SM-Ca: Expansive appearance, erosion/ulceration, fold convergence, and deformation/stiffness[28]. In univariate models, most lesions of ECRC had the following characteristics based on WLI: Hyperemia, erosion, acanthosis, lobulation, depression, expansive (sun-burst) appearance, larger nodules, and an uneven surface. In multivariate models, five independent risk factors, size, location, acanthosis, depression, and an uneven surface, were predictive indicators of ECRC. Thus, a simple online calculator to predict the pathological nature of CRTs based on the WLI was established, with an AUC value of 90.6% and high diagnostic specificity and accuracy. Internal and external validation of this model indicated good consistency of CRC risk with postoperative pathology and good agreement in application between endoscopists with various levels of experience.

CONCLUSION

In conclusion, we present a novel online calculator to predict the pathological nature of CRTs. This calculator may play a practical and important role in reducing the cost and duration of colonoscopy. However, this was a single-center study, and further high-quality, multicenter clinical studies should be conducted to assess the stability and generalizability of this scoring system.

ARTICLE HIGHLIGHTS

Research background

No single endoscopic feature can reliably predict the pathological nature of colorectal tumors (CRTs).

Research motivation

Kudo's pit, capillary, and surface vascular patterns that can predict the pathological nature of CRTs require experienced endoscopists who can perform narrow-band imaging and magnification endoscopy. This is difficult for endoscopists who lack experience and for endoscopists in ordinary hospitals.

Research objectives

This study aimed to establish and validate a simple online calculator to predict the pathological nature of CRTs based on white-light endoscopy.

Research methods

This was a single-center study. The endoscopic features of 530 cases of CRTs were analyzed, and logistic regression analysis was performed to establish a novel online calculator that can predict the pathological nature of CRTs. We also conducted internal and external validation on the modified model.

Research results

A novel online calculator including size, location, acanthosis, depression and unevenness to predict the pathological nature of CRTs based on white-light imaging was established. Internal and external validation of this model indicated good consistency of colorectal cancer risk with postoperative pathology.

Research conclusions

We present a novel online calculator to predict the pathological nature of CRTs. This calculator may be instrumental in reducing the cost and duration of colonoscopy.

Research perspectives

This calculator may play a practical and important role in primary-level hospitals and may significantly improve the diagnostic accuracy of primary physicians.

FOOTNOTES

Author contributions: Wang YD and Wu J designed the research study; Huang BY, Guo CM, Wang CH, Su H, Liu H, Wang MM, Wang J, Li L, Ding PP and Meng MM performed the primary literature and data extraction; Wang YD analyzed the data and wrote the manuscript; Wu J was responsible for revising the manuscript for important intellectual content; All authors read and approved the final version.

Supported by Capital's Funds for Health Improvement and Research, No. 2020-4-2085; and Beijing Science and Technology Plan Project, No. Z211100002921028.

Institutional review board statement: The study was reviewed and approved by the Beijing Shijitan Hospital, Capital Medical University Institutional Review Board, No. Sjtkyll-lx-2020 (19); and No. Sjtkyll-lx-2022 (033).

Informed consent statement: Prior to enrollment, all study participants or their legal guardians provided informed written consent for personal and medical data collection.

Conflict-of-interest statement: All the authors report no relevant conflicts of interest for this article.

Data sharing statement: Technical appendix, statistical code, and dataset available from the corresponding author at wujing36youyi@ccmu.edu.cn. Participants gave informed consent for data sharing.

Country/Territory of origin: China

ORCID number: Ya-Dan Wang 0000-0002-7126-9360; Jing Wu 0000-0001-8838-8692; Bo-Yang Huang 0009-0001-3629-8529; Chun-Mei Guo 0000-0002-6103-7849; Cang-Hai Wang 0000-0001-9422-0765; Hui Su 0000-0002-0517-9981; Hong Liu 0000-0003-2443-7808; Miao-Miao Wang 0000-0002-9769-8569; Jing Wang 0000-0002-5723-0566; Li Li 0000-0002-9422-1191; Peng-Peng Ding 0000-0002-0254-8446; Ming-Ming Meng 0000-0003-3560-1052.

S-Editor: Li L
L-Editor: A
P-Editor: Li L

REFERENCES

1 **Sung H**, Ferlay J, Siegel RL, Laversanne M, Soerjomataram I, Jemal A, Bray F. Global Cancer Statistics 2020: GLOBOCAN Estimates of Incidence and Mortality Worldwide for 36 Cancers in 185 Countries. *CA Cancer J Clin* 2021; **71**: 209-249 [PMID: 33538338 DOI: 10.3322/caac.21660]
2 **Chen W**, Zheng R, Baade PD, Zhang S, Zeng H, Bray F, Jemal A, Yu XQ, He J. Cancer statistics in China, 2015. *CA Cancer J Clin* 2016; **66**: 115-132 [PMID: 26808342 DOI: 10.3322/caac.21338]
3 **Vogelstein B**, Fearon ER, Hamilton SR, Kern SE, Preisinger AC, Leppert M, Nakamura Y, White R, Smits AM, Bos JL. Genetic alterations during colorectal-tumor development. *N Engl J Med* 1988; **319**: 525-532 [PMID: 2841597 DOI: 10.1056/NEJM198809013190901]
4 **Allen JI**. Molecular biology of colon polyps and colon cancer. *Semin Surg Oncol* 1995; **11**: 399-405 [PMID: 8607008 DOI: 10.1002/ssu.2980110606]
5 **Kahi CJ**, Rex DK, Imperiale TF. Screening, surveillance, and primary prevention for colorectal cancer: a review of the recent literature. *Gastroenterology* 2008; **135**: 380-399 [PMID: 18582467 DOI: 10.1053/j.gastro.2008.06.026]
6 **Zauber AG**, Winawer SJ, O'Brien MJ, Lansdorp-Vogelaar I, van Ballegooijen M, Hankey BF, Shi W, Bond JH, Schapiro M, Panish JF, Stewart ET, Waye JD. Colonoscopic polypectomy and long-term prevention of colorectal-cancer deaths. *N Engl J Med* 2012; **366**: 687-696 [PMID: 22356322 DOI: 10.1056/NEJMoa1100370]
7 **Tanaka S**, Saitoh Y, Matsuda T, Igarashi M, Matsumoto T, Iwao Y, Suzuki Y, Nozaki R, Sugai T, Oka S, Itabashi M, Sugihara KI, Tsuruta O, Hirata I, Nishida H, Miwa H, Enomoto N, Shimosegawa T, Koike K. Evidence-based clinical practice guidelines for management of colorectal polyps. *J Gastroenterol* 2021; **56**: 323-335 [PMID: 33710392 DOI: 10.1007/s00535-021-01776-1]
8 **Su MY**, Hsu CM, Ho YP, Chen PC, Lin CJ, Chiu CT. Comparative study of conventional colonoscopy, chromoendoscopy, and narrow-band imaging systems in differential diagnosis of neoplastic and nonneoplastic colonic polyps. *Am J Gastroenterol* 2006; **101**: 2711-2716 [PMID: 17227517 DOI: 10.1111/j.1572-0241.2006.00932.x]
9 **Togashi K**, Osawa H, Koinuma K, Hayashi Y, Miyata T, Sunada K, Nokubi M, Horie H, Yamamoto H. A comparison of conventional endoscopy, chromoendoscopy, and the optimal-band imaging system for the differentiation of neoplastic and non-neoplastic colonic polyps. *Gastrointest Endosc* 2009; **69**: 734-741 [PMID: 19251019 DOI: 10.1016/j.gie.2008.10.063]
10 **Rastogi A**, Keighley J, Singh V, Callahan P, Bansal A, Wani S, Sharma P. High accuracy of narrow band imaging without magnification for the real-time characterization of polyp histology and its comparison with high-definition white light colonoscopy: a prospective study. *Am J Gastroenterol* 2009; **104**: 2422-2430 [PMID: 19584829 DOI: 10.1038/ajg.2009.403]
11 **Macken E**, Moreels T, Vannoote J, Siersema PD, Van Cutsem E. Quality assurance in colonoscopy for colorectal cancer diagnosis. *Eur J Surg Oncol* 2011; **37**: 10-15 [PMID: 20951537 DOI: 10.1016/j.ejso.2010.09.013]
12 **Endoscopic Classification Review Group**. Update on the paris classification of superficial neoplastic lesions in the digestive tract. *Endoscopy* 2005; **37**: 570-578 [PMID: 15933932 DOI: 10.1055/s-2005-861352]
13 **Keum N**, Giovannucci E. Global burden of colorectal cancer: emerging trends, risk factors and prevention strategies. *Nat Rev Gastroenterol Hepatol* 2019; **16**: 713-732 [PMID: 31455888 DOI: 10.1038/s41575-019-0189-8]
14 **Courtney RJ**, Paul CL, Carey ML, Sanson-Fisher RW, Macrae FA, D'Este C, Hill D, Barker D, Simmons J. A population-based cross-sectional study of colorectal cancer screening practices of first-degree relatives of colorectal cancer patients. *BMC Cancer* 2013; **13**: 13 [PMID: 23305355 DOI: 10.1186/1471-2407-13-13]
15 **Kudo S**, Hirota S, Nakajima T, Hosobe S, Kusaka H, Kobayashi T, Himori M, Yagyuu A. Colorectal tumours and pit pattern. *J Clin Pathol* 1994; **47**: 880-885 [PMID: 7962600 DOI: 10.1136/jcp.47.10.880]
16 **Sano Y**, Horimatsu T, Fu KI, Katagiri A, Muto M, Ishikawa H. Magnifying observation of microvascular architecture of colorectal lesions using a narrow-band imaging system. *Dig. Endosc* 2006; **18**: 544-551 [DOI: 10.1111/j.1443-1661.2006.00621.x]
17 **Iwatate M**, Sano Y, Tanaka S, Kudo SE, Saito S, Matsuda T, Wada Y, Fujii T, Ikematsu H, Uraoka T, Kobayashi N, Nakamura H, Hotta K, Horimatsu T, Sakamoto N, Fu KI, Tsuruta O, Kawano H, Kashida H, Takeuchi Y, Machida H, Kusaka T, Yoshida N, Hirata I, Terai T, Yamano HO, Nakajima T, Sakamoto T, Yamaguchi Y, Tamai N, Nakano N, Hayashi N, Oka S, Ishikawa H, Murakami Y, Yoshida S, Saito Y; Japan NBI Expert Team (JNET). Validation study for development of the Japan NBI Expert Team classification of colorectal lesions. *Dig Endosc* 2018; **30**: 642-651 [PMID: 29603399 DOI: 10.1111/den.13065]
18 **Oka S**, Tanaka S, Takata S, Kanao H, Chayama K. Clinical usefulness of narrow band imaging magnifying classification for colorectal tumors based on both surface pattern and microvessel features. *Dig Endosc* 2011; **23** Suppl 1: 101-105 [PMID: 21535213 DOI: 10.1111/j.1443-1661.2011.01108.x]
19 **Wada Y**, Kudo SE, Misawa M, Ikehara N, Hamatani S. Vascular pattern classification of colorectal lesions with narrow band imaging magnifying endoscopy. *Dig Endosc* 2011; 23 Suppl 1: 106-111 [PMID: 21535214 DOI: 10.1111/j.1443-1661.2011.01109.x]
20 **Meza R**, Jeon J, Renehan AG, Luebeck EG. Colorectal cancer incidence trends in the United States and United kingdom: evidence of right- to

left-sided biological gradients with implications for screening. *Cancer Res* 2010; **70**: 5419-5429 [PMID: 20530677 DOI: 10.1158/0008-5472.CAN-09-4417]

21 **Cress RD**, Morris C, Ellison GL, Goodman MT. Secular changes in colorectal cancer incidence by subsite, stage at diagnosis, and race/ethnicity, 1992-2001. *Cancer* 2006; **107**: 1142-1152 [PMID: 16835912 DOI: 10.1002/cncr.22011]

22 **Gupta S**, Balasubramanian BA, Fu T, Genta RM, Rockey DC, Lash R. Polyps with advanced neoplasia are smaller in the right than in the left colon: implications for colorectal cancer screening. *Clin Gastroenterol Hepatol* 2012; **10**: 1395-1401.e2 [PMID: 22835574 DOI: 10.1016/j.cgh.2012.07.004]

23 **Qaseem A**, Denberg TD, Hopkins RH Jr, Humphrey LL, Levine J, Sweet DE, Shekelle P; Clinical Guidelines Committee of the American College of Physicians. Screening for colorectal cancer: a guidance statement from the American College of Physicians. *Ann Intern Med* 2012; **156**: 378-386 [PMID: 22393133 DOI: 10.7326/0003-4819-156-5-201203060-00010]

24 **Pickhardt PJ**, Pooler BD, Kim DH, Hassan C, Matkowskyj KA, Halberg RB. The Natural History of Colorectal Polyps: Overview of Predictive Static and Dynamic Features. *Gastroenterol Clin North Am* 2018; **47**: 515-536 [PMID: 30115435 DOI: 10.1016/j.gtc.2018.04.004]

25 **Parsa N**, Ponugoti P, Broadley H, Garcia J, Rex DK. Risk of cancer in 10 - 19 mm endoscopically detected colorectal lesions. *Endoscopy* 2019; **51**: 452-457 [PMID: 30620947 DOI: 10.1055/a-0799-9997]

26 **Halfter K**, Bauerfeind L, Schlesinger-Raab A, Schmidt M, Schubert-Fritschle G, Hölzel D, Engel J. Colonoscopy and polypectomy: beside age, size of polyps main factor for long-term risk of colorectal cancer in a screening population. *J Cancer Res Clin Oncol* 2021; **147**: 2645-2658 [PMID: 33543329 DOI: 10.1007/s00432-021-03532-7]

27 **Zhang YL**, Zhang ZS, Wu BP, Zhou DY. Early diagnosis for colorectal cancer in China. *World J Gastroenterol* 2002; **8**: 21-25 [PMID: 11833064 DOI: 10.3748/wjg.v8.i1.21]

28 **Watanabe T**, Itabashi M, Shimada Y, Tanaka S, Ito Y, Ajioka Y, Hamaguchi T, Hyodo I, Igarashi M, Ishida H, Ishihara S, Ishiguro M, Kanemitsu Y, Kokudo N, Muro K, Ochiai A, Oguchi M, Ohkura Y, Saito Y, Sakai Y, Ueno H, Yoshino T, Boku N, Fujimori T, Koinuma N, Morita T, Nishimura G, Sakata Y, Takahashi K, Tsuruta O, Yamaguchi T, Yoshida M, Yamaguchi N, Kotake K, Sugihara K; Japanese Society for Cancer of the Colon and Rectum. Japanese Society for Cancer of the Colon and Rectum (JSCCR) Guidelines 2014 for treatment of colorectal cancer. *Int J Clin Oncol* 2015; **20**: 207-239 [PMID: 25782566 DOI: 10.1007/s10147-015-0801-z]

World Journal of Gastrointestinal Oncology

Submit a Manuscript: https://www.f6publishing.com

World J Gastrointest Oncol 2023 July 15; 15(7): 1283-1294

DOI: 10.4251/wjgo.v15.i7.1283

ISSN 1948-5204 (online)

ORIGINAL ARTICLE

Retrospective Study

Efficacy of continuous gastric artery infusion chemotherapy in relieving digestive obstruction in advanced gastric cancer

Rui Tang, Guo-Feng Chen, Kai Jin, Guang-Qiang Zhang, Jian-Jun Wu, Shu-Gao Han, Bin Li, Ming Chao

Specialty type: Oncology

Provenance and peer review: Unsolicited article; Externally peer reviewed.

Peer-review model: Single blind

Peer-review report's scientific quality classification

Grade A (Excellent): A
Grade B (Very good): 0
Grade C (Good): C
Grade D (Fair): D
Grade E (Poor): 0

P-Reviewer: Augustin G, Croatia; Kawabata H, Japan

Received: March 27, 2023
Peer-review started: March 27, 2023
First decision: May 4, 2023
Revised: May 17, 2023
Accepted: June 8, 2023
Article in press: June 8, 2023
Published online: July 15, 2023

Rui Tang, Kai Jin, Guang-Qiang Zhang, Jian-Jun Wu, Shu-Gao Han, Bin Li, Ming Chao, Department of Radiology, The Second Affiliated Hospital of Zhejiang University School of Medicine, Hangzhou 310000, Zhejiang Province, China

Guo-Feng Chen, Department of Gastrointestinal Surgery, The Second Affiliated Hospital of Zhejiang University School of Medicine, Hangzhou 310000, Zhejiang Province, China

Corresponding author: Ming Chao, MD, Professor, Department of Radiology, The Second Affiliated Hospital of Zhejiang University School of Medicine, No. 88 Jiefang Road, Hangzhou 310000, Zhejiang Province, China. chaoming@zju.edu.cn

Abstract

BACKGROUND

Obstruction or fullness after feeding is common in gastric cancer (GC) patients, affecting their nutritional status and quality of life. Patients with digestive obstruction are generally in a more advanced stage. Existing methods, including palliative gastrectomy, gastrojejunostomy, endoluminal stent, jejunal nutrition tube and intravenous chemotherapy, have limitations in treating these symptoms.

AIM

To analyze the efficacy of continuous gastric artery infusion chemotherapy (cGAIC) in relieving digestive obstruction in patients with advanced GC.

METHODS

This study was a retrospective study. Twenty-nine patients with digestive obstruction of advanced GC who underwent at least one cycle of treatment were reviewed at The Second Affiliated Hospital of Zhejiang University School of Medicine. The oxaliplatin-based intra-arterial infusion regimen was applied in all patients. Mild systemic chemotherapy was used in combination with local treatment. The clinical response was evaluated by contrast-enhanced computed tomography using Response Evaluation Criteria In Solid Tumors (RECIST) criteria. Digestive tract symptoms and toxic effects were analyzed regularly. A comparison of the Karnofsky Performance Status (KPS) score and Stooler's Dysphagia Score before and after therapy was made. Univariate survival analysis and multivariate survival analysis were also performed to explore the key factors affecting patient survival.

RESULTS

All patients finished cGAIC successfully without microcatheter displacement, as confirmed by arteriography. The median follow-up time was 24 mo (95%CI: 20.24-27.76 mo). The overall response rate was 89.7% after cGAIC according to the RECIST criteria. The postoperative Stooler's Dysphagia Score was significantly improved. Twenty-two (75.9%) of the 29 patients experienced relief of digestive obstruction after the first two cycles, and 13 (44.8%) initially unresectable patients were then considered radically resectable. The median overall survival time (mOS) was 16 mo (95%CI: 9.32-22.68 mo). Patients who received radical surgery had a significantly longer mOS than other patients (P value < 0.001). Multivariate Cox regression analysis indicated that radical resection after cGAIC, intravenous chemotherapy after cGAIC, and immunotherapy after cGAIC were independent predictors of mOS. None of the patients stopped treatment because of adverse events.

CONCLUSION

cGAIC was effective and safe in relieving digestive obstruction in advanced GC, and it could improve surgical conversion possibility and survival time.

Key Words: Intra-arterial infusion chemotherapy; Intravenous chemotherapy; Interventional radiology; Digestive obstruction; Advanced gastric cancer; Response evaluation criteria in solid tumors

Core Tip: This was a retrospective study to evaluate the effectiveness of continuous gastric artery infusion chemotherapy (cGAIC) in relieving digestive obstruction in advanced gastric cancer patients. The overall response rate was 89.7% after cGAIC. A total of 75.9% of patients experienced relief of digestive obstruction after the first two cycles, and 44.8% of initially unresectable patients were then considered radically resectable. The median overall survival was 16 mo. C-arm computed tomography angiography helped to precisely confirm the tumor-feeding artery. Our new treatment can not only help relieve patients with digestive obstruction but also provide a good prognosis in treating tumors.

Citation: Tang R, Chen GF, Jin K, Zhang GQ, Wu JJ, Han SG, Li B, Chao M. Efficacy of continuous gastric artery infusion chemotherapy in relieving digestive obstruction in advanced gastric cancer. *World J Gastrointest Oncol* 2023; 15(7): 1283-1294
URL: https://www.wjgnet.com/1948-5204/full/v15/i7/1283.htm
DOI: https://dx.doi.org/10.4251/wjgo.v15.i7.1283

INTRODUCTION

Gastric cancer (GC) is the fifth most frequently diagnosed cancer and the third most common cause of cancer-related death worldwide[1]. Due to the insidious onset, 80%-90% of patients in China are initially diagnosed at an advanced stage without the possibility of radical surgery. The poor prognosis objective response rate (ORR) varies from 29% to 47%, and the median overall survival time (mOS) ranges from 7.2 to 14.6 mo[2]. Obstruction or fullness after feeding is common, occurring in 31.6% of GC patients, affecting their nutritional status and quality of life[3]. Chen *et al*[3] found that GC with digestive obstruction was more aggressive and metastatic, indicating that patients with digestive obstruction are generally in a more advanced stage. Therefore, relieving these symptoms and resuming oral feeding as much as possible have become the main therapeutic aim of patients with advanced GC accompanied by digestive obstruction.

National Comprehensive Cancer Network (NCCN) gastric cancer guidelines and Japanese gastric cancer treatment guidelines recommend that intravenous chemotherapy should be considered first in patients with advanced GC, while palliative gastrectomy, gastrojejunostomy, endoluminal stent, jejunal nutrition tube and other treatments are available to relieve digestive obstruction[1,4]. However, surgical operations are not suitable for patients in poor general condition. Despite the efficacy of endoluminal stents and jejunal nutritional tubes, the incidence of postoperative complications is high, such as stent displacement (16%-36%) and restenosis (17%-36%)[5]. In addition, no significant oral feeding improvement was obtained in more than 50% of patients following radiotherapy[6]. Previous studies found the potential role of chemotherapy in relieving digestive obstruction[7,8]. Neoadjuvant chemotherapy can also decrease the stage (40.7%-73.3%) in patients with locally advanced GC[9-12]. However, systemic intravenous chemotherapy is hardly tolerated by patients in poor condition.

In recent years, the usage of intra-arterial chemotherapy has gradually increased as an alternative to intravenous chemotherapy, such as hepatic artery infusion chemotherapy[13]. Research has shown mild adverse effects and significant efficacy, with better tolerance than intravenous chemotherapy[9,11,14]. It has also achieved encouraging results (ORR: 59.5%-85.4%, mOS: 9-30 mo) in patients with advanced GC[15-17]. However, no studies on relieving digestive obstruction have been reported. Thus, this study retrospectively analyzed patients with advanced GC-induced cardia or pyloric obstruction treated by constant gastric artery infusion chemotherapy (cGAIC). This study aimed to assess the safety and efficacy of this new method in relieving digestive obstruction.

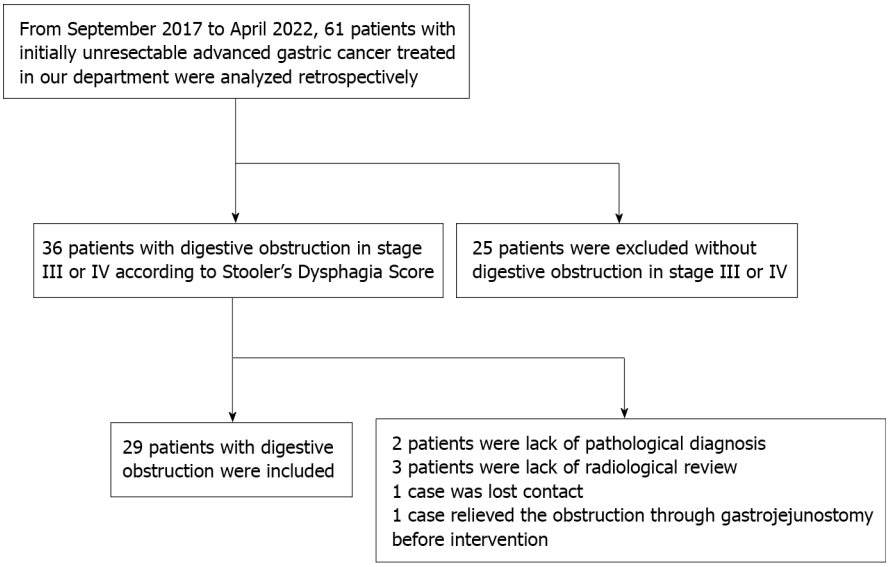

DOI: 10.4251/wjgo.v15.i7.1283

Figure 1 Patients enrollment processes flow diagram.

MATERIALS AND METHODS

Patients

From September 2017 to April 2022, a total of 61 patients with advanced GC were analyzed retrospectively. Among them, 25 patients without obvious digestive obstruction symptoms were excluded. Of the remaining 36 patients, 6 were excluded because of inadequate follow-up, of which 2 lacked a pathological diagnosis, 3 did not undergo radiological review, and 1 lost contact. In addition, 1 case was removed due to having to relieve the obstruction through gastrojejunostomy before intervention. Finally, twenty-nine advanced GC-induced digestive obstruction patients (20 male, 9 female, aged 45-82 years, mean 64.28 ± 8.49 years) who were unable to undergo radical surgery or failed to respond to radiotherapy or intravenous chemotherapy within a sufficient observation time were eligible for this study. All patients passed the examination and approval of the Ethics Committee of The Second Affiliated Hospital of Zhejiang University School of Medicine (Approval No. I2020001737) and gave signed informed consent. All patients were diagnosed by endoscopy and confirmed by pathology. In this study, advanced GC included locally advanced unresectable GC or metastatic GC. Clinical tumor-node-metastasis (cTNM) stage distribution was confirmed by contrast-enhanced computed tomography (CT) according to the 8th edition American Joint Committee and Union International Center Cancer (AJCC/UICC)[18]. Details of the patient selection processes are shown in Figure 1.

Inclusion criteria

Patients with advanced GC who met the following criteria were included: (1) Experienced obstruction or fullness after feeding in stage III or IV according to Stooler's Dysphagia Score; (2) had a Karnofsky Performance Status (KPS) score > 50; (3) had initially unresectable advanced GC according to a gastrointestinal surgeon; (4) had no indication for further radical surgery; and (5) had no contraindications for interventional therapy and chemotherapy.

Exclusion criteria

Patients with inadequate follow-up, acute infection, severe liver and kidney dysfunction or blood coagulation disturbance and pregnant and breastfeeding women were excluded.

Treatment regimens

The framework of the chemotherapy regimen is based on the SOX (S-1 and oxaliplatin) intravenous chemotherapy regimen according to The NCCN Clinical Practice Guidelines for Gastric Cancer. In this study, the treatment regimen consisted of intra-arterial infusion of oxaliplatin 100 mg in 5 h and oral S-1 40 mg/m^2 twice a day for 14 d[14,19,20]. 5-Fluorouracil 2600 mg/m^2 d1 was administered intravenously if the patients could not take S-1 orally. Symptomatic antiemetic treatment and rehydration were used postcGAIC. Laboratory examination and abdominal contrast-enhanced CT were performed after 2 wk[21]. The KPS score and Stooler's Dysphagia Score were obtained from telephone follow-up after leaving the hospital. This cycle was repeated once every 3 wk.

Interventional approaches

Interventional treatments were performed by two interventional radiologists with more than 10 years of experience. After femoral artery puncture using Seldinger's approach, a microcatheter was used for angiography of possible tumor-feeding arteries, including the left gastric artery, right gastric artery, right gastroepiploic artery or anomalous origin of the gastric

Table 1 Infusion area in interventional approaches

Infusion area	Gastroesophageal junction obstruction, *n*	Pyloric obstruction, *n*	Anastomosis obstruction, *n*
Left gastric artery	13	5	1
Right gastric artery	1	3	0
Right gastroepiploic artery	0	13	2
Left gastric artery and right gastroepiploic artery	5	0	0
Right gastric artery and right gastroepiploic artery	0	23	0
Left gastric artery and right gastric artery	1	1	0
Others	7[1]	6[2]	1[2]

[1]Including left gastroepiploic artery, left Inferior phrenic artery, superior mesenteric artery branch.
[2]Including common hepatic artery, coeliac trunk artery.

artery. C-arm computed tomographic angiography (CACTA) during interventional operation was then used to confirm the tumor-feeding artery according to preoperative abdominal contrast-enhanced CT. When selection of the tumor-feeding artery was complete, a vascular sheath and catheters were fixed to the skin, and a mixture of oxaliplatin 100 mg and 250 mL 5% glucose solution was infused by a chemotherapy pump over 5 h (50 mL/h). If 2 tumor-feeding arteries existed, 2 microcatheters were placed at the same time through the bilateral femoral artery, and oxaliplatin 50 mg was equally infused into these arteries (Table 1). After infusion, angiography was performed again to confirm the location of the microcatheter.

The cycles of cGAIC depended on the following stop criteria: (1) The patient could not tolerate continuing chemotherapy; (2) the patient was evaluated as having progressive disease after 2 cycles of cGAICs; (3) the patient was evaluated as having a complete response after cGAIC; (4) the initially unresectable patient was considered resectable and received radical distal subtotal gastrectomy; and (5) the digestive obstruction was relieved, but the patient was still not resectable, and palliative treatment continued.

Evaluation criteria

Radiology responses were assessed by two experienced radiologists independent from the clinical teams. Response Evaluation Criteria In Solid Tumors (RECIST) criteria were used to evaluate tumor response[22]. Complete disappearance of the tumor was considered to be complete response (CR); at least 30% decrease in tumor size was defined as partial response (PR); at least 20% increase in tumor size was defined as progressive disease (PD); and neither sufficient shrinkage to qualify for partial response nor sufficient increase to qualify for progressive disease was considered stable disease (SD). KPS scores from 0 to 100 were used to reflect general physical condition. Digestive obstruction was divided into five levels according to Stooler's Dysphagia Score: 0, normal swallowing; I, semidry food; II, soft food; III, fluid; and IV, completely unable to feed orally. Adverse events in this study included postoperative nausea and vomiting, abdominal pain, gastrointestinal hemorrhage, bone marrow hypocellular, paresthesia and increased levels of liver enzyme. Adverse events were assessed according to Common Terminology Criteria for Adverse Events (CTCAE) Version 5.0.

Statistical analysis

Comparison of the KPS score and Stooler's Dysphagia Score before and after therapy was performed using the Wilcoxon signed-rank test. Comparisons of parameter variables were performed using the paired samples test. Univariate survival analysis was performed using the Kaplan-Meier method, and multivariate survival analysis was performed using a Cox regression model. Factors with $P < 0.05$ in univariate survival analysis were included in the Cox regression model. Statistical analysis was performed using SPSS version 19.0 (SPSS Inc., Chicago, IL, United States). Two-tailed $P < 0.05$ was considered significant.

RESULTS

Among all patients, the median follow-up time was 24 mo (95%CI: 20.24-27.76 mo). All patients were given a total of 82 cGAIC cycles, and the median number of cycles was 3 (1-6). Of these patients, 6 had gastroesophageal junction cancer (Siewert III), 2 had recurrent tumors on anastomosis, and the remaining 21 had GC in the pylorus. During the follow-up, 13 (44.8%) initially unresectable patients were still unresectable and received radical distal subtotal gastrectomy (Billroth II) combined with D2 lymph node dissection, including 1, 3, 4 sb, 5, 6, 7, 8a, 9, 11p, 12a, and 14 V if necessary. Further postoperative intravenous chemotherapy was applied in these 12 patients, excluding 1 patient with poor health status

after gastrectomy. Metastatic disease is mainly treated by systemic therapy, including intravenous chemotherapy or immunotherapy. Only in a few patients were implantation metastases dissected for biopsy; details are shown in the Supplementary Table 1. Other patients continued to carry immune checkpoint inhibitor treatment only (2 patients), intravenous chemotherapy only (5 patients), immune checkpoint inhibitors combined with intravenous chemotherapy (2 patients), best supportive care (5 patients), or gave up further treatments for poor health status and death (2 patients). All patients finished cGAIC successfully without microcatheter displacement, as confirmed by arteriography.

None of the twenty-nine patients showed PD after the treatment evaluated by the RECIST criteria, while the overall response (OR) was 89.7%, and the objective response rate (ORR) was 86.2% after the first cGAIC, 88.9% after the second cGAIC, 84.2% after the third cGAIC, and 100% after the 4-6th cycles of cGAIC by the RECIST criteria (Table 2).

Significant differences were found in Stooler's Dysphagia Score before and after treatment (before: 3.24 ± 0.43, after: 2.13 ± 0.78, P value < 0.001). Nineteen patients experienced relief of digestive obstruction after the first cGAIC, 3 patients experienced relief of digestive obstruction after the second cGAIC, and 7 patients did not recover from digestive obstruction (Table 3). Two temporarily recovered patients developed obstruction again after the third cGAIC. The KPS (before: 61.79 ± 6.58, after: 71.43 ± 5.15, P value < 0.001) score increased after cGAIC.

The median overall survival time (mOS) was 16 mo (95%CI: 9.32-22.68 mo, Figure 2A). Subgroup analysis showed that patients who were relieved of obstruction had a slightly longer mOS than patients who were not (21 *vs* 7 mo, P = 0.078, Figure 2B). Patients who received radical surgery had a significantly longer mOS than other patients (unobtained for low follow-up time *vs* 10 mo, P value < 0.001, Figure 2C).

In the exploratory univariate analysis shown in Table 4, there were significant associations between mOS and intravenous chemotherapy history, pathology, radical resection after cGAIC, intravenous chemotherapy after cGAIC, and immunotherapy after cGAIC (all P < 0.05). In addition, multivariate Cox regression analysis indicated that radical resection after cGAIC, intravenous chemotherapy after cGAIC, and immunotherapy after cGAIC were independent predictors of mOS (all P < 0.05). We also observed that relieving digestive obstruction was not significantly associated with mOS.

Obvious imaging changes were found in the review of abdominal contrast-enhanced CT compared with preoperative CT. Pyloric obstruction or gastroesophageal junction obstruction (Figure 3A and B) manifested as thickening of the gastric wall, blurring of the boundary, and narrowing or disappearance of the digestive tract. After the first cGAIC, the abnormally thick gastric wall became thin, the blurred boundary became clear, and the blocked digestive tract opened again (Figure 3E and F).

Adverse events after intra-arterial infusion chemotherapy show a similar representation but a lower degree compared with those in intravenous chemotherapy in past studies (Table 5). No serious complications, such as gastrointestinal perforation or hemorrhage, were found. All the chemotherapy-related adverse events during cGAIC were not greater than grade 2 according to CTCAE and disappeared rapidly in the following week. None of the patients stopped treatment because of severe adverse events.

DISCUSSION

The efficacy and safety of intra-arterial infusion chemotherapy have been confirmed in the treatment of advanced GC by inhibiting cell proliferation and inducing apoptosis. Zhang *et al*[16] found that preoperative intra-arterial infusion chemotherapy was an independent factor for the long-term survival of patients with advanced GC. Zhang *et al*[17] found an mOS of 25 mo in advanced GC while using intra-arterial chemotherapy, which was better than the mOS of 9 mo when using single intravenous chemotherapy. In addition, studies have shown that weight loss or malnutrition during neoadjuvant chemotherapy are independent risk factors for the effect, which indicates the importance of relieving digestive obstruction[23]. However, relief of digestive obstruction is not mentioned in the previous literature, and the intra-arterial infusion chemotherapy regimen lacks standardized guidance. Therefore, this study aimed to explore the efficacy and safety of cGAIC in advanced GC patients with digestive obstruction.

After the first treatment, patients immediately achieved an 86.2% ORR, which is better than the ORR (29%-47%) in a previous study in advanced GC with digestive obstruction, and no patient exhibited disease progression in the following treatment[1]. In addition, the clinical symptoms of digestive obstruction were relieved quickly in the follow-up visits, indicated by most patients beginning to resume oral feeding, which was an encouraging result for advanced GC patients with poor oral feeding. The KPS score was also improved compared with that before treatment, with better quality of life. No patients stopped treatment because of severe adverse events, which represented good clinical compliance. There may be some key factors in our regimen that are important for the satisfactory clinical effect.

The first key factor is to infuse the tumor-feeding artery accurately using CACTA. In recent studies, the infusion area of intra-arterial chemotherapy was chosen empirically according to the tumor location instead of being guided by CACTA. This may lead to choosing the wrong infusion area, resulting in weak responses compared with intravenous chemotherapy and unnecessary adverse reactions such as ischemia and ulcers. Tao *et al*[24] and Ji *et al*[25] found that the clear tumor blood supply in GC is an independent risk factor for OS. Wang *et al*[26] also confirmed that distinct tumor staining intraoperatively could affect prognosis. Therefore, it is important to place the microcatheter in the right location. In this study, the combination of intraoperative CACTA with preoperative contrast-enhanced CT may help with accurate treatment (Figure 3C and D) and avoid injuring important organs. For example, we should place the microcatheter in the right gastroepiploic artery when possible and avoid the pancreaticoduodenal artery and duodenal artery to prevent pancreatitis or duodenal ulcers. One case in this study failed to relieve digestive obstruction because of an error in evaluating the dual feeding artery. In the following treatment, both arteries were infused, and the obstruction was

Table 2 Tumor radiologic response evaluated by Response Evaluation Criteria In Solid Tumors criteria

	After the first cGAIC, *n* (%)	After the second cGAIC, *n* (%)	After the third cGAIC, *n* (%)	After the fourth cGAIC, *n* (%)	After the fifth cGAIC, *n* (%)	After the sixth cGAIC, *n* (%)
CR	0 (0)	1 (3.7)	4 (21.1)	0 (0)	0 (0)	0 (0)
PR	25 (86.2)	23 (85.2)	12 (63.2)	3 (100)	2 (100)	2 (100)
SD	4 (13.8)	3 (11.1)	3 (15.8)	0 (0)	0 (0)	0 (0)
PD	0 (0)	0 (0)	0 (0)	0 (0)	0 (0)	0 (0)
Total	29	27	19	3	2	2

Date in parentheses are percentages. Total = number of patients finished the treatments. cGAIC: Continuous gastric artery infusion chemotherapy; CR: Complete response; PR: Partial response; SD: Stable disease; PD: Progressive disease.

Table 3 Comparison of Stooler's Dysphagia Score

	Before cGAIC, *n*	After cGAIC, *n*	*P* value
Stooler's Dysphagia Score			< 0.001
I	0	6	
II	0	14	
III	22	8	
IV	7	1	

Stooler's Dysphagia Score reflected the degree of digestive obstruction. I: Semi dry food; II: Soft food; III: Fluid; IV: Completely unable to feed orally; cGAIC: Continuous gastric artery infusion chemotherapy.

relieved.

Another reason contributing to the better treatment may be the infusion time. Compared to 2-6 h continuous infusion in standard intravenous chemotherapy regimens, we infused concentration-dependent drugs through the arterial pathway persistently by a chemotherapy pump in 5 h. In previous studies, drugs were injected into the target area within a few minutes to produce a higher local drug concentration, which is simple and convenient but is not conducive to maintaining blood concentration for a long period[15]. In the postoperative biopsy in Zhang *et al*'s study, they found gastric mucosal necrosis and scarring in the area of intra-arterial infusion treatment[17]. A high concentration of drugs was confirmed in blood samples from the portal vein by the left gastric intra-arterial route, which was 4-40-fold of the group by intravenous administration[26]. This higher local drug concentration may lead to arterial inflammation, promoting tumor cell ischemia and necrosis. A constant higher drug concentration may induce tumor cell apoptosis more effectively, which may be the pathophysiological mechanism of this treatment.

Therefore, in our accurate and constant intra-arterial infusion chemotherapy, the mOS was 16 mo, which was greater than expected. Because cGAIC has a high efficiency in shrinking the local lesion in the cardia or pylorus, the obstruction symptoms can be quickly relieved in the first two cycles of treatment in most patients, which results in a better nutritional status. In addition, 13 unresectable patients were then considered resectable and had an obviously longer median OS time than the others ($P < 0.001$, Figure 2C). Furthermore, based on the effectiveness of local treatment, a single oral or intravenous chemotherapy drug was used in combination. This combination obtained better regional benefits and systemic control in distant metastasis and reduced the dosage of chemotherapy drugs and adverse events. Thus, locally advanced GC patients could acquire higher surgical conversion possibilities and better prognoses.

In another aspect from multivariate Cox regression analysis, appropriate treatments after cGAIC were more relevant with a higher mOS, including radical resection, intravenous chemotherapy and immunotherapy after cGAIC. Although digestive obstruction symptoms of 76% of patients were relieved and life quality and nutritional status improved, relieving digestive obstruction did not become an independent predictor for long-term survival because cGAIC only made up a part of the whole comprehensive treatment. We believe that this treatment indirectly improved survival by improving the radical surgery rate. Two patients with squamous cell carcinoma were also treated with this treatment. In the following univariate survival analysis, this pathological type had a higher hazard ratio than signet ring cell carcinoma and adenocarcinoma, which demonstrated that this treatment was more suitable for advanced gastric or gastroesophageal junction cancer (Siewert type III). In addition, we found that patients with no chemotherapy history were more likely to benefit from cGAIC.

Although intra-arterial chemotherapy has been suggested to be safe and effective, there is still controversy surrounding chemotherapeutic drug selection and the speed of administration[27]. In this study, fluorouracil plus oxaliplatin was used as the preferred chemotherapy regimen for GC recommended by the NCCN, while the dosage of

Table 4 Univariate and Multivariate survival analysis for overall survival

Variables	*n* (%)	Univariate survival analysis			Multivariate survival analysis		
		HR	95%CI	*P* value	HR	95%CI	*P* value
Gender							
Male	20 (69)	1.53	0.49-4.85	0.466			
Female	9 (31)	1					
Intravenous chemotherapy history							
No	22 (76)	0.30	0.11-0.83	0.020			
Yes	7 (24)	1					
Gastric cancer surgery history							
No	27 (93)	0.51	0.12-2.29	0.381			
Yes	2 (7)	1					
Pathology							
Squamous cell carcinoma	2 (7)	9.24	1.62-52.69	0.012			
Signet ring cell carcinoma	8 (27)	0.66	0.18-2.44	0.535			
Adenocarcinoma	19 (66)	1					
Tumor invasion							
≤ T4a	19 (66)	0.48	0.17-1.32	0.153			
T4b	10 (34)	1					
Metastasis							
No	9 (31)	0.63	0.20-1.98	0.425			
Yes	20 (69)						
Obstructive location							
Gastroesophageal junction	6 (21)	1.21	2.24-6.10	0.816			
Pylorus	21 (72)	0.35	0.07-1.68	0.188			
Anastomosis	2 (7)	1					
Stooler's Dysphagia Score							
III	22 (76)	0.34	0.11-1.02	0.055			
IV	7 (24)	1					
Relieve digestive obstruction							
No	7 (24)	2.55	0.84-7.72	0.098			
Yes	22 (76)						
Radical resection after cGAIC							
No	16 (55)	9.56	2.11-43.44	0.003	8.48	1.27-56.51	0.027
Yes	13 (45)						
Intravenous chemotherapy after cGAIC							
No	10(34)	6.20	2.14-18.00	0.001	8.61	1.42-52.17	0.019
Yes	19(66)						
Immunotherapy after cGAIC							
No	18(62)	4.12	0.93-18.28	0.063	13.09	1.64-104-12	0.015
Yes	11(38)						

HR: Hazard ratio; CI: Confidence interval; cGAIC: Continuous gastric artery infusion chemotherapy.

Table 5 Adverse events after constant gastric artery infusion chemotherapy

Adverse events	Grade 1, *n* (%)	Grade 2, *n* (%)
Nausea and vomiting	4 (13.8)	2 (6.9)
Abdominal pain	3 (10.3)	1 (3.4)
Gastrointestinal hemorrhage	0 (0)	0 (0)
Neutropenia	2 (6.9)	2 (6.9)
Anemia	1 (3.4)	0 (0)
Thrombocytopenia	2 (6.9)	2 (6.9)
Paresthesia	1 (3.4)	1 (4.3)
Liver enzyme increased	1 (3.4)	3 (10.3)

Common Terminology Criteria for Adverse Events Version 5.0. Date in parentheses are percentages.

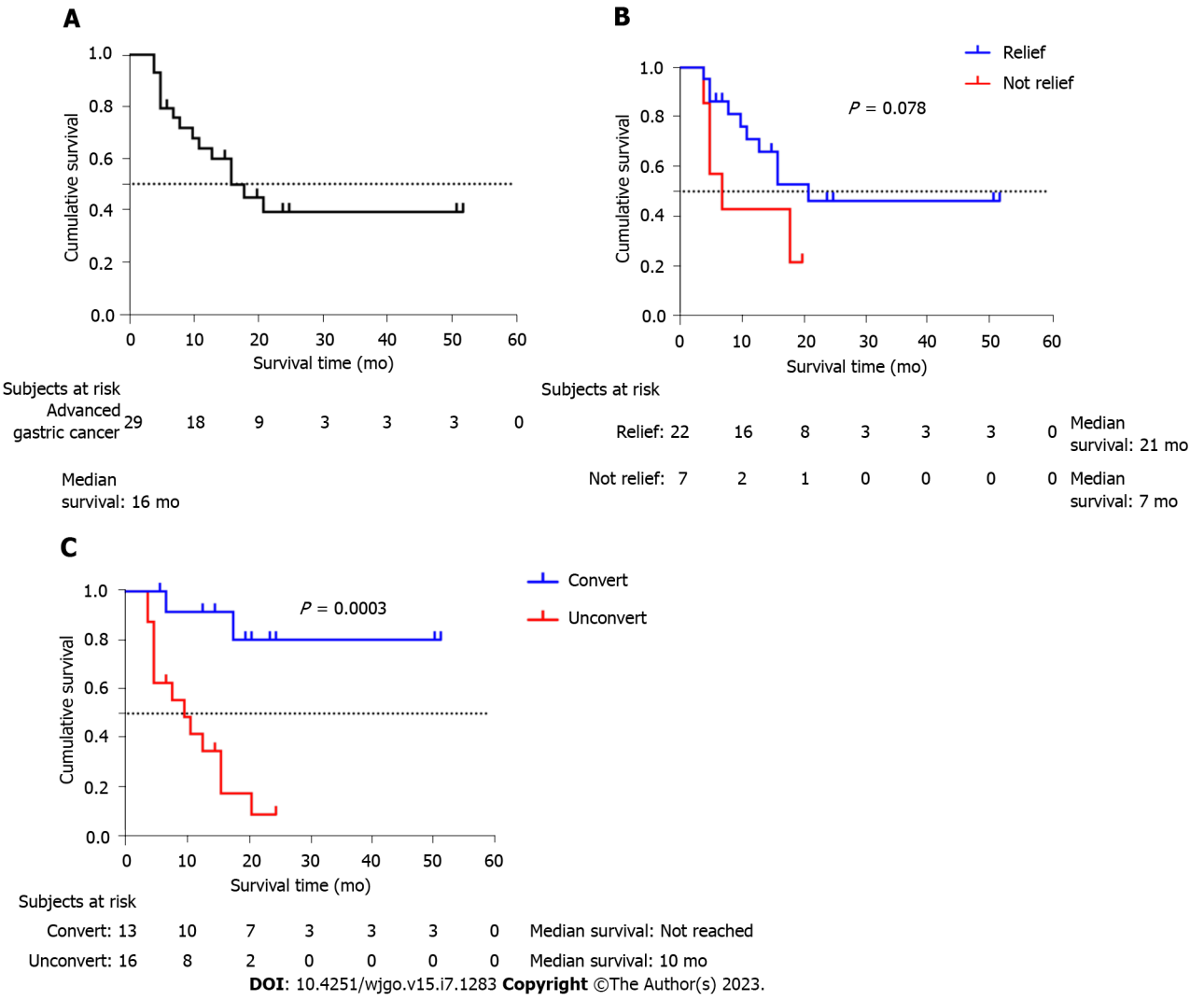

DOI: 10.4251/wjgo.v15.i7.1283

Figure 2 Overall survival time of advanced gastric cancer patients and subgroup analysis. A: The overall survival time of advanced gastric cancer patients with digestive obstruction after continuous gastric artery infusion chemotherapy (cGAIC). The mOS was 16 mo; B: Subgroup analysis between patients who got obstruction relieved and patients not; C: Subgroup analysis between patients who received radical surgery and patients not. Relief: Patients with digestive obstruction got relieved after cGAIC. Not relief: Patients with digestive obstruction didn't get relieved after cGAIC. Convert: Initially unresectable gastric cancer patients converted into resectable successfully. Unconvert: Initially unresectable gastric cancer patients failed to convert into resectable.

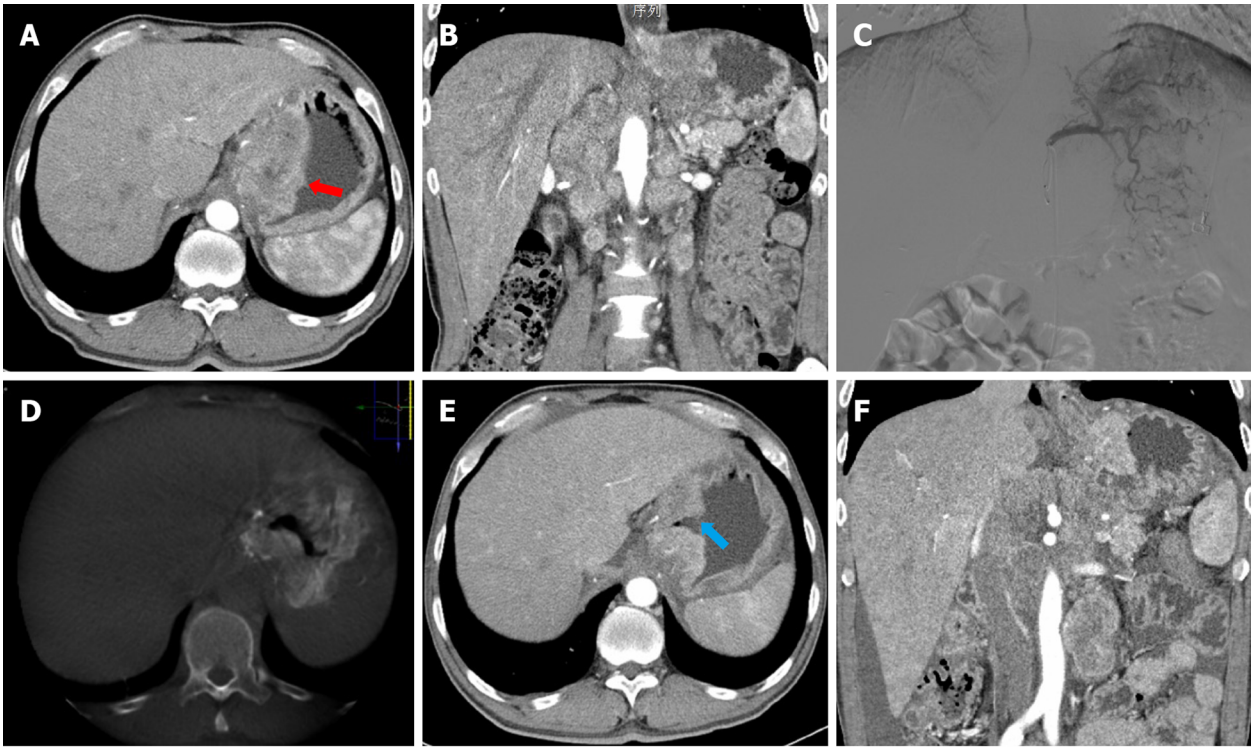

DOI: 10.4251/wjgo.v15.i7.1283 **Copyright** ©The Author(s) 2023.

Figure 3 Comparison between pre and post continuous gastric artery infusion chemotherapy in patient with gastroesophageal junction obstruction. A and B: gastroesophageal junction obstruction (red arrow) in abdominal contrast-enhanced computed tomography (CT) before continuous gastric artery infusion chemotherapy (cGAIC); C and D: C-arm computed tomographic angiography was used to find the tumor-feeding artery accurately in right gastroepiploic artery; E and F: Tumor in gastric fundus shrank obviously, blurred boundary became clear, and blocked digestive tract opened again in gastroesophageal junction (blue arrow), shown in abdominal contrast-enhanced CT in 2 wk after first cGAIC.

oxaliplatin was reduced by half for patients in poor general condition. A few patients with mild gastrointestinal reactions and leukopenia quickly returned to normal after symptomatic treatment.

This study was limited by the small sample size and short observation period. As a new effective method in theory, we did not set a control group at the same period, so we can only compare the effectiveness with the external control group. Moreover, this was a retrospective analysis but not prospective randomized, which may cause selection and recall biases. In addition, we did not embolize the tumor-feeding artery. In addition, the optimal cycles of cGAIC need to be explored in the future. The safety of embolization needs to be verified in randomized trials to avoid the occurrence of serious adverse effects, such as ischemia, ulcer, perforation and bleeding.

CONCLUSION

In conclusion, this study preliminarily demonstrated the efficacy and safety of cGAIC in relieving digestive obstruction in advanced GC, which improved radical resection possibility after cGAIC and survival time. Intraoperative CACTA can help with precise definition of the perfusion area.

ARTICLE HIGHLIGHTS

Research background

Patients with digestive obstruction generally have advanced gastric cancer, affecting their quality of life and survival.

Research motivation

Existing methods cannot relieve digestive obstruction very well.

Research objectives

Continuous gastric artery infusion chemotherapy (cGAIC) was effective and safe in relieving digestive obstruction.

Research methods

Twenty-nine patients with digestive obstruction of advanced gastric cancer treated by cGAIC were reviewed retrospectively. Interventional treatments combined with C-arm computed tomographic angiography were performed to accurately infuse oxaliplatin into the tumor-feeding artery. Radiology responses, Stooler's Dysphagia Score and toxic effects were evaluated.

Research results

The overall response rate was 89.7% after cGAIC. The postoperative Stooler's Dysphagia Score was significantly reduced. Twenty-two (75.9%) of the 29 patients experienced relief of digestive obstruction after the first two cycles, and 13 (44.8%) initially unresectable patients were then considered radically resectable. The median overall survival time was 16 mo.

Research conclusions

The efficacy and safety of cGAIC in relieving digestive obstruction were demonstrated, and cGAIC could improve radical resection after cGAIC and survival time. Intraoperative CACTA can help with precise definition of the perfusion area.

Research perspectives

To improve the efficacy of chemotherapy using interventional methods.

ACKNOWLEDGEMENTS

We gratefully acknowledge the assistance of all the patients and their families volunteer to participate in the clinical study.

FOOTNOTES

Author contributions: Tang R reviewed the literature and contributed to article drafting and statistical analysis; Li B was responsible for data acquisition and revision of the manuscript; Chao M was in charge of this project and responsible for the final revision of the manuscript; Chen GF was a surgeon from Department of Gastrointestinal Surgery, and was responsible for the evaluation of surgical indications of all patients; Jin K, and Zhang GQ were interventional physicians from the Department of Radiology, and participated in the diagnosis and treatment of patients; Wu JJ, and Han SG were experienced radiologists responsible for assessment of radiology response; all authors gave final approval for the version to be submitted.

Institutional review board statement: The study was reviewed and approved by the Ethics Committee of The Second Affiliated Hospital of Zhejiang University School of Medicine (Approval No. I2020001737).

Informed consent statement: All study participants or their legal guardian gave signed informed consent.

Conflict-of-interest statement: The authors declare that the research was conducted in the absence of any commercial or financial relationships that could be construed as a potential conflict of interest.

Data sharing statement: Dataset available from the corresponding author at chaoming@zju.edu.cn. Participants gave informed consent for data sharing.

Country/Territory of origin: China

ORCID number: Rui Tang 0000-0002-6169-9543; Kai Jin 0000-0002-1769-2328; Guang-Qiang Zhang 0000-0002-0004-2951; Jian-Jun Wu 0000-0002-3810-1101; Shu-Gao Han 0000-0002-4842-1790; Bin Li 0000-0002-4469-752X; Ming Chao 0000-0003-0513-0683.

S-Editor: Yan JP
L-Editor: A
P-Editor: Yan JP

REFERENCES

1 **Ajani JA**, D'Amico TA, Almhanna K, Bentrem DJ, Chao J, Das P, Denlinger CS, Fanta P, Farjah F, Fuchs CS, Gerdes H, Gibson M, Glasgow RE, Hayman JA, Hochwald S, Hofstetter WL, Ilson DH, Jaroszewski D, Johung KL, Keswani RN, Kleinberg LR, Korn WM, Leong S, Linn C, Lockhart AC, Ly QP, Mulcahy MF, Orringer MB, Perry KA, Poultsides GA, Scott WJ, Strong VE, Washington MK, Weksler B, Willett CG,

Wright CD, Zelman D, McMillian N, Sundar H. Gastric Cancer, Version 3.2016, NCCN Clinical Practice Guidelines in Oncology. *J Natl Compr Canc Netw* 2016; **14**: 1286-1312 [PMID: 27697982 DOI: 10.6004/jnccn.2016.0137]

2 **Chen W**, Zheng R, Zeng H, Zhang S. The incidence and mortality of major cancers in China, 2012. *Chin J Cancer* 2016; **35**: 73 [PMID: 27484217 DOI: 10.1186/s40880-016-0137-8]

3 **Chen JH**, Wu CW, Lo SS, Li AF, Hsieh MC, Shen KH, Lui WY. Outcome of distal gastric cancer with pyloric stenosis after curative resection. *Eur J Surg Oncol* 2007; **33**: 556-560 [PMID: 17329063 DOI: 10.1016/j.ejso.2007.01.020]

4 **Japanese Gastric Cancer Association**. Japanese gastric cancer treatment guidelines 2018 (5th edition). *Gastric Cancer* 2021; **24**: 1-21 [PMID: 32060757 DOI: 10.1007/s10120-020-01042-y]

5 **Jain P**. Self-expanding metallic esophageal stents: a long way to go before a particular stent can be recommended. *World J Gastroenterol* 2011; **17**: 5327-5328 [PMID: 22219604 DOI: 10.3748/wjg.v17.i48.5327]

6 **Tey J**, Zheng H, Soon YY, Leong CN, Koh WY, Lim K, So JBY, Shabbir A, Tham IWK, Lu J. Palliative radiotherapy in symptomatic locally advanced gastric cancer: A phase II trial. *Cancer Med* 2019; **8**: 1447-1458 [PMID: 30790469 DOI: 10.1002/cam4.2021]

7 **Jiao X**, Zhou Y. Investigation of the potential role of preoperative chemotherapy in treatment for gastric cancer with outlet obstruction. *Mol Clin Oncol* 2015; **3**: 1177-1183 [PMID: 26623073 DOI: 10.3892/mco.2015.587]

8 **Long B**, Yu ZY, Li Q, Du HR, Wang ZJ, Zhan H, Jiao ZY. A systematic review and network meta-analysis protocol of neoadjuvant treatments for patients with gastric cancer. *Medicine (Baltimore)* 2018; **97**: e0392 [PMID: 29642200 DOI: 10.1097/MD.0000000000010392]

9 **Al-Batran SE**, Homann N, Pauligk C, Goetze TO, Meiler J, Kasper S, Kopp HG, Mayer F, Haag GM, Luley K, Lindig U, Schmiegel W, Pohl M, Stoehlmacher J, Folprecht G, Probst S, Prasnikar N, Fischbach W, Mahlberg R, Trojan J, Koenigsmann M, Martens UM, Thuss-Patience P, Egger M, Block A, Heinemann V, Illerhaus G, Moehler M, Schenk M, Kullmann F, Behringer DM, Heike M, Pink D, Teschendorf C, Löhr C, Bernhard H, Schuch G, Rethwisch V, von Weikersthal LF, Hartmann JT, Kneba M, Daum S, Schulmann K, Weniger J, Belle S, Gaiser T, Oduncu FS, Güntner M, Hozaeel W, Reichart A, Jäger E, Kraus T, Mönig S, Bechstein WO, Schuler M, Schmalenberg H, Hofheinz RD; FLOT4-AIO Investigators. Perioperative chemotherapy with fluorouracil plus leucovorin, oxaliplatin, and docetaxel versus fluorouracil or capecitabine plus cisplatin and epirubicin for locally advanced, resectable gastric or gastro-oesophageal junction adenocarcinoma (FLOT4): a randomised, phase 2/3 trial. *Lancet* 2019; **393**: 1948-1957 [PMID: 30982686 DOI: 10.1016/S0140-6736(18)32557-1]

10 **Zhang X**, Liang H, Li Z, Xue Y, Wang Y, Zhou Z, Yu J, Bu Z, Chen L, Du Y, Wang X, Wu A, Li G, Su X, Xiao G, Cui M, Wu D, Wu X, Zhou Y, Zhang L, Dang C, He Y, Zhang Z, Sun Y, Li Y, Chen H, Bai Y, Qi C, Yu P, Zhu G, Suo J, Jia B, Li L, Huang C, Li F, Ye Y, Xu H, Yuan Y, E JY, Ying X, Yao C, Shen L, Ji J; RESOLVE study group. Perioperative or postoperative adjuvant oxaliplatin with S-1 versus adjuvant oxaliplatin with capecitabine in patients with locally advanced gastric or gastro-oesophageal junction adenocarcinoma undergoing D2 gastrectomy (RESOLVE): an open-label, superiority and non-inferiority, phase 3 randomised controlled trial. *Lancet Oncol* 2021; **22**: 1081-1092 [PMID: 34252374 DOI: 10.1016/S1470-2045(21)00297-7]

11 **Guo H**, Ding P, Sun C, Yang P, Tian Y, Liu Y, Lowe S, Bentley R, Li Y, Zhang Z, Wang D, Zhao Q. Efficacy and safety of sintilimab plus XELOX as a neoadjuvant regimen in patients with locally advanced gastric cancer: A single-arm, open-label, phase II trial. *Front Oncol* 2022; **12**: 927781 [PMID: 36091139 DOI: 10.3389/fonc.2022.927781]

12 **Newman E**, Marcus SG, Potmesil M, Sewak S, Yee H, Sorich J, Hayek M, Muggia F, Hochster H. Neoadjuvant chemotherapy with CPT-11 and cisplatin downstages locally advanced gastric cancer. *J Gastrointest Surg* 2002; **6**: 212-23; discussion 223 [PMID: 11992807 DOI: 10.1016/s1091-255x(01)00054-3]

13 **Ouyang G**, Pan G, Xu H, Wu Y, Liu Z, Lu W, Yi B, Chen X. Sorafenib Plus Hepatic Arterial Infusion Chemotherapy in Advanced Hepatocellular Carcinoma: A Systematic Review and Meta-Analysis. *J Clin Gastroenterol* 2020; **54**: 675-681 [PMID: 32569032 DOI: 10.1097/MCG.0000000000001384]

14 **Satake H**, Miki A, Kondo M, Kotake T, Okita Y, Hatachi Y, Yasui H, Imai Y, Ichikawa C, Murotani K, Hashida H, Kobayashi H, Kotaka M, Kato T, Kaihara S, Tsuji A. Phase I study of neoadjuvant chemotherapy with S-1 and oxaliplatin for locally advanced gastric cancer (Neo G-SOX PI). *ESMO Open* 2017; **2**: e000130 [PMID: 28761726 DOI: 10.1136/esmoopen-2016-000130]

15 **Li Y**, Chen J, He Q, Ji X, Wang X, Fan C, Li G. Clinical efficacy of neoadjuvant chemotherapy regimens FLEEOX vs. XELOX in patients with initially unresectable advanced gastric cancer: a propensity score analysis. *Oncotarget* 2017; **8**: 86886-86896 [PMID: 29156843 DOI: 10.18632/oncotarget.19004]

16 **Zhang CW**, Zou SC, Shi D, Zhao DJ. Clinical significance of preoperative regional intra-arterial infusion chemotherapy for advanced gastric cancer. *World J Gastroenterol* 2004; **10**: 3070-3072 [PMID: 15378797 DOI: 10.3748/wjg.v10.i20.3070]

17 **Zhang C**, Li G, Fan C, Xu J, Cao J, Liu S, Li N. Comparison of efficacy of different route of administration of chemotherapy on unresectable, advanced gastric cancer. *World J Surg Oncol* 2012; **10**: 162 [PMID: 22891660 DOI: 10.1186/1477-7819-10-162]

18 **Washington K**. 7th edition of the AJCC cancer staging manual: stomach. *Ann Surg Oncol* 2010; **17**: 3077-3079 [PMID: 20882416 DOI: 10.1245/s10434-010-1362-z]

19 **Inoue K**, Nakane Y, Kogire M, Fujitani K, Kimura Y, Imamura H, Tamura S, Okano S, Kwon AH, Kurokawa Y, Shimokawa T, Takiuchi H, Tsujinaka T, Furukawa H. Phase II trial of preoperative S-1 plus cisplatin followed by surgery for initially unresectable locally advanced gastric cancer. *Eur J Surg Oncol* 2012; **38**: 143-149 [PMID: 22154885 DOI: 10.1016/j.ejso.2011.11.009]

20 **Wang M**, Wu M, Wang W, Wang Q, Wang Y. Docetexal plus S-1 versus oxaliplatin plus S-1 for first-line treatment of patients with advanced gastric cancer: a retrospective study. *Oncol Res Treat* 2014; **37**: 24-28 [PMID: 24613905 DOI: 10.1159/000358162]

21 **Kruk-Bachonko J**, Krupski W, Czechowski M, Kurys-Denis E, Mądro P, Sierocińska-Sawa J, Dąbrowski A, Wallner G, Skoczylas T. Perfusion CT - A novel quantitative and qualitative imaging biomarker in gastric cancer. *Eur J Radiol* 2017; **95**: 399-408 [PMID: 28987697 DOI: 10.1016/j.ejrad.2017.08.033]

22 **Therasse P**, Arbuck SG, Eisenhauer EA, Wanders J, Kaplan RS, Rubinstein L, Verweij J, Van Glabbeke M, van Oosterom AT, Christian MC, Gwyther SG. New guidelines to evaluate the response to treatment in solid tumors. European Organization for Research and Treatment of Cancer, National Cancer Institute of the United States, National Cancer Institute of Canada. *J Natl Cancer Inst* 2000; **92**: 205-216 [PMID: 10655437 DOI: 10.1093/jnci/92.3.205]

23 **Jiang L**, Ma Z, Ye X, Kang W, Yu J. Clinicopathological factors affecting the effect of neoadjuvant chemotherapy in patients with gastric cancer. *World J Surg Oncol* 2021; **19**: 44 [PMID: 33563277 DOI: 10.1186/s12957-021-02157-x]

24 **Tao HQ**, Zou SC. Effect of preoperative regional artery chemotherapy on proliferation and apoptosis of gastric carcinoma cells. *World J Gastroenterol* 2002; **8**: 451-454 [PMID: 12046068 DOI: 10.3748/wjg.v8.i3.451]

25 **Ji X**, Yang Q, Qin H, Zhou J, Liu W. Tumor blood supply may predict neoadjuvant chemotherapy response and survival in patients with gastric cancer. *J Int Med Res* 2019; **47**: 2524-2532 [PMID: 31039658 DOI: 10.1177/0300060519845491]

26 **Wang J**, Shi H, Yang G, Han G, Zhao M, Duan X, Mi L, Han X, Li N, Shi J, Yin X, Yin F. Combined intra-arterial and intravenous chemotherapy for unresectable, advanced gastric cancer has an improved curative effect compared with intravenous chemotherapy only. *Oncol Lett* 2018; **15**: 5662-5670 [PMID: 29556303 DOI: 10.3892/ol.2018.8068]

27 **Li M**, Zhang J, Wang D, Zhong B, Tucker S, Lu C, Cheng J, Cao C, Xu J, Pan H. A phase II study of intra-arterial chemotherapy of 5-fluorouracil, cisplatin, and mitomycin C for advanced nonresectable gastric cancer. *Anticancer Drugs* 2009; **20**: 941-945 [PMID: 19745719 DOI: 10.1097/CAD.0b013e328331af3a]

World Journal of Gastrointestinal Oncology

Submit a Manuscript: https://www.f6publishing.com

World J Gastrointest Oncol 2023 July 15; 15(7): 1295-1310

DOI: 10.4251/wjgo.v15.i7.1295

ISSN 1948-5204 (online)

EVIDENCE-BASED MEDICINE

Comprehensive bioinformatic analysis of mind bomb 1 gene in stomach adenocarcinoma

Di Wang, Qi-Hong Wang, Ting Luo, Wen Jia, Jing Wang

Specialty type: Oncology

Provenance and peer review: Unsolicited article; Externally peer reviewed.

Peer-review model: Single blind

Peer-review report's scientific quality classification

Grade A (Excellent): 0
Grade B (Very good): B, B, B
Grade C (Good): 0
Grade D (Fair): 0
Grade E (Poor): 0

P-Reviewer: Ballini A, Italy; Inchingolo F, Italy; Santacroce L, Italy

Received: February 27, 2023
Peer-review started: February 27, 2023
First decision: March 14, 2023
Revised: March 27, 2023
Accepted: May 8, 2023
Article in press: May 8, 2023
Published online: July 15, 2023

Di Wang, Qi-Hong Wang, Ting Luo, Wen Jia, Jing Wang, Department of Digestive Endoscopy, The General Hospital of Northern Theater Command, Shenyang 110840, Liaoning Province, China

Di Wang, Qi-Hong Wang, Ting Luo, Postgraduate College, China Medical University, Shenyang 110840, Liaoning Province, China

Corresponding author: Jing Wang, MS, Deputy Director, Department of Digestive Endoscopy, The General Hospital of Northern Theater Command, No. 83 Wenhua Road, Shenhe District, Shenyang 110840, Liaoning Province, China. 13309882063@163.com

Abstract

BACKGROUND

The carcinogenesis of stomach adenocarcinoma (STAD) involves many different molecules and multiple pathways, including the NOTCH signaling pathway. As a key factor that functions as a critical link in the NOTCH pathway, mind bomb 1 (*MIB1*) is upregulated in various tumors and has been reported to promote cell metastasis and invasion. However, studies on the role of *MIB1* in STAD are limited. Here, we evaluated the prognostic value of *MIB1* in STAD and its association with immune infiltration and copy number variation.

AIM

To elucidate the relationship between *MIB1* gene and gastric cancer (GC) and provide a new idea for the treatment of GC.

METHODS

We identified mutations in the *MIB1* gene by searching the cBioPortal database and then analyzed their relationship with the overall survival rate and disease-free survival rate using the Kaplan-Meier method. The Cancer Genome Atlas (TCGA) database provided transcript levels for *MIB1* in STADs and normal tissues. As a method of distinguishing the STAD tissues from adjacent normal tissues, a receiver operating characteristic (ROC) curve was generated. Kaplan-Meier plotter was used to determine the effect of *MIB1* expression on survival. Based on the LinkedOmics database, we were able to identify the coexpressed genes of the *MIB1* gene, the top 50 positively correlated genes, and the top 50 negatively correlated genes. STRING was used to construct protein-protein interaction networks related to the *MIB1* gene. An analysis of functional enrichment was carried out using the R package "Cluster Profiler". The relationships between mRNA expression of *MIB1* and immune infiltrates were assessed by

Tumor IMmune Estimation Resource (TIMER) and the "GSVA package" in R.

RESULTS

According to the cBioPortal database, the *MIB1* mutation rate in 287 patients in the TCGA dataset was approximately 6%. Kaplan-Meier survival analysis showed that patients with STAD in the mutated group had a worse prognosis than those in the unmutated group (P = 0.0156). There was a significant upregulation of *MIB1* expression in STAD tissues compared to adjacent normal tissues. A high T stage was associated with increased *MIB1* mRNA expression. The ROC curve analysis revealed 59.4% sensitivity and 85.6% specificity of *MIB1* for differentiating STAD tissues from adjacent normal tissues at a truncation level of 2.248. Kaplan-Meier plotter indicated that patients with higher *MIB1* levels had a worse prognosis than those with lower levels (26.4 mo *vs* 56.2 mo, P = 0.0330). A correlation analysis demonstrated an association between immune infiltrates and *MIB1* mRNA expression.

CONCLUSION

Upregulation of *MIB1* expression is significantly associated with poor survival rate and immune infiltration in gastric adenocarcinoma. *MIB1* may be a biomarker for the poor prognosis of STAD patients and a potential immunotherapeutic target.

Key Words: Stomach adenocarcinoma; Mind bomb 1; Mutation; Prognosis; Biomarker; Immune infiltration

Core Tip: NOTCH signaling pathway is involved in the occurrence and development of many tumors. Mind bomb 1 (*MIB1*) is one of many E3 ubiquitin ligases in ubiquitin proteasome system, which plays a key role in NOTCH signaling pathway. Several studies showed that *MIB1* participated in the proliferation and metastasis of certain tumor cells, but its role in gastric cancer (GC) remained still unclear. The purpose of our study was to elucidate the relationship between *MIB1* gene and GC and provide a new idea for the treatment of GC.

Citation: Wang D, Wang QH, Luo T, Jia W, Wang J. Comprehensive bioinformatic analysis of mind bomb 1 gene in stomach adenocarcinoma. *World J Gastrointest Oncol* 2023; 15(7): 1295-1310
URL: https://www.wjgnet.com/1948-5204/full/v15/i7/1295.htm
DOI: https://dx.doi.org/10.4251/wjgo.v15.i7.1295

INTRODUCTION

Gastric cancer (GC) was the world's leading cause of cancer deaths until the 1980s, when it was surpassed by lung cancer. Currently, the incidence of GC ranks fifth in the world and the fatality rate ranks fourth[1]. Despite its worldwide decline in morbidity and mortality rates in the past five years, GC has maintained a high mortality rate of 75% in most parts of the world, which is also the main cause of the global DALY-adjusted life year burden[2], and it is the most burdensome gastrointestinal disease in China[3]. Despite worldwide advances in clinical diagnosis and treatment, GC is still characterized by a low early diagnosis rate, low radical resection rate, and low 5-year survival rate, and most patients are first diagnosed when the disease is in an advanced stage[4]. Although many therapeutic advances, including surgical treatment, targeted therapy and immunological therapy, have been made in GC[5,6], the 5-year survival rate of patients primarily diagnosed with advanced stage is still as low as 18%[7], and the peritoneal recurrence rate after surgery is as high as 60%[8]. These findings indicate that there is a huge demand for more precise diagnosis and treatment of GC. Therefore, there is an urgent need to find new molecular markers to judge the prognosis of patients with GC.

GC is a multifactorial disease, and the recognized risk factors include age, male sex, genetic predisposition, *Helicobacter pylori* (*H. pylori*) infection, gastroesophageal reflux disease, and lifestyle factors such as smoking, alcohol consumption, and dietary composition[9,10]. Among the different types, 95% of GC cases are stomach adenocarcinoma (STAD)[11]. The combination of several variables, including genetics, epigenetics and the external environment, that may collectively result in the unregulated signaling pathway of cancer pathogenesis can be characterized as the pathogenesis of GC[12,13]. In addition, it is widely believed that dysfunctional oncogenic pathways contribute to the pathogenesis of GC, which might include the epidermal growth factor receptor, Notch, Hedgehog, nuclear factor-κB, and Wnt/β-catenin pathways [14]. Among these pathways, the Notch signaling pathway is involved in direct cell-to-cell communication, cell differentiation, proliferation and apoptosis[15].

Notch signaling is a highly conserved pathway in multicellular animals that regulates the cell fates and upholds homeostasis in adult tissues. Numerous reports have confirmed the role of Notch signaling in both carcinogenesis and antitumor effects in different backgrounds[16,17]. Notch secretion signaling can modulate heterotypic interactions between the stroma and tumor and vice versa. These interactions have been shown to regulate many aspects of oncobiology, such as angiogenesis, cancer stem cell maintenance, immune infiltration, and resistance to therapy. These

functions provide evidence for the environmental dependence of Notch-induced cellular responses[18].

Mind bomb 1 (*MIB1*), a large multidomain RING-type E3 ubiquitin-protein ligase[19], which activates Notch signaling by promoting ubiquitination, endocytosis and subsequent activation of Notch ligands, plays a central role in the conduction of Notch signaling pathway. Inhibition of *MIB1* leaded to the decrease of Notch signal activation in mammalian cells, which was fatal to mouse embryos with Notch activation deficiency[20,21]. Vitro experiments confirmed that *MIB1* can induce degradation of suppressor of tumorigenicity 7 protein (ST7) to upregulate the IQ motif containing GTPase activating protein 1 (IQGAP1) in pancreatic cancer cells to promote tumor growth and progression, and also regulate the resistance of pancreatic cancer cells to gemcitabine[22,23]. It has been reported that *MIB1* was ubiquitous in breast cancer to mediate JAG1 ubiquitination and activate Notch signal[24]. Aside from ubiquitinating the NOTCH ligand, *MIB1* also ubiquitinated Ctnnd1 to regulate the migration of cells[25]. However, it remains unclear that the influence of *MIB1* gene on GC because of the limited research on *MIB1*. Our study aimed to determine whether *MIB1* was associated with prognosis in STAD and whether *MIB1* could be regarded as a potential therapeutic target.

MATERIALS AND METHODS

Study design

Briefly, the design of this study was as follows: First, the mutation of *MIB1* in The Cancer Genome Atlas (TCGA)-STAD data was investigated, and the differences in overall survival (OS) and disease-free survival (DFS) between the patient group with mutations and the group without mutations in *MIB1* were obtained. Second, data on the expression of *MIB1* in pan-cancer and STAD were acquired. Survival analysis was performed to study the prognostic value of *MIB1* in STAD from the aspect of receiver operating characteristic (ROC) curve and OS. Then, we obtained coexpressed genes from LinkedOmics, conducted Gene Ontology (GO) enrichment analysis and Kyoto Encyclopedia of Genes and Genomes (KEGG) pathway analysis on the top 200 related genes, and subsequently displayed the top 50 positively and negatively correlated genes. Finally, enrichment analysis of differentially expressed genes was conducted to determine the biological function of *MIB1* significantly differentially enriched genes (DEGs). In addition, the role of *MIB1* in STAD was explored by studying the correlation between *MIB1* and immune infiltrating cells.

cBioPortal analysis

The cBioPortal for Cancer Genomics (https://www.cbioportal.org/) was used to study the relationship between the mutation of the *MIB1* gene in STAD and the OS or DFS of patients, and visual analysis was performed. In this database, STAD (TCGA, Nature 2014) was selected for analysis.

Expression of MIB1 gene

The official website of the TCGA (https://portal.gdc.cancer.gov/) was used to download the RNA-seq expression data of *MIB1* for STAD. Thirty-two examples of neighboring normal tissues and a total of 375 cases of gastric adenocarcinoma were preserved. The chosen samples included data on *MIB1* gene expression as well as pertinent clinical data, such as age, sex, HP, T stage, N stage, and M stage. The mean and standard deviation were used to describe the mRNA expression data. No permission from the ethical committee was needed for this investigation because all of the data were downloaded from the public database.

Survival analysis

Kaplan-Meier curves were drawn using the Kaplan-Meier Plotter Web tool (https://kmplot.com/). Based on median gene expression, patients were split into two groups, and the log-rank test was used to compare the survival rates between the "high" expression group (red line) and the "low" expression group (blue line). We evaluated predictive factors, specifically OS.

LinkedOmics database and protein-protein interaction networks

With the use of LinkedOmics database (http://www.linkedomics.org/), a volcano plot showing the relationship between *MIB1* members and 200 co-expressed genes in GC was created and the top 50 positively and negatively correlated genes were analyzed. The Metascape database (https://metascape.org/) was used to provide GO enrichment analysis and KEGG pathway keywords for these top 200 genes. STRING (https://string-db.org/) was used to find the genes having the strongest interactions with *MIB1*, and generated the associated protein-protein interaction network with an interaction score > 0.4.

Functional enrichment analysis

The median *MIB1* expression level was used to categorize expression data (HTseq-Counts) into high and low expression groups, which were then further examined using the DESeq2 R package (3.6.3). Adjusted $P < 0.05$ and $|\log2(FC)| > 1.5$ were considered the thresholds to obtain DEGs, and GO enrichment analysis and KEGG pathway analysis of DEGs were performed by the "Cluster Profiler" package and visualized by the "ggplot2" package.

Tumor Immune Evaluation Resource database

Tumor Immune Evaluation Resource (TIMER, https://cistrome.shinyapps.io/timer/) is a comprehensive online resource for systematically analyzing immune infiltration in various cancer types. The connection between *MIB1* expression and

six different immune infiltrating cells in gastric adenocarcinomas, including B cells, $CD4^+$ T cells, $CD8^+$ T cells, neutrophils, macrophages, and dendritic cells, was examined in our study by using TIMER. We also obtained the correlation between *MIB1* and 24 tumor-infiltrating lymphocytes (TILs) by single-sample gene set enrichment analysis (ssGSEA), which was realized by the GSVA package. The Spearman test was used to measure the correlation between *MIB1* and TILs.

Statistical analysis

All statistical analyses were performed using R (V 3.6.3). The differences between the gastric adenocarcinoma tissues and surrounding normal tissues were assessed using paired *t* tests and Mann-Whitney tests. The pROC software program was used to create a ROC curve in order to determine the *MIB1* cutoff value. The impact of *MIB1* on survival was assessed using Kaplan-Meier and log-rank testing.

RESULTS

Mutation and mRNA expression of the MIB1 gene in STAD

Mutation of the *MIB1* gene was analyzed in STAD patients using the online cBioPortal database, and the genetic alterations of *MIB1* in STAD were 6% (Figure 1A). Mutation data and copy number alteration (CNA) data were shown in Figure 1B. Patients with and without mutations did not have a significantly different OS rate ($P = 0.8900$). Nevertheless, the DFS rate of the group with mutations was much lower than that of the group without mutations ($P = 0.0156$) (Figure 1C and 1D). As shown in Figure 2A, *MIB1* was considerably upregulated in a range of tumor tissues when compared to adjacent normal tissues, demonstrating that mRNA expression of *MIB1* was abnormally expressed in several cancer types. Analysis of unpaired data showed that the *MIB1* mRNA in STAD tissues ($n = 375$) was significantly higher than that in adjacent normal tissues ($n = 32$) (Figure 2B; 2.807 ± 0.584 *vs* 2.218 ± 0.495, Mann-Whitney *U* test, $P < 0.001$). Paired data analysis also showed that the mRNA expression level of *MIB1* in gastric adenocarcinoma tissues was significantly higher than that in adjacent normal tissues ($n = 27$) (Figure 2C; 2.562 ± 0.696 *vs* 2.239 ± 0.506, $P < 0.01$).

Relationship between the mRNA level of MIB1 and clinicopathological features in patients with gastric adenocarcinoma

The Mann-Whitney *U* test and logistic regression analysis were performed to evaluate the relationship between the mRNA expression of *MIB1* and the clinicopathological characteristics of gastric adenocarcinoma samples. As shown in Table 1, the expression level of *MIB1* was higher in patients with a high T stage ($P = 0.017$) and pathological stage ($P = 0.032$). However, the expression level of *MIB1* was associated with other clinicopathological features, such as age ($P = 0.423$), sex ($P = 0.884$), N stage ($P = 0.433$), M stage ($P = 1.000$), tissue type ($P = 0.448$), and *H. pylori* infection ($P = 0.470$). In conclusion, *MIB1* was associated with high T stage and pathological stage, which further suggested that *MIB1* might be used as a biomarker for the poor prognosis of gastric adenocarcinoma.

Diagnostic value of MIB1 gene expression in STAD

The usefulness of *MIB1* in separating GC samples from normal samples was investigated using ROC curve analysis. As shown in Figure 2D, the ROC curve showed that the area under the curve (AUC) value of *MIB1* was 0.783 (95%CI: 0.704-0.861). The sensitivity and specificity of *MIB1* were respectively 59.4% and 85.6% at the cutoff value of 2.248. Positive and negative predictive values were 26.0% and 96.1%, respectively. These findings suggested that *MIB1* might be a potential biomarker to differentiate between normal tissues and stomach cancer tissues.

Relationship between gene expression level of MIB1 and OS

As shown in Figure 2E, patients with gastric adenocarcinoma who had high *MIB1* Levels compared to those who had low *MIB1* Levels had significantly worse OS (26.4 mo *vs* 56.2 mo, $P = 0.033$). This suggested that high mRNA expression of *MIB1* was a biomarker for poor prognosis in gastric adenocarcinoma.

Correlation and interaction analyses

A volcano plot of *MIB1* and coexpressed genes in GC was generated in the LinkedOmics database (Figure 3A). The Metascape database was then used to examine the GO and KEGG pathway terms of these top 200 genes. GO analysis was used to investigate the functional mechanism of *MIB1* in GC. The BP terms "proteolysis involved in cellular protein catabolic process", "mitochondrion organization", "phosphatidylinositol-3-phosphate biosynthetic process", and "protein phosphorylation" were significantly enriched (Figure 3B). Among the enriched CC terms was "mitochondrial protein-containing complex" (Figure 3C). "Protein serine/threonine/tyrosine kinase activity", "ubiquitin-like protein transferase activity", and "enzyme activator activity" were the most commonly enriched MF phrases (Figure 3D). The target genes were primarily linked to the phrases "chemical carcinogenesis-reactive oxygen species", "platinum drug resistance", and "ubiquitin mediated proteolysis", according to KEGG pathway analysis (Figure 3E). The top 50 genes with positive relationship (Figure 3F) and the top 50 genes with negative relationship (Figure 3G) with *MIB1* were displayed in a heatmap to further investigate the processes of *MIB1* and its coexpressed genes. The ten coexpressed genes of *MIB1* in the STRING database were NOTCH1, NOTCH2, NOTCH3, DLL1, DLL4, UBB, MARK2, JAG1, JAG2, and RPS27A (Figure 3H). These genes were analyzed by GO and KEGG, most of which were related to NOTCH pathway (Figure 3I and J).

Table 1 Demographic and clinicopathological parameters of patients with gastric cancer with high and low expression of mind bomb 1 in The Cancer Genome Atlas-stomach adenocarcinoma, *n* (%)

Characteristics	Total	Low expression of *MIB1*	High expression of *MIB1*	*P* value
T stage				**0.017**
T1	19 (5.2)	11 (3.0)	8 (2.2)	
T2	80 (21.8)	37 (10.1)	43 (11.7)	
T3	168 (45.8)	99 (27.0)	69 (18.8)	
T4	100 (27.2)	40 (10.9)	60 (16.3)	
N stage				0.433
N0	111 (31.1)	61 (17.1)	50 (14.0)	
N1	97 (27.2)	49 (13.7)	48 (13.4)	
N2	75 (21.0)	32 (9.0)	43 (12.0)	
N3	74 (20.7)	38 (10.6)	36 (10.1)	
M stage				1.000
M0	330 (93.0)	164 (46.2)	166 (46.8)	
M1	25 (7.0)	12 (3.4)	13 (3.7)	
Pathologic stage				**0.032**
Stage I	53 (15.1)	24 (6.8)	29 (8.2)	
Stage II	111 (31.5)	69 (19.6)	42 (11.9)	
Stage III	150 (42.6)	72 (20.5)	78 (22.2)	
Stage IV	38 (10.8)	15 (4.3)	23 (6.5)	
Gender				0.884
Female	134 (35.7)	68 (18.1)	66 (17.6)	
Male	241 (64.3)	119 (31.7)	122 (32.5)	
Histological type				0.448
Diffuse type	63 (16.8)	36 (9.6)	27 (7.2)	
Mucinous type	19 (5.1)	11 (2.9)	8 (2.1)	
Not otherwise specified	207 (55.3)	103 (27.5)	104 (27.8)	
Papillary type	5 (1.3)	1 (0.3)	4 (1.1)	
Signet ring type	11 (2.9)	4 (1.1)	7 (1.9)	
Tubular type	69 (18.4)	32 (8.6)	37 (9.9)	
Histologic grade				0.305
G1	10 (2.7)	4 (1.1)	6 (1.6)	
G2	137 (37.4)	63 (17.2)	74 (20.2)	
G3	219 (59.8)	117 (32.0)	102 (27.9)	
H. pylori infection				0.470
No	145 (89.0)	63 (38.7)	82 (50.3)	
Yes	18 (11.0)	10 (6.1)	8 (4.9)	
OS event				**0.022**
Alive	228 (60.8)	125 (33.3)	103 (27.5)	
Dead	147 (39.2)	62 (16.5)	85 (22.7)	
Age, mean ± SD		65.39 ± 10.80	66.28 ± 10.51	0.423

The bold means statistical significance. *MIB1*: Mind bomb 1; OS: Overall survival; *H. pylori*: *Helicobacter pylori*.

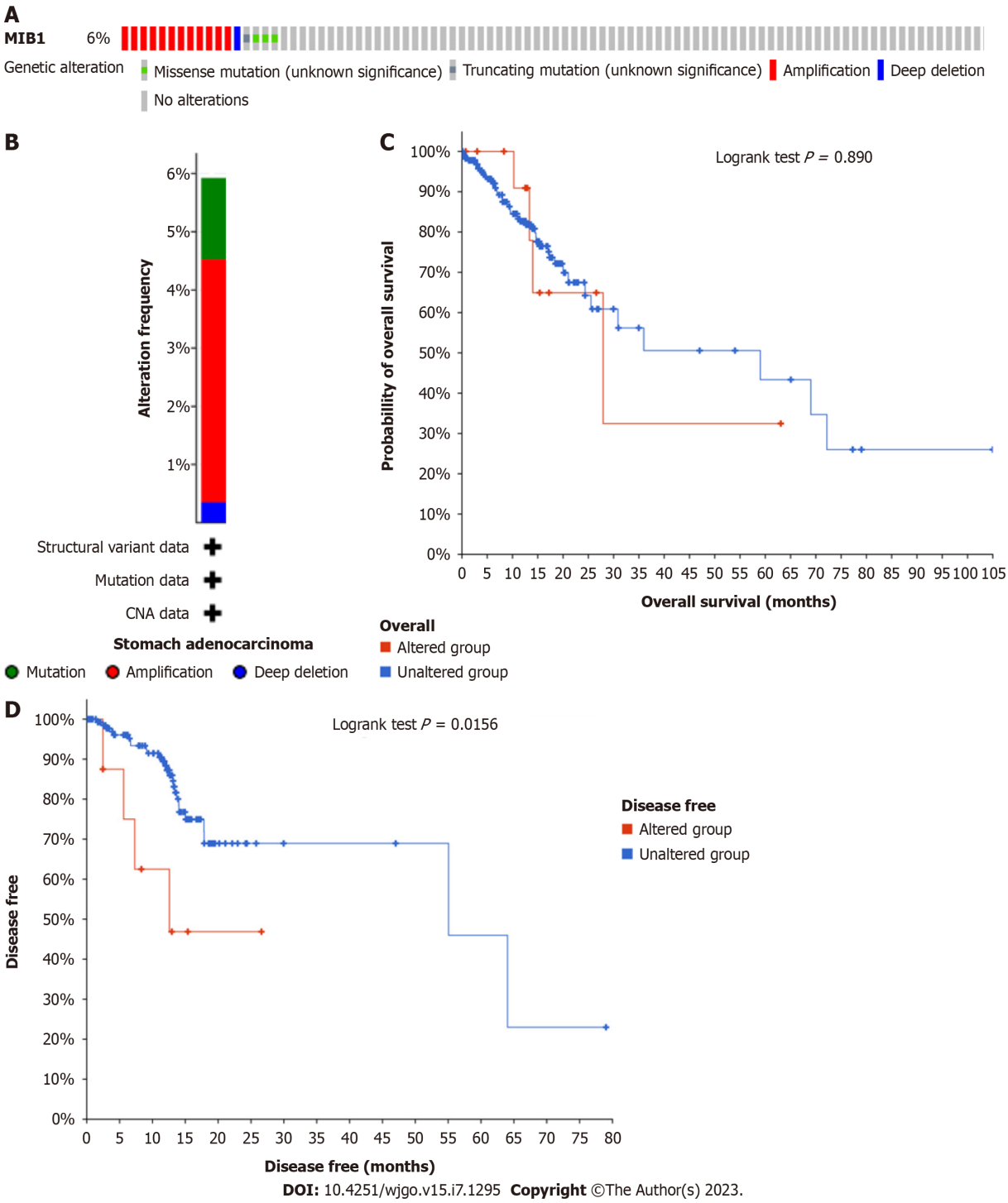

DOI: 10.4251/wjgo.v15.i7.1295

Figure 1 Mutation of mind bomb 1 gene in stomach adenocarcinoma is found in cBioPortal database. A: OncoPrint indicate different types and proportions of mind bomb 1 (*MIB1*) mutations; B: Summary of cancer types shows the type of genomic alterations in stomach adenocarcinoma; C: Kaplan-Meier showed the overall survival rate of patients with and without copy number alteration (CNA) of *MIB1*; D: Kaplan-Meier showed the disease-free survival rate of patients with and without CNA of *MIB1*.

Volcano map and enrichment analysis of the differentially expressed genes

With a threshold of |logFC| < 1.5 and adjusted $P < 0.05$, 506 DEGs in total were discovered, of which 454 showed upregulation and 52 showed downregulation. The DEG expression was visualized in a volcano diagram (Figure 4A). The DEG-related *MIB1* had strongly regulatory effects on the endoplasmic reticulum lumen, cornified envelope, keratin filament, endosome lumen, epidermal cell differentiation, and keratinocyte differentiation, keratinization, cornification and peptide

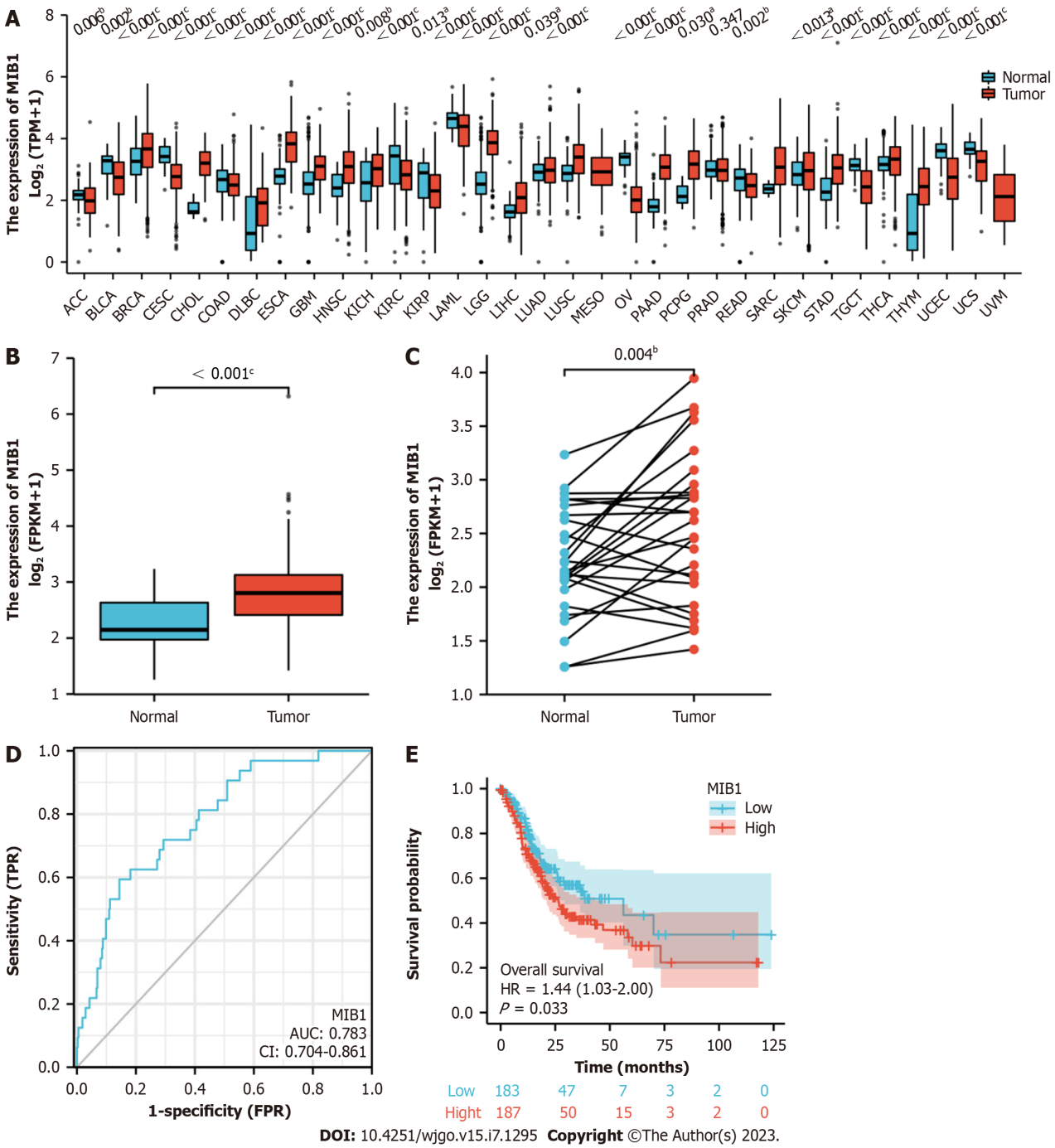

DOI: 10.4251/wjgo.v15.i7.1295

Figure 2 Expression,diagnostic value and prognosis of mind bomb 1 gene. A: Mind bomb 1 (*MIB1*) expression from pan-cancer perspective; B: *MIB1* mRNA expression levels in 375 gastric adenocarcinoma samples and 32 normal samples; C: *MIB1* mRNA expression levels in 27 gastric adenocarcinomas and matched adjacent normal samples; D: Receiver operating characteristic curve showed that the area under the curve value of *MIB1* in distinguishing gastric adenocarcinoma tissues from healthy controls was 0.783. The cutoff was 2.248, and the sensitivity, specificity and accuracy were 59.4% and 85.6%, respectively; E: Kaplan-Meier showed that the overall survival of gastric adenocarcinoma patients with high mRNA expression of *MIB1* was shorter than that of patients with low expression (26.4 mo *vs* 56.2 mo, $P = 0.033$). $^{a}P < 0.05$; $^{b}P < 0.01$, $^{c}P < 0.001$.

cross-linking processes, according to GO enrichment analysis (Figure 4B). KEGG analysis showed that DEG-related *MIB1* was associated with protein digestion and absorption, pancreatic secretion, and cholesterol metabolism pathways (Figure 4C).

Correlation between MIB1 expression and immune cell infiltration in gastric adenocarcinoma

We analyzed the correlation between the expression of *MIB1* and six types of tumor invasive immune cells in the TIMER database. As demonstrated in Figure 5A, *MIB1* expression was favorably linked with B cells ($r = 0.222$, $P = 1.61E-05$), $CD4^+$ T cells ($r = 0.201$, $P = 1.08E-04$), and macrophages ($r = 0.139$, $P = 7.22E-03$) and negatively connected with $CD8^+$ T cells ($r = -0.143$, $P = 5.77E-03$). Figure 5B showed the relationship between *MIB1* and 24 kinds of tumor immune infiltrating cells. Tcm, helper T cells, Tem, Tgd and NK CD56 bright cells were positively correlated with *MIB1*. *MIB1* was

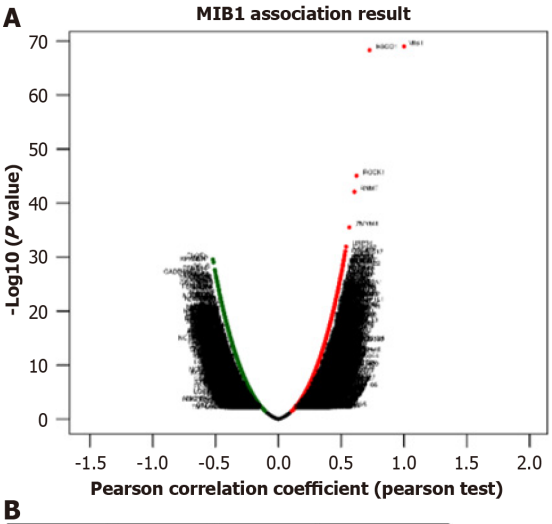
A
MIB1 association result
-Log10 (P value)
Pearson correlation coefficient (pearson test)

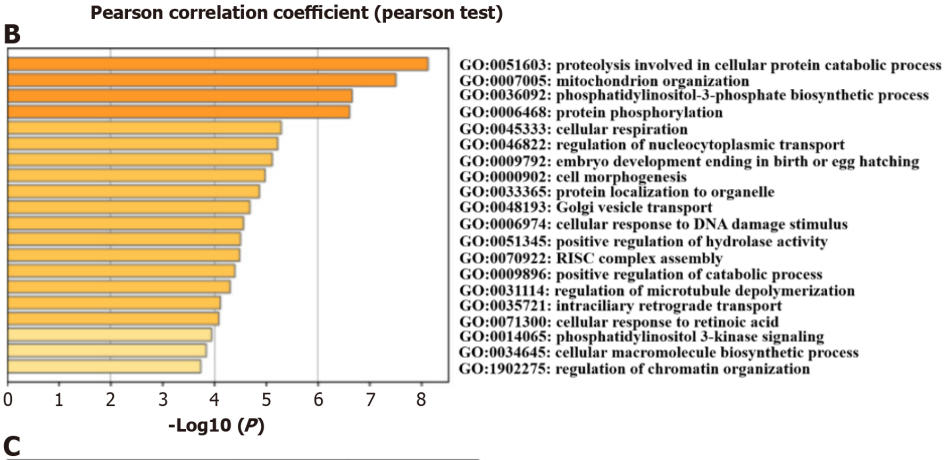
B
GO:0051603: proteolysis involved in cellular protein catabolic process
GO:0007005: mitochondrion organization
GO:0036092: phosphatidylinositol-3-phosphate biosynthetic process
GO:0006468: protein phosphorylation
GO:0045333: cellular respiration
GO:0046822: regulation of nucleocytoplasmic transport
GO:0009792: embryo development ending in birth or egg hatching
GO:0000902: cell morphogenesis
GO:0033365: protein localization to organelle
GO:0048193: Golgi vesicle transport
GO:0006974: cellular response to DNA damage stimulus
GO:0051345: positive regulation of hydrolase activity
GO:0070922: RISC complex assembly
GO:0009896: positive regulation of catabolic process
GO:0031114: regulation of microtubule depolymerization
GO:0035721: intraciliary retrograde transport
GO:0071300: cellular response to retinoic acid
GO:0014065: phosphatidylinositol 3-kinase signaling
GO:0034645: cellular macromolecule biosynthetic process
GO:1902275: regulation of chromatin organization
-Log10 (P)

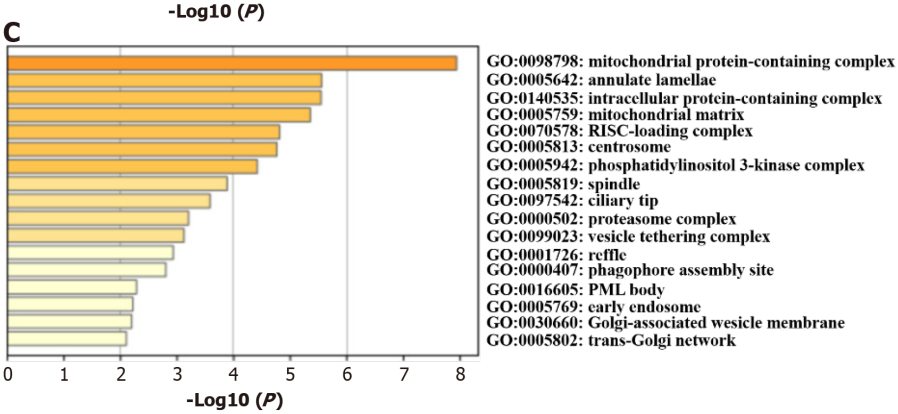
C
GO:0098798: mitochondrial protein-containing complex
GO:0005642: annulate lamellae
GO:0140535: intracellular protein-containing complex
GO:0005759: mitochondrial matrix
GO:0070578: RISC-loading complex
GO:0005813: centrosome
GO:0005942: phosphatidylinositol 3-kinase complex
GO:0005819: spindle
GO:0097542: ciliary tip
GO:0000502: proteasome complex
GO:0099023: vesicle tethering complex
GO:0001726: ruffle
GO:0000407: phagophore assembly site
GO:0016605: PML body
GO:0005769: early endosome
GO:0030660: Golgi-associated vesicle membrane
GO:0005802: trans-Golgi network
-Log10 (P)

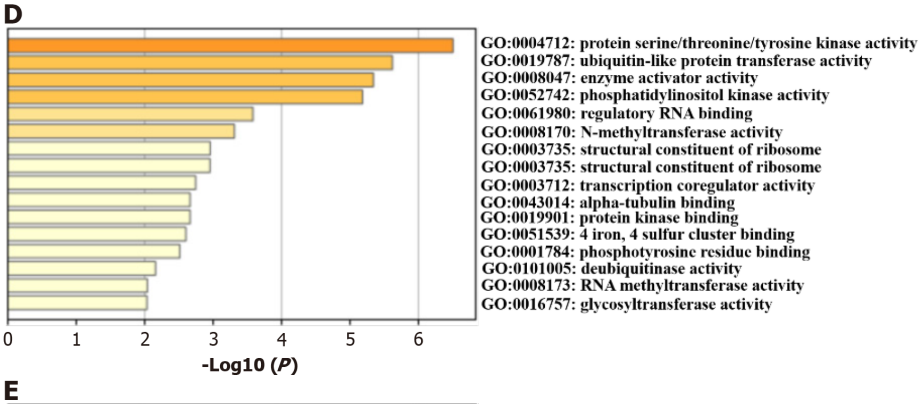
D
GO:0004712: protein serine/threonine/tyrosine kinase activity
GO:0019787: ubiquitin-like protein transferase activity
GO:0008047: enzyme activator activity
GO:0052742: phosphatidylinositol kinase activity
GO:0061980: regulatory RNA binding
GO:0008170: N-methyltransferase activity
GO:0003735: structural constituent of ribosome
GO:0003735: structural constituent of ribosome
GO:0003712: transcription coregulator activity
GO:0043014: alpha-tubulin binding
GO:0019901: protein kinase binding
GO:0051539: 4 iron, 4 sulfur cluster binding
GO:0001784: phosphotyrosine residue binding
GO:0101005: deubiquitinase activity
GO:0008173: RNA methyltransferase activity
GO:0016757: glycosyltransferase activity
-Log10 (P)

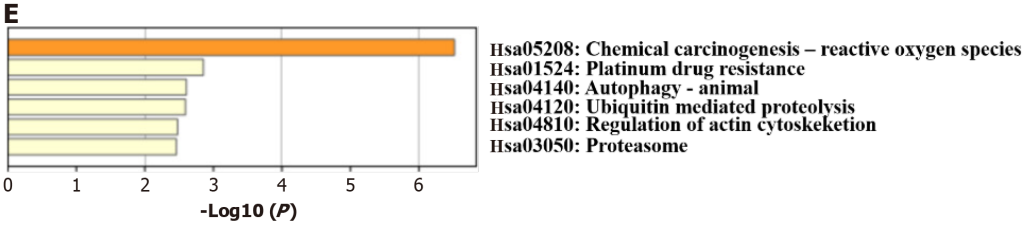
E
Hsa05208: Chemical carcinogenesis – reactive oxygen species
Hsa01524: Platinum drug resistance
Hsa04140: Autophagy - animal
Hsa04120: Ubiquitin mediated proteolysis
Hsa04810: Regulation of actin cytoskeketion
Hsa03050: Proteasome
-Log10 (P)

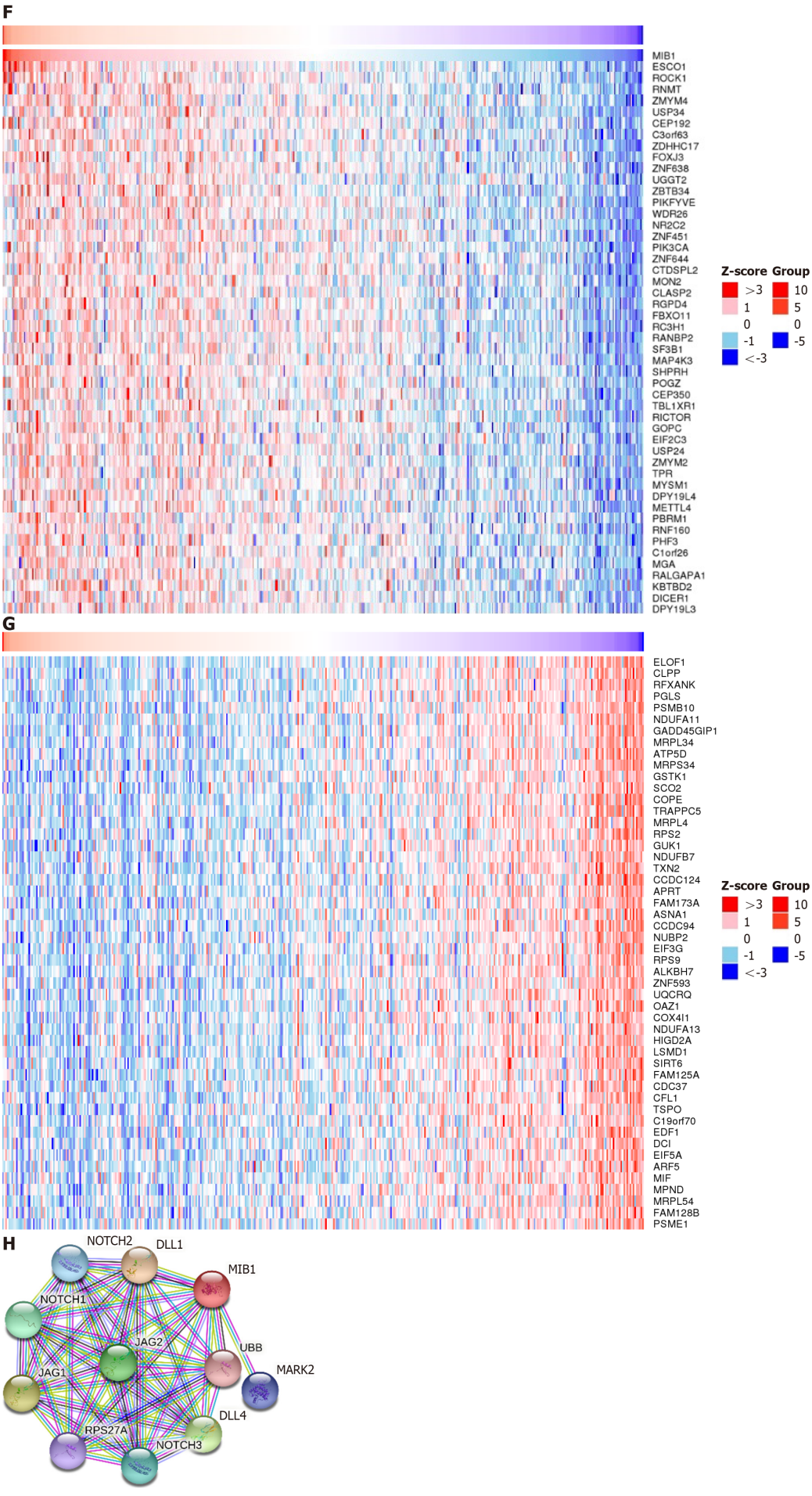
F
MIB1
ESCO1
ROCK1
RNMT
ZMYM4
USP34
CEP192
C3orf63
ZDHHC17
FOXJ3
ZNF638
UGGT2
ZBTB34
PIKFYVE
WDR26
NR2C2
ZNF451
PIK3CA
ZNF644
CTDSPL2
MON2
CLASP2
RGPD4
FBXO11
RC3H1
RANBP2
SF3B1
MAP4K3
SHPRH
POGZ
CEP350
TBL1XR1
RICTOR
GOPC
EIF2C3
USP24
ZMYM2
TPR
MYSM1
DPY19L4
METTL4
PBRM1
RNF160
PHF3
C1orf26
MGA
RALGAPA1
KBTBD2
DICER1
DPY19L3
Z-score
Group
>3
1
0
-1
<-3
10
5
0
-5
G
ELOF1
CLPP
RFXANK
PGLS
PSMB10
NDUFA11
GADD45GIP1
MRPL34
ATP5D
MRPS34
GSTK1
SCO2
COPE
TRAPPC5
MRPL4
RPS2
GUK1
NDUFB7
TXN2
CCDC124
APRT
FAM173A
ASNA1
CCDC94
NUBP2
EIF3G
RPS9
ALKBH7
ZNF593
UQCRQ
OAZ1
COX4I1
NDUFA13
HIGD2A
LSMD1
SIRT6
FAM125A
CDC37
CFL1
TSPO
C19orf70
EDF1
DCI
EIF5A
ARF5
MIF
MPND
MRPL54
FAM128B
PSME1
Z-score
Group
>3
1
0
-1
<-3
10
5
0
-5
H
NOTCH2
DLL1
MIB1
NOTCH1
JAG2
UBB
MARK2
JAG1
DLL4
RPS27A
NOTCH3

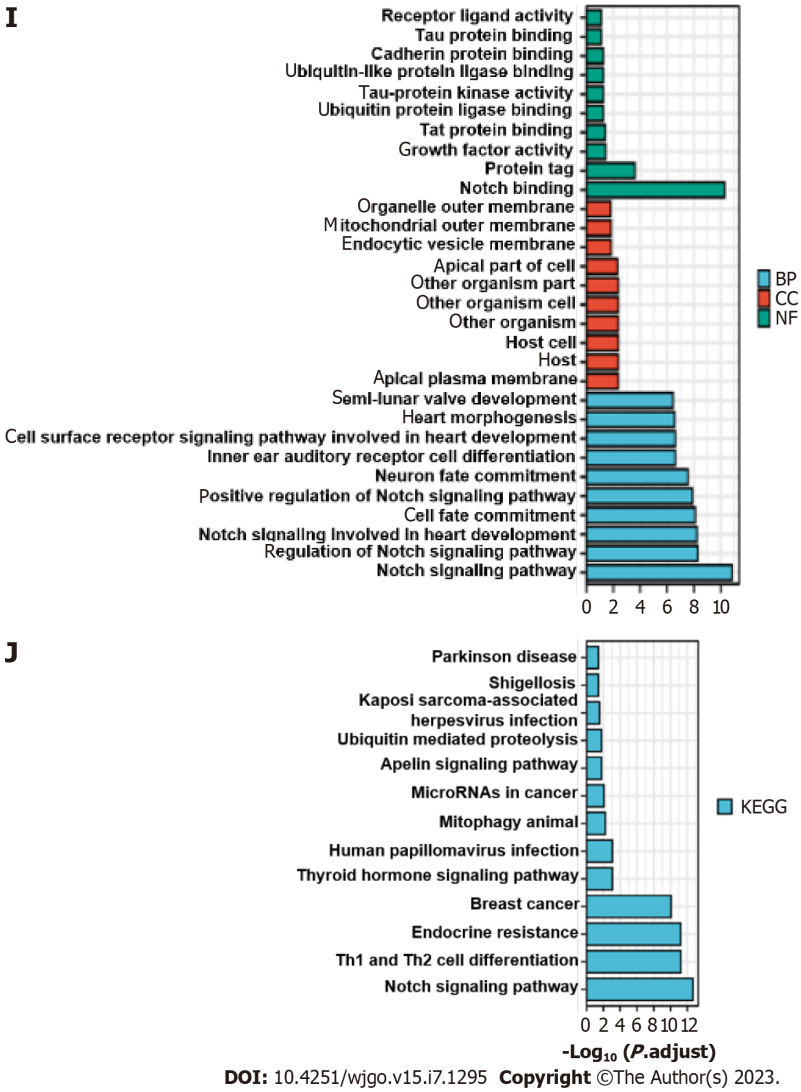

DOI: 10.4251/wjgo.v15.i7.1295

Figure 3 Coexpression analysis of mind bomb 1 gene. A: A volcano plot of the mind bomb 1 (*MIB1*) and its co-expressed genes in gastric cancer; B: The Gene Ontology (GO) enrichment of the BP terms of 200 co-expressed genes; C: The GO enrichment of the CC terms of 200 co-expressed genes; D: The GO enrichment of the MF terms of 200 co-expressed genes; E: The Kyoto Encyclopedia of Genes and Genomes (KEGG) enrichment of the 200 co-expressed genes; F: The top 50 genes with a positive correlation with *MIB1* gene are visualized in a heatmap; G: The top 50 genes with a negative correlation with the *MIB1* gene are visualized in a heatmap; H: The protein-protein interaction network associated with the *MIB1* in gastric cancer; I: The GO enrichment of the 11 genes with the strongest interaction with *MIB1* proteins; J: The KEGG pathway terms of the 11 genes with the strongest interaction with *MIB1* proteins. MIB1: Mind bomb 1.

inversely linked with cytotoxic cells, NK CD56dim cells, pDCs, aDCs, CD8 T cells, and Th17 cells. The relationship between the level of *MIB1* expression and the degree of immune cell infiltration measured by the ssGSEA score was investigated using Spearman correlation. The extent of NK CD56dim cell infiltration was negatively correlated with *MIB1* expression (r = -0.292, P < 0.001) (Figure 5C) and considerably decreased in the *MIB1* high expression group (P < 0.001) (Figured 5D). These results demonstrated that *MIB1* played an important role in the immune infiltration of GC. The proportions of 24 different subsets of tumor-infiltrating immune cells were compared using a heatmap to ascertain the degrees of association (Figure 5E).

DISCUSSION

Notch signaling is an evolutionarily conserved pathway that controls cell fate, determines cell differentiation, proliferation, tumor angiogenesis, stem cell maintenance, apoptosis and other cellular processes, and promotes the occurrence of GC through crosstalk with different signaling pathways, such as the Wnt, Ras, and NF-κB pathways[26,27]. Studies have indicated that endocytosis of Notch ligands is required to activate the receptor in the Notch pathway[28]. However, ubiquitination of the intracellular tail of Notch ligands is a critical event in the subsequent endocytosis and signal transduction of these molecules[29]. Initial genetic studies in flies and zebrafish identified two E3 ubiquitin ligase families capable of ligand ubiquitination: Mind Bomb (Mib) and Neuralized (Neur) proteins[30]. Then a series of studies concluded that *MIB1*, a member of the E3 ubiquitin-protein ligase family, played a major, possibly exclusive role in Notch

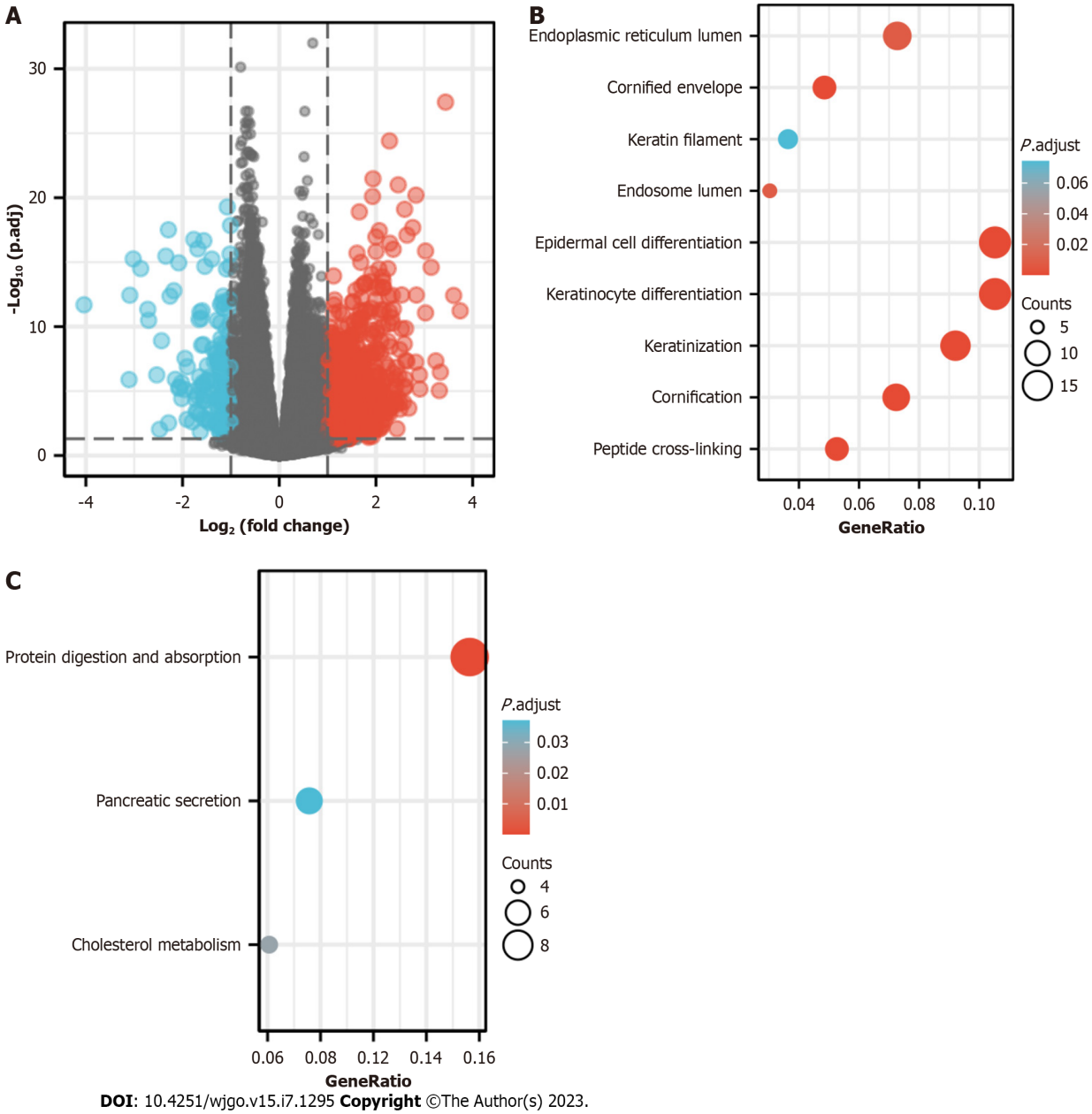

DOI: 10.4251/wjgo.v15.i7.1295 **Copyright** ©The Author(s) 2023.

Figure 4 Enrichment analysis of mind bomb 1 in stomach adenocarcinoma. A: Volcanic map of differential expression in gastric adenocarcinoma with |logFC| < 1.5 and adjusted *P* < 0.05; B: Gene Ontology enrichment analysis of differentially expressed genes; C: Kyoto Encyclopedia of Genes and Genomes enrichment analysis of differentially expressed genes.

ligand ubiquitination and transport in mammals[31].

The roles of some Notch family members in GC have not yet been fully understood, despite the fact that the impact of Notch signaling on GC has been extensively established[32,33]. In this work, we performed a thorough examination of *MIB1*, a NOTCH family member, in patients with GC to determine its mutation, expression, prognostic value, and immune infiltration.

The mRNA expression of *MIB1* was observed to be increased in STAD tissues in our research. And positive correlation was found between the increase of mRNA expression and a high T stage. *MIB1* might be a viable diagnostic biomarker for separating stomach cancer tissues from normal tissues, according to a ROC curve analysis. Kaplan-Meier curves and univariate analysis allowed us to demonstrate that increased mRNA expression of *MIB1* was associated with short OS and might be used as a feasible biomarker for poor prognosis of GC. Additionally, *MIB1* might have a unique function in the immunological infiltration of GC.

MIB1 is a ubiquitin-protein ligase. It was reported that overexpression of *MIB1* significantly promoted cell proliferation, migration and invasion[25]. Recent studies have found that *MIB1* played a carcinogenic function in a variety of human malignancies, including pancreatic, prostate, and lung cancer[23,34,35]. Studies have shown that *MIB1* was an important biomarker leading to poor prognosis, and upregulation of *MIB1* expression was associated with poor OS[22]. Furthermore, mutation of the *MIB1* gene could lead to congenital heart disease by reducing Notch signaling activation [36]. Overexpression of E3 ubiquitin ligase *MIB1* could reduce the apoptosis and inflammation of cardiac microvascular

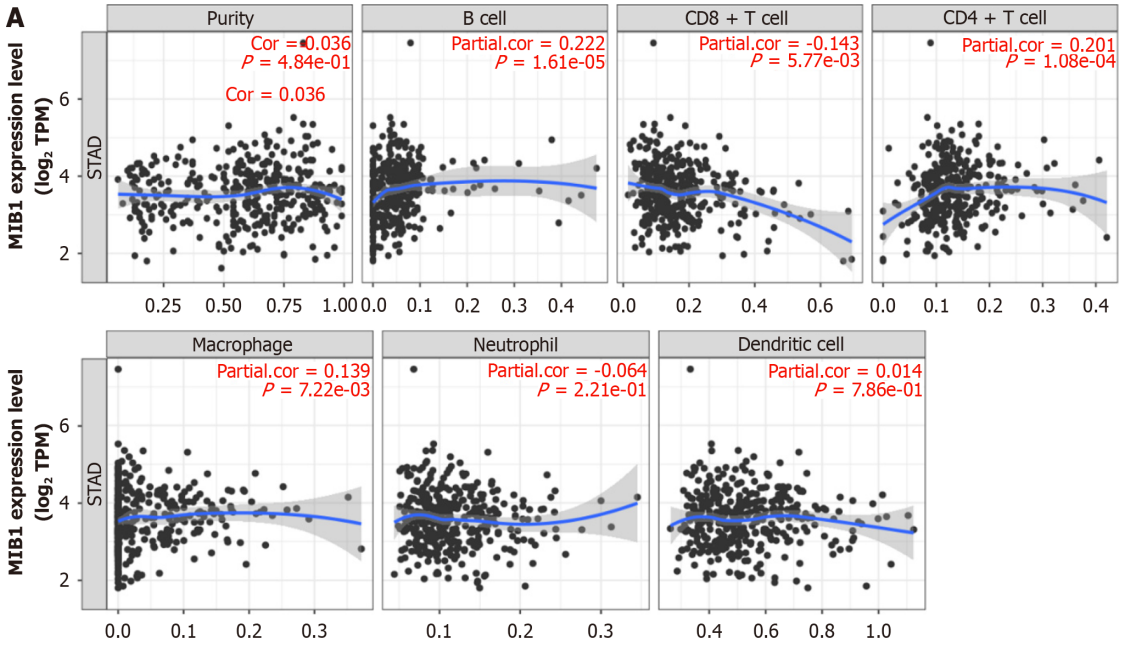
A
Purity
B cell
CD8 + T cell
CD4 + T cell
Cor = 0.036
P = 4.84e-01
Cor = 0.036
Partial.cor = 0.222
P = 1.61e-05
Partial.cor = -0.143
P = 5.77e-03
Partial.cor = 0.201
P = 1.08e-04
MIB1 expression level (log2 TPM)
STAD
Macrophage
Neutrophil
Dendritic cell
Partial.cor = 0.139
P = 7.22e-03
Partial.cor = -0.064
P = 2.21e-01
Partial.cor = 0.014
P = 7.86e-01

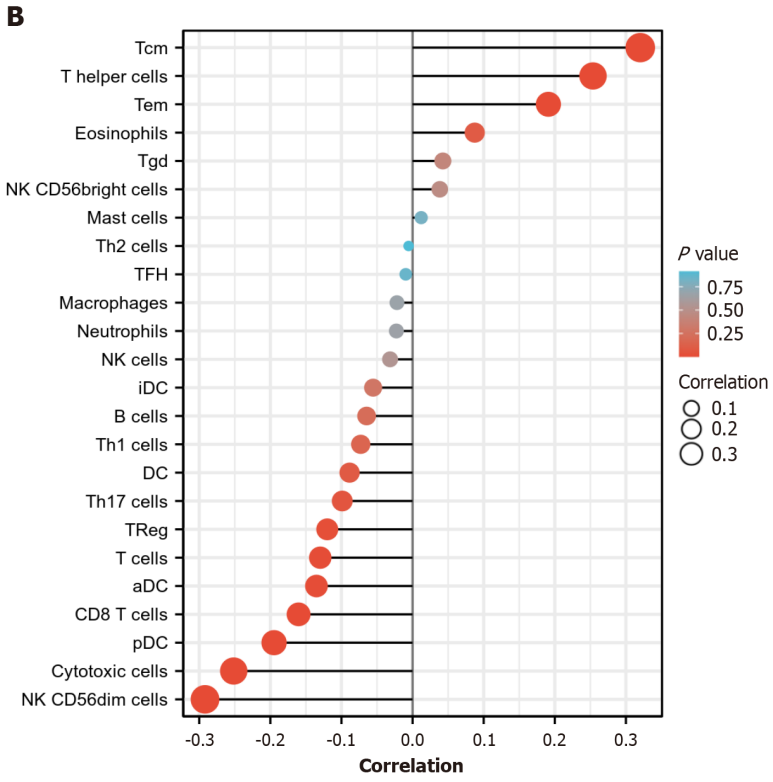
B
Tcm
T helper cells
Tem
Eosinophils
Tgd
NK CD56bright cells
Mast cells
Th2 cells
TFH
Macrophages
Neutrophils
NK cells
iDC
B cells
Th1 cells
DC
Th17 cells
TReg
T cells
aDC
CD8 T cells
pDC
Cytotoxic cells
NK CD56dim cells
Correlation
P value
0.75
0.50
0.25
Correlation
0.1
0.2
0.3

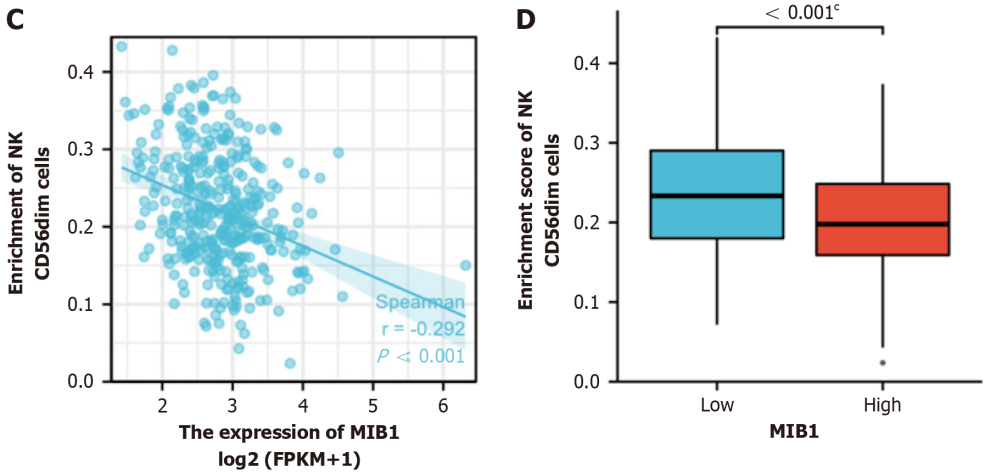
C
Enrichment of NK CD56dim cells
Spearman
r = -0.292
P < 0.001
The expression of MIB1 log2 (FPKM+1)
D
< 0.001c
Enrichment score of NK CD56dim cells
Low
High
MIB1

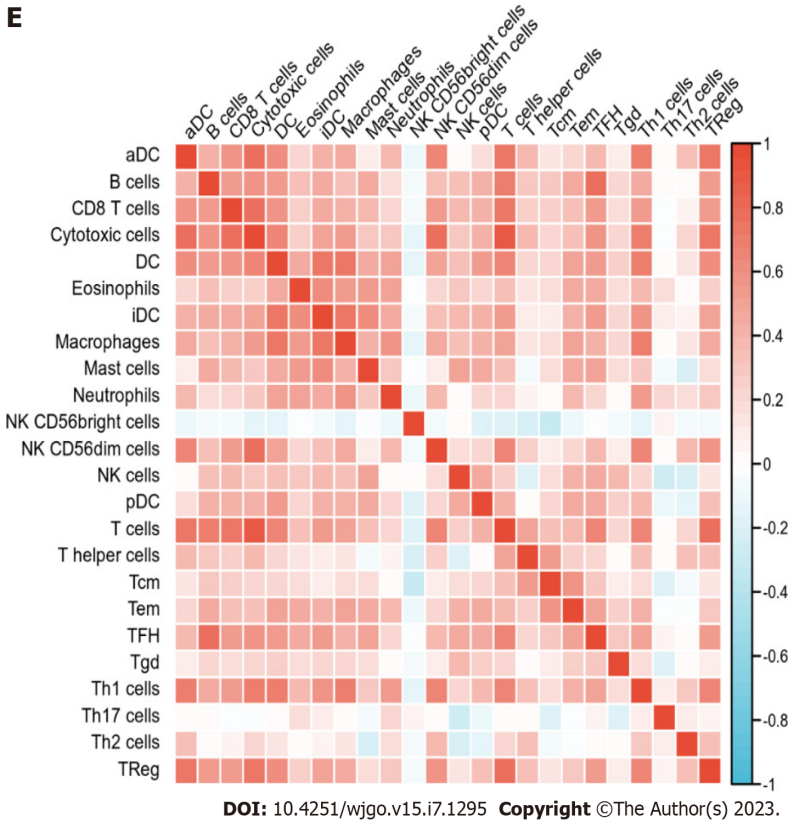

DOI: 10.4251/wjgo.v15.i7.1295

Figure 5 Analysis of the relationship between mind bomb 1 expression and immune infiltration. A: In gastric adenocarcinoma, the expression of mind bomb 1 (*MIB1*) was negatively correlated with $CD8^+$ T cells, and correlated with B cells, $CD4^+$ T cells and macrophages; B: The correlation between the expression level of *MIB1* and the relative abundance of 24 immune cells; C: The expression of *MIB1* was negatively correlated with NK CD56dim cells; D: NK CD56dim cell infiltration level in different expression groups of *MIB1*; E: Heat map of 24 immune infiltrating cells in stomach adenocarcinoma.

endothelial cells in coronary microvascular dysfunction[37].

In this study, analysis of the cBioportal database showed that the *MIB1* mutation rate in 287 patients in the TCGA dataset was approximately 6%, and most of the changes were copy number amplification (CNA). In cancer, CNAs and deletions result in altered expression of tumor suppressor genes and oncogenes, respectively. It was reported that copy number variation of E3 ubiquitin ligase was associated with the occurrence and development of colorectal cancer[38]. We further analyzed the correlation between *MIB1* gene changes and prognosis. We found no significant difference between *MIB1* gene changes and OS, but the DFS of the patient group with mutations was much shorter than that of the group without mutations. Moreover, what we discovered were consistent with previous studies that *MIB1* mRNA was abnormally expressed in many cancers, and we found that *MIB1* was greatly increased in gastric adenocarcinoma *via* the TCGA database. According to this, gastric adenocarcinoma with a poor clinical prognosis might be identified using *MIB1* as a possible biomarker for poor prognosis.

At present, the role of *MIB1* in tumors and whether it acts through the NOTCH pathway have not been fully reported. There have been relatively many studies on *MIB1* in pancreatic cancer. Some studies have shown that *MIB1* can be used as a direct target of miRNA-198 and miRNA-195-5p. *MIB1* has been considered as a new target of miRNA-198, which reduced the proliferation, migration and invasion of prostate cancer. However, this tumor inhibition role appeared to be independent of the Notch pathway[39]. MicroRNA-195-5p might regulate the proliferation and invasion of tumor cells by regulating *MIB1*, suggesting that miRNA-195-5p might be used to treat prostate cancer in the future[34]. Our results indicated that *MIB1* may be an intriguing biomarker or an emerging target for cancer therapy. In addition, ectopic expression of *MIB1* could induce epithelial-to-mesenchymal transition and stimulate cell migration through the Notch-dependent pathway, which might provide new insights into the treatment of *MIB1*-overexpressing cancer[35]. Other studies have shown that *MIB1* promoted the progression of pancreatic cancer by inducing ST7 degradation and downregulating IQGAP1, suggesting that the *MIB1*/ST7/IQGAP1 axis was crucial in the advancement of pancreatic cancer, and inhibiting *MIB1* might become a new therapeutic strategy for pancreatic cancer patients[22]. A study proved that *MIB1* promoted pancreatic cancer proliferation by activating the β-catenin signaling pathway[23]. Therefore, whether *MIB1* affects the progression of GC through the NOTCH pathway needs further *in vivo* and *in vitro* experiments.

A ROC curve analysis was performed to verify the clinical value of *MIB1* in diagnosing gastric adenocarcinoma. With a sensitivity of 59.4% and a specificity of 85.6%, our findings demonstrated that *MIB1* had a relatively higher AUC value to discover the patients with GC. Based on our research, we came to the conclusion that *MIB1* might function as an applicable diagnostic biomarker to separate gastric adenocarcinoma from normal controls.

In addition, *MIB1* was highly expressed in patients with gastric adenocarcinoma. *MIB1* was correlated with multiple clinical features, such as pathological stage, T stage and OS, further suggesting that *MIB1* was a prospective biomarker that merited additional clinical testing.

Cytotoxic cells, NK CD56dim cells, pDCs, aDCs, CD8 T cells and Th17 cells were negatively correlated with *MIB1*. Antitumor immunity was influenced by cytotoxic cells, including NK cells. The function of NK cells in innate immune surveillance is crucial in the fight against cancer[24]. In the course of transformation into toxic T cells, $CD8^+$ T cells display cytotoxic abilities against tumor cells[25]. IFN-I produced by pDCs has antitumor activity[26], Th17 cells have a close connection to neutrophils and are essential for the immune response to tumors[27]. The decrease of these immune cells might contribute to the further development of GC. The results of ssGSEA further demonstrated that *MIB1* was essential in controlling immune infiltration.

Our research revealed the complex role of *MIB1* gene mutation and abnormal expression in the prognosis of GC. In addition, we also preliminarily discussed the relationship between the *MIB1* gene and immune infiltration, as well as its mechanism and biological function in GC. However, our research also had some limitations. This study lacked *in vivo* or *in vitro* experiments to verify the role of the *MIB1* gene, which will allow us to draw more general and accurate conclusions.

CONCLUSION

In brief, we found that *MIB1* mRNA expression increased in STAD was positively attached with high T stage and pathological stage and negatively correlated with OS. According to our research, higher expression of *MIB1* may be a useful predictive biomarker for identifying individuals with gastric adenocarcinomas who have a poor clinical prognosis and may have a special function in immune infiltration.

ARTICLE HIGHLIGHTS

Research background

Gastric cancer (GC) is a disease with multi-etiology and multi-pathway involvement, and it is characterized by a low 5-year survival rate. NOTCH signaling pathway is also involved in the occurrence and development of GC. Mind bomb 1 (*MIB1*), an E3 ubiquitin ligase, plays a central role in activating the NOTCH pathway by mediating ubiquitination of NOTCH ligand. However, the effect of *MIB1* on GC has not been reported.

Research motivation

To investigate the effect of *MIB1* gene on the prognosis of GC.

Research objectives

To investigate the effect of expression and mutation of *MIB1* gene on the prognosis of GC, the function of *MIB1* in GC and its relationship with immune infiltration.

Research methods

TCGA database, cBioPortal database, a receiver operating characteristic (ROC) curve, Kaplan-Meier plotter, LinkedOmics database, STRING database, The Gene Ontology enrichment , Kyoto Encyclopedia of Genes and Genomes pathway and TIMER database were used in this study.

Research results

The level of *MIB1* expression had a certain impact on the survival rate of patients with GC. The prognosis of patients with high *MIB1* was worse than that of patients with low *MIB1*. The increased expression of *MIB1* gene was associated with high TNM staging, suggesting that *MIB1* may play a role in the development of GC. The expression of *MIB1* gene was associated with immune infiltration.

Research conclusions

The up-regulation of *MIB1* expression was significantly related to the low survival rate and immune infiltration in gastric adenocarcinoma.

Research perspectives

MIB1 may be a biomarker for poor prognosis of gastric adenocarcinoma and a potential immunotherapeutic target.

FOOTNOTES

Author contributions: Wang J contributed to conceptualization; Wang D wrote the paper; Wang QH, Luo T, and Jia W collected and

analyzed data.

Supported by the Science and Technology Program of Liaoning Province, No. 2021-MS-040.

Conflict-of-interest statement: The authors declare that they have no known competing financial interests or personal relationships that could have appeared to influence the work reported in this paper.

PRISMA 2009 Checklist statement: We have read the PRISMA 2009 Checklist, and the manuscript was prepared and revised according to the PRISMA 2009 Checklist.

Country/Territory of origin: China

ORCID number: Di Wang 0000-0003-3725-5288; Qi-Hong Wang 0000-0002-7264-2905; Ting Luo 0000-0003-3725-5288; Wen Jia 0000-0003-3725-5288; Jing Wang 0000-0003-3725-5288.

S-Editor: Chen YL
L-Editor: A
P-Editor: Ju JL

REFERENCES

1 **Sung H**, Ferlay J, Siegel RL, Laversanne M, Soerjomataram I, Jemal A, Bray F. Global Cancer Statistics 2020: GLOBOCAN Estimates of Incidence and Mortality Worldwide for 36 Cancers in 185 Countries. *CA Cancer J Clin* 2021; **71**: 209-249 [PMID: 33538338 DOI: 10.3322/caac.21660]
2 **Soerjomataram I**, Lortet-Tieulent J, Parkin DM, Ferlay J, Mathers C, Forman D, Bray F. Global burden of cancer in 2008: a systematic analysis of disability-adjusted life-years in 12 world regions. *Lancet* 2012; **380**: 1840-1850 [PMID: 23079588 DOI: 10.1016/S0140-6736(12)60919-2]
3 **Xie W**, Yang T, Zuo J, Ma Z, Yu W, Hu Z, Song Z. Chinese and Global Burdens of Gastrointestinal Cancers From 1990 to 2019. *Front Public Health* 2022; **10**: 941284 [PMID: 35910886 DOI: 10.3389/fpubh.2022.941284]
4 **Smyth EC**, Nilsson M, Grabsch HI, van Grieken NC, Lordick F. Gastric cancer. *Lancet* 2020; **396**: 635-648 [PMID: 32861308 DOI: 10.1016/S0140-6736(20)31288-5]
5 **Song Z**, Wu Y, Yang J, Yang D, Fang X. Progress in the treatment of advanced gastric cancer. *Tumour Biol* 2017; **39**: 1010428317714626 [PMID: 28671042 DOI: 10.1177/1010428317714626]
6 **Chen Z**, Li Y, Tan B, Zhao Q, Fan L, Li F, Zhao X. Progress and current status of molecule-targeted therapy and drug resistance in gastric cancer. *Drugs Today (Barc)* 2020; **56**: 469-482 [PMID: 32648857 DOI: 10.1358/dot.2020.56.7.3112071]
7 **Asplund J**, Kauppila JH, Mattsson F, Lagergren J. Survival Trends in Gastric Adenocarcinoma: A Population-Based Study in Sweden. *Ann Surg Oncol* 2018; **25**: 2693-2702 [PMID: 29987609 DOI: 10.1245/s10434-018-6627-y]
8 **Nakagawa N**, Kanda M, Ito S, Mochizuki Y, Teramoto H, Ishigure K, Murai T, Asada T, Ishiyama A, Matsushita H, Tanaka C, Kobayashi D, Fujiwara M, Murotani K, Kodera Y. Pathological tumor infiltrative pattern and sites of initial recurrence in stage II/III gastric cancer: Propensity score matching analysis of a multi-institutional dataset. *Cancer Med* 2018; **7**: 6020-6029 [PMID: 30411544 DOI: 10.1002/cam4.1868]
9 **Machlowska J**, Baj J, Sitarz M, Maciejewski R, Sitarz R. Gastric Cancer: Epidemiology, Risk Factors, Classification, Genomic Characteristics and Treatment Strategies. *Int J Mol Sci* 2020; **21** [PMID: 32512697 DOI: 10.3390/ijms21114012]
10 **Yusefi AR**, Bagheri Lankarani K, Bastani P, Radinmanesh M, Kavosi Z. Risk Factors for Gastric Cancer: A Systematic Review. *Asian Pac J Cancer Prev* 2018; **19**: 591-603 [PMID: 29579788 DOI: 10.22034/APJCP.2018.19.3.591]
11 **Rawla P**, Barsouk A. Epidemiology of gastric cancer: global trends, risk factors and prevention. *Prz Gastroenterol* 2019; **14**: 26-38 [PMID: 30944675 DOI: 10.5114/pg.2018.80001]
12 **Houghton J**, Wang TC. Helicobacter pylori and gastric cancer: a new paradigm for inflammation-associated epithelial cancers. *Gastroenterology* 2005; **128**: 1567-1578 [PMID: 15887152 DOI: 10.1053/j.gastro.2005.03.037]
13 **Kankeu Fonkoua L**, Yee NS. Molecular Characterization of Gastric Carcinoma: Therapeutic Implications for Biomarkers and Targets. *Biomedicines* 2018; **6** [PMID: 29522457 DOI: 10.3390/biomedicines6010032]
14 **Wu WK**, Cho CH, Lee CW, Fan D, Wu K, Yu J, Sung JJ. Dysregulation of cellular signaling in gastric cancer. *Cancer Lett* 2010; **295**: 144-153 [PMID: 20488613 DOI: 10.1016/j.canlet.2010.04.025]
15 **Previs RA**, Coleman RL, Harris AL, Sood AK. Molecular pathways: translational and therapeutic implications of the Notch signaling pathway in cancer. *Clin Cancer Res* 2015; **21**: 955-961 [PMID: 25388163 DOI: 10.1158/1078-0432.CCR-14-0809]
16 **Aster JC**, Pear WS, Blacklow SC. The Varied Roles of Notch in Cancer. *Annu Rev Pathol* 2017; **12**: 245-275 [PMID: 27959635 DOI: 10.1146/annurev-pathol-052016-100127]
17 **Ntziachristos P**, Lim JS, Sage J, Aifantis I. From fly wings to targeted cancer therapies: a centennial for notch signaling. *Cancer Cell* 2014; **25**: 318-334 [PMID: 24651013 DOI: 10.1016/j.ccr.2014.02.018]
18 **South AP**, Cho RJ, Aster JC. The double-edged sword of Notch signaling in cancer. *Semin Cell Dev Biol* 2012; **23**: 458-464 [PMID: 22309843 DOI: 10.1016/j.semcdb.2012.01.017]
19 **Guo B**, McMillan BJ, Blacklow SC. Structure and function of the Mind bomb E3 ligase in the context of Notch signal transduction. *Curr Opin*

Struct Biol 2016; **41**: 38-45 [PMID: 27285058 DOI: 10.1016/j.sbi.2016.05.012]

20 **Koo BK**, Lim HS, Song R, Yoon MJ, Yoon KJ, Moon JS, Kim YW, Kwon MC, Yoo KW, Kong MP, Lee J, Chitnis AB, Kim CH, Kong YY. Mind bomb 1 is essential for generating functional Notch ligands to activate Notch. *Development* 2005; **132**: 3459-3470 [PMID: 16000382 DOI: 10.1242/dev.01922]

21 **Yamamoto M**, Morita R, Mizoguchi T, Matsuo H, Isoda M, Ishitani T, Chitnis AB, Matsumoto K, Crump JG, Hozumi K, Yonemura S, Kawakami K, Itoh M. Mib-Jag1-Notch signalling regulates patterning and structural roles of the notochord by controlling cell-fate decisions. *Development* 2010; **137**: 2527-2537 [PMID: 20573700 DOI: 10.1242/dev.051011]

22 **Zhang B**, Cheng X, Zhan S, Jin X, Liu T. MIB1 upregulates IQGAP1 and promotes pancreatic cancer progression by inducing ST7 degradation. *Mol Oncol* 2021; **15**: 3062-3075 [PMID: 33793053 DOI: 10.1002/1878-0261.12955]

23 **Fu X**, Tang N, Xie W, Mao L, Qiu Y. Mind Bomb 1 Promotes Pancreatic Cancer Proliferation by Activating β-Catenin Signaling. *J Nanosci Nanotechnol* 2020; **20**: 7276-7282 [PMID: 32711591 DOI: 10.1166/jnn.2020.18755]

24 **Lanier LL**. NK cell recognition. *Annu Rev Immunol* 2005; **23**: 225-274 [PMID: 15771571 DOI: 10.1146/annurev.immunol.23.021704.115526]

25 **Iwahori K**. Cytotoxic CD8(+) Lymphocytes in the Tumor Microenvironment. *Adv Exp Med Biol* 2020; **1224**: 53-62 [PMID: 32036604 DOI: 10.1007/978-3-030-35723-8_4]

26 **Saulep-Easton D**, Vincent FB, Le Page M, Wei A, Ting SB, Croce CM, Tam C, Mackay F. Cytokine-driven loss of plasmacytoid dendritic cell function in chronic lymphocytic leukemia. *Leukemia* 2014; **28**: 2005-2015 [PMID: 24721775 DOI: 10.1038/Leu.2014.105]

27 **Amicarella F**, Muraro MG, Hirt C, Cremonesi E, Padovan E, Mele V, Governa V, Han J, Huber X, Droeser RA, Zuber M, Adamina M, Bolli M, Rosso R, Lugli A, Zlobec I, Terracciano L, Tornillo L, Zajac P, Eppenberger-Castori S, Trapani F, Oertli D, Iezzi G. Dual role of tumour-infiltrating T helper 17 cells in human colorectal cancer. *Gut* 2017; **66**: 692-704 [PMID: 26719303 DOI: 10.1136/gutjnl-2015-310016]

28 **Gordon WR**, Zimmerman B, He L, Miles LJ, Huang J, Tiyanont K, McArthur DG, Aster JC, Perrimon N, Loparo JJ, Blacklow SC. Mechanical Allostery: Evidence for a Force Requirement in the Proteolytic Activation of Notch. *Dev Cell* 2015; **33**: 729-736 [PMID: 26051539 DOI: 10.1016/j.devcel.2015.05.004]

29 **Itoh M**, Kim CH, Palardy G, Oda T, Jiang YJ, Maust D, Yeo SY, Lorick K, Wright GJ, Ariza-McNaughton L, Weissman AM, Lewis J, Chandrasekharappa SC, Chitnis AB. Mind bomb is a ubiquitin ligase that is essential for efficient activation of Notch signaling by Delta. *Dev Cell* 2003; **4**: 67-82 [PMID: 12530964 DOI: 10.1016/s1534-5807(02)00409-4]

30 **Haddon C**, Jiang YJ, Smithers L, Lewis J. Delta-Notch signalling and the patterning of sensory cell differentiation in the zebrafish ear: evidence from the mind bomb mutant. *Development* 1998; **125**: 4637-4644 [PMID: 9806913 DOI: 10.1242/dev.125.23.4637]

31 **Koo BK**, Yoon MJ, Yoon KJ, Im SK, Kim YY, Kim CH, Suh PG, Jan YN, Kong YY. An obligatory role of mind bomb-1 in notch signaling of mammalian development. *PLoS One* 2007; **2**: e1221 [PMID: 18043734 DOI: 10.1371/journal.pone.0001221]

32 **Brzozowa M**, Mielańczyk L, Michalski M, Malinowski L, Kowalczyk-Ziomek G, Helewski K, Harabin-Słowińska M, Wojnicz R. Role of Notch signaling pathway in gastric cancer pathogenesis. *Contemp Oncol (Pozn)* 2013; **17**: 1-5 [PMID: 23788953 DOI: 10.5114/wo.2013.33765]

33 **Du X**, Cheng Z, Wang YH, Guo ZH, Zhang SQ, Hu JK, Zhou ZG. Role of Notch signaling pathway in gastric cancer: a meta-analysis of the literature. *World J Gastroenterol* 2014; **20**: 9191-9199 [PMID: 25083094 DOI: 10.3748/wjg.v20.i27.9191]

34 **Chen B**, Bai G, Ma X, Tan L, Xu H. MicroRNA1955p is associated with cell proliferation, migration and invasion in prostate cancer and targets MIB1. *Oncol Rep* 2021; **46** [PMID: 34698358 DOI: 10.3892/or.2021.8210]

35 **Wang H**, Huang Q, Xia J, Cheng S, Pei D, Zhang X, Shu X. The E3 Ligase MIB1 Promotes Proteasomal Degradation of NRF2 and Sensitizes Lung Cancer Cells to Ferroptosis. *Mol Cancer Res* 2022; **20**: 253-264 [PMID: 34670864 DOI: 10.1158/1541-7786.MCR-21-0342]

36 **Li B**, Yu L, Liu D, Yang X, Zheng Y, Gui Y, Wang H. MIB1 mutations reduce Notch signaling activation and contribute to congenital heart disease. *Clin Sci (Lond)* 2018; **132**: 2483-2491 [PMID: 30322850 DOI: 10.1042/CS20180732]

37 **Qin XF**, Shan YG, Gao JH, Li FX, Guo YX. E3 ubiquitin ligase mind bomb 1 overexpression reduces apoptosis and inflammation of cardiac microvascular endothelial cells in coronary microvascular dysfunction. *Cell Signal* 2022; **91**: 110223 [PMID: 34954392 DOI: 10.1016/j.cellsig.2021.110223]

38 **Bi H**, Tian T, Zhu L, Zhou H, Hu H, Liu Y, Li X, Hu F, Zhao Y, Wang G. Copy number variation of E3 ubiquitin ligase genes in peripheral blood leukocyte and colorectal cancer. *Sci Rep* 2016; **6**: 29869 [PMID: 27417709 DOI: 10.1038/srep29869]

39 **Ray J**, Hoey C, Huang X, Jeon J, Taeb S, Downes MR, Boutros PC, Liu SK. MicroRNA198 suppresses prostate tumorigenesis by targeting MIB1. *Oncol Rep* 2019; **42**: 1047-1056 [PMID: 31322262 DOI: 10.3892/or.2019.7234]

World Journal of Gastrointestinal Oncology

Submit a Manuscript: https://www.f6publishing.com

World J Gastrointest Oncol 2023 July 15; 15(7): 1311-1316

DOI: 10.4251/wjgo.v15.i7.1311

ISSN 1948-5204 (online)

CASE REPORT

Treatment of *Candida albicans* liver abscess complicated with COVID-19 after liver metastasis ablation: A case report

Wen Hu, Xi Lin, Meng Qian, Tao-Ming Du, Xi Lan

Specialty type: Infectious diseases

Provenance and peer review: Unsolicited article; Externally peer reviewed.

Peer-review model: Single blind

Peer-review report's scientific quality classification

Grade A (Excellent): 0
Grade B (Very good): B
Grade C (Good): C, C
Grade D (Fair): 0
Grade E (Poor): 0

P-Reviewer: Sudhamshu KC, Nepal; Meena DS, India

Received: April 15, 2023
Peer-review started: April 15, 2023
First decision: May 4, 2023
Revised: May 14, 2023
Accepted: May 26, 2023
Article in press: May 26, 2023
Published online: July 15, 2023

Wen Hu, Meng Qian, Xi Lan, Department of Oncology, Chengdu Seventh People's Hospital, Chengdu 610000, Sichuan Province, China

Xi Lin, Department of Oncology, Yanting County People's Hospital, Mianyang 621600, Sichuan Province, China

Tao-Ming Du, Department of Radiology, Chengdu Seventh People's Hospital, Chengdu 610000, Sichuan Province, China

Corresponding author: Xi Lan, MM, Doctor, Department of Oncology, Chengdu Seventh People's Hospital, No. 1188 Shuangxing Street, Shuangliu District, Chengdu 610000, Sichuan Province, China. lanxi2020ys@163.com

Abstract

BACKGROUND

Liver interventional surgery is a relatively safe and minimally invasive surgery. However, for patients who have undergone Whipple surgery, the probability of developing a liver abscess after liver interventional surgery is very high. Fungal liver abscess has a high mortality rate, especially when complicated with malignant tumors, diabetes, coronavirus disease 2019 (COVID-19) and other complications. Fungal liver abscess is rare, and there are no guidelines or expert consensus on the course of antifungal therapy.

CASE SUMMARY

A 54-year-old woman with pancreatic head cancer received albumin-bound paclitaxel in combination with gemcitabine chemotherapy after laparoscopic pancreaticoduodenectomy. Liver metastasis was found 1 mo after completion of 8 cycles of chemotherapy, followed by ablation of the liver metastasis. After half a month of liver metastasis ablation, the patient experienced fever after chemotherapy and was diagnosed with liver abscess complicated with COVID-19 by contrast-enhanced abdominal computed tomography and real-time polymerase chain reaction detection. The results of pus culture showed *Candida albicans*, which was sensitive to fluconazole. The patient underwent percutaneous catheter drainage, antifungal therapy with fluconazole, and antiviral therapy with azvudine. During antifungal therapy, the patient showed a significant increase in liver enzyme levels and was discharged after liver protection therapy. Oral fluconazole was continued for 1 wk outside the hospital, and fluconazole was used for a total of 5 wk. The patient recovered well and received 4 cycles of fluorouracil, leucovorin, oxaliplatin, and irinotecan after 2 mo of antifungal

therapy.

CONCLUSION
Effective treatment of *Candida albicans* liver abscess requires early detection, percutaneous catheter drainage, and 5 wk of antifungal therapy. Meanwhile, complications such as COVID-19 should be actively managed and nutritional support should be provided.

Key Words: Fungal; Liver abscess; COVID-19; Liver metastasis ablation; Pancreatic head cancer; Case report

Core Tip: Fungal liver abscess is rare and has a high mortality rate, especially when combined with malignant tumor, diabetes, coronavirus disease 2019 (COVID-19), and other complications, which increase the difficulty of treatment. However, there are no guidelines or expert consensus on the course of antifungal drugs. We present a rare case of *Candida albicans* liver abscess complicated with COVID-19 after ablation of liver metastasis from pancreatic head cancer. The patient was successfully cured after percutaneous catheter drainage, antifungal therapy, therapeutic management of comorbidities and nutritional support.

Citation: Hu W, Lin X, Qian M, Du TM, Lan X. Treatment of *Candida albicans* liver abscess complicated with COVID-19 after liver metastasis ablation: A case report. *World J Gastrointest Oncol* 2023; 15(7): 1311-1316
URL: https://www.wjgnet.com/1948-5204/full/v15/i7/1311.htm
DOI: https://dx.doi.org/10.4251/wjgo.v15.i7.1311

INTRODUCTION

The incidence of liver abscess after liver intervention is very high in patients who have undergone Whipple surgery. Despite aggressive and appropriate treatment, the mortality rate for liver abscess remains high, particularly when combined with coronavirus disease 2019 (COVID-19). Fungal liver abscess is rare, and there are no guidelines or expert consensus on the timing of antifungal drug use for this condition. In this report, we present a rare case of *Candida albicans* liver abscess complicated by COVID-19 after liver metastasis ablation for pancreatic head cancer. The patient was treated with percutaneous catheter drainage, antifungal therapy, therapeutic management of comorbidities and nutritional support.

CASE PRESENTATION

Chief complaints

A 54-year-old woman was diagnosed with pancreatic head cancer for 8 mo and had liver metastasis ablation for 2 wk.

History of present illness

Eight months ago, the patient was hospitalized for sprained right wrist. It was unexpected to discover that she had pancreatic head cancer and diabetes. She subsequently underwent laparoscopic pancreaticoduodenectomy, and histopathologic results revealed pancreatic adenocarcinoma with mucinous adenomas (about 5%-10% of which were sig-ring cell carcinomas), G3/poorly differentiated, and invasion of nerves and lymphatic vessels. Following surgery, she completed 8 cycles of chemotherapy with albumin-bound paclitaxel and gemcitabine. One month after completing chemotherapy, contrast-enhanced abdominal computed tomography (CT) revealed liver metastasis in the right lobe, with a maximum cross-section of approximately 2.0 cm × 1.9 cm. Two weeks ago, the patient underwent CT-guided ablation of liver metastasis and was discharged after receiving treatment for infection prevention and liver protection. The patient had no discomfort and was admitted to the hospital for chemotherapy.

History of past illness

The patient sprained her right wrist more than 8 mo ago, and she had no other known medical conditions.

Personal and family history

Her father died of an unknown type of cancer at the age 49.

Physical examination

The patient's vital signs were stable, and her skin and sclera showed no signs of yellowing. The abdomen was flat and

soft, and the right lower abdomen was tender and percussive.

Laboratory examinations

Blood routine, renal function, coagulation, carcinoembryonic antigen, and carbohydrate antigen (CA) 19-9 results were all within the normal range. However, some laboratory results were abnormal, including C-reactive protein, 4.62 mg/L (normal range: < 4 mg/L); alanine aminotransferase, 50 IU/L (normal range: 7-40 IU/L); aspartate aminotransferase, 45 IU/L (normal range: 13-35 IU/L); CA125, 62.8 U/mL (normal range: ≤ 25 ng/mL) (Table 1). Real-time polymerase linked reaction (RT-PCR) indicated positive nucleic acid of novel coronavirus, and pus culture revealed *Candida albicans*, which was sensitive to fluconazole.

Imaging examinations

Chest CT examination indicated viral pneumonia, and contrast-enhanced abdominal CT revealed a liver abscess with a maximum cross-section of 6.9 cm × 6.0 cm, accompanied by fluid and gas (Figure 1A).

FINAL DIAGNOSIS

The patient was diagnosed as *Candida albicans* liver abscess, COVID-19, and Stage IV pancreatic head cancer.

TREATMENT

The patient was admitted to the hospital on December 14, 2022, for chemotherapy with fluorouracil, leucovorin, oxaliplatin, and irinotecan (FOLFOXIRI) regimen. On December 17, 2022, the patient developed a fever with a body temperature as high as 39.6 °C. Blood tests showed an increased white blood cell count, neutrophil percentage, C-reactive protein (CRP) and procalcitonin (PCT). Liver function indicated that the aminotransferase value was doubled (Table 1). Chest CT showed no abnormalities. Acute bronchitis was considered in combination with the patient's cough. Given that the patient was a chemotherapy patient with advanced malignant tumor complicated with diabetes mellitus and a weakened immune system, she was given cefoperazone sulbactam sodium (3 g *i.v.* q12h), continued liver protection, immune enhancement, nutritional support, and other treatments. After 3 d of antibiotic use, the patient's temperature still peaked at 39.6 °C, and her RT-PCR indicated COVID-19, while chest CT examination indicated viral pneumonia. She was treated with azvudine tablets (5 mg po qd). In addition, the patient experienced vomiting, poor appetite, and right upper abdominal pain. Contrast-enhanced abdominal CT showed a liver abscess with a maximum cross-section of 6.9 cm × 6.0 cm, accompanied by fluid and gas (Figure 1A). On January 20, 2022, the patient underwent CT-guided percutaneous catheter drainage for hepatic abscess. The pus was brown and turbid with flocculent substance and it was sent for microbial culture. The antibiotic was upgraded to Meropenem (1 g *i.v.* q8h). On December 22, 2022, the patient's blood routine showed a very low white blood cell count of 1.24 × 10^9/L, a platelet count of 49 × 10^9/L, and CRP and PCT were still significantly elevated, while liver function was basically normal (Table 1). To improve both the white blood cell and platelet counts, the patient was injected with recombinant human granulocyte stimulating factor plus recombinant human thrombopoietin. On December 25, 2022, pus culture revealed *Candida albicans*, which was sensitive to fluconazole. Then the patient was treated with fluconazole injection (0.4 g *i.v.* qd, double the first dose). With the use of fluconazole, the patient's symptoms and signs gradually improved. On December 29, 2022, contrast-enhanced abdominal CT showed no gas or fluid in the abscess space (Figure 1B). The patient had no pus coming out of the drain, and the drain was removed. On January 14, 2023, the patient's laboratory results showed normal blood routine, slightly elevated CRP and PCT, and significantly elevated aminotransferase (Table 1). The significant elevated aminotransferases were considered a side effect of fluconazole, but fluconazole had to be continued, so liver protection therapy was strengthened. On January 20, 2023, the patient had no discomfort such as fever or abdominal pain, and her routine blood, CRP, PCT, and liver function were basically normal (Table 1). At this time, the patient received intravenous fluconazole for 4 wk and continued to take oral fluconazole (0.45 g po qd) and hepatoprotective drugs for 1 wk after discharge. In total, the antifungal course lasted for 5 wk.

OUTCOME AND FOLLOW-UP

The patient recovered well and received 4 cycles of FOLFOXIRI chemotherapy after 2 mo of antifungal therapy. The patient's routine blood, liver function, kidney function, and coagulation were normal, tumor markers decreased, and contrast-enhanced abdominal CT did not indicate liver tissue absence, cavity, or gas any longer (Figure 1C).

DISCUSSION

The pancreas is made up of acinar cells that secrete digestive enzymes, ductal cells that secrete bicarbonate, central acinar cells that act as a transition zone between acinar and ductal cells, endocrine islets that secrete hormones, and relatively

Table 1 Laboratory test results

Date	White blood cell count, × 10^9/L	Neutrophil percentage, %	Hemoglobin, g/L	Platelet count, × 10^9/L	hs-CRP, mg/L	PCT, ng/mL	ALT, IU/L	AST, IU/L	GGT, IU/L
2022.12.14	6.35	66.9	123	410	4.62	0.13	50	45	35
2022.12.17	16.97	96.5	138	235	73.08	3.10	96	80	68
2022.12.19	8.22	93.2	112	122	169.78	-	-	-	-
2022.12.22	1.24	72.0	95	49	76.13	0.89	24	27	60
2022.12.28	18.81	88.8	98	212	74.18	0.19	35	47	41
2023.01.14	8.85	68.4	126	323	32.94	0.46	258	316	167
2023.01.20	3.86	56.2	110	224	-	-	47	39	78

Normal values of laboratory tests (routine blood test): White blood cell count: 3.5-9.5 × 10^9/L; neutrophil percentage: 40%-75%; hemoglobin: 115-150 g/L; platelet count: 125-350 × 10^9/L; hypersensitive C-reactive protein: < 4 mg/L; procalcitonin: < 0.05 ng/mL; alanine aminotransferase: 7-40 IU/L; aspartate aminotransferase: 13-35 IU/L; γ-glutamyltransferase: 7-45 IU/L. ALT: Alanine aminotransferase; AST: Aspartate aminotransferase; GGT: γ-glutamyltransferase; hs-CRP: Hypersensitive C-reactive protein; PCT: Procalcitonin.

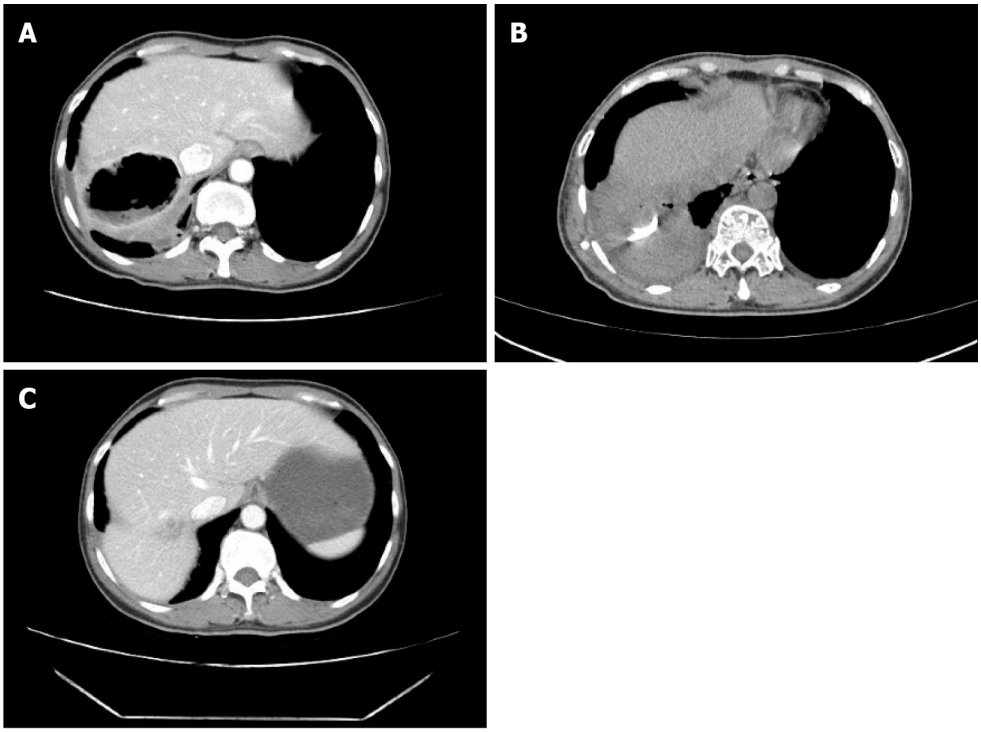

DOI: 10.4251/wjgo.v15.i7.1311

Figure 1 Contrast-enhanced abdominal computed tomography. A: Contrast-enhanced abdominal computed tomography (CT) on December 19, 2022 showed liver abscess, with a maximum section of 6.9 cm × 6.0 cm, accompanied by fluid and gas; B: Contrast-enhanced abdominal CT on December 29, 2022 showed a cavity shadow in the right posterior lobe of the liver, and a drainage tube shadow was seen inside the cavity. The cavity was smaller than before, and no gas-liquid level was observed; C: Contrast-enhanced abdominal CT on March 27, 2023 showed the filling of solid components in the primary cavity of the right posterior lobe of the liver, and the enhancement of the cavity wall was relatively uniform.

inactive stellate cells. Cancer occurs when abnormal DNA mutations in the pancreas cause pancreatic cells to grow and divide uncontrollably[1]. Risk factors for early hepatic metastasis of pancreatic cancer include age over 70 years, lymph node metastasis, adenocarcinoma or neuroendocrine carcinoma, large tumor size, poor differentiation, no surgery, no chemotherapy. Pancreatic cancer is one of the most aggressive and fatal malignancies[2].

The treatment of hepatic metastasis of pancreatic cancer includes chemotherapy, radiotherapy, and surgery. Ablation is one of the most effective and minimally invasive techniques for the treatment of liver tumors, with a low complication rate. Compared with chemotherapy alone, ablation combined with chemotherapy can further prolong the survival period of patients. However, in some rare cases, complications such as liver abscess, bronchobiliary fistula, hollow visceral perforation, diaphragmatic perforation, and hernia may occur[3,4]. The clinical symptoms of hepatic abscess are nons-

pecific, including abdominal pain, fever, nausea, and poor appetite. Routine blood and liver function tests are abnormal, but the extent of the abnormality depends on the pathogen, extent, and site of the abscess. The diagnosis of liver abscess needs to be confirmed by ultrasound, CT, or magnetic resonance imaging (MRI), especially the differentiation between liver abscess and liver metastasis[5-7]. The incidence of liver abscess in ablation patients was 0.1% to 0.7%, while the incidence of liver abscess was significantly increased in patients with enterobiliary anastomosis[8]. The incidence of liver abscess after liver intervention in patients who had undergone Whipple surgery was up to 86%. This was closely related to the fact that pathogenic bacteria can directly enter the biliary tract system and led to the formation of an abscess. The pathogens of liver abscesses were mostly bacteria, partly parasites, and rarely fungi[9]. Patients with liver abscesses had a high mortality rate, which was as high as 75%-80% in the early 20th century. Now the mortality rate for patients with liver abscesses has decreased significantly, but it is still close to 15%. Factors that increase the risk of death in patients with liver abscess include advanced age, malignancy, diabetes, abscess > 5 cm, low immunity, multiple organ failure, PPI use, and cirrhosis, *etc*[8]. When patients with liver abscess are complicated by COVID-19, the mortality is still as high as 55% even after early drainage and antibiotic treatment[10,11]. This is linked to severe sepsis caused by COVID-19, which reduces mitochondrial efficiency and leads to respiratory chain dysfunction[12]. The prognosis of patients with hepatic abscess is closely related to appropriate treatment. Liver abscesses that are smaller than 3 cm to 5 cm, especially when they are multiple, can be treated with antibiotics alone without drainage, although there is no general consensus on this. It has been reported that the cure rate of liver abscess < 3 cm with antibiotics alone is 100%, while the cure rate of liver abscess < 5 cm is about 80%. It is not clear to know the duration of antibiotic use, usually between 2 wk and 6 wk. Surgical drainage in combination with antibiotics is usually necessary if the patient has failed medication, has an abscess greater than 5 cm, or has other causes. If conservative treatment fails, patients may even need a hepatectomy[9].

Fungal liver abscess cases are rare, especially for patients with pancreatic head cancer, diabetes, bone marrow transplantation after chemotherapy, or COVID-19. There are no guidelines or expert consensus on the course of antifungal therapy to guide clinical treatment. For patients with *Candida albicans*, liver abscess complicated with various underlying diseases such as malignant tumor and diabetes, continuous antifungal therapy for 5 wk is effective. In the early stage, the efficacy can be judged according to the patient having no fever, abdominal pain has disappeared and leukocyte, CRP, PCT has decreased. It can also be combined with ultrasound, CT, or MRI to judge the treatment effect. However, the use of antifungal drugs for a long course should make the physician wary of liver function damage and other side effects while liver function and kidney function should be monitored.

CONCLUSION

The incidence of liver abscess after liver intervention is very high in patients who have undergone Whipple surgery. Effective treatment of *Candida albicans* liver abscess requires early detection, percutaneous catheter drainage, and antifungal therapy for 5 wk. Meanwhile, complications such as COVID-19 should be actively dealt with, and nutritional support should be provided.

ACKNOWLEDGEMENTS

Grammar consulting and writing assistance were kindly provided by Ying Liu and Tao Qin.

FOOTNOTES

Author contributions: Hu W contributed to the writing of the original draft; Qian M and Lin X were involved in editing the manuscript; Du TM participated in manuscript editing and provided computed tomography images; Lan X participated in manuscript writing and review.

Informed consent statement: Informed written consent was obtained from the patient for publication of this report and any accompanying images.

Conflict-of-interest statement: The authors declare that they have no conflict of interest to disclose.

CARE Checklist (2016) statement: The authors have read the CARE Checklist (2016), and the manuscript was prepared and revised according to the CARE Checklist (2016).

Country/Territory of origin: China

ORCID number: Xi Lan 0000-0002-9893-3030.

S-Editor: Chen YL
L-Editor: Filipodia
P-Editor: Chen YL

REFERENCES

1 **Hu JX**, Zhao CF, Chen WB, Liu QC, Li QW, Lin YY, Gao F. Pancreatic cancer: A review of epidemiology, trend, and risk factors. *World J Gastroenterol* 2021; **27**: 4298-4321 [PMID: 34366606 DOI: 10.3748/wjg.v27.i27.4298]
2 **Cao BY**, Tong F, Zhang LT, Kang YX, Wu CC, Wang QQ, Yang W, Wang J. Risk factors, prognostic predictors, and nomograms for pancreatic cancer patients with initially diagnosed synchronous liver metastasis. *World J Gastrointest Oncol* 2023; **15**: 128-142 [PMID: 36684042 DOI: 10.4251/wjgo.v15.i1.128]
3 **Yan X**, Ning ZY, Wang P, Zhuang LP, Xu LT, Zhu ZF, Sheng J, Shen YH, Hua YQ, Meng ZQ. Combined ablation-chemotherapy *versus* chemotherapy alone for pancreatic cancer with liver metastasis: a propensity score matching study. *Expert Rev Gastroenterol Hepatol* 2021; **15**: 1047-1056 [PMID: 33356652 DOI: 10.1080/17474124.2021.1869937]
4 **Dai H**, Cui D, Li D, Zhai BO, Zhang J. Hepatic abscess with hepatobronchial fistula following percutaneous radiofrequency ablation for hepatocellular carcinoma: A case report. *Oncol Lett* 2015; **9**: 2289-2292 [PMID: 26137058 DOI: 10.3892/ol.2015.3044]
5 **Lardière-Deguelte S**, Ragot E, Amroun K, Piardi T, Dokmak S, Bruno O, Appere F, Sibert A, Hoeffel C, Sommacale D, Kianmanesh R. Hepatic abscess: Diagnosis and management. *J Visc Surg* 2015; **152**: 231-243 [PMID: 25770745 DOI: 10.1016/j.jviscsurg.2015.01.013]
6 **Oh JG**, Choi SY, Lee MH, Lee JE, Yi BH, Kim SS, Min JH, Lee B. Differentiation of hepatic abscess from metastasis on contrast-enhanced dynamic computed tomography in patients with a history of extrahepatic malignancy: emphasis on dynamic change of arterial rim enhancement. *Abdom Radiol (NY)* 2019; **44**: 529-538 [PMID: 30196363 DOI: 10.1007/s00261-018-1766-y]
7 **Lee CM**, Kang BK, Kim M. Differentiation of Small Hepatic Abscess From Hepatic Metastasis With a Combination of Imaging Parameters. *J Comput Assist Tomogr* 2022; **46**: 514-522 [PMID: 35483061 DOI: 10.1097/RCT.0000000000001307]
8 **Mavilia MG**, Molina M, Wu GY. The Evolving Nature of Hepatic Abscess: A Review. *J Clin Transl Hepatol* 2016; **4**: 158-168 [PMID: 27350946 DOI: 10.14218/JCTH.2016.00004]
9 **Thomas KT**, Bream PR Jr, Berlin J, Meranze SG, Wright JK, Chari RS. Use of percutaneous drainage to treat hepatic abscess after radiofrequency ablation of metastatic pancreatic adenocarcinoma. *Am Surg* 2004; **70**: 496-499 [PMID: 15212401]
10 **Elliott R**, Ohene Baah N, Grossman VA, Sharma AK. COVID-19 Related Mortality During Management of a Hepatic Abscess. *J Radiol Nurs* 2020; **39**: 271-274 [PMID: 32982611 DOI: 10.1016/j.jradnu.2020.09.001]
11 **Deif MA**, Mounir AM, Abo-Hedibah SA, Abdel Khalek AM, Elmokadem AH. Outcome of percutaneous drainage for septic complications coexisted with COVID-19. *World J Radiol* 2022; **14**: 91-103 [PMID: 35646292 DOI: 10.4329/wjr.v14.i4.91]
12 **Shenoy S**. Coronavirus (Covid-19) sepsis: revisiting mitochondrial dysfunction in pathogenesis, aging, inflammation, and mortality. *Inflamm Res* 2020; **69**: 1077-1085 [PMID: 32767095 DOI: 10.1007/s00011-020-01389-z]

Published by **Baishideng Publishing Group Inc**
7041 Koll Center Parkway, Suite 160, Pleasanton, CA 94566, USA
Telephone: +1-925-3991568
E-mail: bpgoffice@wjgnet.com
Help Desk: https://www.f6publishing.com/helpdesk
https://www.wjgnet.com